
The role of the Polycomb protein L3MBTL1 in hematopoiesis

Fabiana Perna (dottoranda)

Dottorato in Scienze Biotecnologiche – 25 ciclo
Indirizzo Biotecnologie mediche
Università di Napoli Federico II





The role of the Polycomb protein L3MBTL1 in hematopoiesis

Fabiana Perna (dottoranda)

Dottoranda: Dr. Fabiana Perna

Relatore: Prof. Fabrizio Pane

Coordinatore: Prof. Giovanni Sannia

INDICE

RIASSUNTO (IT)	pag. 8-12
SUMMARY (EN)	pag 13-16
1. INTRODUCTION	pag 17-20
1.1 L3MBTL1	
1.2 Epigenetic roles for class I and class II genes	
1.3 PRMT5	
2. MATERIALS and METHODS	pag 21-26
2.1 Purification and in vitro primary culture of human cord blood CD34+ cells	
2.2. Generation of lentiviruses and infection of primary hematopoietic CD34+ cells	
2.3 Flow cytometry	
2.4 Isolation of MPN samples	
2.5 Cytospin preparations, GIEMSA staining and Benzidine staining	
2.6 RNA extraction and quantitative Real-Time PCR (qRT-PCR)	
2.7 Methylcellulose colony and LTC-IC assays.	
2.8 Antibodies	
2.9 Ras Activation Assay	
2.10 Overexpression assays	
2.11 Chromatin Immunoprecipitation (ChIP) assays	
2.12 Gene expression profile (GEP) and Gene set enrichment analysis (GSEA)	
2.13 Human embryonic stem cell culture and differentiation protocols	
2.14 Immunofluorescence	
2.15 Western blot analysis	
2.16 Cell Cycle/DNA and flowcytometry analysis	
2.17 Immunoassays	
2.18 Statistical analysis	
2.19 Immunoblotting and Coimmunoprecipitations	
2.20 Comet Assay	
2.21 Immunocytochemistry	
2.22 DNA Fiber Analyses	
2.23 Metaphase Spreads	
2.24 Cell Culture, Transfection, and Plasmids	
2.25 In Vitro Kinase Assay	
2.26 In Vitro Methylation Assay	
2.27 Microarray Analysis	
3. RESULTS	pag 27-40
3.1. L3MBTL1 and the erythroid lineage differentiation of HSPCs	
3.2. L3MBTL1 and the DNA damage response	
3.3. L3MBTL1 and pluripotency of human embryonic stem cells	
3.4. L3MBTL1 and the BMP4/smad5 signaling pathway	
3.5 PRMT5	
4. DISCUSSION	pag 41-46
4.1. L3MBTL1 and erythroid differentiation	
4.2. L3MBTL1 and the DNA damage	
4.3. L3MBTL1 and the pluripotency of human embryonic stem cells	
4.4. L3MBTL1 and the BMP4/smad5 signaling pathway	
4.5 PRMT5	
4.6 Overall conclusions	
5. FIGURES	
6. FIGURE LEGENDS	pag 47-55

7. ACKNOWLEDGEMENTS	pag 56
8. REFERENCES	pag 57-62
9. LIST OF HONORS AND AWARDS	pag 63
10. LIST OF COMMUNICATIONS	pag 64
11. LIST AND COPIES OF PUBLISHED PAPERS	pag 67-

RIASSUNTO

Mutazioni epigenetiche ricorrenti nelle malattie mieloidi

Negli ultimi 40 anni, tramite studi di citogenetica sono state identificate diverse alterazioni somatiche ricorrenti nei pazienti con neoplasie ematologiche mieloidi, tra cui le malattie mieloproliferative (MPN), le sindromi mielodisplastiche (MDS) e le leucemie mieloidi acute (AML). Studi genetici e funzionali di queste anomalie hanno consentito di classificarle in un modello definito "two hit" della trasformazione delle cellule emopoietiche (leucemogenesi), che comprende: le mutazioni di classe I, che conferiscono un vantaggio proliferativo attraverso l'attivazione di diverse cascate del segnale (tali mutazioni includono quelle di geni che codificano per membri stessi della trasduzione del segnale o attivatori a valle della trascrizione); e mutazioni di classe II, che determinano il differenziamento mieloido delle cellule staminali attraverso la regolazione dell'espressione genica di target trascrizionali specifici della linea mieloido.

Piu' recentemente, sono state identificate nuove mutazioni in aggiunta a quelle precedentemente descritte, che pur verificandosi di frequente nei pazienti con malattie ematologiche neoplastiche, non possono essere classificate come di prima o seconda classe. Queste mutazioni, recentemente identificate, sono a carico di geni che codificano per proteine che regolano la metilazione del DNA (DNMT3a, TET2, IDH1/2 ecc) o le modificazioni post-traslazionali degli istoni (L3MBTL1, PRMT5, ASXL1, MLL, EZH2 ecc). E' di grosso interesse scientifico comprendere il ruolo funzionale di queste alterazioni epigenetiche nella patogenesi delle malattie ematologiche, per poter identificare nuovi target (target epigenetici) terapeutici.

In questa dissertazione saranno discussi gli studi che abbiamo condotto per elucidare il ruolo di una delle alterazioni somatiche epigenetiche ricorrenti nelle malattie mieloidi (la delezione della proteina Polycomb L3MBTL1). Questi lavori hanno consentito di dimostrare che questi eventi ricorrenti contribuiscono alla leucemogenesi mieloido.

Inoltre, abbiamo dimostrato che diverse mutazioni di classe I e II (per esempio JAK2V617F o AML1/ETO) alterano l'epigenoma delle cellule maligne, in aggiunta ai ruoli classici nel promuovere la proliferazione e il differenziamento delle cellule emopoietiche. Questi dati sottolineano l'importanza delle anomalie epigenetiche nella patofisiologia delle malattie mieloidi.

L3MBTL1

L3MBTL1 rappresenta l'omologo umano del gene oncosoppressore della drosophila, *l(3)mbt* [*lethal(3)malignant brain tumor*], la cui inattivazione determina aumentata proliferazione dei neuroblasti ottici della mosca adulta e delle cellule gangliari del cervello della larva. Dopo aver cristallizzato i tre domini in tandem (di circa 100 aminoacidi) MBT fu dimostrato che L3MBTL1 umano compatta la cromatina attraverso il legame con residui lisinici mono- e di-metilati sugli istoni H1 (H1K26) e H4 (H4K20) attraverso il secondo dei suoi tre domini MBT. Subito dopo l'identificazione molecolare di *l(3)mbt*, Bornemann et al. riportarono che un altro gene della *Drosophila*, *Sex comb on midleg* (*Scm*), codificava per una proteina che conteneva due domini MBT in tandem in posizione N-terminale. *Scm* fu originariamente identificata come un gene richiesto per l'accurato mantenimento della distribuzione dei geni omeotici durante lo sviluppo e fu pertanto classificato come un repressore *Polycomb* group (PcG). Infatti, gli embrioni mutant *Scm* presentano un classico fenotipo PcG di sviluppo in cui i segmenti anteriori del corpo assumono l'identita' di quelli posteriori (per esempio il torace nell'addome), dovuto alla mancanza di repressione dei geni nel locus *bithorax*.

Il gene umano L3MBTL1, e' localizzato sul braccio lungo del cromosoma 20, in posizione 20q12, nell'ambito della regione comunemente deleta nei pazienti con sindromi mielodisplastiche, malattie mieloproliferative o leucemia mieloide acuta, associate alla delezione del cromosoma 20.

La delezione del cromosoma 20 (20q-) rappresenta la seconda anormalita' cromosomica piu' comune nelle neoplasie ematologiche, dopo il cromosoma Philadelphia. L'anormalita' 20q- viene osservata nel 10% dei pazienti con malattie mieloproliferative, di cui la piu' comune e' la Policitemia Vera, nel 4% dei pazienti con malattie mielodisplastiche, e nell'1-2% dei pazienti con Leucemia mieloide acuta. L'inattivazione (o aploinsufficienza) di geni oncosoppressori su 20q potrebbe spiegare la patogenesi di questi disordini.

L'espressione di L3MBTL1 nel compartimento ematopoietico (nelle cellule CD34+ che rappresentano le cellule staminali/progenitrici ematopoietiche) e l'assenza di mutazioni a carico dell'allele non deleta, hanno fatto a lungo ipotizzare che l'aploinsufficienza di L3MBTL1 possa contribuire alla patogenesi delle neoplasie ematologiche mieloidi associate alla delezione del cromosoma 20.

1) Per definire il suo ruolo in ematopoiesi e la possibilita' che la sua ridotta espressione nelle malattie mieloidi associate a delezione del cromosoma 20 contribuisca alla patogenesi di questi disordini, abbiamo silenziato l'espressione di L3MBTL1 nelle cellule staminali/progenitrici (CD34+) isolate da sangue cordonale (usando short hairpin RNAs). Abbiamo osservato che le cellule staminali emopoietiche deplete per L3MBTL1 dimostrano un aumentato differenziamento verso la linea eritroide. In maniera consistente la overespressione di L3MBTL1 nelle cellule staminali/progenitrici CD34+ come nelle linee cellulari 20q- riduceva il differenziamento eritroide. Inoltre, i livelli endogeni di espressione di L3MBTL1 si riducevano durante il differenziamento eritroide indotto da emina o dall'esposizione a eritropoietina, suggerendo un ruolo specifico per la ridotta espressione di L3MBTL1 nell'indurre le decisioni di differenziamento delle cellule emopoietiche verso la linea eritroide. Il silenziamento di L3MBTL1 aumentava anche la sensibilita' delle cellule staminali progenitrici all'eritropoietina (Epo), con aumentata fosforilazione (indotta da Epo) di STAT5, AKT, and MAPK ed evidente fosforilazione anche in assenza di Epo. Questi dati suggerirono che l'aploinsufficienza di L3MBTL1 contribuisce ad alcune neoplasie mieloproliferative (20q), specialmente la Policitemia Vera, attraverso la promozione del differenziamento eritroide.

La Policitemia Vera infatti e' una malattia clonale della cellula staminale emopoietica, caratterizzata da una proliferazione persistente ed incontrollata della linea eritropoietica indipendentemente dai meccanismi che fisiologicamente regolano l'eritropoiesi. Nella policitemia vera, la proliferazione eritroide e' predominante e determina un aumento numerico dei globuli rossi nel sangue periferico.

2) Per investigare il ruolo di L3MBTL1 come oncosoppressore, abbiamo continuato ad utilizzare un approccio "loss-of-function", attraverso l'utilizzo di vettori lentivirali che consentono l'espressione di shRNA diretti contro L3MBTL1. Abbiamo trovato che la deplezione di L3MBTL1 nelle cellule umane causa stress replicativo, rottura del DNA, attivazione della risposta al danno del DNA e instabilita' genomica. L3MBTL1 interagisce infatti con Cdc45, MCM2-7 and PCNA, componenti dell'apparato replicativo, necessari per la progressione della replicazione. Questi dati suggeriscono che la delezione di L3MBTL1 causa danno del DNA, tramite la perturbazione della replicazione del DNA. Un'attivata risposta al danno del DNA e l'instabilita' genomica sono aspetti comuni nella tumorigenesi e rappresentano una conseguenza dell'overespressione di molti oncogeni. Questi studi ci hanno consentito di proporre un modello in cui la delezione di L3MBTL1 contribuisce allo sviluppo delle neoplasie ematologiche associate alla delezione del braccio lungo del

cromosoma 20 attraverso l'induzione di stress replicativo, danno al DNA e instabilità genomica.

3) Per definire come L3MBTL1, una proteina del gruppo Polycomb con attività trascrizionali di repressione, regola gli eventi iniziali del differenziamento, abbiamo creato delle linee cellulari embrionali che costitutivamente esprimono shRNA diretti contro L3MBTL1. Il silenziamento di L3MBTL1 nelle cellule umane embrionali consentiva una normale morfologia, proliferazione, cinetica di ciclo cellulare, normali marcatori di superficie e cariotipo dopo 40 passaggi. Però, sotto condizioni che promuovevano il differenziamento spontaneo, le cellule embrionali senza L3MBTL1 si differenziavano in una popolazione relativamente omogenea di cellule larghe, piatte, tipo trofoblasti, a differenza del differenziamento multilineare delle cellule di controllo. Le cellule senza L3MBTL1 esprimevano numerosi marcatori della linea trofoblastica e secernevano ormoni placentari. Nonostante le cellule senza L3MBTL1 potevano essere indotte a differenziare in varie linee embrionali, esse adottavano un destino esclusivamente trofoblastico durante il differenziamento spontaneo. Questi dati dimostrano che la deplezione di L3MBTL1 non disturba il self-renewal delle cellule embrionali, ma piuttosto aumenta il differenziamento verso tessuti trofoblastici extraembrionali.

Questo fenotipo risultava molto simile a quello delle cellule embrionali trattate con BMP4 e infatti il trattamento con BMP4 riduceva il livello di espressione endogena di L3MBTL1. Questi dati suggerivano che la deplezione di L3MBTL1 potrebbe essere responsabile dell'attivazione della cascata del segnale di BMP4.

4) Infine, più recentemente abbiamo dimostrato che L3MBTL1 regola l'espressione di un fattore di trascrizione specifico per la linea eritroide EKLF. L3MBTL1, che generalmente funziona come repressore trascrizionale, regola la trascrizione di smad5 e controlla pertanto la cascata del segnale BMP4/smad5 e i suoi effettori a valle, incluso EKLF. Data la rilevanza clinica di regolare l'espressione dei geni globinici da parte di EKLF nelle emoglobinopatie, abbiamo utilizzato un modello umano di beta-emoglobinopatia, cioè le cellule staminali pluripotenti indotte da pazienti. Queste cellule sono state infettate con vettori lentivirali per esprimere shRNA contro L3MBTL1 e si sono mostrate capaci di generare una progenie eritroide che esprime alti livelli di espressione dei geni globinici e di fattori della trascrizione a valle di BMP4, incluso EKLF. Pertanto, pensiamo che L3MBTL1 possa modulare l'induzione dell'espressione di EKLF, attraverso la modulazione del pathway BMP4/smad5, regolando infine l'espressione dei geni globinici e servendo pertanto come potenziale approccio terapeutico per le emoglobinopatie.

PRMT5

PRMT5 è un'arginina metiltransferasi di tipo II che fu inizialmente identificata come una proteina che lega JAK (JAK-binding protein 1 - JBP1) nei lieviti. PRMT5 media la dimetilazione simmetrica dei residui arginici sugli istoni H2A, H3, e H4, e metila altre proteine cellulari come p53, SPT5, e MBD2. Insieme a MEP50, che contiene il dominio WD40 e con pICln, PRMT5 forma un grosso complesso proteico 20S con funzione di metiltransferasi, chiamato il "metilosoma". Questo complesso funziona nel processamento dell'RNA attraverso la metilazione di proteine Sm e ha un ruolo anche nella biogenesi delle snRNP. PRMT5 è stata anche ritrovata nei complessi che rimodellano la struttura della cromatina hSWI/SNF e NURD, dove può esercitare controllo trascrizionale sulla espressione dei geni bersaglio. Per studiare le malattie mieloproliferative indotte dalla mutazione JAK2V617F, abbiamo ricercato l'interazione in vivo tra PRMT5 e le chinasi oncogeniche mutanti JAK2 (JAK2V617F e JAK2K539L), e abbiamo determinato come questa interazione contribuisce al fenotipo mieloproliferativo che inducono.

La mutazione JAK2V617F costitutivamente attiva la tirosina chinasi JAK2 ed è espressa nella maggior parte dei pazienti con malattie mieloproliferative. Abbiamo trovato che la proteina mutata JAK2V617F (e JAK2K539L) si lega a PRMT5 in maniera più forte della proteina JAK2 wild-type. Queste chinasi oncogeniche (mutazioni di classe I) acquisiscono anche la capacità di fosforilare PRMT5, riducendo la sua capacità di metilare i suoi substrati istonici, e rappresentando una specifica acquisizione di funzione che consente loro di regolare le modificazioni cromatiniche. Abbiamo documentato la fosforilazione di PRMT5 nei campioni di pazienti positivi per JAK2V617F e quando abbiamo silenziato l'espressione di PRMT5 nelle cellule umane CD34+ usando shRNA, abbiamo osservato un'aumentata formazione di colonie e differenziamento eritroide. Questi risultati indicano che la fosforilazione di PRMT5 (con funzione epigenetica) contribuisce al fenotipo delle malattie mieloproliferative indotte dalla mutazione classica di JAK2.

CONCLUSIONI

La nostra conoscenza dei meccanismi che promuovono la trasformazione mieloide si è molto evoluta negli ultimi anni grazie all'approfondimento degli eventi genetici che sono stati identificati nei pazienti con questi disordini. Inoltre l'identificazione di mutazioni nei geni coinvolti nella regolazione epigenetica ha rivelato nuovi meccanismi di trasformazione. Regulatori della metilazione del DNA (come TET2, IDH1, IDH2 e DNMT3A) e delle modificazioni degli istoni (come L3MBTL1, PRMT5, MLL, ASXL1 e EZH2) rappresentano il bersaglio di alterazioni somatiche in una percentuale significativa di pazienti con malattie mieloidi. Questo suggerisce un ruolo cruciale per i modificatori epigenetici nella regolazione della emopoiesi normale e illustra come la perdita della funzionalità epigenetica normale può contribuire alla leucemogenesi. Pertanto, elucidare l'impatto delle mutazioni epigenetiche sulla leucemogenesi e la risposta terapeutica sarà essenziale per l'avanzare delle nostre conoscenze e il trattamento delle malattie mieloidi.

La nostra comprensione delle conseguenze biologiche di questi cambiamenti epigenetici è ancora a uno stadio iniziale. Nonostante possiamo capire l'attività specifica di un singolo gene e derivare modelli generali di come le modificazioni epigenetiche influenzano la trascrizione, non conosciamo ancora i componenti cruciali che sono alterati da queste modificazioni epigenetiche e come queste influenzano l'andamento epigenetico, l'espressione genica e le alterazioni fenotipiche delle cellule emopoietiche. Per definizione, le mutazioni in questa classe di geni influenzano globalmente la mappa cromatinica e molti geni e pathway ne risultano alterati; per cui, è improbabile che una spiegazione semplice e lineare possa spiegare come queste mutazioni contribuiscono allo sviluppo della leucemia. L'espressione genica e l'analisi epigenomica hanno identificato un gruppo di geni bersaglio dei modificatori epigenetici, come il cluster genico HOX, che sono essenziali per la trasformazione maligna da parte di specifiche mutazioni epigenetiche. Quel che abbiamo imparato è che queste mutazioni nei modificatori epigenetici non ricadono nella classificazione precedentemente stabilita di mutazioni di classe I o II della leucemogenesi. Clinicamente, le mutazioni epigenetiche si verificano in combinazione con una delle mutazioni di classe I o II o con entrambe. I dati attuali genetici e funzionali suggeriscono che le mutazioni nei modificatori epigenetici ricadono in almeno due nuove classi: quella delle mutazioni che influenzano la idrossimetilazione del DNA (TET2, IDH1 and IDH2), e quella delle mutazioni che direttamente regolano la metilazione del DNA e/o degli istoni (L3MBTL1, PRMT5, MLL, ASXL1 e DNMT3A). Queste due nuove classi di mutazioni epigenetiche probabilmente contribuiscono alla trasformazione leucemica influenzando la regolazione epigenetica, pertanto generando un panorama dello stato della cromatina che può mantenere e cooperare con l'effetto delle mutazioni di classe I o II. Studi ulteriori sono necessari per chiarire queste possibilità e capire come

diverse combinazioni di genotipi di alleli associate alla leucemia risultano in fenotipi di leucemia mieloide distinti in termini biologici, terapeutici e prognostici.

SUMMARY

Recurrent epigenetic modifications in myeloid malignancies

In the past four decades, cytogenetic and candidate-gene studies have identified recurrent somatic alterations in patients with myeloid malignancies, including myeloproliferative neoplasms (MPNs), myelodysplastic syndrome (MDS) and acute myeloid leukaemia (AML). Genetic and functional studies have suggested that there are at least two classes of myeloid leukaemia disease alleles that contribute to haematopoietic transformation: class I alleles, which confer a growth advantage by activating downstream effectors of various signalling pathways including members of the signal transducer and activator of transcription (STAT), PI3K and RAS–MAPK pathways; and class II alleles, which alter the expression of key transcriptional targets in myelopoiesis. However, several lines of evidence suggest that there are leukaemia disease alleles that cannot be classified into this widely accepted two-hit model of myeloid leukaemogenesis. Emerging genetic data suggest that there are additional classes of mutations that commonly occur in patients with myeloid malignancies. The most prominent examples are from recent genome-wide and candidate-gene studies that have identified somatic alterations in genes that encode proteins regulating DNA methylation and post-translational histone modifications. These data suggest that somatic alterations in epigenetic regulators are a common genetic event in myeloid malignancies and contribute to haematopoietic transformation. These data suggest that the classical two-hit model of myeloid malignancy pathogenesis must be modified to account for novel classes of mutant disease alleles, most notably mutations in epigenetic modifiers. These include mutations in tet methylcytosine dioxygenase 2 (TET2), isocitrate dehydrogenase 1 (IDH1), IDH2, additional sex combs-like 1 (ASXL1), enhancer of zeste homologue 2 (EZH2) and DNA methyltransferase 3A (DNMT3A), L3MBTL1 and PRMT5, which have recently been shown to have biological, clinical and potential therapeutic relevance in myeloid malignancies. These data underscore the importance of aberrant epigenetic programming in the biology of myeloid malignancies. Here, we discuss how a specific somatic alteration in epigenetic regulators (deletion of the Polycomb protein L3MBTL1) leads to repatterning of the epigenome and contribute to myeloid leukaemogenesis. Moreover, we have found that several class I and class II alterations (such as JAK2V617F or AML1-ETO) that are central to the pathogenesis of myeloid malignancies have direct epigenetic functions in addition to their canonical roles in promoting haematopoietic cell proliferation.

L3MBTL1

L3MBTL1 is the human homolog of the *Drosophila* tumor suppressor gene, *l(3)mbt* [*lethal(3)malignant brain tumor*], whose inactivation results in overgrowth of adult optic neuroblasts and ganglion mother cells of the larval brain. After crystallizing the structure of human L3MBTL1, we showed that it compacts chromatin by binding mono- and dimethylated lysines on histones H1 (H1K26) and H4 (H4K20), through the second of its three tandem MBT domains. Shortly after the molecular identification of *l(3)mbt*, Bornemann et al. reported that another *Drosophila* gene, *Sex comb on midleg* (*Scm*), encoded a protein containing two tandem MBT repeats at the N-terminus. *Scm* was originally identified as a gene required for the proper maintenance of expression patterns of homeotic genes during development, and was therefore classified as a *Polycomb* group (PcG) repressor. *Scm* mutant embryos have a classic PcG developmental phenotype, in

which anterior segments of the body plan assume the identity of more posterior ones (e.g. thorax into abdomen), due to the loss of repression of genes in the *bithorax* locus.

L3MBTL1 is located on chromosome 20q12, within the common deleted region identified in patients with 20q deletion-associated polycythemia vera, myelodysplastic syndrome, and acute myeloid leukemia. Deletion of the long arm of chromosome 20 (20q-) represents the second most common primary chromosomal abnormality in the hematological malignancies, after the Philadelphia chromosome. The 20q- abnormality is observed in 10% of patients with myeloproliferative neoplasms (MPN), most commonly polycythemia vera (PV), in 4% of patients with MDS, and in 1-2% of patients with AML. Inactivation (or haploinsufficiency) of putative tumor suppressors on 20q has been proposed to explain the pathogenesis of these disorders.

The fact that L3MBTL1 is expressed within the hematopoietic CD34+ cells (which represent the hematopoietic stem/progenitor cells) and that no mutations were found within the non-deleted alleles, suggests that haploinsufficiency of L3MBTL1 may contribute to the pathogenesis of these disorders.

1) To define its role in hematopoiesis, we knocked down L3MBTL1 expression in primary hematopoietic stem/progenitor (ie, CD34⁺) cells isolated from human cord blood (using short hairpin RNAs) and observed an enhanced commitment to and acceleration of erythroid differentiation. Consistent with this effect, overexpression of L3MBTL1 in primary hematopoietic CD34⁺ cells as well as in 20q- cell lines restricted erythroid differentiation. Furthermore, L3MBTL1 levels decrease during hemin-induced erythroid differentiation or erythropoietin exposure, suggesting a specific role for L3MBTL1 down-regulation in enforcing cell fate decisions toward the erythroid lineage. Indeed, L3MBTL1 knockdown also enhanced the sensitivity of hematopoietic stem/progenitor cells to erythropoietin (Epo), with increased Epo-induced phosphorylation of STAT5, AKT, and MAPK as well as detectable phosphorylation in the absence of Epo. Our data suggest that haploinsufficiency of L3MBTL1 contributes to some (20q-) myeloproliferative neoplasms, especially polycythemia vera, by promoting erythroid differentiation.

Polycythemia vera is a myeloproliferative blood disorder in which the bone marrow produces too many red blood cells.

2) We used the loss-of-function approach to explore the possible tumor suppressive mechanism of L3MBTL1 and found that depletion of L3MBTL1 from human cells causes replicative stress, DNA breaks, activation of the DNA damage response, and genomic instability. L3MBTL1 interacts with Cdc45, MCM2-7 and PCNA, components of the DNA replication machinery, and is required for normal replication fork progression, suggesting that L3MBTL1 causes DNA damage, at least in part, by perturbing DNA replication. An activated DNA damage response and genomic instability are common features in tumorigenesis and a consequence of overexpression of many oncogenes. We propose that the loss of L3MBTL1 contributes to the development of 20q(-) hematopoietic malignancies by inducing replicative stress, DNA damage, and genomic instability.

3) To define how L3MBTL1, a chromatin-associated polycomb group protein with transcriptional repressive activities, regulates early events in differentiation, we created hESC lines that constitutively express shRNAs directed against L3MBTL1. Although the L3MBTL1 KD cells could be induced to differentiate into embryonic neuroectoderm, they adopted an exclusive trophoblast fate during spontaneous differentiation. The data suggest that L3MBTL1 depletion does not affect hESC self-renewal but impacts pluripotency; depletion of L3MBTL1 directs hESC differentiation toward extra-embryonic tissues, rather than embryoderived tissues.

To further examine the differentiation of L3MBTL1 KD cells into trophoblasts, we directed control cells toward trophoblasts using BMP4. We compared the gene expression pattern of the BMP4-treated control (LUC shRNA) cells with the spontaneously differentiated L3MBTL1 KD cells and found similar but higher trophoblast marker expression (CG- β and

HAND1) in the BMP4-treated control cells. Of note, L3MBTL1 expression decreased at least 4-fold in the control cells treated with BMP4 compared with untreated LUC shRNA control, which is also consistent with the notion that downregulation of L3MBTL1 allows trophoblast formation to proceed in hESCs. To further investigate the role of BMP signaling, we measured the level of phosphorylated SMAD proteins (SMAD 1/5/8) during the spontaneous differentiation of the LUC shRNA and L3MBTL1 KD cells. We found an increased level of phospho-SMAD 1/5/8 in differentiated L3MBTL1 KD cells compared with the control cells. We also measured the secretion of the placental hormones CG- β and progesterone into the medium from spontaneously differentiated L3MBTL1 KD cells and also the untreated and BMP4-treated controls. L3MBTL1 KD and BMP4-treated control cells show a continuous increase in the concentration of both hormones, with the hormone secretion by the knockdown cells being nearly as high as from the BMP-treated control. These results show that L3MBTL1 KD cells differentiate into functional trophoblast cells, which indicates the role of L3MBTL1 in regulating the spontaneous differentiation of embryonic derivatives.

4) Finally, we more recently found that L3MBTL1 also regulates erythropoiesis and globin gene expression by regulating the expression of the erythroid-specific transcription factor EKLf. We found that L3MBTL1, which generally functions as a transcriptional repressor, regulates the transcription of *smad5*, thereby controlling the BMP4/*smad5* signaling pathway and its downstream targets, such as EKLf. Given the clinical relevance of regulating globin gene expression in beta-hemoglobinopathies, we then utilized a human model of beta thalassemia, i.e. patient-specific induced pluripotent stem (iPS) cells, which we lentivirally infected to express shRNAs against L3MBTL1. The L3MBTL1-KD iPS cells generated high-fetal globin gene expressing erythroid progeny, which manifested a strong BMP4 transcriptional signature including increased EKLf expression. Thus, we propose a model, where L3MBTL1 fine-tunes the induction of EKLf expression, by modulating the BMP4/*smad5* signaling pathway, ultimately regulating fetal globin gene expression and serving as a potential approach to treating the hemoglobinopathies.

PRMT5

The type II arginine methyltransferase PRMT5 was first identified as JAK-binding protein 1 (JBP1) in a yeast two-hybrid assay. It mediates the symmetrical dimethylation of arginine residues within histones H2A, H3, and H4, and methylates other cellular proteins as well, such as p53, SPT5, and MBD2. Together with the WD40-repeat containing MEP50 protein and with pICln, PRMT5 forms a large 20S protein arginine methyltransferase complex, termed the "methylosome." This complex functions in RNA processing by methylating Sm proteins and affecting snRNP biogenesis. PRMT5 has been also found in the hSWI/SNF and NURD chromatin-remodeling complexes, where it can exert transcriptional control on target gene expression. To gain insight into JAK2V617F-induced MPN, we investigated the *in vivo* interaction between PRMT5 and the oncogenic mutant JAK2 kinases (JAK2V617F and JAK2K539L), and determined how this interaction contributes to the myeloproliferative phenotype that they induce.

The JAK2V617F constitutively activated tyrosine kinase is found in most patients with myeloproliferative neoplasms. While examining the interaction between JAK2 and PRMT5, an arginine methyltransferase originally identified as JAK-binding protein 1, we found that JAK2V617F (and JAK2K539L) bound PRMT5 more strongly than did wild-type JAK2. These oncogenic kinases also acquired the ability to phosphorylate PRMT5, greatly impairing its ability to methylate its histone substrates, and representing a specific gain-of-function that allows them to regulate chromatin modifications. We readily detected PRMT5 phosphorylation in JAK2V617F-positive patient samples, and when we knocked down

PRMT5 in human CD34+ cells using shRNA, we observed increased colony formation and erythroid differentiation. These results indicate that phosphorylation of PRMT5 contributes to the mutant JAK2-induced myeloproliferative phenotype.

CONCLUSIONS

Our knowledge of the mechanisms that promote malignant myeloid transformation has evolved as a result of an improved understanding of the range of genetic events that are found in patients with these disorders. The recent identification of mutations in genes involved in epigenetic regulation has elucidated novel mechanisms of transformation. Regulators of DNA methylation (such as TET2, IDH1, IDH2 and DNMT3A) and of histone modifications (such as L3MBTL1, PRMT5, MLL translocations, ASXL1 and EZH2) are targeted by somatic alterations in a significant subset of patients with myeloid malignancies. This suggests a crucial role for epigenetic modifiers in the regulation of normal haematopoiesis and illustrates how the loss of normal epigenetic functionality can contribute to leukaemogenesis. As such, elucidating the impact of epigenetic mutations on leukaemogenesis and therapeutic response will be essential for advancing our understanding and treatment of myeloid malignancies.

Our comprehension of the biological consequences of these epigenetic changes is still at a nascent stage. Although we may understand the specific activity of an individual gene and/or have derived general models of how epigenetic modifications affect transcription, we do not yet have a grasp of the crucial components that are altered by these epigenetic mutations and how this affects epigenetic patterning, gene expression and phenotypic alterations in haematopoietic cells. By definition, mutations in this class of genes affect global chromatin landscapes and many genes and pathways are altered; thus, simple linear explanations are unlikely to precisely show how these mutations contribute to leukaemia development. Gene expression and epigenomic analyses have identified a subset of downstream targets of epigenetic modifiers, such as the HOX gene clusters, that are essential for malignant transformation by specific epigenetic mutations. Greater efforts in this regard, coupled with advances in epigenomic platforms, will help to gain greater insight into the role of these mutations in MDS, MPN and AML. However, what we have learned is that mutations in epigenetic modifiers do not fit neatly into the established framework of class I and class II mutations in leukaemogenesis. Clinically, epigenetic mutations occur in combination with both class I and class II genes and also occasionally with each other. Current genetic and functional data suggest that mutations in epigenetic modifiers fall into at least two novel classes: one set of mutations that affect DNA hydroxymethylation (including TET2, IDH1 and IDH2), and a second set that directly regulate DNA methylation and/or the histone state (including L3MBTL1, PRMT5, MLL, ASXL1 and DNMT3A). These two novel classes of epigenetic mutations probably contribute to leukaemic transformation by affecting epigenetic regulation, thus generating a chromatin landscape that can sustain, and cooperate with, the effect of class I and class II mutations. Further study will be needed to clarify these possibilities and to understand how different genotypic combinations of leukaemia-associated disease alleles result in biologically, therapeutically and prognostically distinct myeloid leukaemia phenotypes.

1. INTRODUCTION

1.1 L3MBTL1

L3MBTL1 is the human homolog of the *Drosophila* tumor suppressor gene, lethal(3)malignant brain tumor¹, whose inactivation results in overgrowth of adult optic neuroblasts and ganglion mother cells of the larval brain².

The L3MBTL1 protein contains three MBT repeats, which assume a three-bladed propeller-like architecture, as well as a Zn finger and an SPM dimerization domain^{3,4}. We previously demonstrated that human L3MBTL1 functions as a HDAC-independent transcriptional repressor⁵ and after crystallizing the MBT repeat domain³ determined that L3MBTL1 compacts chromatin by binding mono- and dimethylated lysine residues in histones H1 (H1K26) and H4 (H4K20)^{6,7} via the second of its three MBT repeats.

L3MBTL1 is located on the long arm of chromosome 20, within the common deleted region identified in patients with myeloid malignancies. Deletion of the long arm of chromosome 20 (20q-) represents the second most common primary chromosomal abnormality in the hematological malignancies, after the Philadelphia chromosome⁸. The 20q- abnormality is observed in 10% of patients with myeloproliferative neoplasms (MPN), most commonly polycythemia vera (PV)⁹, in 4% of patients with MDS¹⁰, and in 1-2% of patients with AML¹¹. Inactivation (or haploinsufficiency) of putative tumor suppressors on 20q has been proposed to explain the pathogenesis of these disorders. Two mutational analyses of small numbers of 20q- patient samples found no mutation in the non-deleted allele of *L3MBTL1*^{12,13}, suggesting that haploinsufficiency of *L3MBTL1* would have to contribute to these disorders. Somatic, focal deletions of other human L3MBTL family members, the *I3mbtl2* and *I3mbtl3* genes, have recently been found in human medulloblastoma¹⁴. These findings suggest that L3MBTL1 is a candidate tumor suppressor gene in myeloid malignancies associated with 20q12 deletions.

Despite the known role of L3MBTL1 in affecting chromatin structure, the function of L3MBTL1 in human hematopoiesis has remained largely unknown.

1) To define the role of L3MBTL1 in normal human hematopoiesis, and its potential role in the 20q- myeloid disorders, we utilized RNA interference to reduce *L3MBTL1* expression in human cord blood (CB) CD34⁺ hematopoietic stem/progenitor cells (HSPCs).

2) L3MBTL1 binds to chromatin most prominently during the S phase of the cell cycle, concomitant with the appearance of the monomethylated H4K20 (H4K20me1) mark⁶, suggesting that the biological function of L3MBTL1 may be related to DNA replication. The accurate duplication of DNA during replication is essential for maintaining genomic stability, as uncorrected errors made during this process can lead to DNA breaks, which generate mutations and/or chromosomal translocations that can promote tumorigenesis¹⁵. DNA breaks resulting from replicative stress trigger an ATM/ATR-dependent DNA damage response (DDR), which prevents the proliferation of cells with damaged DNA by inducing either cell cycle arrest or apoptosis. An activated DDR is present in precancerous lesions from tissues of different origins, and many overexpressed oncogenes cause replicative stress and activation of the DDR. When coupled with mutations in checkpoint and/or DNA repair genes, these abnormalities can lead to cancer¹⁶⁻¹⁸. We examined the function of L3MBTL1 in mammalian cells and found that L3MBTL1 interacts with several components of the DNA replication machinery.

3) In order to further investigate the role of L3MBTL1, we utilized human embryonic stem cells. Human embryonic stem cells (hESCs) can be used to study the early events in

human development and, hopefully, to understand how to differentiate human pluripotent cells for clinical use. To define how L3MBTL1, a chromatin-associated polycomb group protein with transcriptional repressive activities, regulates early events in embryonic cell differentiation, we created hESC lines that constitutively express shRNAs directed against L3MBTL1. Human embryonic stem cells (hESCs) are derived from the inner cell mass of early preimplantation blastocysts; they self-renew and are pluripotent. They can be maintained in an undifferentiated state, but can also be induced to differentiate into cell types characteristic of all 3 germ layers and of extra-embryonic tissues, offering the potential to model aspects of mammalian development and disease. Indeed, progress made over the past decade has determined that directing hESCs toward specific cell fates requires similar kinetics and signaling pathways as those required during development¹⁹. The trophoblast is an essential extra-embryonic tissue that arises from pluripotent trophectoderm (TE) during mammalian development. Interplay between transcriptional, epigenetic, and physiological factors governs TE cell fate. Several transcription factors including Cdx2, Tead4, Eomes, Gata3, Elf5, Ets2, and Tcfap2c are involved in TE lineage specification and its further expansion²⁰⁻²⁴. Differential epigenetic modifications including DNA methylation and the distribution of histone modifications and their modifying enzymatic complexes²⁵⁻²⁸ contribute to lineage identity in the early embryo by regulating the appropriate gene expression profiles. Because in vitro cell fate decisions are similar to those made during development in vivo, hESCs can be exploited to reveal critical aspects of human development.

We hypothesized that as a chromatin-associated protein with repressor properties, changes in the level of L3MBTL1 activity could alter the chromatin structure and influence the ability of hESCs to either self-renew or commit to differentiation. To test this hypothesis, we generated and characterized 2 independent and stable clones of L3MBTL1-depleted hESCs, using a lentiviral vector system to express short hairpin RNAs (shRNAs) directed against L3MBTL1 mRNA.

4) By utilizing embryoid bodies (EB) as a model of hematopoietic development, it was shown that the level of erythroid-specific transcription factor EKLF expression resulted proportional to the amount of BMP4 added^{29,30}; however, the effect of BMP4 on EKLF has never been proven to be directly conveyed by smad proteins, although ten conserved smad binding motifs were identified within three main regulatory regions of EKLF gene. In addition to its role in affecting erythroid differentiation of HSPCs, we found that L3MBTL1 regulates the expression of EKLF in a smad-dependent manner. EKLF functions as a critical regulator of beta-like globin genes^{31,32}. Its expression, restricted to the hematopoietic organs, has been shown also in pre-erythroid differentiation stages, where it is suggested to be mediated by the BMP/Smad signaling pathway.

BMP4 interacts with the BMP receptor, enabling the interaction between its two subunits (BMPR-IA or IB and II), which then leads to phosphorylation of Smad1, Smad5 and/or Smad8 prior to their association with Smad4 and translocation to the nucleus³³. Extensive literature indicates that the BMP4 signaling pathway is required throughout development for the establishment of hematopoietic fate from mesoderm^{30,34,35}. Indeed, exogenous BMP4 can augment the hematopoietic differentiation of hESCs, as well as substantially increase the proportion of committed hematopoietic cells generated from iPSCs³⁶. The addition of EKLF to the growing list of BMP4-regulated genes hints that the BMP4 signaling pathway and Smad activity are required throughout hematopoiesis and specifically in erythropoiesis, as opposed to being necessary only for the initial establishment of hematopoietic fate. Indeed, knock-down of Smad5 impairs maintenance of the erythroid program³⁷⁻³⁹ and stress conditions trigger BMP4 pathway to promote erythropoiesis⁴⁰ and to cooperate with lineage regulators enhancing transcription of cell-type-specific target genes during hematopoietic regeneration⁴¹.

In this study we determined that the regulation of EKLF by the BMP4 signaling pathway exists in definitive hematopoietic / erythroid cells and that it is directly mediated by smad proteins.

Our previous studies identified the role of the Polycomb protein L3MBTL1 in regulating erythroid lineage differentiation of HSPCs⁴², functioning as a transcriptional repressor⁴³ and yet regulating differentiation of human embryonic stem cells in a BMP4-like manner⁴⁴. We have subsequently investigated whether L3MBTL1 functions in erythropoiesis via the BMP4 signaling pathway regulating EKLF. We found that L3MBTL1 represses SMAD5-mediated targets, including EKLF. Moreover we found that knock-down of L3MBTL1 can efficiently increase expression of fetal globin gene in primary hematopoietic cells as well as in patient-specific beta-thalassemic induced pluripotent stem (iPS) cells. Thus, we propose a model of EKLF regulation, which involves a crosstalk between a chromatin-related protein (L3MBTL1) and a cytoplasmic signaling pathway (BMP4) and mediates globin gene expression in a clinically relevant setting, i.e. human models of beta-thalassemia.

1.2 Epigenetic roles for class I and class II genes

In addition to the discovery in patients with myeloid malignancies of mutations in genes that primarily function in regulating DNA methylation or post-translational histone modifications, various previously characterized class I and class II alleles have recently been found to affect the epigenome as part of their transforming activity. This includes the discovery of the direct histone modifying activity of janus kinase 2 (JAK2), as well as identification of interactions between the fusion oncoproteins that are characteristic of APL and PcG proteins. The first JAK2 mutation (JAK2-V617F) was identified in patients with MPN and was found to be an activating mutation within the JH2 pseudokinase domain⁴⁵. JAK2 mutations are known to activate canonical cytokine signalling pathways through the phosphorylation of STAT proteins. However, recent studies have demonstrated a novel role for JAK2 in epigenetic regulation. Dawson et al. showed that JAK2 localizes to the nucleus and phosphorylates Y41 of histone H3⁴⁶. This phosphorylation results in reduced binding of heterochromatin protein 1 α (HP1 α), a chromatin-binding protein that leads to transcriptional silencing.

1.3 PRMT5

The myeloproliferative neoplasms (MPNs) are stem cell disorders whose proliferation is thought to be driven by activating tyrosine kinase gene mutations, such as the BCR-ABL fusion gene in chronic myelogenous leukemia (CML)⁴⁷. The JAK2 kinase V617F mutation is found in most patients with non-CML MPN⁴⁸⁻⁵¹. It is a constitutively active kinase that can phosphorylate STAT5 in the absence of upstream signals, confer cytokine-independent growth to Ba/F3 cells, and induce a myeloproliferative disease in mouse models^{49,52-55}.

Upon activation, the receptor-bound JAK2 phosphorylates specific tyrosine residues of its downstream targets, activating cell survival/proliferation-promoting signaling pathways⁵⁶. Several kinase cascades are activated by JAK2V617F, including the STAT5/BCL-XL, PI3K/AKT, and ERK/MAPK pathways^{49,57}; however, they may not completely account for the MPN phenotype.

The type II arginine methyltransferase PRMT5 was first identified as JAK-binding protein 1 (JBP1) in a yeast two-hybrid assay⁵⁸. It mediates the symmetrical dimethylation of arginine residues within histones H2A, H3, and H4⁵⁹⁻⁶¹ and methylates other cellular proteins as well, such as p53, SPT5, and MBD2^{62,63}. Together with the WD40-repeat containing MEP50 protein and with pICln, PRMT5 forms a large 20S protein arginine methyltransferase complex, termed the “methylosome.” This complex functions in RNA processing by methylating Sm proteins and affecting snRNP biogenesis⁶⁴⁻⁶⁷. PRMT5 has been also found in the hSWI/SNF and NURD chromatin-remodeling complexes^{61,68}, where it can exert transcriptional control on target gene expression.

2. MATERIALS AND METHODS

2.1 Purification and in vitro primary culture of human cord blood CD34+ cells

Mononuclear cells were isolated from CB by Ficoll-Hypaque Plus density centrifugation. CD34+ HSPCs were purified by positive selection using the Midi MACS (magnetic-activated cell sorting) LS+ separation columns and isolation Kit (Miltenyi). CD34+ cells were cultured in Iscove's modified Dulbecco's medium (IMDM, Cellgro) containing 20% BIT 9500 medium (Stem Cell Technologies) supplemented with SCF (100 ng/ml), FLT-3 (10 ng/ml), IL-6 (20 ng/ml) and TPO (100 ng/ml) (these cytokines were purchased from Peprotech, NJ).

2.2. Generation of lentiviruses and infection of primary hematopoietic CD34+ cells

Lentiviral vectors were produced by transfection of 293T cells, according to standard protocols⁶⁹. After 24 hours of growth, cells were infected with high-titer lentiviral concentrated suspensions, in the presence of 8 µg/ml polybrene (Aldrich). Lentiviral shRNA constructs were purchased from the TRC shRNA library at Thermo Scientific Open Biosystems and modified by subcloning the GFP gene instead of the puromycin gene into the pLKO.1 vector as a marker of viral integration. Sequences targeted by short hairpin RNAs (shRNAs) were: GGAAAGACGATGACGGAAA (shLUC), GTAGTGAGTTGTAGATAAA (sh1), GGTCAGTCATAGTGGAGAA (sh2), and GCCTGCACTTTGATGGGTATT (sh3). shRNAs were cloned into the H1p HygroEGFP⁷⁰ (shLUC, sh1 and sh2) or LKO vectors (empty vector and sh3). The luciferase-directed shRNA, cloned into the H1 vector, was used as control⁷¹. RNA sequences were selected using the Dharmacon SMARTselection design software. Forward and reverse oligonucleotides were resuspended at a concentration of 5 mM, heated to 95°C for 5 min, and allowed to cool to RT overnight. After annealing, the duplexes were cloned into SmaI/XbaI sites of an H1P shRNA cassette.

shRNA targeting PRMT5 or a scrambled shRNA was cloned into the pLKO.1-GFP lentiviral vector. HA-PRMT5 WT or M6 cDNAs were cloned into the lentiviral vector pBGJR (modified by replacing the CMV promoter with the EF1α promoter). Viruses were produced by transfecting pLKO.1-GFP or pBGJR vector with helper plasmids into 293T cells, according to standard protocols. GFP-positive cells were sorted 2 days after infection.

2.3 Flow cytometry

Transduced CB CD34+ cells were sorted for green fluorescence (GFP) and CD34 expression after staining with an APC-conjugated anti-CD34 antibody (BD Pharmingen), using a fluorescence-activated cell sorting (FACS) Vantage cell sorter. Transduced K562 cells, cultured in RPMI medium supplemented with 10% fetal bovine serum, were sorted for GFP at 72 hrs after the infection. Cells were harvested for flow cytometry on days +7, +9, +11 in cytokine-driven liquid culture. Cells were stained with the following antibodies: CD34-APC (BD Pharmingen), CD11b-PE (Immunotech), CD14-PE (Immunotech), CD71-APC (BD Pharmingen), GlycophorinA-PE (Invitrogen), CD41-PE (Immunotech) and analyzed by FACS.

2.4 Isolation of MPN samples

CD34+ cells were isolated from PV patient phlebotomy samples or ET/MF patient peripheral blood samples and cultured in SFEM (serum-free stem cell expansion media) supplemented with SCF (100 ng/mL), IL-3 (20 ng/mL), IL-6 (10 ng/mL) and Epo (0.5 IU/mL) every other day. Cells were harvested at day 7 or day 9 for Western blot assays. The cells were >70% CD71/GlyA double-positive at these times of collection.

2.5 Cytospin preparations, GIEMSA staining and Benzidine staining

2×10^5 cells were centrifuged into slides for 5 minutes at 500 rpm and air dried. Cells were stained with May-Grunwald Giemsa stains and observed under light microscope for morphologic analysis. Benzidine staining was performed as described previously⁷².

2.6 RNA extraction and quantitative Real-Time PCR (qRT-PCR)

For qRT-PCR, total RNA was isolated from 2×10^5 cells using the RNeasy mini kit (QIAGEN, Germany), and then subjected to reverse-transcription with random hexamers (SuperScript III kit, Invitrogen). Real-time PCR reactions were performed using an ABI 7500 sequence detection system.

2.7 Methylcellulose colony and LTC-IC assays.

For the CFU assays: 1×10^4 GFP+ CD34+ transduced cells were plated (in duplicate) in methylcellulose with erythropoietin (5 IU/ml), SCF (50 ng/ml), IL-3 (20 ng/ml), IL-6 (20 ng/ml), G-CSF (20 ng/ml) and GM-CSF (20 ng/ml). BFU-E, CFU-GM and CFU-GEMM colonies were scored 14 days after seeding.

For the LTC-IC assays: 4×10^5 GFP+ CD34+ cells were grown on MS-5 stromal cells in IMDM, supplemented with 12.5% horse serum, 12.5% fetal bovine serum (FBS), 4 mmol/L L-glutamine, 100 U/mL penicillin and 100 µg/mL streptomycin and 1 µM hydrocortisone. Medium was half-replenished every week and cobblestone areas were scored at week five. At week five, cells were harvested and plated in methylcellulose medium with cytokines, as described for the CFU assay.

2.8 Antibodies

The following antibodies were used for western blot assays: the affinity purified anti-L3MBTL1 antibody, pSTAT5 (Cell Signaling), STAT5 (Cell Signaling), pMAPK1/2 (Cell Signaling), MAPK (Cell Signaling), pAKT (Cell Signaling), AKT (Cell Signaling), pFOXO1/3 (Cell Signaling), JNK (Santa Cruz), JAK2 (Cell Signaling), p16 (Santa Cruz), Raf-1 (Santa Cruz), phospho smad1,5,8, smad1, smad5, phospho smad2, smad2, (Cell Signaling), HEX (Chemicon), EKLF (abcam), HA (santa cruz).

2.9 Ras Activation Assay

Ras-GTP was precipitated from total cell lysates using the Ras activation assay kit, purchased from Millipore, according to the manufacturer's instructions.

2.10 Overexpression assays

Retroviral vectors were produced by transfection of Phoenix A cells with MIGR1 control or MIGR1 full length L3MBTL1-HA c-DNA plasmids⁹, according to standard protocols⁶⁹. CMK, U937, HEL and K562 cells were grown in RPMI medium supplemented with 10% FBS and infected with high-titer retroviral suspensions in the presence of 8 µg/ml polybrene (Aldrich). 72 hours after infection, the GFP-positive cells were sorted by FACS.

2.11 Chromatin Immunoprecipitation (ChIP) assays

Approximately 4×10^6 cells were used per Chip reaction (per antibody) after cross-linking with 1% formaldehyde for 10 minutes at room temperature. Chip was performed according to the previously reported methodology⁷³. The associated DNA after purification was subjected to qRT-PCR to detect specific DNA sequences. Quantitative results are represented as percentages to 10% DNA input.

2.12 Gene expression profile (GEP) and Gene set enrichment analysis (GSEA)

RNA was extracted and hybridized to Affymetrix U133A arrays, scanned, and subjected to quality control parameters and normalization as described. GSEA contains gene sets that

relate to common biological functions. GSEA first ranks the expression of each gene based on its correlation with one of two phenotypes being compared (in this case L3MBTL1-KD vs controls). It then identifies this rank position within the independent gene set being queried. From this ranking it calculates an enrichment score that reflects the degree to which genes within the independent gene set are over represented within those genes most highly correlating with one of the two phenotypes. The normalized enrichment score (NES) takes into account the number of genes within the independent gene set. Permutation on the phenotype class labels is used to obtain the null distribution of NES and the nominal *P*-value. The false discovery rate (FDR) is computed by comparing the tails of the observed and null distributions for the NES (<http://www.broadinstitute.org/gsea>)⁷⁴.

2.13 Human embryonic stem cell culture and differentiation protocols

hESC line H9 (WA-09) cells were cultured on a feeder layer of mouse embryonic fibroblast (MEFs), purchased from GlobalStem, and plated on gelatin-coated tissue culture plates. ES cells were maintained in an undifferentiated state in human ES (HES) media (DMEM:F12; Invitrogen) supplemented with 20% knockdown serum replacement (Invitrogen), 1% nonessential amino acids (Invitrogen), 0.1 mmol/L 2 mercaptoethanol (Invitrogen), 1 mmol/L L-glutamine (Invitrogen), and 6 ng/ mL FGF2 (R&D Systems). Cells were passaged using Dispase (neural protease; Worthington Bioscience). Spontaneous differentiation was induced by plating control and L3MBTL1KD cells in feeder-free conditions on Matrigel (BD Bioscience)-coated dishes in HES medium without FGF2 for 2 weeks; cells were fed daily. The day on which the cells were seeded was defined as day 1.

Embryoid bodies (EBs) were generated by culturing control and L3MBTL1 KD cells in low-cell-binding dishes for 14 days with the same medium used in spontaneous differentiation. EBs were collected by gravity and fed every other day.

The directed differentiation to trophoblast was achieved by culturing the cells on Matrigel-coated dishes in HES medium in the presence of exogenous BMP4 (100 ng/mL). Briefly, control and L3MBTL1 KD cells were cocultured on MS-5 stroma cells and fed with KSR medium supplemented with SB431542 (10 mM/mL) and dorsomorphin (600 nM/mL) during the first 7 days; then cells were fed only with KSR medium until day 14.

2.14 Immunofluorescence

Cultured cells were washed twice with PBS before being fixed in 4% paraformaldehyde at room temperature. Cells were washed 3 times with PBS before permeabilization with wash buffer (0.3% Triton X-100 and 1.0% bovine serum albumin in PBS) for at least 5 min. The primary antibody (diluted in wash buffer) was added to the cells for 2 h at room temperature, and then the cells were washed 3 times in wash buffer before the addition of the secondary antibody (diluted in wash buffer) for 1 h at room temperature. The cells were washed 3 times with PBS and stored at 4°C. The primary antibodies OCT-3/4 (4 µg/mL; sc-5279), HAND1 (0.4 mg/mL; Ab11846), and L3MBTL1 (1:50 dilution) were detected using the appropriate secondary antibodies conjugated with Alexa Fluor 546 (Molecular Probes). Negative controls consisted of no primary antibody, no secondary antibody, or the appropriate IgG isotype controls as indicated. DAPI counterstaining was performed on fixed cells to visualize all cellular nuclei.

2.15 Western blot analysis

Total cellular protein extracts were prepared using RIPA buffer (SIGMA R0278) supplemented with Halt Protease Inhibitor Cocktail (Thermo Scientific 78430) according to the manufacturer's instructions. Nuclear and cytoplasmic extracts were prepared using the PIERCE kit (78833) for subcellular fractionation; 40 mg of protein extracts were electrophoresed on a 4–12% denaturing gel and electroblotted onto a nitrocellulose

membrane. The membrane was incubated with different antibodies at 4 °C overnight and then incubated with the indicated secondary antibodies at room temperature for 1 h. The Pierce Enhanced Chemiluminescence kit was used to detect antibody reactivity, according to the manufacturer's instructions.

2.16 Cell cycle/DNA and flow cytometry analysis

To analyze DNA content, cells were washed with PBS, and fixed in 70% EtOH at 4 °C. The cells were washed with PBS, resuspended in propidium iodide solution (5 µg/mL) containing 10mg/mL RNase, mixed, and incubated 45min at 37 °C. Flow cytometric data were acquired on a BD FACSCalibur (BD Biosciences) using CellQuest Pro version 6.0. Propidium iodide was excited by the 488 nm laser and fluorescence emission was measured in fluorescence parameter 3 (FL3) with the standard 670LP filter. Doublets were excluded by gating out high FL3-W (width) cells. Single cells were analyzed for percentages of G1/G0, S, and G2/M in MultiCycle AV (Innovative Cell Technologies). Detection of trophoblast marker HLA-G in L3MBTL1 KD spontaneously differentiated cells was performed by immunostaining with an APC-labeled anti-human HLA-G (eBioscience 17-9957 clone 87G) using 0.125 µg/sample; 7-AAD (5 µg/mL) staining served to exclude dead cells from subsequent analysis. For each sample, $5 \cdot 10^4$ cells were analyzed on a FACS Calibur flow cytometer (BD Biosciences) using CELLQuest (BD Biosciences); data analysis was performed using the FlowJo software (Tree Stars, Inc.).

For BrdU/propidium iodide staining, cells were incubated with 1 mM BrdU for 1 h and then stained with BrdU-APC antibody and propidium iodide, according to the instructions in the BrdU Flow Kit (BD Biosciences). Minimally, 10^5 cells were analyzed on the BD FACSCalibur flow cytometer, and the data were collected using BD Cell Quest Pro software and analyzed using FlowJo software (Tree Star).

2.17 Immunoassays

Media were collected from growing cells and stored at - 20 °C until assay. Chorionic gonadotropin (CG-β) and progesterone levels were measured using ELISA kits, as indicated by the manufacturer (Calbiotech).

2.18 Statistical analysis

Data were analyzed using PRISM Version 5.04 (GraphPad Software, Inc.). Sample comparison was performed using 1- way analysis of variance (ANOVA) followed by a post hoc Tukey test or 2-way ANOVA followed by a post-hoc Bonferroni test, with the level of significance set at $P < 0.05$.

2.19 Immunoblotting and Coimmunoprecipitations.

U2OS cells were lysed in lysis buffer [20 mM Tris-HCl (pH 8), 0.5% Nonidet P40, 0.5% Tween 20, 1 mM EDTA, 1 mM DTT, 150 mM NaCl, 1 mM PMSF and protease inhibitor mixture (Calbiochem)], and then briefly sonicated and centrifuged. The protein concentration was measured using the Bradford assay (Bio-Rad), and equal amounts of protein were loaded on NuPage gels (Invitrogen). Protein transfer was conducted onto Immobilon-P PVDF membrane (Millipore), and the membranes immunoblotted with antibodies to the following proteins: phospho-Ser-317 Chk1, phospho-Ser354 Chk1, phospho-Thr68 Chk2, phospho-Tyr15 Cdc2, p53 (all from Cell Signaling), actin, Rad51, p21, geminin (all from Santa Cruz), α-tubulin (Sigma Aldrich), γH2A.x (Biolegend), H4K20me1, H4K20me3, H3 (all from Millipore). For coimmunoprecipitations, whole-cell extracts were prepared from 293T cells overexpressing HA-tagged L3MBTL1 using the same lysis buffer as above. The lysates for coimmunoprecipitations were treated with 1,000 units/mL of benzonase (Sigma Aldrich) overnight at 4 °C to degrade DNA and RNA. They were also treated with 50 µg/mL ethidium bromide to disrupt DNA-protein complexes

and exclude DNA-mediated protein-protein interactions. The lysates were incubated overnight at 4 °C with HA-agarose beads (Roche) or normal rat IgG serum (Santa Cruz) followed by protein A agarose beads (Roche). The coimmunoprecipitates were washed four times with lysis buffer containing 250 mM NaCl before immunoblotting for the following proteins: MCM2-7 (all from Bethyl Laboratories), PCNA (Millipore), Cdc45, Fen-1, Sld5 (all from Santa Cruz). For reciprocal coimmunoprecipitation, Flag-tagged L3MBTL1 was overexpressed in 293T cells, and lysates treated as above were immunoprecipitated with antibodies against Mcm2, Mcm5, or rabbit IgG, followed by adsorption to protein A agarose beads.

2.20 Comet Assay.

DNA breaks were measured using the Comet Assay Reagent Kit (Trevigen) with minor modifications. Briefly, cells embedded in low-melting point agarose on a slide were lysed, treated with alkali, and electrophoresed in 1× TBE buffer for 40 min at 1 V/cm, stained with propidium iodide, and imaged under the fluorescent microscope. To evaluate the extent of DNA damage present in each sample, the average tail moment (a product of percent DNA in tail and tail length) of 100 cells was calculated using CometScore software (Tritek).

2.21 Immunocytochemistry.

Cells were plated on coverslips, then fixed in methanol, permeabilized with 0.25% Triton-X/PBS, blocked in 2% FBS/PBS, and incubated with primary antibody for 1 h, followed by secondary antibody conjugated with a fluorescent probe for 30 min, both at room temperature. Cells were stained with DAPI, mounted onto coverslips in mounting medium (Vector Labs), and imaged on Leica Upright confocal microscope or Carl Zeiss fluorescent microscope using appropriate filters. The primary antibodies used were directed against γ H2A.x (Millipore), 53BP1 (Novus Biologicals), and phospho-Ser1981 ATM (Cell Signaling), and secondary antibodies used were anti-rabbit Alexa488 and anti-mouse Alexa568 (both from Invitrogen). Quantitation of the DNA damage foci was determined by scoring foci of at least 100 cells per treatment used.

2.22 DNA Fiber Analyses.

Control and L3MBTL1 knockdown U2OS and MRC5 cells were sequentially labeled with 50- μ M IdU and 250- μ M CldU for 1 h each. DNA fiber spreads were prepared as described previously with some modifications. Briefly, three aliquots of cells were resuspended in PBS at 1×10^6 cells/mL, spotted onto a microscope slide, and lysed with 15 μ L of spreading buffer [0.5% SDS in 200 mM Tris-HCl (pH 7.4), 50 mM EDTA]. After 6 min, slides were tilted 15° to allow lysates to slowly move down the slide, and the resulting DNA spreads were air-dried, fixed in 3:1 methanol/acetic acid, and stored at 4 °C overnight. The slides were then treated with 2.5 M HCl for 30 min, incubated in blocking buffer (1% BSA/0.05% Tween 20/PBS) for 1 h followed by 1 h at room temperature with 1:500 rat anti-BrdU antibody (Abcam; to detect CldU) plus 1:100 mouse anti-BrdU (BD Biosciences; to detect IdU), diluted in blocking buffer, followed by incubation for 30 min in 1:350 Alexa488-conjugated goat anti-rat antibody and 1:350 Alexa595-conjugated goat anti-mouse antibody (Invitrogen). Slides were air-dried and mounted in Prolong Gold antifade reagent (Invitrogen). Microscopy was carried out using a Zeiss LSM 5 Live Confocal microscope, and the fiber lengths were measured using Volocity software (PerkinElmer).

2.23 Metaphase Spreads.

Cal51 cells were treated with Karyomax solution (Invitrogen) for 5 h and then lysed with 75 mM KCl. Cells were fixed with a 3:1 methanol/acetic acid solution, dropped onto slides, dried, and stained with DAPI. The metaphase chromosomes were imaged under the Carl

Zeiss microscope and evaluated for abnormalities such as chromatid and chromosome breaks, gaps, and exchanges.

2.24 Cell Culture, Transfection, and Plasmids

The human leukemia cell lines TF-1, HEL, and Ba/F3 were grown in RPMI Media 1640 with 10% FBS (Invitrogen), supplemented with recombinant human IL-3 (2 ng/ml) for TF-1 and Ba/F3 cells. To inhibit JAK2 activity in HEL and TF-1 cells, cells were treated with three distinct JAK2 inhibitors: JAK Inhibitor I (Calbiochem), CEP701 (LC Laboratories), and TG101348 at the indicated concentrations (DMSO was used as the diluent control). In the time course experiment, HEL cells were treated with 3 μ M TG101348 for 0, 1, 2, and 4 hr. To activate JAK2 in TF-1 cells, the cells were deprived of cytokine for 12–16 hr, and then GM-CSF (25 ng/ml) or Epo (20 U/ml) was added to the growth medium for 20 min. Transient transfection of 293T cells was performed using the PolyFect Transfection Reagent (QIAGEN) per the manufacturer's instructions. To express the mutant or wild-type JAK2 proteins in 293T cells, the wild-type JAK2, JAK2V617F, and JAK2K539L cDNAs were subcloned into the CMV promoter-driven pCDNA3 vector (Invitrogen) using EcoRV and Not1 sites. FLAG-tagged or HA-tagged PRMT5 and HA-tagged STAT5 cDNAs were also subcloned into the pCDNA3 vector through appropriate restriction sites. For in vitro kinase assays, the full-length PRMT5 open reading frame was subcloned into the bacterial expression vector pSBET, which contains a glutathione S-transferase (GST) tag and a 6 \times Histidine tag at the N and C termini of the inserted sequence, respectively.

2.25 In Vitro Kinase Assay

In vitro kinase assays were performed using commercially available JAK2 kinase (Upstate), which contains only the kinase domain (from amino acid 800 to C-terminal end), and bacterial-purified GST-PRMT5. For each reaction, 0.5 or 2.5 μ g of GST-PRMT5, 0.5 or 1.25 ng of JAK2, and 5 μ Ci of [γ -³²P] ATP were added to the kinase buffer (8 mM MOPS [pH 7.0], 0.2 mM EDTA, 10 mM MgAc, and 0.1 mM cold ATP). Reactions were incubated at 30°C for 20 min, and proteins resolved by gel electrophoresis.

2.26 In Vitro Methylation Assay

HA-PRMT5 was purified from transfected 293T cells by anti- HA immunoprecipitation. The immobilized proteins were then incubated with 25 μ l of HMT buffer (20 mM Tris [pH 8.8], 4 mM EDTA, 1 mM PMSF, 0.5 mM DTT) supplemented with 2.5 μ g of recombinant histone H4 or H2A (New England Biolabs) and 1 μ Ci 3H-SAM (Amersham) at 30°C for 4 hr. The reaction was stopped by adding SDS loading buffer, and the proteins were resolved on SDS-PAGE gels.

2.27 Microarray Analysis

RNA was isolated from HEL cells expressing control shRNA or PRMT5-directed shRNA using the RNAeasy Plus Kit (QIAGEN), transcribed into cDNA using random hexamer priming and Superscriptase (Invitrogen), and then hybridized to the Affymetrix HG-U133 GeneChips. The data were analyzed using Partek Genomic Suites, version 6.5, using a false discovery rate (FDR) of 1% to filter our data and identify differentially expressed genes. Duplicate, independent samples were prepared for each condition.

3. RESULTS

3.1. L3MBTL1 and the erythroid lineage differentiation of HSPCs

a) Knock-down of *L3MBTL1* accelerates erythroid differentiation of human hematopoietic CD34+ progenitor cells

To investigate the function of *L3MBTL1* in human hematopoiesis we knocked down *L3MBTL1* in CD34+ human CB cells, using lentiviruses expressing shRNAs targeting *L3MBTL1*, and 72 hrs after infection documented the efficient knock-down of *L3MBTL1* mRNA and protein in the sorted GFP+ CD34+ cells by qRT-PCR and Western blot, for several different shRNAs constructs (Fig 1A). These cells were then placed in Epo-driven liquid culture (6 IU/ml), and the expression of CD71 and Glycophorin A (GlyA) was monitored by flow cytometry at different time points. The generation of mature erythroid precursor cells (CD71/GlyA-double positive cells) was consistently faster and more efficient for the *L3MBTL1*-KD cells, compared to the control vector infected cells (Fig 1B). Furthermore, while CD71/GlyA double-negative cells were prominently found among the control cells, there were no CD71/GlyA double-negative cells after *L3MBTL1*- KD. These observations were consistently seen using several different shRNAs constructs targeting *L3MBTL1*, demonstrating enhanced erythroid differentiation following *L3MBTL1* depletion.

To evaluate the sensitivity of *L3MBTL1*-KD cells to Epo, we measured GlyA and CD71 expression by FACS analysis in the *L3MBTL1*-KD HSPCs after plating these cells in culture with SCF (100 ng/ml) and different doses of Epo (0.5, 2, 4 and 6 units per ml). At the lowest concentration of Epo (0.5 UI/ml), and at all tested concentrations of Epo, the *L3MBTL1*-KD cells showed accelerated erythroid maturation compared to control cells (2.4, 1.8, 1.6 and 1.6 fold, respectively) (Fig 1C).

Consistent with the immunophenotypic evidence, these cells also showed morphologic evidence of erythroid differentiation following *L3MBTL1*- KD. As erythroid differentiation proceeds, erythroblasts display a gradual decrease in cell size, increase in chromatin condensation and increase in hemoglobin (Hb) concentration⁷⁵, and indeed, the *L3MBTL1*-KD cells appeared smaller with more condensed chromatin than the control cells (which displayed a larger, more homogeneous, and eccentrically placed nucleus, as seen in Fig 1D). Likewise, benzidine staining also revealed 6.6 fold enrichment of Hb-containing cells compared to controls at day 7 of culture, consistent with the time of highest immunophenotypic difference, with a 1.7 fold and 1.3 enrichment at days 9 and 11 of culture (Figure 1E). These results further indicate a role for *L3MBTL1* in regulating the erythroid differentiation of human HSPCs.

b) *L3MBTL1* expression decreases during normal erythroid differentiation of human HSPCs

To investigate whether changes in *L3MBTL1* expression are only seen during erythroid differentiation, we cultured normal CB CD34+ cells in various cytokine cocktails that preferentially support erythroid, myeloid or megakaryocytic differentiation and evaluated *L3MBTL1* expression (by qRT-PCR) at different time points. *L3MBTL1* is downregulated upon differentiation generally, but especially in cells exposed to the erythroid promoting cytokines SCF plus Epo (Fig 2A). These cells maintain a low level *L3MBTL1* expression over time, whereas the cells grown under other culture conditions show a rebound in *L3MBTL1* expression by day 7.

Given the increased erythroid differentiation following *L3MBTL1*- KD, we also assessed whether *L3MBTL1*-KD altered myeloid and megakaryocytic differentiation. *L3MBTL1*-KD and control GFP+ CD34+ cells grown in G-CSF-driven liquid culture showed similar expression of myeloid-specific cell surface markers (CD11b, CD14 or CD33) (Fig 2B and data not shown). Similarly, we observed no effect on the expression of the

megakaryocyte marker CD41 in thrombopoietin (TPO)-driven cultures (Fig 2C), demonstrating that L3MBTL1 depletion specifically affects erythroid differentiation (Fig 2D).

c) Knock-down of *L3MBTL1* induces leukemia cell differentiation towards the erythroid lineage

To determine if L3MBTL1-KD can also affect the differentiation of leukemia cells, we used lentiviral vectors to express shRNA targeting luciferase (shLUC) or *L3MBTL1* (sh1 and sh2) in K562 cells. We sorted GFP⁺ cells (by FACS) 72 hours post-infection and as seen in CB cells, KD of *L3MBTL1* in K562 cells increased GlyA expression, compared to control cells (Fig 3A), and led to higher benzidine staining before and after hemin-exposure (Fig 3B). As hemin is known to trigger the erythroid differentiation of K562 cells⁷², and activate globin gene expression⁷⁶, we studied *L3MBTL1* expression in K562 erythroleukemia cells following hemin exposure. Four days of hemin exposure (at 50 μ M) markedly decreased the level of L3MBTL1 mRNA (Fig 3C) commensurate with an increase in benzidine-positive cells and increased globin gene expression (data not shown). Thus, L3MBTL1 loss can induce erythroid differentiation in leukemia cells as well as in normal human HSPCs.

d) Loss of *L3MBTL1* leads to expansion of erythroid progenitors in long-term cultures

To elucidate the role of L3MBTL1 in the earliest stem/progenitor cells, we performed LTC-IC assays, culturing 4 x 10⁵ GFP⁺ CD34⁺ transduced cells on MS5 stromal cells. We observed an impressive expansion of progenitor cells from the L3MBTL1-KD cells at week 5. The L3MBTL1-KD cells grew mostly on top of the MS5 layer, in sheets of cells rather than cobblestones, while the control cells formed normal cobblestones that grew underneath the stromal layer (Fig 4A). To define the nature of these cells we used flow cytometry to define their lineage-specific cell surface marker profile. The L3MBTL1-KD showed strikingly higher GlyA expression compared to control cells, suggesting that these cells are erythroid progenitors (Fig 4B). KD of L3MBTL1 led to a reduction in stem cell frequency in both limiting dilution and bulk CAFC assays (Fig 4C). Furthermore, when the week 5 culture of the LTC-IC assay cells were plated in methylcellulose, we observed a greater number of BFU-E among the KD-cells than the control cells (Fig 4D).

While CD34 expression was initially higher in the KD-cells, by day +11 we found no difference in CD34 expression between the KD and the control cells (Fig 5A). Given these findings, we evaluated whether the commitment towards the erythroid lineage that follows L3MBTL1 down-modulation impairs the proliferative potential of HSPCs. Cell counts at each time point (day +7, +9 and +11) revealed slower growth of KD-HSPCs compared to control cells in liquid cultures with SCF, IL-3, TPO and FLT-3 (Fig 5B), or Epo-, G-CSF- and TPO (data not shown). We also evaluated the clonogenic ability of sorted CD34⁺ L3MBTL1-KD HSPCs in CFU assays and found decreased progenitor frequency compared to controls; all types of colonies were less frequent (Fig 5C).

As the cell's proliferative potential appears to be slightly decreased following L3MBTL1-KD, we tested the sensitivity of HSPCs to TGF β . We treated CD34⁺ cells with 200pM TGF β , which induces the expression of p57⁷⁷; we observed a greater induction of p57 mRNA in L3MBTL1-KD cells at two hours compared to control cells (Fig 5D); no change in p57 expression was observed in the KD-cells in the absence of TGF β .

e) *L3MBTL1*- KD alters the Epo-dependent and Epo-independent phosphorylation of STAT5, AKT, and MAP Kinase

To investigate the effect of L3MBTL1-KD on intracellular signaling pathways, we prepared lysates from CD34⁺ L3MBTL1-KD cells cultured in Epo for one week and performed

Western blot analyses. We found increased signaling downstream of the Epo receptor, with consistently greater phosphorylation of AKT, FOXO 1/3 and MAPK and variably increased phosphorylation of JAK2 and STAT5 to controls (Fig 6A and 6B). RAS-GTP and Raf-1 protein levels were decreased in the L3MBTL1-KD cells, consistent with the enhanced erythroid maturation (Fig 6C and 6E). Moreover, this pattern of activation mirrors the activation of signaling pathways seen in similarly cultured CD34⁺ HSPCs isolated from JAK2V617F⁺ MPN patients (Fig 6A).

To determine if knock-down of L3MBTL1 can contribute to the Epo-independent erythroid cell growth found in MPN patients, we placed sorted CD34⁺ L3MBTL1-KD cells in Epo-free culture media supplemented with SCF, IL-6, FLT-3 and TPO for one week and found a small GlyA-positive, i.e. erythroid progenitor, cell population in the L3MBTL1-KD cells (Fig 6D). Despite the absence of Epo, phosphorylation of STAT5 and AKT was clearly seen (Fig 6E). Moreover, L3MBTL1-KD cells also displayed increased p16^{INK4a} expression (Fig 6E), protein associated with the induction of erythropoiesis in primary PV samples^{78,79}.

To assess whether decreased L3MBTL1 expression may be implicated in the pathogenesis of non 20q- MPN, we evaluated the expression of L3MBTL1 in granulocytes obtained from 75 MPN patients (who did not show loss of 20q), and compared it with the level of expression in granulocytes obtained from 10 normal donors using the Affymetrix HGU133a.2 array. Granulocyte mRNA from 28 patients with Polycythemia Vera and 47 patients with Essential Thrombocythemia was studied using gene expression array. We observed a $\geq 20\%$ decrease in the expression of L3MBTL1 in 43% of the PV samples (12/28) and 62% of the ET samples (29/47) compared to the normal controls ($p=0.000027$ and $p=0.0004$ respectively) (data not shown). This suggests that downregulation of L3MBTL1 may also play a role in the non 20q- myeloproliferative neoplasms.

f) L3MBTL1 restricts erythroid differentiation

To address the function of L3MBTL1 in 20q- disorders and to explore the mechanism by which L3MBTL1 affects erythroid differentiation, we overexpressed the full length L3MBTL1-HA c-DNA in three human 20q- hematopoietic cell lines (i.e. HEL, CMK and U937 cells) and in K562 cells. We sorted the GFP positive cells and evaluated Glycophorin A expression by FACS analysis: L3MBTL1-HA expressing cells showed decreased expression of Glycophorin A (Figure 7A), suggesting that L3MBTL1 restricts erythroid differentiation. The decreased GlyA expression was seen in CMK (58% vs 86%) and U937 cells (0.5% vs 9%), as well as in HEL (85% vs 93%) and K562 cells (71% vs 84%).

We have also overexpressed L3MBTL1 in primary human CD34⁺ cells, obtaining an almost 200-fold increase in L3MBTL1 expression, as documented by qRT-PCR (Fig 7D). We placed the sorted GFP⁺ CD34⁺ cells in Epo-induced liquid culture, and consistently found a decreased percentage (62% vs 70%) of CD71⁺/GlyA⁺ cells after three days of culture (Fig 7C). The milder decrease in GlyA expression seen in primary human CD34⁺ cells, compared to the 20q- cells, may reflect the normal genetic background of the transduced cells and their intrinsic growth rates. Overexpression of L3MBTL1 in HEL cells decreased the expression of p16^{INK4} (Figure 7B), further suggesting that L3MBTL1 may affect erythropoiesis by regulating (i.e. repressing) p16 expression. Further studies are needed to address this issue.

3.2. L3MBTL1 and the DNA damage response

a) Depletion of L3MBTL1 Inhibits Cell Proliferation and Causes G2/M Arrest.

To assess the role of L3MBTL1 in cell cycle regulation, we depleted L3MBTL1 mRNA and protein in U2OS cells using lentiviral vectors that expressed several shRNAs directed against its ORF. Down-regulation of L3MBTL1 mRNA and protein was achieved efficiently with three different shRNAs ($\geq 90\%$ knockdown; Fig 8 A e B). The depleted cells were monitored for S phase entry by using BrdU incorporation, and we detected a marked decrease of S phase cells and the accumulation of cells in the G2/M phase (Fig 8C). These findings indicate that these cell cycle effects are relevant to the myeloid compartment.

b) Depletion of L3MBTL1 Generates DNA Breaks.

Cell cycle alterations triggered by L3MBTL1 depletion suggest that cells may be experiencing replicative stress, leading to DNA damage. To verify this hypothesis, we examined two DNA damage markers, the production of the phosphorylated histone H2A.x (γ H2A.x), which localizes to sites of double-stranded DNA breaks (DSBs), and the distribution of 53BP1, which is recruited to DNA within minutes following DNA damage by binding to H4K20me2 and possibly other modified histone. We observed an increase in both γ H2A.x and 53BP1 foci following L3MBTL1 depletion with all three shRNAs in U2OS (Fig 9 A e B). We also measured the formation of DNA strand breaks in L3MBTL1-depleted cells using the comet assay, which visualizes damaged DNA on a single-cell level (15). Comet tails were detected in depleted U2OS cells (Fig 9C), MRC5 and Cal51 cells (Fig 9D), indicating DNA strand breakage. We treated MRC5 fibroblasts with varying doses of gamma irradiation to establish a range of tail moments (Fig 9D) and determined that depletion of L3MBTL1 caused extensive DNA damage, similar to that induced by 5 Gy of irradiation.

c) Loss of L3MBTL1 Activates the DDR and Affects H4K20 Methylation Status.

DNA damage triggers a checkpoint response that prevents cells from progressing into mitosis. To explore this pathway, we first examined the phosphorylation of the ATM kinase, one hallmark of the DDR pathway, and detected increased phospho-ATM foci that overlapped with 53BP1 foci in L3MBTL1-depleted cells (Fig 10 A). We also examined whether the downstream components of the ATR/ATM-triggered DDR pathway were activated following L3MBTL1 depletion using immunoblotting to monitor changes in phosphorylation of the key components of this system, including Chk1 and Chk2. As shown in Fig 10 B, increased levels of phospho-Ser317-Chk1, phospho-Ser345-Chk1, and phospho-Thr68-Chk2 were detected in cells at 24, 48, and 72 h postinfection, similar to that observed in cells irradiated with 10 Gy.

Depletion of L3MBTL1 altered the activities as well as the levels of a number of proteins associated with checkpoint regulation and the DDR pathway (Fig 10 B-D). These include: (i) the formation of phospho-Tyr15-Cdc2, a modification that inhibits Cdc2 kinase activity, which is required for cell cycle progression into mitosis (Fig 10B); (ii) the up-regulation of p21 and p53, downstream effectors of the DDR pathway, as well as Rad51, which plays a key role in double-strand break repair by homologous recombination, and (iii) an increase in the level of γ H2A.x (Fig 10D), in keeping with the data shown in Fig. 2. We also observed an increase in the amount of H4K20me2 (40- to 90-fold), which plays important roles in DNA replication and DNA damage recognition, but detected little effect on the levels of H4K20me1. Conversely, overexpression of L3MBTL1 in U937 cells that have monoallelic loss of the commonly deleted region of 20q had the opposite effect,

namely, a decrease in H4K20me2 and an increase in H4K20me1 (Fig 10E). Collectively, these data show that the DDR pathway is strongly activated following depletion of L3MBTL1 and suggest that changes in the level of H4K20 dimethylation could contribute to these effects.

d) L3MBTL1 Depletion Slows the DNA Replication Forks Movement.

The presence of DNA damage and activation of the DDR suggest that depletion of L3MBTL1 may trigger defects in DNA replication. We examined DNA replication fork progression by DNA fiber analyses. For this purpose, control and L3MBTL1-depleted cells were sequentially pulsed for 1 h each with IdU and CldU, lysed, and DNA fibers spread on slides. The fibers were labeled with antibodies to IdU and CldU and fluorescence-labeled secondary antibodies. Fibers containing green IdU fluorescent label flanked on each side with the red CldU fluorescent label represent DNA molecules formed by bidirectional movement of replication forks. Fig 11A shows DNA fibers isolated from control and L3MBTL1-depleted MRC5 fibroblasts. The length of the green IdU-labeled fibers, indicating DNA replicated from origins, was shorter in depleted cells than in fibers isolated from control cells. Furthermore, the total length of red CldU- and green IdU-labeled fibers was shorter in L3MBTL1-depleted cells than in control cells, indicating slower replication fork movement. The average length of DNA fibers from L3MBTL1-depleted cells and control cells was 16.8 μ M and 31.7 μ M, respectively (Fig 11B); 78% of the DNA fibers from L3MBTL1-depleted cells were <20 μ M, whereas 33% of fibers from control cells were this length (Fig 11C). Similar data were obtained using U2OS cells, indicating that this effect is not cell-type specific (Fig 11D and E). The average rate of fork progression in L3MBTL1-depleted cells was ~40% slower than in control cells, indicating that L3MBTL1 is required for the normal progression of DNA replication forks.

e) L3MBTL1 Interacts with Components of DNA Replication Machinery.

Because L3MBTL1 appears to play a role in replication fork progression, we tested whether it interacted with components of the DNA replication machinery. We overexpressed HA-tagged L3MBTL1 in 293T cells, and examined its interaction with members of the MCM2-7 complex, a critical component of the putative replicative helicase. As shown in Fig 12A, HA-tagged L3MBTL1 interacted with the MCM2-7 complex, and L3MBTL1 was immunoprecipitated by antibodies against MCM2 and MCM5 (Fig 12B). Cdc45 and the GINS complex form a replicative helicase complex with MCM2-7 (CMG complex) that travels with the replication fork. These findings prompted us to examine whether L3MBTL1 interacted with these components as well as other replication proteins. As shown in Fig 12A, the interaction of L3MBTL1 with Cdc45 was detected, whereas an interaction with Sld5 (a subunit of the GINS complex) was not observed. Interactions with PCNA, the DNA sliding clamp required for processivity of the replicative DNA polymerases, were also noted, whereas interaction with Fen-1, an enzyme involved in DNA repair and lagging strand processing, was not observed (Fig 12A). We also examined whether the levels of replication proteins were affected by depletion of L3MBTL1 in U2OS cells. Thus, L3MBTL1 interacts with a number of proteins that play roles in different stages of DNA replication, consistent with the notion that it affects replication. The mechanisms contributing to these effects remain to be investigated.

3.3. L3MBTL1 and pluripotency of human embryonic stem cells

a) L3MBTL1 knockdown does not affect embryonic stem cell renewal

We initially screened 10 different shRNAs that target L3MBTL1 using K562 cells (data not shown) and used the 4 most efficient shRNAs to transduce H9 hESCs. Ultimately, 2 shRNAs were used (shRNA1 and shRNA2) (Fig. 13A) that most consistently knocked down L3MBTL1 in H9 cells compared with the H9 cells expressing a nontargeting, luciferase-specific hairpin (LUC shRNA) and the parental H9 cell line. Overall, 11 L3MBTL1 KD ES cell clones were generated.

Although the self-renewal properties of L3MBTL1 knockdown (KD) hESCs were retained, we observed striking morphological changes when L3MBTL1 KD hESCs spontaneously differentiated and established that they spontaneously differentiate into trophoblast-like cells. L3MBTL1 appears to be an important regulator of early cell fate decisions during mammalian development.

The L3MBTL1 KD hESCs showed normal colony morphology (Fig. 13C), normal cell cycle kinetics (Fig. 13D), an unchanged pattern of cell surface markers, and a normal karyotype in prolonged culture (data not shown) when cultured under normal hESC growth conditions. We obtained an *70% reduction in L3MBTL1 mRNA levels (using either shRNA1 or shRNA2) and observed a small decrease in the levels of the pluripotency-promoting OCT-4, NANOG, and SOX2 transcription factor mRNAs (Fig. 13E). Immunofluorescence analysis confirmed the normal expression and localization of OCT-4 protein in all cell lines (Fig. 13F). Thus, L3MBTL1 depletion does not detectably affect the undifferentiated state of hESCs. L3MBTL1 knockdown impairs embryonic cell production during spontaneous differentiation

b) L3MBTL1 knockdown impairs embryonic cell production during spontaneous differentiation

To determine whether loss of L3MBTL1 affects differentiation, we withdrew FGF2 from HES media and grew the hESCs under either adherent or nonadherent conditions, inducing their spontaneous differentiation. hESCs were maintained for 2 weeks under adherent culture conditions as colonies, using Matrigel-coated dishes. Depletion of L3MBTL1 had clear morphological consequences, as all 11 clones derived from the shRNA1- or shRNA2-expressing hESCs generated differentiated colonies composed of large, flat mononucleated cells by days 7–14. In contrast, the control luciferase knockdown H9 cells and the parental line H9 generated mixed colonies composed of many different cell, morphologies (Fig. 14A and data not shown). We also observed morphological consequences in the EBs generated from L3MBTL1 KD cells under nonadherent conditions; in contrast to the control cells, the L3MBTL1 KD cells failed to give rise to typical EB structures containing differentiated cell types. Starting at day 5 of differentiation, the L3MBTL1 KD EBs underwent significant cell death that continued until day 14, indicating defects in differentiation, whereas control cells developed into characteristic EB structures (Fig. 14B). Flow cytometric analysis for Annexin V binding and 7-AAD permeability confirmed an increased cell death in the L3MBTL1 KD cells compared with the control cells at day 7 of differentiation (Fig. 14C).

To characterize the differentiation state of the L3MBTL1 KD cells in monolayer cultures, we performed reverse transcriptase qPCR analysis to quantify the expression of a variety of pluripotent and lineage-specific markers.

Differentiated control and L3MBTL1 KD cells were evaluated and significant differences were seen. As expected, the pluripotency markers OCT-4 and NANOG were reduced in both the L3MBTL1 KD and the control KD cells compared with the undifferentiated cells (Fig. 14D). Of note, L3MBTL1 levels were upregulated at least 3-fold in the differentiated controls compared with the undifferentiated controls, suggesting a potential role for

L3MBTL1 in the earliest stages of differentiation. However, the shRNA constructs continued to suppress L3MBTL1 mRNA levels despite the increased expression that have occurred during normal differentiation (Fig. 14D). Quantification of lineage marker expression shows downregulation of the SOX1 (ectoderm) and AFP (endoderm) markers in the L3MBTL1 KD cells, compared with their increased levels in the differentiated controls. Interestingly, we observed a substantial upregulation in the expression of ACTC1 (mesoderm) and the trophoblast marker chorionic gonadotropin (CG- β) in the L3MBTL1 KD in contrast to the differentiated control cells (Fig. 14E). We also performed reverse transcriptase qPCR analysis to assess the expression of additional lineage markers including NEUROD1, SOX2, MAP2 (ectoderm); HNFA4, FOXA2, PECAM1 (endoderm); and MIXL1, RUNX1, and RUNX2 (mesoderm).

c) L3MBTL1 knockdown promotes differentiation of hESCs toward trophoctoderm

The flat cell morphology (Fig. 14A) and the greater than 18-fold upregulation of CG-**b** in the differentiated L3MBTL1 KD cells (Fig. 14E) led us to examine the expression of other trophoblast markers, including CDX2, HAND1, KRT7, KRT8, and GCM1. CDX2 mRNA upregulation parallels the appearance of morphological changes in spontaneously differentiated L3MBTL1 KD cells by days 6–7, reaching a peak on day 9; in contrast, HAND1, KRT7, KRT8, and GCM1 mRNAs peak at day 14. The expression pattern of these markers further indicates that L3MBTL1 KD cells primarily differentiate into trophoblast cells (Fig. 15A, B). We have confirmed that HAND1 protein is expressed in differentiated L3MBTL1 KD cells by immunofluorescence (Fig. 15C) and that more than 80% of the cells analyzed at day 14 of differentiation have trophoctoderm phenotype, as indicated by the expression of HLA-G (Fig. 15D).

To further examine the differentiation of L3MBTL1 KD cells into trophoblasts, we directed control cells toward trophoblasts using BMP4. We compared the gene expression pattern of the BMP4-treated control (LUC shRNA) cells with the spontaneously differentiated L3MBTL1 KD cells and found similar but higher trophoblast marker expression (CG- β and HAND1) in the BMP4-treated control cells (Fig. 16A). Of note, L3MBTL1 expression decreased at least 4-fold in the control cells treated with BMP4 compared with untreated LUC shRNA control, which is also consistent with the notion that downregulation of L3MBTL1 allows trophoblast formation to proceed in hESCs (Fig 16A). To further investigate the role of BMP signaling, we measured the level of phosphorylated SMAD proteins (SMAD 1/5/8) during the spontaneous differentiation of the LUC shRNA and L3MBTL1 KD cells. We found an increased level of phospho-SMAD 1/5/8 in differentiated L3MBTL1 KD cells compared with the control cells (Fig. 16B). We also measured the secretion of the placental hormones CG-**b** and progesterone into the medium from spontaneously differentiated L3MBTL1 KD cells and also the untreated and BMP4-treated controls. L3MBTL1 KD and BMP4-treated control cells show a continuous increase in the concentration of both hormones, with the hormone secretion by the knockdown cells being nearly as high as from the BMP-treated control (Fig. 16C).

These results show that L3MBTL1 KD cells differentiate into functional trophoblast cells, which indicates the role of L3MBTL1 in regulating the spontaneous differentiation of embryonic derivatives.

d) Directed differentiation is not impaired in L3MBTL1 KD cells

L3MBTL1 KD cells did not express ectoderm markers under conditions that allow spontaneous differentiation (Fig. 14D). However, to determine whether directed differentiation was affected in L3MBTL1 KD cells, we induced neural differentiation by coculturing them on MS-5 stromal cells for 2 weeks. We observed neuronal rosette formation on day 8 with all clones (Fig. 16D, upper panel), demonstrating that L3MBTL1 KD cells can differentiate into neuroectoderm if provided with a sufficiently strong signal.

Further, reverse transcriptase qPCR analysis found a similar level of induction of the neuroectodermal markers SOX1 and PAX6 in the knockdown versus the control cell lines (Fig. 16D, lower panel). We also directed the differentiation of L3MBTL1 KD hESC toward hematoendothelial cells (CD31⁺CD34⁺) and found that the KD cells responded to these differentiation signals as well, albeit less efficiently than to the controls (data not shown). These results indicate that L3MBTL1 KD does not impair hESC differentiation toward embryonic neuroectoderm or hematoendothelial cells when potent differentiation-promoting signals are provided.

3.4. L3MBTL1 and the BMP4/smad5 signaling pathway

a) L3MBTL1 regulates EKLf expression via SMAD5 in hematopoietic and embryonic stem cells

Our previous data implied that the Polycomb protein L3MBTL1 regulates erythroid lineage differentiation of hematopoietic stem/progenitor cells (HSPCs)⁴² and titrates BMP4-like events in human embryonic stem cells⁴⁴. To evaluate whether L3MBTL1 regulates EKLf expression, we lentivirally expressed shRNAs targeting L3MBTL1 in primary cord blood (CB) CD34⁺ cells and evaluated expression of several master erythroid transcription factors by qRT-PCR. Interestingly, EKLf was the most induced among the erythroid-specific genes (Fig. 17A). By screening ten potential smad binding sites across the entire length of the upstream enhancer, the proximal promoter and the intronic enhancer of the EKLf gene, which were previously identified in EBs³⁰, we determined the in vivo direct recruitment of Smad5 at most of these regions with chromatin immuno-precipitation experiments (ChIP) in K562 erythroleukemia cells (Fig17B). This finding indicates that smad5 plays a direct functional role in the transcriptional control of EKLf expression in definitive hematopoietic cells, beyond the EBs. As confirmation, the identification of blocks of perfect conservation within each of the three cis-elements of the EKLf gene, that are mostly GC-rich in nature, indicate a feature that has been described to serve smad binding as well⁸⁰. Next, we evaluated whether L3MBTL1 affects the binding of smad5 to these regions. We retrovirally overexpressed L3MBTL1-HA in K562 cells and performed ChIP experiments by using smad5 antibody. We found that overexpression of L3MBTL1 impairs recruitment of Smad5 on EKLf regulatory regions (Fig17B).

Indeed, activation of BMP4 signaling is required for the enhanced EKLf expression in L3MBTL1-KD cells, as the specific BMP signaling inhibitors (Dorsomorphin and SB431542) block the rise in EKLf expression seen in L3MBTL1-KD hES cells (Fig. 17C). Indeed, we previously generated a stable human embryonic stem cell line lacking L3MBTL1 and showed that these cells mirror the phenotype of cells treated with BMP4: they spontaneously undergo trophoblastic differentiation, and in fact, L3MBTL1 expression decreased in response to BMP4 treatment⁴⁴. Therefore, in order to determine whether regulation of EKLf by L3MBTL1 is due to direct regulation of smad5 expression, we performed ChIP experiments in hES cells by utilizing smad5 antibody and found recruitment of L3MBTL1 at the smad5 promoter (Fig 17D).

Overall, these data indicate that L3MBTL1 regulates EKLf expression via SMAD5 in hematopoietic and embryonic stem cells.

b) Modulation of L3MBTL1 expression affects globin gene expression

In order to evaluate the significance of regulating EKLf via smad5 in terms of globin gene expression, we lentivirally expressed shRNAs targeting L3MBTL1 in primary CB

CD34+ cells and found increased expression of fetal globin gene compared to controls (Fig. 18A-B). Conversely, we observed downregulation of gamma globin gene expression when we overexpressed HA tagged L3MBTL1 (L3MBTL1-HA) in CB CD34+ cells or K562 erythroleukemia cells (Fig. 18C-D). To determine whether this effect on fetal globin gene expression was restricted to erythroid or even hematopoietic cells, we also examined primary hES cells after lentiviral KD of L3MBTL1 and found detectable fetal globin gene mRNA in the KD hES cells (Fig. 18E). These data indicate that L3MBTL1 is a repressor of fetal globin gene expression.

In fact, treating L3MBTL1-overexpressing K562 cells with BMP4 (40 ng/ml) restored fetal globin gene expression, overcoming the repression mediated by L3MBTL1 (Fig. 18F). Therefore, to determine whether EKLF is essential for the effects of L3MBTL1 on globin genes, we knocked down both L3MBTL1 and EKLF in K562 cells and could no longer induce high-level gamma globin gene expression (Fig. 18G).

c) Knock-down of L3MBTL1 activates smad-mediated transcriptional response in patient-specific beta-thalassemia iPS cells and allows generation of high-fetal globin gene expressing erythroid progeny

Given the relevance of inducing fetal hemoglobin production in patients with β -hemoglobinopathies to ameliorate the clinical severity, we depleted L3MBTL1 from induced-Pluripotent Stem (iPS) cells, that were either derived from patients with β -thalassemia major⁸¹ or from CB CD34+ cells. We infected the iPS cells with H1P-hygro-EGFP+ lentiviral vectors expressing shRNAs targeting L3MBTL1, or Luciferase (the control vector), and obtained efficient KD of L3MBTL1 in GFP+ cells that still retained stem cell-related cell surface markers, such as Tra-181 (Fig. 19A). We then analyzed L3MBTL1-KD beta-thalassemic iPS cells that had been induced to differentiate towards the erythroid lineage, and in fact expressed the CD71 and GlyA erythroid cell surface markers; these cells showed high levels of fetal globin gene, compared to control cells (Fig. 19B). This represents an important proof of principle, implying that the regulatory network involving chromatin modifiers could impact on the course of red cell disorders, and represent an innovative strategy for treatment of hemoglobin disorders.

To further investigate the mechanisms mediating the effects of L3MBTL1 in regulating globin gene expression, we analyzed the gene expression profile (GEP) of the L3MBTL1-KD iPS cells. We found increased expression of several BMP/Smad target genes, as well as downregulation of negative modulators of TGF β -superfamily ligand signaling (Fig. 19C-D). Upregulated genes included HHEX, ID2, ID3 and MAFF, all of which have been implicated in regulating HbF expression⁸². HHEX is known to regulate globin gene expression during ontogeny and its promoter contains a 71-nucleotide BMP-responsive element (BRE)⁸³. ID genes are direct targets of BMP4 and Id proteins can regulate HSPC fate decisions³⁶. Expression of the inhibitory Smad, Smad7, which inhibits TGF β -related signaling⁸⁴ was downregulated, as were Lefty1 and Lefty2, extracellular inhibitors which antagonize Nodal signaling⁸⁵. Overall, we found enrichment of many Smad-related genes (Fig. 19E) and hematopoietic transcription factors (data not shown) using Gene Set Enrichment Analysis (GSEA).

To identify which Smad-related signaling pathway is triggered by L3MBTL1 depletion, we evaluated the level of phosphorylation of Smad1/5/8 and Smad2/3, which primarily function downstream of the BMP receptors, and the TGF β , activin and Nodal receptors, respectively. We found enhanced Smad1/5/8 phosphorylation, indicating enhanced BMP signaling (Fig. 19F). Finally, EKLF expression was found upregulated in both iPS cell lines lacking L3MBTL1 by WB (Fig 19G-H).

Overall, these data confirm that L3MBTL1 titrates BMP signaling and indicate that activation of this signaling and of its downstream targets correlates with generation of high-fetal globin gene expressing erythroid progeny in patient-specific iPS cells (Fig 19I).

3.5 PRMT5

a). PRMT5 Interacts with JAK2V617F and JAK2K539L More Strongly than Wild-Type JAK2

First, we examined whether PRMT5 interacts with JAK2 and if the V617F (and K539L) activating mutations in JAK2 affect this interaction. We coexpressed FLAG-PRMT5 with HA-tagged wild-type JAK2 and JAK2V617F, or HA-PRMT5 with nontagged versions of the wild-type JAK2, JAK2V617F, and JAK2K539L proteins in 293T cells, and found that whereas the wild-type JAK2 interacts with PRMT5, both the JAK2V617F and JAK2K539L mutants bound PRMT5 more strongly than wild-type JAK2 (Fig 20A and B), demonstrating that both constitutively activated forms of JAK2 have increased affinity for PRMT5. Next, to determine whether the endogenous JAK2V617F and PRMT5 proteins interact in leukemia cells, we performed co-immunoprecipitation (Co-IP) assays using two different anti-JAK2 antibodies and the JAK2V617F-positive HEL cell line. The interaction of JAK2V617F with PRMT5 was readily detected using either antibody (Figure 20 C). Because none of the commercially available anti-PRMT5 antibodies efficiently immunoprecipitates PRMT5, we also utilized a HEL cell line that we engineered to stably express HA-tagged PRMT5. Using an anti-HA antibody, we could detect a robust interaction between PRMT5 and the mutant JAK2 (Figure 20D). To map the region(s) in JAK2 that interacts with PRMT5, we constructed a series of N-terminal deletion mutants of HA-tagged JAK2 with or without the V617F substitution, and expressed these proteins with FLAG-tagged PRMT5 in 293T cells (Figure 20E). Co-IP experiments showed that deletion of the first 382 amino acids (which contain the receptor-binding FERM domain) from JAK2V617F greatly reduced its interaction with PRMT5. Given that the C terminus of JAK2 (808-1132) does not bind PRMT5, this indicates that the N-terminal portion of JAK2 is responsible for binding PRMT5. The JAK2 Δ 382WT deletion mutant protein also binds weakly to PRMT5, suggesting that loss of the FERM domain may expose other epitopes in wild-type JAK2 that can bind PRMT5.

b) Oncogenic JAK2 Kinases Phosphorylate PRMT5 In Vivo

To determine if JAK2 kinase can directly phosphorylate PRMT5, we performed an in vitro kinase assay using bacterially purified GST-PRMT5 as the substrate (Fig 21A). JAK2-dependent phosphorylation of GST-PRMT5 was readily detected because a JAK2 inhibitor (JAK Inhibitor I) (1 μ M) completely abrogated the phosphorylation (lane 8). We next determined if JAK2 phosphorylates PRMT5 in vivo, by coexpressing HA-PRMT5 with wild-type JAK2 or the JAK2 mutants in 293T cells, and using anti-HA immunoprecipitation followed by anti-phosphotyrosine immunoblotting. We found that PRMT5 was phosphorylated by the mutant JAK2V617F and JAK2K539L kinases, but not the wild-type JAK2 kinase (Fig 21B and C). To determine whether wild-type JAK2 can phosphorylate PRMT5 when it is activated by signaling through the erythropoietin receptor (EpoR), we transfected 293T cells with JAK2 wild-type or V617F mutant with or without the EpoR, and added 20 U/ml of Epo to the cells for 20 min (Figure 21D). Wild-type JAK2 was activated by the presence of Epo and its receptor (as shown by JAK2 autophosphorylation and phosphorylation of HA-STAT5, lane 10). However, unlike JAK2V617F, the activated wild-type JAK2 kinase did not detectably phosphorylate PRMT5, indicating that PRMT5

phosphorylation is indeed an acquired function of the mutant JAK2 kinase. Interestingly, phosphorylation of PRMT5 by JAK2V617F was reduced in cells overexpressing the EpoR, suggesting that the level of EpoR expression can affect the ability of JAK2V617F to phosphorylate PRMT5.

We next determined whether phosphorylation of endogenous PRMT5 by JAK2V617F occurs in JAK2V617F-positive HEL leukemia cells. HEL cells were treated with either DMSO or JAK Inhibitor I for 16 hr, and the phosphorylated proteins were immunoprecipitated using an anti-phosphotyrosine antibody (Fig 21E). Although PRMT5 (and STAT5) is phosphorylated in DMSO-treated HEL cells, and the phosphorylation of both proteins is greatly reduced by the JAK2 inhibitor, PRMT5 is not phosphorylated in the TF-1 hematopoietic cells (which express wild-type JAK2), even when the JAK2 kinase is activated by Epo (or GM-CSF), which clearly triggers STAT5 phosphorylation (Figure 21F). These results identify PRMT5 as a bona fide *in vivo* substrate of JAK2V617F, but not activated wild-type JAK2.

c). Phosphorylation of PRMT5 by JAK2V617F Greatly Impairs Its Methyltransferase Activity

PRMT5 has been shown to methylate histones H2A, H3, and H4 *in vitro* and *in vivo*. To determine whether phosphorylation of PRMT5 affects its enzymatic activity, we purified HA-tagged PRMT5 protein from 293T cells engineered to express either wild-type or mutant JAK2 and HA-PRMT5. After we confirmed the phosphorylation of PRMT5 by JAK2V617F, we incubated the purified PRMT5 with [³H] S-adenosylmethionine and recombinant histone H4 (Fig 22A) or histone H2A (Fig 22B) in an *in vitro* methylation assay. Although coexpression of wild-type JAK2 had little effect on PRMT5 methyltransferase activity (Fig 22A lanes 8–10), JAK2V617F significantly impaired the ability of PRMT5 to methylate histone H4 (lanes 11–13). As expected, coexpression of MEP50 with PRMT5 greatly enhanced its enzymatic activity (lanes 2–4). Similar results were seen for JAK2V617F (and JAK2K539L) on histone H2A methylation (Fig 22B).

We next examined whether JAK2V617F and JAK2K539L expression affects global H2A/H4 R3 symmetric dimethylation levels *in vivo* using 293T cells transiently expressing JAK2 wild-type, JAK2V617F, or JAK2K539L. Wild-type JAK2 had no effect on the global level of H2A/H4 R3 methylation; however, both oncogenic JAK2 kinases nearly abolished H2A/H4 R3 methylation (Fig 22C). We next assessed histone arginine methylation levels in HEL cells, in the presence or absence of JAK Inhibitor I, CEP701, which is a JAK2 (and FLT3) inhibitor and TG101348, the most specific JAK2 inhibitor tested. Treatment with all three JAK2 inhibitors markedly increased H2A R3 symmetric dimethylation in the cell (Fig 22D and 22E) (H4 R3 symmetric dimethylation is not found in HEL cells in the presence or absence of the JAK2 inhibitor). To determine how rapidly JAK2 inhibition affects the level of H2A/H4 R3 methylation, we performed a time course experiment using HEL cells treated with TG101348 (Fig 22E). An increase in H2A/H4 R3 methylation was seen within 1 hr, which peaked at the 2-hr time point. At 4 hr, the effect on H2A/H4 R3 methylation began to reverse, likely due to instability of the inhibitor because both STAT5 and PRMT5 phosphorylation began to increase at the 4-hr time point. In contrast, these JAK2 inhibitors had minimal effect on H2A/H4 R3 methylation levels in TF-1 cells, even though they blocked STAT5 phosphorylation (Fig 22F). Thus, the oncogenic JAK2 proteins gain the ability to regulate global H2A/H4 R3 symmetric dimethylation levels, presumably via phosphorylation of PRMT5.

Although JAK2 regulates gene transcription through the canonical JAK2-STAT5 pathway, as well as other pathways, our data suggest that the oncogenic JAK2 kinases (like V617F and K539L) can also regulate gene expression via repression of PRMT5 activity and possibly changes in the methylation of the histone H2A and H4 tails. We performed gene

expression profile analysis on DMSO-treated versus CEP701-treated HEL cells and on PRMT5-directed shRNA-expressing HEL cells versus control shRNA-expressing cells using Affymetrix HG133 GeneChips. We found 881 genes whose mRNA levels changed more than 1.5-fold in both duplicate samples of the CEP701-treated cells, and 585 genes whose expression reproducibly changed ≥ 1.5 -fold in cells where PRMT5 was knocked down. Because inhibition of JAK2 activity derepresses PRMT5 activity, we hypothesize that genes that are reciprocally regulated between the inhibitor-treated samples and the shPRMT5-treated samples will be regulated by JAK2-induced PRMT5 phosphorylation. Indeed, we found 90 such genes (42 upregulated by the inhibitor and downregulated by the shRNA, and 48 downregulated by the inhibitor and upregulated by the shRNA), including genes involved in ribosomal biogenesis and autophagy (Fig 22G).

d). The Major Phosphorylation Sites in PRMT5 Map to Its N-Terminal Region

There are six tyrosine residues in this region (at position 280, 283, 286, 297, 304, and 307), and we mutated the first three (M3), first four (M4), and all six tyrosine residues (M6) to phenylalanine, and examined the extent of PRMT5 phosphorylation in transfected 293T cells (Fig 23A). Compared to wild-type PRMT5, the M6 form of PRMT5 had markedly reduced phosphorylation when coexpressed with JAK2V617F. The residual phosphorylation could be due to dimerization with endogenous wild-type PRMT5, or to the presence of other phosphorylation sites within the protein. In contrast the M3 form of PRMT5 had a similar degree of phosphorylation as wild-type PRMT5, suggesting that the last three tyrosines are the major sites of JAK2 phosphorylation in PRMT5.

To demonstrate that PRMT5 is phosphorylated at these tyrosine residues, we generated a phospho-specific anti-PRMT5 antibody (P-PRMT5-747) using a mixture of peptides containing all combinations of phosphorylated Y297, Y304, and Y307 tyrosine residues. A dot blot assay confirmed that this antibody recognizes the phosphorylated and not the unphosphorylated peptides (data not shown). To confirm that endogenous PRMT5 is phosphorylated by JAK2V617F in HEL cells, we treated the cells with the JAK inhibitor I, CEP701 (Fig 23B) and TG101348 (Fig 23C) and performed several immunoblots. These JAK2 inhibitors significantly reduced the phosphorylation of PRMT5 and STAT5, demonstrating that endogenous PRMT5 is phosphorylated within these three tyrosine residues by JAK2V617F.

e). Phosphorylation of PRMT5 by JAK2V617F Disrupts Its Association with MEP50

Because MEP50 markedly enhances the enzymatic activity of PRMT5 (Fig 24A and B), we examined whether JAK2V617F impairs PRMT5 activity by disrupting the PRMT5/MEP50 complex. Using 293T cells that transiently express HA-PRMT5, and either the wild-type JAK2 or the V617F mutant protein, we could readily co-immunoprecipitate endogenous MEP50 protein from cells expressing wild-type JAK2 with an anti-HA antibody (Fig 24C). However, coexpression of JAK2V617F significantly reduced the interaction between PRMT5 and MEP50. The kinase activity of JAK2V617F is required to disrupt the PRMT5/MEP50 association because treating the cells with JAK Inhibitor I blocked the phosphorylation of PRMT5 and restored the interaction between PRMT5 and MEP50 (Fig 24D). To determine whether phosphorylation of PRMT5 affects the PRMT5/MEP50 complex in JAK2V617F-positive HEL cells, we established a stable HEL cell line that expresses myc-tagged MEP50 and purified the PRMT5/MEP50 complex using an anti-myc antibody (Fig 24E). Although the unphosphorylated form of PRMT5 bound to MEP50, the phosphorylated form of PRMT5 was exclusively in the flowthrough following the immunoprecipitation. Thus, phosphorylation of PRMT5 by JAK2V617F blocks its association with MEP50 in hematopoietic cells.

f). PRMT5 Negatively Regulates Hematopoietic Stem/Progenitor Cell Expansion and Erythroid Differentiation

We examined whether decreased PRMT5 activity promotes myeloproliferation and/or erythroid differentiation, by knocking down PRMT5 expression in human CD34⁺ CB cells using shRNA. We achieved only 60%–70% knockdown of PRMT5 mRNA but still observed a 2-fold increase in CFUs (Fig 25A). We then overexpressed HA-tagged wild-type PRMT5, or the M6 mutant form of PRMT5 (PRMT5M6), in CD34⁺ CB cells and performed CFU assays. Consistent with the knockdown experiments, PRMT5 overexpression significantly decreased colony formation (Fig 25B), indicating that PRMT5 negatively regulates progenitor cell proliferation and expansion.

We also examined whether PRMT5 activity regulates erythroid differentiation, using *in vitro* liquid culture assays. We knocked down PRMT5 or overexpressed wild-type PRMT5 or the PRMT5M6 mutant in CD34⁺ CB cells and cultured the GFP⁺ cells in medium supporting erythroid differentiation for 1 or 2 weeks. Although PRMT5 knockdown cells showed a significant increase in CD71/Ter-119-positive cells, overexpression of either the wild-type or the M6 mutant form of PRMT5 blocked erythroid differentiation (Fig 25C and D). To further determine whether downregulation of PRMT5 activity is important for JAK2V617F-induced myeloproliferation, we overexpressed the wild-type or mutant PRMT5 (PRMT5M6) proteins in JAK2V617F-positive CD34⁺ cells isolated from therapeutic phlebotomy specimens of patients with PV and performed CFU assays using 1×10^4 GFP⁺ cells (Fig 25E). The control JAK2V617F-positive CD34⁺ cells formed predominantly BFU-E colonies. However, the cells overexpressing PRMT5M6 showed no BFU-E or CFU-GEMM colonies, suggesting that the phosphorylation-defective form of PRMT5 can abrogate the erythroid differentiation potential of these cells.

To determine if PRMT5 is phosphorylated in JAK2V617F-positive patient samples, we isolated CD34⁺ cells from therapeutic phlebotomy specimens taken from patients with PV (Fig 25F), using normal CB CD34⁺ cells as a control. Of the ten patient samples tested, all of the JAK2V617F- positive (or exon 12 mutation-positive) samples had higher PRMT5 phosphorylation than the CD34⁺ CB cells or the JAK2V617F-negative CD34⁺ cells. We found less phospho-PRMT5 in two of the three JAK2V617F-negative patient samples analyzed, compared to the JAK2V617F+ MPN patient samples (Figure 5F, lane 6 and 11). The weak positivity in CB CD34⁺ cells and the high level of phospho-PRMT5 in the one JAK2 wild-type patient sample suggest that other tyrosine kinases can also phosphorylate PRMT5 in hematopoietic cells.

4. Discussion

4.1. L3MBTL1 and erythroid differentiation

Haploinsufficiency of the polycomb group gene (PcG) *L3MBTL1* has been identified in patients with 20q- associated myeloid malignancies^{12,13}, but whether this has functional relevance for these disorders has not been previously determined. We have demonstrated that *L3MBTL1* loss induces the erythroid differentiation of human HSPCs and therefore could contribute to the most common 20q- associated hematologic disorder, polycythemia vera. Further, *L3MBTL1*-KD CD34+ cells show an enhanced response to erythropoietin, resulting in the more rapid development of immunophenotypically and morphologically mature erythroblasts with increased hemoglobin content, compared to control cells. We have demonstrated the increased sensitivity of *L3MBTL1* knock-down hematopoietic stem/progenitor cells to erythropoietin at different concentrations of Epo and at very early time points. The erythroid commitment that follows *L3MBTL1*- KD occurs early, based on the erythroid progenitor cell expansion seen in the LTC-IC assay.

L3MBTL1 is classified as a Polycomb group protein and recent evidence suggests that PcG proteins regulate stem cell pluripotency by maintaining the repression of lineage-specifying genes that trigger the differentiation process^{86,87}. *L3MBTL1* is downregulated upon Epo- or hemin-induced erythroid differentiation. *L3MBTL1* is also downregulated, or at least is less abundant in MEP cells compared to more immature stem cells or progenitor cell populations (such as CMP), which suggests that erythroid differentiation may require “silencing” of *L3MBTL1* function. As a compactor of euchromatin, *L3MBTL1* could serve as an epigenetic brake on erythroid commitment. Gene expression profiling of cells treated with Epo supports this hypothesis, as *L3MBTL1* is one of the genes most strongly downregulated upon Epo exposure⁸⁸. Pr-Set7, an H4K20 specific methyltransferase that physically associates with *L3MBTL1* and is responsible for the H4K20 methyl mark that serves as a docking site for *L3MBTL1* binding, is also downregulated in hemin-treated K562 cells^{6,89}, which also suggests that the ability of *L3MBTL1* to bind chromatin and maintain repression of its target genes impairs erythroid differentiation.

Recently, the ability of reactive oxygen species (ROS) to trigger the precocious differentiation of *Drosophila* stem cells into all three mature blood cell types has been linked to downregulation of PcG expression⁹⁰. This downregulation is associated with JNK activation and it triggers differentiation towards lamellocyte but not plasmatocyte or crystal cell differentiation, somewhat similar to the effects of *L3MBTL1* KD on erythroid but not myeloid or megakaryocytic lineages. ROS triggers FOXO activation⁹⁰ and similarly we found increased phosphorylation/activation of the STAT5, AKT/FOXO, and MAPK pathways in *L3MBTL1*- KD HSPCs, even in the absence of Epo. Such Epo-independent signaling is a hallmark of the MPNs, especially polycythemia vera. PcG members specifically repress the JAK-STAT pathway in the *Drosophila* eye imaginal disc⁹¹ and our data suggest that *L3MBTL1* acts in a similar fashion to regulate erythroid differentiation.

We also found increased expression of p16^{INK4a} in *L3MBTL1*-KD cells. Increased expression of p16^{INK4A} is also found in erythroid colony-forming cells isolated from patients with PV⁷⁸. p16 has been linked to erythroid differentiation and apoptosis in erythroleukemia cells⁷⁹ and may play a role in mediating the effects of *L3MBTL1* in erythropoiesis, since we also observed downregulation of p16 following *L3MBTL1* overexpression. Downregulation of FoxOs by *L3MBTL1*- KD could also contribute to the decreased CAFC frequency seen following *L3MBTL1*-KD⁹². While we previously reported that *L3MBTL1*-KD can increase c-myc levels in some cell types, and cyclin E or A levels in others^{7,93}; we did not observe such increases in the human CD34+ cells at the time points assayed (data not shown). Such increases are seen in terminally differentiated cells (such as 293T cells) and may be needed to observe a strong proliferative response to *L3MBTL1*-KD.

In future studies we wish to determine whether L3MBTL1 loss can cooperate with the constitutively activated mutant JAK2 kinases found in patients with MPNs. There appears to be a relationship between del20q and the occurrence of the JAK2 V617F mutation. In one study of 29 patients with 20q deletion, 28 were found to be JAK2 V617F+⁹⁴. In another study of MPN patient samples, the JAK2V617F/JAK2 burden was 2-25% of the clonal cells, even though all of the clonal cells had del20q⁹⁵. While these studies suggest that the 20q deletion may represent one of several potential pre-JAK2 events (others being mutations in TET2, ASXL1, c-CBL or currently unknown proteins)^{96,97}, Schaub et al. have reported that del20q may occur after the acquisition of *JAK2V617F* in some clones⁹⁸. It is likely that during the genesis of the MPNs the acquisition of additional genetic mutations (i.e. JAK2V617F) may allow the cells to override the anti-proliferative mechanisms elicited by p16 or MAPK activation.

L3MBTL1 plays a key role in hematopoiesis by regulating the erythroid differentiation of HSPCs. Given that *L3MBTL1* is located within the common deleted region on 20q seen in patients with PV, our data suggests that loss of L3MBTL1 is important in the pathogenesis of such disorders.

4.2. L3MBTL1 and the DNA damage

L3MBTL1 interacts with components of the DNA replication machinery (MCM2-7 proteins, Cdc45, and PCNA) and is required for the normal movement of DNA replication forks. These findings suggest that L3MBTL1 influences multiple aspects of DNA replication and repair. The methylation status of H4K20 is important in DNA replication and DDR pathways⁹⁹. SUV4-20 methyltransferase catalyzes the di- and trimethylation of H4K20, and Suv4-20 knockout mice, which can only form the H4K20me1 derivative, are more sensitive to DNA damage than wild-type mice¹⁰⁰. Loss of Pr-Set7, a histone methyltransferase that monomethylates lysine 20 on histone H4, induces DNA damage in human, mouse, and Drosophila cells. Pr-Set7 has also been implicated in DNA replication. We previously established that L3MBTL1 binds to mono- and dimethylated H4K20, and interacts directly with PR-Set7. The binding of L3MBTL1 to chromatin occurs during S phase, coincidental with the appearance of H4K20me1, suggesting that it binds to the mark to exert its effects⁶. Depletion of L3MBTL1 resulted in a marked increase in H4K20me2 levels (Fig 10D), possibly by allowing dimethylation of H4K20 by Suv4-20 histone methyltransferase. The biological effects observed following depletion of L3MBTL1 closely parallel those resulting from the loss of Pr-Set7, suggesting that the ability of L3MBTL1 to recognize and bind to the H4K20me1 mark produced by Pr-Set7 plays an important role in maintaining genomic stability.

At present, it is unclear how L3MBTL1 contributes to genomic stability and influences fork progression. Its role in fork progression may relate to its function in maintaining genomic stability, as L3MBTL1 depletion triggers the DDR, which leads to checkpoint activation and a halt in replication. Recently, Qin et al. found that loss of L3MBTL1 in mice does not alter H4K20 methylation or result in tumor formation¹⁰¹. Differences between the Qin et al. study and ours may reflect the effects caused by the acute loss of L3MBTL1 vs. its chronic absence in the knockout mice, where functional compensation by another L3MBTL family member could occur. Furthermore, H4K20 methylation levels may be controlled differently in ES cells than in the normal, human diploid fibroblasts that we have studied. As oncogenesis is a multistep process, it seems highly likely that additional molecular events are needed to induce tumorigenesis.

Interactions between L3MBTL1 and Cdc45 and MCM2-7 suggest that L3MBTL1 may have a more direct role in DNA replication; however, further studies will be required to define the functional significance of these interactions and to determine whether the position of L3MBTL1 is within or external to nucleosomes, because nucleosome deposition occurs behind the fork on newly synthesized DNA. L3MBTL1 may also prevent the conversion of

the H4K20me1 mark to H4K20me2 by Suv4-20, as we detected an increase in H4K20me2 in cells depleted of L3MBTL1. Though L3MBTL1 is degraded during mitosis⁶, depletion of L3MBTL1 before the G2/M transition leads to the generation of the H4K20me2, which recruits 53BP1, thereby promoting the DDR and hindering normal replication. Normally, Suv4-20 acts during the M and G1 phases to convert H4K20me1 to H4K20me2¹⁰². This methylation step may occur primarily in the absence of chromatin-bound L3MBTL1. Consistent with this notion, we found that L3MBTL1 depletion slowed replication fork progression and increased the formation of 53BP1 foci. Whether removal of L3MBTL1 from the H4K20me1 mark is required for the DDR, by triggering the H4K20me2 generation and subsequent binding of 53BP1, will require further investigation.

DNA damage and genomic instability promote oncogenesis¹⁰³, and tumor samples isolated from patients at diagnosis often show constitutive activation of DNA damage signaling^{16,17}. Mechanistic studies implicate oncogene-induced DNA replication stress, including replication fork collapse and formation of double-stranded breaks, as the stimulus that evokes the DDR response¹⁸. We have shown that the depletion of L3MBTL1, a candidate tumor suppressor gene, leads to the activation of the DDR. Failure to correct DNA damage caused by the loss of L3MBTL1 could lead to genomic instability and the development of a myeloid malignancy. These observations suggest that the role of L3MBTL1 in DNA replication and genome stability may be evolutionary conserved, implying that the loss of L3MBTL1 contributes to the development of 20q12 hematopoietic malignancies by causing DNA damage and genomic instability.

4.3. L3MBTL1 and the pluripotency of human embryonic stem cells

Undifferentiated ES cells generally contain more permissive chromatin with higher levels of activating marks (lysine acetylation) and lower levels of repressive marks (H3 lysine K9 and K27 methylation), whereas differentiated ES cells generally display silenced chromatin structure¹⁰⁴. One of the great challenges in human stem cell biology is to understand the mechanisms that selectively silence certain gene-rich regions of the genome, to allow the production of the full range of cell types found in the adult. Compacted chromatin is generally found during differentiation, but very little is known about the individual proteins that differentially silence genes and affect the outcome of differentiation.

In this study, we found that knocking down the epigenetic “reader” L3MBTL1 strongly influences the differentiation potential of hESCs toward trophoblast under conditions wherein spontaneous differentiation occurs, without affecting hESC self-renewal in the undifferentiated state.

L3MBTL1 KD hESCs can be cultured continuously with no noticeable changes in their behavior, morphology, or cell cycle status and only minor changes in the RNA levels of the pluripotency markers OCT-4, NANOG, or SOX2 (Fig. 13C–E), which suggests that L3MBTL1 does not play a critical role in maintaining the undifferentiated status or self-renewal potential of hESCs.

Nonetheless, L3MBTL1 KD clearly impaired the developmental potential of hESCs in spontaneous differentiation assays. Withdrawal of FGF2 triggered profound changes in the differentiated L3MBTL1 KD cells under adherent conditions with loss of ectoderm, endoderm, and mesoderm marker expression; this implies that L3MBTL1 KD cells have limited pluripotency. The differentiated L3MBTL1 KD cells do express trophoblast markers (Figs. 15B, D), and in fact, the increased expression of CDX2 is consistent with the L3MBTL1 KD cells being restricted to a trophoblast fate (Fig. 15A)¹⁰⁵. Cdx2 acts early in the lineage hierarchy and its overexpression triggers embryonic stem cells to differentiate into trophoblast stem cells¹⁰⁶. Overall, these changes could explain the failure of these cells to form typical EB structures in nonadherent assays. It is also possible that genomic instability during EB development could explain the increased cell death seen in L3MBTL1 KD cells (Fig. 14B,C). In contrast, the differentiated control cells maintained

expression of embryonic lineage markers, and consistent with their upregulation of L3MBTL1, the expression of trophoblast markers was absent.

The production of extra-embryonic trophoblast cells from the L3MBTL1 KD cells resembles the effect of BMP4 on hESCs. BMP4 directs hESCs toward trophoblast with increased SMAD 1/5/8 phosphorylation, CG- β secretion, and HAND1 expression, which occurs concomitantly with a marked decrease in L3MBTL1 expression (Fig. 16A and B). Both the BMP4-stimulated hESCs and the L3MBTL1 KD cells secrete placental hormones, demonstrating that knockdown of L3MBTL1 drives hESCs to become trophoblast-like cells (Fig. 16C). The lack of other embryonic cell types derived from L3MBTL1KD cells is not absolute, as L3MBTL1 KD cells can still form neural tissue and hematoendothelial cells in response to strong inductive signals. This suggests that L3MBTL1 may promote the retention of pluripotency of hESCs, at least in part by blocking trophoblast differentiation.

Thus, L3MBTL1 may play a role in the earliest cell fate decisions involved in human development, most likely by repressing genes involved in trophectoderm differentiation.

Such a phenotype was recently described for Mbd3, a component of the Mi-2/NURD repressor complex¹⁰⁷. L3MBTL1 may promote chromatin compaction via its recognition of mono- and dimethylated states of H4K20 by L3MBTL1⁶ or by recruiting additional chromatin remodelers to block the trophectoderm differentiation of hESCs. In *Drosophila*, dl(3)MBT has been shown to bind histone H4 K20 monomethyl in close association with the dRPD3 histone deacetylase, resulting in deacetylation of histone H4 K5/K12¹⁰⁸.

Mass spectrometry (MS) studies have revealed that a large percentage of histone H4 is dimethylated in undifferentiated hESCs (*65%) with some unmethylated (*20%) and some monomethylated (*10%) or trimethylated (*5%) residues.

Nonetheless, epigenetic disturbance during the early events of differentiation may be a consequence of knocking down L3MBTL1, explaining the lineage selectivity of hESCs toward the trophectoderm fate.

In summary, L3MBTL1 KD hESCs proliferate normally in the undifferentiated state, but are impaired in their ability to spontaneously differentiate toward embryonic tissues, and preferentially differentiate into trophoblast tissue. Further studies are required to establish the molecular basis of the lineage selectivity that occurs after L3MBTL1 knockdown.

4.4 L3MBTL1 and the BMP4 signaling

Combinatorial crosstalk among transcription factors is essential to direct the lineage specification of hematopoietic stem/progenitor cells. Our study supports a model where the erythroid transcriptional network, which is dominated by the transcription factor EKLF, is facilitated by the L3MBTL1-mediated regulation of BMP4/Smad5 signaling. In agreement with larger maps of combinatorial interactions among transcription factors¹⁰⁹, our work implies that lineage specification (erythroid in our case) is not completely determined by tissue-specific transcription factors (specifiers like EKLF), but can be modulated by crosstalk with transcription factors that are broadly-expressed (like smad5). A similar effect is seen in the regulation of monocyte differentiation by SMAD3 (generally expressed) and FLI1 (whose expression is restricted primarily to macrophage-related tissues such as spleen and lymph-nodes)¹⁰⁹.

BMP4 was previously identified as a critical regulator of hematopoietic lineage differentiation from mesoderm during development, while more recent evidence indicates that it functions as a dynamic player during hematopoietic regeneration following stress^{40,41}. The cell-specific context and the transcriptional status of a gene can alter SMAD1 binding: in erythroid cells SMAD1 binds the same targets as GATA1, which helps activate these genes, while in CD34+ non-erythroid progenitor cells, SMAD1 binds with GATA2 on progenitors expressed genes being largely absent from erythroid genes^{41,110,111}.

We speculated that manipulating the pathways regulating hematopoietic regeneration (like the BMP/smud pathway) could therapeutically affect the differentiation of hematopoietic stem/progenitor cells. It appears that, human stress erythropoiesis exhibits properties similar to fetal erythropoiesis, and fetal erythrocyte antigens as well as the expression of fetal hemoglobin (HbF) are observed during the recovery from erythropoietic stress^{112,113}. These characteristics are also observed following bone marrow transplantation^{114,115}, in acute anemia syndromes like childhood transient erythroblastopenia^{116,117} and in patients with thalassemia and sickle cell anemia¹¹⁸. Analysis of peripheral blood and bone marrow progenitors from sickle cell anemia patients identified a population of progenitor cells that express CD34 and glycophorin A (GPA) on their surface, and also CD71 and KIT. These cells give rise to a higher proportion of HbF+ cells than normal bone marrow progenitors^{119,120}. We have identified a BMP4-dependent erythropoiesis pathway in human definitive hematopoiesis, and the downstream target genes of this pathway in erythroid cells, such as EKLF. Moreover, we found that manipulation of this regulatory network, through knock-down of L3MBTL1, enhances the function of EKLF and the expression of fetal globin gene even in cells that are not committed to an erythroid fate. This unveils an additional layer to the regulation of the EKLF transcription factor in hematopoiesis, especially in the erythroid lineage, as initially suggested in embryoid bodies during the BMP4-mediated promotion of the hematopoietic differentiation from mesoderm^{29,30}. L3MBTL1 fine-tunes the BMP4 signaling pathway in ES cells, iPS cells and mature hematopoietic cells, affecting smad5 binding on EKLF gene and consequently regulating its expression and its function on globin gene regulation. The beta-thalassemic iPS cells, which we generated lacking L3MBTL1, show activation of the BMP4 signaling and higher ability to generate erythroid progeny expressing fetal globin gene. These findings suggest that targeting L3MBTL1, or promoting BMP/Smad signaling, could have beneficial effects in patients with b-hemoglobinopathies. Characterization of this regulatory network is important to identify potential novel therapeutic approaches for treatment of inherited red cell disorders like beta-thalassemia, as well as for bone marrow failure syndromes with Epo-resistant anemia.

4.5 PRMT5

We have determined that oncogenic mutations within the JAK2 tyrosine kinase (V617F and K539L) enhance its interaction with PRMT5, leading to PRMT5 phosphorylation *in vivo*. Although both the wild-type and mutant forms of JAK2 proteins interact with PRMT5, phosphorylation of PRMT5 is a “gain-of-function” of the mutant JAK2 kinases, which reduces PRMT5 methyltransferase activity and decreases global histone H2A/H4 R3 methylation.

The PRMT5-interacting region in the JAK2 protein maps to its N terminus, making it unlikely that the mutated residues in the JH2 domain play a critical role in this interaction. Furthermore, it appears that the active conformation of the mutant JAK2 proteins, and not necessarily their kinase activity, allows them to bind PRMT5 more strongly because the increased binding persists in the presence of JAK2 kinase inhibitors (data not shown).

We find that PRMT5 that is phosphorylated by JAK2V617F no longer binds MEP50, even though we can detect an interaction of MEP50 with unphosphorylated PRMT5 in HEL cells. It is possible that much of the PRMT5:MEP50 complex that contains unphosphorylated PRMT5 is cytoplasmic, rather than nuclear, because we and others have shown that both proteins are found in the nucleus and the cytoplasm, and PRMT5 is known to complex with MEP50 in both locations. Given the enhanced proliferation seen following knockdown of PRMT5 in normal CD34+ cells, it would seem “easier” for the JAK2V617F+ mutant cells to simply degrade, or not express PRMT5. However, PRMT5

preferentially promotes p53-dependent cell cycle arrest at the expense of p53-dependent apoptosis⁶² and indeed, we find that knocking down PRMT5 in HEL cells triggers cell death (data not shown). Thus, JAK2V617F-expressing hematopoietic cells may require that some PRMT5 protein be present, to complex with MEP50. Given our confirmation of the recent demonstrations that JAK2 can be found in the nucleus⁴⁶, PRMT5 phosphorylation may be differentially regulated in the nucleus versus the cytoplasm of the cell, and in hematopoietic cells versus other cell types.

The kinase-dependent regulation of global H2A/H4 R3 symmetric methylation reveals a link between an oncogenic tyrosine kinase and this particular chromatin modification. We have also shown the dynamic nature of this regulation. To gain insight into how JAK2V617F could regulate gene expression through phosphorylation of PRMT5, we performed gene expression profiling comparing the JAK2-regulated genes (defined using a JAK2 inhibitor) with the PRMT5-regulated genes (defined using shRNA directed against PRMT5) and found 90 genes that were reciprocally regulated.

Forced expression of JAK2V617F induces a PV-like disease in mouse models⁵²⁻⁵⁴, and our studies suggest that in addition to activating the STAT5 pathway, this mutant JAK2 kinase can induce myeloproliferation and erythrocytosis by abrogating PRMT5 activity. Although knockdown of PRMT5 in many cell lines, such as HEL and K562, led to apoptosis and/or growth arrest, its downregulation in normal CB CD34+ cells provides a proliferative signal. We too find that PRMT5 regulates globin gene expression in HEL, CB CD34+ cells as well as in K562 cells (data not shown). However, the distinct effects of PRMT5 knockdown on gene expression in HEL versus CD34+ cells (data not shown) demonstrate the importance of cell context on PRMT5 function.

Although PRMT5 is most highly phosphorylated in JAK2V617F-positive MPN patient CD34+ cells (and in granulocytes), it is also phosphorylated to some degree in JAK2V617F-negative MPN and normal CB CD34+ cells. Overexpressing PRMT5 (wild-type and, in particular, the M6 mutant form of PRMT5) in JAK2V617F-positive CD34+ patient cells resulted in a block in cell expansion and erythroid differentiation, providing further evidence that phosphorylation and abrogation of PRMT5 activity are important functions of this oncogenic kinase. Nonetheless, further experiments are needed to assess the relative contribution of PRMT5 phosphorylation to the various clinical syndromes associated with the JAK2V617F mutation.

In conclusion, we have identified a “gain of function” for the constitutively activated forms of JAK2 kinase (JAK2V617F and JAK2K539L), namely phosphorylation of PRMT5, which allows them to control transcription by regulating histone H2A and H4 arginine methylation. Given the diverse functions of PRMT5 in the cell, further studies of the proteins methylated by PRMT5 and the pathways affected in JAK2V617F-expressing cells will shed additional light on the molecular pathogenesis of the MPNs.

4.6 Overall Conclusions

These studies have identified crucial roles for epigenetic modifiers (L3MBTL1 and PRMT5) in the regulation of normal haematopoiesis and illustrates how the loss of normal epigenetic functionality can contribute to leukaemogenesis. As such, elucidating the impact of epigenetic mutations on leukaemogenesis and therapeutic response will be essential for advancing our understanding and treatment of myeloid malignancies.

Figure 1

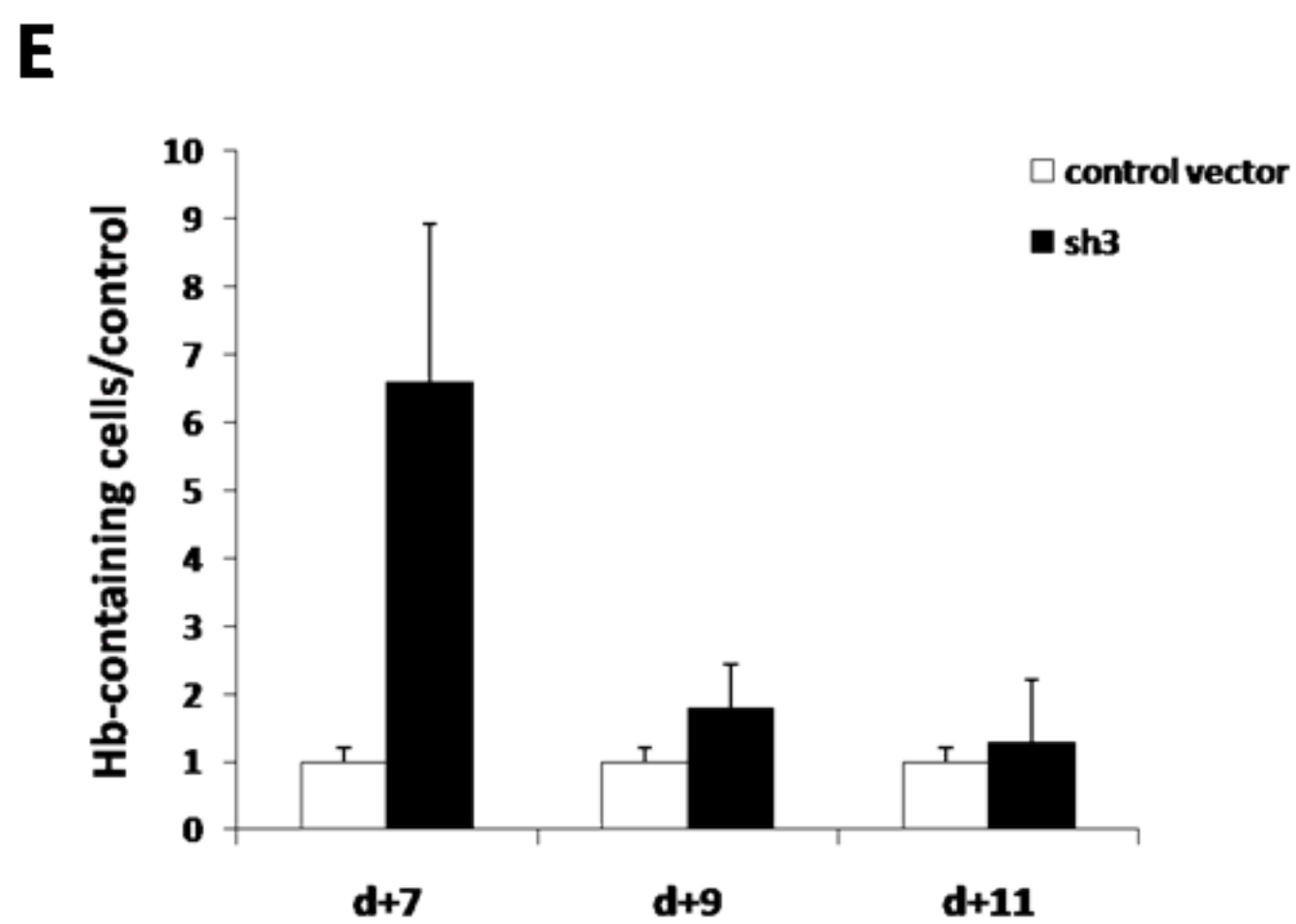
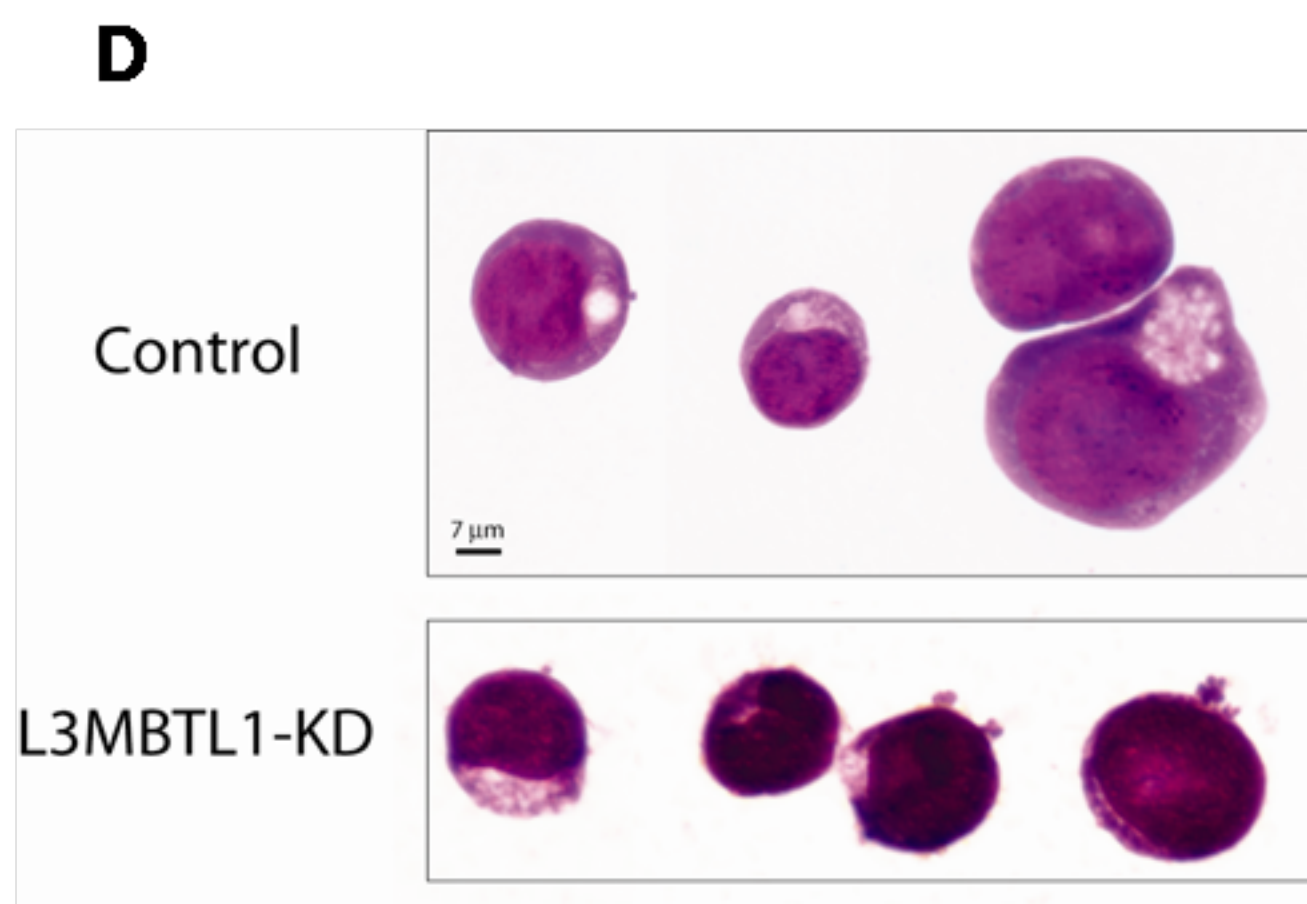
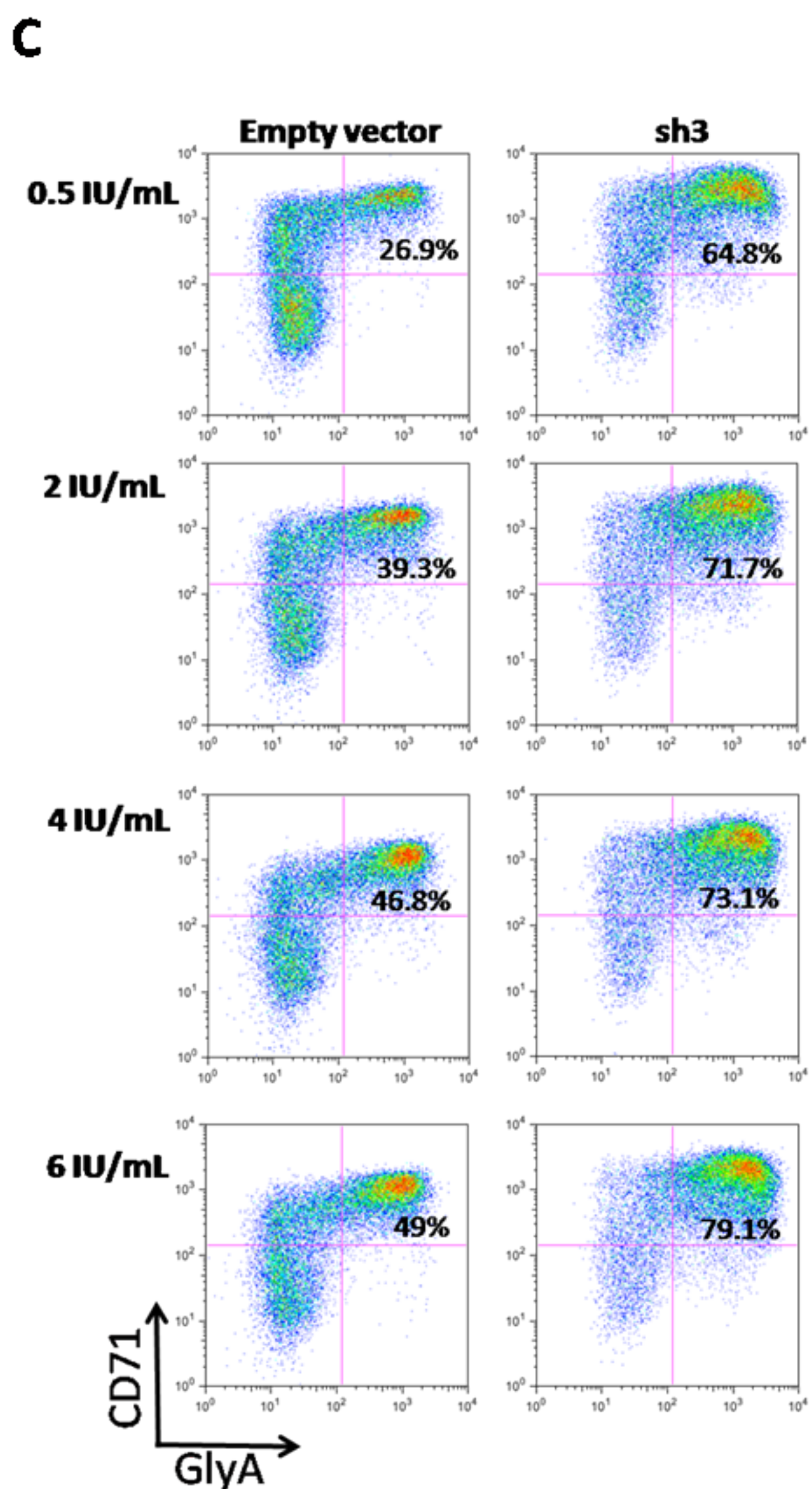
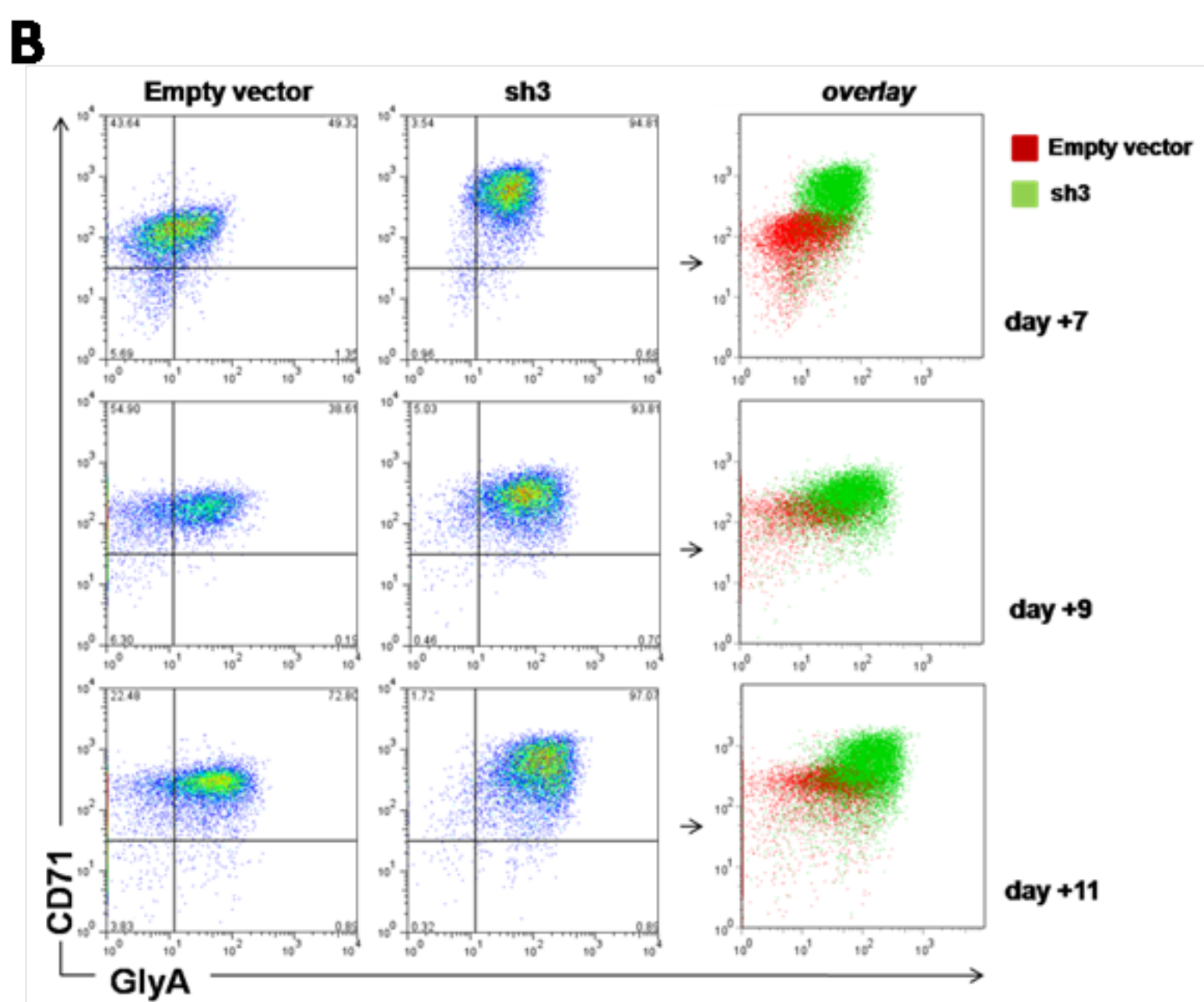
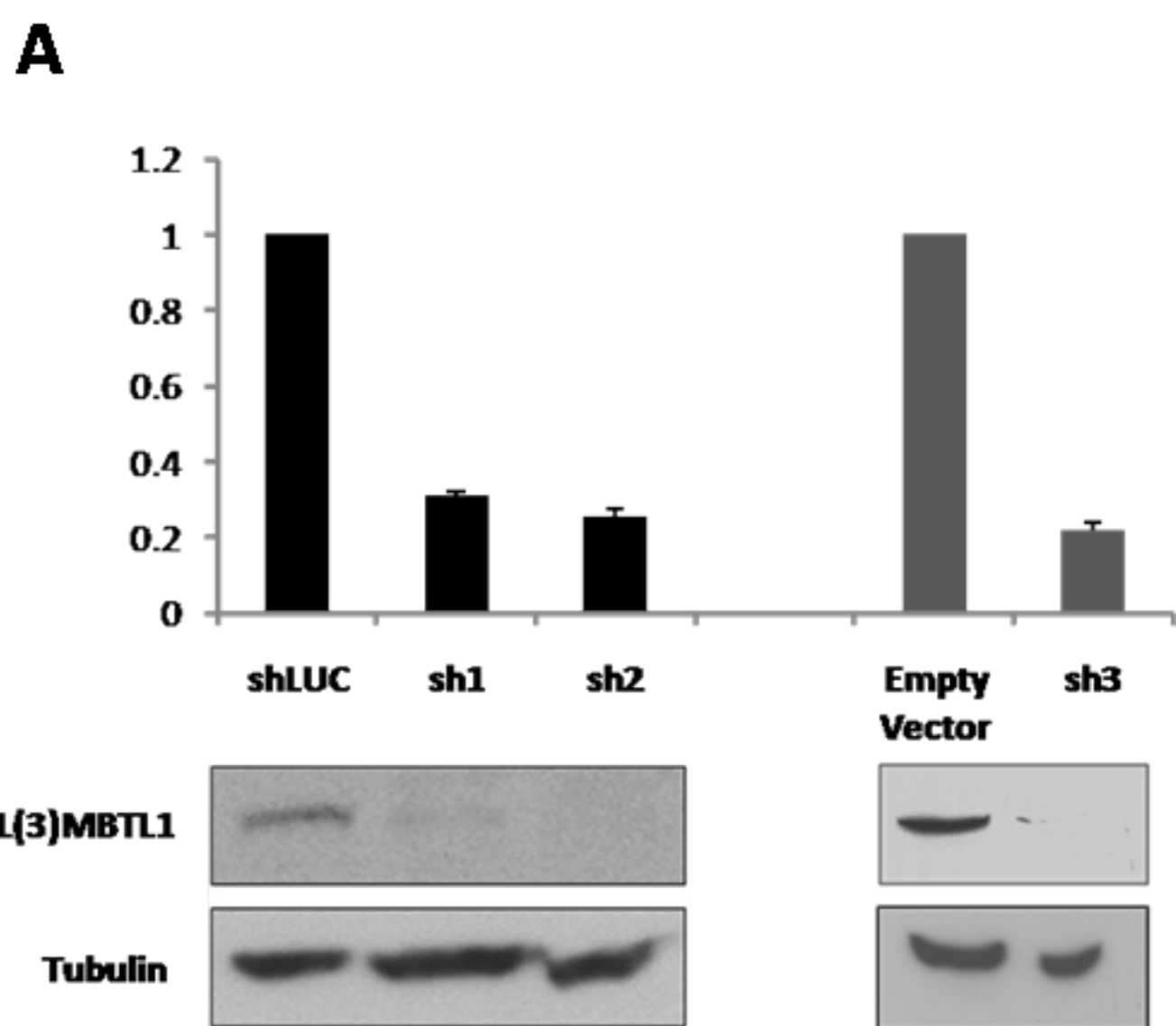


Figure 2

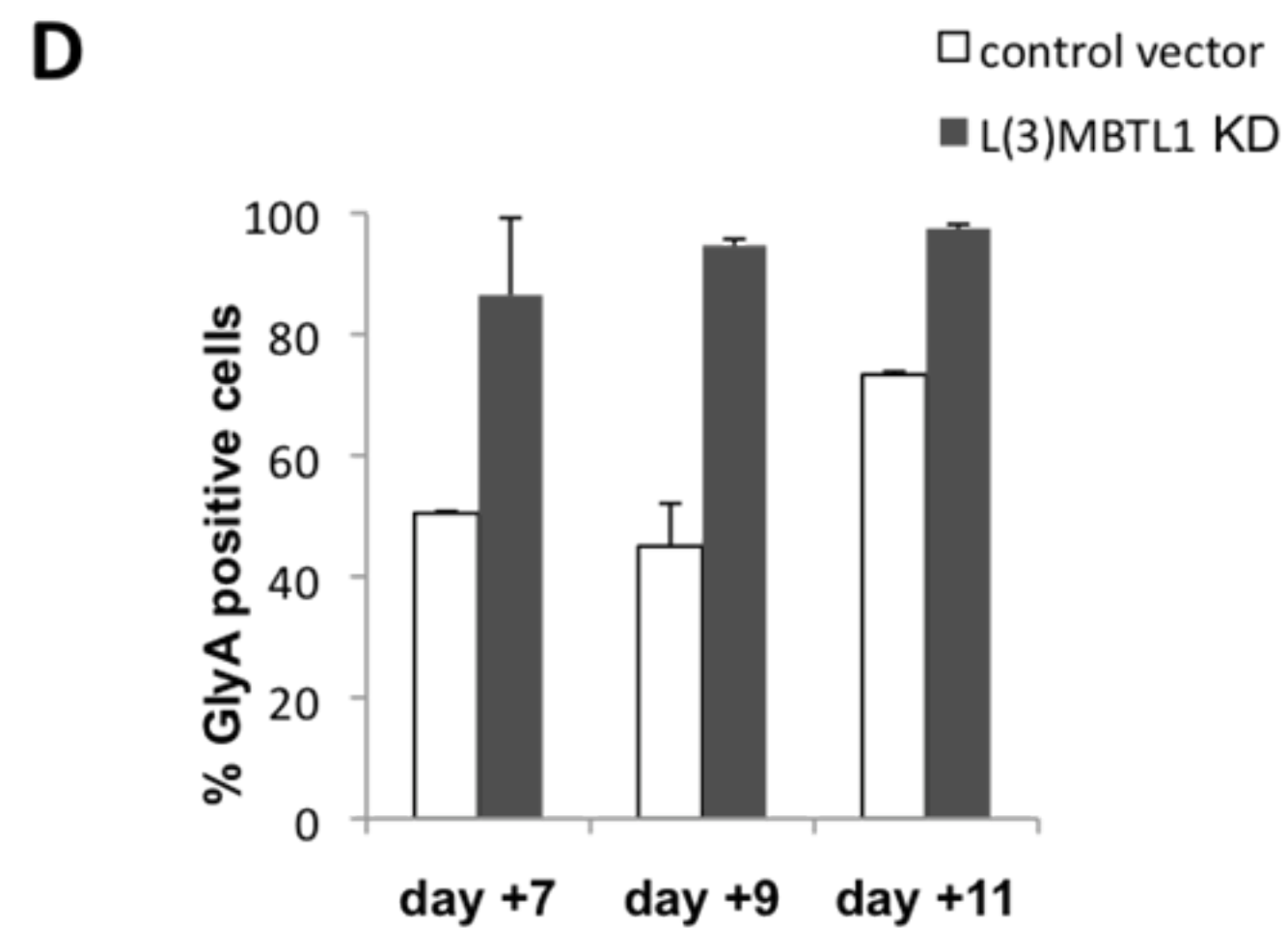
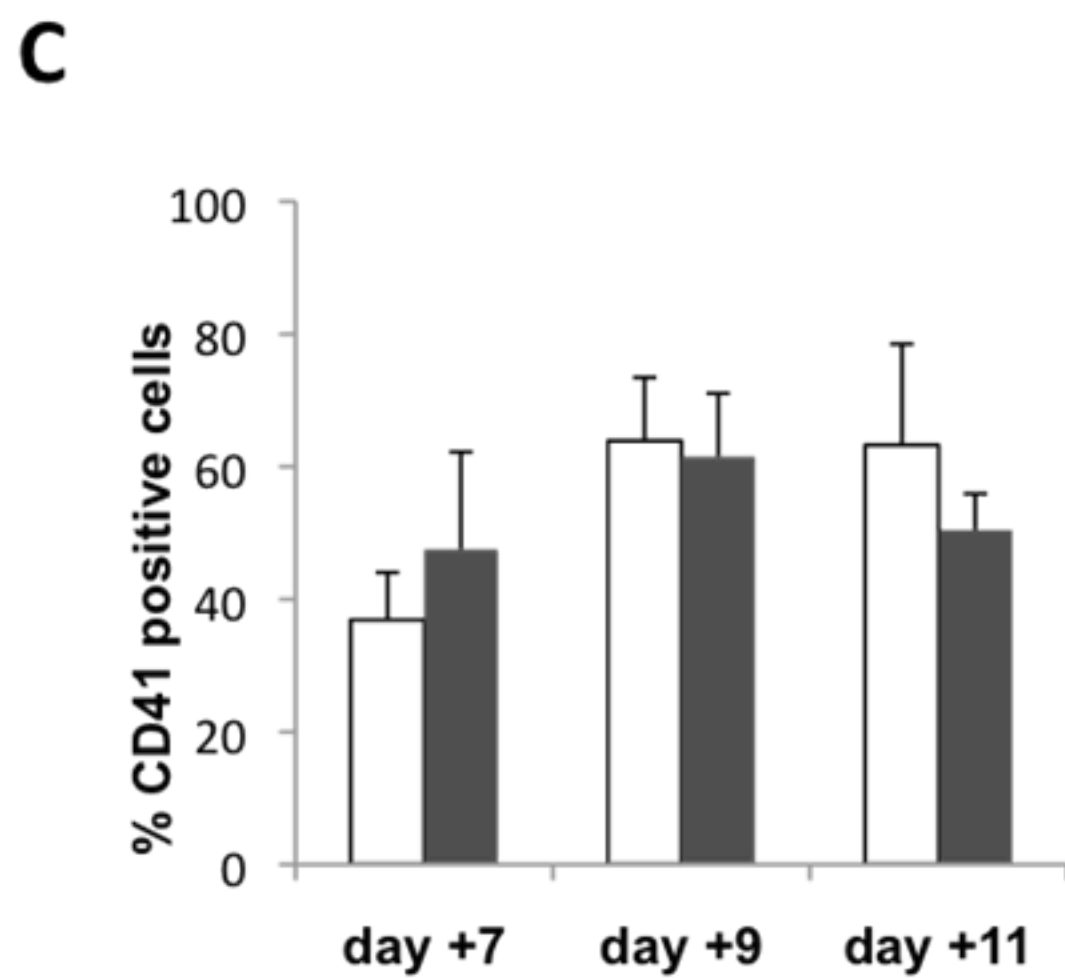
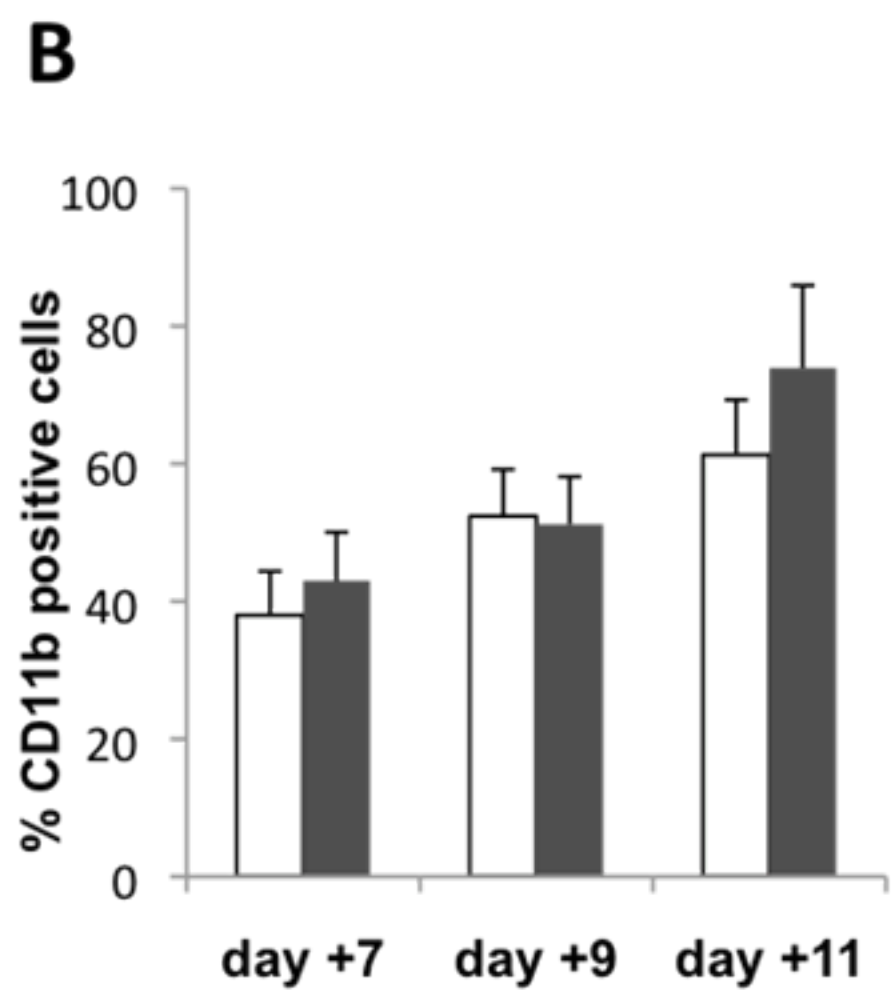
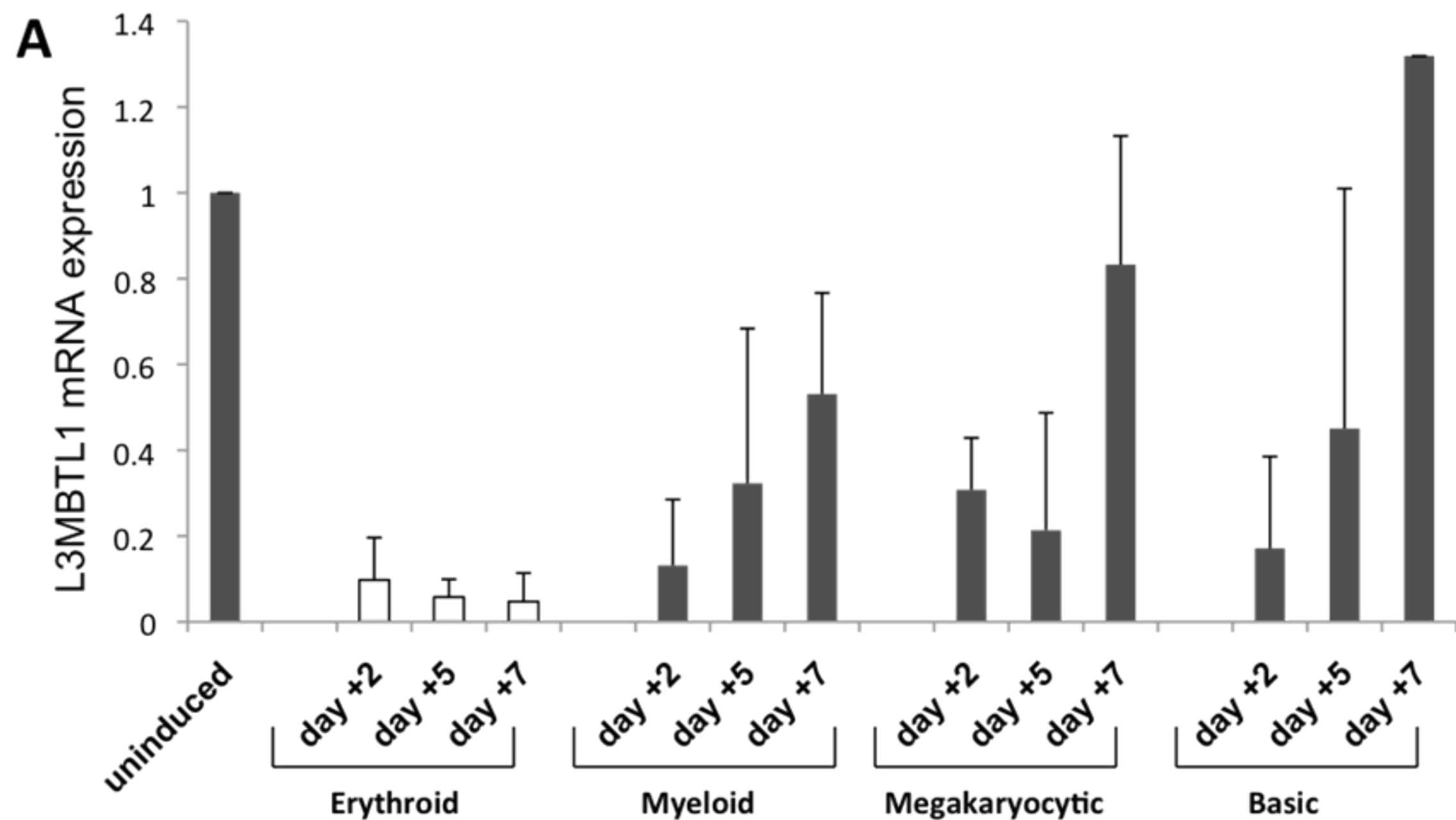


Figure 3

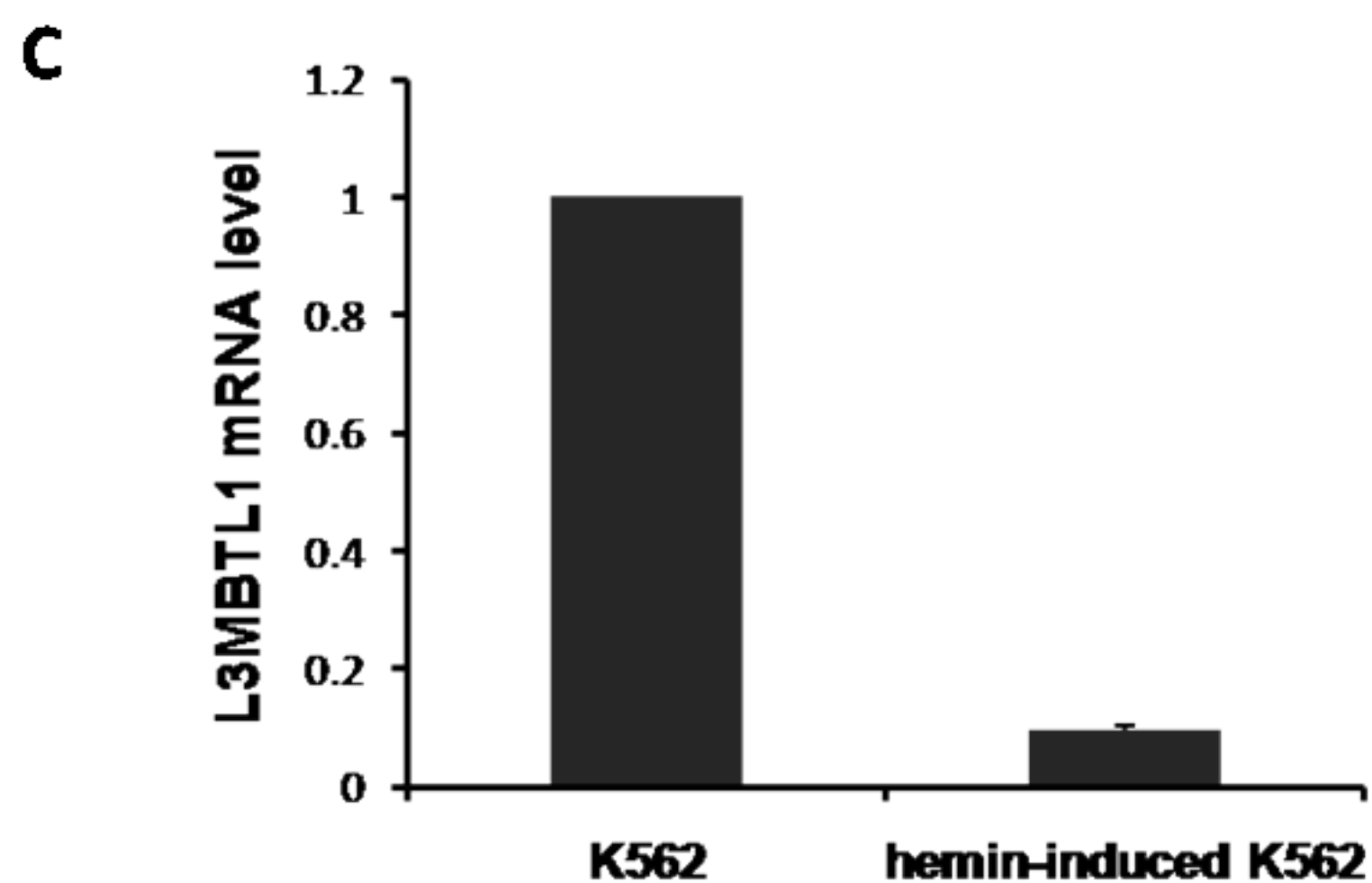
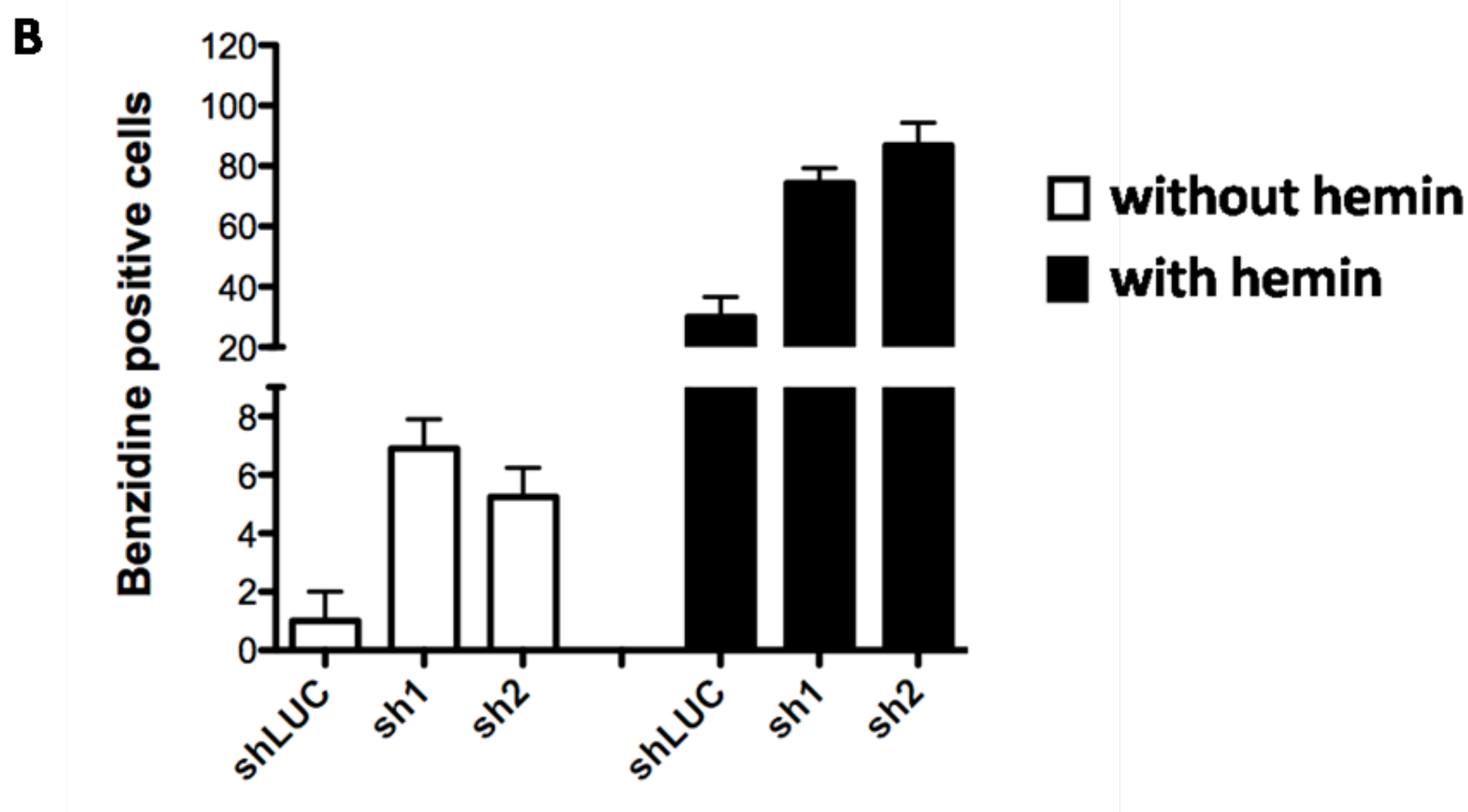
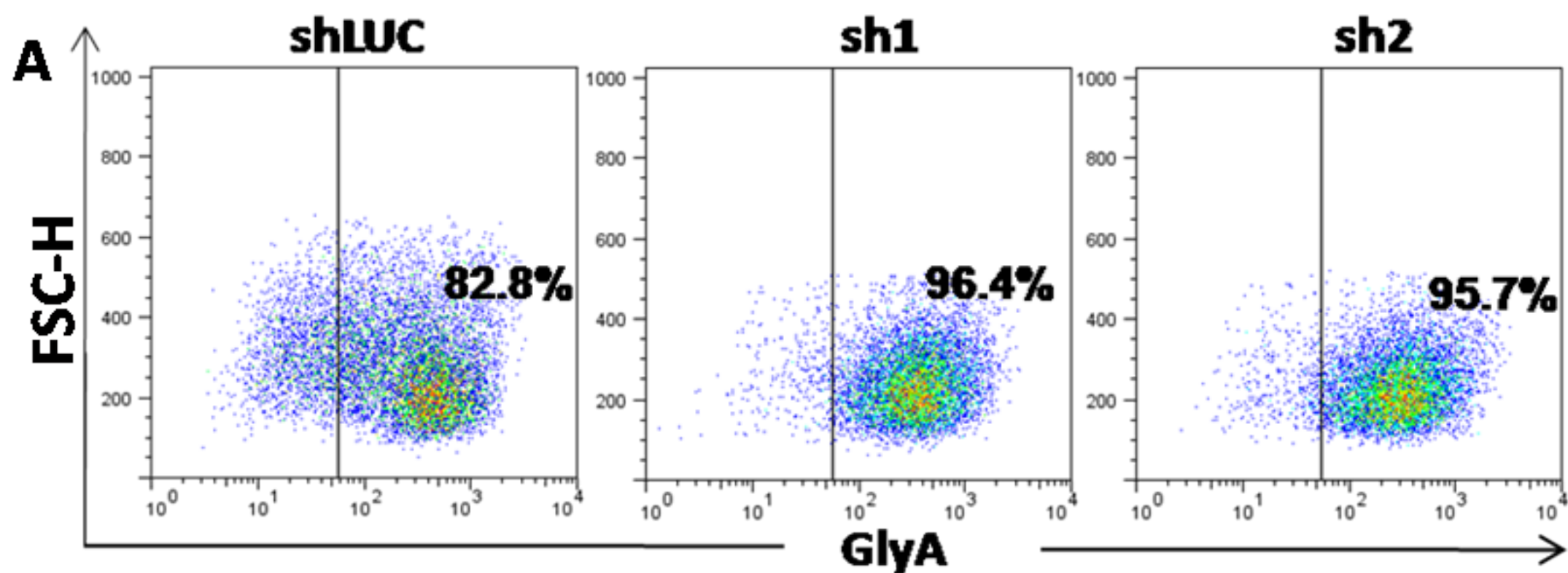


Figure 4

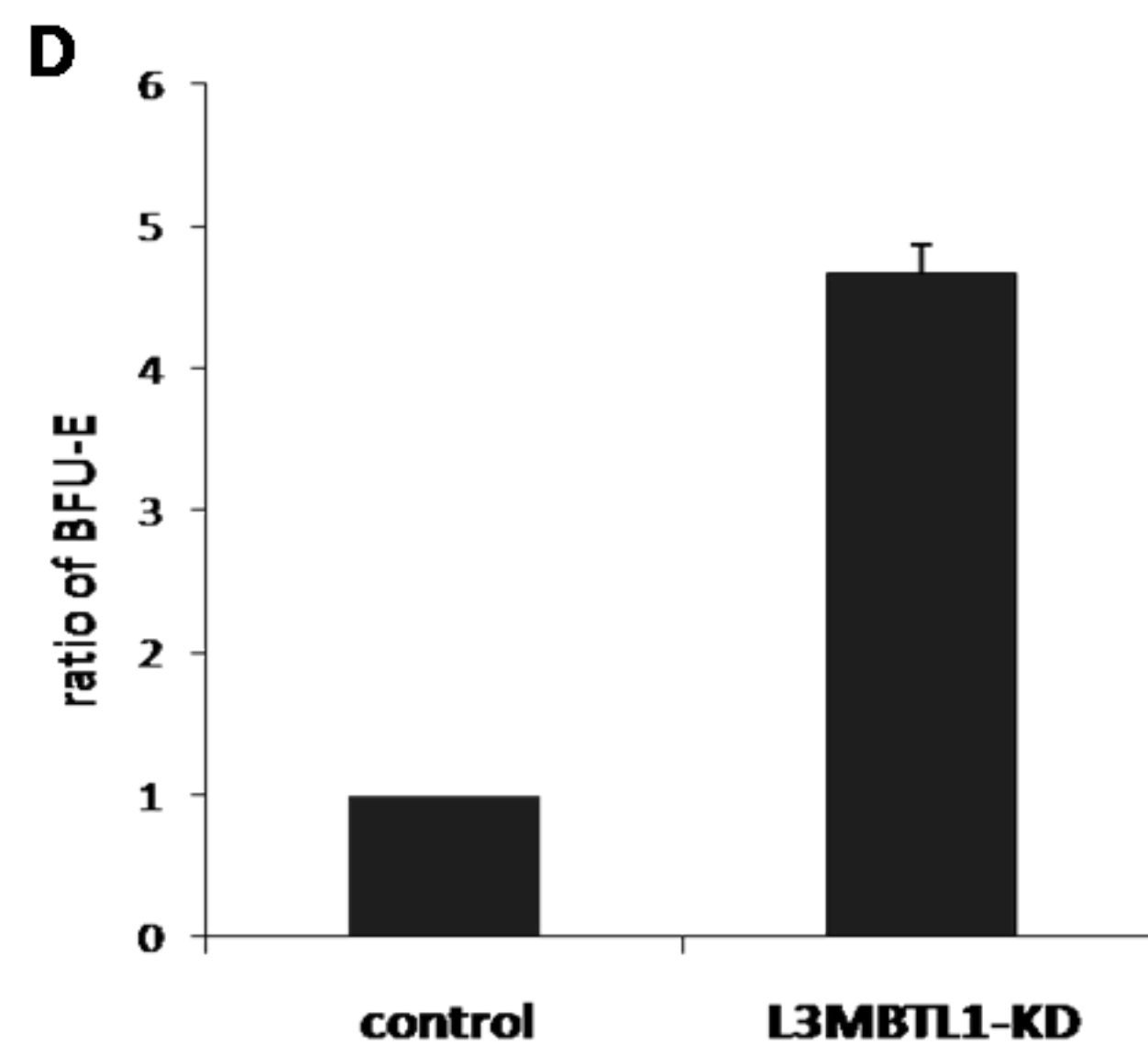
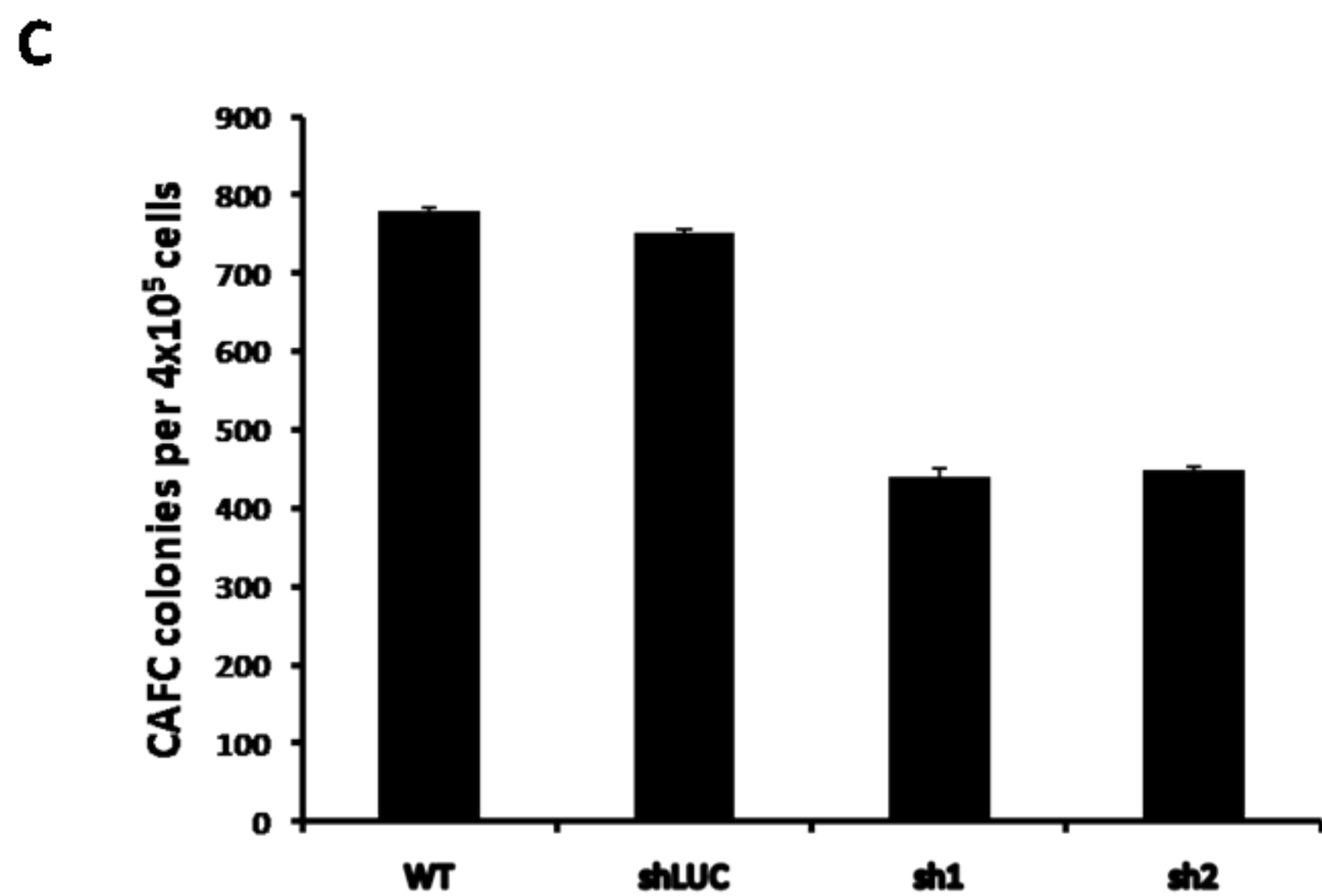
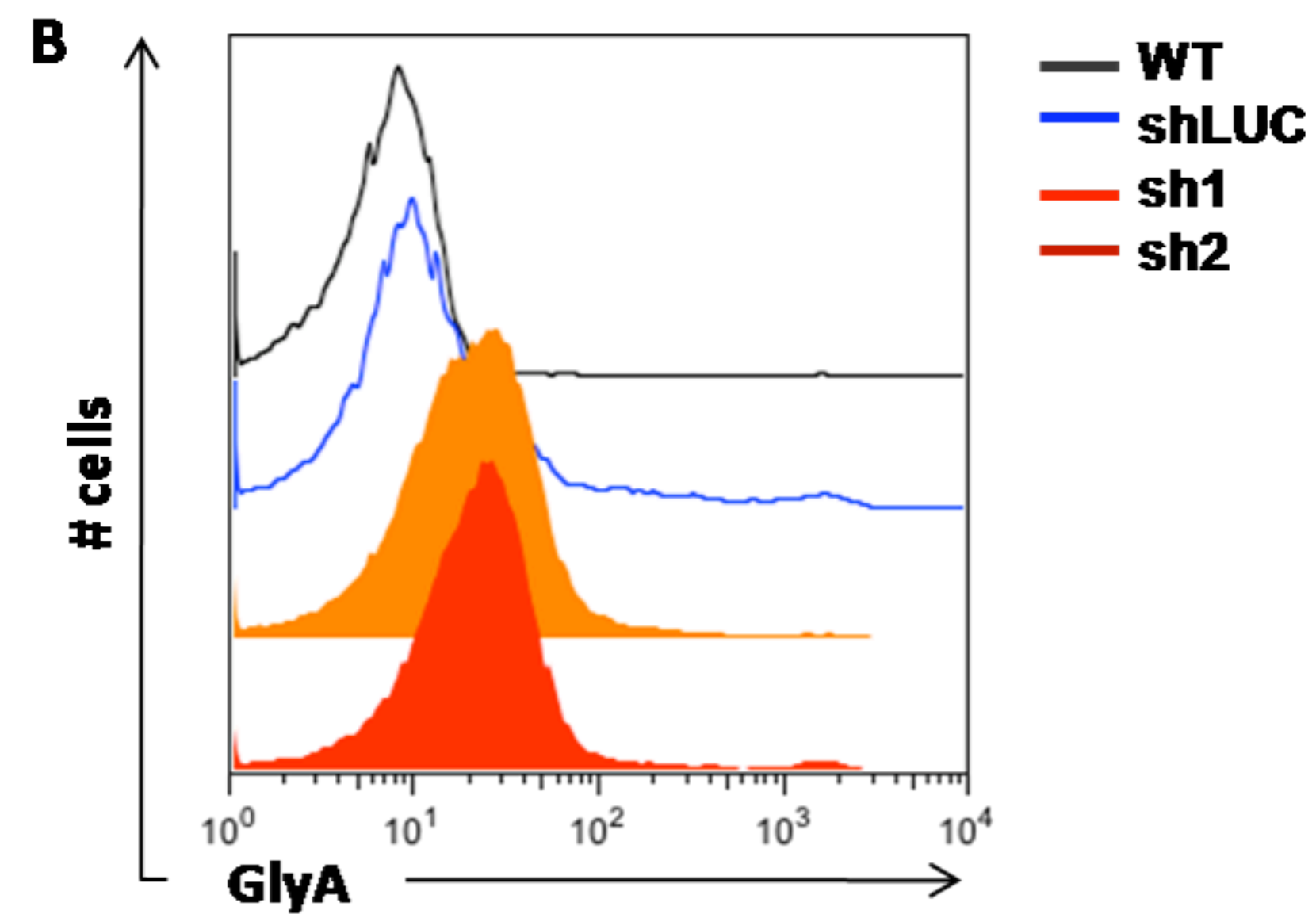
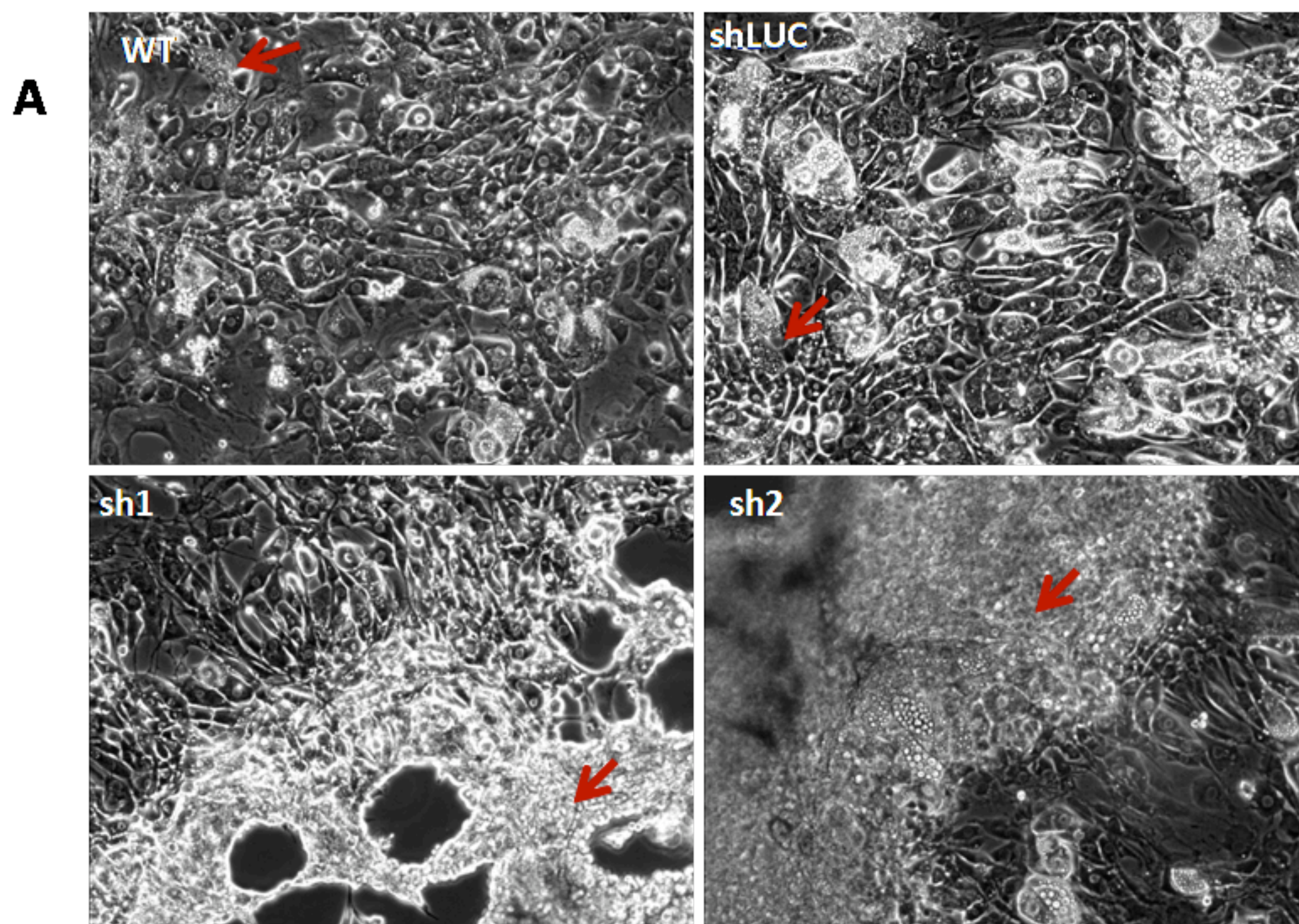
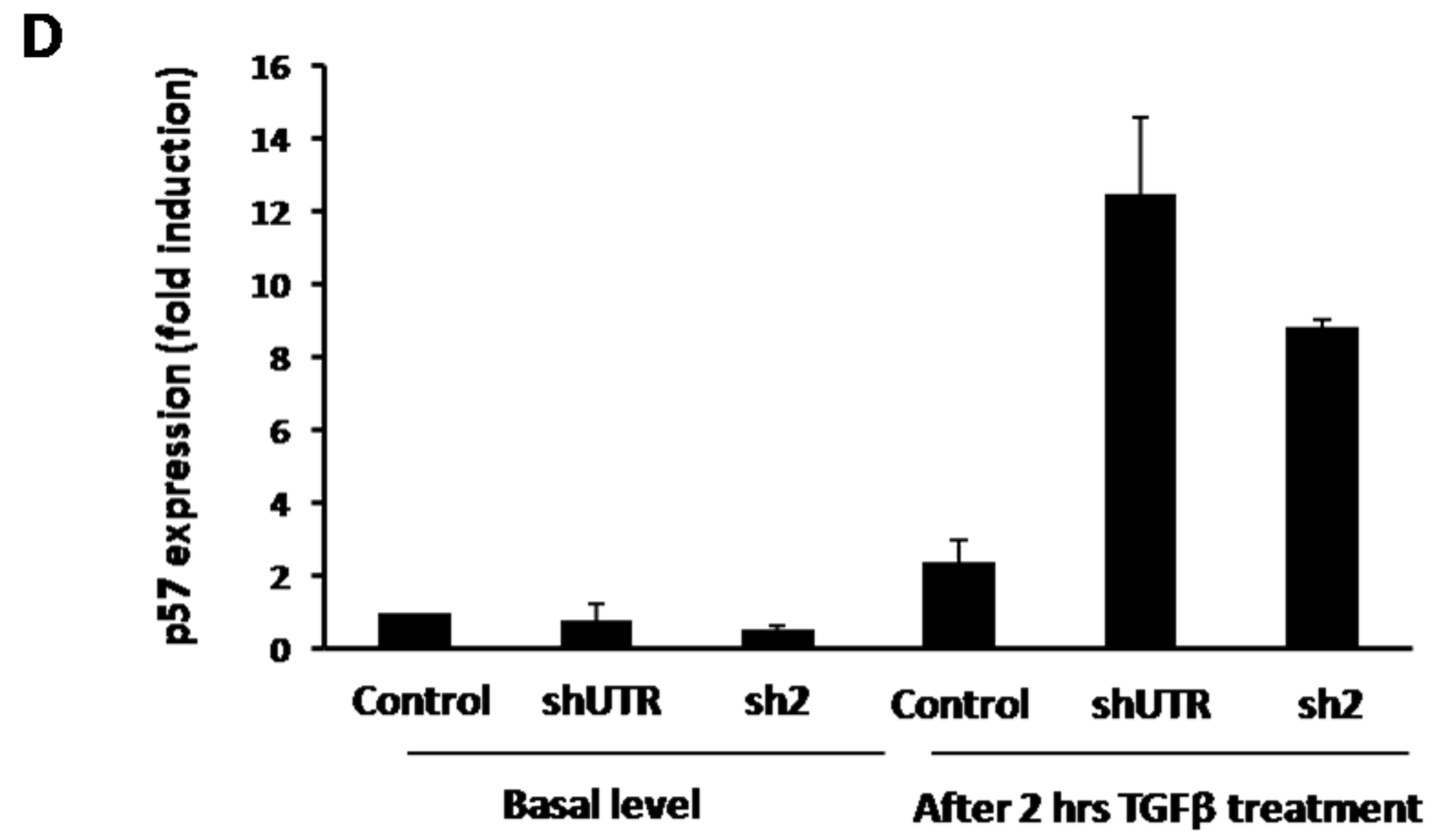
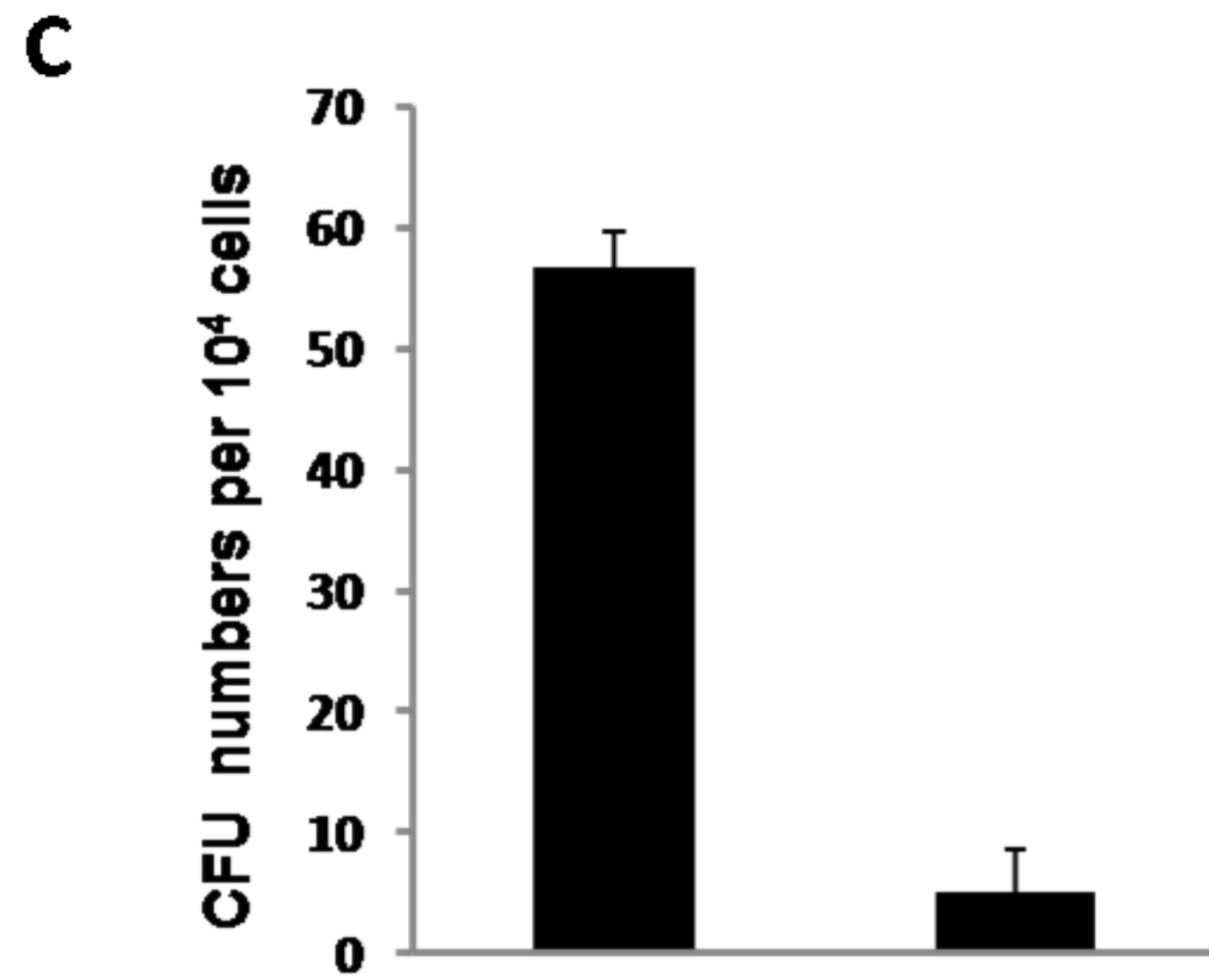
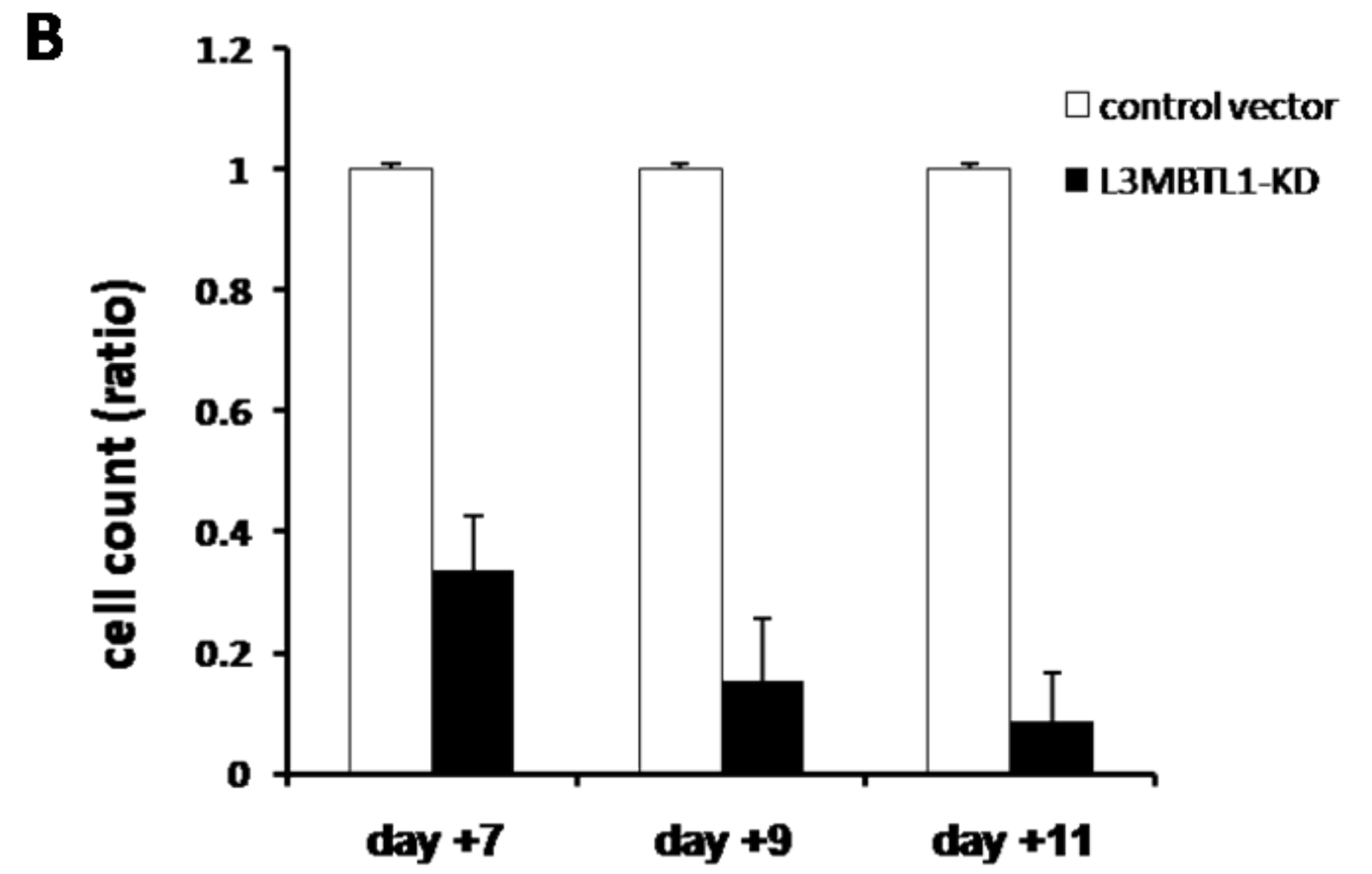
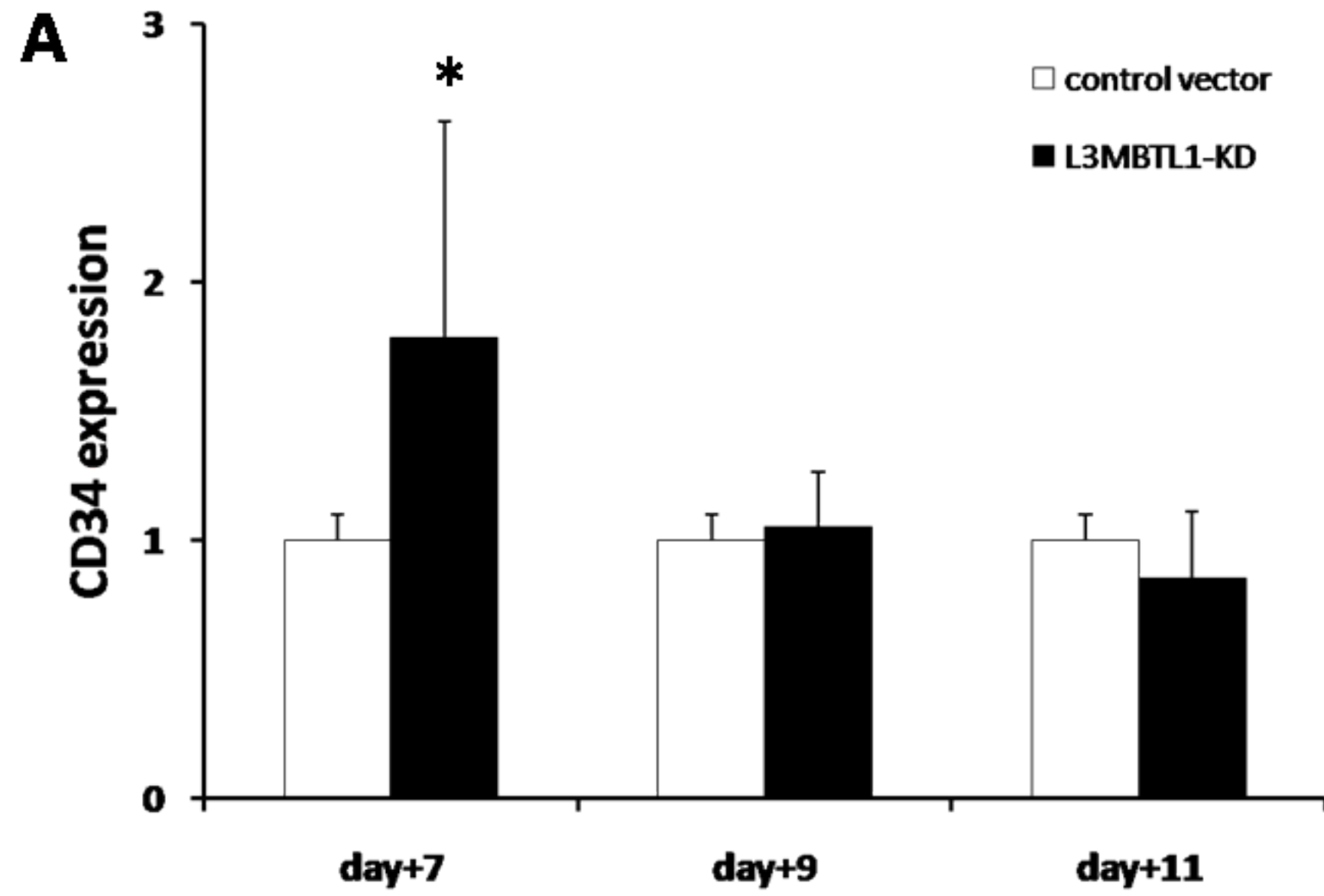


Figure 5



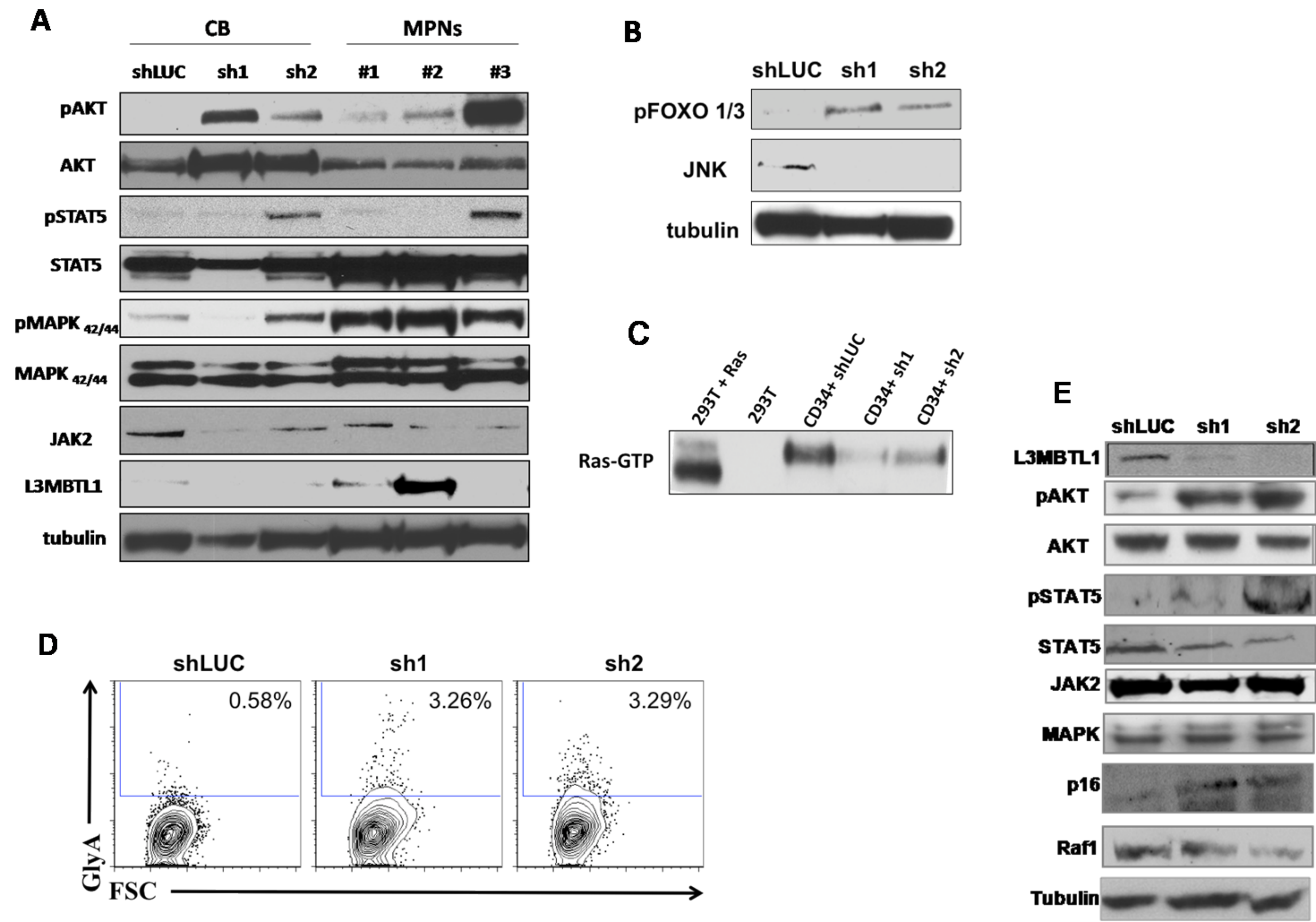
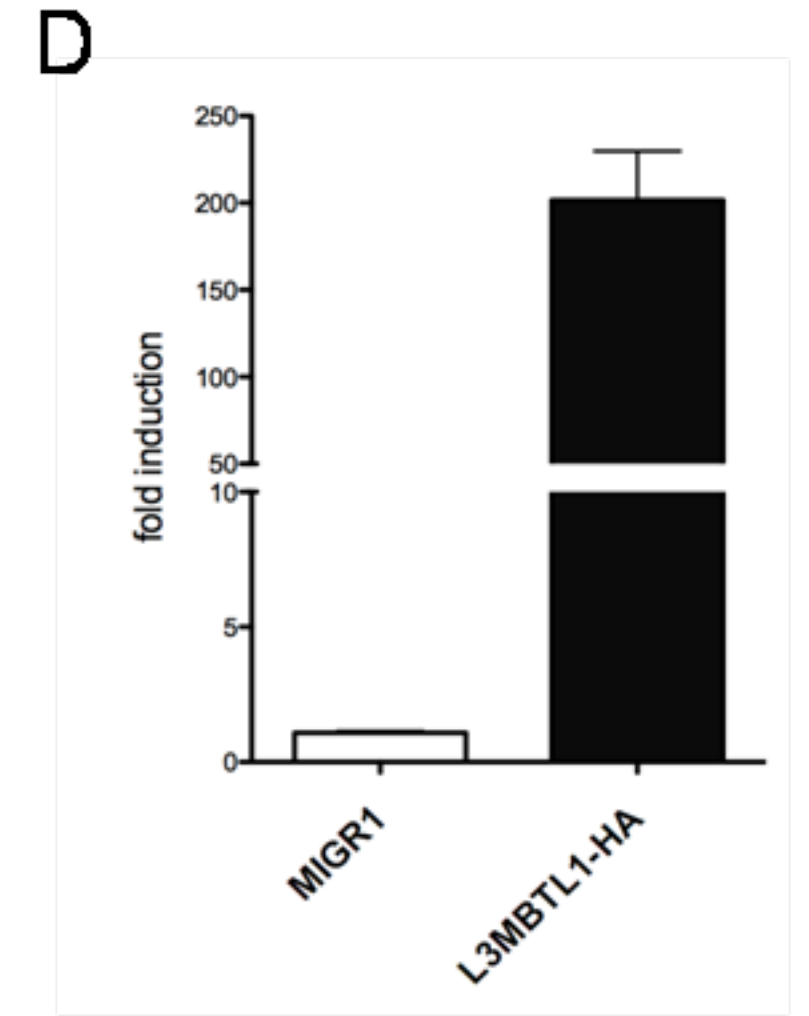
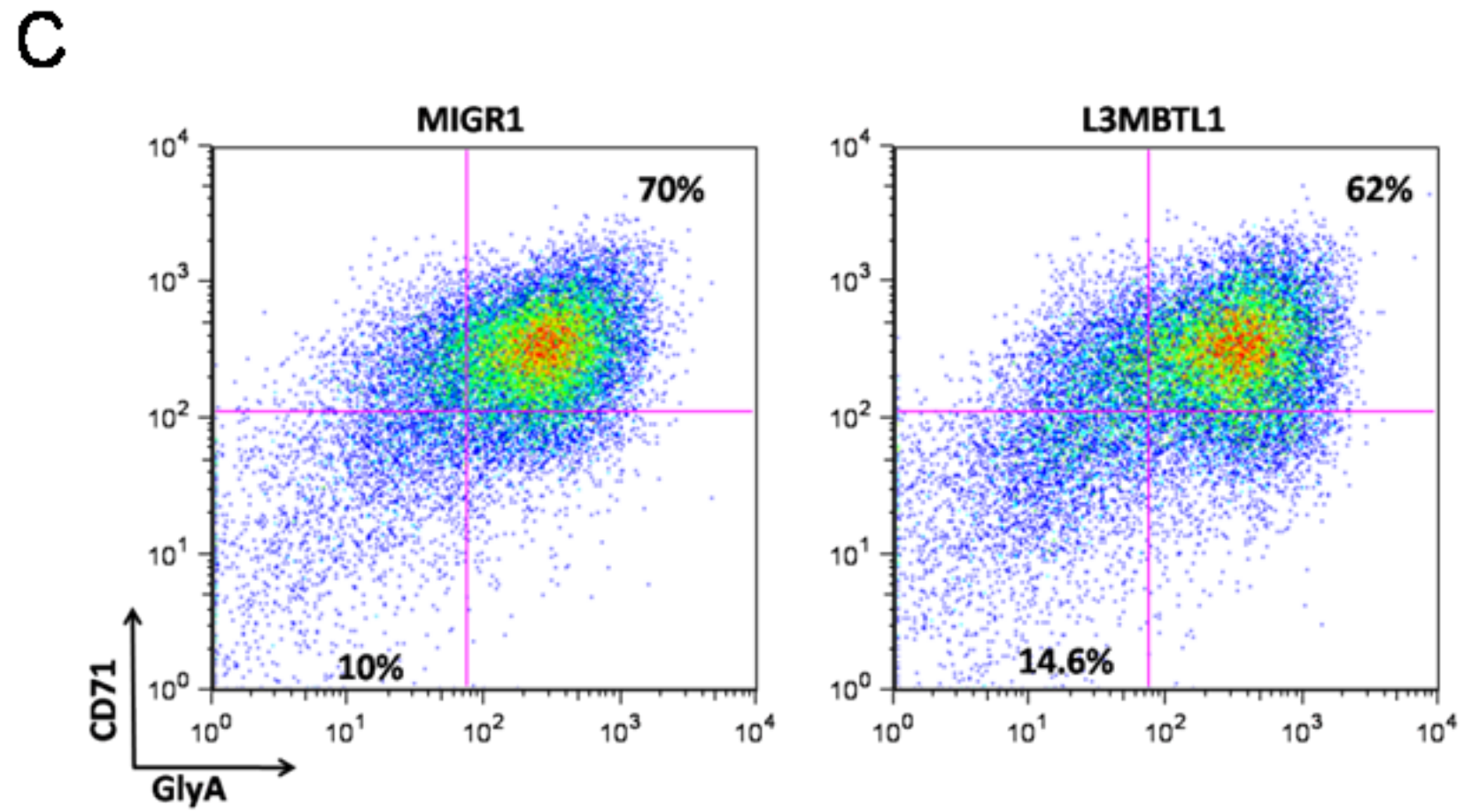
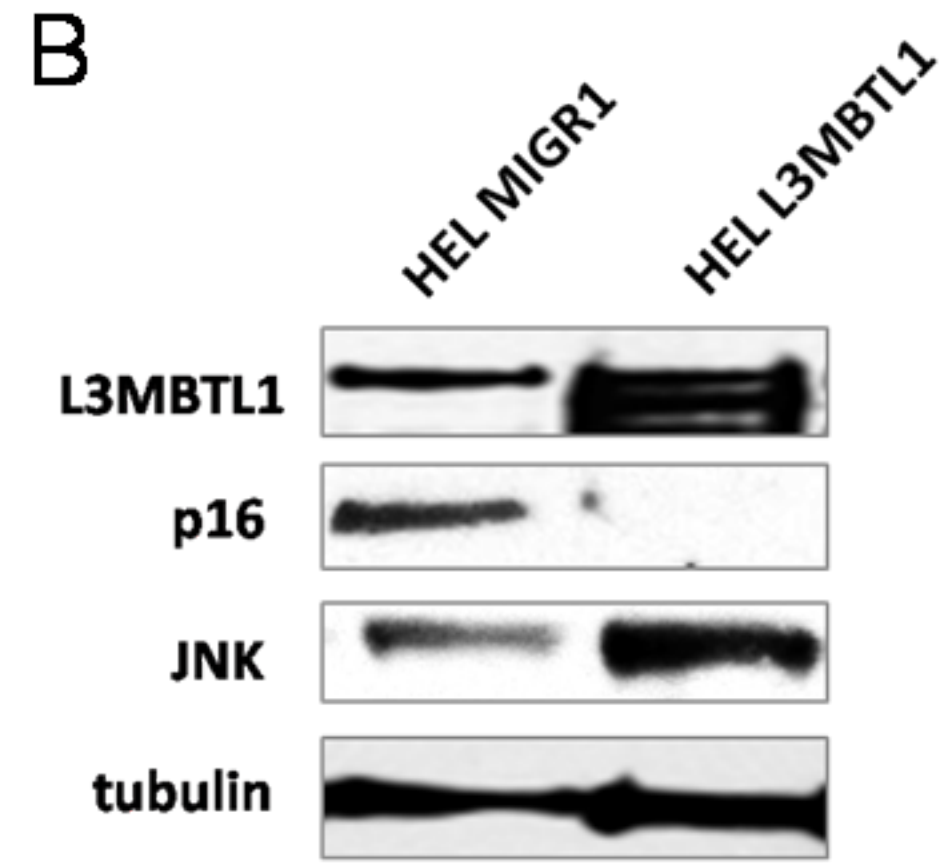
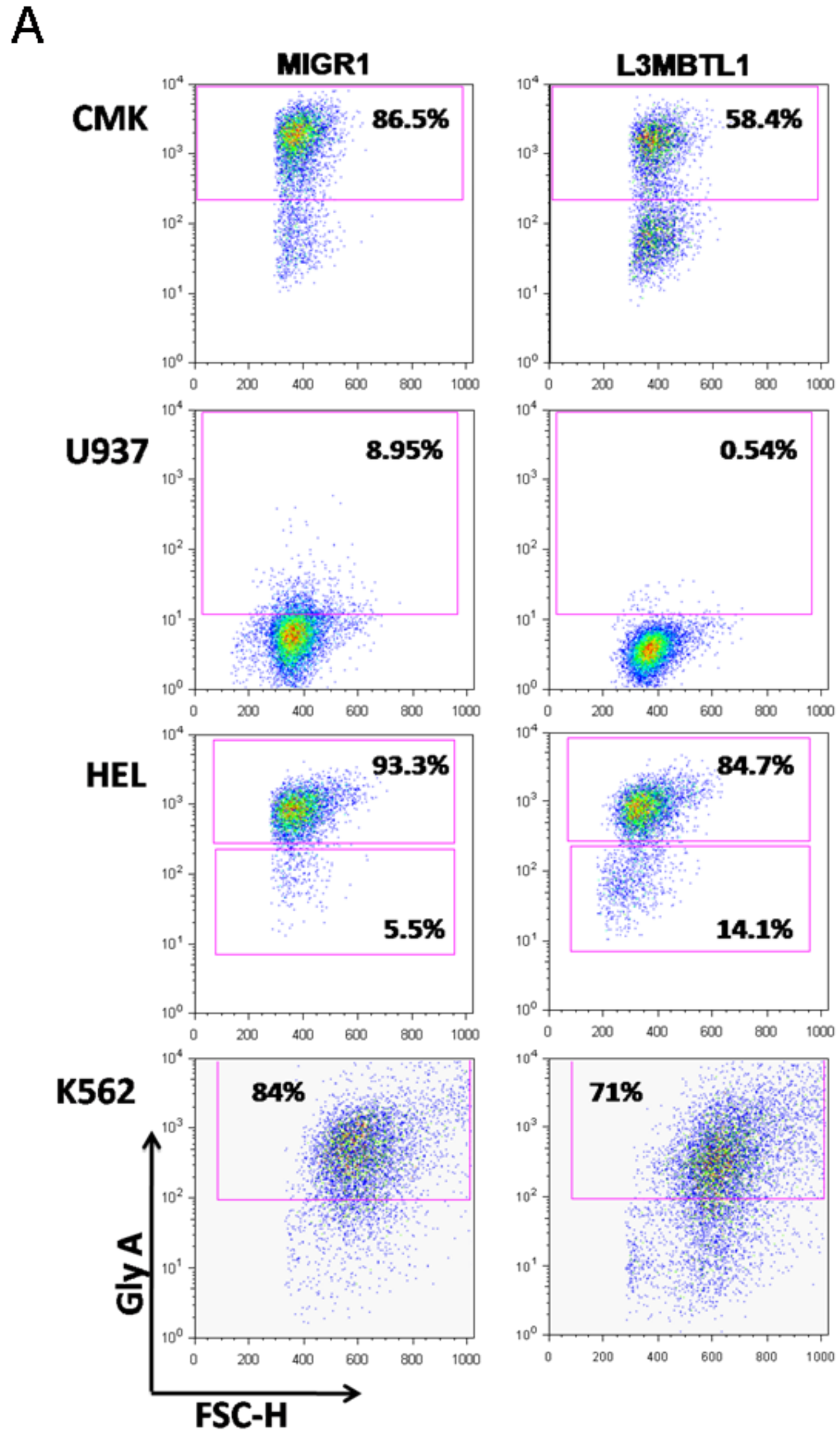
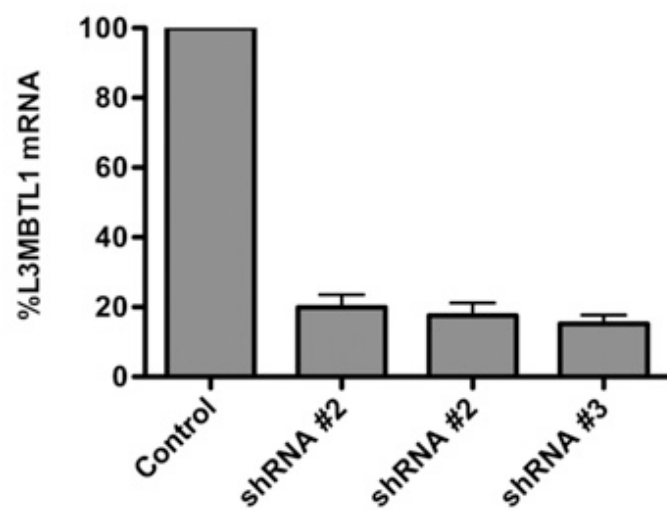
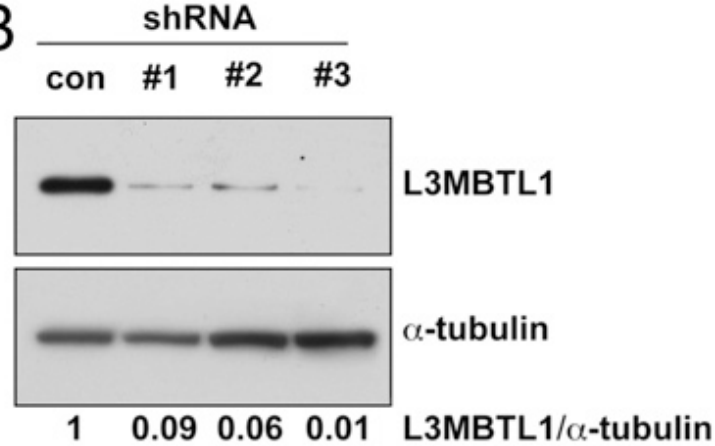
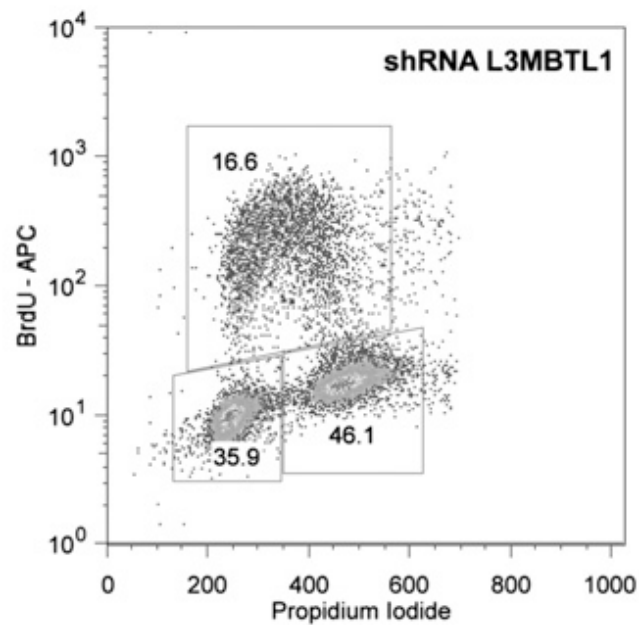
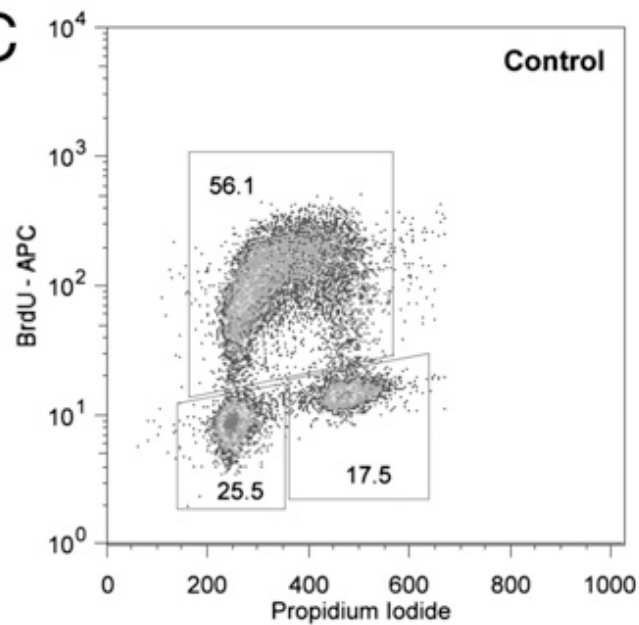
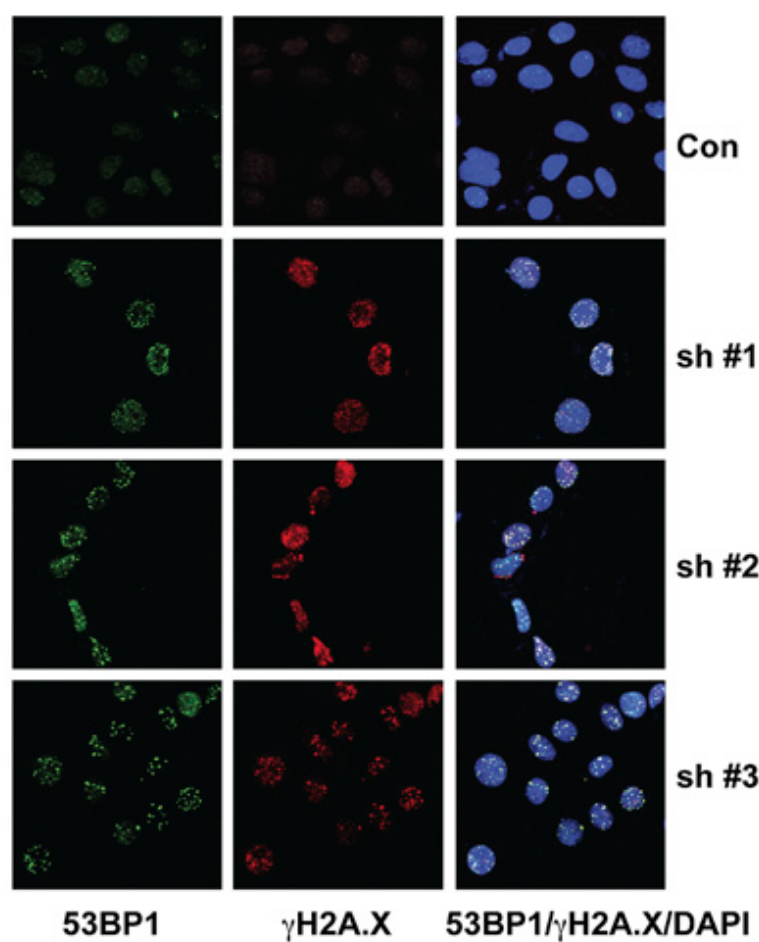
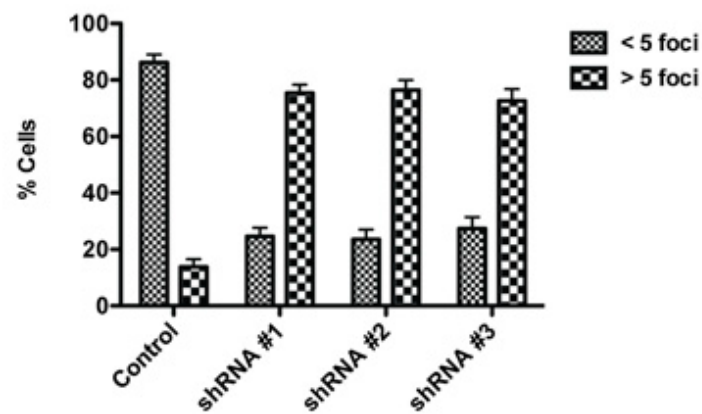
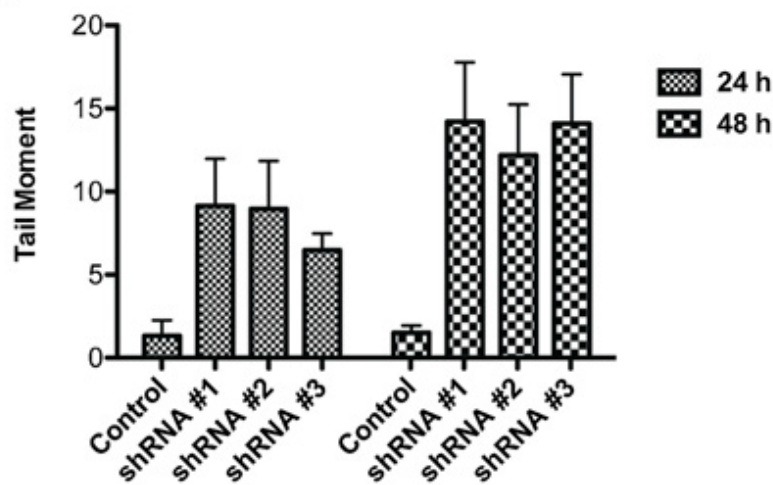
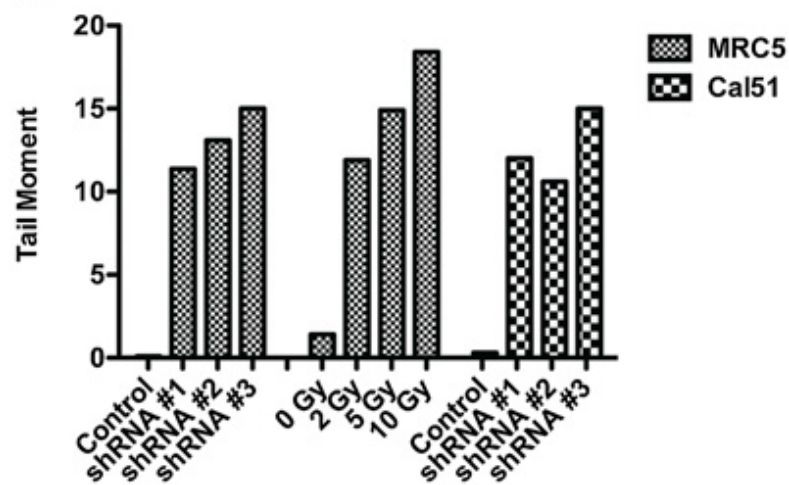
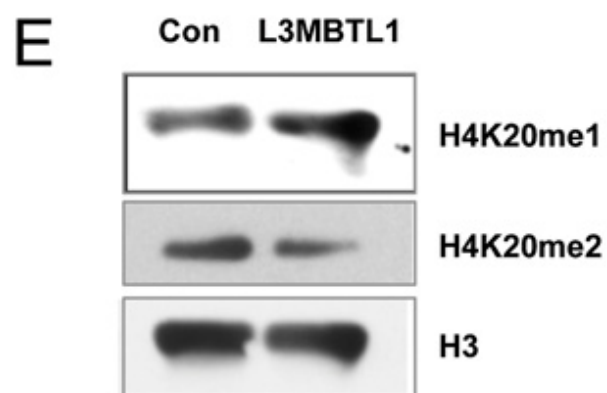
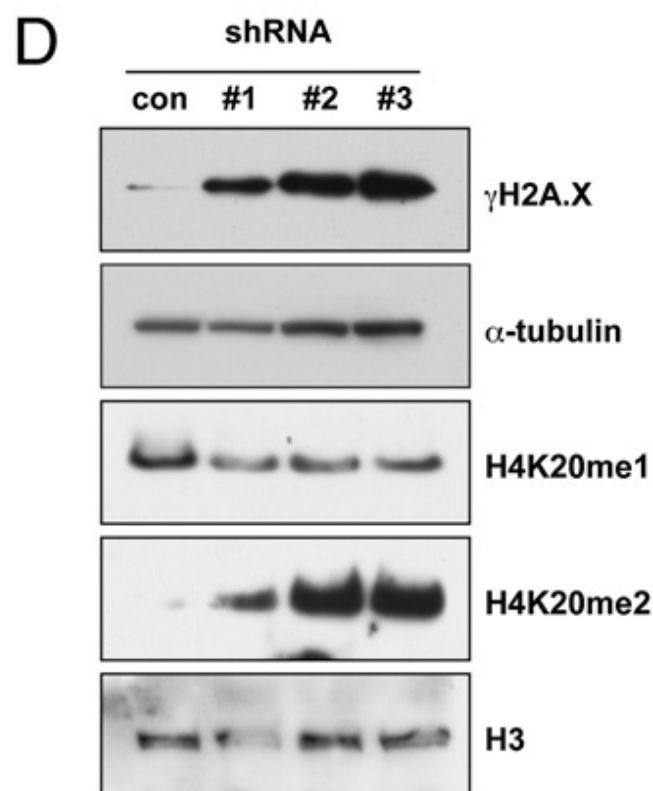
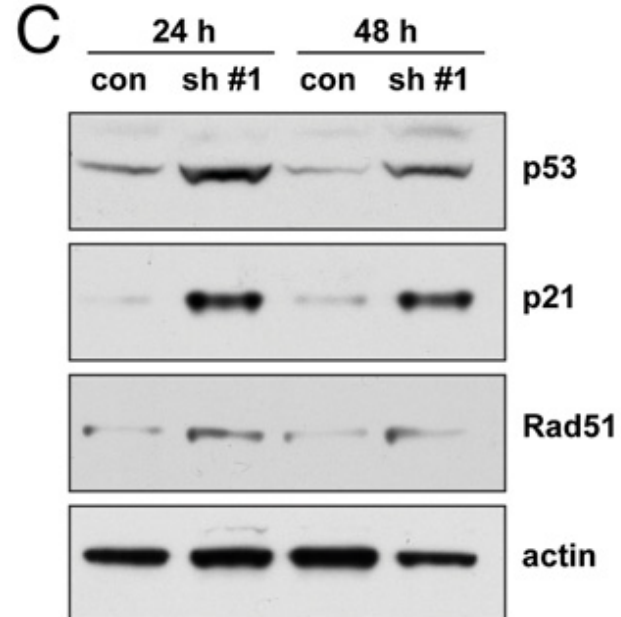
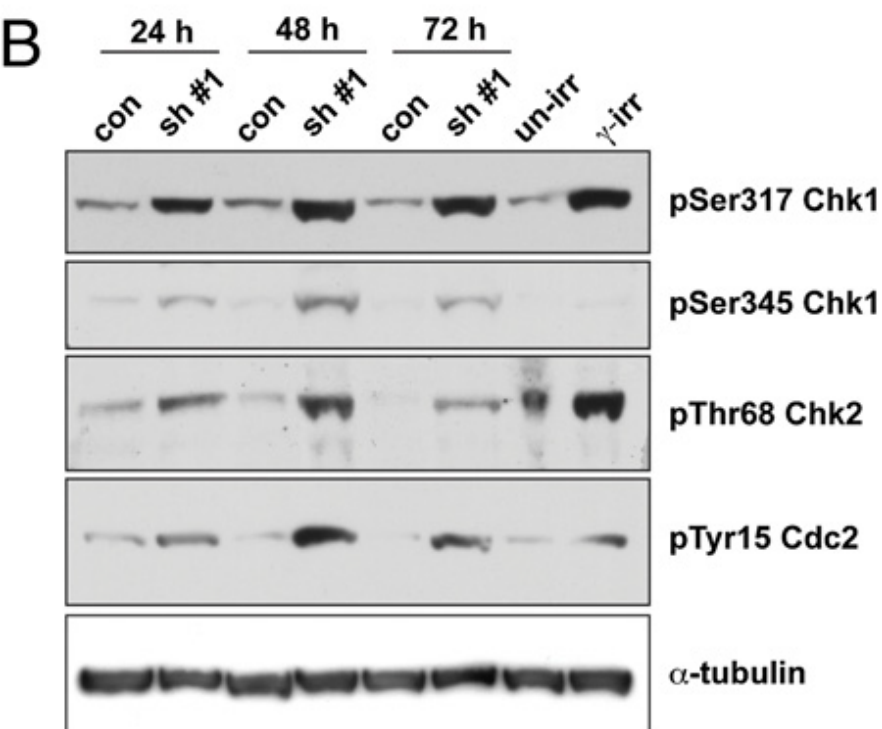
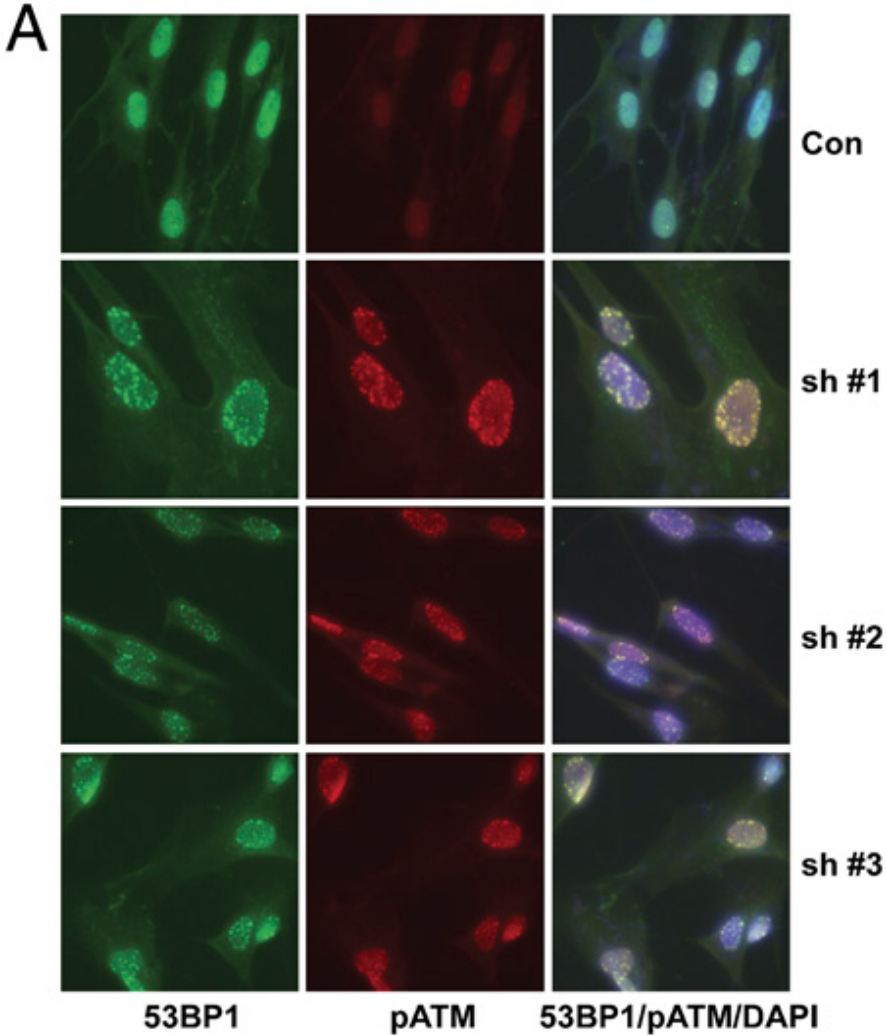


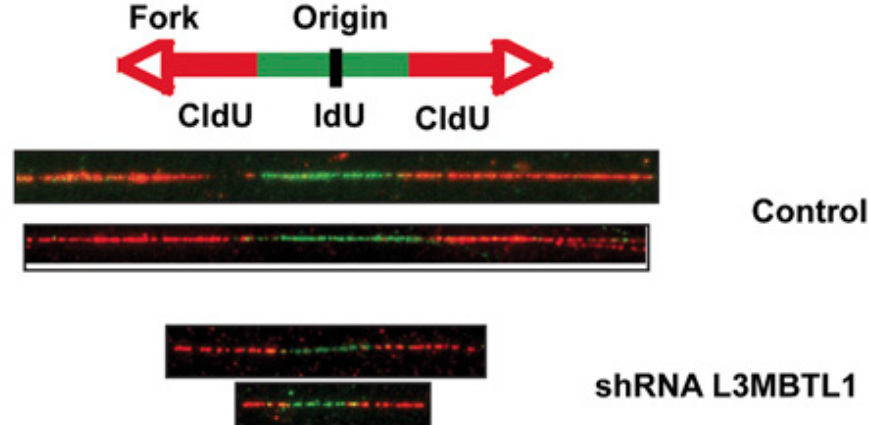
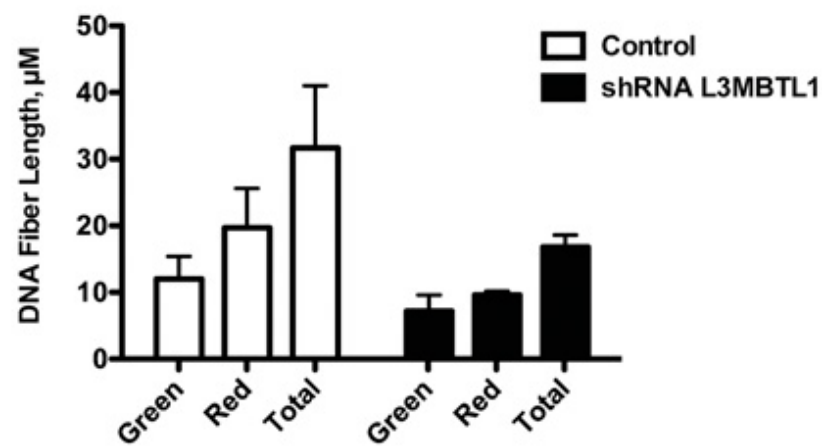
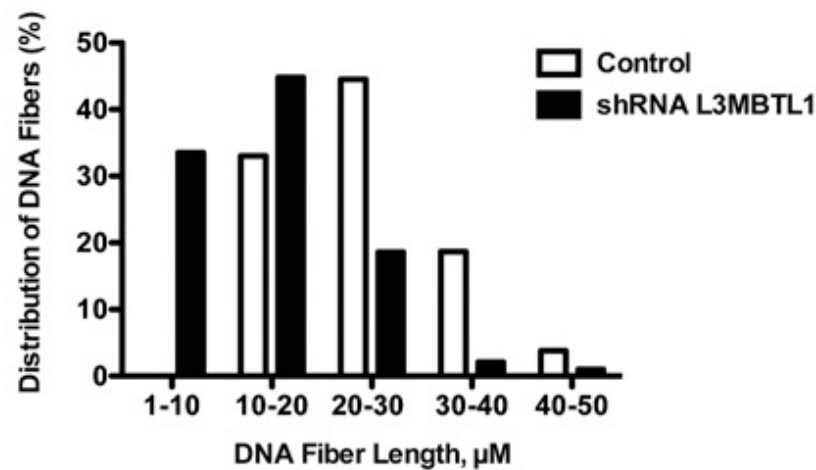
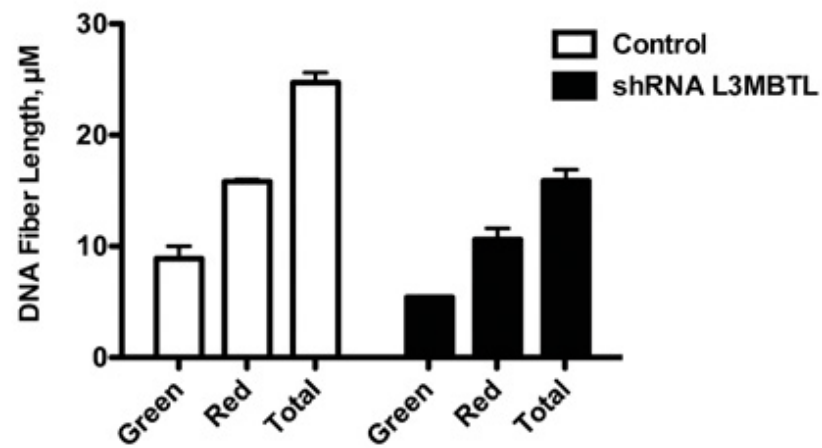
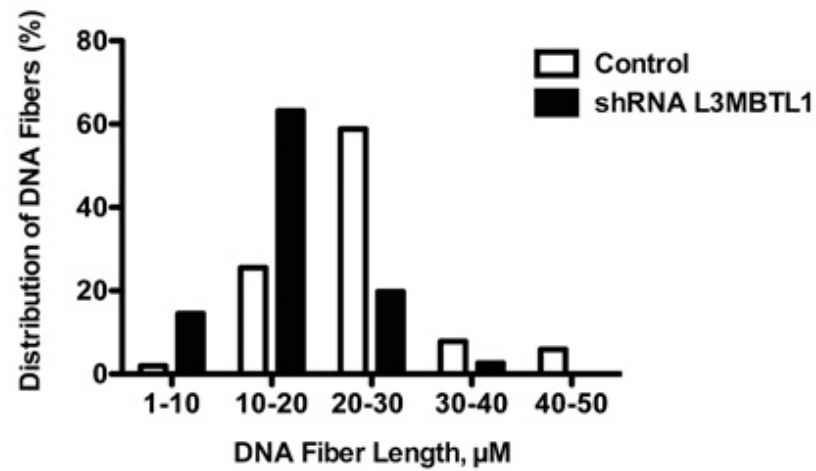
Figure 7

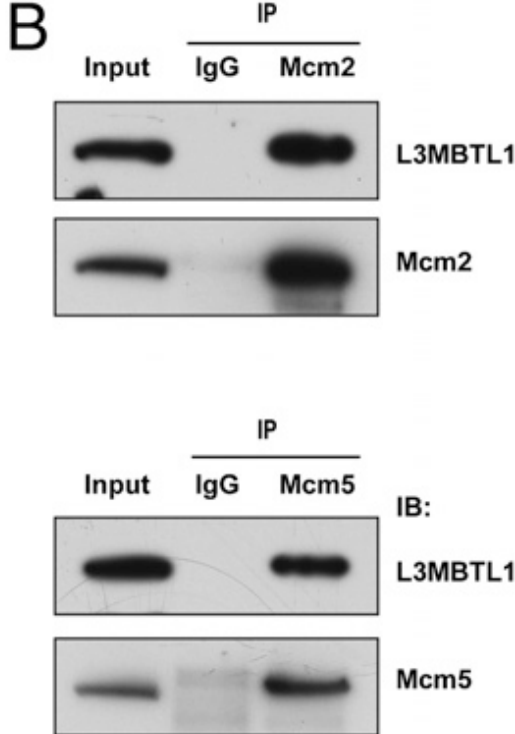
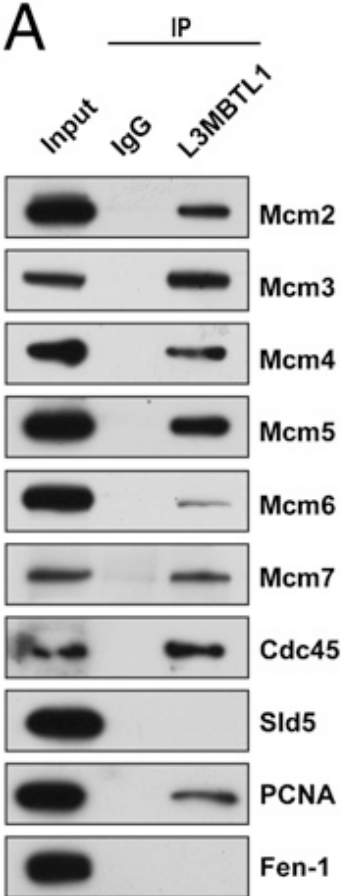


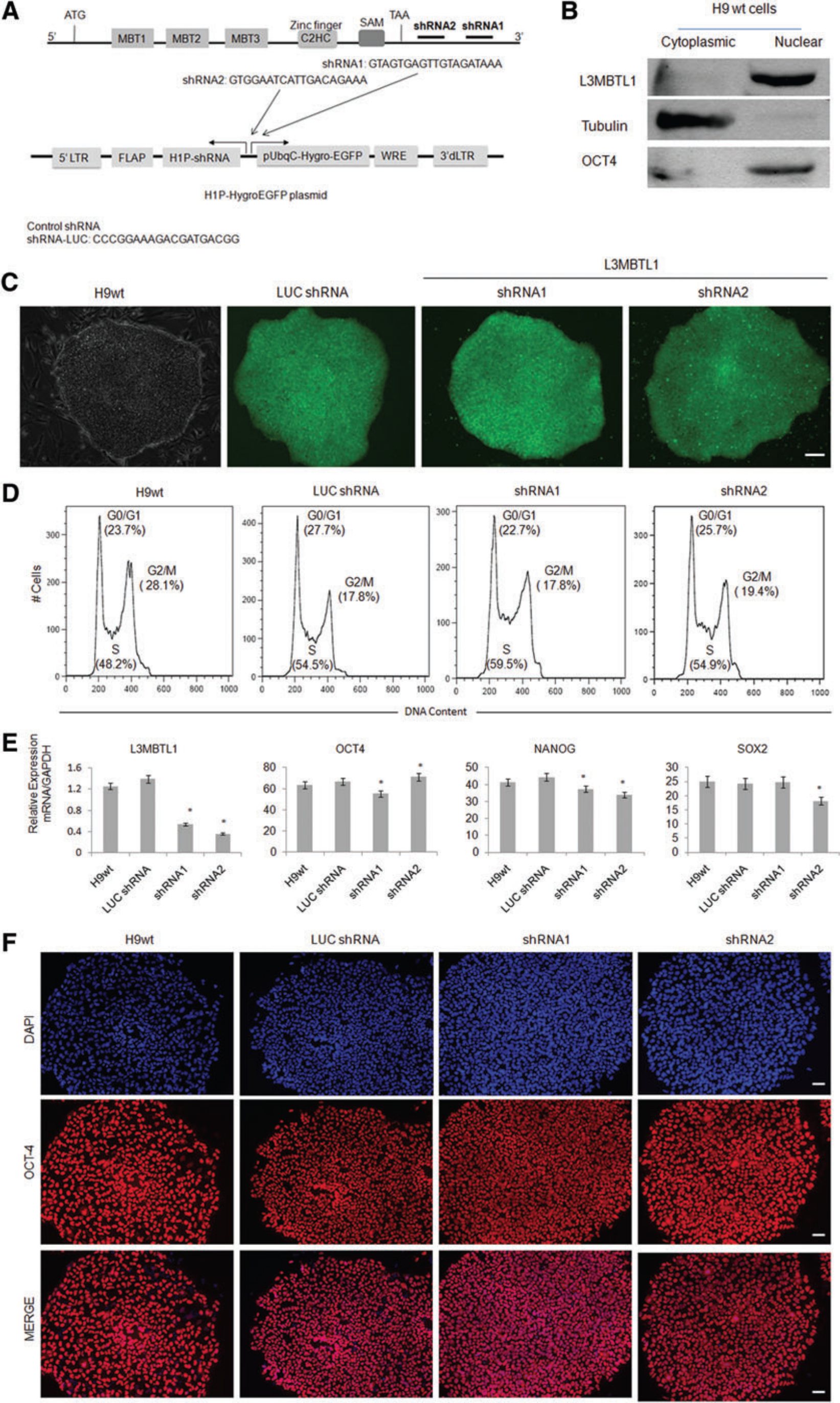
A**B****C**

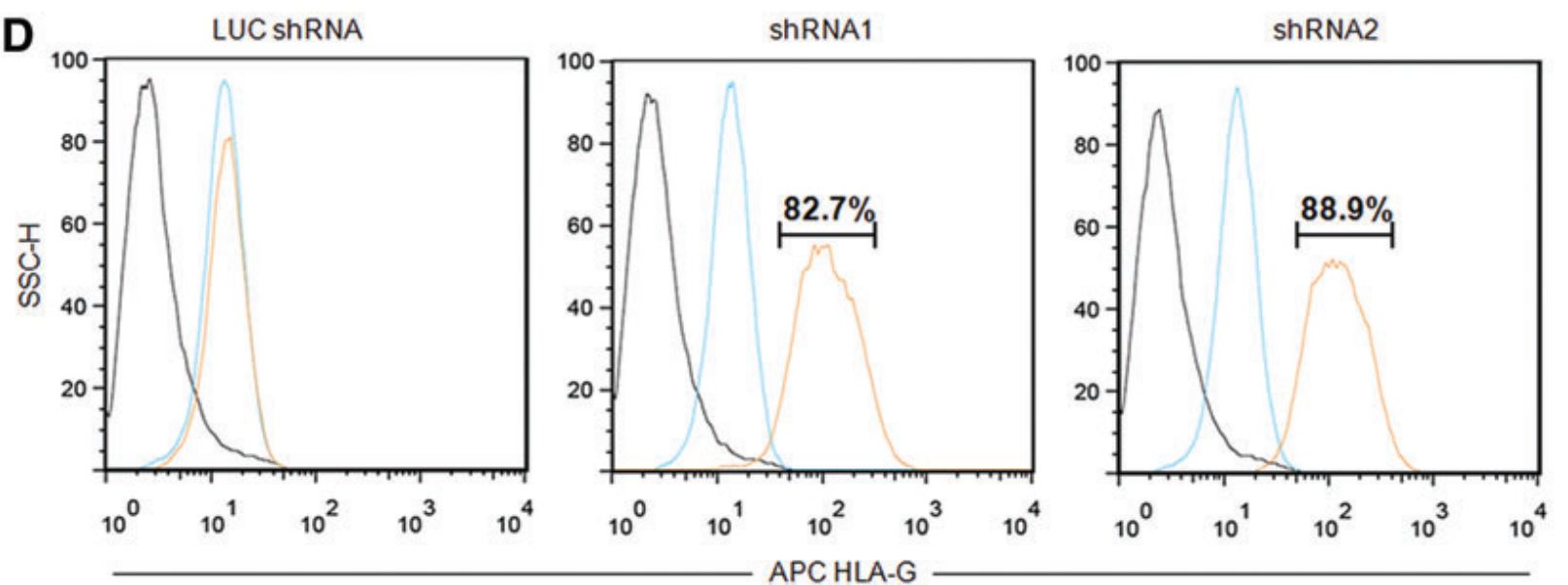
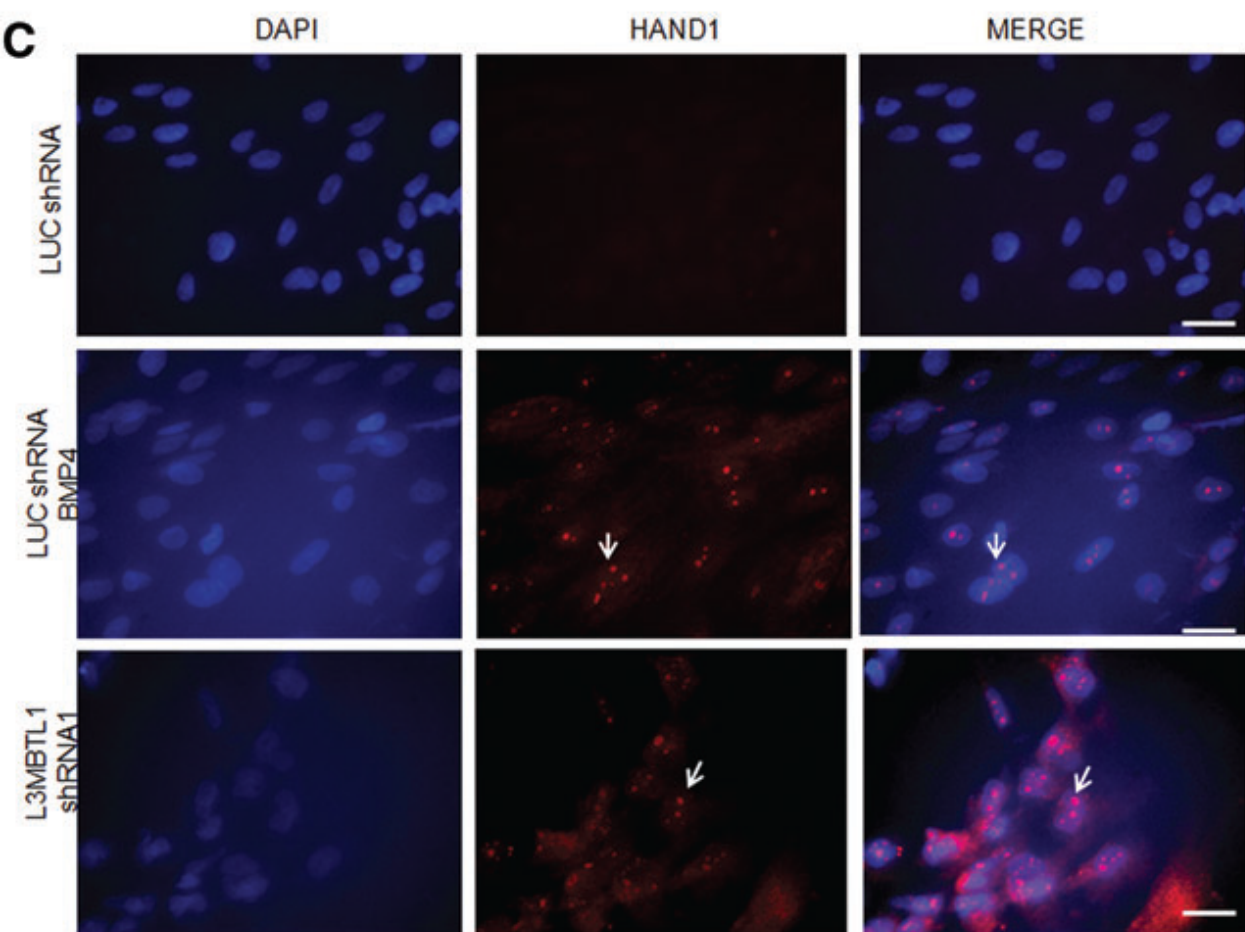
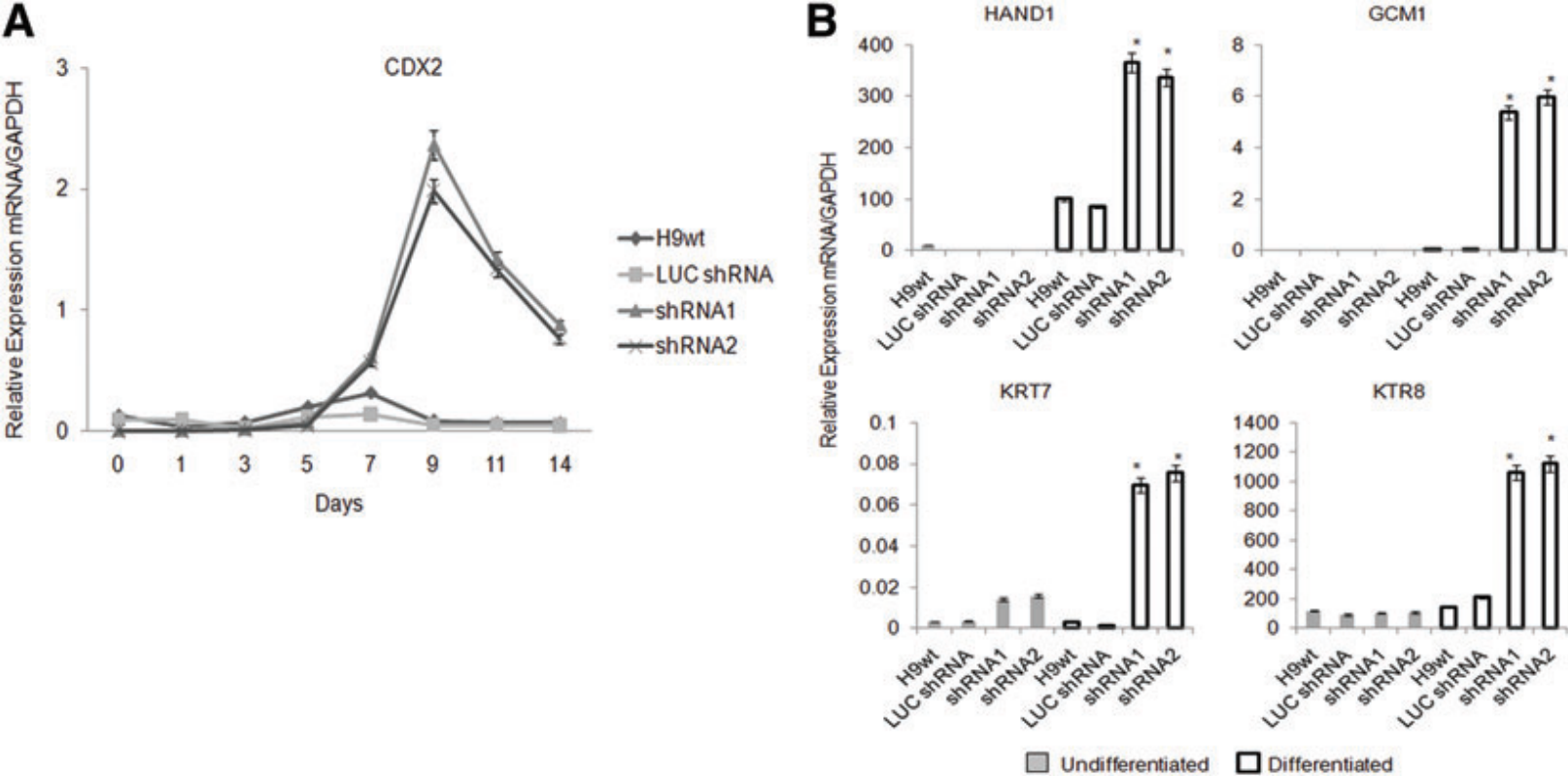
A**B****C****D**

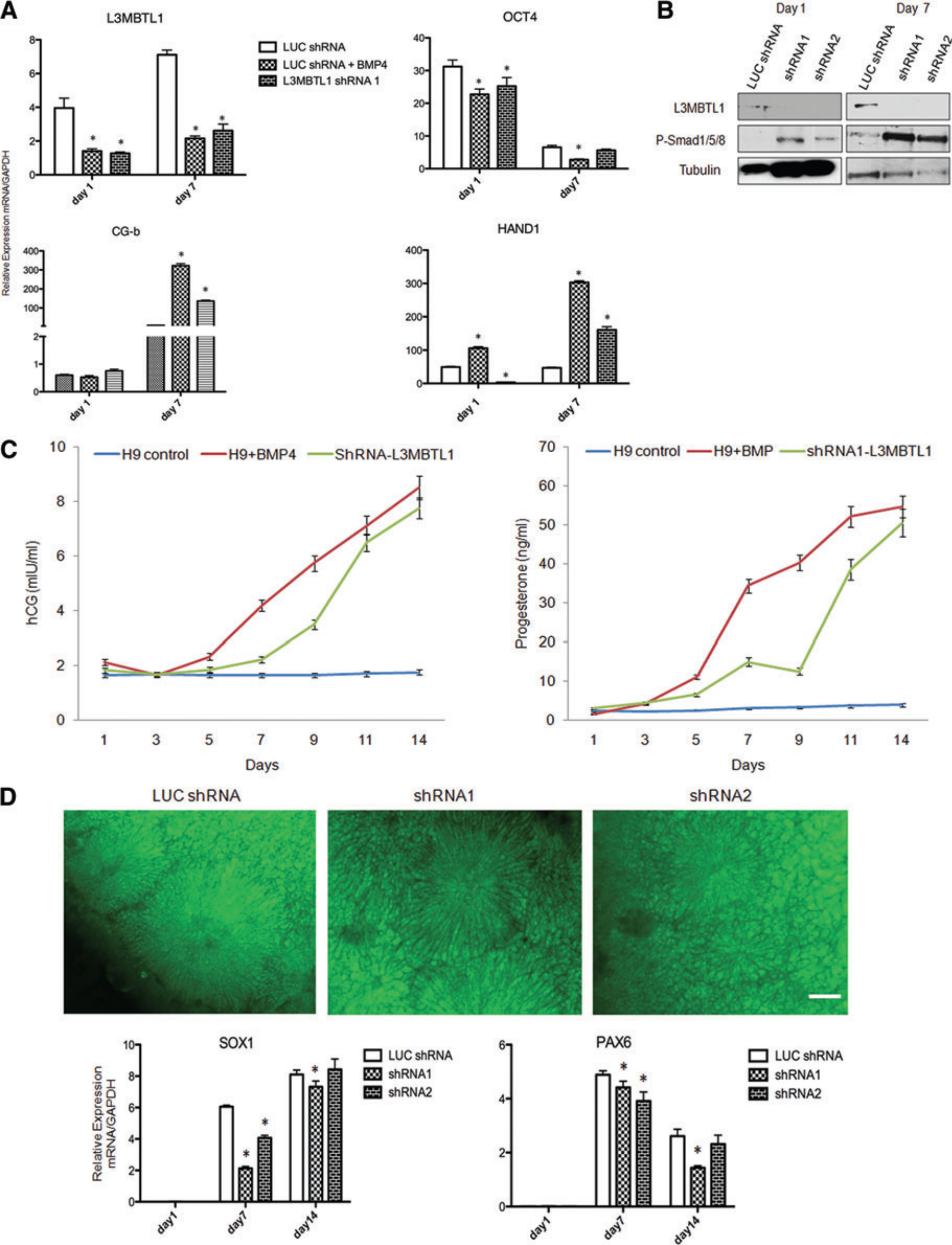


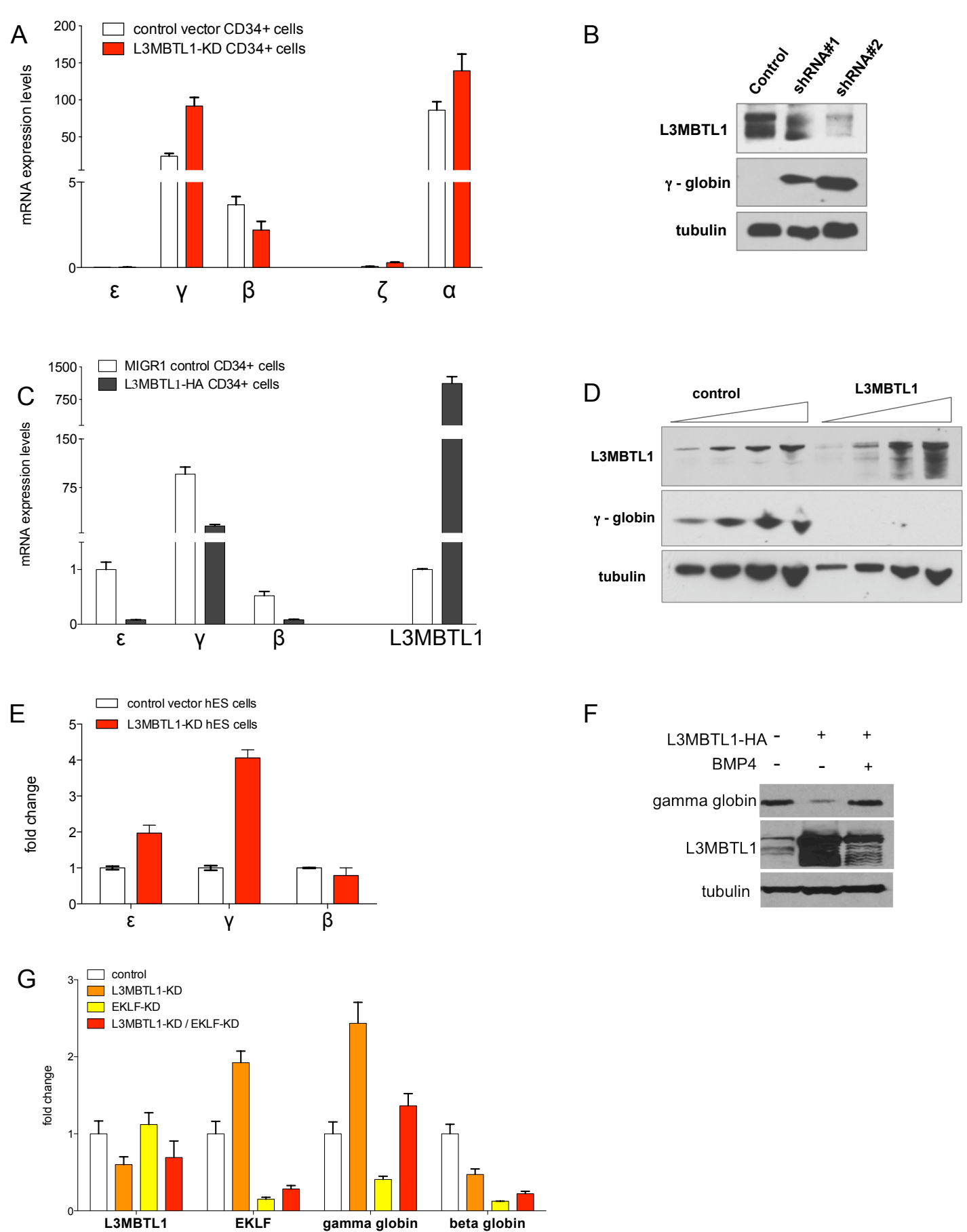
A**B****C****D****E**



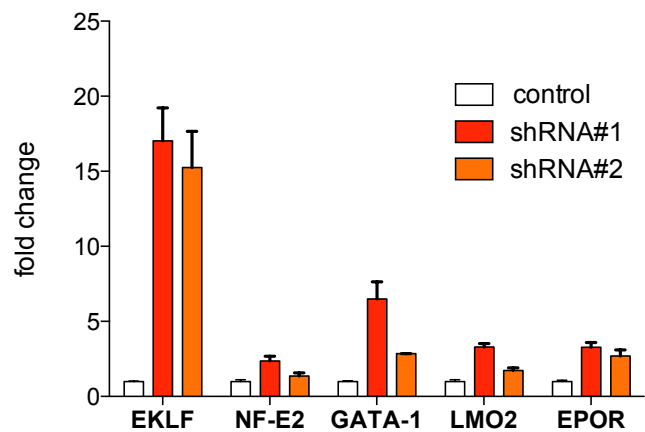




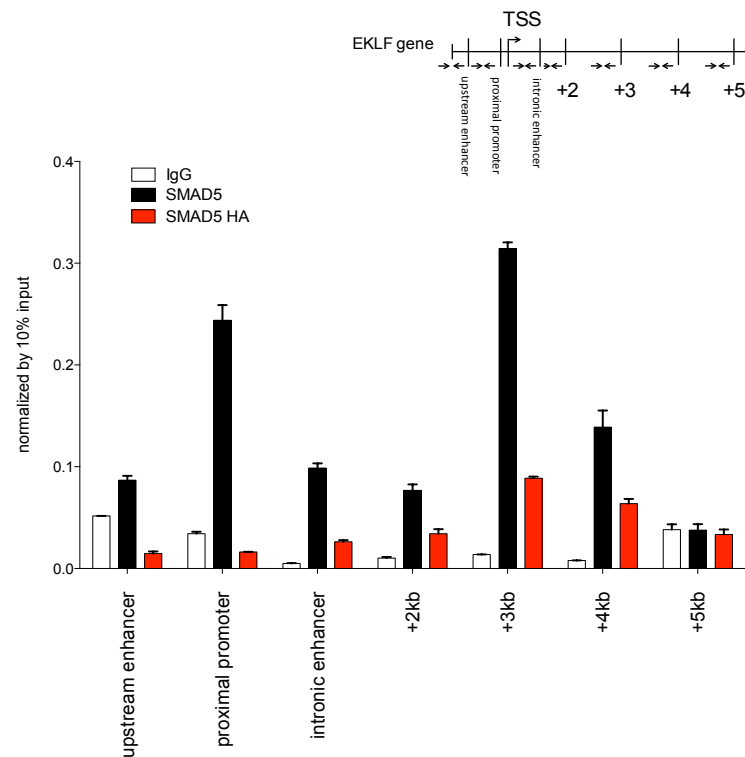




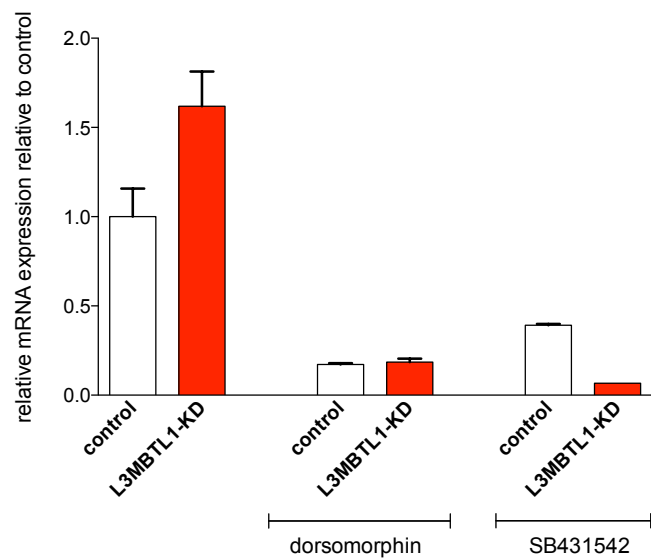
A



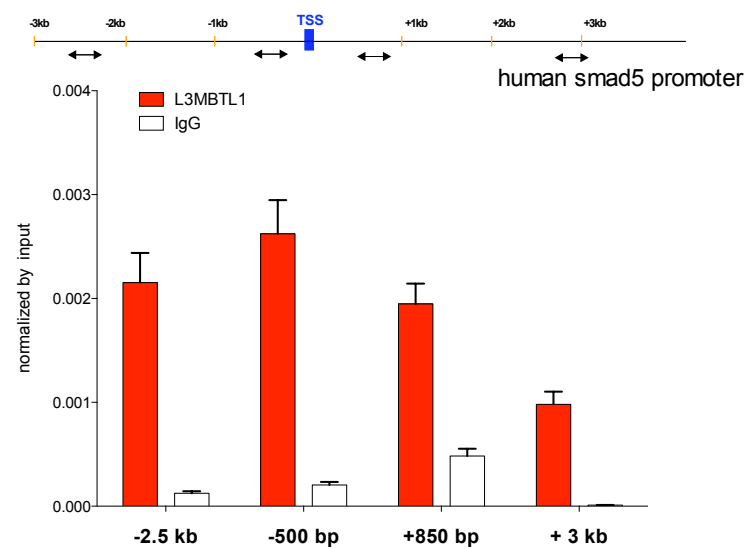
B



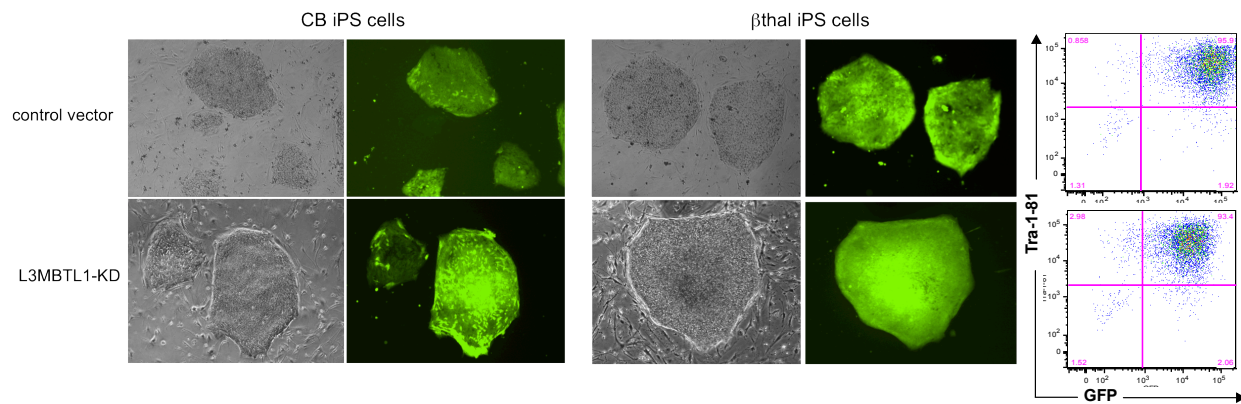
C



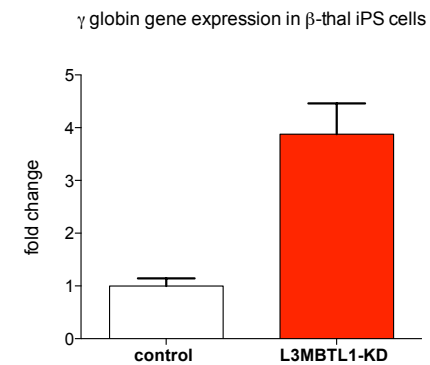
D



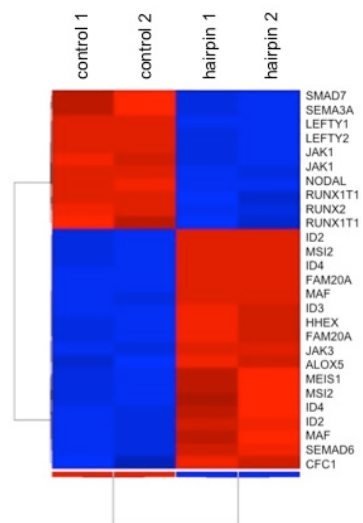
A



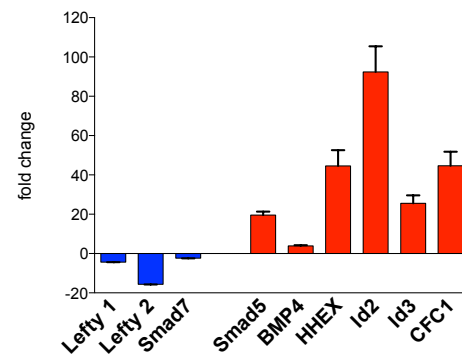
B



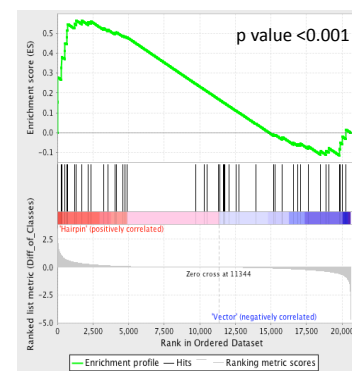
C



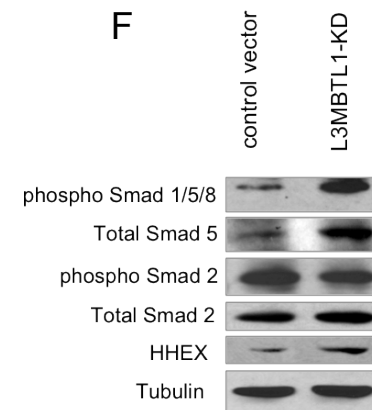
D



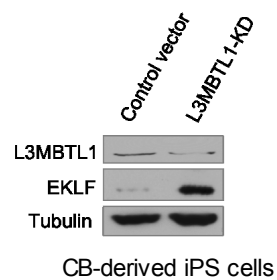
E



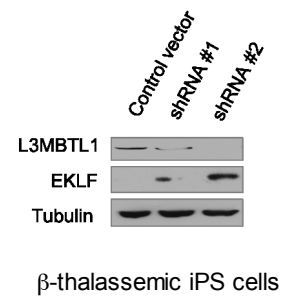
F



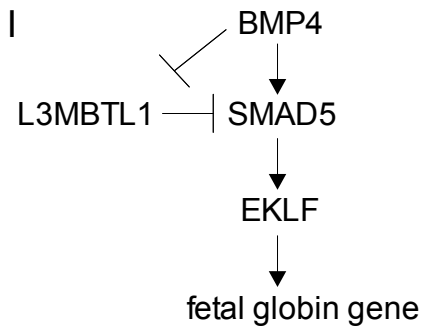
F

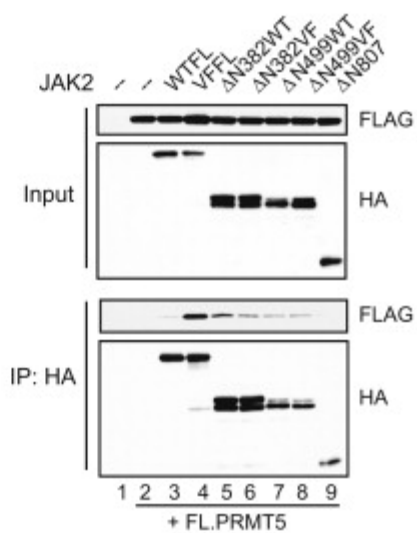
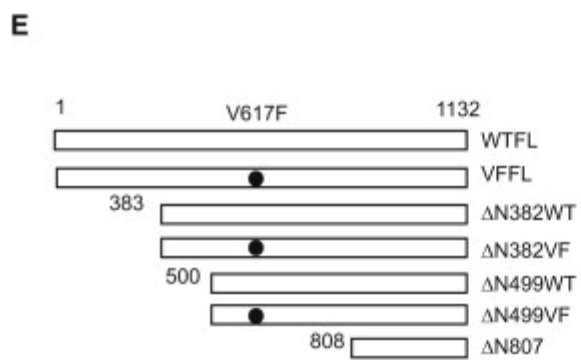
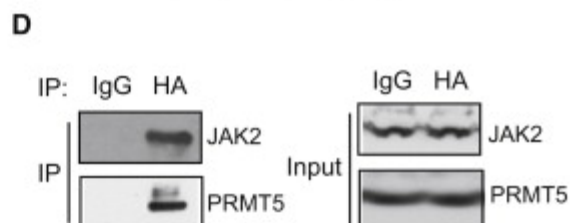
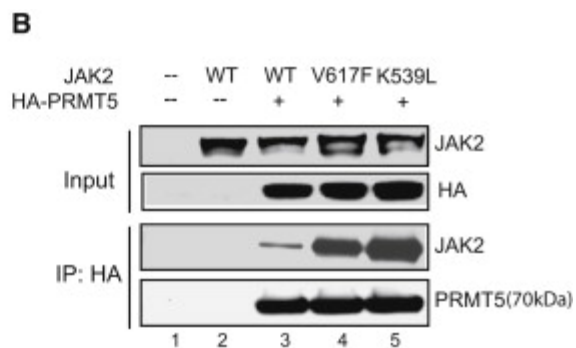
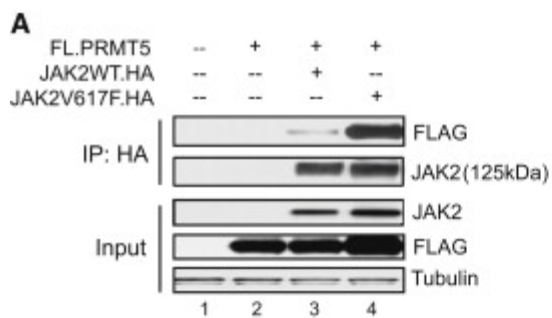


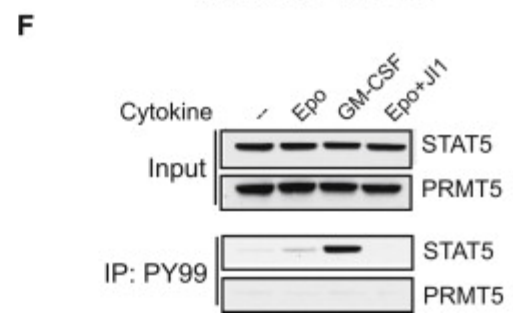
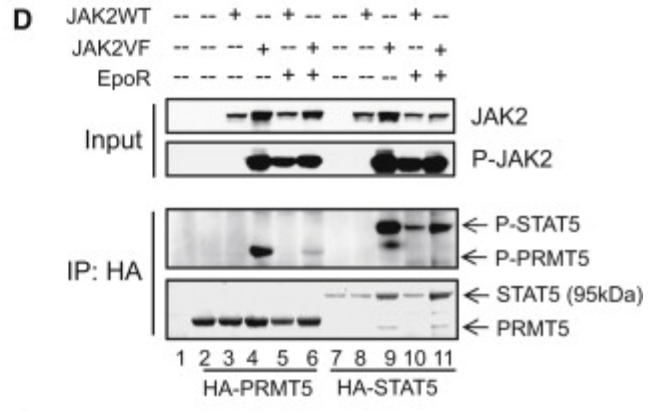
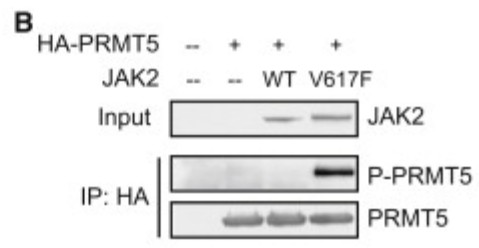
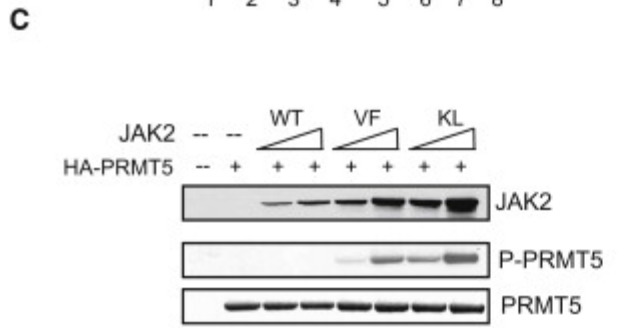
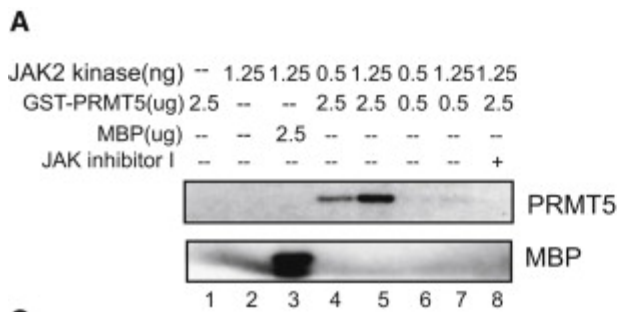
G

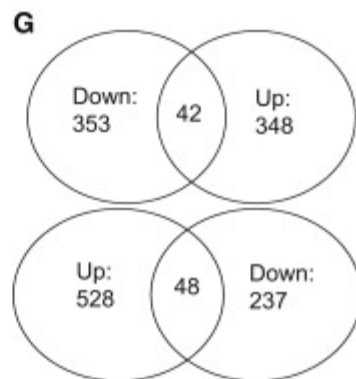
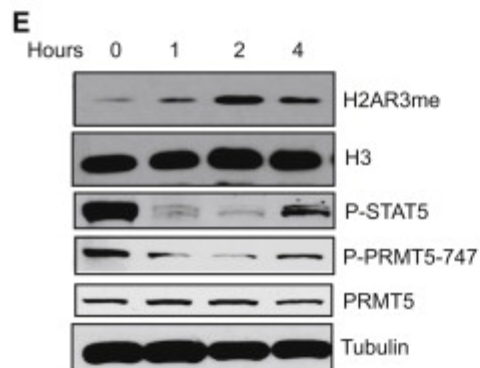
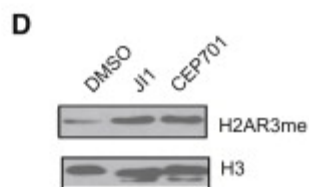
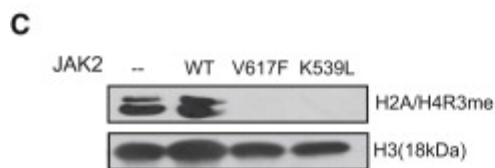
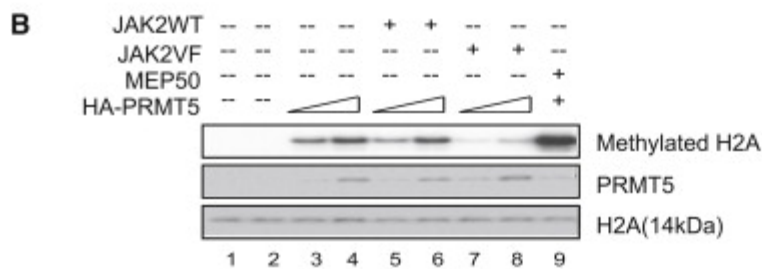
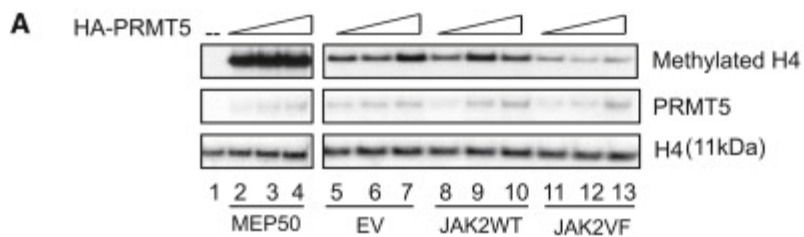


I

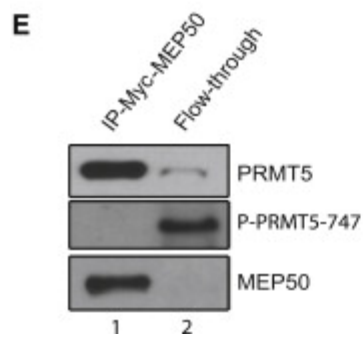
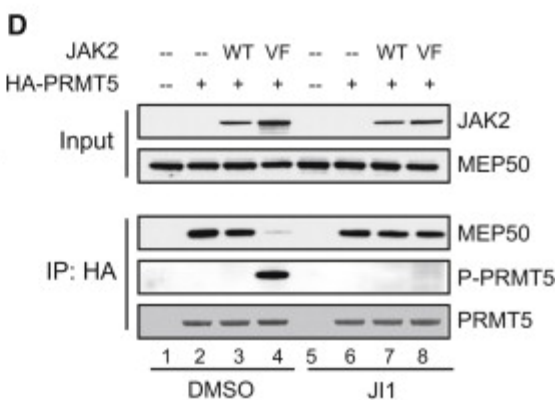
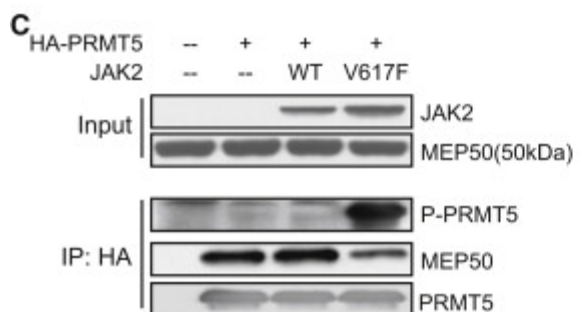
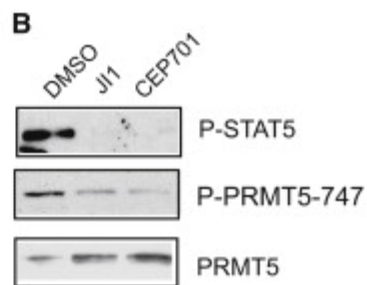
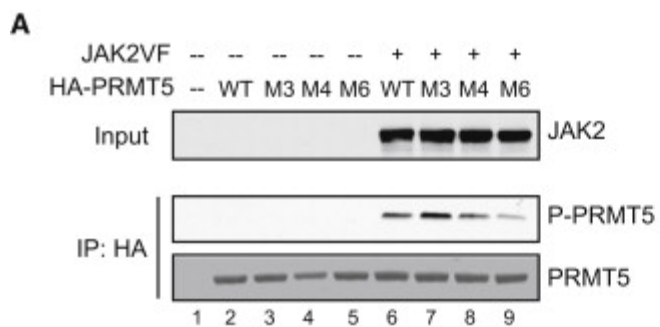


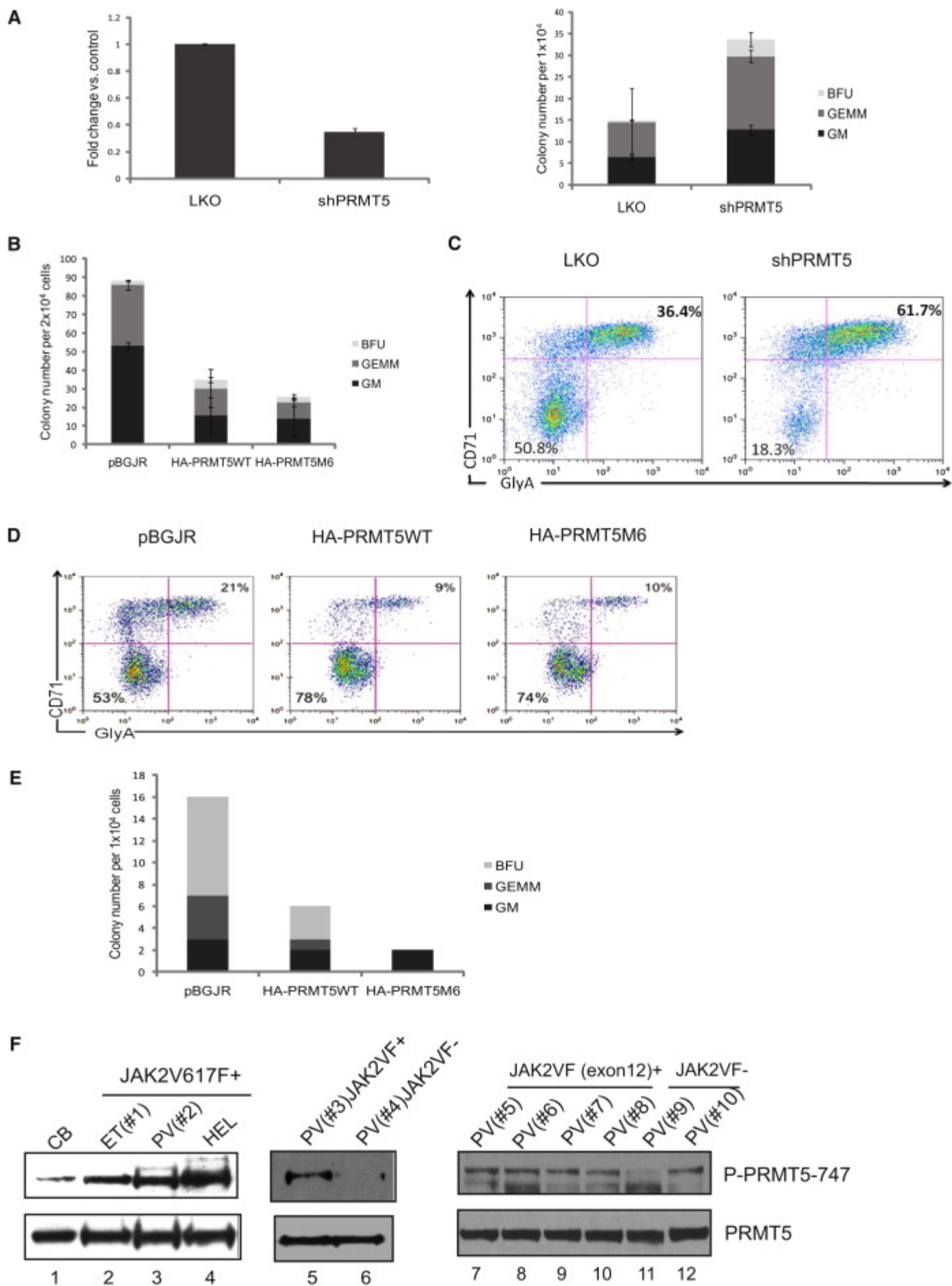






Genes regulated by JAK2 Genes regulated by PRMT5





6. FIGURE LEGENDS

Figure 1. Knock-down of L3MBTL1 promotes the erythroid differentiation of human hematopoietic CD34+ progenitor cells. (A) Lentiviral constructs expressing shRNAs targeting luciferase (control) or L3MBTL1 (sh1 and sh2) lead to efficient knock-down in primary cord blood CD34+ cells, as assessed by Western blot and qRT-PCR. ShRNAs of a different backbone (empty vector and sh3) also yielded efficient knock-down of L3MBTL1. All the presented data were confirmed using both sets of constructs. (B) Expression of CD71 and Glycophorin A on human HSPCs, as assayed by flow cytometric analysis at days 7, 9 and 11 of Epo-induced culture. (C) Expression of CD71 and Glycophorin A on human HSPCs, cultured with different concentrations of Epo, as assayed by flow cytometric analysis at 7 days. (D) Cells, from figure 1B, were stained with May-Grunwald Giemsa on day 7 of Epo-induced culture and their morphology captured by light microscopy. (E) Epo-exposed cells at day 7, 9 and 11 of Epo-induced culture were resuspended in benzidine solution and the cells that stain dark blue-green were scored as positive.

Figure 2. L3MBTL1 knock-down specifically promotes erythroid but not myeloid or megakaryocytic differentiation of human CD34+ cells. (A) L3MBTL1 expression levels were assessed by qRT-PCR in normal CD34+ cord blood cells. The cells were placed in different culture conditions stimulating erythroid, myeloid and megakaryocytic differentiation for 2, 5 and 7 days. Total RNA was extracted from 2×10^5 cells. (B) 72 hrs after lentiviral infection, GFP+ CD34+ cells, were cultured in myeloid conditions for 7, 9 and 11 days and the expression of myeloid-specific markers CD11b (CD14 and CD33 not shown) were assessed by flow cytometric analysis (n=3). (C) 72 hrs after lentiviral vector infection, the GFP+ CD34+ cells, were cultured in megakaryocytic conditions for 7, 9 and 11 days and expression of the megakaryocytic specific marker CD41 was assessed by flow cytometric analysis (n=3). (D) GFP+ CD34+ cells, 72 hrs after lentiviral vector infection, were cultured in erythroid conditions for 7, 9 and 11 days and expression of the erythroid-specific marker GlyA was assessed by flow cytometric analysis (n=3).

Figure 3. Knock-down of L3MBTL1 induces further erythroid differentiation of K562 erythroleukemia cells. (A) K562 cells, grown in RPMI medium supplemented with 10% fetal bovine serum, without exogenous cytokines or hemin, were infected with lentiviral constructs targeting luciferase (shLUC) or L3MBTL1 (sh1 and sh2). GFP+ cells, sorted by FACS at 72 hrs post-infection, were analyzed for GlyA expression by flow cytometry. (B) GFP+ K562 cells, before and after exposure to hemin (50 μ M) for 4 days, were stained with benzidine to assess their Hb-content. (C) K562 cells were treated with 50 μ M hemin for 4 days and the L3MBTL1 mRNA level assessed in the hemin- exposed vs the non-treated cells by qRT-PCR (n=3).

Figure 4. L3MBTL1-KD leads to expansion of erythroid progenitors in long-term culture. (A) Sorted 4×10^5 GFP+ CD34+ were plated on MS5 stromal cell layer and cultured for five weeks. At week five, the colonies were examined using an inverted optical microscope. The red arrows indicate the cobblestone area forming cells in the wt and shLUC figures. The red arrows indicate the overgrowth of progenitor cells (predominantly erythroid) in the sh1 and sh2 photographs. (B) The expression of GlyA on floating cells from 5-week LTC-IC cultures was evaluated by flow cytometry. (C) CAFC colony numbers were evaluated at week five of MS-5 stromal cell based culture (n=2) (D) Week 5 LTC-IC cells were plated on methylcellulose, and the secondary BFU-E colonies were scored after 10 days. The ratio of BFU-E is shown, based on BFU-E numbers in the control cells.

Figure 5. Proliferation potential of L3MBTL1-KD human hematopoietic progenitor cells. (A) The maintenance of CD34 expression was evaluated in L3MBTL1-KD CB cells by flow cytometry. GFP⁺ CD34⁺ CB cells were cultured with SCF, FLT-3, IL-6 and TPO. (* indicates the p value, =0.0046) (B) Cell counts of L3MBTL1-KD CB cells were monitored at different time points in liquid culture with SCF, FLT-3, IL-6 and TPO. (C) 72 hrs after lentiviral infection sorted GFP⁺ CD34⁺ HPC were placed in CFU assays and the number of CFUs quantified. (D) p57 mRNA expression was assessed by qRT-PCR in L3MBTL1-KD HPCs, with and without exposure to 200pM TGFβ1 for 2 hours (n=2).

Figure 6. Primary hematopoietic cells lacking L3MBTL1 show Epo-independent phosphorylation of STAT5, AKT, and MAP Kinase. (A) Primary GFP⁺ CD34⁺ cells were harvested after one week in erythroid culture and lysed, according to standard protocols. Cultured CD34⁺ cells from MPN patients bearing the *JAK2V617F* mutation were harvested after one week of culture in Epo. Phosphorylation of STAT5, AKT and MAPK was assessed by Western blot. The protein levels of JAK2, STAT5, AKT, MAPK and L3MBTL1 were also assessed. (B) Primary GFP⁺ CD34⁺ cells were harvested after one week in erythroid culture and FOXO phosphorylation and JNK expression levels were assessed by Western Blot assay. Tubulin serves as a loading control for figures 6A, 6B and 6E. (C) 2×10^7 GFP⁺ CD34⁺ cells, plated in erythroid culture conditions, were tested for Ras activation, by detection of GTP-bound Ras. Cells were lysed and incubated with (GST)-Raf-RBD fusion protein (Millipore) coupled to glutathione agarose beads. GTP-bound Ras was detected by Western blotting with an isoform-specific antibody. (D) Expression of the erythroid markers CD71 and GlyA was evaluated on L3MBTL1-KD CB cells cultured without Erythropoietin, in SCF, FLT-3, IL-6 and TPO. (E) After one week in culture without EPO, the GFP⁺ CD34⁺ cells were lysed and phosphorylation of STAT5 and AKT were assessed by Western blot analysis. The protein levels of JAK2, STAT5, AKT, MAPK, Raf-1, p16 and L3MBTL1 were also assessed.

Figure 7. L3MBTL1 restricts erythroid differentiation. (A) GlyA expression was assessed by FACS in the L3MBTL1-HA expressing CMK, U937, HEL and K562 cells compared to the MIGR1 (empty vector) transduced cells. (B) p16 protein expression levels were determined by Western blot analysis in L3MBTL1-HA HEL cells vs. the MIGR1 (empty vector) control HEL cells. JNK and L3MBTL1 levels are also shown. Tubulin serves as the loading control. (C) GlyA expression in L3MBTL1-HA expressing CD34⁺ cells after three days of culture with SCF 100ng/ml and Erythropoietin 6IU/ml, compared to the MIGR1 (empty vector) transduced cells. (D) L3MBTL1 mRNA expression levels in retrovirally infected CD34⁺ cells, quantified by qPCR (n=3).

Figure 8. L3MBTL1 depletion inhibits cell proliferation and causes G2/M arrest. U2OS cells were infected with control shRNA or one of several different lentiviral shRNAs targeting L3MBTL1. Levels of L3MBTL1 mRNA (A) and protein (B) were measured by quantitative RT-PCR and immunoblotting 48 h after infection. L3MBTL1 mRNA levels detected were adjusted for loading discrepancies using Hprt mRNA as the loading standard, and the levels of mRNA detected were plotted as a percent of the L3MBTL1 observed in U2OS cells infected with control shRNA. To quantitate depletion of L3MBTL1, the relative protein levels of L3MBTL1 were adjusted using the α-tubulin loading control and quantified relative to the protein level present in the control sample (set as 1). (C) U2OS cells were infected with control shRNA or with L3MBTL1 shRNA #3. After 48 h, cells were incubated with BrdU, stained with BrdU-APC antibody and propidium iodide (PI), and analyzed by flow cytometry. The distribution of BrdU (y axis) and PI (x axis) is plotted.

Figure 9. Depletion of L3MBTL1 generates DNA breaks. (A) U2OS cells infected with one of several shRNAs against L3MBTL1 or with control shRNA were stained with antibodies against 53BP1 and γ H2A.x. (B) DNA damage foci were quantitated in control and L3MBTL1 knockdown cells based on whether they contained more or less than five foci per cell. (C) The tail moment was calculated and plotted from three independent comet assays of U2OS cells treated with control shRNA or L3MBTL1 shRNA U2OS cells at 24 and 48 h after infection. (D) Calculated tail moments from comet assays of control and L3MBTL1-depleted MRC5 and Cal51 cells 48 h after infection are plotted. The tail moment was calculated from comet assays of control MRC5 cells vs. cells irradiated with the indicated dose of gamma irradiation and the data plotted.

Figure 10. Depletion of L3MBTL1 activates the DDR. (A) Control and L3MBTL1-depleted U2OS cells were stained with antibodies against 53BP1 and phospho-ATM (pATM) 48 h postinfection. (B) U2OS cells infected with control or L3MBTL1 shRNAs were harvested 24, 48, and 72 h postinfection and immunoblotted with the indicated antibodies to detect activation of the DDR. Unirradiated cells (unirr) and cells harvested 1 h following 10 Gy of gamma irradiation (γ -irr) were used as negative and positive controls for activated DDR proteins. (C) Lysates from control and L3MBTL1-depleted U2OS cells were isolated 24 and 48 h postinfection, and the levels of Rad51, p53, p21, and actin determined by immunoblotting with the indicated antibodies. (D) Lysates from U2OS cells infected with three different shRNAs against L3MBTL1 were harvested at 48 h and immunoblotted with antibodies directed against γ H2A.x, H4K20me1, H4K20me2, histone H3, and tubulin. (E) Histones were extracted from U937 cells that overexpress L3MBTL1 or that contain empty vector control and immunoblotted for H4K20me1, H4K20me2, and histone H3 (loading control).

Figure 11. Depletion of L3MBTL1 alters the progression of DNA replication forks. MRC5 and U2OS cells infected with control or L3MBTL1 shRNA were incubated for 1 h with IdU followed by 1 h incubation with CldU and then subjected to analysis of replication fork movement. (A) Individual replication units were visualized by immunofluorescence for incorporated halogenated nucleotides in isolated DNA fibers, as described in Materials and Methods. Images of fibers from MRC5 cells infected with control or L3MBTL1 shRNAs are shown. (B) The mean DNA fiber length from MRC5 cells infected with control or L3MBTL1 shRNA was calculated by measuring at least 100 fibers in each experiment, and the results plotted. (C) The data for one representative experiment with MRC5 cells are plotted as percentage of DNA fibers with each specified length. (D) Mean DNA fiber length for U2OS cells infected with control or L3MBTL1 shRNA was calculated by measuring at least 100 fibers in each experiment and plotted. (E) The data derived from an experiment using U2OS cells are plotted as percentage of replication forks with the specified DNA fiber length indicated.

Figure 12. L3MBTL1 interacts with components of the DNA replication machinery. (A) HA-L3MBTL1 was overexpressed in 293T cells, and cell lysates were immunoprecipitated and immunoblotted with the HA or rabbit IgG antibodies. (B) Flag-L3MBTL1 was overexpressed in 293T cells, and cell lysates were immunoprecipitated with antibodies against Mcm2, Mcm5, or rabbit IgG. Following SDS/PAGE separation, gels were immunoblotted with Flag antibody to detect L3MBTL1. The immunoprecipitation of Mcm2 and Mcm5 proteins was verified by immunoblotting with the corresponding antibodies, using rabbit IgG as a control.

Figure 13. Characterization of undifferentiated control and L3MBTL1 knockdown (KD) human embryonic stem cells. (A) Schematic representation of L3MBTL1 gene showing the location for the short hairpin (shRNA) sequences cloned into the H1P-HygroEGFP lentiviral plasmid. (B) Western blot of cytoplasmic and nuclear fractions from

H9 parental cells shows nuclear location of L3MBTL1. Oct4 (nuclear) and tubulin (cytoplasmic) were used as controls. (C) Microscopic images showing the undifferentiated stage for the wt parental, LUC shRNA, L3MBTL1-shRNA1, and shRNA2 H9 cells based on their expression of GFP. Whole colonies were imaged on an Olympus epifluorescence system under a 10× objective. Scale bar represents 100µm. (D) Cell cycle analysis of undifferentiated control and L3MBTL1KD ES cells. Relative DNA content, assessed by PI staining, shows the proportion of cells in the G1, G2, and S phases. A representative example of 3 independent experiments is shown. (E) Reverse transcriptase qPCR analysis comparing the level of L3MBTL1, OCT-4, NANOG, and SOX2 mRNA expression in control and L3MBTL1-depleted cells. Statistical analysis was performed by 1-way ANOVA and Tukey posttest (* $P < 0.05$). Error bars represent the standard deviation ($n=3$). (F) Fluorescent microscopy images of OCT-4 with a DAPI DNA counterstain using the Olympus epifluorescence system under a 20× objective. Scale bar represents 50µm.

Figure 14. Morphological changes of spontaneously differentiated control and L3MBTL1 KD cells. (A) Photographs showing the morphological contrast between LUC shRNA and L3MBTL1 KD cells (left and right upper row, respectively); images were acquired using the Gel Doc System Quantity One software (BioRad). Lower row shows a magnified view of the differentiated L3MBTL1 KD cells (white circle); black lines show a phase-contrast image (left) and a DAPI/GFP fluorescence image (right). (B) L3MBTL1 KD cells fail to develop proper embryoid bodies. Fluorescent microscopic images showing EB derivation based on GFP expression for the LUC shRNA, shRNA1, and shRNA2 cell lines. Representative images of 3 independent experiments are shown. (C) Flow cytometry assay shows increasing cell death for the differentiated L3MBTL1 KD EB cells. Top plots show unstained control and L3MBTL1 KD EB cells and bottom plots show PE-Annexin V versus 7-AAD permeability profiles in the same cells. Apoptotic cells on the plots are Annexin V positive and PI negative (lower right quadrant), whereas necrotic cells are Annexin V positive and PI positive (upper right quadrant). (D) Expression of L3MBTL1, OCT-4, and NANOG in undifferentiated and differentiated state measured as relative level of mRNA/GAPDH. (E) mRNA expression levels of lineage cell markers SOX1 (ectoderm), AFP (endoderm), ACTC1 (mesoderm), and CG-β (trophoblast) in undifferentiated and differentiated states measured as relative level of mRNA/GAPDH. Statistical analysis was performed by 1-way ANOVA and Tukey posttest (* $P < 0.05$). Error bars represent the standard deviation ($n = 3$).

Figure 15. Reverse transcriptase qPCR analysis for lineage cell markers. (A) Relative levels of mRNA expression of trophoblast marker CDX2. Error bars represent the standard deviation ($n = 3$). (B) Trophoblast cell markers HAND1, GCM1, KRT7, and KRT8 in undifferentiated and differentiated states measured as relative level of mRNA/GAPDH. Statistical analysis was performed by 1-way ANOVA and Tukey posttest (* $P < 0.05$). Error bars represent the standard deviation ($n = 3$). (C) Immunofluorescent detection of HAND1. White arrows indicate the nuclear location of HAND1 protein. Microscopy performed with Olympus epifluorescence system under a 40 · objective. Scale bar represents 50 µm. Representative images of 3 independent experiments are shown. (D) FACS analysis shows the percentage of spontaneously differentiated control and L3MBTL1 shRNA1 and shRNA2 cells expressing the trophodermal (TE) marker HLA-G (red). Isotype control antibody staining is shown (black). Undifferentiated LUC shRNA and L3MBTL1 KD cells were used as negative controls for HLA-G staining (blue).

Figure 16. L3MBTL1 knockdown mimics trophoblast differentiation induced by BMP4. Luciferase control with or without BMP4 and L3MBTL1 KD cells were cultured for 7 days. (A) Reverse transcriptase qPCR analysis for L3MBTL1, OCT-4, CG-β, and HAND1

mRNA expression. Statistical analysis was by 2-way ANOVA and Bonferroni posttest (*P < 0.05). Error bars represent the standard deviation (n = 3). (B) Phosphorylation of SMADS1/5/8 was examined by Western blot analysis in the homogenates of undifferentiated (day 1) and spontaneously differentiated (day 7) control LUC shRNA and L3MBTL1-KD cells. (C) Immunoassay for placental hormones CG- β and progesterone. Error bars represent the standard deviation (n = 3). (D) L3MBTL1 KD cells differentiate under defined conditions. Fluorescence images of typical neuronal rosette structures at day 9 of directed neuroectoderm differentiation for control LUC shRNA and L3MBTL1 KD cell lines (upper panel) are shown. Scale bar represents 50 μ m. Representative images of 3 independent experiments are shown. Reverse transcriptase qPCR analysis results for neuroectoderm markers SOX-1 and PAX6 mRNA expression (bottom panel) are also shown. Statistical analysis was performed by 2-way ANOVA and Bonferroni posttest (*P < 0.05). Error bars represent the standard deviation (n = 3).

Figure 17. L3MBTL1 regulates EKLf expression via SMAD5 in hematopoietic and embryonic stem cells. A) EKLf, NF-E2, GATA-1, LMO2, and EPOR expression levels were evaluated by qRT-PCR in L3MBTL1-KD CB CD34+ cells after 7 days of erythroid-supporting culture (with SCF 100 ng/ml and Epo 6U/ml) compared to controls. GAPDH served as housekeeping control B) K562 erythroleukemia cells were crosslinked with 1% formaldehyde and immunoprecipitated with smad5 (cell signaling) and IgG antibody. Primers covering the smad binding motifs²⁹ across the upstream enhancer, the proximal promoter and the intronic enhancer of the EKLf were utilized. Data were normalized by 10% input. K562-L3MBTL1-HA were retrovirally infect to express L3MBTL1-HA or MIGR1 control c-DNA and crosslinked with 1% formaldehyde and immunoprecipitated with smad5 (cell signaling) and IgG antibody. C) EKLf mRNA expression levels was evaluated by qRT-PCR in human ES cells +/- treatment with Dorsomorphin and SB431542 inhibitors. GAPDH served as housekeeping control. D) human embryonic stem cells were crosslinked with 1% formaldehyde and immunoprecipitated with L3MBTL1 and IgG antibody. Data were normalized by 10% input. The graph shows the location of the primers of the human smad5 promoter.

Figure 18. Modulation of L3MBTL1 expression affects globin gene expression A) Globin gene expression was measured by qRT-PCR in cord blood (CB) derived L3MBTL1-KD CD34+ cells after 7 days in liquid culture that supports erythroid differentiation. Data were calculated according to standard curve analysis, and normalized to GAPDH expression. B) Gamma globin gene expression was measured by WB in cord blood (CB) derived L3MBTL1-KD CD34+ cells after 7 days in liquid culture that supports erythroid differentiation. Tubulin served as loading control C) Globin gene mRNA levels were evaluated by qRT-PCR in L3MBTL1-HA overexpressing CB CD34+ cells after 3 days in liquid culture that supports erythroid differentiation. GAPDH served as the housekeeping gene and the data were calculated using a standard curve analysis. D) Gamma globin gene expression was measured in L3MBTL1-HA overexpressing. Tubulin served as loading control E) Globin gene mRNA expression was measured in stable L3MBTL1-KD human embryonic stem cells by qRT-PCR. Data were normalized by GAPDH expression and calculated as fold induction relative to controls. F) L3MBTL1-HA overexpressing K562 cells were treated with 40 ng/ml BMP4 and gamma globin gene expression was evaluated by WB. Tubulin served as loading control. G) Gamma and beta globin gene expression levels in K562 cells +/- knock-down of L3MBTL1 and +/- Knock-down of EKLf. GAPDH served as housekeeping control

Figure 19. knock-down of L3MBTL1 activates smad-mediated transcriptional response in patient-specific beta-thalassemic iPS cells A) Undifferentiated iPS cells

were transduced with a lentiviral vector expressing shRNA targeting L3MBTL1 or luciferase (and GFP). GFP⁺ cells maintain the morphologic and immunophenotypic features of stemness, based on Tra-181 expression B) Globin gene mRNA expression is analyzed by qRT-PCR in CD71⁺GlyA⁺ cells, which were differentiated from L3MBTL1-KD and control b-thal iPS cells. Data were normalized by GAPDH expression C) Gene expression profile (GEP) of undifferentiated L3MBTL1-KD iPS cells, compared to controls, based on microarray analysis. Results indicate duplicate experiments (control and hairpin 1 and 2). D) mRNA expression levels of several genes, identified by microarray analysis, was confirmed by qPCR. Data were normalized by GAPDH expression and shown as shRNA vs control E) Gene Set Enrichment Analysis of L3MBTL1-KD iPS cells F) Expression levels of phospho smad 1/5/8, total smad5, phospho smad2, total smad2, and HHEX were evaluated in L3MBTL1-KD and control iPS cells by WB. Tubulin served as loading control. G) EKLf and L3MBTL1 expression were evaluated by WB assay in CB-derived iPS cells. Tubulin served as loading control H) EKLf and L3MBTL1 expression were evaluated by WB assay in patient-specific derived iPS cells. Tubulin served as loading control. I) working model

Figure 20. The Oncogenic JAK2 Mutants Interact More Strongly with PRMT5 than Wild-Type JAK2 and Gain the Ability to Phosphorylate PRMT5 (A) The V617F mutation enhances the interaction between JAK2 and PRMT5. 293T cells were transiently transfected with vectors expressing FLAG-PRMT5 alone (lane 2) or with HA-tagged wild-type (lane 3), or V617F (lane 4) JAK2 proteins. Immunoprecipitation was performed using an anti-HA antibody and immunoblotting with anti-FLAG or anti-JAK2 antibodies.(B) Both the V617F and K539L mutations enhance the PRMT5/JAK2 association. HA-tagged PRMT5 was coexpressed in 293T cells with wild-type (lane 3), V617F (lane 4), or K539L (lane 5) JAK2 proteins. Proteins were precipitated by anti-HA immunoprecipitation, and the blots were probed with antibodies specific for HA, JAK2, or PRMT5.(C) Endogenous interaction between PRMT5 and JAK2V617F is detected in HEL cells. Proteins were precipitated from HEL cell extracts using two different anti- JAK2 antibodies; normal rabbit IgG was used as a control for the immunoprecipitation.(D) Interaction between HA-PRMT5 and endogenous JAK2V617F is detected in HEL cells. Co-IP was performed using a HEL cell line stably expressing HA-PRMT5. Proteins were precipitated by either a normal mouse IgG or anti-HA antibody. Immunoblotting was performed using antibodies specific for JAK2 and PRMT5.(E) The N-terminal region of JAK2 interacts with PRMT5. The left diagram is of full-length JAK2 and various amino terminal-deleted JAK2 proteins with or without the V617F mutation. Numbers indicate the relevant amino acids. Right panel shows that HA-tagged JAK2 full-length or various amino terminal-deletion mutants were coexpressed in 293T cells with FLAG-PRMT5. JAK2 and any associated PRMT5 were pulled down using anti-HA immunoprecipitation. Membranes were immunoblotted with an anti-HA antibody to detect JAK2 and an anti-FLAG antibody to detect PRMT5. WTFL, wild-type full-length JAK2 protein; VFFL, JAK2V617F full-length protein.

Figure 21. The Constitutively Active JAK2 Mutants Phosphorylate PRMT5 In Vivo(A) JAK2 phosphorylates PRMT5 in vitro. In vitro kinase assays were performed using bacterial-purified GST-PRMT5 and the active JAK2 kinase. The amount of protein in the reaction is indicated. Myelin basic protein (MBP) was used as a positive control (lane 3).(B) PRMT5 is phosphorylated by JAK2V617F in vivo. HA-PRMT5 was cotransfected into 293T cells with an empty vector or with vectors expressing wild-type or V617F mutant JAK2 protein. PRMT5 was precipitated by anti-HA immunoprecipitation, and phosphorylation of PRMT5 was detected using a phosphotyrosine-specific antibody (PY350).(C) Both JAK2V617F and JAK2K539L phosphorylate PRMT5 in vivo. 293T cells

were transiently transfected with HA-PRMT5 alone or cotransfected with an increasing concentration of JAK2 wild-type, JAK2V617F- or JAK2K539L-expressing vector. HA-PRMT5 was purified by anti-HA immunoprecipitation, and phosphorylation of PRMT5 was detected by immunoblotting with the PY350 antibody.(D) Activated wild-type JAK2 is unable to phosphorylate PRMT5 in vivo. 293T cells were transfected with vectors expressing the proteins indicated in the figure. Proteins were purified by anti-HA immunoprecipitation, and phosphorylation of PRMT5 and STAT5 was detected using an anti-phosphotyrosine antibody. Input was from 5% of the total lysate. JAK2 phosphorylation was detected using an antibody specific for phospho-JAK2.(E) Endogenous PRMT5 is phosphorylated in HEL cells. HEL cells were treated with either DMSO or 2 μ M JAK Inhibitor I for 16 hr. Phosphorylated proteins were purified using the PY99 anti-phosphotyrosine antibody. Normal mouse IgG was used as a control for the immunoprecipitation. The precipitated STAT5 and PRMT5 proteins were detected using anti-STAT5 and anti-PRMT5 antibodies, respectively. JI1, JAK Inhibitor I.(F) Phosphorylated PRMT5 is not detected in TF-1 cells. TF-1 cells cultured in growth medium supplemented with 2 ng/ml of recombinant human IL-3 were deprived of cytokine for 16 hr. The cells (5×10^6) were then treated with GM-CSF (25 ng/ml), Epo (20 U/ml), or Epo plus 2 μ M of JAK Inhibitor I (JI1) for 20 min. Phosphorylated STAT5 and PRMT5 proteins were immunoprecipitated using the PY99 antibody.

Figure 22. Phosphorylation of PRMT5 by JAK2V617F Impairs Its Histone Methyltransferase Activity(A) Coexpression of JAK2V617F, but not the wild-type JAK2, impairs the ability of PRMT5 to methylate histone H4 in vitro. An in vitro methylation assay was performed using HA-PRMT5 purified from 293T cells transfected with HA-PRMT5 alone (lanes 5–7) or cotransfected with MEP50 (lanes 2–4), wild-type JAK (lanes 8–10), or JAK2V617F (lanes 11–13). Increasing amount of proteins (10, 15, or 20 μ l) were added to each methylation reaction with 2.5 μ g recombinant H4 and 1 μ Ci of 3 H-SAM. Even loading of the proteins (PRMT5 and histone H4) was visualized using Coomassie blue staining. EV, empty vector.(B) In vitro methylation assays were performed with recombinant H2A and similarly purified HA-PRMT5. Increasing amount of purified protein (10 or 20 μ l) was added to the reaction.(C) Overexpression of the mutant JAK2 proteins, but not the wild-type JAK2 protein, downregulates H2A/H4 R3 methylation. The core histones were purified from 293T cells transfected with either an empty vector or with vectors expressing the JAK2 proteins indicated in the figure. Methylation of H2A/H4 R3 was detected using a rabbit polyclonal antibody specific for H2A/H4 R3 symmetric dimethylation (H2A/H4R3me2s). An anti-histone H3 antibody was used to show the equal loading.(D) Inhibition of JAK2 kinase activity increases H2A R3 methylation in HEL cells. HEL cells were treated with DMSO or with the JAK2 inhibitors JAK Inhibitor I (1 μ M) or CEP701 (0.2 μ M) for 2 hr. Histone methylation was detected in cell lysates using an antibody specific for symmetric dimethylation of H2A/H4 R3. JI1, JAK Inhibitor I.(E) Inhibition of JAK2 rapidly upregulates H2A R3 methylation in HEL cells. HEL cells were treated with TG101348 (3 μ M) for 0, 1, 2, and 4 hr. JAK2 kinase inhibition was monitored by measuring STAT5 phosphorylation using an anti-phospho-STAT5 antibody. Phosphorylation of PRMT5 was detected with the phospho-specific PRMT5 antibody (P-PRMT5-747). Histones were purified by acidic extraction, and H2A R3 methylation was detected using an anti-H2A/H4R3me2s antibody. The levels of histone H3 and tubulin are shown as loading controls.(F) JAK2 inhibitors do not change the level of H2A R3 methylation in TF-1 cells. TF-1 cells growing in medium supplemented with recombinant human IL-3 were treated with DMSO or JAK2 inhibitors (as indicated in the figure) for 2 hr. Histone methylation was detected using an anti-H2A/H4R3me2s antibody and STAT5 phosphorylation detected using a phospho-STAT5 antibody. SS, steady state. Starved cells were deprived of IL-3 for 2 hr.(G) Gene expression profiles were generated using

Affymetrix HG133 GeneChips and CEP701 (0.5 μ M)-treated or shPRMT5-treated HEL cells, versus controls (DMSO or a lentivirus expressing a scrambled shRNA, respectively). Genes reciprocally up- or downregulated ≥ 1.5 -fold in both duplicate samples from drug-treated samples, and the shPRMT5-treated samples are compared. The top shows the number of genes that are downregulated by CEP701 treatment and upregulated by knockdown of PRMT5. The bottom illustrates the number of genes that are upregulated by CEP701 treatment and downregulated by PRMT5 knockdown.

Figure 23. Phosphorylation of PRMT5 by JAK2V617F Disrupts Its Association with MEP50

(A) Tyrosine residues within PRMT5 that are potential sites of phosphorylation (279,282,285, 296,303,306) were converted to phenylalanine residues by site-directed mutagenesis. Wild-type or mutant HA-PRMT5 proteins were coexpressed with JAK2V617F protein in 293T cells and immunoprecipitated with an anti-HA antibody. Phosphorylation of PRMT5 was detected using a rabbit polyclonal anti-phosphotyrosine antibody (PY350). (B) HEL cells were treated with DMSO, JAK Inhibitor I (1 μ M), or CEP701 (0.2 μ M) overnight, and the phosphorylation of PRMT5 was detected by immunoblotting using a phospho-PRMT5 antibody (P-PRMT5-747) specific for the Y297, Y304, and Y307 phosphotyrosine residues in the PRMT5 protein. The level of PRMT5 and phospho-STAT5 are also shown. (C) Coexpression of JAK2V617F disrupts the PRMT5/MEP50 association. The HA-PRMT5/MEP50 complex was purified using an anti-HA antibody from 293T cells expressing the proteins indicated in the figure. Phosphorylation of PRMT5 was confirmed by immunoblotting with an anti-phosphotyrosine antibody. Coprecipitated MEP50 was detected with an anti-MEP50 antibody. (D) The kinase activity of JAK2V617F is required to disrupt the PRMT5/MEP50 complex. DMSO or 4 μ M JAK Inhibitor I (JI1) was added to the 293T cells after transfection. Cells were collected 48 hr after transfection, and the HA-PRMT5/MEP50 complex was immunoprecipitated using an anti-HA antibody. (E) Phosphorylated PRMT5 isolated from HEL cells does not bind MEP50. HEL cells stably expressing myc-tagged MEP50 were subjected to immunoprecipitation using an anti-myc antibody. After overnight incubation, the flowthrough was saved, and the PRMT5/MEP50 complex was eluted from the beads. Proteins in the eluate and the flowthrough were precipitated by TCA precipitation and resolved by SDS-PAGE gels. The membranes were blotted using anti-PRMT5 and anti-MEP50 antibodies, and the P-PRMT5-747 antibody, to quantify the amount of each protein in the various lanes.

Figure 24. PRMT5 Activity Regulates Progenitor Cell Expansion/Differentiation in Human CD34+ Cells

(A) Knockdown of PRMT5 promotes CFU formation. Isolated human CB CD34+ cells were transduced with lentiviruses expressing a scrambled shRNA or shRNA specific to PRMT5. GFP-positive cells were sorted 2 days after infection. Left panel shows that PRMT5 mRNA expression was detected by real-time PCR. Right panel illustrates that approximately 1×10^4 GFP-positive CD34+ cells were plated in methylcellulose culture supplemented with cytokines to support the formation of CFU-GM, CFU-GEMM, and BFU-E. Colonies were scored 2 weeks after the plating. The results shown here are the averages of two independent experiments with error bars indicating \pm SD. (B) Overexpression of PRMT5 inhibits colony formation. Isolated human CB CD34+ cells were transduced with lentiviruses expressing either GFP alone, or GFP together with HA-tagged wild-type PRMT5 or an HA-tagged M6 mutant form of PRMT5. GFP-positive cells were sorted, and 2×10^4 cells were used for CFU assays. The average results of two independent experiments are shown here. The error bars indicate \pm SD. (C) Knockdown of PRMT5 promotes erythroid differentiation. GFP+ CD34+ cells were cultured in serum-free medium supplemented with cytokines supporting erythroid differentiation for 14 days. CD71-positive/Ter-115-positive cells were determined by FACS analysis. (D) PRMT5

overexpression inhibits erythroid differentiation. HA-PRMT5 or HA-PRMT5M6 was overexpressed in CB CD34+ cells, which were cultured in erythroid-promoting medium for 7 days; erythroid differentiation was determined by FACS analysis, staining for CD71 (y axis) and Glycophorin A (x axis). pBGJR refers to the control lentiviral vector.(E) PRMT5 overexpression inhibits colony formation in JAK2V617F-positive CD34+ cells isolated from patients with PV. CD34+ cells were isolated from phlebotomy units of patients with PV and transduced by control lentivirus or lentiviruses expressing HA-PRMT5 or HA-PRMT5M6. The 1×10^4 GFP+ cells were plated in methylcellulose with cytokines supporting GM, GEMM, and BFU colony formation. Colonies were scored 14 days after plating.(F) Phosphorylation of PRMT5 was detected in CD34+ cells isolated from patients with MPN. CD34+ cells were isolated from human umbilical cord blood (lane 1) or from ten phlebotomy units taken from patients with MPN (lanes 2–3 and 5–12). HEL cells were used as a positive control (lane 4). Phosphorylation of PRMT5 was detected using the P-PRMT5-747 antibody. The total amount of PRMT5 was also assessed by immunoblotting. ET, essential thrombocythemia; PV, polycythemia vera; HEL, HEL leukemia cells.

7. ACKNOWLEDGEMENTS

This work was supported by an ASH scholar award, by the Dana Foundation MSKCC Clinical Scholar Award in biomedical research, by the Associazione Cristina Bassi contro le leucemie acute dell'adulto, by the American Italian Cancer Foundation postdoctoral fellowships and by the Italian Society of Experimental Hematology (SIES) to F.P; by NCI R01 grant 102202, the Starr Foundation and by Lymphoma Research Foundation to S.D.N.

8. References

1. Wismar J, Loffler T, Habtemichael N, et al. The *Drosophila melanogaster* tumor suppressor gene lethal(3)malignant brain tumor encodes a proline-rich protein with a novel zinc finger. *Mech Dev.* 1995;53:141-154.
2. Gateff E, Loffler T, Wismar J. A temperature-sensitive brain tumor suppressor mutation of *Drosophila melanogaster*: developmental studies and molecular localization of the gene. *Mech Dev.* 1993;41:15-31.
3. Wang WK, Tereshko V, Boccuni P, MacGrogan D, Nimer SD, Patel DJ. Malignant brain tumor repeats: a three-leaved propeller architecture with ligand/peptide binding pockets. *Structure.* 2003;11:775-789.
4. Min J, Allali-Hassani A, Nady N, et al. L3MBTL1 recognition of mono- and dimethylated histones. *Nat Struct Mol Biol.* 2007;14:1229-1230.
5. Boccuni P, MacGrogan D, Scandura JM, Nimer SD. The human L(3)MBT polycomb group protein is a transcriptional repressor and interacts physically and functionally with TEL (ETV6). *J Biol Chem.* 2003;278:15412-15420.
6. Kalakonda N, Fischle W, Boccuni P, et al. Histone H4 lysine 20 monomethylation promotes transcriptional repression by L3MBTL1. *Oncogene.* 2008;27:4293-4304.
7. Trojer P, Li G, Sims RJ, 3rd, et al. L3MBTL1, a histone-methylation-dependent chromatin lock. *Cell.* 2007;129:915-928.
8. Dewald GW, Schad CR, Lilla VC, Jalal SM. Frequency and photographs of HGM11 chromosome anomalies in bone marrow samples from 3,996 patients with malignant hematologic neoplasms. *Cancer Genet Cytogenet.* 1993;68:60-69.
9. Bench AJ, Nacheva EP, Hood TL, et al. Chromosome 20 deletions in myeloid malignancies: reduction of the common deleted region, generation of a PAC/BAC contig and identification of candidate genes. UK Cancer Cytogenetics Group (UKCCG). *Oncogene.* 2000;19:3902-3913.
10. Fenaux P, Morel P, Lai JL. Cytogenetics of myelodysplastic syndromes. *Semin Hematol.* 1996;33:127-138.
11. Heim S, Mitelman F. Cytogenetic analysis in the diagnosis of acute leukemia. *Cancer.* 1992;70:1701-1709.
12. MacGrogan D, Kalakonda N, Alvarez S, et al. Structural integrity and expression of the L3MBTL gene in normal and malignant hematopoietic cells. *Genes Chromosomes Cancer.* 2004;41:203-213.
13. Bench AJ, Li J, Huntly BJ, et al. Characterization of the imprinted polycomb gene L3MBTL, a candidate 20q tumour suppressor gene, in patients with myeloid malignancies. *Br J Haematol.* 2004;127:509-518.
14. Northcott PA, Nakahara Y, Wu X, et al. Multiple recurrent genetic events converge on control of histone lysine methylation in medulloblastoma. *Nat Genet.* 2009;41:465-472.
15. Paulsen RD, Cimprich KA. The ATR pathway: fine-tuning the fork. *DNA Repair (Amst).* 2007;6:953-966.
16. Bartkova J, Horejsi Z, Koed K, et al. DNA damage response as a candidate anti-cancer barrier in early human tumorigenesis. *Nature.* 2005;434:864-870.
17. Gorgoulis VG, Vassiliou LV, Karakaidos P, et al. Activation of the DNA damage checkpoint and genomic instability in human precancerous lesions. *Nature.* 2005;434:907-913.
18. Halazonetis TD, Gorgoulis VG, Bartek J. An oncogene-induced DNA damage model for cancer development. *Science.* 2008;319:1352-1355.
19. Keller G. Embryonic stem cell differentiation: emergence of a new era in biology and medicine. *Genes Dev.* 2005;19:1129-1155.

20. Auman HJ, Nottoli T, Lakiza O, Winger Q, Donaldson S, Williams T. Transcription factor AP-2gamma is essential in the extra-embryonic lineages for early postimplantation development. *Development*. 2002;129:2733-2747.
21. Donnison M, Beaton A, Davey HW, Broadhurst R, L'Huillier P, Pfeffer PL. Loss of the extraembryonic ectoderm in Elf5 mutants leads to defects in embryonic patterning. *Development*. 2005;132:2299-2308.
22. Russ AP, Wattler S, Colledge WH, et al. Eomesodermin is required for mouse trophoblast development and mesoderm formation. *Nature*. 2000;404:95-99.
23. Strumpf D, Mao CA, Yamanaka Y, et al. Cdx2 is required for correct cell fate specification and differentiation of trophectoderm in the mouse blastocyst. *Development*. 2005;132:2093-2102.
24. Yagi R, Kohn MJ, Karavanova I, et al. Transcription factor TEAD4 specifies the trophectoderm lineage at the beginning of mammalian development. *Development*. 2007;134:3827-3836.
25. Bernstein BE, Mikkelsen TS, Xie X, et al. A bivalent chromatin structure marks key developmental genes in embryonic stem cells. *Cell*. 2006;125:315-326.
26. Peters AH, O'Carroll D, Scherthan H, et al. Loss of the Suv39h histone methyltransferases impairs mammalian heterochromatin and genome stability. *Cell*. 2001;107:323-337.
27. Pasini D, Bracken AP, Jensen MR, Lazzarini Denchi E, Helin K. Suz12 is essential for mouse development and for EZH2 histone methyltransferase activity. *EMBO J*. 2004;23:4061-4071.
28. Torres-Padilla ME, Parfitt DE, Kouzarides T, Zernicka-Goetz M. Histone arginine methylation regulates pluripotency in the early mouse embryo. *Nature*. 2007;445:214-218.
29. Adelman CA, Chattopadhyay S, Bieker JJ. The BMP/BMPR/Smad pathway directs expression of the erythroid-specific EKLF and GATA1 transcription factors during embryoid body differentiation in serum-free media. *Development*. 2002;129:539-549.
30. Lohmann F, Bieker JJ. Activation of Eklf expression during hematopoiesis by Gata2 and Smad5 prior to erythroid commitment. *Development*. 2008;135:2071-2082.
31. Siatecka M, Bieker JJ. The multifunctional role of EKLF/KLF1 during erythropoiesis. *Blood*. 2011;118:2044-2054.
32. Alhashem YN, Vinjamur DS, Basu M, Klingmuller U, Gaensler KM, Lloyd JA. Transcription factors KLF1 and KLF2 positively regulate embryonic and fetal beta-globin genes through direct promoter binding. *The Journal of biological chemistry*. 2011;286:24819-24827.
33. Massague J, Chen YG. Controlling TGF-beta signaling. *Genes & development*. 2000;14:627-644.
34. Pimanda JE, Donaldson IJ, de Bruijn MF, et al. The SCL transcriptional network and BMP signaling pathway interact to regulate RUNX1 activity. *Proceedings of the National Academy of Sciences of the United States of America*. 2007;104:840-845.
35. Zafonte BT, Liu S, Lynch-Kattman M, et al. Smad1 expands the hemangioblast population within a limited developmental window. *Blood*. 2007;109:516-523.
36. Hong SH, Lee JH, Lee JB, Ji J, Bhatia M. ID1 and ID3 represent conserved negative regulators of human embryonic and induced pluripotent stem cell hematopoiesis. *Journal of cell science*. 2011;124:1445-1452.
37. Fuchs O, Simakova O, Klener P, et al. Inhibition of Smad5 in human hematopoietic progenitors blocks erythroid differentiation induced by BMP4. *Blood cells, molecules & diseases*. 2002;28:221-233.
38. Liu B, Sun Y, Jiang F, et al. Disruption of Smad5 gene leads to enhanced proliferation of high-proliferative potential precursors during embryonic hematopoiesis. *Blood*. 2003;101:124-133.
39. McReynolds LJ, Gupta S, Figueroa ME, Mullins MC, Evans T. Smad1 and Smad5 differentially regulate embryonic hematopoiesis. *Blood*. 2007;110:3881-3890.
40. Lenox LE, Perry JM, Paulson RF. BMP4 and Madh5 regulate the erythroid response to acute anemia. *Blood*. 2005;105:2741-2748.

41. Trompouki E, Bowman TV, Lawton LN, et al. Lineage regulators direct BMP and Wnt pathways to cell-specific programs during differentiation and regeneration. *Cell*. 2011;147:577-589.
42. Perna F, Gurvich N, Hoya-Arias R, et al. Depletion of L3MBTL1 promotes the erythroid differentiation of human hematopoietic progenitor cells: possible role in 20q- polycythemia vera. *Blood*. 2010;116:2812-2821.
43. Boccuni P, MacGrogan D, Scandura JM, Nimer SD. The human L(3)MBT polycomb group protein is a transcriptional repressor and interacts physically and functionally with TEL (ETV6). *The Journal of biological chemistry*. 2003;278:15412-15420.
44. Hoya-Arias R, Tomishima M, Perna F, Voza F, Nimer SD. L3MBTL1 deficiency directs the differentiation of human embryonic stem cells toward trophectoderm. *Stem cells and development*. 2011;20:1889-1900.
45. Tefferi A, Levine RL, Kantarjian H. Oncogenic signals as treatment targets in classic myeloproliferative neoplasms. *Biol Blood Marrow Transplant*. 2009;15:114-119.
46. Dawson MA, Bannister AJ, Gottgens B, et al. JAK2 phosphorylates histone H3Y41 and excludes HP1alpha from chromatin. *Nature*. 2009;461:819-822.
47. De Keersmaecker K, Cools J. Chronic myeloproliferative disorders: a tyrosine kinase tale. *Leukemia*. 2006;20:200-205.
48. Baxter EJ, Scott LM, Campbell PJ, et al. Acquired mutation of the tyrosine kinase JAK2 in human myeloproliferative disorders. *Lancet*. 2005;365:1054-1061.
49. James C, Ugo V, Le Couedic JP, et al. A unique clonal JAK2 mutation leading to constitutive signalling causes polycythaemia vera. *Nature*. 2005;434:1144-1148.
50. Kralovics R, Passamonti F, Buser AS, et al. A gain-of-function mutation of JAK2 in myeloproliferative disorders. *N Engl J Med*. 2005;352:1779-1790.
51. Levine RL, Wadleigh M, Cools J, et al. Activating mutation in the tyrosine kinase JAK2 in polycythemia vera, essential thrombocythemia, and myeloid metaplasia with myelofibrosis. *Cancer Cell*. 2005;7:387-397.
52. Akada H, Yan D, Zou H, Fiering S, Hutchison RE, Mohi MG. Conditional expression of heterozygous or homozygous Jak2V617F from its endogenous promoter induces a polycythemia vera-like disease. *Blood*. 2010;115:3589-3597.
53. Marty C, Lacout C, Martin A, et al. Myeloproliferative neoplasm induced by constitutive expression of JAK2V617F in knock-in mice. *Blood*. 2010;116:783-787.
54. Mullally A, Lane SW, Ball B, et al. Physiological Jak2V617F expression causes a lethal myeloproliferative neoplasm with differential effects on hematopoietic stem and progenitor cells. *Cancer Cell*. 2010;17:584-596.
55. Xing S, Wanting TH, Zhao W, et al. Transgenic expression of JAK2V617F causes myeloproliferative disorders in mice. *Blood*. 2008;111:5109-5117.
56. Ihle JN, Gilliland DG. Jak2: normal function and role in hematopoietic disorders. *Curr Opin Genet Dev*. 2007;17:8-14.
57. Wang Y, Fiskus W, Chong DG, et al. Cotreatment with panobinostat and JAK2 inhibitor TG101209 attenuates JAK2V617F levels and signaling and exerts synergistic cytotoxic effects against human myeloproliferative neoplastic cells. *Blood*. 2009;114:5024-5033.
58. Pollack BP, Kotenko SV, He W, Izotova LS, Barnoski BL, Pestka S. The human homologue of the yeast proteins Skb1 and Hsl7p interacts with Jak kinases and contains protein methyltransferase activity. *J Biol Chem*. 1999;274:31531-31542.
59. Ancelin K, Lange UC, Hajkova P, et al. Blimp1 associates with Prmt5 and directs histone arginine methylation in mouse germ cells. *Nat Cell Biol*. 2006;8:623-630.
60. Branscombe TL, Frankel A, Lee JH, et al. PRMT5 (Janus kinase-binding protein 1) catalyzes the formation of symmetric dimethylarginine residues in proteins. *J Biol Chem*. 2001;276:32971-32976.
61. Pal S, Vishwanath SN, Erdjument-Bromage H, Tempst P, Sif S. Human SWI/SNF-associated PRMT5 methylates histone H3 arginine 8 and negatively regulates expression of ST7 and NM23 tumor suppressor genes. *Mol Cell Biol*. 2004;24:9630-9645.

62. Jansson M, Durant ST, Cho EC, et al. Arginine methylation regulates the p53 response. *Nat Cell Biol.* 2008;10:1431-1439.
63. Tan CP, Nakielny S. Control of the DNA methylation system component MBD2 by protein arginine methylation. *Mol Cell Biol.* 2006;26:7224-7235.
64. Chari A, Golas MM, Klingenhager M, et al. An assembly chaperone collaborates with the SMN complex to generate spliceosomal SnRNPs. *Cell.* 2008;135:497-509.
65. Friesen WJ, Paushkin S, Wyce A, et al. The methylosome, a 20S complex containing JBP1 and pICln, produces dimethylarginine-modified Sm proteins. *Mol Cell Biol.* 2001;21:8289-8300.
66. Friesen WJ, Wyce A, Paushkin S, et al. A novel WD repeat protein component of the methylosome binds Sm proteins. *J Biol Chem.* 2002;277:8243-8247.
67. Meister G, Fischer U. Assisted RNP assembly: SMN and PRMT5 complexes cooperate in the formation of spliceosomal UsnRNPs. *EMBO J.* 2002;21:5853-5863.
68. Le Guezennec X, Vermeulen M, Brinkman AB, et al. MBD2/NuRD and MBD3/NuRD, two distinct complexes with different biochemical and functional properties. *Mol Cell Biol.* 2006;26:843-851.
69. Moffat J, Grueneberg DA, Yang X, et al. A lentiviral RNAi library for human and mouse genes applied to an arrayed viral high-content screen. *Cell.* 2006;124:1283-1298.
70. Ivanova N, Dobrin R, Lu R, et al. Dissecting self-renewal in stem cells with RNA interference. *Nature.* 2006;442:533-538.
71. Elbashir SM, Lendeckel W, Tuschl T. RNA interference is mediated by 21- and 22-nucleotide RNAs. *Genes Dev.* 2001;15:188-200.
72. Dean A, Erard F, Schneider AP, Schechter AN. Induction of hemoglobin accumulation in human K562 cells by hemin is reversible. *Science.* 1981;212:459-461.
73. Zhao X, Jankovic V, Gural A, et al. Methylation of RUNX1 by PRMT1 abrogates SIN3A binding and potentiates its transcriptional activity. *Genes & development.* 2008;22:640-653.
74. Subramanian A, Tamayo P, Mootha VK, et al. Gene set enrichment analysis: a knowledge-based approach for interpreting genome-wide expression profiles. *Proceedings of the National Academy of Sciences of the United States of America.* 2005;102:15545-15550.
75. Fawcett D, Jensch RP. Hemopoiesis. New York: Chapman and Hall; 1997.
76. Kim A, Dean A. Developmental stage differences in chromatin subdomains of the beta-globin locus. *Proc Natl Acad Sci U S A.* 2004;101:7028-7033.
77. Scandura JM, Boccuni P, Massague J, Nimer SD. Transforming growth factor beta-induced cell cycle arrest of human hematopoietic cells requires p57KIP2 up-regulation. *Proc Natl Acad Sci U S A.* 2004;101:15231-15236.
78. Dai C, Krantz SB. Increased expression of the INK4a/ARF locus in polycythemia vera. *Blood.* 2001;97:3424-3432.
79. Minami R, Muta K, Umemura T, et al. p16(INK4a) induces differentiation and apoptosis in erythroid lineage cells. *Exp Hematol.* 2003;31:355-362.
80. Ishida W, Hamamoto T, Kusanagi K, et al. Smad6 is a Smad1/5-induced smad inhibitor. Characterization of bone morphogenetic protein-responsive element in the mouse Smad6 promoter. *The Journal of biological chemistry.* 2000;275:6075-6079.
81. Papapetrou EP, Lee G, Malani N, et al. Genomic safe harbors permit high beta-globin transgene expression in thalassemia induced pluripotent stem cells. *Nature biotechnology.* 2011;29:73-78.
82. Sripichai O, Kiefer CM, Bhanu NV, et al. Cytokine-mediated increases in fetal hemoglobin are associated with globin gene histone modification and transcription factor reprogramming. *Blood.* 2009;114:2299-2306.
83. Zhang W, Yatskievych TA, Cao X, Antin PB. Regulation of Hex gene expression by a Smads-dependent signaling pathway. *The Journal of biological chemistry.* 2002;277:45435-45441.
84. Nakao A, Afrakhte M, Moren A, et al. Identification of Smad7, a TGFbeta-inducible antagonist of TGF-beta signalling. *Nature.* 1997;389:631-635.

85. Yeo C, Whitman M. Nodal signals to Smads through Cripto-dependent and Cripto-independent mechanisms. *Molecular cell*. 2001;7:949-957.
86. Boyer LA, Plath K, Zeitlinger J, et al. Polycomb complexes repress developmental regulators in murine embryonic stem cells. *Nature*. 2006;441:349-353.
87. Lee TI, Jenner RG, Boyer LA, et al. Control of developmental regulators by Polycomb in human embryonic stem cells. *Cell*. 2006;125:301-313.
88. Bodo E, Kromminga A, Funk W, et al. Human hair follicles are an extrarenal source and a nonhematopoietic target of erythropoietin. *FASEB J*. 2007;21:3346-3354.
89. Sims JK, Rice JC. PR-Set7 establishes a repressive trans-tail histone code that regulates differentiation. *Mol Cell Biol*. 2008;28:4459-4468.
90. Owusu-Ansah E, Banerjee U. Reactive oxygen species prime *Drosophila* haematopoietic progenitors for differentiation. *Nature*. 2009;461:537-541.
91. Classen AK, Bunker BD, Harvey KF, Vaccari T, Bilder D. A tumor suppressor activity of *Drosophila* Polycomb genes mediated by JAK-STAT signaling. *Nat Genet*. 2009;41:1150-1155.
92. Tothova Z, Kollipara R, Huntly BJ, et al. FoxOs are critical mediators of hematopoietic stem cell resistance to physiologic oxidative stress. *Cell*. 2007;128:325-339.
93. Trojer P, Reinberg D. Beyond histone methyl-lysine binding: how malignant brain tumor (MBT) protein L3MBTL1 impacts chromatin structure. *Cell Cycle*. 2008;7:578-585.
94. Campbell PJ, Baxter EJ, Beer PA, et al. Mutation of JAK2 in the myeloproliferative disorders: timing, clonality studies, cytogenetic associations, and role in leukemic transformation. *Blood*. 2006;108:3548-3555.
95. Kralovics R, Teo SS, Li S, et al. Acquisition of the V617F mutation of JAK2 is a late genetic event in a subset of patients with myeloproliferative disorders. *Blood*. 2006;108:1377-1380.
96. Delhommeau F, Dupont S, Della Valle V, et al. Mutation in TET2 in myeloid cancers. *N Engl J Med*. 2009;360:2289-2301.
97. Sanada M, Suzuki T, Shih LY, et al. Gain-of-function of mutated C-CBL tumour suppressor in myeloid neoplasms. *Nature*. 2009;460:904-908.
98. Schaub FX, Jager R, Looser R, et al. Clonal analysis of deletions on chromosome 20q and JAK2-V617F in MPD suggests that del20q acts independently and is not one of the predisposing mutations for JAK2-V617F. *Blood*. 2009;113:2022-2027.
99. Yang H, Mizzen CA. The multiple facets of histone H4-lysine 20 methylation. *Biochem Cell Biol*. 2009;87:151-161.
100. Schotta G, Sengupta R, Kubicek S, et al. A chromatin-wide transition to H4K20 monomethylation impairs genome integrity and programmed DNA rearrangements in the mouse. *Genes Dev*. 2008;22:2048-2061.
101. Qin J, Van Buren D, Huang HS, et al. Chromatin protein L3MBTL1 is dispensable for development and tumor suppression in mice. *J Biol Chem*. 2010;285:27767-27775.
102. Pesavento JJ, Yang H, Kelleher NL, Mizzen CA. Certain and progressive methylation of histone H4 at lysine 20 during the cell cycle. *Mol Cell Biol*. 2008;28:468-486.
103. Luo J, Solimini NL, Elledge SJ. Principles of cancer therapy: oncogene and non-oncogene addiction. *Cell*. 2009;136:823-837.
104. Meshorer E, Misteli T. Chromatin in pluripotent embryonic stem cells and differentiation. *Nat Rev Mol Cell Biol*. 2006;7:540-546.
105. Jedrusik A, Parfitt DE, Guo G, et al. Role of Cdx2 and cell polarity in cell allocation and specification of trophectoderm and inner cell mass in the mouse embryo. *Genes Dev*. 2008;22:2692-2706.
106. Tolkunova E, Cavaleri F, Eckardt S, et al. The caudal-related protein cdx2 promotes trophoblast differentiation of mouse embryonic stem cells. *Stem Cells*. 2006;24:139-144.
107. Zhu D, Fang J, Li Y, Zhang J. Mbd3, a component of NuRD/Mi-2 complex, helps maintain pluripotency of mouse embryonic stem cells by repressing trophectoderm differentiation. *PLoS One*. 2009;4:e7684.

108. Scharf AN, Meier K, Seitz V, Kremmer E, Brehm A, Imhof A. Monomethylation of lysine 20 on histone H4 facilitates chromatin maturation. *Mol Cell Biol.* 2009;29:57-67.
109. Ravasi T, Suzuki H, Cannistraci CV, et al. An atlas of combinatorial transcriptional regulation in mouse and man. *Cell.* 2010;140:744-752.
110. Bresnick EH, Lee HY, Fujiwara T, Johnson KD, Keles S. GATA switches as developmental drivers. *The Journal of biological chemistry.* 2010;285:31087-31093.
111. Grass JA, Boyer ME, Pal S, Wu J, Weiss MJ, Bresnick EH. GATA-1-dependent transcriptional repression of GATA-2 via disruption of positive autoregulation and domain-wide chromatin remodeling. *Proceedings of the National Academy of Sciences of the United States of America.* 2003;100:8811-8816.
112. Alter BP. Fetal erythropoiesis in stress hematopoiesis. *Exp Hematol.* 1979;7 Suppl 5:200-209.
113. Stamatoyannopoulos G, Veith R, Galanello R, Papayannopoulou T. Hb F production in stressed erythropoiesis: observations and kinetic models. *Ann N Y Acad Sci.* 1985;445:188-197.
114. Galanello R, Barella S, Maccioni L, et al. Erythropoiesis following bone marrow transplantation from donors heterozygous for beta-thalassaemia. *Br J Haematol.* 1989;72:561-566.
115. Weinberg RS, Schofield JM, Lenes AL, Brochstein J, Alter BP. Adult 'fetal-like' erythropoiesis characterizes recovery from bone marrow transplantation. *Br J Haematol.* 1986;63:415-424.
116. Link MP, Alter BP. Fetal-like erythropoiesis during recovery from transient erythroblastopenia of childhood (TEC). *Pediatr Res.* 1981;15:1036-1039.
117. Papayannopoulou T, Vichinsky E, Stamatoyannopoulos G. Fetal Hb production during acute erythroid expansion. I. Observations in patients with transient erythroblastopenia and post-phlebotomy. *Br J Haematol.* 1980;44:535-546.
118. Thein SL. Genetic modifiers of the beta-haemoglobinopathies. *Br J Haematol.* 2008;141:357-366.
119. Luck L, Zeng L, Hiti AL, Weinberg KI, Malik P. Human CD34(+) and CD34(+)CD38(-) hematopoietic progenitors in sickle cell disease differ phenotypically and functionally from normal and suggest distinct subpopulations that generate F cells. *Exp Hematol.* 2004;32:483-493.
120. Mathias LA, Fisher TC, Zeng L, et al. Ineffective erythropoiesis in beta-thalassemia major is due to apoptosis at the polychromatophilic normoblast stage. *Exp Hematol.* 2000;28:1343-1353.

9. List of honors and awards

2012-2014	ASH scholar award, clinical/translational category
2012	ASH abstract achievement award
2011	ASH abstract achievement award
2011	ASH/EHA Translational Research Training in Hematology (TRTH) Award
2010/2012	Clinical Scholar Biomedical Research Training Fellowship-Dana Foundation Memorial Sloan-Kettering Cancer Center, New York, USA
2010/2011	American Italian Cancer Foundation Post-doctoral Fellowship (renewal)
2010/2011	Research Fellowship of the Italian Society of Experimental Hematology (SIES)
2009/2010	American Italian Cancer Foundation Post-doctoral Fellowship

10. List of communications

Perna F, Vu L, Themeli M et al. L3MBTL1: A Polycomb Protein At the Node of Crosstalk Between the BMP4 and Hippo Signaling Pathways in Erythropoiesis. ASH 2012 selected for poster presentation.

Perna F, Vu L, Themeli M et al. Targeting a novel epigenetic silencing mechanism to efficiently upregulate fetal globin gene expression. ASH 2011 selected for oral presentation and ASH abstract achievement award.

Vu L, Zhao X, **Perna F** et al. Regulation of AML1/RUNX1 Function by Protein Arginine Methyltransferase 4 (PRMT4) in Myeloid Differentiation. ASH 2011 selected for oral presentation

Perna F, Hoya-Arias R, Vu PL et al. The PcG protein L3MBTL1 transcriptionally represses human embryonic and fetal globin genes: a novel prospect for HbF activation. *ASH 2010, selected for oral presentation*.

Liu F, Zhao X, **Perna F** et al. JAK2V617F-mediated phosphorylation of PRMT5 down-regulates its methyltransferase activity. *ASH 2010, selected for oral presentation*.

Vu L, Zhao X, **Perna F** et al. Downregulation of Protein Arginine Methyltransferase-4 (PRMT4) promotes mir-223 expression and myeloid differentiation. *ASH 2010, poster*.

Perna F, Nadia Gurvich, Ruben Hoya-Arias et al. An erythroid differentiation signature characterizes the depletion of the PcG TSG *L3MBTL1* in human hematopoietic stem/progenitor cells: possible function in 20q- syndromes. *Aplastic Anemia & MDS Symposium 2010 poster*

Perna F, Nadia Gurvich, Ruben Hoya-Arias et al. Deletion of L3MBTL1 in 20q- myeloid disorders: a functional abnormality. *Italian Meeting of Experimental Hematology (SIES) 2010 selected for award*

Invited speaker at the following meetings:

- Translational Hematology “meeting in memory of Piernicola Bocconi”, Federico II University of Naples, Italy 2011
- Translational Hematology, Italian Society of Experimental Hematology, University of Perugia, Italy 2011

11. List and PDF of published papers during the years 2010-2013

1. Bazzoli E, Pulvirenti T, Oberstadt M, **Perna F** et al. MEF promotes stemness in the pathogenesis of gliomas. *Cell Stem Cell* 2012 Dec 7;11(6):836-844.
2. Abdel-Wahab O, Adli M, Lafave LM, Gao J, Hricik T, Shih AH, Pandey S, Patel JP, Chung YR, Koche R, **Perna F** et al. ASXL1 Mutations Promote Myeloid Transformation through Loss of PRC2-Mediated Gene Repression. *Cancer Cell*. 2012 Aug 14;22(2):180-93
3. Wang L, Gural A, Sun X, Zhao X, **Perna F** et al. The leukemogenicity of AML1-ETO is dependent on site-specific lysine acetylation. *Science* 2011 Aug 5;333(6043):765-9.
4. Liu F*, Zhao X*, **Perna F** et al. JAK2V617F-Mediated Phosphorylation of PRMT5 Downregulates Its Methyltransferase Activity and Promotes Myeloproliferation. *Cancer Cell*. 2011 Feb 15;19(2):283-94.*These authors contribute equally to this work
5. Moran-Crusio K, Reavie L, Shih A, Abdel-Wahab O, Ndiaye-Lobry D, Lobry C, Figueroa M, Vasanthakumar A, Patel J, Zhao X, **Perna F** et al. Tet2 loss leads to increased hematopoietic stem cell self-renewal and myeloid transformation. *Cancer Cell* 2011 Jul 12;20(1):11-24.
6. Moulik K, Ahn J, Zong H, Rodina A, Cerchietti L, DaGama E, Cladas-Lopes E, Beebe K, **Perna F** et al. A small molecule Hsp90 inhibitor provides a global overview of proteome alterations in cancer. *Nature Chemical Biology* 2011 Sep 25. doi: 10.1038/nchembio.670.
7. **Perna F**, Gurvich N, Hoya-Arias R et al. Depletion of L3MBTL1 promotes the erythroid differentiation of human hematopoietic progenitor cells: possible role in 20q- polycythemia vera. *Blood*. 2010 Oct 14;116(15):2812-21.
8. **Perna F**, Abdel-Wahab O, Levine RL et al. ETV6-ABL1-positive "chronic myeloid leukemia": clinical and molecular response to tyrosine kinase inhibition. *Haematologica*. 2011 Feb;96(2):342-3.
9. Gurvich N, **Perna F**, Farina A et al. L3MBTL1 polycomb protein, a candidate tumor suppressor in del(20q12) myeloid disorders, is essential for genome stability. *Proc Natl Acad Sci U S A*. 2010 Dec 28;107(52):22552-7.
10. Hoya-Arias R, Tomishima M, **Perna F** et al. L3MBTL1 deficiency directs the differentiation of human embryonic stem cells towards trophectoderm. *Stem Cells Dev*. 2011 Apr 3
11. Battipaglia G, Avilia S, Morelli E, Caranci F, **Perna F** et al. Posterior reversible encephalopathy syndrome (PRES) during induction chemotherapy for acute myeloblastic leukemia (AML). *Ann Hematol*. 2012 Jan 13.
12. Risitano A, **Perna F**. Aplastic Anemia: Immunosuppressive therapy in 2010. *Pediatr Rep*. 2011 Jun 22;3 Suppl 2:e7.
13. Risitano AM, **Perna F** and Selleri C. Achievements and Limitations of Complement Inhibition by Eculizumab in Paroxysmal Nocturnal Hemoglobinuria: The Role of Complement Component 3. *Mini Rev Med Chem* 2011 Jun 1;11(6):528-35.
14. Strianese D, Tranfa F, Finelli M, De Renzo A, Stabaino S, Schiemer R, Cardone D, Pacelli R, **Perna F** et al. Hepatitis C Virus Infection in Ocular Adnexal Lymphomas. *Arch Ophthalmol*. 2010 Oct;128(10):1295-9.
15. Storto G, De Renzo A, Pellegrino T, **Perna F** et al. Assessment of Metabolic Response to Radioimmunotherapy with 90Y-Ibritumomab Tiuxetan in Patients with Relapsed or Refractory B-Cell Non-Hodgkin Lymphoma. *Radiology* 2010 Jan; 254(1):245-52.

MEF Promotes Stemness in the Pathogenesis of Gliomas

Elena Bazzoli,^{1,2,3,5,9} Teodoro Pulvirenti,⁴ Moritz C. Oberstadt,^{1,2,10} Fabiana Perna,⁵ Boyoung Wee,^{1,2} Nikolaus Schultz,⁶ Jason T. Huse,^{2,7} Elena I. Fomchenko,^{1,2} Francesca Voza,⁵ Viviane Tabar,⁸ Cameron W. Brennan,^{2,8} Lisa M. DeAngelis,^{2,3} Stephen D. Nimer,^{2,5} Eric C. Holland,^{1,2,8,*} and Massimo Squatrito^{1,2,11,*}

¹Cancer Biology and Genetics Program

²Brain Tumor Center

³Department of Neurology

⁴Cell Biology Program

⁵Molecular Pharmacology and Chemistry Program

⁶Computational Biology Program

⁷Department of Pathology

⁸Department of Neurosurgery

Memorial Sloan Kettering Cancer Center, New York, NY 10021, USA

⁹Department of Neurological, Neuropsychological, Morphological and Motor Sciences, Azienda Ospedaliera Universitaria Integrata, 37134 Verona, Italy

¹⁰Department of Pharmacology, Ernst-Moritz-Arndt University of Greifswald, 17487 Greifswald, Germany

¹¹Present address: FSB Brain Tumor Group, F-BBVA Cancer Cell Biology Programme, Centro Nacional de Investigaciones Oncológicas (CNIO), Melchor Fernández Almagro 3, Madrid E-28029, Spain

*Correspondence: hollande@mskcc.org (E.C.H.), msquatrito@cnio.es (M.S.)

<http://dx.doi.org/10.1016/j.stem.2012.09.012>

SUMMARY

High-grade gliomas are aggressive and uniformly fatal tumors, composed of a heterogeneous population of cells that include many with stem-cell-like properties. The acquisition of stem-like traits might contribute to glioma initiation, growth, and recurrence. Here we investigated the role of the transcription factor myeloid Elf-1 like factor (MEF, also known as ELF4) in gliomas. We found that MEF is highly expressed in both human and mouse glioblastomas and its absence impairs gliomagenesis in a PDGF-driven glioma mouse model. We show that modulation of MEF levels in both mouse neural stem cells and human glioblastoma cells has a significant impact on neurosphere formation. Moreover, we identify Sox2 as a direct downstream target of MEF. Taken together, our studies implicate MEF as a previously unrecognized gatekeeper gene in gliomagenesis that promotes stem cell characteristics through Sox2 activation.

INTRODUCTION

Malignant gliomas represent the most prevalent primary brain tumor in adults and inevitably have a poor prognosis. Despite the implementation of new therapeutic strategies, the median survival of patients with Glioblastoma multiforme (GBM), the most aggressive glioma variant, is only 14–16 months and these tumors remain rapidly and uniformly fatal (Wen and Kesari, 2008).

GBMs are very heterogeneous tumors that contain both neoplastic and nonneoplastic cells, including endothelial, stromal, and inflammatory cells (Charles et al., 2011). A fraction of cells within the tumor, identified as glioma stem-like cells (GSCs), share some common features with normal neural stem cells (NSCs); they are multipotent and have the property of self-renewal. These cells may either derive from adult undifferentiated stem and progenitor cells or could acquire stem-like properties as a result of the genetic alterations that promote the tumorigenic process (Holmberg et al., 2011). When implanted into the brain of immunodeficient animals, these GSCs are capable of generating new tumors at high efficiency (Galli et al., 2004). Moreover, GSCs are remarkably resistant to the chemotherapy and radiotherapy (Dean et al., 2005) used as standard first-line treatment of patients with malignant gliomas. Indeed, acquisition of stem-like characteristics likely contributes to the malignant nature of high-grade gliomas and may be responsible for the initiation, growth, and recurrence of these tumors.

Myeloid Elf-1 like factor (MEF, also known as ELF4) is a member of the ETS family of transcription factors, which contains over 30 family members. Several ETS proteins can function as oncogenes and show aberrant expression in solid tumors as well as in hematological malignancies (Sashida et al., 2010). While MEF has been proposed to function as a tumor suppressor gene in some contexts, it could contribute to tumor formation in mice as well as in humans (Mikkers et al., 2002) (Sashida et al., 2010). Insight into its mechanism of action has come from studies done in fibroblasts demonstrating MEF's ability to induce transformation by stimulating Mdm2 expression, thereby downregulating p53-dependent responses, and by inhibiting activation of Ink4a, thereby allowing unrestrained phosphorylation of the retinoblastoma (Rb) protein (Sashida et al., 2009). Some of the ETS proteins are known to play

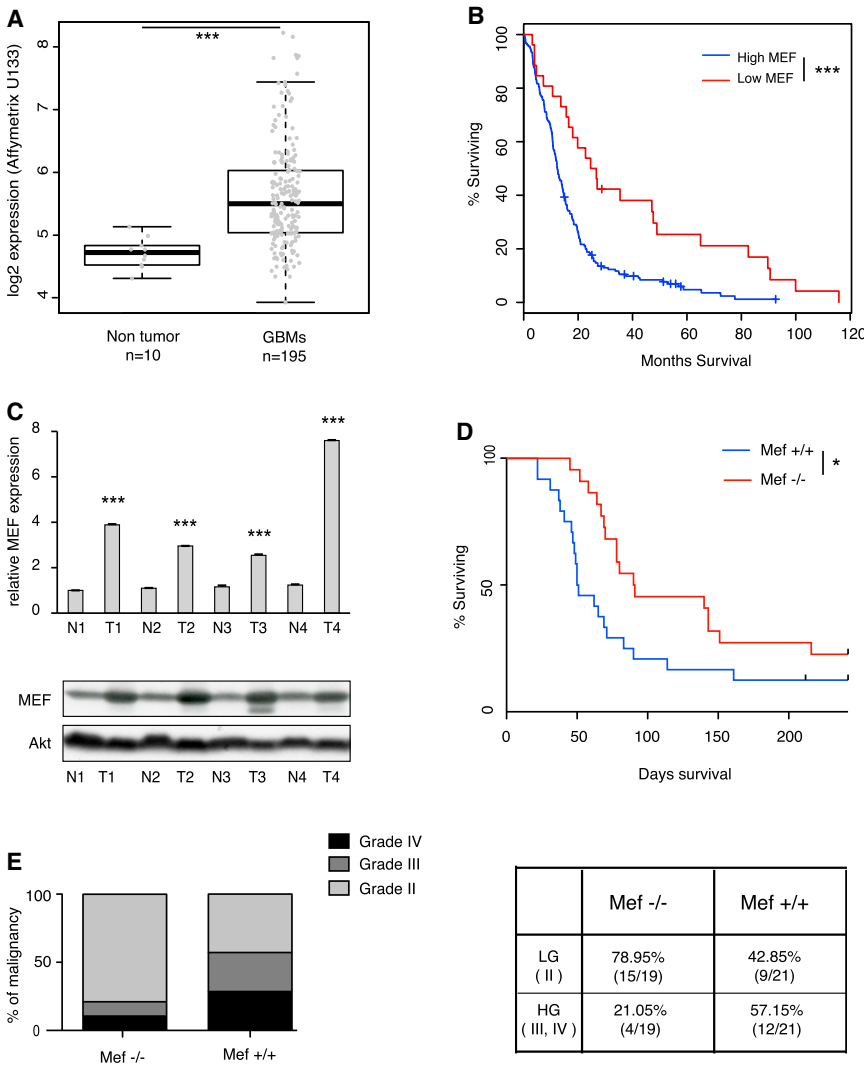


Figure 1. MEF in Human and Mouse Gliomas

(A) MEF expression in the TCGA data set obtained from human GBM samples (n = 195) and nontumor brain tissue (n = 10) (**p = 2.366e⁻⁰⁹, Student's t test).

(B) Kaplan Meier survival curves of TCGA GBM patients: low level of MEF (calculated as less than one standard deviation from the mean of diploid tumors) significantly correlates with better overall survival (***)log-rank p value, p = 0.000386).

(C) Top panel: MEF mRNA level detected by RT-PCR is higher in PDGF-driven mouse GBMs (T) compared to normal tissue (N). Data are normalized to GAPDH expression. Results are presented as mean ± SD (***)p < 0.0001, Student's t test). Bottom panel: western blot showing that MEF protein level is higher in PDGF-driven mouse GBMs compared to normal tissue.

(D) Kaplan Meier survival curves of PDGF gliomas generated in Ntv-a *Mef*^{+/+} versus *Mef*^{-/-} mice. MEF loss increases overall survival and reduces gliomagenesis (log-rank p value, *p = 0.02).

(E) Left panel: mouse gliomas lacking MEF show significantly lower percentage of high-grade tumors versus low-grade tumors (Fisher's exact test, *p = 0.027); right panel: contingency table presenting the number of high-grade (HG) tumors versus low-grade (LG) tumors in the two different genetic backgrounds.

See also Figure S1.

a role in brain tumors (Uht et al., 2007), though so far no published data are available regarding the role of MEF in normal brain or in brain tumor biology. Here we show that MEF is highly expressed in GBMs and it contributes to gliomagenesis by promoting stem cell traits through direct activation of Sox2 expression.

RESULTS

MEF Is Highly Expressed in Human Gliomas and Its Loss Impairs Glioma Formation in Mice

GBM represents a heterogeneous disease and recent genomic analyses have quantified the expression level of a wide variety of genes (Cancer Genome Atlas Research Network, 2008). We analyzed the data set from The Cancer Genome Atlas (TCGA) for GBMs and found MEF expression significantly elevated in the tumor samples (n = 195) as compared to nontumor brain tissue (n = 10) (p < 0.0001; Student's t test) (Figure 1A and Table S1 available online), without evidence for amplification at the genomic level. Because MEF has previously been shown to block the p53 pathway, we examined the p53 status of these

tumors and found no correlation between MEF expression levels and p53 mutation or deletion, suggesting that MEF may function in a p53-independent manner in glioma (Figure S1A available online). A search conducted in the Oncomine website (<https://www.oncomine.org/>) revealed that in the Sun data set (Sun et al., 2006), which includes 81 human GBMs (grade IV), 25 anaplastic astrocytomas (grade III), and 50 oligodendrogliomas (grade II), MEF expression is significantly higher in GBMs than in lower grade gliomas (p < 0.0001) (Figure S1B). To confirm these data we analyzed MEF expression by qPCR in 25 human glioma surgical samples from Memorial Sloan-Kettering Cancer Center (MSKCC) (six oligodendrogliomas, seven anaplastic oligodendrogliomas, two anaplastic astrocytomas, and ten glioblastomas) and found that MEF is significantly elevated in high-grade versus low-grade gliomas (p = 0.02, Student's t test) (Figure S1C). However, this difference might reflect a lower ratio of tumor cells versus nontumor cells in the low-grade samples.

Lower levels of MEF were associated with a better prognosis in a small cohort of acute myeloid leukemia patients (Fukushima et al., 2003). We examined the TCGA GBM patient survival data and found that low levels of MEF significantly correlated with better overall survival in GBMs as well (log rank test, p = 0.0008; Figure 1B). Gene expression profiling studies have identified four molecular subclasses of GBMs based on transcriptional signatures: Classical, Mesenchymal, Proneural and Neural. Each of these subtypes has been associated with

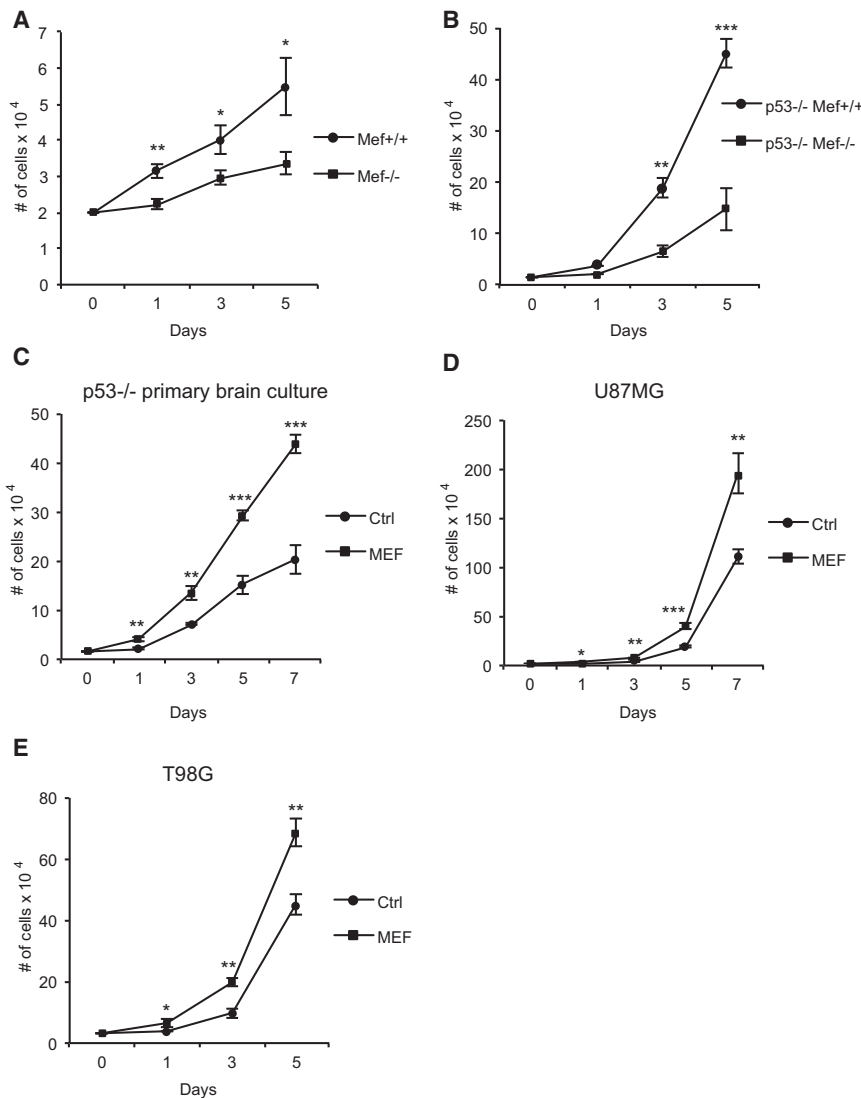


Figure 2. Mef Promotes Proliferation of both Primary Brain Cultures and Human Glioma Cell Lines

(A and B) Growth curve of primary brain cultures derived from *Mef*^{-/-}, *Mef*^{+/+} (A) and *p53*^{-/-}/*Mef*^{+/+}, *p53*^{-/-}/*Mef*^{-/-} (B) newborn mice.

(C–E) Growth curve of primary brain cells derived from *p53*^{-/-} newborn mice (C) and human U87MG and T98G glioma cell lines (D and E).

Results are presented as mean ± SD from a representative of three experiments performed in triplicate. **p* < 0.05; ***p* < 0.001; ****p* < 0.0001 (Student's *t* test). See also Figure S2.

Ink4a/Arf null background, in which PDGF is able to uniformly generate high-grade gliomas that share hallmark histological features with human GBMs (Dai et al., 2001). Using qPCR and Western blot analysis, we found higher levels of MEF mRNA and protein in these tumors as compared to the contralateral normal brain tissues (Figure 1C).

Next, to determine if lack of MEF impacts on PDGF-induced gliomagenesis, *Mef*^{-/-} mice were crossed with *Ntv-a* mice (which carry a wild-type Ink4a/Arf locus) to generate *Ntv-a Mef*^{+/+} and *Ntv-a Mef*^{-/-} mice. A survival analysis of the two cohorts revealed that loss of MEF significantly impaired PDGF-induced glioma formation, with MEF null mice living an average of 129 days (*n* = 22) and wild-type mice living 59 days (*n* = 24) (*p* < 0.02, log rank test) (Figure 1D). The tumors were then scored and graded by histological features (see Experimental Procedures

specific signaling alterations, such as EGFR, Ras, and PDGFR pathway activation, respectively (Verhaak et al., 2010). When the patients were stratified according to GBM subtypes, the Proneural subclass showed the lowest level of MEF expression (Figure S1D) and, within this subtype, lower levels of MEF also correlated with better overall survival (Figure S1E). When we looked at the IDH1 status, we found that the tumors with the lowest MEF levels within the Proneural group were predominantly IDH1 mutant tumors, whereas IDH1 wild-type Proneural tumors had a range of MEF levels similar to the other tumor types (data not shown).

To determine whether MEF plays an active role in gliomagenesis, we used the RCAS/PDGF mouse glioma model, which closely resembles the human Proneural GBM subtype. The RCAS/*tv-a* system utilizes avian leukosis virus based vectors (RCAS) to mediate gene transfer into somatic cells, engineered to be transgenic for its receptor (*tv-a*). Specifically, we used Nestin *tv-a* (*Ntv-a*) mice, where the *tv-a* receptor is under the control of the Nestin promoter, a well-known marker of progenitor and neural/gliial cells. First, we evaluated MEF expression in an

for details). Tumors lacking MEF showed less aggressive features, with significantly fewer high-grade gliomas (*p* = 0.02, Fisher's exact test) (Figure 1E). Thus, MEF can affect both glioma formation and progression.

MEF Promotes Proliferation of both Mouse Primary Brain Cultures and Human Glioma Cell Lines

As MEF has been shown to promote the transition of cells from G1 to S (Liu et al., 2006; Sashida et al., 2009) we evaluated its effect on proliferation, using both mouse primary brain cultures and human glioma cell lines. The primary cultures were generated from the whole brain of newborn pups, and to investigate potential p53-independent effects, we used cells from *Mef*^{+/+} and *Mef*^{-/-} mice and also from *p53*^{-/-}/*Mef*^{+/+} and *p53*^{-/-}/*Mef*^{-/-} mice. Cells lacking MEF grew more slowly than the control cells (Figures 2A and 2B), while its overexpression in *p53*^{-/-} cells (Figure S2A) increased proliferation (Figure 2C). Similarly, the overexpression of MEF in the human U87MG and T98G glioma cell lines (Figures S2B and S2C) resulted in higher rates of cell proliferation (Figures 2D and 2E).

These data confirm the role of MEF in promoting the growth of both mouse primary brain cultures and human glioma cell lines.

MEF Promotes Stem Cell Characteristics in Mouse NSCs and Human Glioma Cell Lines

In recent years, an increasing number of studies have investigated the connection between malignancy and “stemness,” focusing on how stem/progenitor cells, as well as neoplastic cells, change their properties during the process of malignant transformation. Several transcription factors are known to induce pluripotent stem cells from differentiated cells, as well as to maintain multipotency of NSCs (Patel and Yang, 2010). Because MEF contributes to glioma formation and aggressiveness in vivo, we explored the possible role of MEF in promoting stem cell characteristics.

NSCs and GSCs can be grown as spheres in culture, in the absence of serum but in the presence of basic fibroblast growth factor (bFGF) and epidermal growth factor (EGF). Although sphere-forming assays cannot be considered an exact readout of in vivo stem cell activity, they are useful to measure the in vitro potential of cells to exhibit stem-cell-like traits (Pastrana et al., 2011); therefore, we investigated whether MEF could influence the formation of neurospheres.

Freshly isolated *Mef*^{-/-} and *Mef*^{+/+} cells from postnatal non-neoplastic brains were plated at different cell densities (10, 5, and 1 cells/ μ l) in 24-well plates and grown in neurosphere medium for 2 weeks to allow the generation of neurospheres. We then performed serial passages over the course of 8 weeks, generating secondary, tertiary, and quaternary spheres. Spheres were mechanically dissociated every 2 weeks, and at each passage, sphere number was assessed. We found that at a density of 1 cell/ μ l, lack of MEF significantly decreased generation of secondary, tertiary, and quaternary neurospheres (Student's t test, $p < 0.0001$, at each passage) (Figure 3A). Similar results were obtained at higher cell concentrations (5 and 10 cells/ μ l) (Figure S3A). Moreover, cells lacking MEF underwent morphological changes over time, with some of them becoming attached to the bottom of the wells and presenting short elongation processes (Figure S3B). To understand whether the decreased sphere forming ability seen in *Mef*^{-/-} cells was accompanied by increased differentiation, we grew cells from dissociated spheres in 5% serum medium without FGF and EGF to evaluate their differentiation potential. Phase contrast images revealed clear differences in the morphology of the *Mef*^{+/+} and *Mef*^{-/-} cells, suggesting that differentiation is more profound in cells lacking MEF (Figure 3B). Immunofluorescence staining showed a significant reduction in Nestin⁺ cells ($p = 0.0006$), together with a significant increase in both Olig2 and GFAP⁺ cells ($p < 0.0001$ and $p = 0.0481$, respectively, Student's t test) in *Mef*^{-/-} cells (Figures 3C and 3D). These differences were detected also by Western blot analysis (Figure 3E). Interestingly, most of the GFAP-positive *Mef*^{-/-} cells showed the stellate morphology typical of astrocytes and a brighter signal, which was confirmed by increased GFAP protein levels measured by Western blot (Figure 3E). We failed to detect Tuj-1⁺ cells in three of the four *Mef*^{-/-} samples, while an average of 14.4% Tuj-1⁺ cells was found in four different *Mef*^{+/+} samples (data not shown), which suggests that MEF might also contribute to differentiation toward the neuronal lineage.

To determine whether lack of MEF could influence the stem cell potential under more strict conditions, we generated primary cell cultures obtained from the whole brain of newborn pups, forced them to grow in serum for two passages, and switched them to neurosphere medium. To evaluate possible p53-independent effects, primary brain cultures were isolated from different genetic backgrounds (*Mef*^{+/+}, *Mef*^{-/-}, *p53*^{-/-}/*Mef*^{+/+}, and *p53*^{-/-}/*Mef*^{-/-}). Four days after the switch to neurosphere medium, cells lacking MEF failed to form spheres, while both the *Mef*^{+/+} and the *p53*^{-/-}/*Mef*^{+/+} cells were able to do so ($p = 0.0003$ and $p = 0.0001$, respectively, Student's t test) (Figure 3F). The impaired neurosphere formation of the *p53*^{-/-}/*Mef*^{-/-} cells could be rescued by MEF re-expression ($p = 0.00145$, Student's t test) (Figure 3G and Figure S3C).

We then investigated whether MEF overexpression could induce reprogramming signals under the same strict conditions, influencing the sphere-forming ability of different primary and glioma cells. We first overexpressed MEF in primary brain cultures obtained from p53 null pups, using retroviral vectors (Figure S2A). After antibiotic selection, the cells were grown in serum for two passages and then switched to neurosphere medium. We found that cells overexpressing MEF formed more neurospheres than the control cells ($p = 0.0012$ at 24 hr, $p = 0.0017$ at 72 hr; Student's t test) (Figure 3H). Similar differences upon MEF overexpression were observed in the U87MG and T98G human glioma cell lines ($p < 0.0001$ and $p < 0.0001$, respectively, Student's t test) (Figure 3I).

Lastly, we evaluated the impact of MEF on stem-like properties using human primary GSCs, with various genetic profiles. Tumor samples, isolated from patients suffering from GBMs and undergoing surgery at MSKCC, were dissociated and initially grown in neurosphere medium as a monolayer on plastic cell culture dishes coated with 10 ng/ml laminin. Specifically, we used the following cells: GBM1 (++)*PDGFRA*, +*EGFR*, *MET*, *CDK6*, -*PTEN*, -*CDKN2A*), GBM3 (++)*EGFR*, +*MET*, *CDK6*, -*CDKN2A*, *PTEN*, carrying *EGFR**III* mutation), and GBM543 (++)*PDGFRA*, ++*CDK4*, +(*EGFR*, *MET*, *CDK6*), -*PTEN*) (Ozawa et al., 2010; Pulvirenti et al., 2011). Using lentiviral vectors to express shRNAs, we silenced MEF expression (Figure S3D) and found that decreased MEF levels lead to a significant decrease in neurosphere formation in all of these three GSC lines ($p < 0.0001$ for both shRNA#1 and shRNA#2), as compared to nontargeting shRNA control (Figure 3J). Moreover, when we performed limiting dilution neurosphere assays, we confirmed that MEF knockdown leads to a reduced frequency of sphere-forming cells ($p < 0.0001$ for both shRNAs in each GSC line, ELDA software) (Figure 3K).

Taken together, these data suggest a role for MEF in promoting stem-cell-like features in both primary brain cultures and glioma cell lines.

Sox2 Gene Is a Direct Target of MEF and Rescues Sphere-Forming Ability in MEF-Defective Cells

To investigate possible mechanisms behind the ability of MEF to promote stem-cell traits, we measured the expression level of several genes related to pluripotency, including Sox2, Oct4, Nanog, Klf4, Hes1, and Hey1, in MEF-transduced *p53*^{-/-} primary brain cells. Among these genes, we found that Sox2 and Oct4 expression was significantly increased by MEF. We

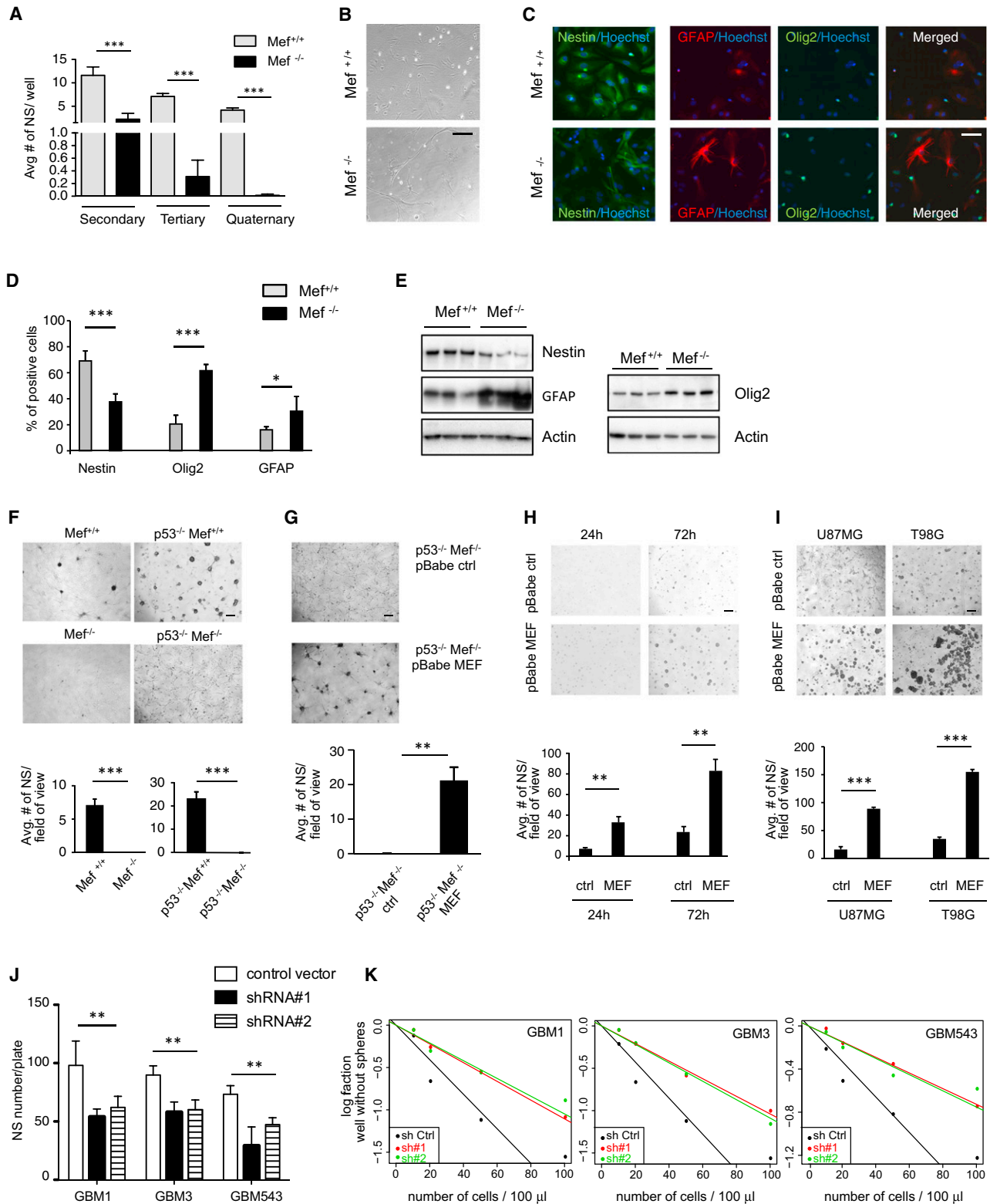


Figure 3. MEF Promotes Stem Cell Traits of both Primary Brain Cultures and Glioma Cell Lines

(A) Neurospheres isolated from newborn pups, with *Mef*^{+/+} and *Mef*^{-/-} genetic background, respectively: MEF loss led to impaired neurosphere formation after serial passages.

(B) Phase contrast images showing morphological changes between *Mef*^{+/+} and *Mef*^{-/-} brain cells grown in 5% serum, without bFGF and EGF, for 5 days to favor differentiation.

observed a 3.6-fold increase in Sox2 gene expression and a 3-fold increase in Oct4 expression level ($p = 0.02$ and $p = 0.013$, respectively, Student's *t* test) (Figure 4A). Similarly, in U87MG and T98G cells, MEF induced a 2.1 ($p = 0.017$) and 1.6 ($p = 0.018$)-fold increase in Sox2 levels and a 1.8 ($p = 0.0025$) and 1.6 ($p = 0.0199$)-fold increase in Oct4 levels (Figure 4B).

The Sox2 promoter is known to contain ETS binding sites (Wiebe et al., 2000), though they have not been identified in the Oct4 promoter; therefore, we focused on Sox2 as a possible direct downstream target of MEF. We analyzed Sox2 expression in *Mef*^{+/+} versus *Mef*^{-/-} and *p53*^{-/-}/*Mef*^{+/+} versus *p53*^{-/-}/*Mef*^{-/-} primary brain cells and found a significant reduction in Sox2 levels in the absence of MEF ($p < 0.0001$, Student's *t* test) (Figures 4C and 4D). To exclude the possibility that developmental adaptation to the lack of MEF resulted in decreased Sox2 expression, we acutely knocked down MEF in p53 null primary brain cultures (~60%) and found a significant reduction in Sox2 expression ($p = 0.015$ and $p = 0.0059$, respectively, Student's *t* test) (Figure 4E). Thus, both the acute loss and chronic absence of MEF substantially decreases Sox2 expression.

To test whether MEF can activate the Sox2 promoter, we transiently transfected a Sox2 promoter-driven luciferase reporter plasmid (Kuwabara et al., 2004) into p53 null primary brain cells, together with MEF or an empty vector control. As shown in Figure 4F, MEF induced a greater than 3-fold increase in luciferase activity from the Sox2 promoter ($p < 0.0001$, Student's *t* test) while having no effect on Hes1 promoter-driven luciferase activity. We also investigated whether MEF activates the Sox2 promoter in human glioma cell lines and found a similar upregulation ($p < 0.0001$, Student's *t* test) (Figures 4G and 4H).

Having identified Sox2 as a transcriptional target of MEF, we investigated whether Sox2 overexpression could rescue the decrease in neurosphere formation seen in cells lacking MEF. We overexpressed Sox2 in *p53*^{-/-}/*Mef*^{-/-} primary brain cultures (Figure S4B) and grew them in neurosphere conditions. The absence of neurospheres seen in cells lacking MEF was rescued by Sox2 overexpression ($p = 0.00018$, Student's *t* test), indicating that Sox2 acts downstream of MEF to promote neurosphere formation (Figure 4I).

To confirm that Sox2 gene regulation by MEF was direct, we performed Chromatin Immunoprecipitation (ChIP) assays using T98G glioma cells that were transduced with a pBabe retroviral

vector expressing a FLAG-tagged MEF cDNA or a control vector. Using an anti-FLAG ChIP assay, we found that in human glioma cells, MEF protein is recruited to specific regions of the Sox2 gene (which covered -1.964, -1.672, and -1.324 kb from the transcription starting site [TSS]; *p* values: 0.0009, 0.003, 0.0008, respectively). No direct binding was observed at the farthest region (-3.841 kb) (Figure 4J).

DISCUSSION

The regulation of stemness is of interest to many disciplines, including developmental biology, regenerative medicine, degenerative disease, and cancer. Normal stem cells are known to play critical roles in tissue development, differentiation, and organogenesis (Vierbuchen et al., 2010). Several transcription factors, such as Notch, Id1, Sox2, Oct4, and others, have been reported to control different aspects of stemness, influencing the delicate balance between stem cell maintenance and the promotion of stem cell differentiation. In recent years, many studies have shown that genes involved in normal stem cell biology also play a relevant role in tumorigenesis (Nam and Ben-zra, 2009) (Venere et al., 2011).

Malignant gliomas are highly aggressive cancers composed of a heterogeneous cell population, a fraction of which exhibits stem-like characteristics (Vescovi et al., 2006). Whether GSCs arise from normal NSCs or from neoplastic cells that have acquired stem cell traits is still unclear; however, it has been proposed that the acquisition of stem cell characteristics through the activation of stem cell gene signatures can confer malignant potential to gliomas (Holmberg et al., 2011).

We have shown that MEF, a member of the ETS family of transcription factors, contributes to gliomagenesis and promotes stem-like characteristics. MEF is highly expressed in both human and mouse GBMs, and GBM patients with low levels of MEF show a significantly better overall survival. This finding was replicated in the RCAS/PDGFR model where gliomas that lack MEF had less aggressive histological features and better overall survival.

Genes overexpressed in cancer can affect many different biological processes including growth, stress response, block of apoptosis, and stemness. Uncontrolled proliferation is a key aspect of cancer cell behavior and we found that MEF promotes the proliferation of both mouse primary brain cultures and human glioma cell lines, contributing to the pathogenesis of gliomas.

(C and D) Immunofluorescence staining and quantification of *Mef*^{+/+} and *Mef*^{-/-} brain cells grown in the above condition to favor differentiation. Positive staining is quantified as percentages of total Hoechst+ cells per image (10 fields of images were taken from four different cell lines for each genotype, *Mef*^{-/-} and *Mef*^{+/+}); scale bars indicate 50 μ m.

(E) Western blot comparing *Mef*^{-/-} to *Mef*^{+/+} brain cells: lack of MEF lead to decreased Nestin and increased Olig2 and GFAP protein levels.

(F) *Mef*^{+/+}, *Mef*^{-/-}, *p53*^{-/-}/*Mef*^{+/+}, and *p53*^{-/-}/*Mef*^{-/-} primary brain cultures grown in neurosphere conditions. Scale bars indicate 100 μ m.

(G) Re-expression of MEF in *p53*^{-/-}/*Mef*^{-/-} cells rescues their ability to form neurospheres when cultured in neurosphere conditions.

(H) Micrograph showing *p53*^{-/-} primary brain cells transfected with pBabe-empty and pBabe-MEF retroviral vectors, cultured in neurosphere conditions. Bar graphs on the bottom show average neurosphere number per field of view.

(I) MEF overexpressing human U87MG and T98G cell lines, cultured in neurosphere conditions, form more neurospheres compared to control. Bar graphs on the bottom show average neurosphere number per field of view.

(J) Graph bar showing decreased neurosphere formation after MEF knockdown in patient-derived human primary GBMs (GBM1, GBM3, and GBM543).

(K) Graph representing limiting dilution neurosphere assays in patient-derived human primary GBMs (GBM1, GBM3, and GBM543) infected with pGipz control vector and pGipz MEF shRNAs #1 and #2.

Results are presented as mean \pm SD from a representative of three experiments performed in triplicate, unless otherwise specified. * $p < 0.05$; ** $p < 0.005$; *** $p < 0.0001$ (Student's *t* test). See also Figure S3.

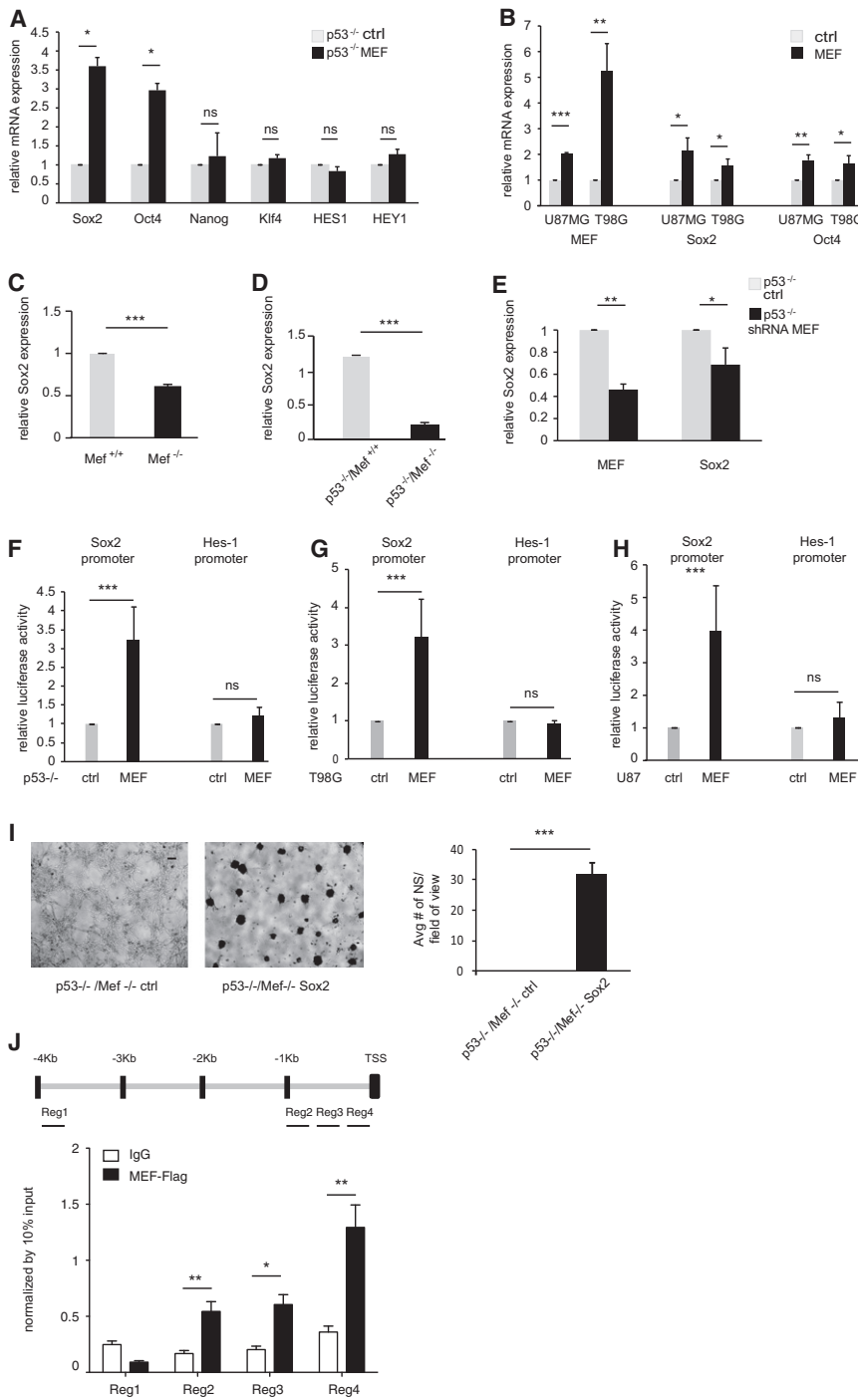


Figure 4. Sox2 Gene Is Regulated by MEF

(A and B) MEF overexpression in *p53*^{-/-} primary brain cells as well as in U87MG and T98G human glioma cell lines led to increased Sox2 expression. Data are normalized to GAPDH expression. (C and D) Lack of MEF decreases Sox2 expression. Data are normalized to GAPDH expression. (E) Acute knockdown of MEF in *p53*^{-/-} primary brain cells led to decreased Sox2 expression. Data are normalized to GAPDH expression. (F–H) Dual luciferase assays showing that MEF activates Sox2 promoter in *p53*^{-/-} primary brain cells as well as T98G and U87MG human glioma cell lines. (I) Sox2 overexpression in *p53*^{-/-}*Mef*^{-/-} primary brain cultures grown in neurosphere conditions rescues their ability to form neurospheres. Scale bar indicates 100 μ m. Bar graph shows average neurosphere number per field of view. (J) ChIP experiments were performed on T98G glioma cells using antibody to Flag. Plotted values are relative enrichments (y axis) to 10% input and measured for sites in the Sox2 promoter (x axis). Antibody against IgG was used as a nonspecific control. Results are presented as mean \pm SD from a representative of three experiments performed in triplicate. **p* < 0.05; ***p* < 0.001; ****p* < 0.0001 (Student's *t* test). See also Figure S4.

which might reflect changes in the stem cell signature of both neoplastic and non-neoplastic cells.

We have further implicated MEF in promoting stem cell traits through direct activation of Sox2 expression. The HMG-box transcription factor Sox2 is known to play an important role in maintaining stem cell self-renewal within the central nervous system (CNS) and this activity is present in gliomas as well (Pevny and Nicolis, 2010). Sox2 has been described to act as an oncogene in different human cancers including gliomas. While the role of Sox2 in normal brain and glioma cells has been well documented, the transcription factors that activate its expression in these contexts are less clear (Denysenko et al., 2010; Ikushima et al., 2009). We identified Sox2 as a direct target of MEF in mouse primary brain cells and human glioma cell lines, because both acute

and chronic modulation of MEF levels affected Sox2 gene expression and promoter activation. MEF directly binds to Sox2 promoter in T98G glioma cells. We observed that overexpression of Sox2 in *p53*^{-/-}*Mef*^{-/-} cells was sufficient to rescue the impaired ability of these cells to form neurospheres. Thus, our data suggest that Sox2 is downstream of MEF and may be responsible for its ability to modulate stem-like characteristics.

Given the cellular heterogeneity and molecular complexity of gliomas, it is unclear in which contexts the stem cell property

of self-renewal might represent a feature associated with increased tumorigenic potential (Barrett et al., 2012). Additionally, the so called “glioma stem-like cells” within different tumors may vary in terms of proliferation rates, which might impact their aggressiveness regardless of their self-renewal properties. To date, it is often difficult to distinguish between the contributions of proliferation versus self-renewal to the process of gliomagenesis; nonetheless, self-renewal inevitably entails proliferative events. Adding to the intricacy, acquisition of reprogramming signals generated by alterations in specific genes or pathways (Notch, Id1, Sox2, Oct4, etc.) might differentially impact on these two diverse aspects.

Our work defines the role of MEF in promoting stem cell features in both primary mouse brain cells and human glioblastoma cells via direct regulation of Sox2 expression, providing insights into the multifaceted regulation of stemness. Further work is necessary to better define the MEF/Sox2-mediated acquisition of stem cell traits and whether it modulates the response to chemotherapy and radiotherapy.

EXPERIMENTAL PROCEDURES

TCGA Analysis

TCGA data was downloaded from the TCGA Data Portal (<https://tcga-data.nci.nih.gov/>) or the cBio Cancer Genomics Portal (Cerami et al., 2012) (<http://cbioportal.org/>). Subtype information was retrieved from Verhaak et al. (2010). Low MEF expression in the TCGA data set was defined using the median expression data (median of three platforms, see Verhaak et al., 2010) as one standard deviation lower than the mean of all tumors. All other analyses were performed using data from the Affymetrix U133 microarray platform. Expression data was available for 195 tumors and 10 normal brain samples (Table S1).

Generation of Primary Brain Cultures and Primary Brain Neurosphere and Neurosphere Formation Assay

The *Mef*^{+/+}, *Mef*^{-/-}, *p53*^{-/-}, and *p53*^{-/-}*Mef*^{-/-} primary brain cultures were prepared with mechanical dissociation of the whole brain from newborn mice. The cells were then filtered through a 70 μm Nylon strainer and plated in 10 cm culture dishes (with the procedure derived with minor modifications from a previously described experimental method) (Dai et al., 2001). Mouse primary brain cultures, as well as T98G and U87MG human glioma cell lines, were plated at 20 cells/μl in neurosphere medium. Mouse primary brain neurospheres were isolated as previously described (Bleau et al., 2009) and plated at different concentrations (10, 5, and 1 cell/μl). Human primary glioblastoma neurospheres were freshly isolated from patients suffering from GBMs and undergoing surgery at MSKCC. Primary GBM samples were dissociated, plated at different concentrations (1, 0.5, 0.2, and 0.1 cells/μl) and grown in neurosphere medium. Neurosphere medium consisted of NSC Basal Medium, NSC proliferation supplements, 10 ng/ml EGF, 20 ng/ml basic-FGF, and 1 mg/ml Heparin (Stem Cell Technologies, Vancouver, Canada). Neurosphere number was established by counting the number of neurospheres per well or, for U87MG and T98G, by taking pictures of the central part of the plates and then counting the neurosphere number per field of view.

SUPPLEMENTAL INFORMATION

Supplemental Information for this article includes four figures, Supplemental Experimental Procedures, and one table and can be found with this article online at <http://dx.doi.org/10.1016/j.stem.2012.09.012>.

ACKNOWLEDGMENTS

We thank J. Finney and Q. Zhang for technical assistance. We extend thanks to Dr. L. Abrey as well as to all members of Dr. E. Holland's and Dr. S. Nimer's

laboratories for their helpful comments and suggestions. We sincerely thank Prof. F.H. Gage for providing the Sox2-promoter-driven luciferase construct, Dr. E.P. Papapetrou for providing the human pLM-YS SOX2 vector, and G. Sashida for providing the pBabe-Puro-lentivirus MEF vector and the pLKO.1-Puro-lentivirus vector containing mouse *Mef*-specific shRNA. This work was supported by a grant from National Brain Tumor Foundation, RO1-DK52208 grant (S.D.N.), and U54CA143798, UO1CA141502 and RO1CA100688 grants (E.C.H.). E.B. has been supported by Brain Tumor Center of Memorial Sloan-Kettering Cancer Center. M.C.O. has been supported by the Rottendorf Foundation, Ennigerloh, Germany, and the Gerhard Domagk Scholarship Program, Greifswald, Germany. This work is dedicated to the memory of Dr. Mark A. Zatzkis, a dear friend of S.D.N., who died of a GBM in 2007.

Received: October 6, 2011

Revised: July 2, 2012

Accepted: September 13, 2012

Published: December 7, 2012

REFERENCES

- Barrett, L.E., Granot, Z., Coker, C., Iavarone, A., Hambardzumyan, D., Holland, E.C., Nam, H.S., and Benezra, R. (2012). Self-renewal does not predict tumor growth potential in mouse models of high-grade glioma. *Cancer Cell* 21, 11–24.
- Bleau, A.M., Hambardzumyan, D., Ozawa, T., Fomchenko, E.I., Huse, J.T., Brennan, C.W., and Holland, E.C. (2009). PTEN/PI3K/Akt pathway regulates the side population phenotype and ABCG2 activity in glioma tumor stem-like cells. *Cell Stem Cell* 4, 226–235.
- Cancer Genome Atlas Research Network. (2008). Comprehensive genomic characterization defines human glioblastoma genes and core pathways. *Nature* 455, 1061–1068.
- Cerami, E., Gao, J., Dogrusoz, U., Gross, B.E., Sumer, S.O., Aksoy, B.A., Jacobsen, A., Byrne, C.J., Heuer, M.L., Larsson, E., et al. (2012). The cBio cancer genomics portal: an open platform for exploring multidimensional cancer genomics data. *Cancer Discov.* 2, 401–404.
- Charles, N.A., Holland, E.C., Gilbertson, R., Glass, R., and Kettenmann, H. (2011). The brain tumor microenvironment. *Glia* 59, 1169–1180.
- Dai, C., Celestino, J.C., Okada, Y., Louis, D.N., Fuller, G.N., and Holland, E.C. (2001). PDGF autocrine stimulation dedifferentiates cultured astrocytes and induces oligodendrogliomas and oligoastrocytomas from neural progenitors and astrocytes in vivo. *Genes Dev.* 15, 1913–1925.
- Dean, M., Fojo, T., and Bates, S. (2005). Tumour stem cells and drug resistance. *Nat. Rev. Cancer* 5, 275–284.
- Denysenko, T., Gennero, L., Roos, M.A., Melcarne, A., Juenemann, C., Faccani, G., Morra, I., Cavallo, G., Reguzzi, S., Pescarmona, G., and Ponzetto, A. (2010). Glioblastoma cancer stem cells: heterogeneity, microenvironment and related therapeutic strategies. *Cell Biochem. Funct.* 28, 343–351.
- Fukushima, T., Miyazaki, Y., Tsushima, H., Tsutsumi, C., Taguchi, J., Yoshida, S., Kuriyama, K., Scadden, D., Nimer, S., and Tomonaga, M. (2003). The level of MEF but not ELF-1 correlates with FAB subtype of acute myeloid leukemia and is low in good prognosis cases. *Leuk. Res.* 27, 387–392.
- Galli, R., Binda, E., Orfanelli, U., Cipelletti, B., Gritti, A., De Vitis, S., Fiocco, R., Foroni, C., Dimeco, F., and Vescovi, A. (2004). Isolation and characterization of tumorigenic, stem-like neural precursors from human glioblastoma. *Cancer Res.* 64, 7011–7021.
- Holmberg, J., He, X., Peredo, I., Orrego, A., Hesselager, G., Ericsson, C., Hovatta, O., Oba-Shinjo, S.M., Marie, S.K., Nistér, M., and Muhr, J. (2011). Activation of neural and pluripotent stem cell signatures correlates with increased malignancy in human glioma. *PLoS ONE* 6, e18454.
- Ikushima, H., Todo, T., Ino, Y., Takahashi, M., Miyazawa, K., and Miyazono, K. (2009). Autocrine TGF-beta signaling maintains tumorigenicity of glioma-initiating cells through Sry-related HMG-box factors. *Cell Stem Cell* 5, 504–514.

- Kuwabara, T., Hsieh, J., Nakashima, K., Taira, K., and Gage, F.H. (2004). A small modulatory dsRNA specifies the fate of adult neural stem cells. *Cell* 116, 779–793.
- Liu, G., Yuan, X., Zeng, Z., Tunici, P., Ng, H., Abdulkadir, I.R., Lu, L., Irvin, D., Black, K.L., and Yu, J.S. (2006). Analysis of gene expression and chemoresistance of CD133+ cancer stem cells in glioblastoma. *Mol. Cancer* 5, 67.
- Mikkers, H., Allen, J., Knipscheer, P., Romeijn, L., Hart, A., Vink, E., and Berns, A. (2002). High-throughput retroviral tagging to identify components of specific signaling pathways in cancer. *Nat. Genet.* 32, 153–159.
- Nam, H.S., and Benezra, R. (2009). High levels of Id1 expression define B1 type adult neural stem cells. *Cell Stem Cell* 5, 515–526.
- Ozawa, T., Brennan, C.W., Wang, L., Squatrito, M., Sasayama, T., Nakada, M., Huse, J.T., Pedraza, A., Utsuki, S., Yasui, Y., et al. (2010). PDGFRA gene rearrangements are frequent genetic events in PDGFRA-amplified glioblastomas. *Genes Dev.* 24, 2205–2218.
- Pastrana, E., Silva-Vargas, V., and Doetsch, F. (2011). Eyes wide open: a critical review of sphere-formation as an assay for stem cells. *Cell Stem Cell* 8, 486–498.
- Patel, M., and Yang, S. (2010). Advances in reprogramming somatic cells to induced pluripotent stem cells. *Stem Cell Rev.* 6, 367–380.
- Pevny, L.H., and Nicolis, S.K. (2010). Sox2 roles in neural stem cells. *Int. J. Biochem. Cell Biol.* 42, 421–424.
- Pulvirenti, T., Van Der Heijden, M., Droms, L.A., Huse, J.T., Tabar, V., and Hall, A. (2011). Dishevelled 2 signaling promotes self-renewal and tumorigenicity in human gliomas. *Cancer Res.* 71, 7280–7290.
- Sashida, G., Liu, Y., Elf, S., Miyata, Y., Ohyashiki, K., Izumi, M., Menendez, S., and Nimer, S.D. (2009). ELF4/MEF activates MDM2 expression and blocks oncogene-induced p16 activation to promote transformation. *Mol. Cell. Biol.* 29, 3687–3699.
- Sashida, G., Bazzoli, E., Menendez, S., Liu, Y., and Nimer, S.D. (2010). The oncogenic role of the ETS transcription factors MEF and ERG. *Cell Cycle* 9, 3457–3459.
- Sun, L., Hui, A.M., Su, Q., Vortmeyer, A., Kotliarov, Y., Pastorino, S., Passaniti, A., Menon, J., Walling, J., Bailey, R., et al. (2006). Neuronal and glioma-derived stem cell factor induces angiogenesis within the brain. *Cancer Cell* 9, 287–300.
- Uht, R.M., Amos, S., Martin, P.M., Riggan, A.E., and Hussaini, I.M. (2007). The protein kinase C-eta isoform induces proliferation in glioblastoma cell lines through an ERK/Elk-1 pathway. *Oncogene* 26, 2885–2893.
- Venere, M., Fine, H.A., Dirks, P.B., and Rich, J.N. (2011). Cancer stem cells in gliomas: identifying and understanding the apex cell in cancer's hierarchy. *Glia* 59, 1148–1154.
- Verhaak, R.G., Hoadley, K.A., Purdom, E., Wang, V., Qi, Y., Wilkerson, M.D., Miller, C.R., Ding, L., Golub, T., Mesirov, J.P., et al.; Cancer Genome Atlas Research Network. (2010). Integrated genomic analysis identifies clinically relevant subtypes of glioblastoma characterized by abnormalities in PDGFRA, IDH1, EGFR, and NF1. *Cancer Cell* 17, 98–110.
- Vescovi, A.L., Galli, R., and Reynolds, B.A. (2006). Brain tumour stem cells. *Nat. Rev. Cancer* 6, 425–436.
- Vierbuchen, T., Ostermeier, A., Pang, Z.P., Kokubu, Y., Südhof, T.C., and Wernig, M. (2010). Direct conversion of fibroblasts to functional neurons by defined factors. *Nature* 463, 1035–1041.
- Wen, P.Y., and Kesari, S. (2008). Malignant gliomas in adults. *N. Engl. J. Med.* 359, 492–507.
- Wiebe, M.S., Wilder, P.J., Kelly, D., and Rizzino, A. (2000). Isolation, characterization, and differential expression of the murine Sox-2 promoter. *Gene* 246, 383–393.

ASXL1 Mutations Promote Myeloid Transformation through Loss of PRC2-Mediated Gene Repression

Omar Abdel-Wahab,^{1,12} Mazhar Adli,^{2,12} Lindsay M. LaFave,^{1,3,12} Jie Gao,⁵ Todd Hricik,¹ Alan H. Shih,¹ Suveg Pandey,¹ Jay P. Patel,¹ Young Rock Chung,¹ Richard Koche,² Fabiana Perna,⁴ Xinyang Zhao,⁶ Jordan E. Taylor,⁷ Christopher Y. Park,¹ Martin Carroll,⁸ Ari Melnick,⁹ Stephen D. Nimer,¹¹ Jacob D. Jaffe,⁷ Iannis Aifantis,⁴ Bradley E. Bernstein,^{2,*} and Ross L. Levine^{1,10,*}

¹Human Oncology and Pathogenesis Program and Leukemia Service, Memorial Sloan-Kettering Cancer Center, 1275 York Avenue, Box 20, New York, NY 10065, USA

²Howard Hughes Medical Institute, Broad Institute of Harvard and MIT, Department of Pathology, Massachusetts General Hospital, and Harvard Medical School, MGH-Simches Research Building, CPZN 8400, 185 Cambridge Street, Boston, MA 02114, USA

³Gerstner Sloan Kettering School of Biomedical Sciences

⁴Molecular Pharmacology and Chemistry Program
Memorial Sloan-Kettering Cancer Center, New York, NY 10065, USA

⁵Howard Hughes Medical Institute and Department of Pathology, New York University School of Medicine, New York, NY 10016, USA

⁶Department of Biochemistry and Molecular Genetics, University of Alabama, Birmingham, AL 35233, USA

⁷Broad Institute of Harvard and MIT, Cambridge, MA 02142, USA

⁸Division of Hematology and Oncology, University of Pennsylvania, Philadelphia, PA 19104, USA

⁹Division of Hematology/Oncology

¹⁰Biochemistry and Molecular Biology Program
Weill Cornell Medical College, New York, NY 10065, USA

¹¹Sylvester Comprehensive Cancer Center, University of Miami, Miami, FL 33136, USA

¹²These authors contributed equally to this work

*Correspondence: bernstein.bradley@mgh.harvard.edu (B.E.B.), leviner@mskcc.org (R.L.L.)
<http://dx.doi.org/10.1016/j.ccr.2012.06.032>

SUMMARY

Recurrent somatic *ASXL1* mutations occur in patients with myelodysplastic syndrome, myeloproliferative neoplasms, and acute myeloid leukemia, and are associated with adverse outcome. Despite the genetic and clinical data implicating *ASXL1* mutations in myeloid malignancies, the mechanisms of transformation by *ASXL1* mutations are not understood. Here, we identify that *ASXL1* mutations result in loss of polycomb repressive complex 2 (PRC2)-mediated histone H3 lysine 27 (H3K27) tri-methylation. Through integration of microarray data with genome-wide histone modification ChIP-Seq data, we identify targets of *ASXL1* repression, including the posterior *HOXA* cluster that is known to contribute to myeloid transformation. We demonstrate that *ASXL1* associates with the PRC2, and that loss of *ASXL1* in vivo collaborates with *NRASG12D* to promote myeloid leukemogenesis.

INTRODUCTION

Recent genome-wide and candidate-gene discovery efforts have identified a series of novel somatic genetic alterations in patients with myeloid malignancies with relevance to pathogen-

esis, prognostication, and/or therapy. Notably, these include mutations in genes with known or putative roles in the epigenetic regulation of gene transcription. One such example is the mutations in the gene *Addition of sex combs-like 1* (*ASXL1*), which is mutated in $\approx 15\%$ – 25% of patients with myelodysplastic

Significance

Mutations in genes involved in modification of chromatin have recently been identified in patients with leukemias and other malignancies. Here, we demonstrate a specific role for *ASXL1*, a putative epigenetic modifier frequently mutated in myeloid malignancies, in polycomb repressive complex 2 (PRC2)-mediated transcriptional repression in hematopoietic cells. *ASXL1* loss-of-function mutations in myeloid malignancies result in loss of PRC2-mediated gene repression of known leukemogenic target genes. Our data provide insight into how *ASXL1* mutations contribute to myeloid transformation through dysregulation of Polycomb-mediated gene silencing. This approach also demonstrates how epigenomic and functional studies can be used to elucidate the function of mutations in epigenetic modifiers in malignant transformation.

syndrome and $\approx 10\%$ – 15% of patients with myeloproliferative neoplasms and acute myeloid leukemia (Abdel-Wahab et al., 2011; Bejar et al., 2011; Gelsi-Boyer et al., 2009). Clinical studies have consistently indicated that mutations in *ASXL1* are associated with adverse survival in myelodysplastic syndrome and acute myeloid leukemia (Bejar et al., 2011; Metzeler et al., 2011; Pratorcorona et al., 2012; Thol et al., 2011).

ASXL1 is the human homolog of *Drosophila Additional sex combs (Asx)*. *Asx* deletion results in a homeotic phenotype characteristic of both Polycomb (PcG) and Trithorax group (TxG) gene deletions (Gaebler et al., 1999), which led to the hypothesis that *Asx* has dual functions in silencing and activation of homeotic gene expression. In addition, functional studies in *Drosophila* suggested that *Asx* encodes a chromatin-associated protein with similarities to PcG proteins (Sinclair et al., 1998). More recently, it was demonstrated that *Drosophila Asx* forms a complex with the chromatin deubiquitinase Calypso to form the Polycomb-repressive deubiquitinase (PR-DUB) complex, which removes monoubiquitin from histone H2A at lysine 119. The mammalian homolog of Calypso, BAP1, directly associates with ASXL1, and the mammalian BAP1-ASXL1 complex was shown to possess deubiquitinase activity in vitro (Scheuermann et al., 2010).

The mechanisms by which *ASXL1* mutations contribute to myeloid transformation have not been delineated. A series of in vitro studies in non-hematopoietic cells have suggested a variety of activities for ASXL1, including physical cooperativity with HP1a and LSD1 to repress retinoic acid-receptor activity and interaction with peroxisome proliferator-activated receptor gamma (PPAR γ) to suppress lipogenesis (Cho et al., 2006; Lee et al., 2010; Park et al., 2011). In addition, a recent study using a gene-trap model reported that constitutive disruption of *Asx1* results in significant perinatal lethality; however, the authors did not note alterations in stem/progenitor numbers in surviving *Asx1* gene trap mice (Fisher et al., 2010a, 2010b). Importantly, the majority of mutations in *ASXL1* occur as nonsense mutations and insertions/deletions proximal or within the last exon prior to the highly conserved plant homeo domain. It is currently unknown whether mutations in *ASXL1* might confer a gain-of-function due to expression of a truncated protein, or whether somatic loss of ASXL1 in hematopoietic cells leads to specific changes in epigenetic state, gene expression, or hematopoietic functional output. The goals of this study were to determine the effects of *ASXL1* mutations on ASXL1 expression as well as the transcriptional and biological effects of perturbations in ASXL1 which might contribute toward myeloid transformation.

RESULTS

ASXL1 Mutations Result in Loss of ASXL1 Expression

ASXL1 mutations in patients with myeloproliferative neoplasms, myelodysplastic syndrome, and acute myeloid leukemia most commonly occur as somatic nonsense mutations and insertion/deletion mutations in a clustered region adjacent to the highly conserved PHD domain (Abdel-Wahab et al., 2011; Gelsi-Boyer et al., 2009). To assess whether these mutations result in loss of ASXL1 protein expression or in expression of a truncated isoform, we performed western blots using N- and C-terminal anti-ASXL1 antibodies in a panel of human myeloid

leukemia cell lines and primary acute myeloid leukemia samples, which are wild-type or mutant for *ASXL1*. We found that myeloid leukemia cells with homozygous frameshift/nonsense mutations in *ASXL1* (NOMO1 and KBM5) have no detectable ASXL1 protein expression (Figure 1A). Similarly, leukemia cells with heterozygous *ASXL1* mutations have reduced or absent ASXL1 protein expression. Western blot analysis of ASXL1 using an N-terminal anti-ASXL1 antibody in primary acute myeloid leukemia samples wild-type and mutant for *ASXL1* revealed reduced/absent full-length ASXL1 expression in samples with *ASXL1* mutations compared to *ASXL1* wild-type samples (Figure S1A available online). Importantly, we did not identify truncated ASXL1 protein products in mutant samples using N- or C-terminal directed antibodies in primary acute myeloid leukemia samples or leukemia cell lines. Moreover, expression of wild-type ASXL1 cDNA or cDNA constructs bearing leukemia-associated mutant forms of ASXL1 revealed reduced stability of mutant forms of ASXL1 relative to wild-type ASXL1, with more rapid degradation of mutant ASXL1 isoforms following cycloheximide exposure (Figure S1B). These data are consistent with ASXL1 functioning as a tumor suppressor with loss of ASXL1 protein expression in leukemia cells with mutant *ASXL1* alleles.

ASXL1 Knockdown in Hematopoietic Cells Results in Upregulated HOXA Gene Expression

Given that *ASXL1* mutations result in loss of ASXL1 expression, we investigated the effects of ASXL1 knockdown in primary hematopoietic cells. We used a pool of small interfering RNAs (siRNA) to perform knockdown of ASXL1 in primary human CD34+ cells isolated from umbilical cord blood. ASXL1 knockdown was performed in triplicate and confirmed by qRT-PCR analysis (Figure 1B), followed by gene-expression microarray analysis. Gene-set enrichment analysis (GSEA) of this microarray data revealed a significant enrichment of genes found in a previously described gene expression signature of leukemic cells from bone marrow of *MLL-AF9* knock-in mice (Kumar et al., 2009), as well as highly significant enrichment of a gene signature found in primary human cord blood CD34+ cells expressing *NUP98-HOXA9* (Figure S1C and Table S1) (Takeda et al., 2006). Specifically, we found that ASXL1 knockdown in human primary CD34+ cells resulted in increased expression of 145 genes out of the 279 genes, which are overexpressed in the *MLL-AF9* gene expression signature ($p < 0.05$, FDR < 0.05). These gene expression signatures are characterized by increased expression of posterior *HOXA* cluster genes, including *HOXA5-9*.

In order to ascertain whether loss of ASXL1 was associated with similar transcriptional effects in leukemia cells, we performed short hairpin RNA (shRNA)-mediated stable knockdown of *ASXL1* in the *ASXL1*-wild-type human leukemia cell lines UKE1 (Figures 1C and 1D) and SET2 (Figure 1D) followed by microarray and qRT-PCR analysis. Gene expression analysis in UKE-1 cells expressing ASXL1 shRNA compared to control cells revealed significant enrichment of the same *HOXA* gene expression signatures as were seen with ASXL1 knockdown in CD34+ cells (Figure 1C and Table S2). Upregulation of 5' *HOXA* genes was confirmed by qRT-PCR in UKE1 (Figure 1D) cells and by western blot analysis (Figure 1D) in SET2 cells expressing ASXL1 shRNA compared to control. Quantitative mRNA profiling (Nanostring nCounter) of the entire *HOXA* cluster revealed

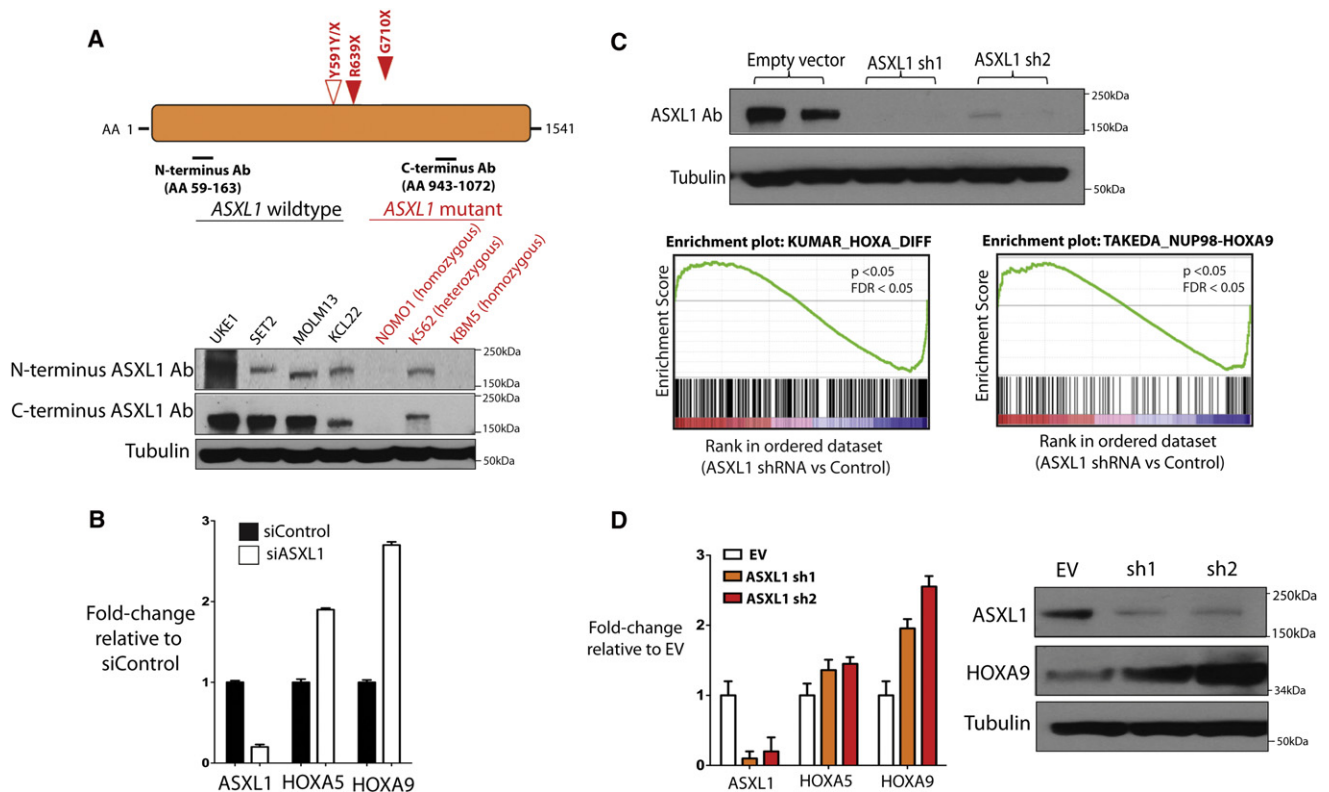


Figure 1. Leukemogenic ASXL1 Mutations Are Loss-of-Function Mutations and ASXL1 Loss Is Associated with Upregulation of HOXA Gene Expression

(A) Characterization of ASXL1 expression in leukemia cells with nonsense mutations in ASXL1 reveals loss of ASXL1 expression at the protein level in cells with homozygous ASXL1 mutations as shown by western blotting using N- and C-terminal anti-ASXL1 antibodies.

(B) Displayed are the ASXL1-mutant cell line lines NOMO1 (homozygous ASXL1 R639X), K562 (heterozygous ASXL1 Y591Y/X), and KBM5 (homozygous ASXL1 G710X) and a panel of ASXL1-wild-type cell lines. ASXL1 siRNA in human primary CD34+ cells from cord blood results in upregulation of HOXA5 and HOXA9 with ASXL1 knockdown (KD) as revealed by quantitative real-time PCR (qRT-PCR) analysis.

(C and D) Stable KD of ASXL1 in ASXL1-wild-type transformed human myeloid leukemia UKE1 cells (as shown by western blot) followed by GSEA reveals significant enrichment of gene sets characterized by upregulation of 5' HOXA genes (C) as was confirmed by qRT-PCR (D). Statistical significance is indicated in (D) by the p value and false-discovery rate (FDR). Similar upregulation of HOXA9 is seen by the western blot following stable ASXL1 KD in the ASXL1-wild-type human leukemia SET2 cells.

Error bars represent standard deviation of expression relative to control. See also Figure S1 and Tables S1 and S2.

upregulation of multiple HOXA members, including HOXA5, 7, 9, and 10, in SET2 cells with ASXL1 knockdown compared to control cells (Figure S1D). These results indicate consistent upregulation of HOXA gene expression following ASXL1 loss in multiple hematopoietic contexts.

ASXL1 Forms a Complex with BAP1 in Leukemia Cells, but BAP1 Loss Does Not Upregulate HoxA Gene Expression in Hematopoietic Cells

Mammalian ASXL1 forms a protein complex in vitro with the chromatin deubiquitinase BAP1, which removes monoubiquitin from histone H2A at lysine 119 (H2AK119) (Scheuermann et al., 2010). In Drosophila loss of either Asx or Calypso resulted in similar effects on genome-wide H2AK119 ubiquitin levels and on target gene expression. Recent studies have revealed recurrent germline and somatic loss-of-function BAP1 mutations in mesothelioma and uveal melanoma (Bott et al., 2011; Harbour et al., 2010; Testa et al., 2011). However, we have not identified BAP1 mutations in patients with myeloproliferative neoplasms or

acute myeloid leukemia (O.A.-W., J.P.P., and R.L.L., unpublished data). Co-immunoprecipitation studies revealed an association between ASXL1 and BAP1 in human myeloid leukemia cells wild-type for ASXL1 but not in those cells mutant for ASXL1 due to reduced/absent ASXL1 expression (Figure 2A). Immunoprecipitation of FLAG-tagged wild-type ASXL1 and FLAG-tagged leukemia-associated mutant forms of ASXL1 revealed reduced interaction between mutant forms of ASXL1 and endogenous BAP1 (Figure S2A). Despite these findings, BAP1 knockdown did not result in upregulation of HOXA5 and HOXA9 in UKE1 cells, although a similar extent of ASXL1 knockdown in the same cells reproducibly increased HOXA5 and HOXA9 expression (Figure 2B). We obtained similar results with knockdown of Asxl1 or Bap1 in the Ba/F3 murine hematopoietic cell line (Figure 2C). In Ba/F3 cells, knockdown of Asxl1 resulted in upregulated Hoxa9 gene expression commensurate with the level of Asxl1 downregulation, whereas knockdown of Bap1 does not impact Hoxa expression (Figure 2C). ASXL1 knockdown in SET-2 cells failed to reveal an effect of ASXL1

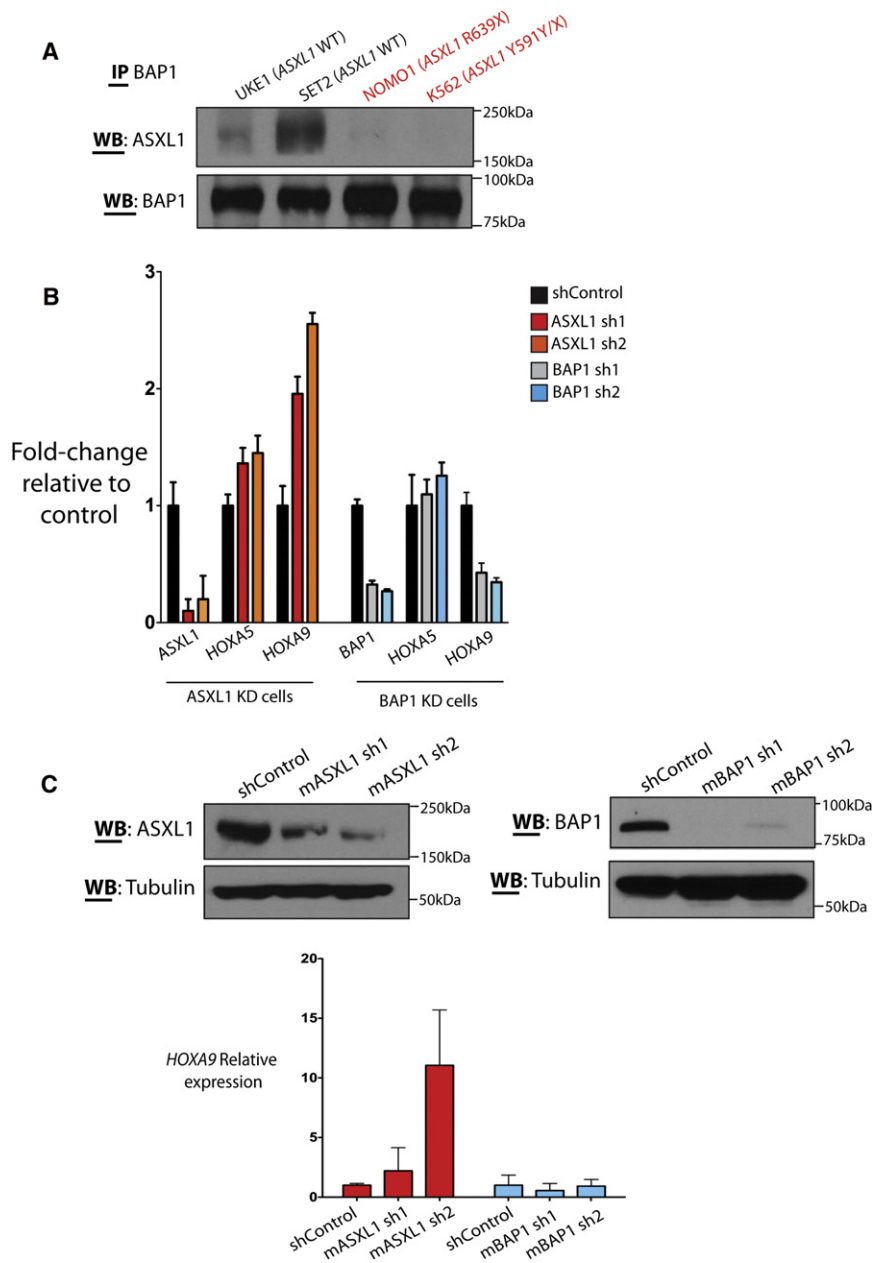


Figure 2. ASXL1 and BAP1 Physically Interact in Human Hematopoietic Cells but BAP1 Loss Does Not Result in Increased *HoxA* Gene Expression

(A) Immunoprecipitation of BAP1 in a panel of ASXL1-wild-type and mutant human myeloid leukemia cells reveals co-association of ASXL1 and BAP1.

(B) Cells with heterozygous or homozygous mutations in ASXL1 with reduced or absent ASXL1 expression have minimal interaction with BAP1 in vitro. BAP1 knockdown in the ASXL1/BAP1 wild-type human leukemia cell line UKE1 fails to alter *HOXA* gene expression. In contrast, stable knockdown of ASXL1 in the same cell type results in a significant upregulation of *HOXA9*.

(C) Similar results are seen with knockdown of *Asx1* or *Bap1* in murine precursor-B lymphoid Ba/F3 cells.

Error bars represent standard deviation of expression relative to control. See also Figure S2.

loss on H2AK119Ub levels as assessed by western blot of purified histones from shRNA control and ASXL1 knockdown cells (Figure S2B). By contrast, SET2 cells treated with MG132 (25 μ M) had a marked decrease in H2AK119Ub, as has been previously described (Dantuma et al., 2006). These data suggest that ASXL1 loss contributes to myeloid transformation through a BAP1-independent mechanism.

Loss of ASXL1 Is Associated with Global Loss of H3K27me3

The results described above led us to hypothesize that ASXL1 loss leads to BAP1-independent effects on chromatin state and on target gene expression. To assess the genome-wide effects of ASXL1 loss on chromatin state, we performed chro-

matin immunoprecipitation followed by next generation sequencing (ChIP-seq) for histone modifications known to be associated with PcG [histone H3 lysine 27 trimethylation (H3K27me3)] or TxG activity [histone H3 lysine 4 trimethylation (H3K4me3)] in UKE1 cells expressing empty vector or two independent validated shRNAs for ASXL1. ChIP-Seq data analysis revealed a significant reduction in genome-wide H3K27me3 transcriptional start site occupancy with ASXL1 knockdown compared to empty vector ($p = 2.2 \times 10^{-16}$; Figure 3A). Approximately 20% of genes ($n = 4,686$) were initially marked by H3K27me3 in their promoter regions (defined as 1.5 kb downstream and 0.5 kb upstream of the transcriptional start site). Among these genes, ~27% had a 2-fold reduction in H3K27me3 ($n = 1,309$) and ~66% had a 1.5-fold reduction in H3K27me3 ($n = 3,092$), respectively, upon ASXL1 knockdown. No significant

effect was seen on H3K4me3 transcriptional start site occupancy with ASXL1 depletion (Figure 3A). We next evaluated whether loss of ASXL1 might be associated with loss of H3K27me3 globally by performing western blot analysis on purified histones from UKE1 cells transduced with empty vector or shRNAs for ASXL1 knockdown. This analysis revealed a significant decrease in global H3K27me3 with ASXL1 loss (Figure 3B), despite preserved expression of the core polycomb repressive complex 2 (PRC2) members EZH2, SUZ12, and EED. Similar effects on total H3K27me3 levels were seen following *Asx1* knockdown in Ba/F3 cells (Figure S3A). These results demonstrate that ASXL1 depletion leads to a marked reduction in genome-wide H3K27me3 in hematopoietic cells.

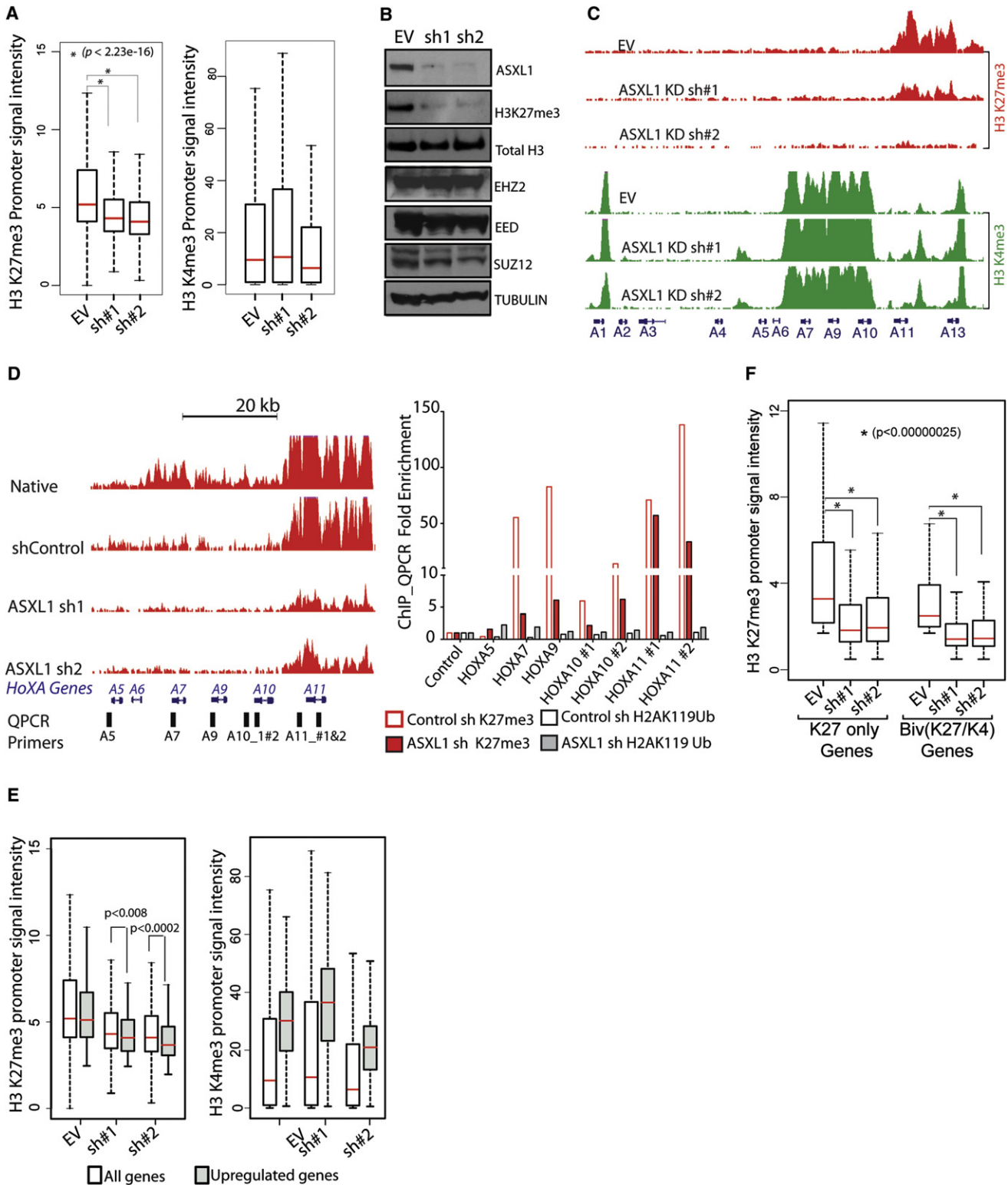


Figure 3. ASXL1 Loss Is Associated with Loss of H3K27me3 and with Increased Expression of Genes Poised for Transcription

(A) ASXL1 loss is associated with a significant genome-wide decrease in H3K27me3 as illustrated by box plot showing the 25th, 50th, and 75th percentiles for H3K27me3 and H3K4me3 enrichment at transcription start sites in UKE1 cells treated with an empty vector or shRNAs directed against ASXL1. The whiskers indicate the most extreme data point less than 1.5 interquartile range from box and the red bar represents the median.

(B) Loss of ASXL1 is associated with a global loss of H3K27me3 without affecting PRC2 component expression as shown by western blot of purified histones from cells with UKE1 knockdown and western blot for core PRC2 component in whole cell lysates from ASXL1 knockdown UKE1 cells.

Detailed analysis of ChIP-seq data revealed that genomic regions marked by large H3K27me3 domains in control cells displayed more profound loss of H3K27me3 upon loss of ASXL1. Genome-wide analysis of the ChIP-Seq data from control and ASXL1 shRNA treated cells revealed that the sites that lose H3K27me3 in the ASXL1 knockdown cells were on average ~6.6 kb in length, while the sites that maintained H3K27me3 were on average ~3.1 kb in length ($p < 10^{-16}$) (Figure S3B). This is visually illustrated by the reduction in H3K27me3 at the posterior *HOXA* cluster (Figure 3C) and at the *HOXB* and *HOXC* loci (Figure S3C). The association of ASXL1 loss with loss of H3K27me3 abundance at the *HOXA* locus was confirmed by ChIP for H3K27me3 in control and ASXL1 knockdown cells followed by qPCR (ChIP-qPCR) across the *HOXA* locus (Figure 3D). ChIP-qPCR in control and knockdown cells revealed a modest increase in H2AK119Ub with ASXL1 loss at the *HOXA* locus (Figure 3D), in contrast to the more significant reduction in H3K27me3. In contrast to the large decrease in H3K27me3 levels at the *HOXA* locus with ASXL1 knockdown, a subset of loci had much less significant reduction in H3K27me3, in particular at loci whose promoters were marked by sharp peaks of H3K27me3 (Figure S3D). Intersection of gene expression and ChIP-Seq data revealed that genes overexpressed in ASXL1 knockdown cells were simultaneously marked with both activating (H3K4me3) and repressive (H3K27me3) domains in control cells (Figures 3E and 3F). This finding suggests that the transcriptional repression mediated by ASXL1 in myeloid cells is most apparent at loci poised for transcription with bivalent chromatin domains. Indeed, the effects of ASXL1 loss on H3K27me3 occupancy were most apparent at genes whose promoters were marked by the dual presence of H3K27me3 and H3K4me3 (Figure 3F). We cannot exclude the possibility that H3K4me3 and H3K27me3 exist in different populations within the homogeneous cell lines being studied, but the chromatin and gene expression data are consistent with an effect of ASXL1 loss on loci with bivalent chromatin domains (Bernstein et al., 2006; Mikkelsen et al., 2007).

Enforced Expression of ASXL1 in Leukemic Cells Results in Suppression of *HOXA* Gene Expression, a Global Increase in H3K27me3, and Growth Suppression

We next investigated whether reintroduction of wild-type ASXL1 protein could restore H3K27me3 levels in ASXL1 mutant leukemia cells. We stably expressed wild-type ASXL1 in NOMO1 and KBM5 cells, homozygous ASXL1 mutant human

leukemia cell lines, which do not express ASXL1 protein (Figure 4A and Figure S4A). ASXL1 expression resulted in a global increase in H3K27me3 as assessed by histone western blot analysis (Figure 4A). Liquid chromatography/mass spectrometry of purified histones in NOMO1 cells expressing ASXL1 confirmed a ~2.5-fold increase in trimethylated H3K27 peptide and significant increases in dimethylated H3K27 in NOMO1 cells expressing ASXL1 compared to empty vector control (Figure 4B). ASXL1 add-back resulted in growth suppression (Figure 4C) and in decreased *HOXA* gene expression in NOMO1 cells (Figure 4D). ASXL1 add-back similarly resulted in decreased expression of *HOXA* target genes in KBM5 cells (Figures S4A and S4B). ChIP-qPCR revealed a strong enrichment in ASXL1 binding at the *HOXA* locus in NOMO1 cells expressing ASXL1, demonstrating that the *HOXA* locus is a direct target of ASXL1 in hematopoietic cells (Figure 4E).

ASXL1 Loss Leads to Exclusion of H3K27me3 and EZH2 from the *HoxA* Cluster Consistent with a Direct Effect of ASXL1 on PRC2 Recruitment

We next investigated whether the effects of ASXL1 loss on H3K27me3 was due to inhibition of PRC2 recruitment to specific target loci. ChIP-qPCR for H3K27me3 in SET2 cells with ASXL1 knockdown or control revealed a loss of H3K27me3 enrichment at the posterior *HoxA* locus with ASXL1 knockdown (Figures 5A and 5B). We observed a modest, variable increase in H3K4me3 enrichment at the *HOXA* locus with ASXL1 depletion in SET2 cells (Figure 5C). We similarly assessed H3K27me3 enrichment in primary bone marrow leukemic cells from acute myeloid leukemia patients, wild-type and mutant for ASXL1, which likewise revealed decreased H3K27me3 enrichment across the *HOXA* cluster in primary acute myeloid leukemia samples with ASXL1 mutations compared to ASXL1-wild-type acute myeloid leukemia samples (Figure 5D).

Given the consistent effects of ASXL1 depletion on H3K27me3 abundance at the *HOXA* locus, we then evaluated the occupancy of EZH2, a core PRC2 member, at the *HoxA* locus. ChIP-Seq for H3K27me3 in native SET2 and UKE1 cells identified that H3K27me3 is present with a dome-like enrichment pattern at the 5' end of the posterior *HOXA* cluster (Figure 5A); ChIP-qPCR revealed that EZH2 is prominently enriched in this same region in parental SET2 cells (Figure 5E). Importantly, ASXL1 depletion resulted in loss of EZH2 enrichment at the *HOXA* locus (Figure 5E), suggesting that ASXL1 is required for EZH2 occupancy and for PRC2-mediated repression of the posterior *HOXA* locus.

(C) Loss of H3K27me3 is evident at the *HOXA* locus as shown by ChIP-Seq promoter track signals across the *HOXA* locus in UKE1 cells treated with an EV or shRNA knockdown of ASXL1.

(D) H3K27me3 ChIP-Seq promoter track signals from *HOXA5* to *HOXA13* in UKE1 cells treated with shRNA control or one of 2 anti-ASXL1 shRNAs with location of primers used in ChIP-quantitative PCR (ChIP-qPCR) validation. ChIP for H3K27me3 and H2AK119Ub followed by ChIP-qPCR in cells treated with control or ASXL1 knockdown confirms a significant decrease in H3K27me3 at the *HOXA* locus with ASXL1 knockdown but minimal effects of ASXL1 knockdown on H2AK119Ub levels at the same primer locations.

(E) Integrating gene-expression data with H3K27me3/H3K4me3 ChIP-Seq identifies a significant correlation between alterations in chromatin state and increases in gene expression following ASXL1 loss at loci normally marked by the simultaneous presence of H3K27me3 and H3K4me3 in control cells.

(F) Loss of H3K27me3 is seen at promoters normally marked by the presence of H3K27me3 alone or at promoters co-occupied by H3K27me3 and H3K4me3 in the control state.

See also Figure S3.

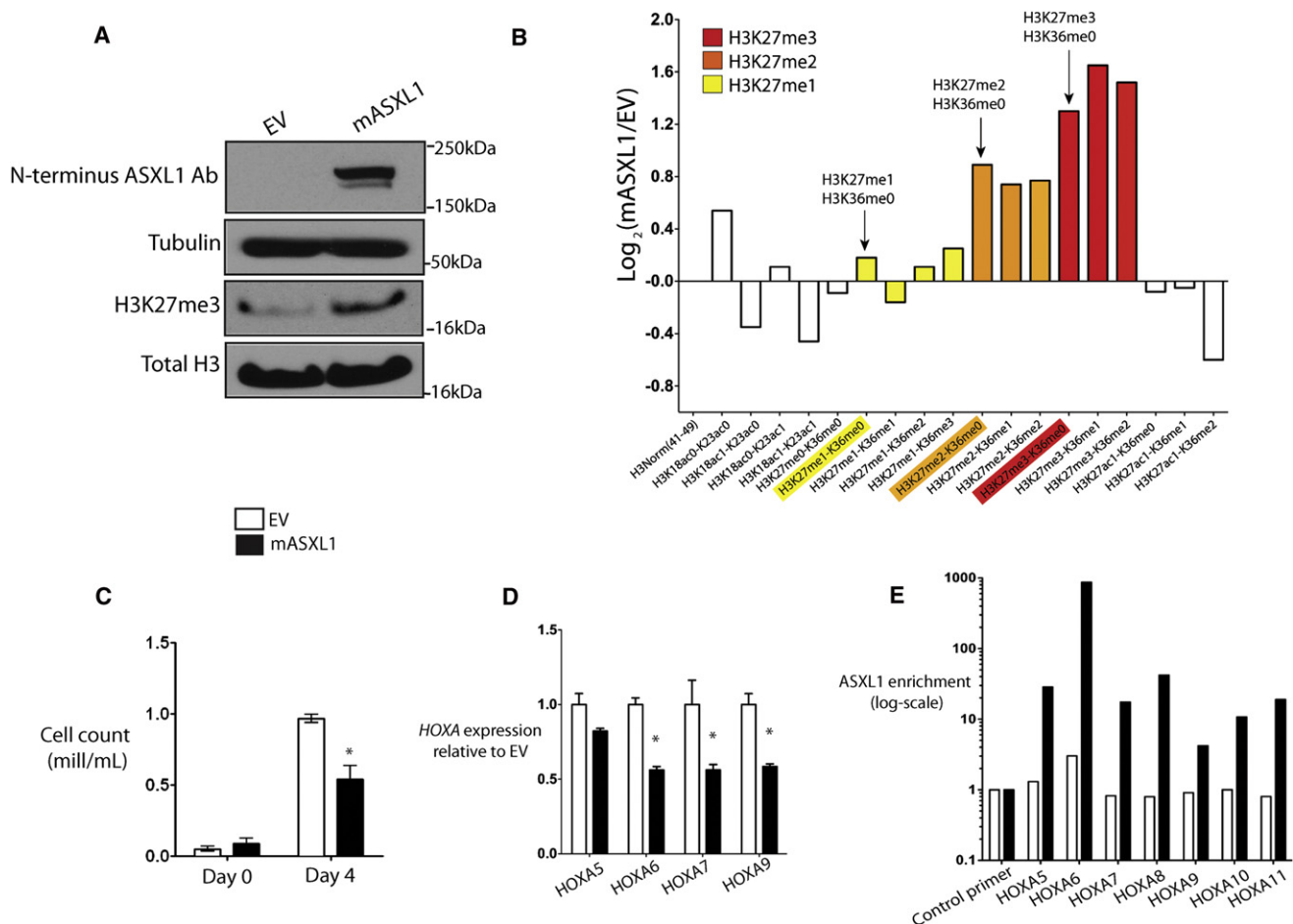


Figure 4. Expression of ASXL1 in ASXL1-Null Leukemic Cells Results in Global Increase in H3K27me2/3, Growth Suppression, and Suppression of *HoxA* Gene Expression

(A and B) ASXL1 expression in ASXL1 null NOMO1 cells is associated with a global increase in H3K27me3 as detected by western blot of purified histones (A) as well as by quantitative liquid-chromatography/mass spectrometry of H3 peptides from amino acids 18–40 (B) (arrows indicate quantification of H3K27me1/2/3). (C) ASXL1 overexpression results in growth suppression in 7-day growth assay performed in triplicate.

(D) Overexpression of ASXL1 was associated with a decrement in posterior *HoxA* gene expression in NOMO1 cells as shown by qRT-PCR for *HOXA5*, *6*, *7*, and *9*. (E) This downregulation in *HOXA* gene expression was concomitant with a strong enrichment of ASXL1 at the loci of these genes as shown by chromatin immunoprecipitation of ASXL1 followed by quantitative PCR with *BCRRP1* as a control locus.

Error bars represent standard deviation of target gene expression relative to control. See also Figure S4.

ASXL1 Physically Interacts with Members of the PRC2 in Human Myeloid Leukemic Cells

Given that ASXL1 localizes to PRC2 target loci and ASXL1 depletion leads to loss of PRC2 occupancy and H3K27me2, we investigated whether ASXL1 might physically interact with the PRC2 complex in hematopoietic cells. Co-immunoprecipitation studies using an anti-FLAG antibody in HEK293T cells expressing empty vector, hASXL1-FLAG alone, or hASXL1-FLAG plus hEZH2 cDNA revealed a clear co-immunoprecipitation of FLAG-ASXL1 with endogenous EZH2 and with ectopically expressed EZH2 (Figure 6A). Similarly, co-immunoprecipitation of FLAG-ASXL1 revealed physical association between ASXL1 and endogenous SUZ12 in 293T cells (Figure 6A). Immunoprecipitations were performed in the presence of benzonase to ensure that the protein-protein interactions observed were DNA-independent (Figure 6B) (Muntean et al., 2010). We then assessed whether endogenous ASXL1 formed a complex with

PRC2 members in hematopoietic cells. We performed IP for EZH2 or ASXL1 followed by western blotting for partner proteins in SET2 and UKE1 cells, which are wild-type for *ASXL1*, *SUZ12*, *EZH2*, and *EED*. These co-immunoprecipitation assays all revealed a physical association between ASXL1 and EZH2 in SET2 (Figure 6B) and UKE1 cells (Figure S5). By contrast, immunoprecipitation of endogenous ASXL1 did not reveal evidence of protein-protein interactions between ASXL1 and BMI1 (Figure S5). Likewise, immunoprecipitation of BMI1 enriched for PRC1 member RING1A, but failed to enrich for ASXL1, suggesting a lack of interaction between ASXL1 and the PRC1 repressive complex (Figure 6C).

ASXL1 Loss Collaborates with NRasG12D In Vivo

We and others previously reported that *ASXL1* mutations are most common in chronic myelomonocytic leukemia and frequently co-occur with *N/K-Ras* mutations in chronic

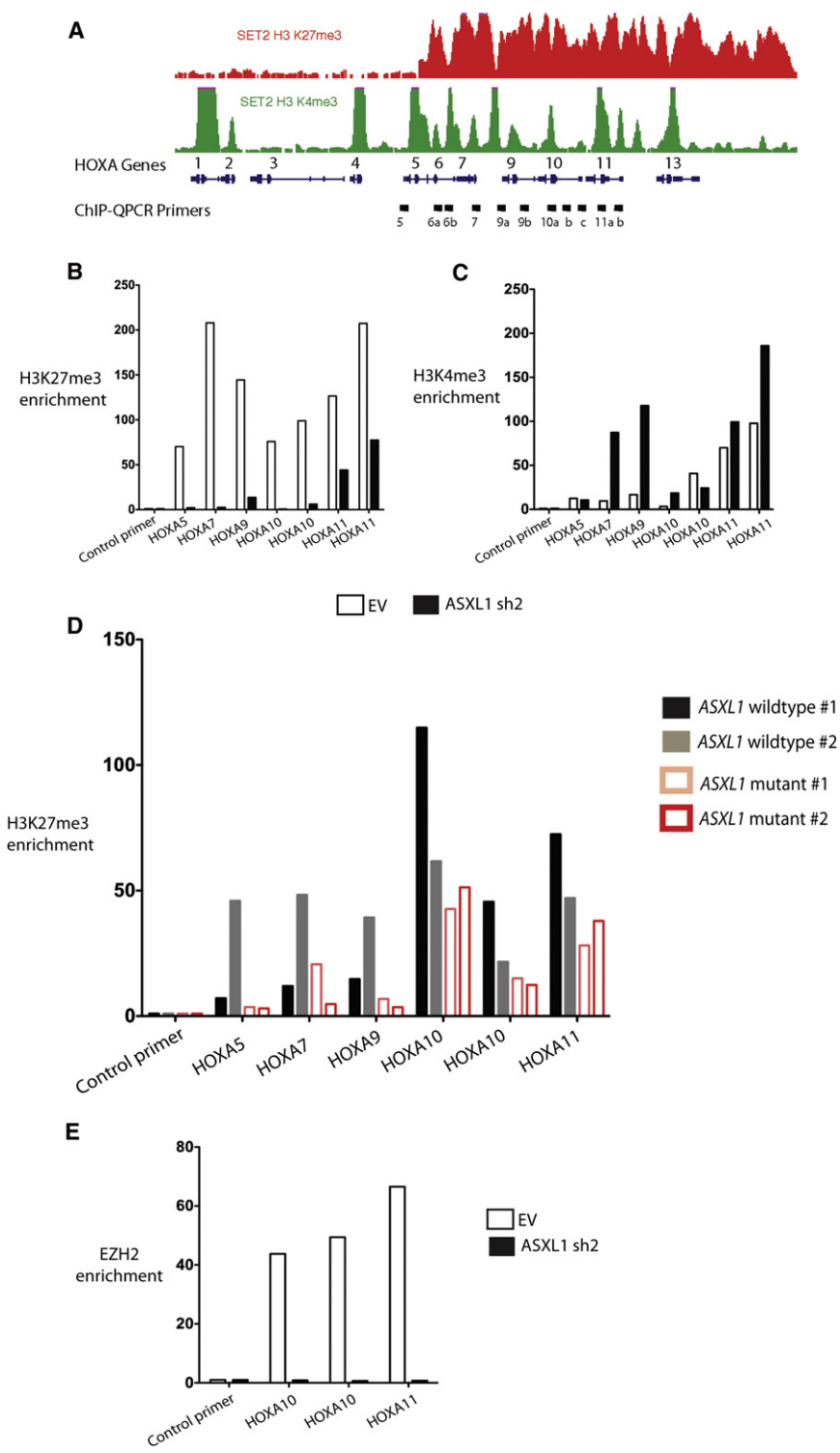


Figure 5. ASXL1 Loss Is Associated with Loss of PRC2 Recruitment at the HOXA Locus

(A) Chromatin-immunoprecipitation (ChIP) for H3K27me3 and H3K4me3 followed by next-generation sequencing reveals the abundance and localization of H3K27me3 and H3K4me3 at the *HoxA* locus in SET2 cells.

(B and C) ChIP for H3K27me3 (B) and H3K4me3 (C) followed by quantitative PCR (qPCR) across the 5' *HOXA* locus in SET2 cells treated with an empty vector or stable knockdown of ASXL1 reveals a consistent downregulation of H3K27me3 across the 5' *HOXA* locus following ASXL1 loss and a modest increase in H3K4me3 at the promoters of 5' *HOXA* genes with ASXL1 loss [primer locations are shown in (A)].

(D) Similar ChIP for H3K27me3 followed by qPCR across the *HOXA* locus in primary leukemic blasts from two patients with ASXL1 mutations versus two without ASXL1 mutations reveals H3K27me3 loss across the *HOXA* locus in ASXL1 mutant cells.

(E) ChIP for EZH2 followed by qPCR at the 5' end of *HOXA* locus in SET2 cells reveals loss of EZH2 enrichment with ASXL1 loss in SET2 cells. ChIP-qPCR was performed in biologic duplicates and ChIP-qPCR data is displayed as enrichment relative to input. qPCR at the gene body of *RRP1*, a region devoid of H3K4me3 or H3K27me3, is utilized as a control locus.

The error bars represent standard deviation.

myelomonocytic leukemia (Abdel-Wahab et al., 2011; Patel et al., 2010). We therefore investigated the effects of combined *NRasG12D* expression and *Asxl1* loss in vivo. To do this, we expressed *NRasG12D* in combination with an empty vector expressing GFP alone or one of two different *Asxl1* shRNA constructs in whole bone marrow cells and transplanted these

cells into lethally irradiated recipient mice. We validated our ability to effectively knock down ASXL1 in vivo by performing qRT-PCR in hematopoietic cells from recipient mice (Figure 7A and Figure S6A). Consistent with our in vitro data implicating the *HoxA* cluster as an ASXL1 target locus, we noted a marked increase in *HoxA9* and *HoxA10* expression in bone marrow nucleated cells from mice expressing *NRasG12D* in combination with *Asxl1* shRNA compared to mice expressing *NRasG12D* alone (Figure 7B).

Expression of oncogenic *NRasG12D* and an empty shRNA vector control led to a progressive myeloproliferative disorder as previously described (Mackenzie et al., 1999). In contrast, expression of *NRasG12D* in combination with validated *mASXL1* knockdown vectors resulted in accelerated myeloproliferation and impaired survival compared with mice transplanted with *NRasG12D/EV* (median survival 0.8 month for ASXL1 shRNA versus 3 months for control shRNA vector: $p < 0.005$; Figure 7C) We also noted impaired survival with an independent *mASXL1* shRNA construct ($p < 0.01$; Figure S6B) Mice transplanted with *NRasG12D/Asxl1*

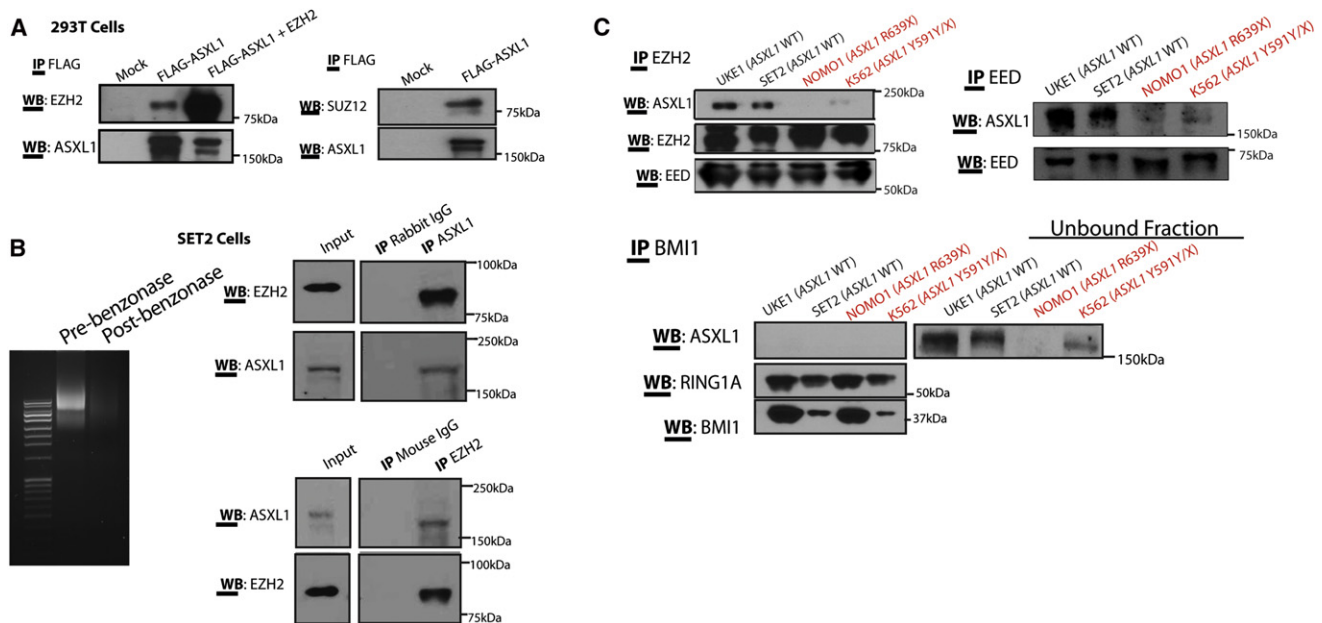


Figure 6. ASXL1 Interacts with the PRC2 in Hematopoietic Cells

(A) Physical interaction between ASXL1 and EZH2 is demonstrated by transient transfection of HEK293T cells with FLAG-hASXL1 cDNA with or without hEZH2 cDNA followed by immunoprecipitation (IP) of FLAG epitope and western blotting for EZH2 and ASXL1.

(B) HEK293T cells were transiently transfected with FLAG-hASXL1 cDNA followed by IP of FLAG epitope and western blotting for SUZ12 and ASXL1. Endogenous interaction of ASXL1 with PRC2 members was also demonstrated by IP of endogenous EZH2 and ASXL1 followed by western blotting of the other proteins in whole cell lysates from SET2 cells.

(C) Lysates from the experiment shown in (B) were treated with benzonase to ensure nucleic acid free conditions in the lysates prior to IP as shown by ethidium bromide staining of an agarose gel before and after benzonase treatment. IP of endogenous EZH2 and embryonic ectoderm development (EED) in a panel of ASXL1-wild-type and mutant human leukemia cells reveals a specific interaction between ASXL1 and PRC2 members in ASXL1-wildtype human myeloid leukemia cells. In contrast, IP of the PRC1 member BMI1 failed to pull down ASXL1.

See also Figure S5.

shRNA had increased splenomegaly and hepatomegaly compared with *NRasG12D/EV* transplanted mice (Figures 7D and 7E; Figure S6C). Histological analysis revealed a significant increase in myeloid infiltration of the spleen and livers of mice transplanted with *NRasG12D/Asx1* shRNA (Figure S6D).

Mice transplanted with *NRasG12D/Asx1* shRNA, but not *NRasG12D/EV*, experienced progressive, severe anemia (Figure 7F). It has previously been identified that expression of oncogenic *K/N-Ras* in multiple models of human/murine hematopoietic systems results in alterations in the erythroid compartment (Braun et al., 2006; Darley et al., 1997; Zhang et al., 2003). We noted an expansion of CD71^{high}/Ter119^{high} erythroblasts in the bone marrow of mice transplanted with *NRasG12D/Asx1* shRNA compared with *NRasG12D/EV* mice (Figure S6E). We also noted increased granulocytic expansion in mice engrafted with *NRasG12D/Asx1* shRNA positive cells, as shown by the presence of increased neutrophils in the peripheral blood (Figure S6D) and the expansion of Gr1/Mac1 double-positive cells in the bone marrow by flow cytometry (Figure S6F).

Previous studies have shown that hematopoietic cells from mice expressing oncogenic *Ras* alleles or other mutations that activate kinase signaling pathways do not exhibit increased self-renewal in colony replating assays (Braun et al., 2004; MacKenzie et al., 1999). This is in contrast to the immortalization of hematopoietic cells in vitro seen with expression of *MLL-AF9*

(Somerville and Cleary, 2006) or deletion of *Tet2* (Moran-Crusio et al., 2011). Bone marrow cells from mice with combined overexpression of *NRasG12D* plus *Asx1* knockdown had increased serial replating (to five passages) compared to bone marrow cells from mice engrafted with *NRasG12D/EV* cells (Figure 7G). These studies demonstrate that *Asx1* loss cooperates with oncogenic *NRasG12D* in vivo.

DISCUSSION

The data presented here identify that ASXL1 loss in hematopoietic cells results in reduced H3K27me3 occupancy through inhibition of PRC2 recruitment to specific oncogenic target loci. Recent studies have demonstrated that genetic alterations in the PRC2 complex occur in a spectrum of human malignancies (Bracken and Helin, 2009; Margueron and Reinberg, 2011; Sauvageau and Sauvageau, 2010). Activating mutations and overexpression of *EZH2* occur most commonly in epithelial malignancies and in lymphoid malignancies (Morin et al., 2010; Varambally et al., 2002). However, there are increasing genetic data implicating mutations that impair PRC2 function in the pathogenesis of myeloid malignancies. These include the loss-of-function mutations in *EZH2* (Abdel-Wahab et al., 2011; Ernst et al., 2010; Nikoloski et al., 2010) and less common somatic loss-of-function mutations in *SUZ12*, *EED*, and *JARID2* (Score

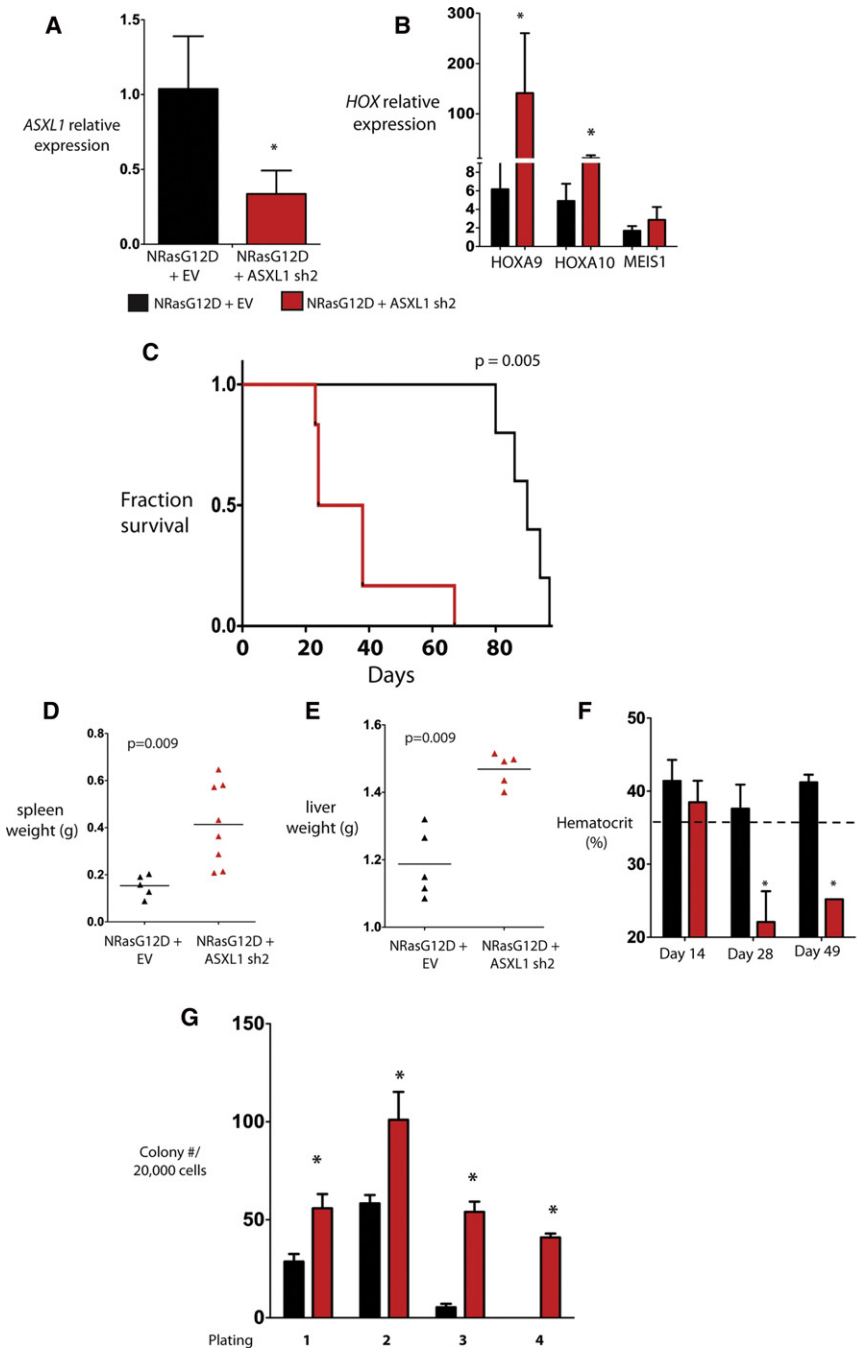


Figure 7. Asx1 Silencing Cooperates with NRasG12D In Vivo

(A) Retroviral bone marrow transplantation of NRasG12D with or without an shRNA for Asx1 resulted in decreased *Asx1* mRNA expression as shown by qRT-PCR results in nucleated peripheral blood cells from transplanted mice at 14 days following transplant.

(B) qRT-PCR revealed an increased expression of *HOXA9* and *HOXA10* but not *MEIS1* in the bone marrow of mice sacrificed 19 days following transplantation.

(C) Transplantation of bone marrow cells bearing overexpression of NRasG12D in combination with downregulation of *Asx1* led to a significant hastening of death compared to mice transplanted with NRasG12D/EV.

(D–F) Mice transplanted with NRasG12D/ASXL1 shRNA experienced increased splenomegaly (D) and hepatomegaly (E), and progressive anemia (F) compared with mice transplanted with NRasG12D + an empty vector (EV).

(G) Bone marrow cells from mice with combined NRasG12D overexpression/Asx1 knockdown revealed increased serial replating compared with cells from NRasG12D/EV mice. Error bars represent standard deviation relative to control. Asterisk indicates $p < 0.05$ (two-tailed, Mann Whitney U test).

See also Figure S6.

myeloid malignancies. In many cases, patients present with concomitant heterozygous mutations in multiple PRC2 members or in *EZH2* and *ASXL1*; these data suggest that haploinsufficiency for multiple genes that regulate PRC2 function can cooperate in hematopoietic transformation through additive alterations in PRC2 function.

Many studies have investigated how mammalian PcG proteins are recruited to chromatin in order to repress gene transcription and specify cell fate in different tissue contexts. Recent in silico analysis suggested that ASXL proteins found in animals contain a number of domains that likely serve in the recruitment of chromatin modulators and transcriptional effectors to DNA (Aravind and

et al., 2012) in patients with myeloproliferative neoplasms, myelodysplastic syndrome, and chronic myelomonocytic leukemia. The data from genetically-engineered mice also support this concept with *Ezh2* overexpression models, revealing evidence of promotion of malignant transformation (Herrera-Merchan et al., 2012), and recent studies demonstrate a role for *Ezh2* loss in leukemogenesis (Simon et al., 2012). Thus, it appears that alterations in normal PRC2 activity and/or H3K27me3 abundance in either direction may promote malignant transformation. Our data implicate *ASXL1* mutations as an additional genetic alteration that leads to impaired PRC2 function in patients with

Iyer, 2012). Data from ChIP and co-immunoprecipitation experiments presented here suggest a specific role for ASXL1 in epigenetic regulation of gene expression by facilitating PRC2-mediated transcriptional repression of known leukemic oncogenes. Thus, ASXL1 may serve as a scaffold for recruitment of the PRC2 complex to specific loci in hematopoietic cells, as has been demonstrated for JARID2 in embryonic stem cells (Landeira et al., 2010; Pasini et al., 2010; Peng et al., 2009; Shen et al., 2009).

Recent data suggested that ASXL1 might interact with BAP1 to form a H2AK119 deubiquitinase (Scheuermann et al., 2010).

However, our data suggest that ASXL1 loss leads to BAP1-independent alterations in chromatin state and gene expression in hematopoietic cells. These data are consonant with recent genetic studies, which have shown that germline loss of BAP1 increases susceptibility to uveal melanoma and mesothelioma (Testa et al., 2011; Wiesner et al., 2011). In contrast, germline loss of ASXL1 is seen in the developmental disorder Bohring-Opitz Syndrome (Hoischen et al., 2011), but has not, to date, been observed as a germline solid tumor susceptibility locus. Whether alterations in H2AK119 deubiquitinase function due to alterations in BAP1 and/or ASXL1 can contribute to leukemogenesis or to the pathogenesis of other malignancies remains to be determined.

Integration of gene expression and chromatin state data following ASXL1 loss identified specific loci with a known role in leukemogenesis that are altered in the setting of ASXL1 mutations. These include the posterior *HOXA* cluster, including *HOXA9*, which has a known role in hematopoietic transformation. We demonstrate that ASXL1 normally serves to tightly regulate *HOXA* gene expression in hematopoietic cells, and that loss of ASXL1 leads to disordered *HOXA* gene expression in vitro and in vivo. Overexpression of 5' *HOXA* genes is a well-described oncogenic event in hematopoietic malignancies (Lawrence et al., 1996), and previous studies have shown that *HOXA9* overexpression leads to transformation in vitro and in vivo when co-expressed with *MEIS1* (Kroon et al., 1998). Interestingly, ASXL1 loss was not associated with an increase in *MEIS1* expression, suggesting that transformation by ASXL1 mutations requires the co-occurrence of oncogenic disease alleles which dysregulate additional target loci. These data and our in vivo studies suggest that ASXL1 loss, in combination with co-occurring oncogenes, can lead to hematopoietic transformation and increased self-renewal. Further studies in mice expressing ASXL1 shRNA or with conditional deletion of *Asx1* alone and in concert with leukemogenic disease alleles will provide additional insight into the role of ASXL1 loss in hematopoietic stem/progenitor function and in leukemogenesis.

Given that somatic mutations in chromatin modifying enzymes (Dagliesh et al., 2010), DNA methyltransferases (Ley et al., 2010), and other genes implicated in epigenetic regulation occur commonly in human cancers, it will be important to use epigenomic platforms to elucidate how these disease alleles contribute to oncogenesis in different contexts. The data here demonstrate how integrated epigenetic and functional studies can be used to elucidate the function of somatic mutations in epigenetic modifiers. In addition, it is likely that many known oncogenes and tumor suppressors contribute, at least in part, to transformation through direct or indirect alterations in the epigenetic state (Dawson et al., 2009). Subsequent epigenomic studies of human malignancies will likely uncover novel routes to malignant transformation in different malignancies, and therapeutic strategies that reverse epigenetic alterations may be of specific benefit in patients with mutations in epigenetic modifiers.

EXPERIMENTAL PROCEDURES

Cell Culture

HEK293T cells were cultured in Dulbecco's modified Eagle's medium (DMEM) supplemented with 10% fetal bovine serum (FBS) and nonessential amino

acids. Human leukemia cell lines were cultured in RPMI-1640 medium supplemented with 10% FBS+1 mM hydrocortisone+10% horse serum (UKE1 cells), RPMI-1640 supplemented with 10% FBS (K562, MOLM13, KCL22, KU812 cells), RPMI-1640 supplemented with 20% FBS (SET2, NOMO1, Monomac-6 cells), or IMDM + 20% FBS (KBM5 cells). For proliferation studies, 1×10^3 cells were seeded in 1 ml volume of media in triplicate and cell number was counted manually daily for 7 days by Trypan blue exclusion.

Plasmid Constructs, Mutagenesis Protocol, Short Hairpin RNA, and Small Interfering RNA

See Supplemental Information.

Primary Acute Myeloid Leukemia Patient Samples and ASXL1, BAP1, EZH2, SUZ12, and EED Genomic DNA Sequencing Analysis

Approval was obtained from the institutional review boards at Memorial Sloan-Kettering Cancer Center and at the Hospital of the University of Pennsylvania for these studies, and informed consent was provided according to the Declaration of Helsinki. Please see Supplemental Information for details on DNA sequence analysis.

Western Blot and Immunoprecipitation Analysis

Western blots were carried out using the following antibodies: ASXL1 (Clone N-13; Santa Cruz (sc-85283); N-terminus directed), ASXL1 (Clone 2049C2a; Santa Cruz (sc-81053); C terminus directed), BAP1 [clone 3C11; Santa Cruz (sc-13576)], BMI1 (Abcam ab14389), EED (Abcam ab4469), EZH2 (Active Motif 39933 or Millipore 07-689), FLAG (M2 FLAG; Sigma A2220), Histone H3 lysine 27 trimethyl (Abcam ab6002), Histone H2A Antibody II (Cell Signaling Technologies 2578), Ubiquityl-Histone H2AK119 (Clone D27C4; Cell Signaling Technologies 8240), RING1A (Abcam ab32807), SUZ12 (Abcam ab12073), and total histone H3 (Abcam ab1791), and tubulin (Sigma, T9026). Antibodies different from the above used for immunoprecipitation include: ASXL1 [clone H105X; Santa Cruz (sc-98302)], FLAG (Novus Biological Products; NBP1-06712), and EZH2 (Active Motif 39901). Immunoprecipitation and pull-down reactions were performed in an immunoprecipitation buffer (150 mM NaCl, 20 mM Tris (pH 7.4–7.5), 5 mM EDTA, 1% Triton, 100 mM sodium orthovanadate, protease arrest (Genotec), 1 mM PMSF, and phenylarsene oxide). To ensure nuclease-free immunoprecipitation conditions, immunoprecipitations were also performed using the following methodology (Muntean et al., 2010): cells were lysed in BC-300 buffer (20 mM Tris-HCl (pH 7.4), 10% glycerol, 300 mM KCl, 0.1% NP-40) and the cleared lysate was separated from the insoluble pellet and treated with MgCl₂ to 2.5 mM and benzonase (Emanuel Merck, Darmstadt) at a concentration of 1,250 U/ml. The lysate was then incubated for 1–1.5 hr at 4°. The reaction was then stopped with addition of 5 mM EDTA. DNA digestion is confirmed on an ethidium bromide agarose gel. We then set up our immunoprecipitation by incubating our lysate overnight at 4°.

Histone Extraction and Histone LC/MS Analysis

See Supplemental Information.

Gene Expression Analysis

Total RNA was extracted from cells using QIAGEN's RNeasy Plus Mini kit (Valencia, CA, USA). cDNA synthesis, labeling, hybridization, and quality control were carried out as previously described (Figuroa et al., 2008). Ten micrograms of RNA was then used for generation of labeled cRNA according to the manufacturer's instructions (Affymetrix, Santa Clara, CA, USA). Hybridization of the labeled cRNA fragments and washing, staining, and scanning of the arrays were carried out as per instructions of the manufacturer. Labeled cRNA from CD34+ cells treated with either ASXL1 siRNA or controls were analyzed using the Affymetrix HG-U133-Plus2.0 platform and from UKE1 cells using the Illumina Href8 array. All expression profile experiments were carried out using biological duplicates. "Present" calls in $\geq 80\%$ of samples were captured and quantile normalized across all samples on a per-chip basis. Raw expression values generated by Genome Studio (Illumina) were filtered to exclude probesets having expression values below negative background in $\geq 80\%$ of samples. Probesets remaining after background filtering were log₂ transformed and quantile normalized on a per-chip basis. qRT-PCR was performed on cDNA using SYBR green quantification in an ABI 7500

sequence detection system. The sequences of all qRT-PCR primers are listed in the Supplemental Information.

Chromatin Immunoprecipitation and Antibodies

ChIP experiments for H3K4me3, H3K27me3, and H3K36me3 were carried out as described previously (Bernstein et al., 2006; Mikkelsen et al., 2007). Cells were cross-linked in 1% formaldehyde, lysed, and sonicated with a Branson 250 Sonifier to obtain chromatin fragments in a size range between 200 and 700 bp. Solubilized chromatin was diluted in ChIP dilution buffer (1:10) and incubated with antibody overnight at 4°C. Protein A sepharose beads (Sigma) were used to capture the antibody-chromatin complex and washed with low salt, LiCl, as well as TE (pH 8.0) wash buffers. Enriched chromatin fragments were eluted at 65°C for 10 min, subjected to cross-link reversal at 65°C for 5 hr, and treated with Proteinase K (1 mg/ml), before being extracted by phenol-chloroform-isoamyl alcohol, and ethanol precipitated. ChIP DNA was then quantified by QuantiT Picogreen dsDNA Assay kit (Invitrogen). ChIP experiments for ASXL1 were carried out on nuclear preps. Cross-linked cells were incubated in swelling buffer (0.1 M Tris pH 7.6, 10 mM KOAc, 15 mM MgOAc, 1% NP40), on ice for 20 minutes, passed through a 16G needle 20 times and centrifuged to collect nuclei. Isolated nuclei were then lysed, sonicated, and immunoprecipitated as described above. Antibodies used for ChIP include anti-H3K4me3 (Abcam ab8580), anti-H3K27me3 (Upstate 07-449), anti-H3K36me3 (Abcam ab9050), and anti-ASXL1 [clone H105X; Santa Cruz (sc-98302)], and Ubiquityl-Histone H2AK119 (Clone D27C4; Cell Signaling Technologies 8240).

Sequencing Library Preparation, Illumina/Solexa Sequencing, and Read Alignment and Generation of Density Maps

See Supplemental Information.

HOXA Nanostring nCounter Gene Expression CodeSet

Direct digital mRNA analysis of *HOXA* cluster gene expression was performed using a Custom CodeSet including each *HOXA* gene (NanoString Technologies). Synthesis of the oligonucleotides was done by NanoString Technologies, and hybridization and analysis were done using the Prep Station and Digital Analyzer purchased from the company.

Animal Use, Retroviral Bone Marrow Transplantation, Flow Cytometry, and Colony Assays

Animal care was in strict compliance with institutional guidelines established by the Memorial Sloan-Kettering Cancer Center, the National Academy of Sciences Guide for the Care and Use of Laboratory Animals, and the Association for Assessment and Accreditation of Laboratory Animal Care International. All animal procedures were approved by the Institutional Animal Care and Use Committee (IACUC) at Memorial Sloan-Kettering Cancer Center. See Supplemental Information for more details on animal experiments.

Statistical Analysis

Statistical significance was determined by the Mann-Whitney U test and Fisher's exact test using Prism GraphPad software. Significance of survival differences was calculated using Log-rank (Mantel-Cox) test. $p < 0.05$ was considered statistically significant. Normalized expression data from CD34+ cord blood was used as a Gene Set Enrichment Analysis query of the C2 database (MSig DB) where 1,000 permutations of the genes was used to generate a null distribution. A pre-ranked gene list, containing genes upregulated at least \log_2 0.5-fold, in which the highest ranked genes corresponds to the genes, with the largest fold-difference between *Asxl1* hairpin-treated UKE1 cells and those treated with empty vector, was used to query the C2 MSig DB as described above.

ACCESSION NUMBERS

All microarray data used in this manuscript are deposited in Gene Expression Omnibus (<http://www.ncbi.nlm.nih.gov/geo/>) under GEO accession number GSE38692. The ChIP-Seq data are deposited under GEO accession number GSE38861.

SUPPLEMENTAL INFORMATION

Supplemental Information includes six figures, two tables, and Supplemental Experimental Procedures and can be found with this article online at <http://dx.doi.org/10.1016/j.ccr.2012.06.032>.

ACKNOWLEDGMENTS

This work was supported by a grant from the Starr Cancer Consortium to R.L.L. and B.E.B., by grants from the Gabrielle's Angel Fund to R.L.L. and O.A.-W., by a grant from the Anna Fuller Fund to R.L.L., and by an NHLBI grant to B.E.B. (5U01HL100395). I.A. and B.E.B. are Howard Hughes Medical Institute Early Career Scientists. A.M. is a Burroughs Wellcome Clinical Translational Scholar and Scholar of the Leukemia and Lymphoma Society. X.Z. and S.D.N. are supported by a Leukemia and Lymphoma Society SCOR award, and F.P. is supported by an American Italian Cancer Foundation award. O.A.-W. is an American Society of Hematology Basic Research Fellow and is supported by a grant from the NIH K08 Clinical Investigator Award (1K08CA160647-01). J.P.P. is supported by an American Society of Hematology Trainee Research Award.

Received: January 7, 2012

Revised: May 21, 2012

Accepted: June 28, 2012

Published: August 13, 2012

REFERENCES

- Abdel-Wahab, O., Pardanani, A., Patel, J., Wadleigh, M., Lasho, T., Heguy, A., Beran, M., Gilliland, D.G., Levine, R.L., and Tefferi, A. (2011). Concomitant analysis of EZH2 and ASXL1 mutations in myelofibrosis, chronic myelomonocytic leukemia and blast-phase myeloproliferative neoplasms. *Leukemia* 25, 1200–1202.
- Aravind, L., and Iyer, L.M. (2012). The HARE-HTH and associated domains: Novel modules in the coordination of epigenetic DNA and protein modifications. *Cell Cycle* 11, 119–131.
- Bejar, R., Stevenson, K., Abdel-Wahab, O., Galili, N., Nilsson, B., Garcia-Manero, G., Kantarjian, H., Raza, A., Levine, R.L., Neuberg, D., and Ebert, B.L. (2011). Clinical effect of point mutations in myelodysplastic syndromes. *N. Engl. J. Med.* 364, 2496–2506.
- Bernstein, B.E., Mikkelsen, T.S., Xie, X., Kamal, M., Huebert, D.J., Cuff, J., Fry, B., Meissner, A., Wernig, M., Plath, K., et al. (2006). A bivalent chromatin structure marks key developmental genes in embryonic stem cells. *Cell* 125, 315–326.
- Bott, M., Brevet, M., Taylor, B.S., Shimizu, S., Ito, T., Wang, L., Creaney, J., Lake, R.A., Zakowski, M.F., Reva, B., et al. (2011). The nuclear deubiquitinase BAP1 is commonly inactivated by somatic mutations and 3p21.1 losses in malignant pleural mesothelioma. *Nat. Genet.* 43, 668–672.
- Bracken, A.P., and Helin, K. (2009). Polycomb group proteins: navigators of lineage pathways led astray in cancer. *Nat. Rev. Cancer* 9, 773–784.
- Braun, B.S., Tuveson, D.A., Kong, N., Le, D.T., Kogan, S.C., Rozmus, J., Le Beau, M.M., Jacks, T.E., and Shannon, K.M. (2004). Somatic activation of oncogenic *Kras* in hematopoietic cells initiates a rapidly fatal myeloproliferative disorder. *Proc. Natl. Acad. Sci. USA* 101, 597–602.
- Braun, B.S., Archard, J.A., Van Ziffle, J.A., Tuveson, D.A., Jacks, T.E., and Shannon, K. (2006). Somatic activation of a conditional *KrasG12D* allele causes ineffective erythropoiesis in vivo. *Blood* 108, 2041–2044.
- Cho, Y.S., Kim, E.J., Park, U.H., Sin, H.S., and Um, S.J. (2006). Additional sex comb-like 1 (ASXL1), in cooperation with SRC-1, acts as a ligand-dependent coactivator for retinoic acid receptor. *J. Biol. Chem.* 281, 17588–17598.
- Dalgliesh, G.L., Furge, K., Greenman, C., Chen, L., Bignell, G., Butler, A., Davies, H., Edkins, S., Hardy, C., Latimer, C., et al. (2010). Systematic sequencing of renal carcinoma reveals inactivation of histone modifying genes. *Nature* 463, 360–363.

- Dantuma, N.P., Groothuis, T.A., Salomons, F.A., and Neeffjes, J. (2006). A dynamic ubiquitin equilibrium couples proteasomal activity to chromatin remodeling. *J. Cell Biol.* *173*, 19–26.
- Darley, R.L., Hoy, T.G., Baines, P., Padua, R.A., and Burnett, A.K. (1997). Mutant N-RAS induces erythroid lineage dysplasia in human CD34+ cells. *J. Exp. Med.* *185*, 1337–1347.
- Dawson, M.A., Bannister, A.J., Göttgens, B., Foster, S.D., Bartke, T., Green, A.R., and Kouzarides, T. (2009). JAK2 phosphorylates histone H3Y41 and excludes HP1alpha from chromatin. *Nature* *461*, 819–822.
- Ernst, T., Chase, A.J., Score, J., Hidalgo-Curtis, C.E., Bryant, C., Jones, A.V., Waghorn, K., Zoi, K., Ross, F.M., Reiter, A., et al. (2010). Inactivating mutations of the histone methyltransferase gene EZH2 in myeloid disorders. *Nat. Genet.* *42*, 722–726.
- Figuerola, M.E., Reimers, M., Thompson, R.F., Ye, K., Li, Y., Selzer, R.R., Fridriksson, J., Paietta, E., Wiernik, P., Green, R.D., et al. (2008). An integrative genomic and epigenomic approach for the study of transcriptional regulation. *PLoS One* *3*, e1882.
- Fisher, C.L., Lee, I., Bloyer, S., Bozza, S., Chevalier, J., Dahl, A., Bodner, C., Helgason, C.D., Hess, J.L., Humphries, R.K., and Brock, H.W. (2010a). Additional sex combs-like 1 belongs to the enhancer of trithorax and polycomb group and genetically interacts with Cbx2 in mice. *Dev. Biol.* *337*, 9–15.
- Fisher, C.L., Pineault, N., Brookes, C., Helgason, C.D., Ohta, H., Bodner, C., Hess, J.L., Humphries, R.K., and Brock, H.W. (2010b). Loss-of-function Additional sex combs-like1 mutations disrupt hematopoiesis but do not cause severe myelodysplasia or leukemia. *Blood* *115*, 38–46.
- Gaebler, C., Stanzl-Tschegg, S., Heinze, G., Holper, B., Milne, T., Berger, G., and Vécsei, V. (1999). Fatigue strength of locking screws and prototypes used in small-diameter tibial nails: a biomechanical study. *J. Trauma* *47*, 379–384.
- Gelsi-Boyer, V., Trouplin, V., Adélaïde, J., Bonansea, J., Cervera, N., Carbuccia, N., Lagarde, A., Prebet, T., Nezri, M., Sainty, D., et al. (2009). Mutations of polycomb-associated gene ASXL1 in myelodysplastic syndromes and chronic myelomonocytic leukaemia. *Br. J. Haematol.* *145*, 788–800.
- Harbour, J.W., Onken, M.D., Roberson, E.D., Duan, S., Cao, L., Worley, L.A., Council, M.L., Matatall, K.A., Helms, C., and Bowcock, A.M. (2010). Frequent mutation of BAP1 in metastasizing uveal melanomas. *Science* *330*, 1410–1413.
- Herrera-Merchan, A., Arranz, L., Ligos, J.M., de Molina, A., Dominguez, O., and Gonzalez, S. (2012). Ectopic expression of the histone methyltransferase Ezh2 in haematopoietic stem cells causes myeloproliferative disease. *Nat Commun* *3*, 623.
- Hoischen, A., van Bon, B.W., Rodríguez-Santiago, B., Gilissen, C., Vissers, L.E., de Vries, P., Janssen, I., van Lier, B., Hastings, R., Smithson, S.F., et al. (2011). De novo nonsense mutations in ASXL1 cause Bohring-Opitz syndrome. *Nat. Genet.* *43*, 729–731.
- Kroon, E., Kros, J., Thorsteinsdottir, U., Baban, S., Buchberg, A.M., and Sauvageau, G. (1998). Hoxa9 transforms primary bone marrow cells through specific collaboration with Meis1a but not Pbx1b. *EMBO J.* *17*, 3714–3725.
- Kumar, A.R., Li, Q., Hudson, W.A., Chen, W., Sam, T., Yao, Q., Lund, E.A., Wu, B., Kowal, B.J., and Kersey, J.H. (2009). A role for MEIS1 in MLL-fusion gene leukemia. *Blood* *113*, 1756–1758.
- Landeira, D., Sauer, S., Poot, R., Dvorkina, M., Mazzarella, L., Jorgensen, H.F., Pereira, C.F., Leleu, M., Piccolo, F.M., Spivakov, M., et al. (2010). Jarid2 is a PRC2 component in embryonic stem cells required for multi-lineage differentiation and recruitment of PRC1 and RNA Polymerase II to developmental regulators. *Nat. Cell Biol.* *12*, 618–624.
- Lawrence, H.J., Sauvageau, G., Humphries, R.K., and Largman, C. (1996). The role of HOX homeobox genes in normal and leukemic hematopoiesis. *Stem Cells* *14*, 281–291.
- Lee, S.W., Cho, Y.S., Na, J.M., Park, U.H., Kang, M., Kim, E.J., and Um, S.J. (2010). ASXL1 represses retinoic acid receptor-mediated transcription through associating with HP1 and LSD1. *J. Biol. Chem.* *285*, 18–29.
- Ley, T.J., Ding, L., Walter, M.J., McLellan, M.D., Lamprecht, T., Larson, D.E., Kandath, C., Payton, J.E., Baty, J., Welch, J., et al. (2010). DNMT3A mutations in acute myeloid leukemia. *N. Engl. J. Med.* *363*, 2424–2433.
- MacKenzie, K.L., Dolnikov, A., Millington, M., Shounan, Y., and Symonds, G. (1999). Mutant N-ras induces myeloproliferative disorders and apoptosis in bone marrow repopulated mice. *Blood* *93*, 2043–2056.
- Margueron, R., and Reinberg, D. (2011). The Polycomb complex PRC2 and its mark in life. *Nature* *469*, 343–349.
- Metzeler, K.H., Becker, H., Maharry, K., Radmacher, M.D., Kohlschmidt, J., Mrózek, K., Nicolet, D., Whitman, S.P., Wu, Y.Z., Schwind, S., et al. (2011). ASXL1 mutations identify a high-risk subgroup of older patients with primary cytogenetically normal AML within the ELN Favorable genetic category. *Blood* *118*, 6920–6929.
- Mikkelsen, T.S., Ku, M., Jaffe, D.B., Issac, B., Lieberman, E., Giannoukos, G., Alvarez, P., Brockman, W., Kim, T.K., Koche, R.P., et al. (2007). Genome-wide maps of chromatin state in pluripotent and lineage-committed cells. *Nature* *448*, 553–560.
- Moran-Crusio, K., Reavie, L., Shih, A., Abdel-Wahab, O., Ndiaye-Lobry, D., Lobry, C., Figuerola, M.E., Vasanthakumar, A., Patel, J., Zhao, X., et al. (2011). Tet2 loss leads to increased hematopoietic stem cell self-renewal and myeloid transformation. *Cancer Cell* *20*, 11–24.
- Morin, R.D., Johnson, N.A., Severson, T.M., Mungall, A.J., An, J., Goya, R., Paul, J.E., Boyle, M., Woolcock, B.W., Kuchenbauer, F., et al. (2010). Somatic mutations altering EZH2 (Tyr641) in follicular and diffuse large B-cell lymphomas of germinal-center origin. *Nat. Genet.* *42*, 181–185.
- Muntean, A.G., Tan, J., Sitwala, K., Huang, Y., Bronstein, J., Connelly, J.A., Basur, V., Elenitoba-Johnson, K.S., and Hess, J.L. (2010). The PAF complex synergizes with MLL fusion proteins at HOX loci to promote leukemogenesis. *Cancer Cell* *17*, 609–621.
- Nikoloski, G., Langemeijer, S.M., Kuiper, R.P., Knops, R., Massop, M., Tönnissen, E.R., van der Heijden, A., Scheele, T.N., Vandenberghe, P., de Witte, T., et al. (2010). Somatic mutations of the histone methyltransferase gene EZH2 in myelodysplastic syndromes. *Nat. Genet.* *42*, 665–667.
- Park, U.H., Yoon, S.K., Park, T., Kim, E.J., and Um, S.J. (2011). Additional sex comb-like (ASXL) proteins 1 and 2 play opposite roles in adipogenesis via reciprocal regulation of peroxisome proliferator-activated receptor gamma. *J. Biol. Chem.* *286*, 1354–1363.
- Pasini, D., Cloos, P.A., Walfridsson, J., Olsson, L., Bukowski, J.P., Johansen, J.V., Bak, M., Tommerup, N., Rappilber, J., and Helin, K. (2010). JARID2 regulates binding of the Polycomb repressive complex 2 to target genes in ES cells. *Nature* *464*, 306–310.
- Peng, J.C., Valouev, A., Swigut, T., Zhang, J., Zhao, Y., Sidow, A., and Wysocka, J. (2009). Jarid2/Jumonji coordinates control of PRC2 enzymatic activity and target gene occupancy in pluripotent cells. *Cell* *139*, 1290–1302.
- Pratcorona, M., Abbas, S., Sanders, M., Koenders, J., Kavelaars, F., Erpelinck-Verschueren, C., Zeilemaker, A., Lowenberg, B., and Valk, P. (2012). Acquired mutations in ASXL1 in acute myeloid leukemia: prevalence and prognostic value. *Haematologica* *97*, 388–392.
- Sauvageau, M., and Sauvageau, G. (2010). Polycomb group proteins: multifaceted regulators of somatic stem cells and cancer. *Cell Stem Cell* *7*, 299–313.
- Scheuermann, J.C., de Ayala Alonso, A.G., Oktaba, K., Ly-Hartig, N., McGinty, R.K., Fraterman, S., Wilm, M., Muir, T.W., and Müller, J. (2010). Histone H2A deubiquitinase activity of the Polycomb repressive complex PR-DUB. *Nature* *465*, 243–247.
- Score, J., Hidalgo-Curtis, C., Jones, A.V., Winkelmann, N., Skinner, A., Ward, D., Zoi, K., Ernst, T., Stegelmann, F., Dohner, K., et al. (2012). Inactivation of polycomb repressive complex 2 components in myeloproliferative and myelodysplastic/myeloproliferative neoplasms. *Blood* *119*, 1208–1213.
- Shen, X., Kim, W., Fujiwara, Y., Simon, M.D., Liu, Y., Mysliwiec, M.R., Yuan, G.C., Lee, Y., and Orkin, S.H. (2009). Jumonji modulates polycomb activity and self-renewal versus differentiation of stem cells. *Cell* *139*, 1303–1314.
- Simon, C., Chagraoui, J., Kros, J., Gendron, P., Wilhelm, B., Lemieux, S., Boucher, G., Chagnon, P., Drouin, S., Lambert, R., et al. (2012). A key role

for EZH2 and associated genes in mouse and human adult T-cell acute leukemia. *Genes Dev.* 26, 651–656.

Sinclair, D.A., Milne, T.A., Hodgson, J.W., Shellard, J., Salinas, C.A., Kyba, M., Randazzo, F., and Brock, H.W. (1998). The Additional sex combs gene of *Drosophila* encodes a chromatin protein that binds to shared and unique Polycomb group sites on polytene chromosomes. *Development* 125, 1207–1216.

Somervaille, T.C., and Cleary, M.L. (2006). Identification and characterization of leukemia stem cells in murine MLL-AF9 acute myeloid leukemia. *Cancer Cell* 10, 257–268.

Takeda, A., Goolsby, C., and Yaseen, N.R. (2006). NUP98-HOXA9 induces long-term proliferation and blocks differentiation of primary human CD34+ hematopoietic cells. *Cancer Res.* 66, 6628–6637.

Testa, J.R., Cheung, M., Pei, J., Below, J.E., Tan, Y., Sementino, E., Cox, N.J., Dogan, A.U., Pass, H.I., Trusa, S., et al. (2011). Germline BAP1 mutations predispose to malignant mesothelioma. *Nat. Genet.* 43, 1022–1025.

Thol, F., Friesen, I., Damm, F., Yun, H., Weissinger, E.M., Krauter, J., Wagner, K., Chaturvedi, A., Sharma, A., Wichmann, M., et al. (2011). Prognostic significance of ASXL1 mutations in patients with myelodysplastic syndromes. *J. Clin. Oncol.* 29, 2499–2506.

Varambally, S., Dhanasekaran, S.M., Zhou, M., Barrette, T.R., Kumar-Sinha, C., Sanda, M.G., Ghosh, D., Pienta, K.J., Sewalt, R.G., Otte, A.P., et al. (2002). The polycomb group protein EZH2 is involved in progression of prostate cancer. *Nature* 419, 624–629.

Wiesner, T., Obenauf, A.C., Murali, R., Fried, I., Griewank, K.G., Ulz, P., Windpassinger, C., Wackernagel, W., Loy, S., Wolf, I., et al. (2011). Germline mutations in BAP1 predispose to melanocytic tumors. *Nat. Genet.* 43, 1018–1021.

Zhang, J., Socolovsky, M., Gross, A.W., and Lodish, H.F. (2003). Role of Ras signaling in erythroid differentiation of mouse fetal liver cells: functional analysis by a flow cytometry-based novel culture system. *Blood* 102, 3938–3946.

This copy is for your personal, non-commercial use only.

If you wish to distribute this article to others, you can order high-quality copies for your colleagues, clients, or customers by [clicking here](#).

Permission to republish or repurpose articles or portions of articles can be obtained by following the guidelines [here](#).

The following resources related to this article are available online at www.sciencemag.org (this information is current as of February 26, 2013):

Updated information and services, including high-resolution figures, can be found in the online version of this article at:

<http://www.sciencemag.org/content/333/6043/765.full.html>

Supporting Online Material can be found at:

<http://www.sciencemag.org/content/suppl/2011/07/13/science.1201662.DC1.html>

A list of selected additional articles on the Science Web sites **related to this article** can be found at:

<http://www.sciencemag.org/content/333/6043/765.full.html#related>

This article **cites 29 articles**, 14 of which can be accessed free:

<http://www.sciencemag.org/content/333/6043/765.full.html#ref-list-1>

This article has been **cited by** 6 articles hosted by HighWire Press; see:

<http://www.sciencemag.org/content/333/6043/765.full.html#related-urls>

This article appears in the following **subject collections**:

Medicine, Diseases

<http://www.sciencemag.org/cgi/collection/medicine>

Cellulose-, pectin-, and hemicellulose-degrading enzymes (GH families 5, 61, 3, and 28) were prominent, and GH5 endoglucanase (*S. lacrymans* S7.9 database protein ID, 433209) and GH74 endoglucanase/xyloglucanase (*S. lacrymans* S7.9 database protein ID, 453342) were up-regulated greater than 100-fold.

We conclude that brown rot fungi have cast off the energetically expensive apparatus of ligninolysis and acquired alternative mechanisms of initial attack. Wood decomposition by *S. lacrymans* may involve metabolically driven nonenzymatic disruption of lignocellulose with internal breakage of cellulose chains by highly localized ·OH radical action. Mycelia in split plates mimicking realistic nutrient heterogeneity (fig. S1) produced variegatic acid (VA), an iron-reducing phenolate (Fig. 2, A to C), via the Boletales atromentin pathway, which was recruited in *S. lacrymans* for the Fenton's reaction. The genome was rich in secondary metabolism genes (table S15), including a putative atromentin locus (24). Mycelium imports amino acids to sites of wood colonization (25), which is consistent with observed up-regulation of oligopeptide transporters on wood (table S12). Localizing variegatic acid production to well-resourced parts of the mycelium could enhance Fenton's chemistry in contact with wood.

Wood colonization is presumably followed by coordinated induction of the decay machinery revealed in the wood-induced transcriptome (Fig. 3 and fig. S4). GHs and oxidoreductases accounted for 20.7% of transcripts, accumulating greater than fourfold on wood relative to glucose medium (fig. S4 and table S12). Iron reduction mechanisms included an enzyme harboring a C terminal cellulose-binding module (*S. lacrymans* S7.9 database protein ID, 452187) (fig. S5) that is up-regulated 122-fold on wood substrate (fig. S4 and table S12). This enzyme, which is present in *Ph. chrysosporium* but absent from *P. placenta* (26), is a potential docking mechanism for localizing iron reductase activity, and hence ·OH generation, on the surface of microcrystalline cellulose. Cellulose-targeted iron reduction, combined with substrate induction of variegatic acid biosynthesis, might explain the particular ability of brown rot fungi in Boletales to degrade unassociated microcrystalline cellulose without the presence of lignin (27).

Thus, comparative genomics helps us understand the molecular processes of forest soil fungi that drive the element cycles of forest biomes (28). Sequenced forest Agaricomycetes revealed shared patterns of gene family contractions and expansions associated with emergences of both brown rot saprotrophy and ectomycorrhizal symbiosis. In Boletales, loss of aggressive ligninolysis might have permitted brown rot transitions to biotrophic ectomycorrhiza, which is promoted in soils impoverished in nitrogen by brown rot residues, and by the nutritional advantage conferred by the connection to a mycorrhizal network. *S. lacrymans* and other fungi cultured with conifer roots (29) ensheath *Pinus sylvestris* roots

with a mantle-like layer (fig. S6), suggesting nutrient exchange.

The chronology of divergences in extant fungal nutritional mode (Fig. 1A) matches the predicted major diversification in conifers (18), suggesting that the boreal forest biome may have originated via genetic coevolution of above- and below-ground biota.

References and Notes

1. F. Martin *et al.*, *New Phytol.* **190**, 818 (2011).
2. F. Martin, in *Biology of the Fungal Cell*, R. J. Howard, N. A. R. Gow, Eds. (Springer Berlin, Heidelberg, 2007), vol. 8, pp. 291–308.
3. R. L. Gilbertson, *Mycologia* **72**, 1 (1980).
4. D. S. Hibbett, M. J. Donoghue, *Syst. Biol.* **50**, 215 (2001).
5. K.-E. Eriksson, R. A. Blanchette, P. Ander, *Microbial and enzymatic degradation of wood and wood components* (Springer-Verlag, Berlin, New York, 1990).
6. B. D. Lindahl *et al.*, *New Phytol.* **173**, 611 (2007).
7. R. R. Northup, Z. Yu, R. A. Dahlgren, K. A. Vogt, *Nature* **377**, 227 (1995).
8. B. Goodell *et al.*, *J. Biotechnol.* **53**, 133 (1997).
9. T. Shimokawa, M. Nakamura, N. Hayashi, M. Ishihara, *Holzforchung* **58**, 305 (2005).
10. V. Arantes, A. M. Milagres, T. R. Filley, B. Goodell, *J. Ind. Microbiol. Biotechnol.* **38**, 541 (2011).
11. S. F. Curling, C. A. Clausen, J. E. Winandy, *Int. Biodeterior. Biodegradation* **49**, 13 (2002).
12. M. Binder, D. S. Hibbett, *Mycologia* **98**, 971 (2006).
13. D. Martinez *et al.*, *Proc. Natl. Acad. Sci. U.S.A.* **106**, 1954 (2009).
14. F. Martin *et al.*, *Nature* **464**, 1033 (2010).
15. F. Martin *et al.*, *Nature* **452**, 88 (2008).
16. D. Martinez *et al.*, *Nat. Biotechnol.* **22**, 695 (2004).
17. M. Binder, K. H. Larsson, P. B. Matheny, D. S. Hibbett, *Mycologia* **102**, 865 (2010).
18. A. J. Eckert, B. D. Hall, *Mol. Phylogenet. Evol.* **40**, 166 (2006).
19. H. Kausserud *et al.*, *Mol. Ecol.* **16**, 3350 (2007).
20. O. Schmidt, *Holzforchung* **54**, 221 (2000).
21. Materials and methods are available as supporting material on Science Online.
22. B. L. Cantarel *et al.*, *Nucleic Acids Res.* **37**, D233 (2009).
23. G. Vaaje-Kolstad *et al.*, *Science* **330**, 219 (2010).
24. P. Schneider, S. Bouhired, D. Hoffmeister, *Fungal Genet. Biol.* **45**, 1487 (2008).
25. M. Tialka, M. Fricker, S. Watkinson, *Appl. Environ. Microbiol.* **74**, 2700 (2008).
26. A. Vanden Wymelenberg *et al.*, *Appl. Environ. Microbiol.* **76**, 3599 (2010).
27. T. Nilsson, J. Ginns, *Mycologia* **71**, 170 (1979).
28. B. O. Lindahl, A. F. S. Taylor, R. D. Finlay, *Plant Soil* **242**, 123 (2002).
29. R. Vasiliauskas, A. Menkis, R. D. Finlay, J. Stenlid, *New Phytol.* **174**, 441 (2007).

Acknowledgments: J. Schilling, University of Minnesota, and D. Barbara, University of Warwick, critically reviewed the manuscript; T. Marks designed graphics; and B. Wackler and M. Zomorodi gave technical assistance. Assembly and annotations of *S. lacrymans* genomes are available at www.jgi.doe.gov/Serpula and DNA Data Bank of Japan/European Molecular Biology Laboratory/GenBank, accessions nos. AECQB000000000 and AEQC000000000. The complete microarray expression data set is available at the Gene Expression Omnibus (www.ncbi.nlm.nih.gov/geo/) accession no. GSE27839. The work was conducted by the U.S. Department of Energy Joint Genome Institute and supported by the Office of Science of the U.S. Department of Energy under contract DE-AC02-05CH11231. Further financial support is acknowledged in the supporting online material on Science Online.

Supporting Online Material

www.sciencemag.org/cgi/content/full/science.1205411/DC1
Materials and Methods
SOM Text
Figs. S1 to S6
Tables S1 to S15
References (30–89)

10 March 2011; accepted 20 June 2011
Published online 14 July 2011;
10.1126/science.1205411

The Leukemogenicity of AML1-ETO Is Dependent on Site-Specific Lysine Acetylation

Lan Wang,¹ Alexander Gural,¹ Xiao-Jian Sun,² Xinyang Zhao,¹ Fabiana Perna,¹ Gang Huang,¹ Megan A. Hatlen,¹ Ly Vu,¹ Fan Liu,¹ Haiming Xu,¹ Takashi Asai,¹ Hao Xu,¹ Tony Deblasio,¹ Silvia Menendez,¹ Francesca Voza,¹ Yanwen Jiang,³ Philip A. Cole,⁴ Jinsong Zhang,⁵ Ari Melnick,³ Robert G. Roeder,² Stephen D. Nimer^{1*}

The chromosomal translocations found in acute myelogenous leukemia (AML) generate oncogenic fusion transcription factors with aberrant transcriptional regulatory properties. Although therapeutic targeting of most leukemia fusion proteins remains elusive, the posttranslational modifications that control their function could be targetable. We found that AML1-ETO, the fusion protein generated by the t(8;21) translocation, is acetylated by the transcriptional coactivator p300 in leukemia cells isolated from t(8;21) AML patients, and that this acetylation is essential for its self-renewal-promoting effects in human cord blood CD34⁺ cells and its leukemogenicity in mouse models. Inhibition of p300 abrogates the acetylation of AML1-ETO and impairs its ability to promote leukemic transformation. Thus, lysine acetyltransferases represent a potential therapeutic target in AML.

Histone-modifying enzymes can regulate the binding of specific chromatin-binding proteins to histone marks and can change the affinity of the histones for DNA (1, 2). These

enzymes also affect nonhistone proteins, and posttranslational modifications of transcription factors such as p53 or AML1 (which is required for definitive hematopoietic development) can

regulate their protein-protein interactions and their activity (1–3). For instance, p300 binds to the C terminus of AML1 and acetylates its N terminus, promoting its activating function (4, 5). When AML1 is fused to ETO (a nuclear protein that interacts with co-repressor molecules) by the t(8;21) translocation, the p300-binding region of AML1 is lost from the AML1-ETO fusion protein (hereafter abbreviated as A-E).

Studies of hematopoietic development and specific gene promoter function indicate that A-E is generally considered to act as a transcription repressor via recruitment of co-repressors (such as NCoR and SMRT) and histone deacetylases (6–8). Although A-E also up-regulates target gene expression (9, 10), information about the mechanisms of gene activation or the importance of the up-regulated genes is sparse. We have shown that the NHR1 domain in A-E binds HEB, a class I basic helix-loop-helix protein (i.e., an E protein) (11). To explore the importance of this domain to the leukemia-promoting properties of A-E, we compared the effects of “wild-type” A-E with those of the A-E ΔNHR1 construct (which lacks amino acids 245 to 436) on the self-renewal and differentiation potential of human CD34⁺ hematopoietic stem/progenitor cells (HSPCs) isolated from cord blood.

After confirming the expression of Flag-tagged A-E and A-E ΔNHR1 by Western blotting (fig. S1A), we examined HSPC self-renewal with the use of CAFC (cobblestone area-forming cell) assays (12, 13). Unlike A-E, A-E ΔNHR1 did not increase the number of CAFCs present at week 5 (Fig. 1A and fig. S3C), nor did it promote the maintenance of CD34⁺ HSPCs growing in liquid culture (5.1% for A-E ΔNHR1 versus 22.1% for A-E and 3.7% for the MIGR1 control); these findings indicate the essential role of the NHR1 (amino acids 245 to 436) domain in the self-renewal-promoting effects of A-E in this model (Fig. 1B and fig. S1B).

To determine whether the NHR1 domain is required for the inhibitory effect of A-E on differentiation, we grew A-E and A-E ΔNHR1-transduced cells in liquid culture with erythroid or myeloid differentiation-promoting cytokines for 9 days. Both the A-E- and A-E ΔNHR1-expressing cells showed a similar decrease in glycophorin A, CD71, and CD11b expression (fig. S1C). Thus, loss of the NHR1 domain affects the self-renewal signals provided by A-E, but not the delay (or block) in myelo-erythroid differentiation.

To investigate how the NHR1 domain of A-E promotes self-renewal, we used microarray-based expression assays to compare the transcriptome

of the A-E- and A-E ΔNHR1-transduced human HSPCs (versus control MIGR1-transduced HSPCs). Several potential regulators of HSC

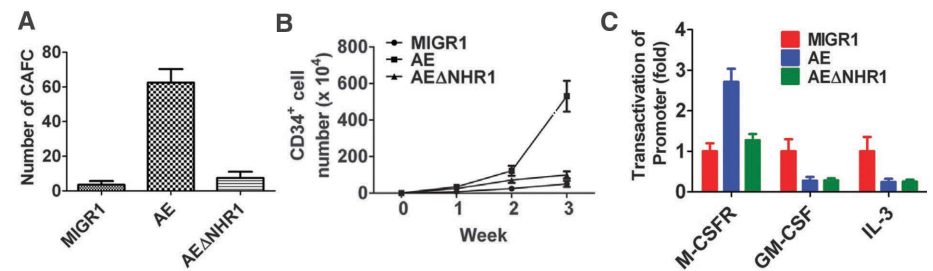


Fig. 1. The enhanced self-renewal capacity and transcriptional activation induced by A-E in human HSPCs requires the NHR1 domain. (A) The NHR1 domain (amino acids 245 to 436) is required for A-E to increase CAFC formation by human CD34⁺ cells transduced with the indicated retroviral vector. The number of cobblestone areas at week 5 is shown (± SD; n = 3). (B) Deletion of NHR1 affects the ability of A-E to promote self-renewal in liquid culture. CD34 expression was examined weekly in MIGR1-, A-E-, and A-E ΔNHR1-transduced human CD34⁺ cells (± SD; n = 3). (C) *M-CSFR*, *GM-CSF*, and *IL-3* promoter activity was examined in cells transfected with MIGR1, A-E, or A-E ΔNHR1 (± SD; n = 3). All values were standardized to the level of *Renilla* luciferase activity.

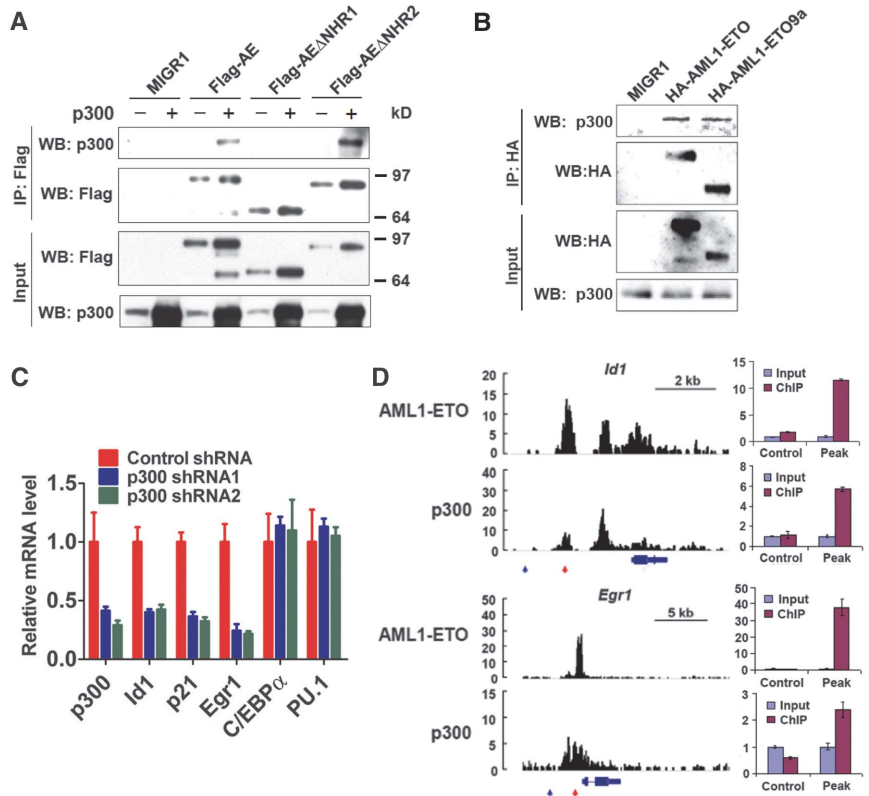


Fig. 2. The NHR1 domain of A-E interacts with p300, which potentiates its transcriptional activating properties. (A) The NHR1 domain is required for the interaction of A-E with p300. An antibody to Flag was used for immunoprecipitation (IP); antibodies to p300 or Flag were used for Western blotting (WB). (B) AE9a also interacts with p300. An antibody to hemagglutinin (HA) was used for immunoprecipitation; antibodies to p300 or HA were used for Western blotting. (C) Knockdown of p300 decreased the expression of A-E-activated target genes. Kasumi-1 cells were transduced with shRNAs against p300 or a control shRNA. Quantitative polymerase chain reaction (qPCR) was performed to quantify the level of target gene expression (± SD; n = 3). (D) A-E and p300 colocalize on some A-E up-regulated genes, as shown by ChIP-seq assays. Representative examples of A-E and p300 co-occupancy are shown as custom tracks in the UCSC genome browser. The locations of the Runx1 consensus binding sites are shown by green lines on the x axis. DNA binding was also analyzed by qPCR amplification of the regions indicated by the red and green arrows on the x axis (± SD; n = 3).

¹Molecular Pharmacology and Chemistry Program, Sloan-Kettering Institute, Memorial Sloan-Kettering Cancer Center, New York, NY 10065, USA. ²Laboratory of Biochemistry and Molecular Biology, Rockefeller University, 1230 York Avenue, New York, NY 10065, USA. ³Division of Hematology/Oncology, Department of Medicine, Weill Cornell Medical College, New York, NY 10065, USA. ⁴Department of Pharmacology and Molecular Sciences, Johns Hopkins University School of Medicine, Baltimore, MD 21205, USA. ⁵Department of Cancer and Cell Biology, University of Cincinnati College of Medicine, 3125 Eden Avenue, Cincinnati, OH 45267, USA.

*To whom correspondence should be addressed. E-mail: nimers@mskcc.org

self-renewal (*Id1*, *p21*, and *Egr1*) were up-regulated by A-E but not by A-E Δ NHR1 (14–16) (fig. S3E). Similarly, A-E Δ NHR1 was much less transactivating than A-E on the *M-CSFR* promoter (Fig. 1C) (17). In contrast, the differentiation-promoting genes, *C/EBP α* and *PU.1*, that are down-regulated by A-E are still down-regulated by A-E Δ NHR1 (18, 19) (fig. S3E), and both the *IL-3* and *GM-CSF* promoters were similarly down-regulated by A-E and A-E Δ NHR1 (Fig. 1C). These results suggest that the NHR1 domain is required for transcriptional activation but not repression by A-E, and is required for the effects of A-E on self-renewal but not differentiation.

We next examined whether A-E directly binds p300. Baculovirus-expressed A-E and p300 directly interact in vitro (fig. S6B), and an antibody to ETO coimmunoprecipitated the endogenous A-E and p300 proteins in human Kasumi-1 leukemia cells, which do not express ETO (fig. S6B). We generated several A-E or ETO deletion mutants in order to map the p300-binding domain in A-E (Fig. 2A and fig. S1D). Both A-E and ETO bound p300, and although deletions of the NHR2 domain in either ETO or A-E had no effect on

p300 binding, deletion of the NHR1 domain (amino acids 245 to 436) completely abrogated this binding (Fig. 2A and fig. S1D). Furthermore, the A-E exon 9a protein, an alternatively spliced form of A-E that lacks NHR3 and NHR4 (depicted in fig. S2A), also interacts with p300 (Fig. 2B). Given that ETO can bind both co-repressor molecules and p300, ETO may function as a fast-response adaptor protein, inducing transcriptional activation or repression depending on the signaling pathways activated in the cell.

To determine whether p300 is important for the up-regulation of A-E target gene expression, we knocked down p300 in Kasumi-1 cells with the use of two different short hairpin RNAs (shRNAs); we found significant decreases in the levels of *Id1*, *p21*, and *Egr1* mRNA but no change in the levels of *C/EBP α* or *PU.1* mRNA (Fig. 2C), indicating that p300 is essential for A-E-mediated transcriptional activation. To identify genes potentially regulated by A-E and p300, we performed ChIP-seq (chromatin immunoprecipitation sequencing) assays using antibodies to p300 and ETO and the A-E-expressing Kasumi-1 cells. We found that the promoters of the *Id1*, *p21*, and *Egr1* genes (genes

activated by A-E) were co-occupied by A-E and p300 (Fig. 2D and fig. S5C). In contrast, p300 did not colocalize with A-E at the promoter (or enhancer) of the *C/EBP α* gene, which is repressed by A-E (Fig. 2D and fig. S5C). Thus, p300 can contribute to the ability of A-E to function as a transcriptional activator, and both can target similar transcriptional regulatory regions.

Given that p300 acetylates a variety of protein targets, we examined whether A-E is acetylated by p300 by overexpressing A-E and p300 in 293T cells. A-E, but not ETO, was acetylated by p300, localizing the potential acetylation sites to the AML1 portion of A-E (amino acids 1 to 177) (fig. S1E). Deletion of the Runt domain (amino acids 49 to 177) did not affect A-E acetylation (fig. S1E), leaving Lys²⁴ and Lys⁴³ as the only candidate acetylation sites (fig. S2A). We mutated Lys²⁴ and Lys⁴³ to arginine, separately and together (i.e., K24R, K43R, and K24R/K43R), and then used an antibody to acetyl lysine to confirm that both Lys²⁴ and Lys⁴³ are acetylated by p300 (Fig. 3A). As predicted, acetylation of Lys⁴³ was abrogated after deletion of the NHR1 domain (amino acids 245 to 436), the region responsible for the A-E/p300 interaction (Fig. 3B). The Lys²⁴ and Lys⁴³ residues are highly conserved in other vertebrates (fig. S2B), which suggests that their acetylation may be conserved throughout evolution.

To define how acetylation of A-E affects its functions, we compared the effects of “wild-type” A-E and the A-E K24R, K43R, and K24R/K43R mutant proteins on the in vitro behavior of transduced human HSPCs (fig. S3A). Like A-E, A-E K24R increased the number of CAFs present at week 5, whereas A-E K43R and A-E K24R/K43R did not (fig. S3, B and C). The K43R mutation also abrogated the effect of A-E on self-renewal, whereas the A-E K24R mutant protein retained this effect (fig. S3D). Thus, acetylation of A-E at Lys⁴³ is essential for its self-renewal-promoting effects in human HSPCs [and for its effects on the self-renewal-promoting genes *Id1*, *p21*, and *Egr1* (fig. S3E)].

To investigate the role of A-E acetylation in leukemogenesis in vivo, we expressed the wild type and the K24R, K43R, and K24R/K43R mutant forms of the AE9a protein (the isoform of A-E that can induce leukemia in mouse models by itself) in fetal liver HSPCs by means of retroviral transduction and transplantation assays (20). We examined the peripheral blood, bone marrow, and spleen of the mice 15 weeks after transplantation, and found large numbers of blast cells in the AE9a and AE9a K24R mice, but not in the AE9a K43R or AE9a K24R/K43R mice (fig. S4D). The AE9a K43R mice also had normal white blood cell counts and platelet counts and displayed less anemia than did the AE9a mice (fig. S4B), whereas the blood counts of the AE9a K24R mice were as abnormal as those of the AE9a mice. The AE9a K43R mice also had far fewer c-kit⁺ immature peripheral blood cells at 15 weeks than did the AE9a mice or the AE9a K24R mice, and

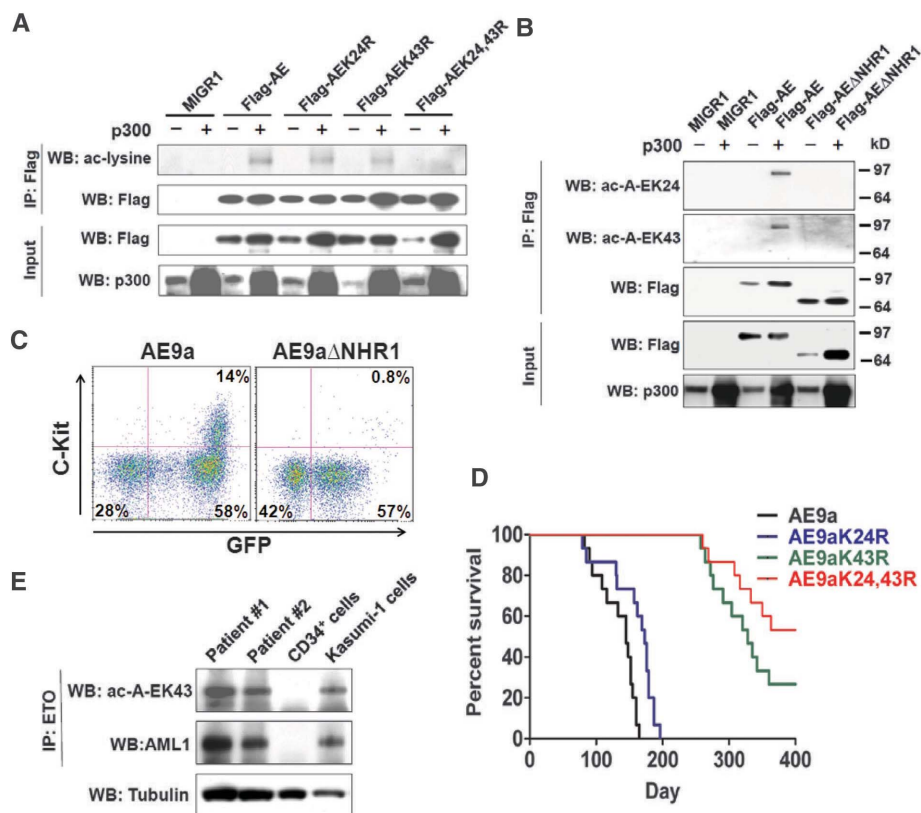


Fig. 3. The acetylation of A-E Lys⁴³ by p300 is required for A-E-induced leukemogenesis. **(A)** Acetylation of Flag-tagged A-E by p300. Antibodies to Flag or to acetyl lysine were used for immunoprecipitation or Western blotting. **(B)** The ability of A-E to bind p300 is required for its lysine acetylation. Antibodies to Flag or to acetyl A-E Lys²⁴ or Lys⁴³ were used for immunoprecipitation or Western blotting. **(C)** Lethally irradiated recipient mice were injected with HSPCs transduced with AE9a or AE9a Δ NHR1. The number of GFP⁺ c-kit⁺ cells in the peripheral blood is shown 15 weeks after transplant. **(D)** Survival of mice receiving AE9a-transduced or AE9a mutant-transduced HSPCs ($P < 0.0001$, $n = 15$ per group). **(E)** Acetylation of A-E Lys⁴³ was detected in blast cells from t(8;21)⁺ leukemia patients. Antibodies to ETO, acetyl A-E Lys⁴³, or AML1 were used for immunoprecipitation or Western blotting (29).

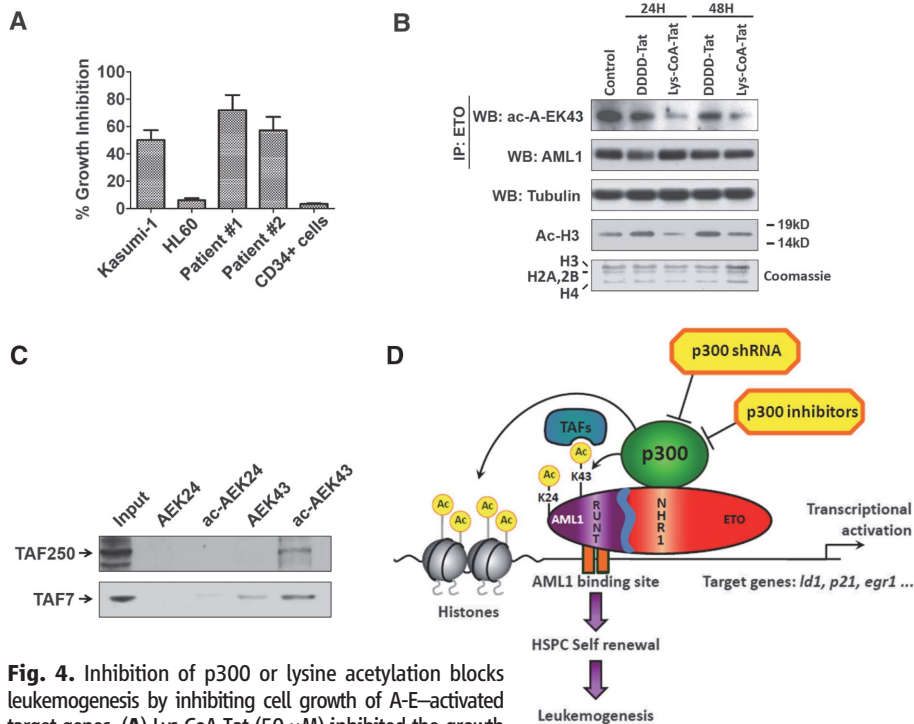


Fig. 4. Inhibition of p300 or lysine acetylation blocks leukemogenesis by inhibiting cell growth of A-E-activated target genes. **(A)** Lys-CoA-Tat (50 μ M) inhibited the growth of primary t(8;21)⁺ leukemia cells and Kasumi-1 cells (\pm SD; $n = 3$) but not HL-60 cells or normal human CD34⁺ HSPCs. **(B)** Lys-CoA-Tat (50 μ M) blocks A-E Lys⁴³ and histone H3 acetylation in Kasumi-1 cells, as detected by antibodies to acetyl A-E Lys⁴³ or to histone H3. **(C)** The binding of TAF_{II}250 and TAF7 to A-E peptides that contain acetylated or unacetylated Lys²⁴ or Lys⁴³ was studied using a peptide pull-down assay. Antibodies to TAF_{II}250 or TAF7 were used for Western blotting. **(D)** A hypothetical model showing how p300, and acetylation of A-E by p300, might cooperate to induce leukemia.

the cells retained expression of CD45 (fig. S4C). All of the mice that received AE9a-transduced HSPCs developed AML; the median survival of the AE9a mice and the AE9a K24R mice was 145 and 173 days, respectively ($P < 0.001$). However, the median survival of the AE9a K43R and AE9a K24R/K43R mice was 328 days and “not reached,” respectively (Fig. 3D). Note that AE9a is also acetylated on Lys⁴³ in vivo, as assessed in AML cells isolated from the spleens of fully leukemic mice (fig. S4E).

Because the NHR1 domain is required for the acetylation of A-E Lys⁴³, we also examined whether its deletion affected the leukemogenicity of AE9a. At 15 weeks after transplantation, the AE9a Δ NHR1 mice had normal white blood cell counts and less anemia than did the AE9a mice (fig. S1F). The AE9a Δ NHR1 mice also had far fewer GFP⁺ c-kit⁺ immature cells in the peripheral blood than did the AE9a mice at 15 weeks (0.8% versus 14%) (Fig. 3C). This in vivo result differs from what has been reported using smaller NHR1 domain deletions, perhaps reflecting the size of the deletion or the use of different model systems (21–24).

Together, these results indicate that acetylation of AE9a at Lys⁴³ is required for AE9a-induced leukemogenesis in mice. Note that A-E, A-E K24R, A-E K43R, and A-E K24R/K43R are expressed at similar levels in the 293T cells

(fig. S5A) and they have similar DNA binding activity in electrophoretic mobility shift assays (fig. S5B) (25). To determine whether A-E is acetylated in t(8;21) leukemia patient samples, we analyzed two A-E–positive patient samples and found detectable A-E Lys²⁴ and A-E Lys⁴³ acetylation in both (Fig. 3E and fig. S3G).

To define whether acetylation of A-E is required to inhibit differentiation, we examined the level of glycophorin A and CD11b expression on transduced cells grown in differentiation-driving cytokines. Both A-E and A-E K24R/K43R triggered a similar decrease in the expression of these differentiation markers (fig. S3F). Thus, the absence of A-E Lys⁴³ acetylation affects the self-renewal signals provided by A-E, but not the delay or block of differentiation, which is consistent with its effects on the myeloid differentiation genes *C/EBP α* and *PUL1* (fig. S3E). We performed mass spectrometry and found that a Lys⁴³-acetylated A-E peptide (but not the non-acetylated peptide) preferentially bound a variety of proteins, including several components of the transcriptional pre-initiation complex (TAF). We performed peptide pull-down assays and found binding of both TAF7 and TAF_{II}250 (Fig. 4C). This suggests that the acetylation of A-E Lys⁴³, which is critical for A-E–induced transcriptional activation, may work at least in part by promoting the recruitment of bromodomain-containing

TAF proteins. Of course, histone acetyltransferases other than p300 may also contribute to the acetylation of A-E, and the Lys⁴³-containing region may recruit transcription factors or other coactivators in addition to bromodomain-containing proteins.

Given the importance of the interaction of A-E with p300, and its subsequent acetylation, we assessed whether inhibiting p300 function by means of RNA interference or chemical inhibitors would alter leukemia cell growth. Knockdown of p300 decreased the level of A-E acetylation (fig. S6A) and decreased the expression of *Id1*, *p21*, and *Egr1* (Fig. 2C). We also treated primary t(8;21)⁺ leukemia cells isolated from patients, as well as t(8;21)⁺ Kasumi-1 cells with the p300 inhibitor Lys-CoA-Tat and a second p300 inhibitor C646 (26, 27); both inhibitors decreased the levels of *Id1*, *p21*, and *Egr1* mRNA as well as the levels of acetylated A-E Lys⁴³ and histone H3 (Fig. 4B and fig. S6A). Lys-CoA-Tat also inhibited the growth of the t(8;21) positive primary patient leukemia cells and Kasumi-1 cells (as did C646), with little effect on the growth of normal human HSPCs (Fig. 4A and fig. S6C). Furthermore, both Lys-CoA-Tat and C646 inhibited the growth of MO-91, U937, and HEL cells, with minimal effect on THP-1, Mono-Mac-1, or HL60 cells (fig. S6C). Thus, other acetylated proteins—perhaps the nonhistone substrates of p300—may regulate the sensitivity of cells to p300 inhibition, which suggests that inhibition of p300 function could have broader therapeutic potential in AML.

We next used two different mouse leukemia models to examine the effect of p300 inhibitors on leukemia cell growth in vivo. We treated 3×10^6 AE9a-expressing or MLL-AF9-expressing leukemia cells ex vivo with Lys-CoA-Tat or C646 for 12 hours before injecting the cells into sublethally irradiated C57Bl/6 mice (day 0) (28). Both p300 inhibitors reduced the number of immature GFP⁺ c-kit⁺ cells in the AE9a mice (fig. S7A), leading to lower white blood cell counts, less anemia, and less thrombocytopenia relative to the recipients of DDDD-Tat-treated or C37-treated AE9a cells (fig. S7B). These p300 inhibitors significantly increased the median survival from 36 days to 54 days for Lys-CoA-Tat and from 32 days to 43 days for C646 ($P < 0.0001$; fig. S7C). In contrast, Lys-CoA-Tat did not affect the survival of the MLL-AF9 leukemia mice, and C646 had only a minimal effect on MLL-AF9-driven leukemia, increasing the median survival from 23 days to 28 days (fig. S7C). Thus, p300 inhibitors can block the transcriptional activating function of A-E and decrease the growth of A-E-expressing leukemia cells, providing a potentially therapeutic approach to t(8;21) AML (and possibly other AML subtypes as well).

Our results show that acetylation of A-E (and AE9a) by p300 is required for their leukemogenic effects in a human preleukemia model and a mouse AML model. The NHR1 domain of A-E

provides a docking site for p300, allowing A-E and p300 to colocalize at the regulatory regions of many A-E up-regulated genes, including those involved in self-renewal (e.g., *Id1*, *p21*, and *Egr1*). The critical consequence of this interaction is that A-E is acetylated—an event essential for its self-renewal-promoting effects and its ability to activate gene expression. Thus, even though A-E can bind p300 and presumably bring it to chromatin where it can acetylate histone residues, it is the acetylation of A-E itself that is the key step, perhaps at least in part by recruiting bromodomain-containing proteins such as TAF_{II}250 or TAF7 (see our model for A-E-induced leukemogenesis in Fig. 4D). The discovery that site-specific lysine acetylation of the AML1-ETO oncogenic fusion protein contributes potently to leukemogenesis suggests that inhibition of its acetylation merits exploration as a possible therapeutic strategy for t(8;21)⁺ leukemia.

References and Notes

- C. Choudhary *et al.*, *Science* **325**, 834 (2009); 10.1126/science.1175371.
- W. Gu, R. G. Roeder, *Cell* **90**, 595 (1997).
- L. Wang *et al.*, *Blood Cells Mol. Dis.* **43**, 30 (2009).
- Y. Yamaguchi *et al.*, *J. Biol. Chem.* **279**, 15630 (2004).
- I. Kitabayashi, A. Yokoyama, K. Shimizu, M. Ohki, *EMBO J.* **17**, 2994 (1998).
- S. D. Nimer, M. A. Moore, *Oncogene* **23**, 4249 (2004).
- J. Wildonger, R. S. Mann, *Development* **132**, 2263 (2005).
- S. Minucci, C. Nervi, F. Lo Coco, P. G. Pelicci, *Oncogene* **20**, 3110 (2001).
- L. Klampfer, J. Zhang, A. O. Zelenetz, H. Uchida, S. D. Nimer, *Proc. Natl. Acad. Sci. U.S.A.* **93**, 14059 (1996).
- Y. Liu *et al.*, *Cancer Cell* **9**, 249 (2006).
- J. Zhang, M. Kalkum, S. Yamamura, B. T. Chait, R. G. Roeder, *Science* **305**, 1286 (2004).
- D. A. Breems, E. A. Blockland, S. Neben, R. E. Ploemacher, *Leukemia* **8**, 1095 (1994).
- J. C. Mulloy *et al.*, *Blood* **99**, 15 (2002).
- V. Jankovic *et al.*, *Proc. Natl. Acad. Sci. U.S.A.* **104**, 1260 (2007).
- A. Viale *et al.*, *Nature* **457**, 51 (2009).
- A. Wilson, E. Laurenti, A. Trumpp, *Curr. Opin. Genet. Dev.* **19**, 461 (2009).
- K. L. Rhoades *et al.*, *Proc. Natl. Acad. Sci. U.S.A.* **93**, 11895 (1996).
- T. Pabst *et al.*, *Nat. Med.* **7**, 444 (2001).
- R. K. Vangala *et al.*, *Blood* **101**, 270 (2003).
- M. Yan *et al.*, *Nat. Med.* **12**, 945 (2006).
- M. Yan, E. Y. Ahn, S. W. Hiebert, D. E. Zhang, *Blood* **113**, 883 (2009).
- C. Kwok, B. B. Zeisig, J. Qiu, S. Dong, C. W. So, *Proc. Natl. Acad. Sci. U.S.A.* **106**, 2853 (2009).
- D. Mannari, D. Gascoyne, J. Dunne, T. Chaplin, B. Young, *Leukemia* **24**, 891 (2010).
- S. Park *et al.*, *Blood* **113**, 3558 (2009).
- A. J. Okumura, L. F. Peterson, F. Okumura, A. Boyapati, D. E. Zhang, *Blood* **112**, 1392 (2008).
- Y. Zheng *et al.*, *J. Am. Chem. Soc.* **127**, 17182 (2005).
- E. M. Bowers *et al.*, *Chem. Biol.* **17**, 471 (2010).
- L. Wang *et al.*, *Cell Death Differ.* **14**, 306 (2007).
- X. Zhao *et al.*, *Genes Dev.* **22**, 640 (2008).

Acknowledgments: We thank members of the Nimer lab for thoughtful suggestions and comments; D. J. Meyers for the HAT inhibitors; E. Chuang for help with manuscript preparation; E. Dolezal for help with patient samples; K. Debeer for help with graphic design; M. E. Figueroa for help with data analysis; S. Pereira Mendez for technical assistance; and the MSKCC Animal Core Facility, Flow Cytometry Core Facility, and Anti-tumor Assessment Core Facility for their help. P.A.C. is a cofounder, paid consultant, and shareholder of Acylin Therapeutics Inc., which is developing p300 HAT inhibitors. P.A.C. and Johns Hopkins University hold a patent on HAT inhibitors that has been licensed to Acylin Therapeutics Inc. Supported by a Leukemia Lymphoma Society SCOR grant (S.D.N., R.G.R.), a Leukemia Lymphoma Society fellowship (L.W.), an Empire State Stem Cell Scholar award (L.W.), a Clinical Scholars award (F.L.), a Starr Foundation grant (X.-J.S., R.G.R., S.D.N.), NIH grant GM62437 (P.A.C.), and the Gabrielle's Angel Foundation. The microarray data have been submitted to the National Center for Biotechnology Information Gene Expression Omnibus (GEO) GSE28317.

Supporting Online Material

www.sciencemag.org/cgi/content/full/science.1201662/DC1
Materials and Methods
Figs. S1 to S7

14 December 2010; accepted 17 June 2011
Published online 14 July 2011;
10.1126/science.1201662

Cartilage Acidic Protein–1B (LOTUS), an Endogenous Nogo Receptor Antagonist for Axon Tract Formation

Yasufumi Sato,^{1*} Masumi Iketani,^{1*} Yuji Kurihara,¹ Megumi Yamaguchi,¹ Naoya Yamashita,¹ Fumio Nakamura,¹ Yuko Arie,¹ Takahiko Kawasaki,² Tatsumi Hirata,² Takaya Abe,³ Hiroshi Kiyonari,³ Stephen M. Strittmatter,⁴ Yoshio Goshima,^{1,5†} Kohtaro Takei^{1,5†}

Neural circuitry formation depends on the molecular control of axonal projection during development. By screening with fluorophore-assisted light inactivation in the developing mouse brain, we identified cartilage acidic protein–1B as a key molecule for lateral olfactory tract (LOT) formation and named it LOT usher substance (LOTUS). We further identified Nogo receptor–1 (NgR1) as a LOTUS-binding protein. NgR1 is a receptor of myelin-derived axon growth inhibitors, such as Nogo, which prevent neural regeneration in the adult. LOTUS suppressed Nogo–NgR1 binding and Nogo-induced growth cone collapse. A defasciculated LOT was present in *lotus*-deficient mice but not in mice lacking both *lotus*- and *ngr1*. These findings suggest that endogenous antagonism of NgR1 by LOTUS is crucial for normal LOT formation.

Spatially represented information in specific regions is a common feature of the nervous system and is essential for higher brain function. Specificity of neural connections that ensures the precise relay of information is required for establishing such spatial representation of information. In these processes, various types of repulsive and attractive guidance molecules and their receptors have crucial roles (1).

The olfactory bulb (OB) is the first relay for olfactory information. The axons of early-generated mitral cells emerge from the OB at embryonic day (E) 12.5 in the mouse; thereafter, they grow

laterally and then elongate caudally at the surface of the telencephalon (2, 3). This projection of mitral cells, termed the lateral olfactory tract (LOT), is stereotypically organized in the higher olfactory centers (4, 5). The LOT is a good experimental system for analysis of the molecular mechanisms underlying neural circuit formation, because LOT formation can be visualized by anterograde tracing with the lipophilic dialkylcarbocyanine (DiI) or by immunohistochemistry of the LOT marker protein neuropilin-1 (Nrp1) in whole-mount samples of brain and its developmental process can be observed in an organotypic

culture system. Therefore, we used these techniques to screen for molecules that function in LOT formation.

We established a molecular targeting method by modifying the fluorophore-assisted light inactivation (FALI) technique (6, 7) (fig. S1). FALI, generally known as chromophore-assisted light inactivation, is an acute protein-ablation technique directed by binding of fluorescein isothiocyanate (FITC)-labeled antibodies. Light irradiation at a wavelength of 490 nm induces local generation of oxygen radicals (singlet oxygen) from the fluorophore, which react chemically with the nearby target antigen and inactivate it (fig. S1A). We modified the technique to perform continuous protein inactivation during periods of 24 hours and longer (fig. S1B). The protein inactivation can be achieved with nonneutralizing antibodies. To identify the molecules that function for LOT formation, we generated monoclonal antibodies (mAbs) produced with a homogenate of protein extract from the developing

¹Department of Molecular Pharmacology and Neurobiology, Yokohama City University Graduate School of Medicine, Yokohama 236-0004, Japan. ²Division of Brain Function, National Institute of Genetics, Graduate School for Advanced Studies, Mishima 411-8540, Japan. ³Laboratory for Animal Resources and Genetic Engineering, RIKEN Center for Developmental Biology, Kobe 650-0047, Japan. ⁴Department of Neurology and Section of Neurobiology, Yale University School of Medicine, New Haven, CT 06520, USA. ⁵Advanced Medical Research Center, Yokohama City University Graduate School of Medicine, Yokohama 236-0004, Japan.

*These authors contributed equally to this study.

†To whom correspondence should be addressed. E-mail: kohtaro@med.yokohama-cu.ac.jp (K.T.); goshima@med.yokohama-cu.ac.jp (Y.G.)

Tet2 Loss Leads to Increased Hematopoietic Stem Cell Self-Renewal and Myeloid Transformation

Kelly Moran-Crusio,^{1,2,11} Linsey Reavie,^{1,2,11} Alan Shih,^{3,4,11} Omar Abdel-Wahab,^{3,4} Delphine Ndiaye-Lobry,^{1,2} Camille Lobry,^{1,2} Maria E. Figueroa,⁵ Aparna Vasanthakumar,⁶ Jay Patel,³ Xinyang Zhao,⁷ Fabiana Perna,⁷ Suveg Pandey,³ Jozef Madzo,⁶ Chunxiao Song,⁸ Qing Dai,⁸ Chuan He,⁸ Sherif Ibrahim,¹ Miloslav Beran,⁹ Jiri Zavadil,¹⁰ Stephen D. Nimer,^{4,7} Ari Melnick,⁵ Lucy A. Godley,⁶ Iannis Aifantis,^{1,2,11,*} and Ross L. Levine^{3,4,11,*}

¹Department of Pathology and NYU Cancer Institute

²Howard Hughes Medical Institute

New York University School of Medicine, New York, NY 10016, USA

³Human Oncology and Pathogenesis Program

⁴Leukemia Service, Department of Medicine

Memorial Sloan-Kettering Cancer, New York, NY 10016, USA

⁵Division of Hematology/Oncology, Weill Cornell Medical College, New York, NY 10016, USA

⁶Department of Medicine, The University of Chicago, Chicago, IL 60637, USA

⁷Molecular Pharmacology and Chemistry Program, Sloan-Kettering Institute, New York, NY 10016, USA

⁸Department of Chemistry and Institute for Biophysical Dynamics, The University of Chicago, Chicago, IL 60637, USA

⁹Department of Leukemia, M.D. Anderson Medical Center, Houston, TX 77030, USA

¹⁰Department of Pathology, NYU Cancer Institute and Center for Health Informatics and Bioinformatics, NYU Langone Medical Center, New York, NY 10016, USA

¹¹These authors contributed equally to this work

*Correspondence: iannis.aifantis@nyumc.org (I.A.), leviner@mskcc.org (R.L.L.)

DOI 10.1016/j.ccr.2011.06.001

SUMMARY

Somatic loss-of-function mutations in the ten-eleven translocation 2 (*TET2*) gene occur in a significant proportion of patients with myeloid malignancies. Although there are extensive genetic data implicating *TET2* mutations in myeloid transformation, the consequences of *Tet2* loss in hematopoietic development have not been delineated. We report here an animal model of conditional *Tet2* loss in the hematopoietic compartment that leads to increased stem cell self-renewal in vivo as assessed by competitive transplant assays. *Tet2* loss leads to a progressive enlargement of the hematopoietic stem cell compartment and eventual myeloproliferation in vivo, including splenomegaly, monocytosis, and extramedullary hematopoiesis. In addition, *Tet2*^{+/-} mice also displayed increased stem cell self-renewal and extramedullary hematopoiesis, suggesting that *Tet2* haploinsufficiency contributes to hematopoietic transformation in vivo.

INTRODUCTION

Genetic studies of patients with myeloid malignancies have identified recurrent somatic alterations in the majority of patients with myeloproliferative neoplasms (MPNs), myelodysplastic syndromes (MDSs), and acute myeloid leukemia (AML). A subset of myeloid disease alleles can be classified into two distinct

complementation groups: one class that includes mutations that activate oncogenic signaling pathways, and a second class of mutations that perturbs myeloid differentiation (Gilliland and Griffin, 2002). However, recent studies have suggested that this model of myeloid transformation does not accurately represent the biologic and clinical heterogeneity of MPN, MDS, and AML, and that not all leukemogenic disease alleles can be

Significance

Recurrent somatic mutations in *TET2* and in other genes that regulate the epigenetic state have been identified in patients with myeloid malignancies and in other cancers. However, the effects of *Tet2* loss have not yet been studied in an in vivo model. We report here that *Tet2* loss leads to increased stem cell self-renewal and to progressive stem cell expansion. Consistent with human mutational data, *Tet2* loss leads to myeloproliferation in vivo, notable for splenomegaly and monocytic proliferation. In addition, haploinsufficiency for *Tet2* confers increased self-renewal and myeloproliferation, suggesting that the monoallelic *TET2* mutations found in most patients can contribute to myeloid transformation. This work demonstrates that reduction in *TET2* expression or function leads to enhanced stem cell function in vivo and myeloid transformation.

classified by their ability to directly affect signaling and/or differentiation. Consonant with this notion, recent studies have identified recurrent mutations of known and putative epigenetic modifiers in patients with myeloid malignancies. These include somatic mutations in chromatin-modifying enzymes (Ernst et al., 2010; Nikoloski et al., 2010) and in DNA methyltransferases (Ley et al., 2010; Yamashita et al., 2010). In addition, biologic studies of recurrent chromosomal translocations, including MLL fusions, have shown that leukemogenic fusion proteins alter epigenetic regulation in hematopoietic cells, resulting in changes in chromatin state at specific loci (Dorrance et al., 2006; Krivtsov et al., 2008). Taken together, these data suggest that somatic alterations in genes that regulate the epigenetic state of hematopoietic cells are a common pathogenetic event in leukemogenesis (Abdel-Wahab and Levine, 2010). Importantly, recent studies have identified recurrent mutations in epigenetic master regulators in lymphoid malignancies (Morin et al., 2010) and in solid tumors (van Haafden et al., 2009; Varela et al., 2011), suggesting that mutational dysregulation of the epigenetic machinery is a common theme in oncogenic transformation.

Recent studies have identified a novel class of somatic mutations in myeloid malignancies. Specifically, somatic deletions and loss-of-function mutations in the ten-eleven translocation 2 (*TET2*) gene were identified in 10%–20% of patients with MDS and MPN (Delhommeau et al., 2009; Langemeijer et al., 2009); subsequent studies identified recurrent *TET2* mutations in patients with chronic myelomonocytic leukemia (CMML) and AML (Abdel-Wahab et al., 2009; Jankowska et al., 2009), and demonstrated that *TET2* mutations were associated with adverse outcome in intermediate-risk AML (Metzeler et al., 2011). Within the TET family of proteins, TET1, TET2, and TET3 have been shown to modify DNA by hydroxylating 5-methylcytosine (5mC) (Ko et al., 2010; Tahiliani et al., 2009), and the *TET2* mutant proteins observed in these patients with myeloid malignancies have been shown to be deficient in this enzymatic function (Ko et al., 2010). In addition, recent work demonstrated that mutations in the metabolic enzymes IDH1 and IDH2 (Mardis et al., 2009; Parsons et al., 2008; Ward et al., 2010; Yan et al., 2009) are mutually exclusive with *TET2* mutations, and that production of 2-hydroxyglutarate by neomorphic IDH1/2 mutant proteins (Dang et al., 2009) inhibits *TET2* catalytic activity (Figuroa et al., 2010; Xu et al., 2011). Taken together, these data indicate that mutations that impair 5-hydroxymethylation represent a novel mechanism of transformation in myeloid malignancies.

Although there are extensive genetic data implicating *TET2* mutations in myeloid transformation, the consequences of *Tet2* loss in hematopoietic development have not been delineated. Recent *in vitro* studies using shRNA-based approaches have suggested a role for *TET2* in regulating myeloid differentiation (Figuroa et al., 2010; Ko et al., 2010) and in regulating stem/progenitor cell proliferation (Figuroa et al., 2010). In order to elucidate the function of *Tet2* in hematopoiesis *in vivo*, we describe here the characterization of conditional deletion of *Tet2* in the hematopoietic compartment demonstrating a role for *Tet2* in regulating hematopoietic stem cell renewal and differentiation. These findings provide a model for human disease in which the loss of *Tet2*, often through the loss of a single allele, leads to increased self-renewal and myeloid transformation,

and provides insight into how mutations in epigenetic modifiers contribute to malignant transformation.

RESULTS

Tet2-Expression Silencing Leads to Increased Replating Capacity

We first investigated the effects of *Tet2* silencing in hematopoiesis by transducing whole mouse bone marrow cells with retroviral vectors encoding validated *Tet2* shRNA vectors (Figuroa et al., 2010), and sorting for GFP-positive cells. Stable shRNA-mediated knockdown led to stable reductions in TET2 expression by 50%–70% (Figure 1A). Because TET2 is an enzyme that hydroxylates 5mC on DNA, its knockdown should lead to loss of 5-hydroxylation of methylcytosine (5hmC). We used a mass spectrometry-based approach (Shah et al., 2010) to demonstrate that *Tet2* silencing results in a significant reduction in 5hmC in GFP⁺ hematopoietic cells stably expressing *Tet2* shRNAs (Figure 1B). GFP⁺ cells were then plated in methylcellulose for CFU *in vitro* assays. We observed no significant differences in the number or the lineage specificity of *Tet2*-expressing and *Tet2*-silenced colonies after the first plating. However, at the second plating there was a 2-fold increase in the number of colonies expressing *Tet2*-specific shRNAs (Figure 1C). Strikingly, *Tet2*-silenced cells retained the ability to serially replat and generate colonies, although essentially no wild-type colonies were detected after the second plating. In agreement with the putative acquisition of a more immature phenotype, *Tet2* shRNA-expressing colonies upregulated c-Kit, a hematopoietic stem and progenitor cell marker (Figure 1D). These initial studies demonstrated that *Tet2* silencing reduces global 5hmC levels and increases the replating capacity of hematopoietic stem and progenitor cells.

Generation of a Conditional *Tet2* Knockout Allele

Although these studies provide important information on TET2 function, hematopoiesis is a dynamic process that is most accurately studied *in vivo*. Thus, we decided to conditionally inhibit *Tet2* gene expression in the hematopoietic compartment. We first assessed *Tet2* expression by performing qRT-PCR of sorted hematopoietic stem/progenitor subsets (LSK: Lin[−] Sca-1⁺ c-Kit⁺; common myeloid progenitor [CMP]: Lin[−] Sca-1[−] c-Kit⁺, FcγR^{lo} CD34⁺; GMP: Lin[−] Sca-1[−] c-Kit⁺ FcγR⁺ CD34⁺, MEP: Lin[−] Sca-1[−] c-Kit⁺ FcγR[−] CD34[−]) and in differentiated hematopoietic lineages. Expression studies revealed that *Tet2* expression was ubiquitously expressed in the hematopoietic compartment, including in stem and progenitor subsets and in mature myeloid and lymphoid cells (Figure 2A). Purified human CD34⁺ peripheral blood-mobilized cells also demonstrated expression of *TET2* in human hematopoietic stem cells (see Figure S1A available online). Two different *TET2* isoforms are expressed, including a shorter isoform b that lacks the C-terminal enzymatic domain. To understand the nature and location of *TET2* mutations in human myeloid malignancies and how this would inform our mouse model, we analyzed *TET2* mutations from 991 patients with a variety of myeloid malignancies (MPN, CMML, and AML). Exon 3 in the murine *Tet2* locus encodes for approximately half of the TET2 protein; analysis from the mutational data identifies the corresponding exon 3 of human *TET2* as the

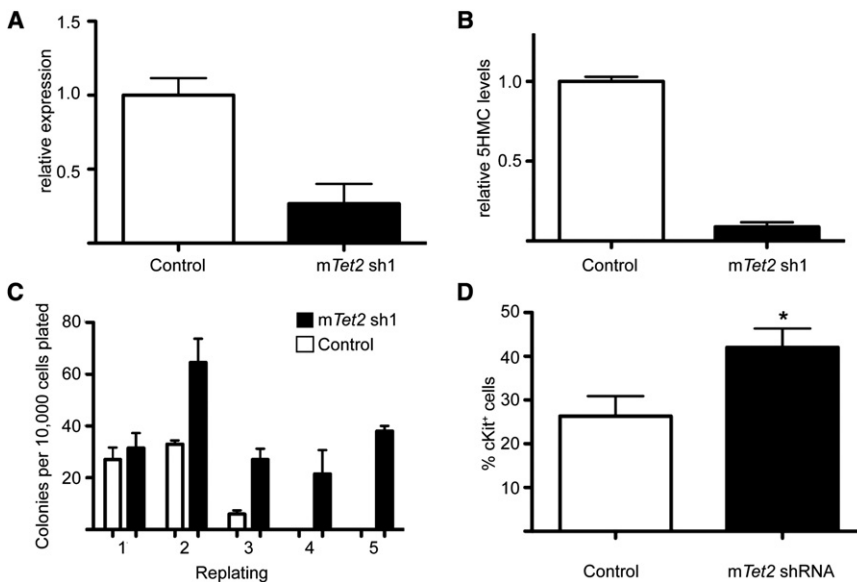


Figure 1. In Vitro *Tet2*-Expression Silencing Leads to Increased Serial Replating

(A) Quantification of the shRNA-mediated *Tet2* knockdown efficiency using qRT-PCR. (B) Quantification of 5hmC by LC/MS of control (MSCV-IRES-GFP) versus *Tet2* knockdown-derived cells after retroviral transduction and GFP sorting. (C) CFU assay of bone marrow-derived cells infected with control or *Tet2* shRNA virus. Colony counts were scored every 14 days. (D) Upregulation of surface c-Kit expression in progenitors expressing *Tet2*-specific shRNA. * $p < 0.026$. Error bars represent \pm SD.

Tet2 Deletion Leads to an Enhanced Repopulating Capacity of Hematopoietic Progenitors In Vitro

Given that RNAi-mediated *Tet2* silencing led to increased replating potential, we assessed whether deletion of TET2 in different hematopoietic subsets led to

most frequently mutated exon in myeloid malignancies, including a large number of nonsense mutations, insertions, and deletion mutations that truncate the protein. Specifically, we found that 41.5% (51 of 123) of *TET2* mutations occurred in the first coding exon of *TET2* (exon 3), whereas 29.3% (36 of 123) of *TET2* mutations occurred in the last coding exon (exon 11) (Abdel-Wahab et al., 2009; Figueroa et al., 2010) (Figure 2B; Figure S1B). Moreover, the largest proportion of mutations that results in a premature stop codon occurs in exon 3 (Figure 2B). In addition, exon 3 of *Tet2* is contained within the two described *Tet2* transcripts (*Tet2a* and *Tet2b*), which are both expressed in the hematopoietic compartment (Figure S1A). Therefore, we decided to target exon 3 using homologous recombination. We utilized ES cell targeting to insert two LoxP sites flanking exon 3, as well as an Frt-flanked neomycin selection cassette in the upstream intron (Figure 2C). The generated mice (*Tet2^{fl/fl}*) were initially crossed to a germline Flp-deleter murine line to eliminate the neomycin cassette, and then subsequently crossed to IFN α -inducible *Mx1-cre*, the hematopoietic-specific *Vav-cre*, and the germline *Ella-cre* mice (Kühn et al., 1995; Lakso et al., 1996; Stadtfeld and Graf, 2005). Figures 2D and 2E demonstrate the efficient targeting of the locus and the generation of a recombinant (E) allele upon Cre recombinase expression in hematopoietic cells. Although *Tet2* was recently suggested to play an important role in ES cell differentiation (Ito et al., 2010; Koh et al., 2011), *Ella-cre⁺Tet2^{-/-}* mice were born with the expected Mendelian ratios with normal growth and organ development. These data suggested that other members of the *Tet* family may have redundant functions in embryonic development and in homeostasis of different tissues. *Vav-Cre*-mediated deletion led to a complete silencing of *Tet2* expression in the bone marrow, thymus, and spleen of *Vav-cre⁺Tet2^{fl/fl}* animals. Interestingly, *Tet2*-expression silencing was not accompanied by changes in expression of either *Tet1* or *Tet3*, which were both expressed in hematopoietic cells at similar levels before and after *Tet2* deletion (Figure 2F).

similar effects. We performed methylcellulose CFU assays using FACS-sorted Lin⁻c-Kit⁺ progenitors and LSK CD150⁺ HSC from *Vav-cre⁺Tet2^{-/-}* and *Vav-cre⁺Tet2^{+/+}* mice. In both cases, *Tet2*-deficient cells demonstrated serial replating capacity (for at least ten replatings followed by continuous liquid culture for 4 additional months), whereas *Tet2^{+/+}* counterparts differentiated and did not generate colonies after the second plating (Figure 3A). *Tet2^{-/-}* colonies were more homogeneous and less differentiated and contained cells with a promyeloblastic morphology (Figure 3B). Indeed, expression of c-Kit, a classical marker of hematopoietic progenitors and the receptor for stem cell factor, was upregulated significantly in *Tet2^{-/-}* and was expressed in nearly all *Tet2^{-/-}* cells in the third plating and beyond (Figure 3C). Furthermore, the c-Kit-expressing cells also upregulated the myeloid progenitor markers CD34 and Fc γ R (Figure 3C). Interestingly, comparison of gene expression profiles of *Tet2^{-/-}* cells at the fifth plating (CFU5) to different stem and progenitor populations showed that *Tet2^{-/-}* cells share a common gene expression program with CMPs, suggesting that these are indeed c-Kit⁺ myeloid progenitors with the ability to replate indefinitely in culture (Figure S2). *Tet2^{-/-}* myeloid progenitor cells were also characterized by increased expression of the self-renewal regulators *Meis1* and *Evi1*, and by reduced expression of multiple myeloid-specific factors (including *Cebpa*, *Cebp δ* , *Mpo*, and *Csf1*), more consistent with multipotent LSK cells than committed CMP or GMP (Figure S2; data not shown). These findings are consistent with the shRNA knockdown experiments shown in Figure 1 and suggest that *Tet2* loss leads to enhanced serial replating ability in vitro.

Tet2 Deletion Leads to Progressive Defects in Hematopoiesis

We next performed detailed analysis of in vivo hematopoiesis in *Tet2^{-/-}* mice. Detailed phenotypic characterization of young (4–6 weeks) *Vav-Cre⁺Tet2^{-/-}* mice failed to reveal gross alterations in bone marrow stem/progenitor numbers or in the

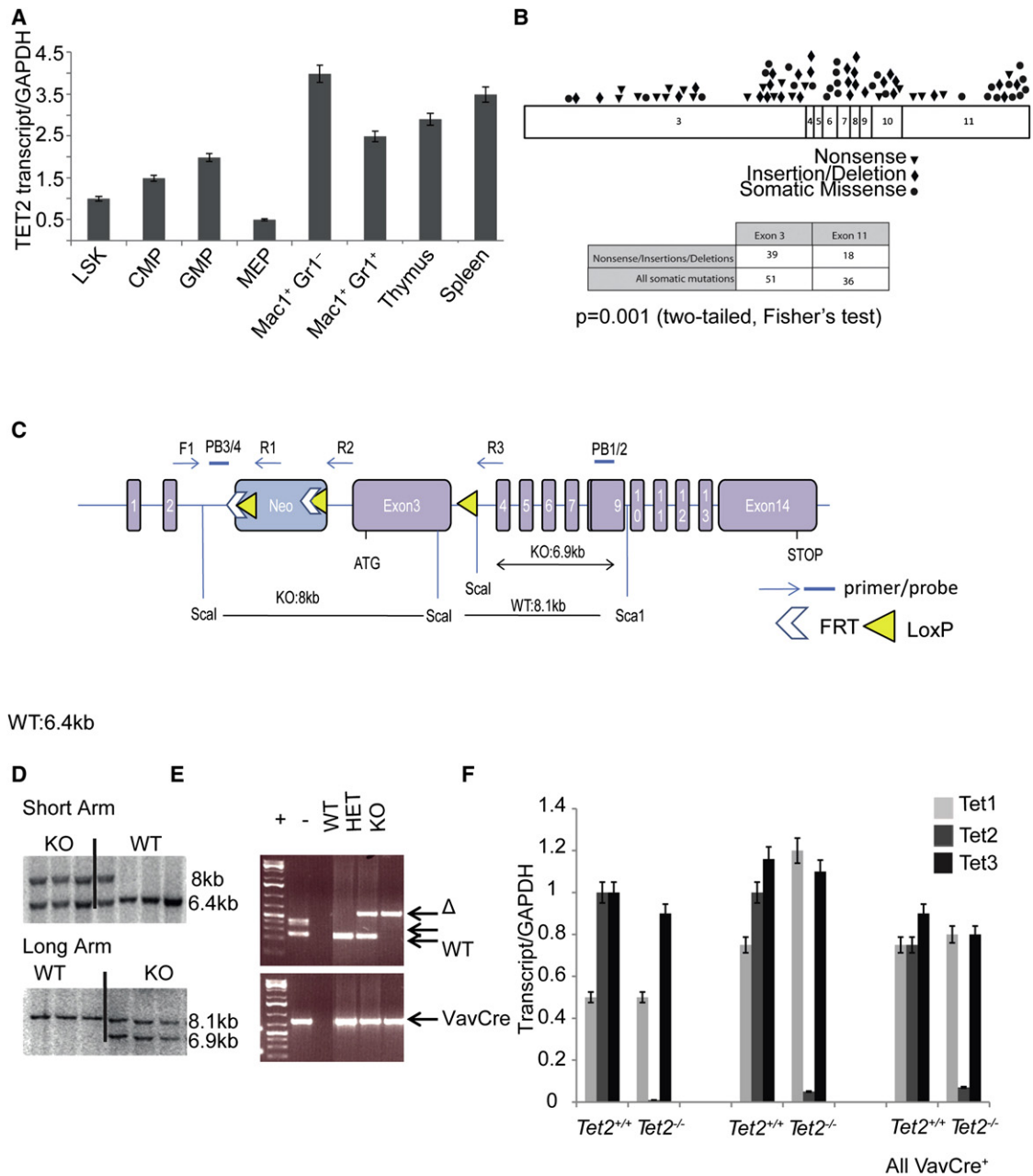


Figure 2. Generation of a Conditional *Tet2* allele

(A) qRT-PCR showing relative expression levels of *Tet2* in purified progenitor and mature mouse hematopoietic stem and progenitor subsets.

(B) Exon distribution of *TET2* mutations found in patients with AML and CMML.

(C) Schematic depiction of the targeted *Tet2* allele. Exon 3 is targeted and flanked by LoxP sites upon Frt-mediated deletion of the NEO cassette.

(D) Verification of correct homologous recombination using Southern blots on targeted ES cells.

(E) Verification of VavCre-mediated excision using genomic PCR. Recombined (Δ), floxed, and wild-type *Tet2* alleles are shown.

(F) Efficiency of *Tet2* knockout using qRT-PCR in purified bone marrow c-Kit⁺ cells, total thymus, and spleen. Expression of *Tet1* and *Tet3* in wild-type and *Tet2*-deficient bone marrow cells reveals no differences in *Tet1* and *Tet3* expression with *Tet2* deletion. Error bars represent \pm SD.

See also Figure S1.

myeloid compartment (Figure 4A, first panel). Likewise, there were no effects on the differentiation of lymphocyte lineages in the bone marrow (data not shown). However, detailed FACS analysis of *Tet2*^{-/-} spleens from young mice identified signifi-

cant extramedullary hematopoiesis, as defined by a significant increase in the absolute numbers of c-Kit⁺ (data not shown), LSK cells (including CD150⁺ HSC), and myeloid progenitors (Figures 4B and 4C). Moreover, purification of *Tet2*^{+/+} and

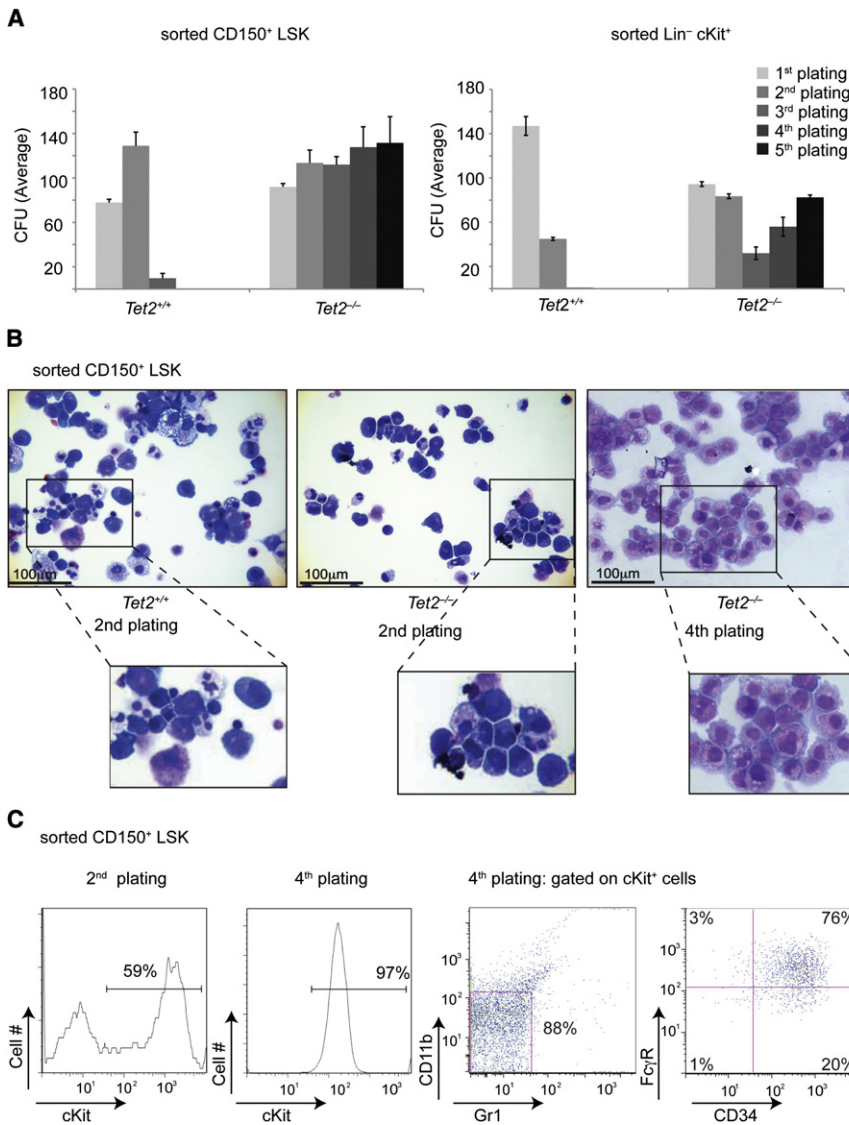


Figure 3. Tet2 Deficiency Leads to Increased Serial Replating Ability In Vitro

(A) Left panel shows a methylcellulose CFU assay using LSK CD150⁺-purified cells. Absolute number of colonies is shown at different platings. A similar CFU assay using Lineage⁻ c-Kit⁺ cells is shown in the right panel.

(B) Morphology of generated colonies either at the 2nd or 4th plating. Cytopins of the colonies are shown.

(C) Left panels illustrate upregulation of surface c-Kit expression at the 2nd and 4th plating. Right panels show cell surface expression of CD34 and FcγR on Lin⁻ cKit⁺ Tet2^{-/-} cells by the 4th plating. A representative example of at least three independent experiments is shown for each assay. Error bars represent ± SD.

See also Figure S2.

with an increase in the proportion of total CD11b⁺ cells (see below). Notably, extramedullary hematopoiesis was prominent, with a significant increase in the absolute number of LSK (Figures 4B and 4C) as well as CD150⁺ HSC (not shown) cells. These combined studies suggested that Tet2 deletion leads to progressive defects in blood differentiation and to a significant elevation of extramedullary hematopoiesis.

Tet2-Deficient Hematopoietic Stem Cells Show Increased Self-Renewal Ability In Vivo

Because we have previously shown that Tet2 deletion leads to increased replating capacity in vitro, we tested the ability of Tet2^{-/-} cells to compete directly against wild-type counterparts in an in vivo transplantation setting. We mixed identical numbers of either Mx1-cre⁺ Tet2^{WT/WT}CD45.2⁺ or Mx1-cre⁺ Tet2^{fl/fl}

Tet2^{-/-} bone marrow progenitor populations (LSK, CMP, GMP) and subsequent transcriptome analysis revealed that Tet2^{-/-} LSK cells display a significant enrichment of a CMP gene expression signature (Figure S3; Experimental Procedures), suggesting that Tet2 loss leads to aberrant hematopoiesis in vivo.

We next analyzed older (20 week) Tet2^{-/-} animals to determine the consequences of Tet2 loss on long-term hematopoiesis. At 20 weeks after Tet2 deletion, we noted an increase in the size of the bone marrow LSK compartment (Figure 4A, second panel). This phenotype was not accompanied by expansion of a specific stem or multipotential progenitor compartment as defined by the utilization of CD150/CD48 marker labeling. Further analysis of the progenitor compartment showed a marked increase in the GMP population, which includes progenitors of monocytes and granulocytes (Figure 4A). However, the most striking effects of Tet2 deletion were noted in the spleen of these animals; Tet2^{-/-} but not Tet2^{+/+} mice displayed splenomegaly at 20 weeks of age, which was associated

CD45.1⁺/CD45.2⁺ BM from littermate mice with wild-type CD45.1⁺ bone marrow and transplanted them in lethally irradiated CD45.1⁺ recipients (Figure 5A). Four weeks after transplantation, equal engraftment (approximately 50:50) rates were detected in peripheral blood, and subsequently, Tet2 deletion was induced by polyI-polyC injections. The presence of the Tet2-recombined allele was verified using genomic PCR of peripheral blood mononuclear cells. Chimerism was followed by FACS assessment of peripheral blood staining for CD45.1 versus CD45.2 (or CD45.1⁺45.2⁺). As evident from Figure 5B, upon Tet2 deletion, Tet2^{-/-} chimerism increased rapidly because these cells outcompeted their wild-type counterparts. Indeed, at 23 weeks after polyI-polyC deletion, more than 95% of the peripheral blood cells (both myeloid and lymphoid) were Tet2^{-/-} (Figure 5C). To define in detail the developmental stage in which Tet2^{-/-} cells outcompete Tet2-expressing cells, we have analyzed transplanted recipients 23 weeks after polyI-polyC injection. Analysis of the LT-HSC compartment indicated

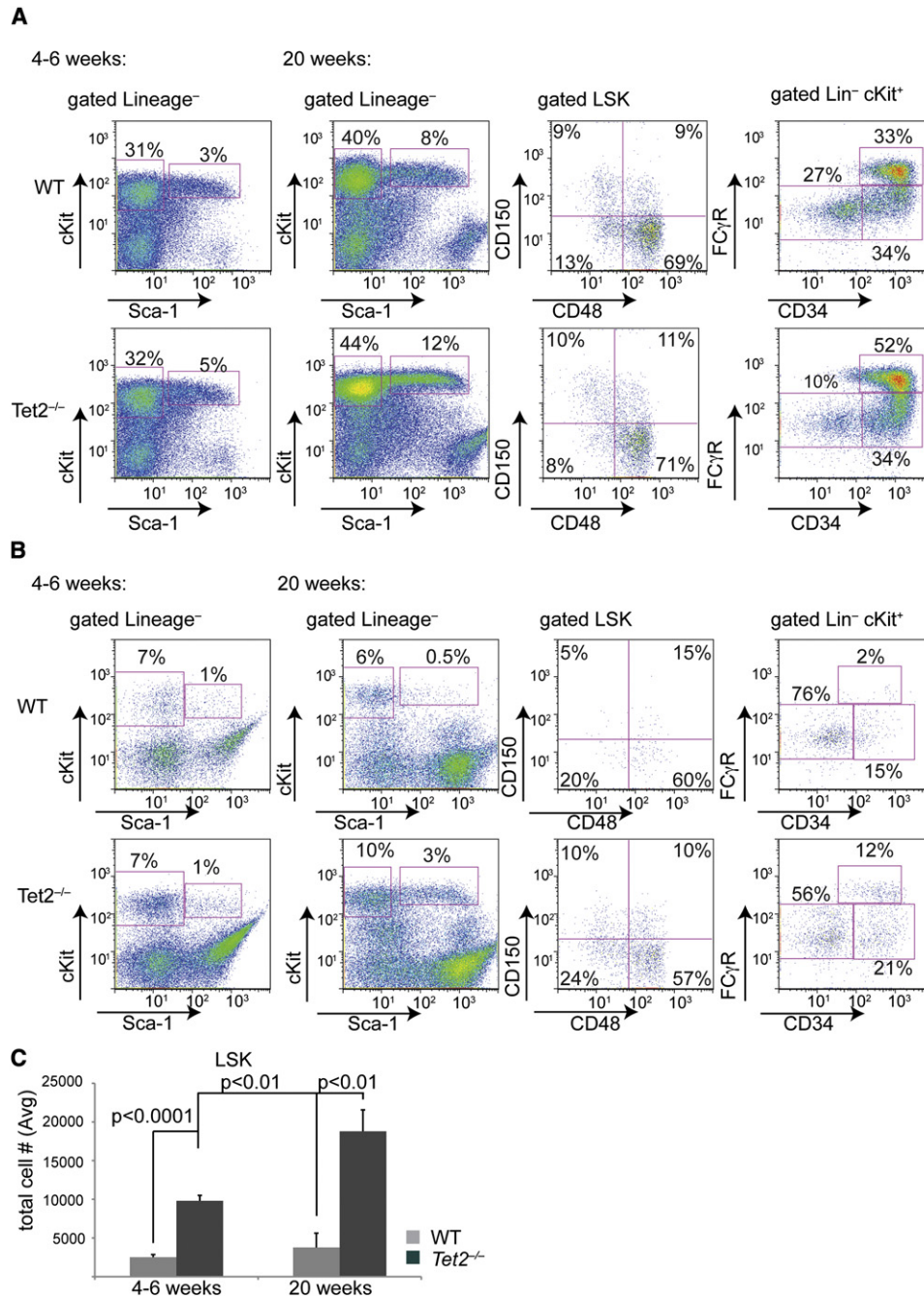


Figure 4. Tet2 Deletion Leads to Progressive Defects in Bone Marrow and Extramedullary Hematopoiesis

(A) FACS analysis of bone marrow stem and progenitor populations of *Tet2*^{-/-} (*vav-Cre*⁺*Tet2*^{fl/fl}) and wild-type (*vav-Cre*⁺*Tet2*^{WT/WT}) at two different ages (4–6 and 20 weeks). Antibody stainings are as indicated.

(B) Identical antibody labeling as in (A) but using spleen cells from *Tet2*^{-/-} (*vav-Cre*⁺*Tet2*^{fl/fl}) and wild-type (*vav-Cre*⁺*Tet2*^{WT/WT}) mice.

(C) Absolute numbers of spleen LSK cells in *Tet2*^{-/-} (*vav-Cre*⁺*Tet2*^{fl/fl}) and wild-type (*vav-Cre*⁺*Tet2*^{WT/WT}) mice at two different ages. p values are shown for each comparison. For all experiments shown in this figure, there are eight for each genotype. Error bars represent ± SD.

See also Figure S3.

that the vast majority (>90%) of these cells were *Tet2*^{-/-}, suggesting that TET2-deficient HSC has the ability to outcompete wild-type counterparts. Once established, this bias toward the *Tet2*^{-/-} cells was also observed in downstream bone

marrow multipotent progenitors (MPP1,2), myeloid progenitors (CMP), bone marrow mature CD11b⁺ monocytes, and B220⁺ lymphocytes (Figures 5D and 5E). Competitive transplant studies using *VavCre*⁺*Tet2*^{-/-} HSC demonstrated that TET2-deficient

cells outcompeted wild-type cells to a similar extent, further supporting our previous findings (Figure S4). These studies confirm that *Tet2* function regulates the self-renewal of adult HSC.

Tet2-Deficient Animals Develop CMML-like Disease

We next performed a detailed phenotypic analysis of *Tet2*^{-/-}*VavCre*⁺ mice 20 weeks after deletion. We found that *Tet2*^{-/-} animals, but not *Tet2*^{+/+} littermates, were characterized by progressive leukocytosis; this was associated with neutrophilia and a marked increase in peripheral monocyte counts (Figures 6A and 6B and Table 1; Table S1). Peripheral blood analysis revealed that by week 20, approximately 70% of the *Tet2*^{-/-}*VavCre*⁺ mice developed significant peripheral blood monocytosis (Figure S5). Myeloid dysplasia was apparent in both bone marrow and peripheral lymphoid tissue, as defined by myeloid left shift (presence of blasts, promyelocytes, myelocytes, or metamyelocytes). In addition, presence of hypogranular cytoplasm or abnormal segmentation of the nuclei was detected in the *Tet2*-deficient animals (Figures 6B and 6D; data not shown).

Moreover, *Tet2*^{-/-} mice had significantly enlarged spleens (Figure 6C) compared to littermate controls (*p* < 0.05). Detailed pathologic analysis revealed that approximately all *Tet2*^{-/-} mice by week 20 developed significant splenomegaly (spleen weight >250 mg), consistent with significant myeloproliferation. Histopathologic analysis revealed that *Tet2*^{-/-} mice, but not *Tet2*^{+/+} littermate controls, had prominent histologic evidence of disease, including significant destruction of spleen architecture, infiltration of the liver and lung, as well as bone marrow neutrophilia and monocytosis (Figure 6D). FACS analysis of the spleen of these mice revealed a significant enlargement of both the CD11b⁺ and CD11b⁺Gr1⁺ populations, consistent with granulocytic and monocytic expansion (Figure 6E). Collectively, these studies demonstrate that *Tet2* loss is associated with myeloproliferation in vivo, and suggest that *TET2* mutations contribute to increased stem cell self-renewal and to progressive myeloid expansion in vivo. Although splenomegaly and leukocytosis are observed in a spectrum of myeloid malignancies, the constellation of splenomegaly, extramedullary hematopoiesis, neutrophilia, and monocytosis is most consistent with human CMML. *TET2* mutations are most commonly observed in human CMML, with somatic loss-of-function mutations in more than 40% of well-annotated CMML patient cohorts (Abdel-Wahab et al., 2009; Jankowska et al., 2009). In agreement with the murine data, detailed clinical and molecular analysis of patients with CMML revealed that patients with *TET2*-mutant CMML presented with splenomegaly, elevated peripheral blood WBC, and monocytosis (Figure S1B). Moreover, *TET2*-mutant CMML was characterized by a paucity of co-occurring cytogenetic abnormalities: 5.9% of patients with *TET2* mutant had cytogenetic abnormalities versus 61.3% of patients with *TET2*-wild-type CMML (*p* = 0.018) (Figures S1B and S1C). These studies suggested that *Tet2* deletion leads to progressive myeloproliferation in vivo with cardinal features of human CMML.

Tet2 Haploinsufficiency Is Sufficient to Initiate Aberrant Hematopoiesis In Vitro and In Vivo

Although a small subset of patients with leukemia presents with biallelic *TET2* mutations and/or deletions, the majority of patients present with monoallelic *TET2* loss (Abdel-Wahab et al., 2009;

Jankowska et al., 2009). We performed DNA and cDNA sequencing of patient samples with monoallelic *TET2* mutations and demonstrated that these patients continue to express the wild-type allele (Figure S6). These data suggest the possibility that haploinsufficiency for *TET2* may result in alterations in self-renewal, hematopoietic differentiation, and susceptibility to myeloid transformation. Therefore, we performed phenotypic analysis of *Tet2*^{+/-} (*Vav-Cre*⁺*Tet2*^{W^{fl}/fl}) mice. We first purified CD150⁺ HSC from the bone marrow of *Tet2* heterozygotes and plated them in methylcellulose cultures. Similar to *Tet2*^{-/-} cells, *Tet2*^{+/-} cells were able to serially replat (Figure 7A), unlike wild-type HSC that failed to generate colonies after the second plating. Likewise, *Tet2*^{+/-} cells generated colonies with a similar immunophenotype as *Tet2*^{-/-} cells. This was demonstrated by an immature, promyeloblastic morphology and the upregulation of the cell surface markers c-Kit, CD34, and FcγR (Figures 7B and 7C; data not shown). Furthermore, competitive reconstitution experiments, performed as described in Figure 5A, demonstrated that *Tet2*^{+/-}, but not *Tet2*^{+/+}, cells were able to outcompete wild-type counterparts, albeit with slower kinetics than *Tet2*^{-/-} cells (Figures 7D–7H). Indeed, 23 weeks post-deletion, more than 70% of peripheral blood cells were *Tet2*^{+/-}, consistent with increased long-term self-renewal with loss of a single *Tet2* allele. Moreover, in a noncompetitive setting, 20-week-old *Vav-Cre*⁺*Tet2*^{W^{fl}/fl} mice showed increased circulating monocytes (Figure 7I) and extramedullary hematopoiesis (Figures 7J and 7K), with a significant increase of both Lineage^{neg} c-Kit⁺ and LSK cells (Figure 7J; data not shown). These data clearly demonstrate that *Tet2* loss leads to dose-dependent effects on hematopoiesis and on myeloid transformation, and that monoallelic *TET2* loss is an important pathogenetic event in myeloid malignancies.

DISCUSSION

The identification of recurrent somatic loss-of-function mutations in *TET2* provides genetic evidence that mutational inactivation of enzymes that regulate cytosine hydroxymethylation is a common pathogenetic event in myeloid malignancies (Delhommeau et al., 2009; Ko et al., 2010; Langemeijer et al., 2009). In addition, genetic and functional studies suggest that neomorphic *IDH* mutations contribute to myeloid transformation, at least in part, by inhibiting TET enzymatic function (Figuroa et al., 2010; Xu et al., 2011). Although genetic and in vitro studies suggested a role for *TET2* in regulating hematopoietic differentiation and stem/progenitor cell expansion, to our knowledge, the in vivo effects of *Tet2* loss had not previously been described. Here, we report the effects of *Tet2* loss in the hematopoietic compartment, which has allowed us to make several important observations. First, we found that *Tet2* loss leads to increased replating capacity in vitro, and that *Tet2*-deficient cells had enhanced repopulating activity in competitive reconstitution assays consistent with enhanced HSC function in vivo. Second, *Tet2* loss led to progressive myeloproliferation in vivo, with features characteristic of human CMML. In addition we found that *Tet2* haploinsufficiency confers increased self-renewal to stem/progenitor cells and to extramedullary hematopoiesis, suggesting that heterozygous loss of *TET2*, as is commonly observed in myeloid malignancies, is sufficient to contribute to myeloid transformation in vivo.

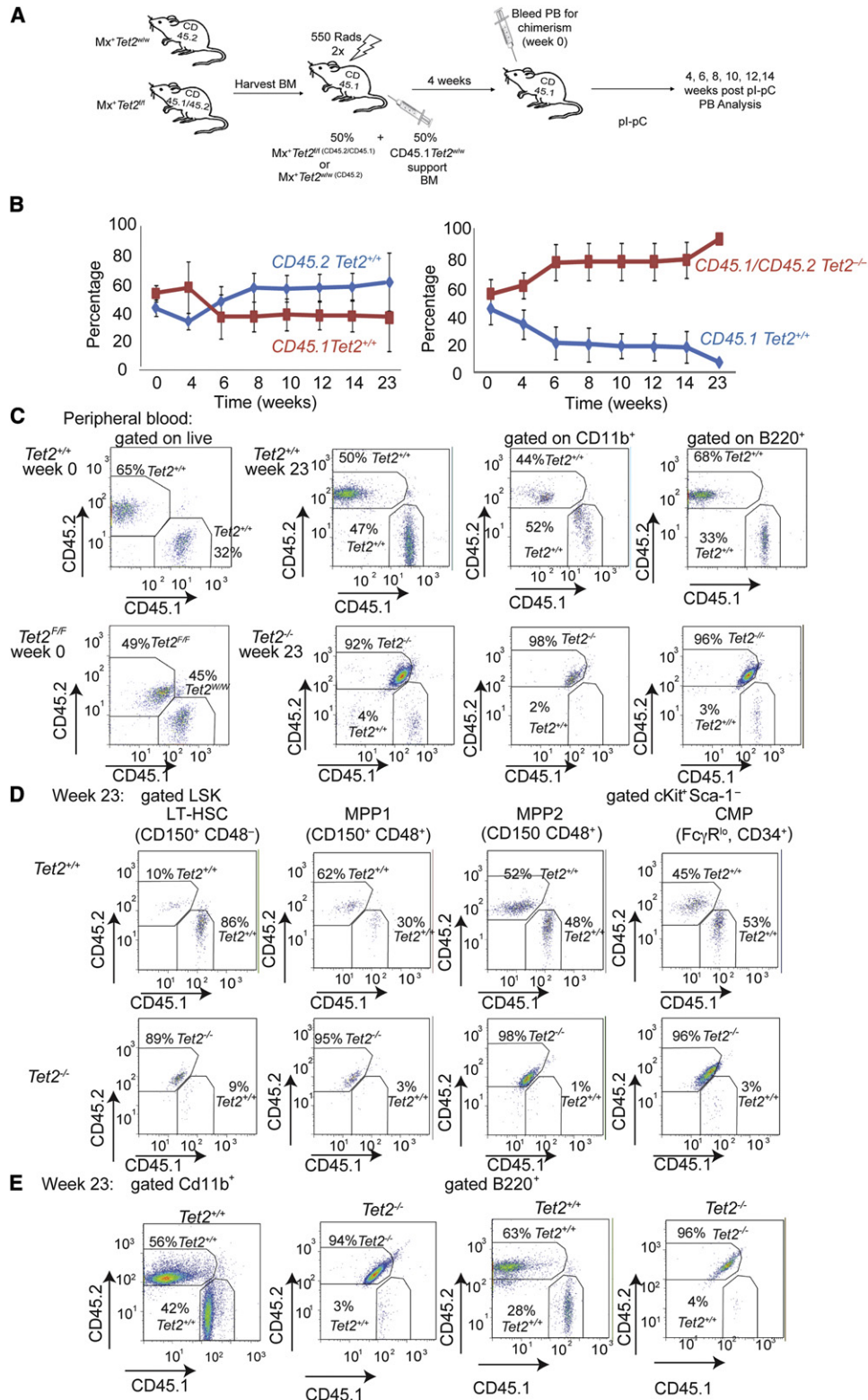


Figure 5. *Tet2*^{-/-} Hematopoietic Stem Cells Show Increased Repopulating Ability Consistent with Increased Self-Renewal

(A) Schematic depiction of the competitive transplantation scheme. *Tet2*^{-/-} cells are double positive for CD45.1/CD45.2 markers. *Tet2* wild-type cells are CD45.2 single positive cells.

(B) Percentage of CD45.1 versus CD45.2 total chimerism in the peripheral blood of recipient animals (n = 15 for each genotype). Time (weeks) denotes the time after the termination of polyI-polyC injections.

Our *in vivo* investigation of the effects of *Tet2* loss is consistent with several observations emanating from previous genetic and functional studies. The presence of *TET2* mutations in a significant proportion of patients with MPN, MDS, and AML is consistent with the notion that *TET2* loss confers increased self-renewal to stem/progenitor cells *in vivo*, which then leads to acquisition of mutations that direct the phenotype of *TET2*-mutant hematopoietic cells (Haeno et al., 2009; Tefferi, 2010). These data are also consistent with previous xenotransplantation studies of a small cohort of *TET2* mutant primary MPN samples that demonstrated that *TET2*-mutant MPN cells could engraft NOD-SCID mice (Delhommeau et al., 2009). In addition, genetic studies of patients with MPN that subsequently transformed to AML identified *TET2* mutations as a recurrent somatic mutation during progression from MPN to AML (Abdel-Wahab et al., 2010; Schaub et al., 2010). Our data implicate increased self-renewal as a putative mechanism of transformation by *TET2* mutations, which contribute to disease initiation and progression. Our transcriptional data suggest that *Tet2* loss leads to increased expression of myeloid-specific and self-renewal gene programs. However, subsequent studies will have to functionally investigate which downstream targets of *Tet2* loss are required to confer enhanced self-renewal on stem/progenitor cells. Recent work suggested that TET proteins regulate embryonic stem cell self-renewal and differentiation (Ito et al., 2010; Koh et al., 2011). Taken together, the data suggest that *Tet2* deletion likely has effects at multiple stages in hematopoietic differentiation, and that regulation of hydroxymethylation by TET enzymes controls stem cell self-renewal and differentiation in different cellular contexts. However, to our knowledge, the exact mechanisms by which perturbations in TET enzyme function remain to be delineated. This is particularly evident given recent studies suggesting a dynamic interplay between changes in TET1-mediated hydroxymethylation and other epigenetic marks in regulating gene expression (Ficz et al., 2011; Williams et al., 2011; Wu et al., 2011), and it is likely additional alterations in the epigenetic state cooperate with *TET2* mutations in malignant transformation.

In addition to effects of *Tet2* loss on self-renewal, we found that *Tet2* loss led to progressive myeloproliferation *in vivo*. Two recent studies used RNAi-mediated *Tet2* knockdown *in vitro* to suggest that *TET2* depletion led to impaired hematopoietic differentiation and to preferential myeloid commitment (Figueroa et al., 2010; Ko et al., 2010). These data are consistent with our *in vivo* data because we observe progressive hematopoietic stem/progenitor cell expansion and myeloproliferation *in vivo* with *Tet2* deletion or haploinsufficiency notable for neutrophilia, monocytosis, and splenomegaly. Although these features are seen, to a varying degree, in different myeloid malignancies, they are most commonly observed in human CMML, suggesting

that *Tet2* loss in the absence of other genetic lesions favors progressive myelomonocytic expansion. This is consistent with the observations that *TET2* mutations are most common in CMML (Abdel-Wahab et al., 2009; Jankowska et al., 2009) and that *TET2*-mutant CMML is characterized by fewer additional somatic cytogenetic alterations compared to *TET2*-wild-type CMML (Figures S1B and S1C). Most importantly, we demonstrate that *Tet2* haploinsufficiency is sufficient to confer increased self-renewal to stem/progenitor cells and to promote myeloproliferation *in vivo*. Given that the vast majority of patients with *TET2*-mutant hematopoietic malignancies retain a wild-type copy of *TET2*, our data provide functional evidence that loss of a single *TET2* allele can contribute to transformation.

Collectively, the presented data implicate *TET2* as a master regulator of normal and malignant hematopoiesis. It is likely that *TET2* has distinct roles in other hematopoietic lineages, and may contribute to transformation in lymphoid malignancies or even in epithelial tumors. These data also suggest that dysregulation of hydroxymethylation by mutations in the TET family of enzymes and by other somatic mutations may contribute to malignant transformation in other contexts. In addition it is possible that therapies that modulate hydroxymethylation levels might be of benefit in malignancies characterized by loss of TET enzyme function by inhibiting malignant stem cell self-renewal. Moreover, our studies provide insight into mechanisms of transformation by a novel class of mutations found in myeloid malignancies and in other tumors, and we predict that subsequent studies will identify additional mutations in epigenetic modifiers, which contribute to neoplasia by similar mechanisms.

EXPERIMENTAL PROCEDURES

Animals

All animals were housed at New York University School of Medicine or at Memorial Sloan-Kettering Cancer Center. All animal procedures were conducted in accordance with the Guidelines for the Care and Use of Laboratory Animals and were approved by the Institutional Animal Care and Use Committees (IACUCs) at New York University School of Medicine and Memorial Sloan-Kettering Cancer Center.

Generation of *Tet2*-Deficient Mice

The *Tet2* allele was deleted by targeting exon 3. Briefly, we have inserted two LoxP sites flanking exon 3, as well as an Frt-flanked neomycin selection cassette in the upstream intron (Figure 3A). Ten micrograms of the targeting vector was linearized by NotI and then transfected by electroporation of BAC-BA1 (C57BL/6 × 129/SvEv) hybrid embryonic stem cells. After selection with G418 antibiotic, surviving clones were expanded for PCR analysis to identify recombinant ES clones. Secondary confirmation of positive clones identified by PCR was performed by Southern blotting analysis. DNA was digested with Scal and electrophoretically separated on a 0.8% agarose gel. After transfer to a nylon membrane, the digested DNA was hybridized with a probe targeted against the 3' or 5' external region. DNA from C57Bl/6 (B6), 129/SvEv (129), and BA1 (C57Bl/6 × 129/SvEv) (Hybrid) mouse strains was

(C) Representative FACS plots showing CD45.1/CD45.2 (*Tet2*^{-/-}) and CD45.2 (*Tet2*^{+/+}) stainings and chimerism in whole peripheral mononuclear cells, myeloid CD11b⁺, and lymphoid B220⁺ cells. Two time points (weeks 0 and 23) are shown.

(D) Representative FACS plots showing CD45.1/CD45.2 (*Tet2*^{-/-}) and CD45.2 (*Tet2*^{+/+}) stainings and chimerism within the bone marrow stem (LT-HSC) and progenitor (MPP1, MPP2, and CMP) compartments. Analysis performed at week 23 after polyI-polyC injection.

(E) Similar stainings quantifying CD45.1/CD45.2 (*Tet2*^{-/-}) and CD45.2 (*Tet2*^{+/+}) expression in bone marrow myeloid (CD11b⁺) and lymphoid (B220⁺) mature populations. Week 23 stainings are shown (n = 5 for each genotype). Error bars represent ± SD.

See also Figure S4.

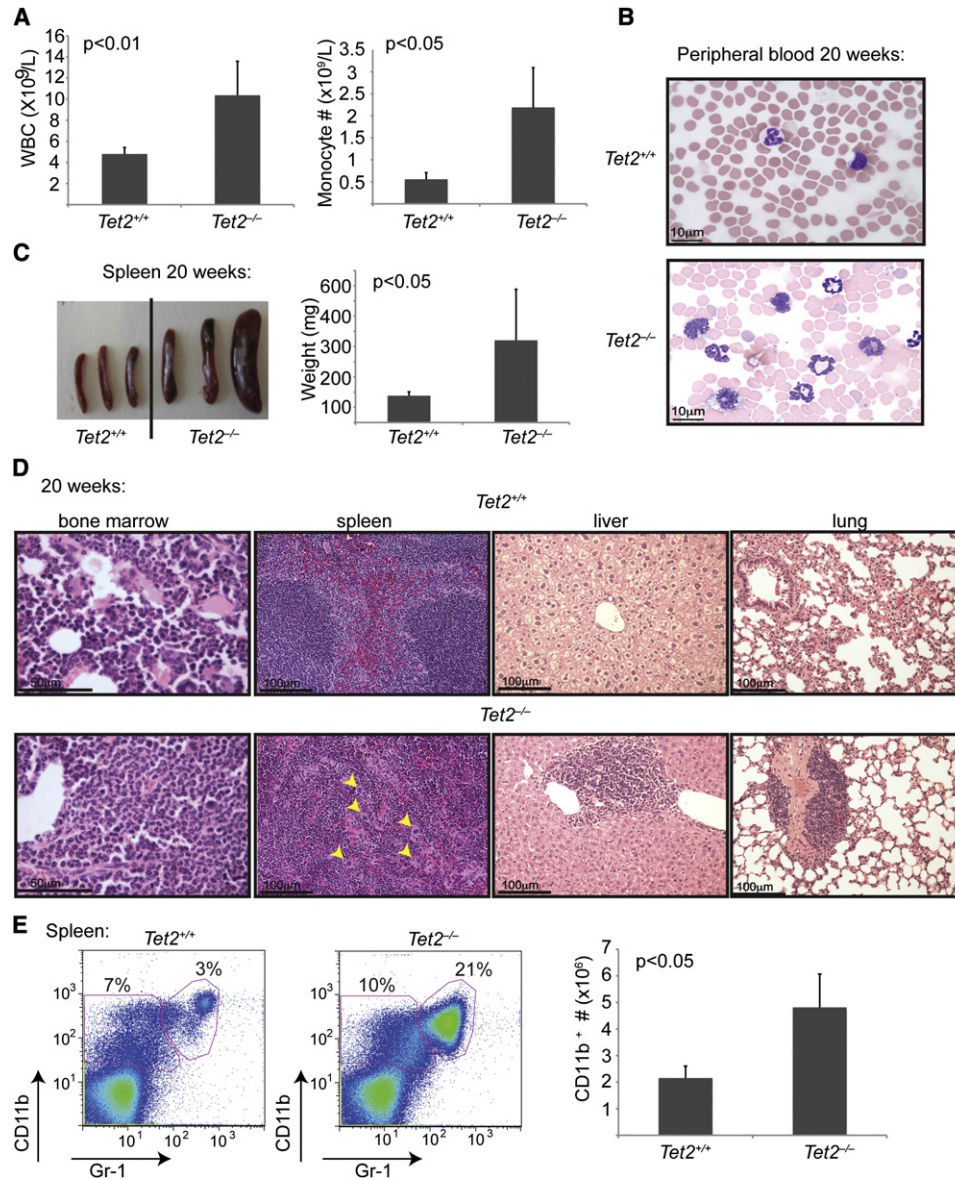


Figure 6. *Tet2*^{-/-} Animals Develop Myeloid Neoplasia Reminiscent of Human CMML

(A) Left panel shows automated peripheral blood enumeration of whole blood cells (WBC). Right panel illustrates manual differential counts of neutrophils and monocytes showing blood monocytosis ($n \geq 3$ for each genotype).

(B) Representative images of peripheral blood smears from *Tet2*^{+/+} and *Tet2*^{-/-} mice at 20 weeks of age ($n \geq 3$ for each genotype).

(C) Splenomegaly in 20-week-old *Tet2*^{-/-} (*Vav-Cre*⁺*Tet2*^{fl/fl}) animals. Littermate wild-type (*Vav-Cre*⁺*Tet2*^{WT/WT}) controls at 20 weeks are used ($n = 5$ mice).

(D) Histologic (H&E) analysis of *Tet2*^{-/-} and control tissues (bone marrow, spleen, liver, and lung) is shown, illustrating disrupted spleen architecture, monocytic infiltrations in liver and lung, and bone marrow neutrophilia ($n = 5$ for each genotype).

(E) Left panels show FACS analysis of spleen CD11b and Gr-1-expressing populations. A representative FACS plot from each genotype is shown. Right panel illustrates total cell number of CD11b⁺ cells in the spleen of *Tet2*^{+/+} and *Tet2*^{-/-} mice at 20 weeks of age. Error bars represent \pm SD.

See also Figure S5.

used as wild-type controls. Positive ES clones were expanded and injected into blastocysts.

The generated mice (*Tet2*^{fl/fl}) were initially crossed to a germline Flp-deleter (Jackson Laboratories), to eliminate the neomycin cassette, and subsequently to the IFN α -inducible Mx1-cre (Jackson Laboratories), the hematopoietic-specific *Vav*-cre, and the germline *Ella*-cre (Kühn et al., 1995; Stadtfeld and Graf, 2005; Lakso et al., 1996). The *Vav*-Cre transgenic line was generated by the Graf laboratory (Stadtfeld and Graf, 2005) and was a gift from Virginia Shapiro (Mayo Clinic).

In Vivo Studies

Tet2 conditional and control mice received five intraperitoneal injections of poly(I:C) every other day at a dose of 20 μ g/g of body weight starting at 2 weeks post-birth. For the hematopoietic-specific *Vav*-cre line, *Tet2*^{fl/fl} *VavCre*⁺, *Tet2*^{fl/w} *VavCre*⁺, and *Tet2*^{wt/w} *VavCre*⁺ mice were analyzed between 2 and 20 weeks of age. Thymus, bone marrow, spleen, and peripheral blood were analyzed by flow cytometry and formalin-fixed paraffin-embedded tissue sections stained with hematoxylin and eosin. Peripheral blood was smeared on a slide and stained using the Giemsa-Wright staining method. Tissue sections and blood

Table 1. Tet2 Deficiency Leads to Progressive Peripheral Leukocytosis

Genotype	WBC ($\times 10^9/l$)	HCT (%)	PLT ($\times 10^9/l$)	No.
4–6 Weeks				
<i>Tet2</i> ^{+/+}	5.48 \pm 1.54	40.32 \pm 8.70	367 \pm 66	11
<i>Tet2</i> ^{+/-}	6.61 \pm 1.95	49.63 \pm 5.90	365 \pm 59	7
<i>Tet2</i> ^{-/-}	6.66 \pm 2.04	50.06 \pm 4.70	352 \pm 85	9
20 Weeks				
<i>Tet2</i> ^{+/+}	5.43 \pm 1.35	46.29 \pm 5.56	498 \pm 171	8
<i>Tet2</i> ^{+/-}	8.77 \pm 1.90 ^a	52.55 \pm 4.42	559 \pm 119	10
<i>Tet2</i> ^{-/-}	10.00 \pm 2.28 ^a	52.45 \pm 11.18	517 \pm 124	13

Peripheral blood analysis (automated) at 4–6 and 20 weeks of age. See also Table S1.

^ap \leq 0.01.

smears were evaluated by a hematopathologist. Deletion of the *Tet2* allele and transcript was measured by genomic PCR and quantitative real-time PCR.

Gene Expression Analysis

LSK and CMP cells were sorted from *Tet2*^{+/+} *Mx-1*⁺, *Tet2*^{-/-} *Mx-1*⁺ littermate mice 4 weeks post-deletion via pIC injection. Additionally, cells were obtained from serial replating of CD150⁺-sorted *Tet2*-deficient cells. RNA was isolated using RNeasy RNA isolation kit (QIAGEN) according to manufacturer's protocol. A portion of total RNA (5 ng) from target cell populations was amplified and then labeled with the Ovation RNA Amplification System v2 and Ovation cDNA Biotin System (NuGEN). The resulting cDNA was hybridized to GeneChip MG 430 2.0 arrays according to the array manufacturer's recommendations (Affymetrix). The Affymetrix gene expression-profiling data were normalized using the previously published Robust Multi-array Average (RMA) algorithm using the GeneSpring GX software (Agilent, Palo Alto, CA, USA). The gene expression intensity presentation was generated with GeneSpring GX software and Multi Experiment Viewer software. Hierarchical clustering on genes and samples was performed using Euclidean distance as a metric and average linkage method (Bolstad et al., 2003).

Gene Set Enrichment Analysis

Gene Set Enrichment Analysis was performed using GSEA (Subramanian et al., 2005) <http://www.broadinstitute.org/gsea/>, using gene set as permutation type, 1000 permutations, and log2 ratio of classes as metric for ranking genes. Independent stem cell gene expression signatures are obtained by <http://franklin.imgen.bcm.tmc.edu> and Ng et al. (2009).

The "CMP signature" gene sets were generated using a systematic approach based on the comparison of gene expression arrays from wild-type LSK and wild-type GMP. Genes that were significantly modulated in CMP compared to LSK (over 1.33-fold; p < 0.05) were used to define CMP versus LSK_UP gene set containing upregulated genes and CMP versus LSK_DWN containing downregulated genes.

In Vitro Colony-Forming Assays

CD150⁺ LSK as well as ckit⁺ cells were sorted from the bone marrow of *Tet2*^{-/-} *VavCre*⁺, *Tet2*^{+/-} *MxCre*⁺, *Tet2*^{-/-} *Mx-1Cre*⁺, *Tet2*^{+/+} *VavCre*⁺, or *Tet2*^{+/+} *Mx-1Cre*⁺ mice and seeded at a density of 500 cells/replicate for the CD150⁺ subset and 2000 cells/replicate for the cKit⁺ subset into cytokine-supplemented methylcellulose medium (Methocult, M3434; STEMCELL Technologies). Colonies propagated in culture were scored at day 7. Representative colonies were isolated from the plate for cytopins. Remaining cells were resuspended, counted, and a portion was stained for c-kit (clone 2B8; BioLegend), and replated (4000 cells/replicate) for a total of 5 platings (7, 14, 21, 28, and 35 days). Cytopins were performed by resuspending in warm PBS and spun onto the slides at 350 \times g for 5 min. Slides were air-dried and stained using the Giemsa-Wright method.

Bone Marrow Transplantation

Freshly dissected femurs and tibias were isolated from *Tet2*^{+/+} *Mx-1Cre*⁺ CD45.2⁺, *Tet2*^{+/-} *Mx-1Cre*⁺ CD45.2⁺, or *Tet2*^{-/-} *Mx-1Cre*⁺ CD45.1⁺/CD45.2⁺ mice. Hence, *Tet2*-deficient animals are expressing both CD45.2 and CD45.1 markers, whereas *Tet2* heterozygous animals and *Tet2* wild-type control animals are expressing only the CD45.2 marker. Bone marrow was flushed with a 1 cc insulin syringe into PBS supplemented with 3% fetal bovine serum. The bone marrow was spun at 0.5 \times g by centrifugation at 4°C, and red blood cells were lysed in ammonium chloride-potassium bicarbonate lysis buffer for 3 min on ice. After centrifugation, cells were resuspended in PBS plus 3% FBS, passed through a cell strainer, and counted. Finally, 0.5 \times 10⁶ total bone marrow cells of *Tet2*^{+/+} *Mx-1Cre*⁺ CD45.2⁺, *Tet2*^{+/-} *Mx-1Cre*⁺ CD45.2⁺, or *Tet2*^{-/-} *Mx-1Cre*⁺ CD45.1⁺/CD45.2⁺ cells were mixed with 0.5 \times 10⁶ wild-type CD45.1⁺-support bone marrow and transplanted via retro-orbital injection into lethally irradiated (two times 550 Gy) CD45.1⁺ host mice. Chimerism was measured by FACS in peripheral blood at 4 weeks post-transplant (week 0, pre-polyI-polyC). Deletion of *Tet2* was initiated at this time point via five intraperitoneal injections of polyI-polyC at a dose of 20 μ g/g of body weight. Chimerism for the duration of the experiment was subsequently followed via FACS in the peripheral blood every 2 weeks (week 0, 2, 4, 6, 8, 10, 12, 14, and 16 after polyI-polyC injection). Additionally, for each bleeding, whole blood cell counts were measured on a blood analyzer, and peripheral blood smears were scored. Chimerism in the bone marrow, spleen, and thymus was evaluated at 10 and 14 weeks via animal sacrifice and subsequent FACS analysis.

Mouse Bone Marrow Infections and shRNA Colony Assays

Bone marrow was harvested from the femur of wild-type C57Bl/6 mice. After red cell lysis, the bone marrow was cultured in media containing RPMI/10% FBS and IL-3 (7 ng/ml), IL-6 (10 ng/ml), and stem cell factor (10 ng/ml). The next day, cells were infected with MSCV retroviral vectors for control and *Tet2* shRNAs containing IRES GFP. Targets for shRNAs can be found in Supplemental Experimental Procedures. Cells were infected twice in the presence of polybrene and then sorted for GFP⁺ cells 48 hr following second infection. A total of 1 \times 10⁴ cells was plated per well in Methocult (STEMCELL Technologies) supplemented with IL-3 (20 ng/ml), IL-6 (10 ng/ml), SCF (10 ng/ml), GM-CSF (10 ng/ml), TPO (50 ng/ml), and Flt3L (100 ng/ml). Colonies were scored 14 days after seeding, recollected in PBS, and then recultured in Methocult at 1 \times 10⁴ cells. *Tet2* knockdown was confirmed by qRT-PCR using Thermo Scientific Verso cDNA Kit and SYBR green quantification in an ABI 7500 sequence detection system.

5hmC Quantification

Genomic DNA was purified using Purge DNA purification kit (QIAGEN). Genomic DNA was hydrolyzed and analyzed in triplicate for the relative levels of 5hmC by liquid chromatography-electrospray ionization tandem mass spectrometry (Shah et al., 2010).

Patient Samples and Sequencing

Approval was obtained from the institutional review boards of Memorial Sloan-Kettering Cancer Center, Dana-Farber Cancer Institute, and MD Anderson Cancer Center. Patients provided written informed consent in all cases at time of enrollment. DNA sequencing methods and primer sequences for TET2 have been described previously (Abdel-Wahab et al., 2009). A total of 389 AML samples were obtained at diagnosis from patients enrolled in the Eastern Cooperative Oncology Group's (ECOG) E1900 clinical trial. Samples were deidentified at the time of inclusion. A total of 354 MPN, 69 CMML, and an additional 119 AML samples were analyzed with characteristics previously described (Abdel-Wahab et al., 2009). Approval was obtained from the institutional review boards of Memorial Sloan-Kettering Cancer Center, Dana-Farber Cancer Institute, and MD Anderson Cancer Center. DNA sequencing methods and primer sequences for TET2 have been described previously (Abdel-Wahab et al., 2009).

Human CD34⁺ Stem Cell Isolation

Peripheral blood was collected from normal bone marrow transplant donors who underwent stem cell mobilization with G-CSF. Remainder excess aliquots were used for CD34⁺ cell isolation. CD34⁺ HSPCs were purified by positive

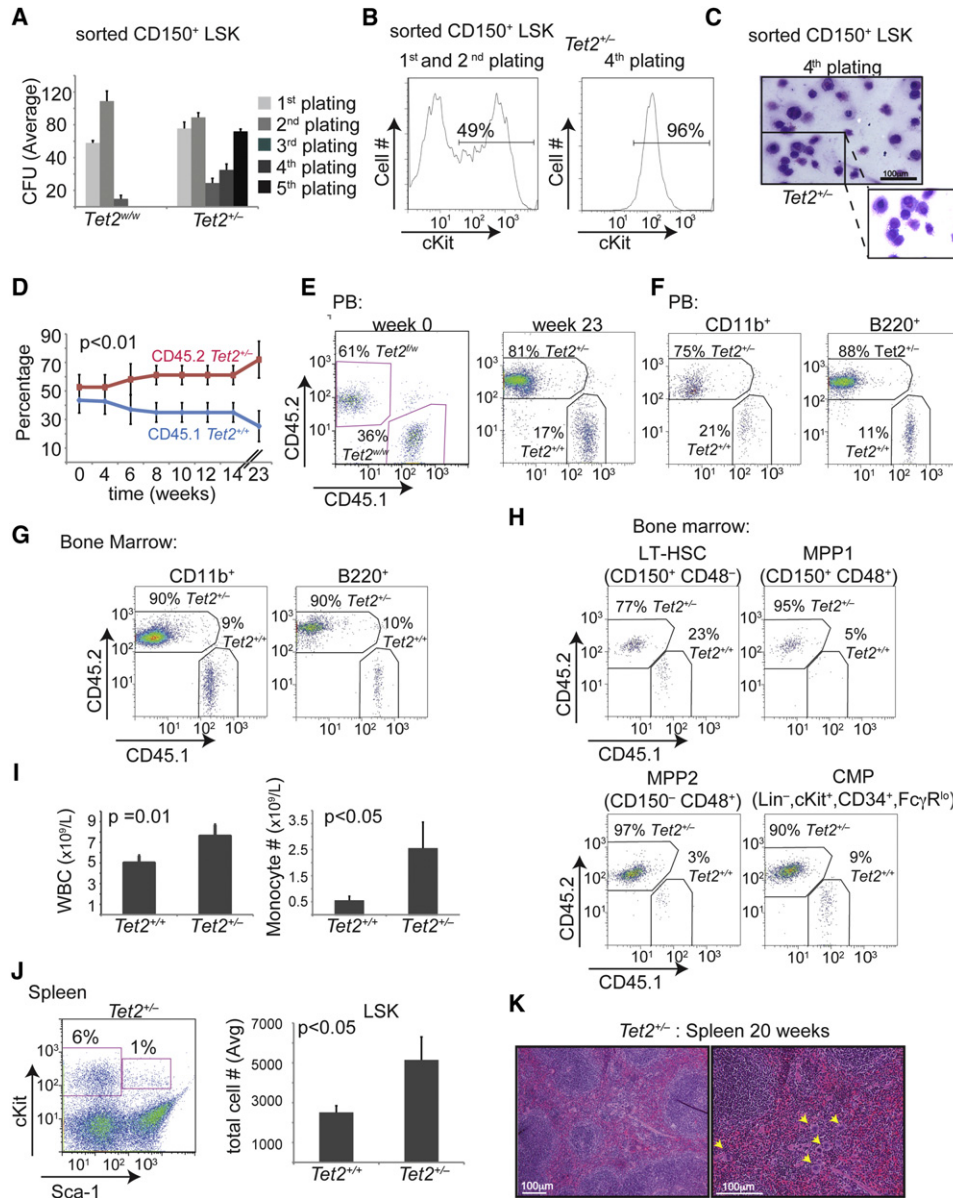


Figure 7. Tet2 Haploinsufficiency Is Able to Initiate Aberrant In Vitro and In Vivo Hematopoiesis

(A) Methylcellulose CFU assay using LSK CD150⁺ cells (Lin⁻, cKit⁺, Sca-1⁺, CD150⁺). An average of the absolute number of colonies is shown for sequential platings (1–5) (n = 5).

(B) Representative FACS plot of colony-forming assay showing c-Kit expression at the 2nd and 4th plating.

(C) Giemsa-Wright staining of colonies formed from Tet2^{+/-} CD150⁺ LSKs (Vav-Cre⁺Tet2^{W^{fl}/fl}). Images of cytopsins are shown.

(D) Graph represents chimerism between CD45.2 (Tet2^{+/-}) and CD45.1 (Tet2^{+/+}) in the peripheral blood from a competitive transplantation assay over time (0–23 weeks). Experimental strategy is described in Figure 5A. Blue line indicates wild-type:wild-type cohorts, and red indicates Tet2^{+/-}:wild-type cohorts (n = 5 mice).

(E) Representative FACS plots showing CD45.1/CD45.2 chimerism in the peripheral blood from CD45.1 (Tet2^{+/+}) and CD45.2 (Tet2^{+/-}) cohorts before (week 0) and after deletion (23 weeks after polyI-polyC).

(F–H) Representative FACS plots showing CD45.1 (Tet2^{+/+})/CD45.2 (Tet2^{+/-}) chimerism at 23 weeks post-deletion in myeloid and lymphoid populations in the peripheral blood (F), in the bone marrow (G), and in the bone marrow stem and progenitor cell compartment (H).

(I) Left panel shows automated peripheral blood enumeration of whole blood cells (WBC). Right panel illustrates manual differential counts of neutrophils and monocytes showing monocytosis (n ≥ 3 for each genotype).

(J) Representative FACS plot showing increased frequency of LSKs in the spleen of Tet2^{+/-} mice. Right panel depicts absolute number of LSKs in the spleen of wild-type and Tet2^{+/-} mice (n = 5 for each genotype).

(K) H&E of spleen from 20-week-old Tet2^{+/-} mice. Error bars represent ± SD.

See also Figure S6.

selection using the Midi-magnetic-activated cell sorting LS⁺ separation columns and isolation kit (Miltenyi). RNA was collected using the QIAGEN RNeasy kit.

ACCESSION NUMBERS

Microarray data can be accessed under GEO accession number GSE27816.

SUPPLEMENTAL INFORMATION

Supplemental Information includes Supplemental Experimental Procedures, six figures, and one table and can be found with this article online at doi:10.1016/j.ccr.2011.06.001.

ACKNOWLEDGMENTS

We would like to thank Hans-Guido Wendel and Dino Mavrikis for assistance with Tet2 shRNA construction. Also, we thank the NYU Genome Technology Center (supported in part by NIH/NCI P30 CA016087-30 grant) for expert assistance with microarray experiments, and the NYU Flow Cytometry facility (supported in part by NIH/NCI 5 P30CA16087-31) for expert cell sorting, the NYU Histology Core (5P30CA16087-31), and the Transgenic Mouse Core (NYU Cancer Institute Center Grant [5P30CA16087-31]). I.A. is supported by the National Institutes of Health (RO1CA133379, RO1CA105129, R21CA141399, RO1CA149655, RO1GM088847), the Leukemia & Lymphoma Society (TRP grant), the American Cancer Society (RSG0806801), the Irma T. Hirschl Trust, and the Dana Foundation. This work was supported in part by grants from the National Institutes of Health (U54CA143798-01, Physical Sciences Oncology Center) and 1R01CA138234-01, and by grants from the Starr Cancer Consortium and Howard Hughes Medical Institute to R.L.L. L.R. is supported by a NIH Ruth L. Kirchstein Award (F31-AG039991). M.E.F. is funded by a Leukemia and Lymphoma Society Special Fellowship award. A.M. is funded by a Leukemia and Lymphoma Society SCOR and TRP award, and is a Burroughs Wellcome Clinical Translational Scholar and Scholar of the Leukemia and Lymphoma Society. A.M. and M.E.F. are also supported by the Sackler Center for Biomedical and Physical Sciences. L.A.G. was supported by the NIH Grants CA129831 and CA129831-03S1. X.Z. and S.D.N. are supported by a Leukemia and Lymphoma Society SCOR award and FP by an American Italian Cancer Foundation award. R.L.L. is a Geoffrey Beene Junior Faculty Chair at Memorial Sloan-Kettering Cancer Center. I.A. is a Howard Hughes Medical Institute Early Career Scientist.

Received: March 4, 2011

Revised: May 3, 2011

Accepted: June 6, 2011

Published online: June 30, 2011

REFERENCES

- Abdel-Wahab, O., and Levine, R.L. (2010). *EZH2* mutations: mutating the epigenetic machinery in myeloid malignancies. *Cancer Cell* **18**, 105–107.
- Abdel-Wahab, O., Mullally, A., Hedvat, C., Garcia-Manero, G., Patel, J., Wadleigh, M., Malinge, S., Yao, J., Kilpivaara, O., Bhat, R., et al. (2009). Genetic characterization of TET1, TET2, and TET3 alterations in myeloid malignancies. *Blood* **114**, 144–147.
- Abdel-Wahab, O., Manshour, T., Patel, J., Harris, K., Yao, J., Hedvat, C., Heguy, A., Bueso-Ramos, C., Kantarjian, H., Levine, R.L., and Verstovsek, S. (2010). Genetic analysis of transforming events that convert chronic myeloproliferative neoplasms to leukemias. *Cancer Res.* **70**, 447–452.
- Bolstad, B.M., Irizarry, R.A., Astrand, M., and Speed, T.P. (2003). A comparison of normalization methods for high density oligonucleotide array data based on variance and bias. *Bioinformatics* **19**, 185–193.
- Dang, L., White, D.W., Gross, S., Bennett, B.D., Bittinger, M.A., Driggers, E.M., Fantin, V.R., Jang, H.G., Jin, S., Keenan, M.C., et al. (2009). Cancer-associated IDH1 mutations produce 2-hydroxyglutarate. *Nature* **462**, 739–744.
- Delhommeau, F., Dupont, S., Della Valle, V., James, C., Trannoy, S., Massé, A., Kosmider, O., Le Couedic, J.P., Robert, F., Alberdi, A., et al. (2009). Mutation in TET2 in myeloid cancers. *N. Engl. J. Med.* **360**, 2289–2301.
- Dorrance, A.M., Liu, S., Yuan, W., Becknell, B., Arnoczky, K.J., Guimond, M., Strout, M.P., Feng, L., Nakamura, T., Yu, L., et al. (2006). Mll partial tandem duplication induces aberrant Hox expression in vivo via specific epigenetic alterations. *J. Clin. Invest.* **116**, 2707–2716.
- Ernst, T., Chase, A.J., Score, J., Hidalgo-Curtis, C.E., Bryant, C., Jones, A.V., Waghorn, K., Zoi, K., Ross, F.M., Reiter, A., et al. (2010). Inactivating mutations of the histone methyltransferase gene *EZH2* in myeloid disorders. *Nat. Genet.* **42**, 722–726.
- Ficz, G., Branco, M.R., Seisenberger, S., Santos, F., Krueger, F., Hore, T.A., Marques, C.J., Andrews, S., and Reik, W. (2011). Dynamic regulation of 5-hydroxymethylcytosine in mouse ES cells and during differentiation. *Nature* **473**, 398–402.
- Figueroa, M.E., Abdel-Wahab, O., Lu, C., Ward, P.S., Patel, J., Shih, A., Li, Y., Bhagwat, N., Vasanthakumar, A., Fernandez, H.F., et al. (2010). Leukemic IDH1 and IDH2 mutations result in a hypermethylation phenotype, disrupt TET2 function, and impair hematopoietic differentiation. *Cancer Cell* **18**, 553–567.
- Gilliland, D.G., and Griffin, J.D. (2002). The roles of FLT3 in hematopoiesis and leukemia. *Blood* **100**, 1532–1542.
- Haeno, H., Levine, R.L., Gilliland, D.G., and Michor, F. (2009). A progenitor cell origin of myeloid malignancies. *Proc. Natl. Acad. Sci. USA* **106**, 16616–16621.
- Ito, S., D'Alessio, A.C., Taranova, O.V., Hong, K., Sowers, L.C., and Zhang, Y. (2010). Role of Tet proteins in 5mC to 5hmC conversion, ES-cell self-renewal and inner cell mass specification. *Nature* **466**, 1129–1133.
- Jankowska, A.M., Szpurka, H., Tiu, R.V., Makishima, H., Afaible, M., Huh, J., O'Keefe, C.L., Ganetzky, R., McDevitt, M.A., and Maciejewski, J.P. (2009). Loss of heterozygosity 4q24 and TET2 mutations associated with myelodysplastic/myeloproliferative neoplasms. *Blood* **113**, 6403–6410.
- Ko, M., Huang, Y., Jankowska, A.M., Pape, U.J., Tahiliani, M., Bandukwala, H.S., An, J., Lamperti, E.D., Koh, K.P., Ganetzky, R., et al. (2010). Impaired hydroxylation of 5-methylcytosine in myeloid cancers with mutant TET2. *Nature* **468**, 839–843.
- Koh, K.P., Yabuuchi, A., Rao, S., Huang, Y., Cunniff, K., Nardone, J., Laiho, A., Tahiliani, M., Sommer, C.A., Mostoslavsky, G., et al. (2011). Tet1 and Tet2 regulate 5-hydroxymethylcytosine production and cell lineage specification in mouse embryonic stem cells. *Cell Stem Cell* **8**, 200–213.
- Krivtsov, A.V., Feng, Z., Lemieux, M.E., Faber, J., Vempati, S., Sinha, A.U., Xia, X., Jesneck, J., Bracken, A.P., Silverman, L.B., et al. (2008). H3K79 methylation profiles define murine and human MLL-AF4 leukemias. *Cancer Cell* **14**, 355–368.
- Kühn, R., Schwenk, F., Aguet, M., and Rajewsky, K. (1995). Inducible gene targeting in mice. *Science* **269**, 1427–1429.
- Lakso, M., Pichel, J.G., Gorman, J.R., Sauer, B., Okamoto, Y., Lee, E., Alt, F.W., and Westphal, H. (1996). Efficient in vivo manipulation of mouse genomic sequences at the zygote stage. *Proc. Natl. Acad. Sci. USA* **93**, 5860–5865.
- Langemeijer, S.M., Kuiper, R.P., Berends, M., Knops, R., Aslanyan, M.G., Massop, M., Stevens-Linders, E., van Hoogen, P., van Kessel, A.G., Raymakers, R.A., et al. (2009). Acquired mutations in TET2 are common in myelodysplastic syndromes. *Nat. Genet.* **41**, 838–842.
- Ley, T.J., Ding, L., Walter, M.J., McLellan, M.D., Lamprecht, T., Larson, D.E., Kandoth, C., Payton, J.E., Baty, J., Welch, J., et al. (2010). DNMT3A mutations in acute myeloid leukemia. *N. Engl. J. Med.* **363**, 2424–2433.
- Mardis, E.R., Ding, L., Dooling, D.J., Larson, D.E., McLellan, M.D., Chen, K., Koboldt, D.C., Fulton, R.S., Delehaunty, K.D., McGrath, S.D., et al. (2009). Recurring mutations found by sequencing an acute myeloid leukemia genome. *N. Engl. J. Med.* **361**, 1058–1066.
- Metzeler, K.H., Maharry, K., Radmacher, M.D., Mrozek, K., Margeson, D., Becker, H., Curfman, J., Holland, K.B., Schwind, S., Whitman, S.P., et al. (2011). TET2 mutations improve the new European LeukemiaNet risk classification of acute myeloid leukemia: a Cancer and Leukemia Group B study. *J. Clin. Oncol.* **29**, 1373–1381.

- Morin, R.D., Johnson, N.A., Severson, T.M., Mungall, A.J., An, J.H., Goya, R., Paul, J.E., Boyle, M., Woolcock, B.W., Kuchenbauer, F., et al. (2010). Somatic mutations altering EZH2 (Tyr641) in follicular and diffuse large B-cell lymphomas of germinal-center origin. *Nat. Genet.* **42**, 181–185.
- Ng, S.Y., Yoshida, T., Zhang, J., and Georgopoulos, K. (2009). Genome-wide lineage-specific transcriptional networks underscore Ikaros-dependent lymphoid priming in hematopoietic stem cells. *Immunity* **30**, 493–507.
- Nikoloski, G., Langemeijer, S.M., Kuiper, R.P., Knops, R., Massop, M., Tönnissen, E.R., van der Heijden, A., Scheele, T.N., Vandenberghe, P., de Witte, T., et al. (2010). Somatic mutations of the histone methyltransferase gene EZH2 in myelodysplastic syndromes. *Nat. Genet.* **42**, 665–667.
- Parsons, D.W., Jones, S., Zhang, X., Lin, J.C., Leary, R.J., Angenendt, P., Mankoo, P., Carter, H., Siu, I.M., Gallia, G.L., et al. (2008). An integrated genomic analysis of human glioblastoma multiforme. *Science* **321**, 1807–1812.
- Schaub, F.X., Looser, R., Li, S., Hao-Shen, H., Lehmann, T., Tichelli, A., and Skoda, R.C. (2010). Clonal analysis of TET2 and JAK2 mutations suggests that TET2 can be a late event in the progression of myeloproliferative neoplasms. *Blood* **115**, 2003–2007.
- Shah, M.Y., Vasanthakumar, A., Barnes, N.Y., Figueroa, M.E., Kamp, A., Hendrick, C., Ostler, K.R., Davis, E.M., Lin, S., Anastasi, J., et al. (2010). DNMT3B7, a truncated DNMT3B isoform expressed in human tumors, disrupts embryonic development and accelerates lymphomagenesis. *Cancer Res.* **70**, 5840–5850.
- Stadtfeld, M., and Graf, T. (2005). Assessing the role of hematopoietic plasticity for endothelial and hepatocyte development by non-invasive lineage tracing. *Development* **132**, 203–213.
- Subramanian, A., Tamayo, P., Mootha, V.K., Mukherjee, S., Ebert, B.L., Gillette, M.A., Paulovich, A., Pomeroy, S.L., Golub, T.R., Lander, E.S., and Mesirov, J.P. (2005). Gene set enrichment analysis: a knowledge-based approach for interpreting genome-wide expression profiles. *Proc. Natl. Acad. Sci. USA* **102**, 15545–15550.
- Tahiliani, M., Koh, K.P., Shen, Y., Pastor, W.A., Bandukwala, H., Brudno, Y., Agarwal, S., Iyer, L.M., Liu, D.R., Aravind, L., and Rao, A. (2009). Conversion of 5-methylcytosine to 5-hydroxymethylcytosine in mammalian DNA by MLL partner TET1. *Science* **324**, 930–935.
- Tefferi, A. (2010). Novel mutations and their functional and clinical relevance in myeloproliferative neoplasms: JAK2, MPL, TET2, ASXL1, CBL, IDH and IKZF1. *Leukemia* **24**, 1128–1138.
- van Haafden, G., Dalgliesh, G.L., Davies, H., Chen, L., Bignell, G., Greenman, C., Edkins, S., Hardy, C., O'Meara, S., Teague, J., et al. (2009). Somatic mutations of the histone H3K27 demethylase gene UTX in human cancer. *Nat. Genet.* **41**, 521–523.
- Varela, I., Tarpey, P., Raine, K., Huang, D., Ong, C.K., Stephens, P., Davies, H., Jones, D., Lin, M.L., Teague, J., et al. (2011). Exome sequencing identifies frequent mutation of the SWI/SNF complex gene PBRM1 in renal carcinoma. *Nature* **469**, 539–542.
- Ward, P.S., Patel, J., Wise, D.R., Abdel-Wahab, O., Bennett, B.D., Collier, H.A., Cross, J.R., Fantin, V.R., Hedvat, C.V., Perl, A.E., et al. (2010). The common feature of leukemia-associated IDH1 and IDH2 mutations is a neomorphic enzyme activity converting alpha-ketoglutarate to 2-hydroxyglutarate. *Cancer Cell* **17**, 225–234.
- Williams, K., Christensen, J., Pedersen, M.T., Johansen, J.V., Cloos, P.A., Rappaport, J., and Helin, K. (2011). TET1 and hydroxymethylcytosine in transcription and DNA methylation fidelity. *Nature* **473**, 343–348.
- Wu, H., D'Alessio, A.C., Ito, S., Xia, K., Wang, Z., Cui, K., Zhao, K., Eve Sun, Y., and Zhang, Y. (2011). Dual functions of Tet1 in transcriptional regulation in mouse embryonic stem cells. *Nature* **473**, 389–393.
- Xu, W., Yang, H., Liu, Y., Yang, Y., Wang, P., Kim, S.H., Ito, S., Yang, C., Wang, P., Xiao, M.T., et al. (2011). Oncometabolite 2-hydroxyglutarate is a competitive inhibitor of α -ketoglutarate-dependent dioxygenases. *Cancer Cell* **19**, 17–30.
- Yamashita, Y., Yuan, J., Suetake, I., Suzuki, H., Ishikawa, Y., Choi, Y.L., Ueno, T., Soda, M., Hamada, T., Haruta, H., et al. (2010). Array-based genomic resequencing of human leukemia. *Oncogene* **29**, 3723–3731.
- Yan, H., Parsons, D.W., Jin, G., McLendon, R., Rasheed, B.A., Yuan, W., Kos, I., Batinic-Haberle, I., Jones, S., Riggins, G.J., et al. (2009). IDH1 and IDH2 mutations in gliomas. *N. Engl. J. Med.* **360**, 765–773.

Affinity-based proteomics reveal cancer-specific networks coordinated by Hsp90

Kamalika Moulick^{1,8}, James H Ahn^{1,8}, Hongliang Zong^{2,8}, Anna Rodina¹, Leandro Cerchietti², Erica M Gomes DaGama¹, Eloisi Caldas-Lopes¹, Kristin Beebe³, Fabiana Perna¹, Katerina Hatzi², Ly P Vu¹, Xinyang Zhao¹, Danuta Zatorska¹, Tony Taldone¹, Peter Smith-Jones⁴, Mary Alpaugh¹, Steven S Gross⁵, Nagavarakishore Pillarsetty⁴, Thomas Ku⁴, Jason S Lewis⁴, Steven M Larson⁴, Ross Levine⁶, Hediye Erdjument-Bromage⁷, Monica L Guzman², Stephen D Nimer^{1*}, Ari Melnick^{2*}, Len Neckers^{3*} & Gabriela Chiosis^{1*}

Most cancers are characterized by multiple molecular alterations, but identification of the key proteins involved in these signaling pathways is currently beyond reach. We show that the inhibitor PU-H71 preferentially targets tumor-enriched Hsp90 complexes and affinity captures Hsp90-dependent oncogenic client proteins. We have used PU-H71 affinity capture to design a proteomic approach that, when combined with bioinformatic pathway analysis, identifies dysregulated signaling networks and key oncoproteins in chronic myeloid leukemia. The identified interactome overlaps with the well-characterized altered proteome in this cancer, indicating that this method can provide global insights into the biology of individual tumors, including primary patient specimens. In addition, we show that this approach can be used to identify previously uncharacterized oncoproteins and mechanisms, potentially leading to new targeted therapies. We further show that the abundance of the PU-H71-enriched Hsp90 species, which is not dictated by Hsp90 expression alone, is predictive of the cell's sensitivity to Hsp90 inhibition.

Most cancers arise from multiple molecular lesions, and functional redundancy of affected pathways limits the utility of specific molecularly targeted drugs. A better understanding of the molecular aberrations that maintain the malignant phenotype of cancer cells would enable more efficient targeting of tumor-promoting molecules and aid the development of more effective and less toxic anticancer treatments.

Application of genomics technologies, including large-scale genome sequencing, has led to the identification of many gene mutations in various cancers, emphasizing the complexity of this disease^{1,2}. However, such genetic analyses intrinsically lack the ability to elucidate the functional complexity of signaling networks that are aberrantly activated as a consequence of the identified genetic defect(s). Thus, the development of complementary proteomic methodologies to identify molecular lesions intrinsic to tumors in a patient- and disease stage-specific manner must follow.

Most proteomic strategies are limited to measuring protein expression in a particular tumor but are unable to provide information on the functional importance of such findings³. Some functional information can be obtained using antibodies directed at specific proteins or post-translational modifications, and by activity-based protein profiling using small molecules targeting the active site of certain enzymes⁴⁻⁷. Although such methods allow one to query a specific pathway or post-translational modification, they are not well suited to capture more global information regarding the malignant state³.

To maintain homeostasis, cells use intricate molecular machineries comprising thousands of proteins that are programmed to execute well-defined functions. Dysregulation of these pathways, through protein misexpression or mutation, provides biological advantages that confer the malignant phenotype. At the molecular level, this requires cells to invest energy in maintaining the stability and function of these proteins, and for this reason cancer cells co-opt molecular chaperones, including Hsp90 (refs. 8,9).

Hsp90 has important roles in maintaining the transformed phenotype^{8,9}. Hsp90 and its associated cochaperones assist in the correct folding of cellular proteins, collectively referred to as 'client proteins', many of which are effectors of signal transduction pathways controlling cell growth, differentiation, the DNA-damage response and cell survival. Tumor cell addiction to these proteins (that is, through mutations, aberrant expression, improper cellular translocation and so on) thus makes them critically reliant on Hsp90 (ref. 9).

Although Hsp90 is expressed in all cells and tissues, tumors preferentially contain Hsp90 in a higher-order multi-chaperone complex with high affinity for certain Hsp90 inhibitors, whereas normal tissues harbor a latent, uncomplexed Hsp90 that has low affinity for these inhibitors¹⁰.

Based on these data, we hypothesize that small molecules able to target tumor-enriched Hsp90 complexes can be used to affinity capture Hsp90-dependent oncogenic client proteins. When combined with bioinformatic analysis, this should enable the creation of

¹Molecular Pharmacology and Chemistry Program, Sloan-Kettering Institute, New York, New York, USA. ²Division of Hematology and Oncology, Weill Cornell Medical College, New York, New York, USA. ³Urologic Oncology Branch, Center for Cancer Research, National Cancer Institute, Bethesda, Maryland, USA. ⁴Department of Radiology, Memorial Sloan-Kettering Cancer Center, New York, New York, USA. ⁵Department of Pharmacology, Weill Cornell Medical College of Cornell University, New York, New York, USA. ⁶Human Oncology and Pathogenesis Program and Leukemia Service, Department of Medicine, Memorial Sloan-Kettering Cancer Center, New York, New York, USA. ⁷Microchemistry and Proteomics Core, Molecular Biology Program, Memorial Sloan-Kettering Cancer Center, New York, New York, USA. ⁸These authors contributed equally to this work. *e-mail: chiosisg@mskcc.org or neckers@nih.gov or amm2014@med.cornell.edu or nimers@mskcc.org.

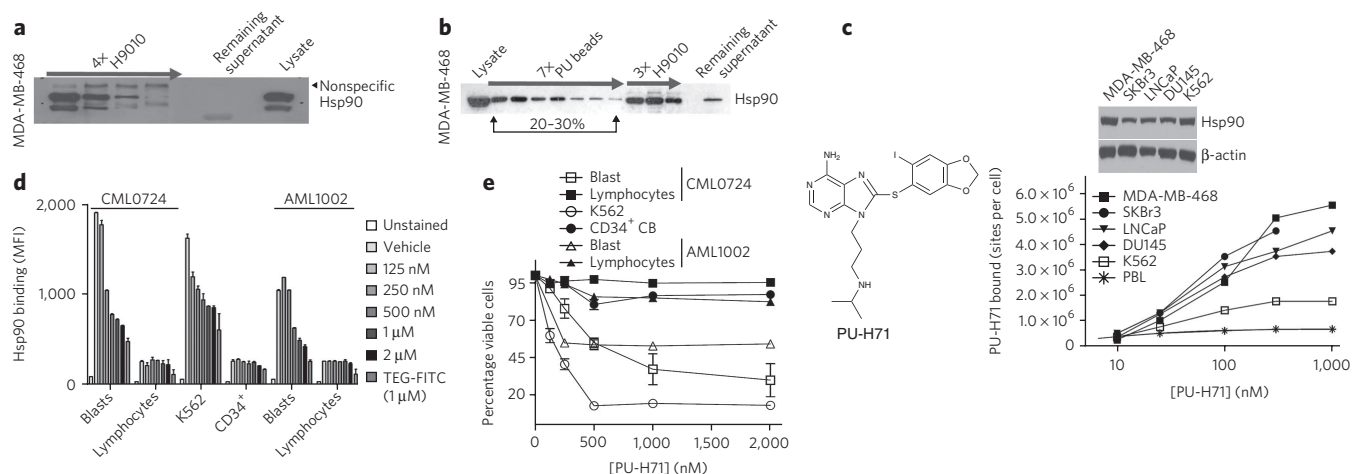


Figure 1 | PU-H71 interacts with a restricted fraction of Hsp90 that is more abundant in cancer cells. (a) Sequential immunoprecipitation steps, as indicated by the arrow, with H9010 (a Hsp90-specific antibody) deplete Hsp90 in the MDA-MB-468 cell extract. Lysate, control cell extract. (b) Hsp90 from MDA-MB-468 extracts was isolated through sequential chemical-purification and immunoprecipitation steps. (c) Saturation studies were performed with ^{125}I -PU-H71 in the indicated cells (below). Expression of Hsp90 in the indicated cells was analyzed by western blotting (above). Representative data of four separate repeats are presented. (d) Binding of PU-FITC, presented as mean fluorescence intensity (MFI), to primary AML and CML, CD34⁺ cord blood cells (CB), or K562 cells pretreated with the indicated doses of PU-H71 for 24 h. TEG-FITC is a nonspecific binding control. (e) Percent viability relative to untreated control for the indicated cells after treatment for 96 h with the indicated doses of PU-H71. Data are presented as means \pm s.e.m. ($n = 3$).

a detailed molecular map of transformation-specific lesions that can guide the development of combination therapies that are optimally effective for a specific patient.

Here we describe an Hsp90 inhibitor-based chemical biology–proteomics–bioinformatics approach to discover oncogenic proteins and pathways in chronic myeloid leukemia (CML). We show that the method provides a global overview of the Hsp90 interactome in malignant cells, and that this interactome represents a substantial fraction of the functional malignant proteome^{8,9}.

RESULTS

Heterogeneous Hsp90 presentation in cancer cells

To investigate the interaction of small-molecule Hsp90 inhibitors with tumor Hsp90 complexes, we used agarose beads that were covalently attached to either geldanamycin or PU-H71 (referred to as GM and PU beads, respectively). Both geldanamycin and PU-H71, which are chemically distinct agents, interact with and inhibit Hsp90 by binding to a regulatory pocket in its N-terminal domain¹¹. For comparison, we generated agarose beads coupled to an anti-Hsp90 antibody (H9010).

First, we evaluated the binding of these agents to Hsp90 in lysates from breast cancer cells and CML cells. Four consecutive immunoprecipitation steps with H9010, but not with a nonspecific IgG, quantitatively depleted Hsp90 from these extracts (Fig. 1a). In contrast, sequential pull-downs with PU or GM beads removed only a limited fraction of total cellular Hsp90 (Fig. 1b and Supplementary Results, Supplementary Fig. 1a,b). Specifically, in MDA-MB-468 breast cancer cells, the combined PU bead fractions represented ~20–30% of the total Hsp90 pool, and further addition of fresh PU bead aliquots failed to precipitate the Hsp90 remaining in the lysate (Fig. 1b, PU beads). This PU-H71-depleted, remaining Hsp90 fraction, although inaccessible to the small molecule, maintained affinity for H9010 (Fig. 1b, H9010). From this we conclude that a substantial fraction of Hsp90 in the MDA-MB-468 cell extracts was still in a native conformation but not reactive with PU-H71.

To exclude the possibility that changes in Hsp90's configuration in cell lysates make it unavailable for binding to immobilized PU-H71 but not to the antibody, we analyzed binding of radiolabeled ^{125}I -PU-H71 to Hsp90 in intact cancer cells (Fig. 1c).

Binding of ^{125}I -PU-H71 to Hsp90 in several cancer cell lines saturated at a well-defined, although distinct, number of sites per cell (Fig. 1c).

We quantified the fraction of cellular Hsp90 bound by PU-H71 in MDA-MB-468 cells. First, we determined that Hsp90 represented 2.66–3.33% of the total protein in these cells, a value in close agreement with the reported abundance of Hsp90 in other tumor cells⁹. Approximately 41.65×10^6 MDA-MB-468 cells were lysed to yield 3,875 μg of protein, of which between 103.07 μg and 129.04 μg was Hsp90. One cell, therefore, contained $(2.47\text{--}3.09) \times 10^{-6}$ μg , $(2.74\text{--}3.43) \times 10^{-11}$ μmol or $(1.64\text{--}2.06) \times 10^7$ molecules of Hsp90. In MDA-MB-468 cells, ^{125}I -PU-H71 bound to, at most, 5.5×10^6 of the available cellular binding sites (Fig. 1c), which amounts to 26.6–33.5% of the total Hsp90 (calculated as $5.5 \times 10^6 / (1.64\text{--}2.06) \times 10^7 \times 100$). This value is markedly similar to that obtained with PU bead pull-downs in cell extracts (Fig. 1b), confirming that PU-H71 binds to a fraction of Hsp90 in MDA-MB-468 cells that represents approximately 30% of the total Hsp90 pool, and validating the use of PU beads to efficiently isolate this pool. In K562 and other established t(9;22)⁺ CML cell lines, PU-H71 bound 10.3–23% of the total cellular Hsp90 (Fig. 1c and Supplementary Fig. 1b,c).

Next, we extended our studies to several primary leukemia cells and to normal blood cells. Among these were primary chronic- and blast-phase CML and acute myeloid leukemia (AML) samples that contained both blasts (malignant cell population) and lymphocytes (normal cell population), CD34⁺ cells isolated from the cord blood of healthy donors, total mononuclear cells from peripheral blood and also peripheral blood leukocytes (PBLs) (Fig. 1c–e and Supplementary Figs. 1d and 2a–h). We used a fluorescein-labeled PU-H71 (PU-FITC) and flow cytometric analysis to determine PU-H71 binding to distinct cell populations.

PU-H71 efficiently bound to Hsp90 in K562 cells and in CML and AML blasts with a half-maximal inhibitory concentration (IC_{50}) of 116 nM, 201 nM and 425 nM, respectively (Fig. 1d). In contrast, its affinity for Hsp90 in normal blood cells was weaker, with IC_{50} values higher than 2,000 nM (Fig. 1d and Supplementary Fig. 1d). Hsp90 is highly expressed in these normal blood cells, as indicated by substantial binding of the Hsp90 antibody (Supplementary Fig. 1d).

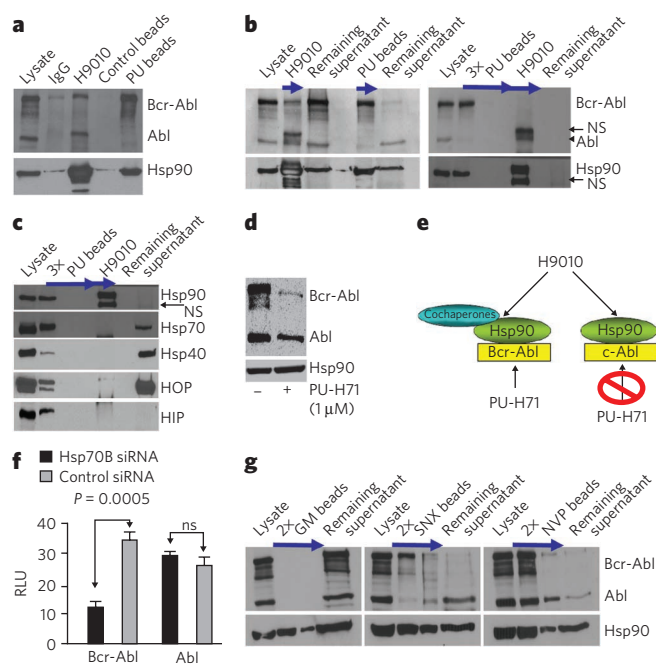


Figure 2 | PU-H71 is selective for and isolates Hsp90 in complex with oncoproteins and cochaperones. (a) Representative western blot of Hsp90 complexes in K562 extracts isolated by precipitation with H9010, a nonspecific IgG, PU beads or control beads containing 2-methoxyethylamine, an Hsp90-inert molecule. (b,c) Single or sequential immunoprecipitations and chemical precipitations, as indicated by arrows, conducted in K562 extracts with H9010 and PU beads. NS, nonspecific. (d) Representative western blot of K562 cells treated for 24 h with vehicle (–) or PU-H71 (+). (e) Proposed Hsp90 species in K562 cells, in complex with both aberrant, Bcr-Abl, and normal, c-Abl, proteins. PU-H71, but not H9010, selects for the Hsp90 population that is Bcr-Abl oncoprotein bound. (f) Expression of proteins in Hsp70-knocked down K562 cells. Changes in protein concentrations are presented in relative luminescence units (RLU). Control, scrambled small interfering RNA (siRNA). Data are presented as means \pm s.e.m. ($n = 3$). ns, nonsignificant. (g) Representative western blot of sequential chemical precipitations, as indicated by arrows, conducted in K562 extracts with GM, SNX and NVP beads.

Cells with the highest avidity for PU-H71 were also the most sensitive to killing by this agent (Fig. 1e and Supplementary Figs. 1e and 2). When evaluated in a panel of CML and AML cell lines and primary samples, we noted a good correlation between PU-H71 binding to Hsp90 and its cell-killing potential (Supplementary Figs. 1e and 2).

Collectively, these data confirm that certain Hsp90 inhibitors bind preferentially to a subset of Hsp90 species that is more abundant in cancer cells than in normal cells (Supplementary Fig. 3a). Abundance of this species is not dictated solely by the amount of Hsp90 expression and is predictive of cellular sensitivity to Hsp90 inhibition.

PU-H71 selects for oncoprotein–Hsp90 complex species

Next we performed immunoprecipitations and chemical precipitations with beads coated with H9010-specific antibody and those carrying PU, and analyzed the associated client cargo in each case. We first investigated K562 CML cells because this cell line coexpresses the aberrant Bcr-Abl protein, a constitutively active kinase, and its normal counterpart c-Abl. These two Abl species are clearly separable by molecular weight and are therefore easily distinguishable by western blot (Fig. 2a, lysate). We observed that H9010, but not a nonspecific IgG, isolated Hsp90 complexed with both Bcr-Abl and Abl (Fig. 2a

and Supplementary Fig. 3b,c, H9010). Comparison of immunoprecipitated Bcr-Abl and Abl (Fig. 2a,b, H9010) with the fraction of each protein remaining in the supernatant (Fig. 2b, remaining supernatant), indicated that H9010 did not preferentially enrich for Hsp90 bound to either mutant or wild-type Abl in K562 cells.

In contrast, PU-H71-bound Hsp90 preferentially isolated Bcr-Abl protein (Fig. 2a,b, PU beads). Following depletion of the Hsp90–Bcr-Abl species by PU beads (Fig. 2b,c, PU beads), H9010 precipitated the remaining Hsp90–Abl species (Fig. 2b,c, H9010). PU beads retained selectivity for Hsp90–Bcr-Abl at substantially saturating conditions (that is, excess of lysate and beads; Supplementary Fig. 4a). As further confirmation of the biochemical selectivity of PU-H71 for the Bcr-Abl–Hsp90 complex, Bcr-Abl was more susceptible to degradation by PU-H71 than was Abl (Fig. 2d). We confirmed the selectivity of PU-H71 for the aberrant Abl in other established t(9;22)⁺ CML cell lines (Supplementary Fig. 4b) and in primary CML samples (Supplementary Fig. 4c).

PU-H71 selects for Hsp90 bound to cochaperones

To further differentiate between the PU-H71-isolated and antibody-isolated Hsp90 fractions, we evaluated the cochaperone constituency of both species⁸. The fraction of Hsp90 bound to Bcr-Abl also associated with several cochaperones, including Hsp70, Hsp40, HOP and HIP (Fig. 2c, PU beads), as well as additional cochaperones (Supplementary Data Set 1a–d). These findings strongly suggest that PU-H71 recognizes cochaperone-associated Hsp90. After depletion by PU beads, the Hsp90 pool detected by H9010, shown to include Hsp90–Abl complexes, did not contain cochaperones (Fig. 2c, H9010), although their abundant expression was detected in the lysate (Fig. 2c, remaining supernatant). Cochaperones were isolated by H9010 in total cell extract (Supplementary Fig. 3b,c).

These findings suggest the existence of distinct pools of Hsp90 that are preferentially bound to either Bcr-Abl or Abl in CML cells (Fig. 2e). H9010 recognizes both pools, whereas PU-H71 selects for the Bcr-Abl–Hsp90 species. Our data also suggest that Hsp90 may use and require more acutely the classical cochaperones Hsp70, Hsp40 and HOP when it modulates the activity of aberrant (that is, Bcr-Abl) but not normal (that is, Abl) proteins (Supplementary Fig. 3a). In accord with this hypothesis, we find that Bcr-Abl is more sensitive than Abl to knockdown of Hsp70 in K562 cells (Fig. 2f and Supplementary Fig. 3d).

Not all Hsp90 inhibitors trap Hsp90–oncoprotein complexes

We next evaluated whether other inhibitors that interact with the N-terminal ATP pocket of Hsp90, including the synthetic inhibitors SNX-2112 and NVP-AUY922 and the natural product geldanamycin¹¹, could selectively isolate similar Hsp90 species (Fig. 2g). SNX beads showed selectivity for Bcr-Abl–Hsp90, whereas NVP beads behaved similarly to H9010 and did not discriminate between Bcr-Abl–Hsp90 and Abl–Hsp90 species (see SNX versus NVP beads, respectively; Fig. 2g). Although GM beads also recognized a subpopulation of Hsp90 in cell lysates (Supplementary Fig. 1a), they were much less efficient than were PU beads in co-precipitating Bcr-Abl (Fig. 2g, GM beads). The ineffectiveness of GM in trapping Hsp90–client protein complexes was previously reported¹².

PU-H71 identifies additional Hsp90 oncoclient proteins

To determine whether selectivity towards oncoprotein–Hsp90 complexes was a general property of PU-H71, we tested several additional well-defined Hsp90 client proteins in other tumor cell lines^{13,14} (Supplementary Fig. 4d–f). In agreement with our results in K562 cells, H9010 precipitated Hsp90 bound to both mutant B-Raf expressed in SKMel28 melanoma cells and to wild-type B-Raf expressed in CCD18Co normal colon fibroblasts (Supplementary Fig. 4e). PU and GM beads, however, selectively recognized Hsp90 bound to mutant B-Raf, showing little recognition of Hsp90 bound

Table 1 | IC₅₀ values for the indicated compounds in cell proliferation assays

Drug or cell line	PU-H71	Gleevec	PP242	AS703026	BMS-345541	KN-93
K562	0.13 ± 0.02	0.33 ± 0.07	2.00 ± 0.10	1.07 ± 0.10	8.60 ± 0.30	5.75 ± 0.60
Mia-PaCa-2	0.15 ± 0.01	>10.00	0.70 ± 0.14	NA	NA	NA

Cells were treated for 72 h with the indicated inhibitors, and the effect on cell growth was analyzed. The half-maximal inhibitory concentration (IC₅₀) is indicated in μM. Data are presented as means ± s.d. (n = 3). NA, not available.

The NF-κB pathway. Activation of nuclear factor-κB (NF-κB) is required for Bcr-Abl transformation of primary bone marrow cells and for Bcr-Abl-transformed hematopoietic cells to form tumors in nude mice²². PU-H71-isolated proteins enriched in this pathway include NF-κB as well as NF-κB activators, including IKBKAP, TANK-binding kinase 1 (TBK-1) and TAK1-binding protein 1 (TAB1)²³ (Supplementary Data Set 1a,d). Recently, Bcr-Abl-induced activation of the NF-κB cascade in myeloid leukemia cells was shown to be largely mediated by tyrosine-phosphorylated PKD2 (or PRKD2)²⁴ which we identify here to be a PU-H71-Hsp90 interactor (Fig. 3b,c, Supplementary Figs. 4c and 6c, and Supplementary Data Set 1a,d).

The Raf-MAPK pathway. Key effectors of the MAPK pathway, also activated in CML^{17,22}, including Raf-1, A-Raf, ERK, p90RSK, Vav and several MAPKs, are included in the PU-H71-Hsp90-bound pool (Fig. 3b,c, Supplementary Figs. 4c and 6b, and Supplementary Data Set 1a,d). IPA connects the MAPK pathway to key elements of many signal transduction pathways including the PI3K-AKT-mTOR, STAT and focal adhesion pathways (Fig. 3a and Supplementary Fig. 6b-e).

The STAT pathway. The STAT pathway is also activated in CML and confers cytokine independence and protection against apoptosis²², and was enriched by PU-H71 chemical precipitation (network 8, 20 focus molecules, score = 14; Supplementary Fig. 6d and Supplementary Data Set 1f). Both STAT5 and STAT3 were associated with PU-H71-Hsp90 complexes (Fig. 3b,c and Supplementary Data Set 1a,d). In CML, STAT5 activation by phosphorylation is driven by Bcr-Abl¹⁷. Bruton agammaglobulinemia tyrosine kinase (BTK), constitutively phosphorylated and activated by Bcr-Abl in pre-B lymphoblastic leukemia cells²⁵, can also signal through STAT5 (ref. 26). BTK is another Hsp90-regulated protein that we identified in CML (Fig. 3b,c, Supplementary Fig. 4c and Supplementary Data Set 1a,d). In addition to phosphorylation, STATs can be activated in myeloid cells by calpain (CAPN1)-mediated proteolytic cleavage, leading to truncated STAT species²⁷. CAPN1 is also found in PU-H71-bound Hsp90 pull-downs, as is activated Ca²⁺-calmodulin-dependent protein kinase IIγ (CaMKIIγ) activated in CML by Bcr-Abl²⁸ (Supplementary Data Set 1a,d).

The focal adhesion pathway. The focal adhesion pathway was well represented in PU-H71 pull-downs (network 12, 16 focus molecules, score = 13; Supplementary Fig. 6e and Supplementary Data Set 1f). The focal adhesion-associated proteins paxillin, FAK, vinculin, talin and tensin are constitutively phosphorylated in Bcr-Abl-transfected cell lines^{29,30}, and these too were isolated in PU-H71-Hsp90 complexes (Fig. 3a).

Other pathways. Other important transforming pathways in CML, driven by MYC³¹ (network 7, 15 focus molecules, score = 22) and TGF-β³² (network 10, 13 focus molecules, score = 18) were identified here as well (Supplementary Fig. 6a,f,g and Supplementary Data Set 1f). Among the identified networks were also those important for disease progression and aberrant cell cycle and proliferation of CML (networks 3-6, 9, 11 and 13; Supplementary Fig. 6a and Supplementary Data Set 1f).

In summary, PU-H71 pull-down enriched for a broad cross-section of proteins that participate in signaling pathways vital to the malignant phenotype of CML. Interaction of PU-H71-bound Hsp90 with the aberrant CML signalosome was retained in primary CML samples (Fig. 3c and Supplementary Fig. 4c).

PU-H71 cargo contributes to the malignant phenotype

To demonstrate that the networks identified by PU beads are important for transformation in K562, we next showed that inhibitors of key nodal proteins from individual networks (Fig. 3a, yellow boxes—Bcr-Abl, NFκB, mTOR, MEK and CAMKII) diminish the growth and proliferation potential of K562 cells (Table 1 and Supplementary Fig. 7a).

Next we showed that PU beads identified a set of Hsp90 interactors with no known role in CML, but which also contribute to the transformed phenotype. The histone-arginine methyltransferase CARM1, a transcriptional coactivator of many genes³³, was validated in the PU bead pull-downs from CML cell lines and primary CML cells (Fig. 3b,c and Supplementary Fig. 4b,c). This is the first reported link between Hsp90 and CARM1, although other arginine methyltransferases, such as PRMT5, have been shown to be Hsp90 clients in ovarian cancer cells³⁴. Although elevated amounts of CARM1 are implicated in the development of prostate and breast cancers, little is known about the importance of CARM1 in CML leukomogenesis³³. CARM1 was essentially entirely captured by the Hsp90 species recognized by PU beads (Fig. 4a), and it was also sensitive to degradation by PU-H71 (Fig. 3b). Therefore, CARM1 may be a previously unreported Hsp90 oncoprotein in CML. Indeed, knockdown experiments with CARM1 but not control short hairpin RNAs (shRNAs), showed reduced viability and enhanced apoptosis in K562 (Fig. 4b).

To demonstrate that the presence of proteins in PU-H71 pull-downs is due to their participation in aberrantly activated signaling and not merely their abundant expression, we compared PU bead pull-downs from K562 and Mia-PaCa-2, a pancreatic cancer cell line (Supplementary Data Set 1a). Although both cell lines express large amounts of STAT5 protein (Fig. 4c), we noted activation of the STAT5 pathway, as demonstrated by STAT5 phosphorylation (Fig. 4c) and DNA binding³⁵, in only the K562 cells. In accordance, this protein was identified only in the K562 PU bead pull-downs (Supplementary Data Set 1a and Supplementary Fig. 7b). In contrast, we identified activated STAT3 in PU-H71-Hsp90 complexes from both K562 (Fig. 3b) and Mia-PaCa-2 cell extracts (Fig. 4d).

We identified the mTOR pathway using PU beads in both K562 and Mia-PaCa-2 cells (Supplementary Fig. 7b) and, indeed, its pharmacological inhibition by PP242, a selective inhibitor that targets the ATP domain of mTOR³⁶, was toxic to both cells. In contrast, the Abl inhibitor Gleevec³⁷ was toxic to only K562 cells (Table 1 and Supplementary Fig. 7a,c). Both cell lines express Abl but only K562 has the oncogenic Bcr-Abl (Fig. 4c), and PU beads identified Abl, as Bcr-Abl, in K562 but not in Mia-PaCa-2 cells (Supplementary Fig. 7b).

PU-H71 identifies a new STAT activation mechanism

PU bead pull-downs contain several proteins, including Bcr-Abl¹⁷, CAMKIIγ²⁸, FAK²⁹, vav-1 (ref. 38) and PRKD2 (ref. 24), that are constitutively activated in CML. These are classical Hsp90-regulated clients that depend on Hsp90 for their stability because their steady-state concentrations decrease upon Hsp90 inhibition^{8,9} (Fig. 3b). Constitutive activation of STAT3 and STAT5 is also reported in CML^{17,22}. These proteins, however, do not fit the criteria of classical Hsp90 client proteins, because STAT5 and STAT3 concentrations remain essentially unchanged upon Hsp90 inhibition (Fig. 3b). The PU-H71 pull-downs also contained proteins that may constitute active signaling megacomplexes, such as mTOR, VPS32, VPS15 and

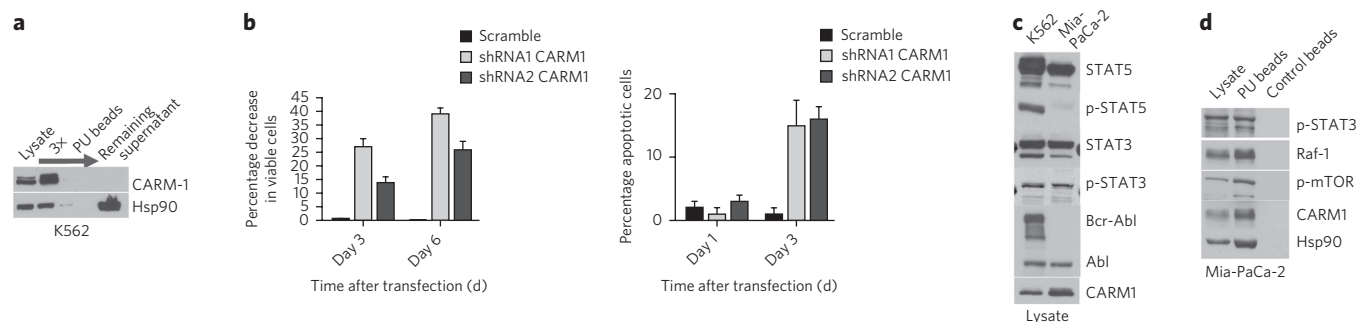


Figure 4 | PU-H71-identified proteins and networks are those important for the malignant phenotype. (a) Representative western blot of sequential chemical precipitations, as indicated by the arrow, conducted in K562 extracts with the PU beads. (b) The effect of CARM1 knockdown on cell viability using trypan blue (left) or acridine orange-ethidium bromide (right) staining was evaluated in K562 cells. Data are presented as means \pm s.e.m. ($n = 3$). (c) The expression of select potential Hsp90-interacting proteins was analyzed by western blotting in K562 leukemia and Mia-PaCa-2 pancreatic cancer cells. (d) Representative western blot of single chemical precipitations conducted in Mia-PaCa-2 cell extracts with PU and control beads.

RAPTOR²⁰. Furthermore, PU-H71–Hsp90 complexes contained adapter proteins such as GRB2, DOCK, CRKL and EPS15, which link Bcr-Abl to key effectors of multiple aberrantly activated signaling pathways in K562 (refs. 6,17; Fig. 3a). Their expression also remained unchanged upon Hsp90 inhibition (Fig. 3b). We therefore wondered whether the contribution of Hsp90 to certain oncogenic pathways extends beyond its classical folding and stabilizing activity. Specifically, we hypothesized that Hsp90 might also act as a scaffolding molecule to maintain signaling complexes in an active configuration, as has been previously postulated^{16,39}.

Hsp90 binds to and influences the conformation of STAT5

To investigate this hypothesis further we focused on STAT5, which is constitutively phosphorylated in CML⁴⁰. The overall concentration of p-STAT5 is determined by the balance of phosphorylation and dephosphorylation events. The high concentrations of p-STAT5 in

K562 cells may reflect either an increase in upstream kinase activity or a decrease in protein tyrosine phosphatase (PTPase) activity. A direct interaction between Hsp90 and p-STAT5 could also modulate the amount of p-STAT5 in cells.

To dissect the relative contributions of these potential mechanisms, we first investigated the effect of PU-H71 on the main kinases and PTPases that regulate STAT5 phosphorylation in K562 cells. Bcr-Abl directly activates STAT5 without the need for JAK phosphorylation⁴⁰. Concordantly, STAT5 phosphorylation rapidly decreased in the presence of the Bcr-Abl inhibitor Gleevec (Fig. 5a, Gleevec). While Hsp90 regulates Bcr-Abl stability, the reduction in steady-state Bcr-Abl concentrations following Hsp90 inhibition requires more than 3 h⁴¹. Indeed, we observed no change in Bcr-Abl expression (Fig. 5a, PU-H71, Bcr-Abl) or function, as evidenced by no decrease in CRKL phosphorylation (Fig. 5a, PU-H71, p-CRKL and CRKL), with PU-H71 in the time interval during which p-STAT5

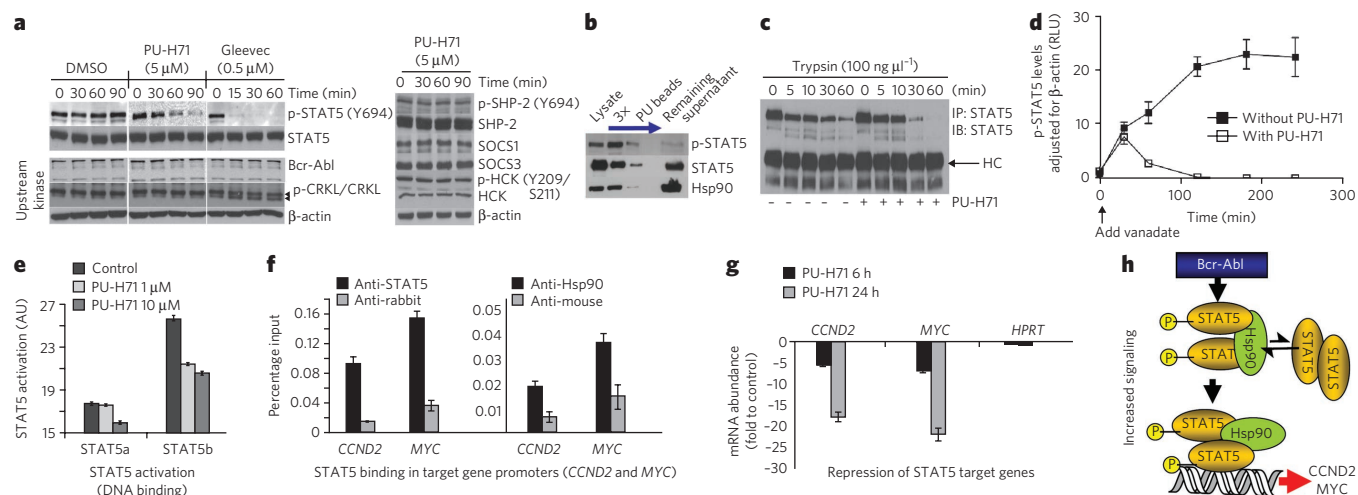


Figure 5 | Hsp90 facilitates an enhanced STAT5 activity in CML. (a) Representative western blot of K562 cells treated for the indicated times with PU-H71 (5 μ M), Gleevec (0.5 μ M) or DMSO (vehicle). (b) Representative western blot of sequential chemical precipitations conducted in K562 cells with PU and control beads, as indicated by the blue arrow. (c) Representative western blot of STAT5 immunocomplexes from cells pretreated with vehicle or PU-H71, and then treated for the indicated times with trypsin. (d) p-STAT5 concentrations in K562 cells treated for the indicated times with vanadate (1 mM) in the presence and absence of PU-H71 (5 μ M). Data are presented as mean \pm s.d. ($n = 3$). (e) The DNA-binding capacity of STAT5 in K562 cells treated for 24 h with the indicated concentrations of PU-H71. (f) Quantitative ChIP performed with STAT5 or Hsp90 antibodies versus an IgG control for two known STAT5 target genes. A primer that amplifies an intergenic region was used as negative control. Results are expressed as a percentage of the input for the specific antibody (STAT5 or Hsp90) over the respective IgG control. (g) The transcript abundance of CCND2 and MYC in K562 cells exposed to 1 μ M of PU-H71. Results are expressed as fold change compared to baseline (time 0 h) and were normalized to RPL13A. HPRT was used as negative control. Data are presented as means \pm s.e.m. (h) Proposed mechanism for Hsp90-facilitated increased STAT5 signaling in CML. Hsp90 binds to and influences the conformation of STAT5 and maintains STAT5 in an active conformation directly within STAT5-containing transcriptional complexes.



concentrations were reduced (Fig. 5a, PU-H71, p-STAT5). Also, we saw no change in the activity and expression of HCK, a kinase activator of STAT5 in 32Dcl3 cells transfected with Bcr-Abl⁴² (Fig. 5a, HCK and p-HCK). We also excluded the possibility of a change in PTPase activity, because the expression and activity of SHP2, the major cytosolic STAT5 phosphatase⁴³, was not altered in this time interval (Fig. 5a, SHP2 and p-SHP2), nor were the concentrations of SOCS1 and SOCS3, which form a negative-feedback loop that switches off STAT signaling³⁷ (Fig. 5a, SOCS1 and SOCS3). Thus, no effect on STAT5 phosphorylation in the 0–90-min interval can be attributed to a change in kinase or phosphatase activity upon Hsp90 inhibition.

Because most p-STAT5, but not STAT5, is bound to Hsp90 in CML cells (Fig. 5b), we hypothesized that the cellular concentrations of activated STAT5 are fine-tuned by direct binding to Hsp90. The activation and inactivation cycle of STATs entails their transition between different dimer conformations⁴⁴. We found that STAT5 is more susceptible to trypsin cleavage when bound to Hsp90 (Fig. 5c), indicating that binding of Hsp90 directly modulates the conformational state of STAT5, potentially keeping it in a conformation unfavorable for dephosphorylation and/or favorable for phosphorylation. To investigate this possibility, we used a pulse-chase strategy in which orthovanadate (Na₃VO₄), a nonspecific PTPase inhibitor, was added to cells to block dephosphorylation of STAT5. We then determined the residual concentration of p-STAT5 at several later time points (Fig. 5d and Supplementary Fig. 7d). In the absence of PU-H71, p-STAT5 accumulated rapidly, whereas in its presence, cellular p-STAT5 concentrations were diminished. The kinetics of this process (Fig. 5d) were similar to the rate of p-STAT5 steady-state reduction (Fig. 5a, PU-H71).

Hsp90 supports STAT5-mediated transcription

The biological activity of STAT5 also requires its nuclear translocation and direct binding to its various target genes^{40,44}. We wondered whether Hsp90 might also facilitate the transcriptional activation of STAT5-regulated genes, and thus participate in promoter-associated STAT5 transcription complexes. We found that STAT5 is constitutively active in K562 cells and binds to a STAT5-binding consensus sequence. STAT5 activation and DNA binding were partially abrogated, in a dose-dependent manner, upon Hsp90 inhibition with PU-H71 (Fig. 5e). Furthermore, quantitative chromatin immunoprecipitation (ChIP) assays in K562 cells revealed the presence of both Hsp90 and STAT5 at the critical STAT5 targets *MYC* and *CCND2* (Fig. 5f). Neither protein was present at intergenic control regions (data not shown). Accordingly, PU-H71 (1 μM) decreased the mRNA abundance of the STAT5 target genes *CCND2*, *MYC*, *CCND1*, *BCL-XL* and *MCL1* (ref. 45), but not of the control genes *HPRT* and *GAPDH* (Fig. 5g).

Collectively, these data show that STAT5 activity is positively regulated by Hsp90 in CML cells (Fig. 5h). Our findings are consistent with a scenario whereby Hsp90 binding to STAT5 modulates the conformation of the protein to alter STAT5 phosphorylation and dephosphorylation kinetics. In addition, Hsp90 maintains STAT5 in an active conformation in STAT5-containing transcriptional complexes. Considering the complexity of the STAT pathway, other potential mechanisms cannot be excluded. Therefore, in addition to its role in promoting protein stability, Hsp90 promotes oncogenesis by maintaining client proteins in an active configuration.

DISCUSSION

We present herein a rapid and simple chemical-proteomics method for surveying tumor oncoproteins (Supplementary Fig. 8). The method takes advantage of PU-H71's ability to (i) preferentially bind to a pool of Hsp90 associated with oncogenic client proteins, and (ii) trap Hsp90 in an oncoclient-bound configuration. We propose that this approach provides a powerful tool to dissect, tumor-by-tumor,

molecular lesions that are characteristic of distinct cancers. Because of the initial chemical-precipitation step, which purifies and enriches the aberrant protein population as part of PU bead-bound Hsp90 complexes, the method does not require expensive SILAC labeling or two-dimensional gel separation of samples. Instead, protein cargo from PU bead pull-downs is simply eluted in SDS buffer and submitted to standard SDS-PAGE, and then the separated proteins are extracted and trypsinized for LC-MS/MS analysis.

Although this method presents a unique approach to identifying the oncoproteins that maintain the malignant phenotype of tumor cells, one needs to be aware that, similar to other chemical or antibody-based proteomics techniques, it has potential limitations⁴⁶. For example, 'sticky' or abundant proteins may bind in a nondiscriminatory way to proteins isolated by PU beads. Second, although we have presented several lines of evidence that PU-H71 is specific for Hsp90, one must consider that, at the high concentration of PU-H71 present on the beads, some nonspecific binding to a few non-Hsp90 proteins is unavoidable.

Despite these potential limitations, we have used this method to carry out the first global evaluation of Hsp90-dependent aberrant signaling pathways in CML. The Hsp90 interactome identified by PU-H71 affinity purification overlaps substantially with the well-characterized CML signalosome, indicating that this method can identify a large part of the complex web of pathways and proteins that define the molecular basis of this leukemia. When applied to less well-characterized tumor types, this method may provide unpredicted targets for combinatorial therapy.

We believe the functional proteomics method described here will assist identification of the critical proteome subset that is dysregulated in individual tumors, including primary patient specimens. Thus, tumor-specific Hsp90 client profiling could ultimately yield an approach for personalized therapeutic targeting of tumors (Supplementary Fig. 8).

Our work also proposes that Hsp90 forms biochemically distinct complexes in cancer cells (Supplementary Fig. 3a). In this view, a major fraction of cancer cell Hsp90 retains 'housekeeping' chaperone functions similar to normal cells, whereas a functionally distinct Hsp90 pool that is enriched or expanded in cancer cells specifically interacts with the oncogenic proteins required to maintain tumor cell survival. Perhaps this Hsp90 fraction represents a cell stress-specific form of chaperone complex that is expanded and constitutively maintained in the tumor cell context. Our data suggest that it may execute functions necessary to maintain the malignant phenotype. One such role is to regulate the folding of mutated (that is, mB-Raf) or chimeric (that is, Bcr-Abl) proteins^{8,9}. We now present experimental evidence for an additional role; that is, to facilitate scaffolding and complex formation of molecules involved in aberrantly activated signaling complexes.

What distinguishes the PU-H71-binding fraction of Hsp90 from the non-PU-H71-binding fraction? This is a complex question that remains under active investigation. Although both Hsp90α and Hsp90β isoforms are recognized by PU-H71, our data provide evidence for at least one difference between Bcr-Abl-Hsp90 (PU-H71 preferring) and Abl-Hsp90 (PU-H71 nonpreferring) chaperone complexes. That is, Bcr-Abl-Hsp90 chaperone complexes contain a number of cochaperones (suggesting that an active chaperoning process is underway, further supported by the sensitivity of Bcr-Abl to the silencing of Hsp70), whereas Abl-Hsp90 complexes lack associated cochaperones (probably representing sequestered but not actively chaperoned Abl, supported by the insensitivity of Abl to Hsp70 knockdown). Finally, we have observed a differential impact of Hsp90 phosphorylation on PU-H71 and geldanamycin binding. These findings, which are being pursued further, suggest that various Hsp90 inhibitors may be uniquely affected by specific post-translational modifications to the chaperone. Taken together, these preliminary observations suggest that PU-H71 recognizes an Hsp90 fraction

that is participating in an active chaperone cycle, and that this characteristic is not necessarily shared by other Hsp90 inhibitors.

Our work uses chemical tools to provide new insights into the heterogeneity of tumor-associated Hsp90 and harnesses the biochemical features of a particular Hsp90 inhibitor to identify tumor-specific biological pathways and proteins. We believe the functional proteomics method described here will allow identification of the critical proteome subset that becomes dysregulated in distinct tumors. This will allow for the identification of new cancer mechanisms, as exemplified by the STAT5 mechanism, the identification of new oncoproteins, as exemplified by CARM1, and the identification of therapeutic targets for the development of rationally combined targeted therapies complementary to Hsp90.

METHODS

Cell lines and primary cells. The CML cell lines K562, Kasumi-4, MEG-01 and KU182, triple-negative breast cancer cell line MDA-MB-468, HER2⁺ breast cancer cell line SKBr3, melanoma cell line SK-Mel-28, prostate cancer cell lines LNCaP and DU145, pancreatic cancer cell line Mia-PaCa-2 and colon fibroblast cell line CCD18Co were obtained from the American Type Culture Collection. The CML cell line KCL-22 was obtained from the Japanese Collection of Research Bioresources. The NIH-3T3 fibroblast cells were transfected as described⁴¹. Cells were cultured in DMEM in F12 (MDA-MB-468, SKBr3 and Mia-PaCa-2), RPMI (K562, SK-Mel-28, LNCaP, DU145 and NIH-3T3) or MEM (CCD18Co) supplemented with 10% (v/v) fetal bovine serum (FBS), 1 × L-glutamine and 1 × penicillin and streptomycin (Pen/Strep). Kasumi-4 cells were maintained in IMDM supplemented with 20% (v/v) FBS, 10 ng ml⁻¹ granulocyte macrophage colony-stimulating factor (GM-CSF) and 1 × Pen/Strep. PBLs (*n* = 3) and cord blood (*n* = 5) were obtained from patient blood purchased from the New York Blood Center. We layered 35 ml of the cell suspension over 15 ml of Ficoll-Paque plus (GE Healthcare). Samples were centrifuged at 2,000 r.p.m. for 40 min at 4 °C, and the leukocyte interface was collected. Cells were plated in RPMI medium with 10% (v/v) FBS and used as indicated. Primary human chronic and blast crisis CML and AML cells were obtained with informed consent. The manipulation and analysis of specimens was approved by the University of Rochester, Weill Cornell Medical College and University of Pennsylvania Institutional Review Boards. Mononuclear cells were isolated using Ficoll-Paque (Pharmacia Biotech) density gradient separation. Cells were cryopreserved in freezing medium consisting of IMDM, 40% (v/v) FBS, and 10% (v/v) DMSO or in CryoStor CS-10 (Biolife). When cultured, cells were kept in a humidified atmosphere of 5% CO₂ at 37 °C.

Cell lysis for chemical precipitation and immunoprecipitation. Cells were lysed by collecting them in Felts buffer (20 mM HEPES, 50 mM KCl, 5 mM MgCl₂, 0.01% (w/v) NP-40, freshly prepared 20 mM Na₂MoO₄ (pH 7.2–7.3)) with added 1 μg μl⁻¹ protease inhibitors (leupeptin and aprotinin), followed by three successive freeze (in dry ice) and thaw steps. Total protein concentration was determined using the BCA kit (Pierce) according to the manufacturer's instructions.

Immunoprecipitation. The Hsp90 antibody (H9010) or normal IgG (Santa Cruz Biotechnology) was added at a volume of 10 μl to the indicated amount of cell lysate, together with 40 μl of protein G agarose beads (Upstate), and the mixture incubated at 4 °C overnight. The beads were washed five times with Felts lysis buffer and separated by SDS-PAGE, followed by a standard western blotting procedure.

Chemical precipitation. Hsp90 inhibitors beads or control beads, containing an Hsp90 inactive chemical (2-methoxyethylamine) conjugated to agarose beads, were washed three times in lysis buffer. Unless otherwise indicated, the bead conjugates (80 μl) were then incubated at 4 °C with the indicated amounts of cell lysate (120–500 μg), and the volume was adjusted to 200 μl with lysis buffer. Following incubation, bead conjugates were washed five times with the lysis buffer and proteins in the pull-down were analyzed by western blotting. For depletion studies, two to four successive chemical precipitations were performed, followed by immunoprecipitation steps, where indicated.

Statistical analysis. Unless otherwise indicated, data were analyzed by unpaired two-tailed *t*-tests as implemented in GraphPad Prism (version 4; GraphPad Software). A *P*-value of less than 0.05 was considered significant. Unless otherwise noted, data are presented as the mean ± s.d or mean ± s.e.m. of duplicate or triplicate replicates. Error bars represent the s.d or s.e.m. of the mean. If a single panel is presented, data are representative of two or three individual experiments.

Additional methods. Detailed methodology is described in the **Supplementary Methods** section on line.

Received 12 April 2011; accepted 27 July 2011;
published online 25 September 2011

References

- Ley, T.J. *et al.* DNA sequencing of a cytogenetically normal acute myeloid leukaemia genome. *Nature* **456**, 66–72 (2008).
- Parsons, D.W. *et al.* An integrated genomic analysis of human glioblastoma multiforme. *Science* **321**, 1807–1812 (2008).
- Hanash, S. & Taguchi, A. The grand challenge to decipher the cancer proteome. *Nat. Rev. Cancer* **10**, 652–660 (2010).
- Kolch, W. & Pitt, A. Functional proteomics to dissect tyrosine kinase signalling pathways in cancer. *Nat. Rev. Cancer* **10**, 618–629 (2010).
- Nomura, D.K., Dix, M.M. & Cravatt, B.F. Activity-based protein profiling for biochemical pathway discovery in cancer. *Nat. Rev. Cancer* **10**, 630–638 (2010).
- Brehme, M. *et al.* Charting the molecular network of the drug target Bcr-Abl. *Proc. Natl. Acad. Sci. USA* **106**, 7414–7419 (2009).
- Ashman, K. & Villar, E.L. Phosphoproteomics and cancer research. *Clin. Transl. Oncol.* **11**, 356–362 (2009).
- Zuehlke, A. & Johnson, J.L. Hsp90 and co-chaperones twist the functions of diverse client proteins. *Biopolymers* **93**, 211–217 (2010).
- Workman, P., Burrows, F., Neckers, L. & Rosen, N. Drugging the cancer chaperone HSP90: combinatorial therapeutic exploitation of oncogene addiction and tumor stress. *Ann. NY Acad. Sci.* **1113**, 202–216 (2007).
- Kamal, A. *et al.* A high-affinity conformation of Hsp90 confers tumour selectivity on Hsp90 inhibitors. *Nature* **425**, 407–410 (2003).
- Janin, Y.L. ATPase inhibitors of heat-shock protein 90, second season. *Drug Discov. Today* **15**, 342–353 (2010).
- Tsaytler, P.A., Krijgsveld, J., Goerdal, S.S., Rudiger, S. & Egmond, M.R. Novel Hsp90 partners discovered using complementary proteomic approaches. *Cell Stress Chaperones* **14**, 629–638 (2009).
- da Rocha Dias, S. *et al.* Activated B-RAF is an Hsp90 client protein that is targeted by the anticancer drug 17-allylamino-17-demethoxygeldanamycin. *Cancer Res.* **65**, 10686–10691 (2005).
- Grbovic, O.M. *et al.* V600E B-Raf requires the Hsp90 chaperone for stability and is degraded in response to Hsp90 inhibitors. *Proc. Natl. Acad. Sci. USA* **103**, 57–62 (2006).
- Taldone, T. & Chiosis, G. Purine-scaffold hsp90 inhibitors. *Curr. Top. Med. Chem.* **9**, 1436–1446 (2009).
- Dezwaan, D.C. & Freeman, B.C. HSP90: the Rosetta stone for cellular protein dynamics? *Cell Cycle* **7**, 1006–1012 (2008).
- Ren, R. Mechanisms of BCR-ABL in the pathogenesis of chronic myelogenous leukaemia. *Nat. Rev. Cancer* **5**, 172–183 (2005).
- Burke, B.A. & Carroll, M. BCR-ABL: a multi-faceted promoter of DNA mutation in chronic myelogenous leukemia. *Leukemia* **24**, 1105–1112 (2010).
- McClellan, A.J. *et al.* Diverse cellular functions of the Hsp90 molecular chaperone uncovered using systems approaches. *Cell* **131**, 121–135 (2007).
- Carayol, N. *et al.* Critical roles for mTORC2- and rapamycin-insensitive mTORC1-complexes in growth and survival of BCR-ABL-expressing leukemic cells. *Proc. Natl. Acad. Sci. USA* **107**, 12469–12474 (2010).
- Nobukuni, T., Kozma, S.C. & Thomas, G. hVps34, an ancient player, enters a growing game: mTOR Complex1/S6K1 signaling. *Curr. Opin. Cell Biol.* **19**, 135–141 (2007).
- McCubrey, J.A. *et al.* Targeting survival cascades induced by activation of Ras/Raf/MEK/ERK, PI3K/PTEN/Akt/mTOR and Jak/STAT pathways for effective leukemia therapy. *Leukemia* **22**, 708–722 (2008).
- Häcker, H. & Karin, M. Regulation and function of IKK and IKK-related kinases. *Sci. STKE* **2006**, re13 (2006).
- Mihailovic, T. *et al.* Protein kinase D2 mediates activation of nuclear factor kappaB by Bcr-Abl in Bcr-Abl⁺ human myeloid leukemia cells. *Cancer Res.* **64**, 8939–8944 (2004).
- Hendriks, R.W. & Kersseboom, R. Involvement of SLP-65 and Btk in tumor suppression and malignant transformation of pre-B cells. *Semin. Immunol.* **18**, 67–76 (2006).
- Mahajan, S. *et al.* Transcription factor STAT5A is a substrate of Bruton's tyrosine kinase in B cells. *J. Biol. Chem.* **276**, 31216–31228 (2001).
- Oda, A., Wakao, H. & Fujita, H. Calpain is a signal transducer and activator of transcription (STAT) 3 and STAT5 protease. *Blood* **99**, 1850–1852 (2002).
- Si, J. & Collins, S.J. Activated Ca²⁺/calmodulin-dependent protein kinase IIgamma is a critical regulator of myeloid leukemia cell proliferation. *Cancer Res.* **68**, 3733–3742 (2008).
- Salgia, R. *et al.* Increased tyrosine phosphorylation of focal adhesion proteins in myeloid cell lines expressing p210BCR/ABL. *Oncogene* **11**, 1149–1155 (1995).
- Le, Y. *et al.* FAK silencing inhibits leukemogenesis in BCR/ABL-transformed hematopoietic cells. *Am. J. Hematol.* **84**, 273–278 (2009).
- Sawyers, C.L. The role of myc in transformation by Bcr-Abl. *Leuk. Lymphoma* **11**, 45–46 (1993).
- Naka, K. *et al.* TGF-beta-FOXO signaling maintains leukemia-initiating cells in chronic myeloid leukemia. *Nature* **463**, 676–680 (2010).
- Bedford, M.T. & Clarke, S.G. Protein arginine methylation in mammals: who, what, and why. *Mol. Cell* **33**, 1–13 (2009).

34. Maloney, A. *et al.* Gene and protein expression profiling of human ovarian cancer cells treated with the heat shock protein 90 inhibitor 17-allylamino-17-demethoxygeldanamycin. *Cancer Res.* **67**, 3239–3253 (2007).
35. Jaganathan, S., Yue, P. & Turkson, J. Enhanced sensitivity of pancreatic cancer cells to concurrent inhibition of aberrant signal transducer and activator of transcription 3 and epidermal growth factor receptor or Src. *J. Pharmacol. Exp. Ther.* **333**, 373–381 (2010).
36. Apsel, B. *et al.* Targeted polypharmacology: discovery of dual inhibitors of tyrosine and phosphoinositide kinases. *Nat. Chem. Biol.* **4**, 691–699 (2008).
37. Deininger, M.W. & Druker, B.J. Specific targeted therapy of chronic myelogenous leukemia with imatinib. *Pharmacol. Rev.* **55**, 401–423 (2003).
38. Katzav, S. Flesh and blood: the story of *Vav1*, a gene that signals in hematopoietic cells but can be transforming in human malignancies. *Cancer Lett.* **255**, 241–254 (2007).
39. Pratt, W.B., Morishima, Y. & Osawa, Y. The Hsp90 chaperone machinery regulates signaling by modulating ligand binding clefts. *J. Biol. Chem.* **283**, 22885–22889 (2008).
40. de Groot, R.P., Raaijmakers, J.A., Lammers, J.W., Jove, R. & Koenderman, L. STAT5 activation by BCR-Abl contributes to transformation of K562 leukemia cells. *Blood* **94**, 1108–1112 (1999).
41. An, W.G., Schulte, T.W. & Neckers, L.M. The heat shock protein 90 antagonist geldanamycin alters chaperone association with p210bcr-abl and v-src proteins before their degradation by the proteasome. *Cell Growth Differ.* **11**, 355–360 (2000).
42. Klejman, A. *et al.* The Src family kinase Hck couples BCR/ABL to STAT5 activation in myeloid leukemia cells. *EMBO J.* **21**, 5766–5774 (2002).
43. Xu, D. & Qu, C.K. Protein tyrosine phosphatases in the JAK/STAT pathway. *Front. Biosci.* **13**, 4925–4932 (2008).
44. Lim, C.P. & Cao, X. Structure, function and regulation of STAT proteins. *Mol. Biosyst.* **2**, 536–550 (2006).
45. Paukku, K. & Silvennoinen, O. STATs as critical mediators of signal transduction and transcription: lessons learned from STAT5. *Cytokine Growth Factor Rev.* **15**, 435–455 (2004).
46. Rix, U. & Superti-Furga, G. Target profiling of small molecules by chemical proteomics. *Nat. Chem. Biol.* **5**, 616–624 (2009).

Acknowledgments

This work was supported in part by the Geoffrey Beene Cancer Research Center of the Memorial Sloan-Kettering Cancer Center (G.C.), Leukemia and Lymphoma Society (G.C., M.L.G., S.D.N., X.Z. and R.L.), Breast Cancer Research Fund (G.C.), the SPORE Pilot Award and Research & Therapeutics Program in Prostate Cancer (G.C.), the Hirshberg Foundation for Pancreatic Cancer (G.C.), the Byrne Fund (G.C.), 1U01 AG032969-01A1 (G.C.), 1R01 CA155226-01 (G.C. and A.M.) and US National Cancer Institute (NCI) Cancer Center Support Grant P30 CA08748 (H.E.B.). K.B. and L.N. were supported by funds from the Intramural Program of the NCI. S.M.L. and P.M.S.-J. are supported by the Ludwig Center for Cancer Immunotherapy at MSKCC and by NCI Grant P50-CA86483. M.L.G. is funded by the US National Institutes of Health (NIH) through the NIH Director's New Innovator Award Program, 1 DP2 OD007399-01 and the V foundation. F.P. is funded by the American Italian Cancer Foundation. We thank D. Toft (Mayo Clinic) and M. Cox (University of Texas) for the gifts of H9010 Hsp90-specific antibodies, L.A. Fabrizio, A.M. Morrishow, H. Deng and J. Fernandez for help with MS analysis, A. Perl, C.T. Jordan, M. Becker and J. Nicoll for providing the primary CML samples or suggestions on their use, and B. Clarkson, J. Bromberg and P. Gregor for suggestions with the manuscript.

Author contributions

K.M., J.H.A., H.Z., L.C., A.R., K.B., P.S.-J., F.P., K.H., L.P.V., X.Z., H.E.-B., N.P. and T.K. performed experiments and D.Z., T.T., A.R., R.L., S.M.L., M.L.G. and S.S.G. provided reagents. All authors participated in the design and analysis of various experiments and G.C., A.M., S.D.N., M.L.G. and L.N. wrote the paper.

Competing financial interests

The authors declare competing financial interests: details accompany the full-text HTML version of the paper at <http://www.nature.com/naturechemicalbiology/>.

Additional information

Supplementary information is available online at <http://www.nature.com/naturechemicalbiology/>. Reprints and permissions information is available online at <http://www.nature.com/reprints/index.html>. Correspondence and requests for materials should be addressed to G.C. or L.N. or A.M. or S.D.N.

blood

2010 116: 2812-2821
Prepublished online June 28, 2010;
doi:10.1182/blood-2010-02-270611

Depletion of *L3MBTL1* promotes the erythroid differentiation of human hematopoietic progenitor cells: possible role in 20q – polycythemia vera

Fabiana Perna, Nadia Gurvich, Ruben Hoya-Arias, Omar Abdel-Wahab, Ross L. Levine, Takashi Asai, Francesca Voza, Silvia Menendez, Lan Wang, Fan Liu, Xinyang Zhao and Stephen D. Nimer

Updated information and services can be found at:
<http://bloodjournal.hematologylibrary.org/content/116/15/2812.full.html>

Information about reproducing this article in parts or in its entirety may be found online at:
http://bloodjournal.hematologylibrary.org/site/misc/rights.xhtml#repub_requests

Information about ordering reprints may be found online at:
<http://bloodjournal.hematologylibrary.org/site/misc/rights.xhtml#reprints>

Information about subscriptions and ASH membership may be found online at:
<http://bloodjournal.hematologylibrary.org/site/subscriptions/index.xhtml>



Depletion of *L3MBTL1* promotes the erythroid differentiation of human hematopoietic progenitor cells: possible role in 20q– polycythemia vera

*Fabiana Perna,¹ *Nadia Gurvich,¹ Ruben Hoya-Arias,¹ Omar Abdel-Wahab,² Ross L. Levine,² Takashi Asai,¹ Francesca Voza,¹ Silvia Menendez,¹ Lan Wang,¹ Fan Liu,¹ Xinyang Zhao,¹ and Stephen D. Nimer¹

¹Molecular Pharmacology and Chemistry Program, Sloan-Kettering Institute and ²Human Oncology and Pathogenesis Program, Memorial Sloan-Kettering Cancer Center, New York, NY

L3MBTL1, the human homolog of the *Drosophila* L(3)MBT polycomb group tumor suppressor gene, is located on chromosome 20q12, within the common deleted region identified in patients with 20q deletion-associated polycythemia vera, myelodysplastic syndrome, and acute myeloid leukemia. *L3MBTL1* is expressed within hematopoietic CD34⁺ cells; thus, it may contribute to the pathogenesis of these disorders. To define its role in hematopoiesis, we knocked down *L3MBTL1* expression in primary hematopoietic

stem/progenitor (ie, CD34⁺) cells isolated from human cord blood (using short hairpin RNAs) and observed an enhanced commitment to and acceleration of erythroid differentiation. Consistent with this effect, overexpression of *L3MBTL1* in primary hematopoietic CD34⁺ cells as well as in 20q– cell lines restricted erythroid differentiation. Furthermore, *L3MBTL1* levels decrease during hemin-induced erythroid differentiation or erythropoietin exposure, suggesting a specific role for *L3MBTL1* down-regulation in enforcing

cell fate decisions toward the erythroid lineage. Indeed, *L3MBTL1* knockdown enhanced the sensitivity of hematopoietic stem/progenitor cells to erythropoietin (Epo), with increased Epo-induced phosphorylation of STAT5, AKT, and MAPK as well as detectable phosphorylation in the absence of Epo. Our data suggest that haploinsufficiency of *L3MBTL1* contributes to some (20q–) myeloproliferative neoplasms, especially polycythemia vera, by promoting erythroid differentiation. (*Blood*. 2010;116(15):2812-2821)

Introduction

Deletion of the long arm of chromosome 20 (20q–) represents the second most common primary chromosomal abnormality in the hematologic malignancies, after the Philadelphia chromosome.¹ The 20q– abnormality is observed in 10% of patients with myeloproliferative neoplasms (MPNs), most commonly polycythemia vera (PV),² in 4% of patients with myelodysplastic syndrome,³ and in 1% to 2% of patients with acute myeloid leukemia.⁴ Inactivation (or haploinsufficiency) of putative tumor suppressors on 20q has been proposed to explain the pathogenesis of these disorders.

We have been studying *L3MBTL1*, the human homolog of the *Drosophila* tumor suppressor gene, lethal(3)malignant brain tumor,⁵ whose inactivation results in overgrowth of adult optic neuroblasts and ganglion mother cells of the larval brain.⁶ We demonstrated that human *L3MBTL1* functions as a transcriptional repressor,⁷ and after crystallizing the MBT repeat domain,⁸ determined that *L3MBTL1* compacts chromatin by binding monomethylated and dimethylated lysine residues in histones H1 (H1K26) and H4 (H4K20).^{9,10} Two mutational analyses of small numbers of 20q– patient samples found no mutation in the nondeleted allele of *L3MBTL1*,^{11,12} suggesting that haploinsufficiency of *L3MBTL1* would have to contribute to these disorders.

Despite the known role of *L3MBTL1* in affecting chromatin structure, the function of *L3MBTL1* in hematopoiesis is largely unknown. To define the role of *L3MBTL1* in normal human hematopoiesis and its potential role in the 20q– myeloid disorders,

we used RNA interference to reduce *L3MBTL1* expression in human cord blood (CB) CD34⁺ hematopoietic stem/progenitor cells (HSPCs). We found that *L3MBTL1* knockdown accelerated erythroid differentiation and increased signaling in response to erythropoietin (Epo), as well as low-level activation of the JAK-STAT, MAP kinase, and AKT signaling pathways in the absence of Epo. Similarly, we were able to impair erythroid differentiation by overexpressing *L3MBTL1* in primary hematopoietic CD34⁺ cells and in 20q– cell lines. Thus, *L3MBTL1* regulates human erythropoiesis, and lack of *L3MBTL1* could contribute to the pathogenesis of 20q– disorders, in particular PV.

Methods

Purification and in vitro primary culture of human CB CD34⁺ cells

Mononuclear cells were isolated from CB (obtained from the New York Blood Center on a contractual basis) by Ficoll-Hypaque Plus density centrifugation. CD34⁺ HSPCs were purified by positive selection using the Midi-magnetic-activated cell sorting LS⁺ separation columns and isolation kit (Miltenyi). CD34⁺ cells were cultured in Iscove modified Dulbecco medium (IMDM, Cellgro) containing 20% BIT 9500 medium (Stem Cell Technologies) supplemented with stem cell factor (SCF; 100 ng/mL), Fms-like tyrosine kinase 3 (FLT-3; 10 ng/mL), interleukin-6 (IL-6; 20 ng/mL), and thrombopoietin (TPO; 100 ng/mL; these cytokines were purchased from PeproTech).

Submitted February 16, 2010; accepted June 13, 2010. Prepublished online as *Blood* First Edition paper, June 28, 2010; DOI 10.1182/blood-2010-02-270611.

*F.P. and N.G. contributed equally to this study.

The online version of this article contains a data supplement.

The publication costs of this article were defrayed in part by page charge payment. Therefore, and solely to indicate this fact, this article is hereby marked "advertisement" in accordance with 18 USC section 1734.

© 2010 by The American Society of Hematology

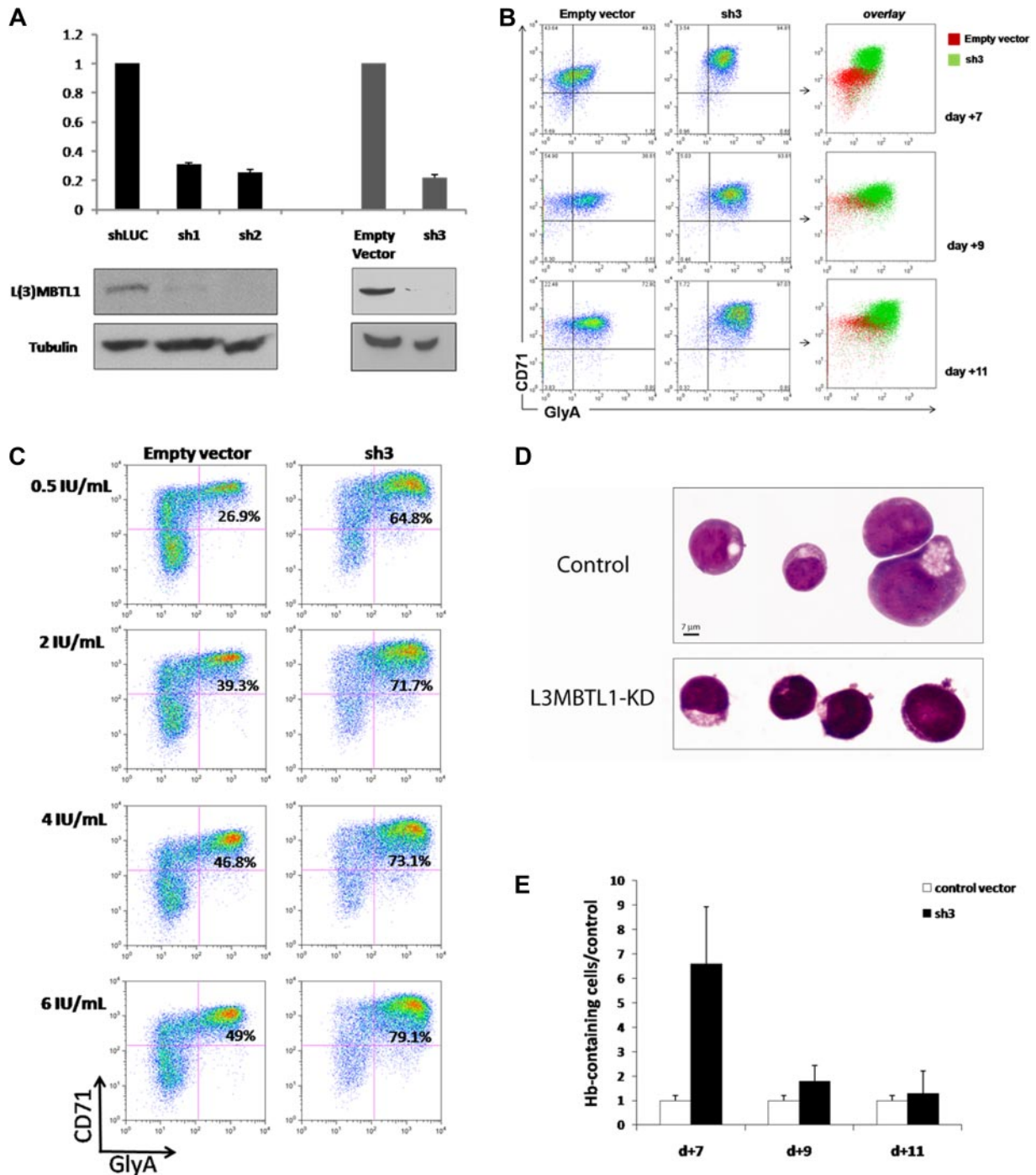


Figure 1. Knockdown of *L3MBTL1* promotes the erythroid differentiation of human hematopoietic CD34⁺ progenitor cells. (A) Lentiviral constructs expressing shRNAs targeting luciferase (control) or *L3MBTL1* (sh1 and sh2) led to efficient knockdown in primary CB CD34⁺ cells, as assessed by Western blot and quantitative RT-PCR. shRNAs of a different backbone (empty vector and sh3) also yielded efficient knockdown of *L3MBTL1*. All the presented data were confirmed using both sets of constructs. (B) Expression of CD71 and GlyA on human HSPCs, as assayed by flow cytometric analysis at days 7, 9, and 11 of Epo-induced culture. (C) Expression of CD71 and GlyA on human HSPCs, cultured with different concentrations of Epo, as assayed by flow cytometric analysis at 7 days. (D) Cells from panel B were stained with May-Grunwald-Giemsa on day 7 of Epo-induced culture, and their morphology was captured by light microscopy. (E) Epo-exposed cells at days 7, 9, and 11 of Epo-induced culture were resuspended in benzidine solution, and cells that stained dark blue-green were scored as positive.

Generation of lentiviruses and infection of primary hematopoietic CD34⁺ cells

Lentiviral vectors were produced by transfection of 293T cells, according to standard protocols.¹³ After 24 hours of growth, CD34⁺ cells were infected with high-titer lentiviral concentrated suspensions, in the presence of 8 μg/mL polybrene (Sigma-Aldrich). Sequences targeted by

short hairpin RNAs (shRNAs) were: GGAAAGACGATGACGGAAA (shLUC), GTAGTGAGTTGTAGATAAAA (sh1), GGTCAGTCATAGTGAGAGAA (sh2), and GCCTGCACTTTGATGGGTATT (sh3). shRNAs were cloned into the H1p HygroEGFP¹⁴ (shLUC, sh1, and sh2) or LKO vectors (empty vector and sh3). The luciferase-directed shRNA, cloned into the H1 vector, was used as control.¹⁵ A detailed description of the

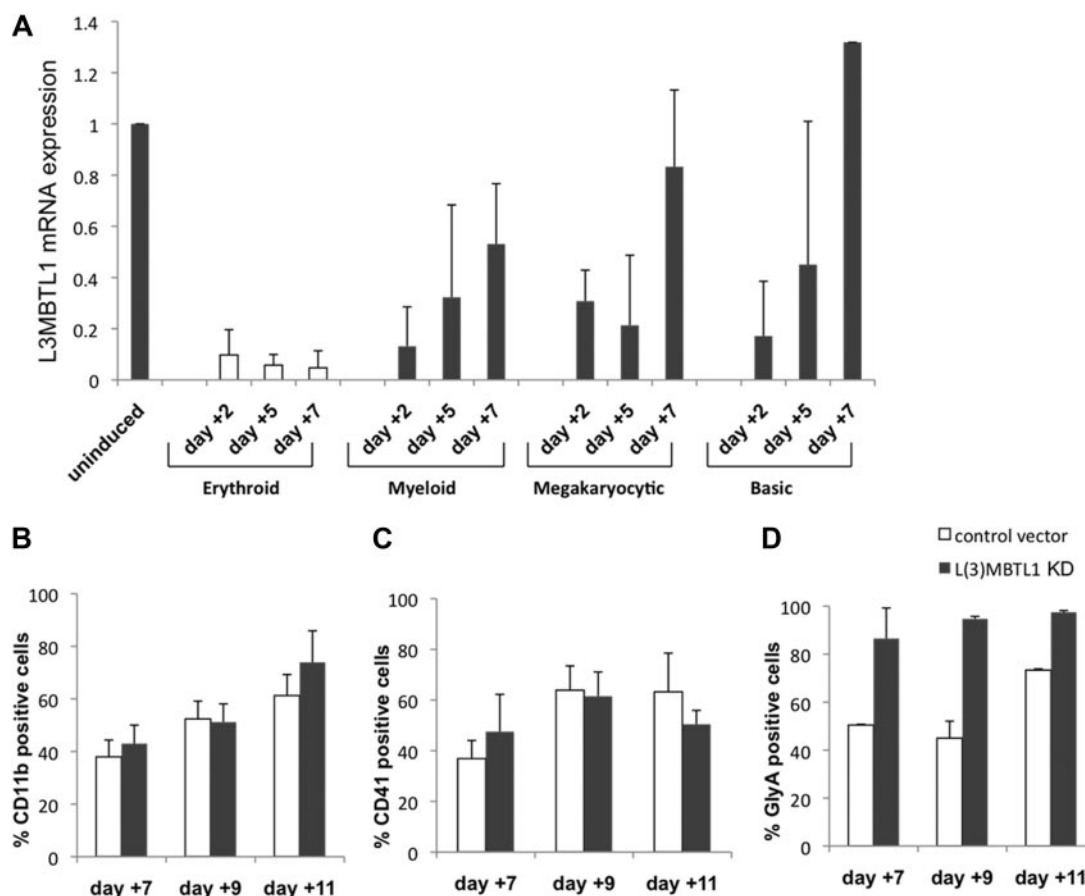


Figure 2. *L3MBTL1* knockdown specifically promotes erythroid, but not myeloid or megakaryocytic, differentiation of human CD34⁺ cells. (A) *L3MBTL1* expression levels were assessed by quantitative RT-PCR in normal CD34⁺ CB cells. The cells were placed in different culture conditions stimulating erythroid, myeloid, and megakaryocytic differentiation for 2, 5, and 7 days. Total RNA was extracted from 2×10^5 cells. (B) Seventy-two hours after lentiviral infection, GFP⁺CD34⁺ cells were cultured in myeloid conditions for 7, 9, and 11 days, and the expression of myeloid-specific markers CD11b (CD14 and CD33 not shown) was assessed by flow cytometric analysis ($n = 3$). (C) Seventy-two hours after lentiviral vector infection, the GFP⁺CD34⁺ cells were cultured in megakaryocytic conditions for 7, 9, and 11 days, and expression of the megakaryocytic-specific marker CD41 was assessed by flow cytometric analysis ($n = 3$). (D) GFP⁺CD34⁺ cells, 72 hours after lentiviral vector infection, were cultured in erythroid conditions for 7, 9, and 11 days, and expression of the erythroid-specific marker GlyA was assessed by flow cytometric analysis ($n = 3$).

constructs is provided in supplemental Figure 1 (available on the *Blood* Web site; see the Supplemental Materials link at the top of the online article).

Flow cytometry

Transduced CB CD34⁺ cells were sorted for green fluorescence (GFP) and CD34 expression after staining with an allophycocyanin (APC)-conjugated anti-CD34 antibody (BD Biosciences PharMingen), using a fluorescence-activated cell sorting (FACS) Vantage cell sorter. Transduced K562 cells, cultured in RPMI medium supplemented with 10% fetal bovine serum, were sorted for GFP 72 hours after the infection. Cells were harvested for flow cytometry on days 7, 9, and 11 in cytokine-driven liquid culture. Cells were stained with the following antibodies: CD34-APC (BD Biosciences PharMingen), CD11b-phycoerythrin (PE; Immunotech), CD14-PE (Immunotech), CD71-APC (BD Biosciences PharMingen), glycophorin A-PE (Invitrogen), and CD41-PE (Immunotech) and analyzed by FACS. Analysis of progenitor cell populations was performed by staining cells with the following antibodies: CD3-PECy5, CD4-PECy5, CD7-PECy5, CD8-PECy5, CD10-PECy5, CD19-PECy5, CD20-PECy5, CD2-PECy5, CD11b-PECy5, CD56-PECy5, GPA-PECy5, CD45RA-FITC, CD38-PECy7, CD34-APC, and IL-3 α -PE (BioLegend) and CD45RA-V450 (BD Biosciences PharMingen). The characterization of specific progenitor cell subsets (common myeloid progenitor [CMP], granulocyte-monocyte progenitor [GMP], and megakaryocyte-erythrocyte progenitor [MEP]) was

performed by FACS analysis according to the methods described by Park et al.¹⁶

Cytokine-driven liquid culture conditions and isolation of MPN samples

CD34⁺ cells were cultured in 20% BIT in IMDM, with different cytokines to support erythroid, myeloid, or megakaryocytic cell differentiation. The erythroid cultures contained Epo (6 IU/mL) and SCF (100 ng/mL); the myeloid cultures SCF (100 ng/mL), FLT-3 (10 ng/mL), IL-3 (20 ng/mL), IL-6 (20 ng/mL), granulocyte-macrophage colony-stimulating factor (GM-CSF; 20 ng/mL), and granulocyte colony-stimulating factor (G-CSF; 20 ng/mL); the megakaryocytic cultures SCF (100 ng/mL), TPO (100 ng/mL), and IL-11 (50 ng/mL); and the basic cultures SCF (100 ng/mL), FLT-3 (10 ng/mL), IL-6 (20 ng/mL), and TPO (100 ng/mL). Epo and G-CSF were purchased from Amgen, and the other cytokines were purchased from PeproTech.

CD34⁺ cells were isolated from PV patient phlebotomy samples or essential thrombocythemia/myelofibrosis patient peripheral blood samples (obtained on an Memorial Sloan-Kettering Cancer Center Institutional Review Board-approved protocol) and cultured in serum-free stem cell expansion media supplemented with SCF (100 ng/mL), IL-3 (20 ng/mL), IL-6 (10 ng/mL), and Epo (0.5 IU/mL) every other day. Cells were harvested at day 7 or day 9 for Western blot assays. The cells were more than 70% CD71/Glycophorin A (GlyA) double-positive at these times of collection.

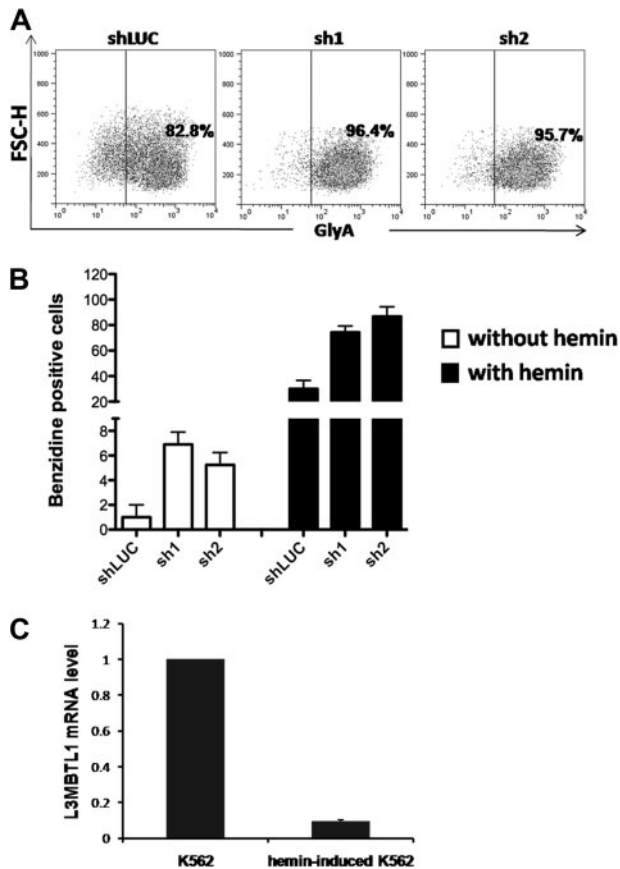


Figure 3. Knockdown of *L3MBTL1* induces further erythroid differentiation of K562 erythroleukemia cells. (A) K562 cells, grown in RPMI medium supplemented with 10% fetal bovine serum, without exogenous cytokines or hemin, were infected with lentiviral constructs targeting luciferase (shLUC) or *L3MBTL1* (sh1 and sh2). GFP⁺ cells, sorted by FACS at 72 hours after infection, were analyzed for GlyA expression by flow cytometry. (B) GFP⁺ K562 cells, before and after exposure to hemin (50 μ M) for 4 days, were stained with benzidine to assess their Hb content. (C) K562 cells were treated with 50 μ M hemin for 4 days and the *L3MBTL1* mRNA level assessed in the hemin-exposed versus the nontreated cells by quantitative RT-PCR (n = 3).

Cytospin preparations, Giemsa staining, and benzidine staining

A total of 2×10^5 cells were centrifuged into slides for 5 minutes at 33g and air dried. Cells were stained with May-Grunwald-Giemsa stains and observed under light microscope for morphologic analysis. Benzidine staining was performed as described previously.¹⁷

RNA extraction and quantitative real-time RT-PCR

For quantitative reverse-transcription polymerase chain reaction (RT-PCR), total RNA was isolated from 2×10^5 cells using the RNeasy mini kit (QIAGEN), and then subjected to reverse transcription with random hexamers (SuperScript III kit; Invitrogen). Real-time PCR reactions were performed using an ABI 7500 sequence detection system. A list of PCR primers is available on request.

Methylcellulose colony and LTC-IC assays

CFU assays. A total of 1×10^4 GFP⁺ CD34⁺ transduced cells were plated (in duplicate) in methylcellulose with Epo (5 IU/mL), SCF (50 ng/mL), IL-3 (20 ng/mL), IL-6 (20 ng/mL), G-CSF (20 ng/mL), and GM-CSF (20 ng/mL). Burst-forming units–erythroid (BFU-E), granulocyte-macrophage colony-forming units (CFU-GM), and CFU-granulocyte erythrocyte macrophage megakaryocyte colonies (GEMM) were scored 14 days after seeding. For the long-term culture–initiating cell (LTC-IC) assays, 4×10^5

GFP⁺CD34⁺ cells were grown on MS-5 stromal cells in IMDM, supplemented with 12.5% horse serum, 12.5% fetal bovine serum, 4mM L-glutamine, 100 U/mL penicillin, 100 μ g/mL streptomycin, and 1 μ M hydrocortisone. Medium was half-replenished every week, and cobblestone areas were scored at week 5. At week 5, cells were harvested and plated in methylcellulose medium with cytokines, as described for the CFU assay.

The images were captured by the Leica MZFL3 Stereoscope with a 0.5 \times plan objective. The camera used was a QImaging RetigaEx and Velocity Software 4.3.0 was used to acquire the images digitally.

Antibodies

The following antibodies were used for Western blot assays: the affinity-purified anti-L3MBTL1 antibody,⁷ pSTAT5 (Cell Signaling), STAT5 (Cell Signaling), pMAPK1/2 (Cell Signaling), MAPK (Cell Signaling), pAKT (Cell Signaling), AKT (Cell Signaling), pFOXO1/3 (Cell Signaling), JNK (Santa Cruz Biotechnology), JAK2 (Cell Signaling), p16 (Santa Cruz Biotechnology), and Raf-1 (Santa Cruz Biotechnology).

Ras activation assay

Ras-GTP was precipitated from total cell lysates using the Ras activation assay kit, purchased from Millipore, according to the manufacturer's instructions.

Overexpression assays

Retroviral vectors were produced by transfection of Phoenix A cells with the MIGR1 control or MIGR1 full-length *L3MBTL1*-HA c-DNA plasmids,⁹ according to standard protocols.¹³ CMK, U937, HEL, and K562 cells were grown in RPMI medium supplemented with 10% fetal bovine serum and infected with high-titer retroviral suspensions in the presence of 8 μ g/mL polybrene (Sigma-Aldrich). Seventy-two hours after infection, the GFP-positive cells were sorted by FACS.

Results

Knockdown of *L3MBTL1* accelerates erythroid differentiation of human hematopoietic CD34⁺ progenitor cells

To investigate the function of *L3MBTL1* in human hematopoiesis, we knocked down *L3MBTL1* in CD34⁺ human CB cells, using lentiviruses expressing shRNAs targeting *L3MBTL1*, and 72 hours after infection documented the efficient knockdown of *L3MBTL1* mRNA and protein in the sorted GFP⁺ CD34⁺ cells by quantitative RT-PCR and Western blot, for several different shRNA constructs (Figure 1A). These cells were then placed in Epo-driven liquid culture (6 IU/mL), and the expression of CD71 and GlyA was monitored by flow cytometry at different time points. The generation of mature erythroid precursor cells (CD71/GlyA double-positive cells) was consistently faster and more efficient for the *L3MBTL1*-KD cells, compared with the control vector-infected cells (Figure 1B; supplemental Figure 2). Furthermore, although CD71/GlyA double-negative cells were prominently found among the control cells, there were no CD71/GlyA double-negative cells after *L3MBTL1*-KD. These observations were consistently seen using several different shRNA constructs targeting *L3MBTL1*, demonstrating enhanced erythroid differentiation after *L3MBTL1* depletion.

To evaluate the sensitivity of *L3MBTL1*-KD cells to Epo, we measured GlyA and CD71 expression by FACS analysis in the *L3MBTL1*-KD HSPCs after plating these cells in culture with SCF (100 ng/mL) and different doses of Epo (0.5, 2, 4, and 6 U/mL). At the lowest concentration of Epo (0.5 IU/mL), and at all tested

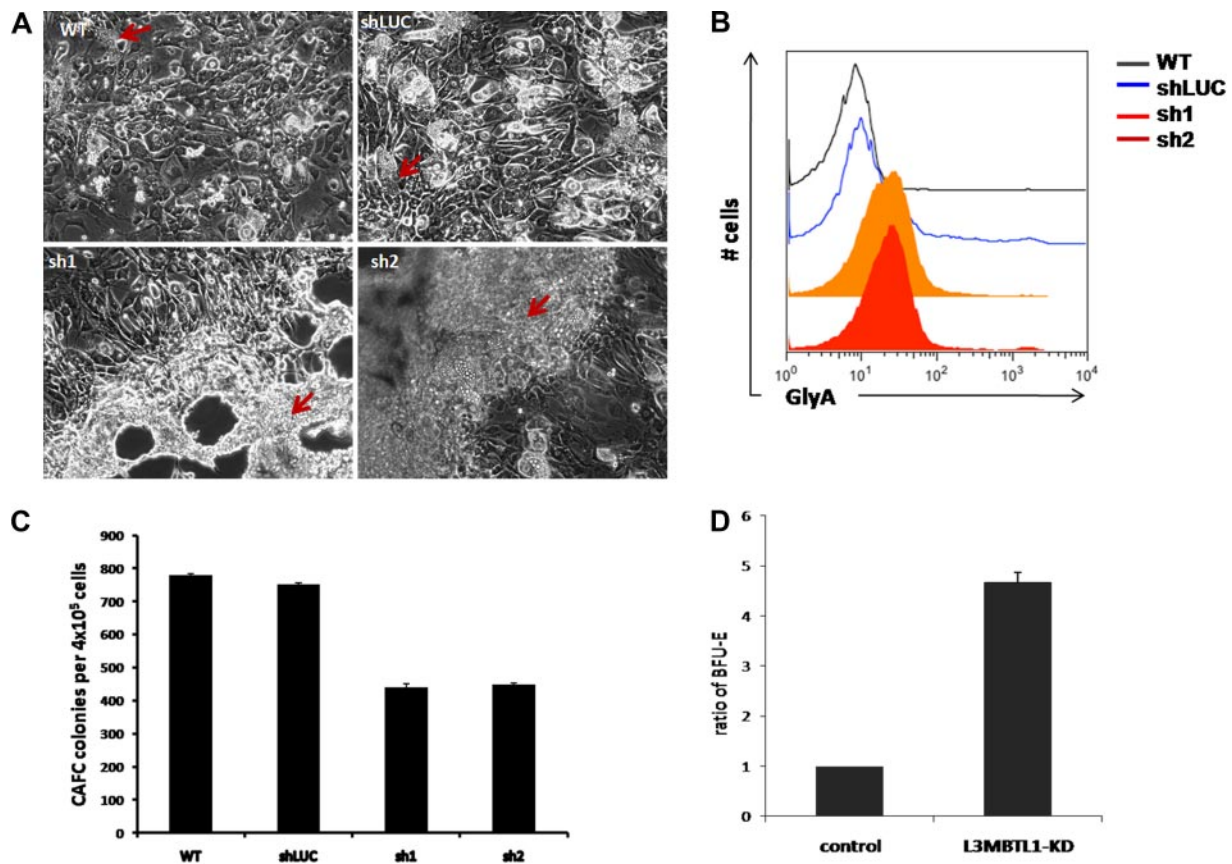


Figure 4. L3MBTL1-KD leads to expansion of erythroid progenitors in long-term culture. (A) Sorted 4×10^5 GFP⁺ CD34⁺ were plated on MS5 stromal cell layer and cultured for 5 weeks. At week 5, the colonies were examined using an inverted optical microscope. The red arrows indicate the cobblestone area forming cells in the wt and shLUC figures. The red arrows indicate the overgrowth of progenitor cells (predominantly erythroid) in the sh1 and sh2 photographs. (B) The expression of GlyA on floating cells from 5-week LTC-IC cultures was evaluated by flow cytometry. (C) CAFC colony numbers were evaluated at week 5 of MS-5 stromal cell-based culture ($n = 2$). (D) Week 5 LTC-IC cells were plated on methylcellulose, and the secondary BFU-E colonies were scored after 10 days. The ratio of BFU-E colonies is shown, based on BFU-E numbers in the control cells.

concentrations of Epo, the L3MBTL1-KD cells showed accelerated erythroid maturation compared with control cells (2.4-, 1.8-, 1.6-, and 1.6-fold, respectively; Figure 1C).

Consistent with the immunophenotypic evidence, these cells also showed morphologic evidence of erythroid differentiation after L3MBTL1-KD. As erythroid differentiation proceeds, erythroblasts display a gradual decrease in cell size, increase in chromatin condensation, and increase in hemoglobin (Hb) concentration,¹⁸ and indeed, the L3MBTL1-KD cells appeared smaller with more condensed chromatin than the control cells (which displayed a larger, more homogeneous, and eccentrically placed nucleus, as seen in Figure 1D). Likewise, benzidine staining revealed a 6.6-fold enrichment of Hb-containing cells compared with controls at day 7 of culture, consistent with the time of highest immunophenotypic difference, with a 1.7-fold and 1.3-fold enrichment at days 9 and 11 of culture (Figure 1E). These results further indicate a role for L3MBTL1 in regulating the erythroid differentiation of human HSPCs.

L3MBTL1 expression decreases during normal erythroid differentiation of human HSPCs

To investigate whether changes in *L3MBTL1* expression are only seen during erythroid differentiation, we cultured normal CB CD34⁺ cells in various cytokine cocktails that preferentially support erythroid, myeloid, or megakaryocytic differentiation and evaluated *L3MBTL1* expression (by quantitative RT-PCR) at differ-

ent time points. *L3MBTL1* is down-regulated on differentiation generally, but especially in cells exposed to the erythroid-promoting cytokines SCF plus Epo (Figure 2A). These cells maintain a low-level *L3MBTL1* expression over time, whereas the cells grown under other culture conditions show a rebound in *L3MBTL1* expression by day 7.

Given the increased erythroid differentiation after L3MBTL1-KD, we also assessed whether L3MBTL1-KD altered myeloid and/or megakaryocytic differentiation. L3MBTL1-KD and control GFP⁺ CD34⁺ cells grown in G-CSF-driven liquid culture showed similar expression of myeloid-specific cell surface markers (CD11b, CD14, or CD33, Figure 2B; and data not shown). Similarly, we observed no effect on the expression of the megakaryocyte marker CD41 in TPO-driven cultures (Figure 2C), demonstrating that L3MBTL1 depletion specifically affects erythroid differentiation (Figure 2D).

To investigate whether known regulators of erythropoiesis were up-regulated after L3MBTL1-KD, we quantified the level of Epo-receptor, GATA-1, FOG-1, NF-E2, LMO2, and FKLf mRNA expression in L3MBTL1-KD CD34⁺ cells plated in Epo-induced liquid cultures and found an “erythroid signature,” as shown in supplemental Figure 3. However, none of these genes was up-regulated in the L3MBTL1-KD CD34⁺ cells, 72 hours after viral infection, before they were plated in cytokine-induced culture conditions, even though we did find down-regulation of PU.1, RUNX1, and CEBP α mRNA (data not shown), genes known to be

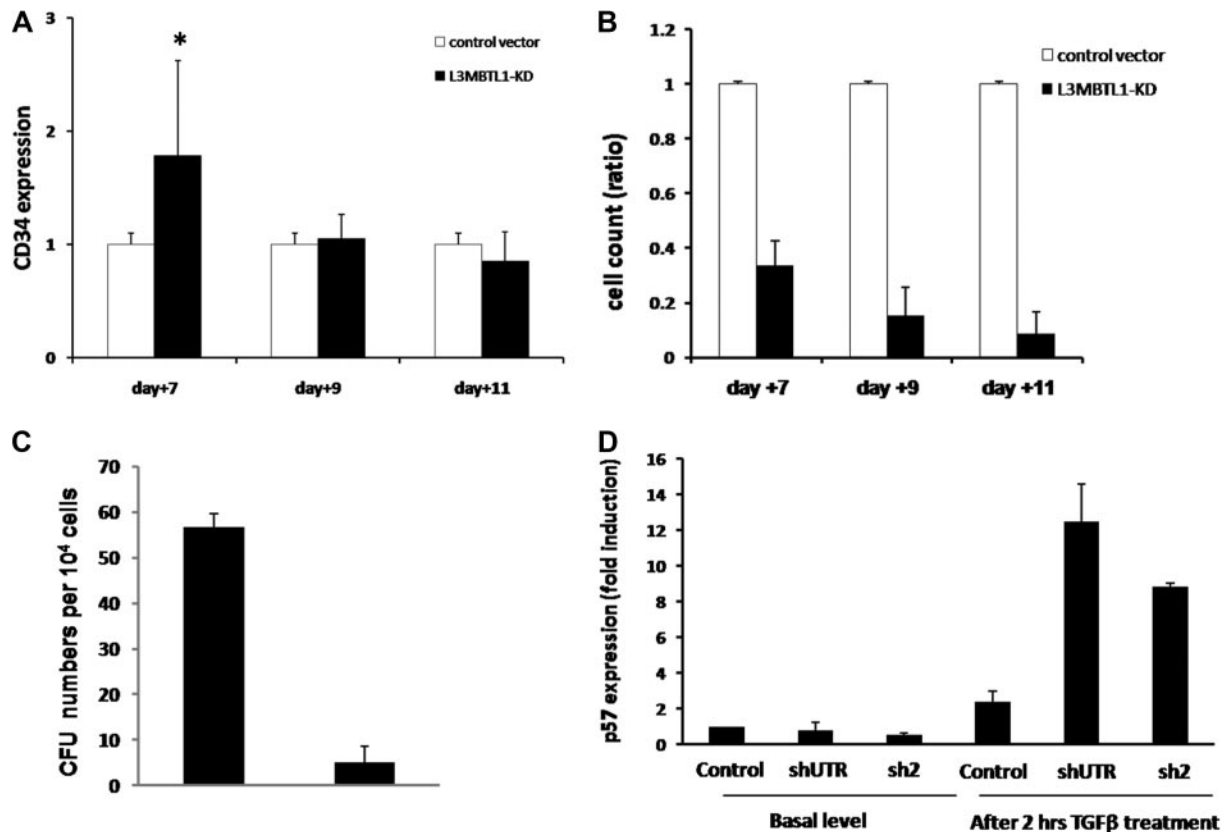


Figure 5. Proliferation potential of L3MBTL1-KD human hematopoietic progenitor cells. (A) The maintenance of CD34 expression was evaluated in L3MBTL1-KD CB cells by flow cytometry. GFP⁺CD34⁺ CB cells were cultured with SCF, FLT-3, IL-6, and TPO. * $P < .005$. (B) Cell counts of L3MBTL1-KD CB cells were monitored at different time points in liquid culture with SCF, FLT-3, IL-6, and TPO. (C) Seventy-two hours after lentiviral infection, sorted GFP⁺CD34⁺ HPCs were placed in CFU assays and the number of CFUs quantified. (D) p57 mRNA expression was assessed by quantitative RT-PCR in L3MBTL1-KD HPCs, with and without exposure to 200pM TGF- β 1 for 2 hours ($n = 2$).

down-regulated during erythropoiesis. Thus, we cannot attribute the pro-erythroid effects of L3MBTL1-KD to changes in any of these “erythroid-associated genes,” at this time.

Knockdown of *L3MBTL1* induces leukemia cell differentiation toward the erythroid lineage

To determine whether L3MBTL1-KD can also affect the differentiation of leukemia cells, we used lentiviral vectors to express shRNA-targeting luciferase (shLUC) or *L3MBTL1* (sh1 and sh2) in K562 cells. We sorted GFP⁺ cells (by FACS) 72 hours after infection and as seen in CB cells, KD of *L3MBTL1* in K562 cells increased GlyA expression, compared with control cells (Figure 3A; supplemental Figure 4), and led to higher benzidine staining before and after hemin exposure (Figure 3B). As hemin is known to trigger the erythroid differentiation of K562 cells¹⁷ and activate globin gene expression,¹⁹ we studied *L3MBTL1* expression in K562 erythroleukemia cells after hemin exposure. Four days of hemin exposure (at 50 μ M) markedly decreased the level of *L3MBTL1* mRNA (Figure 3C) commensurate with an increase in benzidine-positive cells and increased globin gene expression (data not shown). Thus, L3MBTL1 loss can induce erythroid differentiation in leukemia cells as well as in normal human HSPCs.

Loss of *L3MBTL1* leads to expansion of erythroid progenitors in long-term cultures

To elucidate the role of L3MBTL1 in the earliest stem/progenitor cells, we performed LTC-IC assays, culturing 4×10^5 GFP⁺

CD34⁺ transduced cells on MS5 stromal cells. We observed an impressive expansion of progenitor cells from the L3MBTL1-KD cells at week 5. The L3MBTL1-KD cells grew mostly on top of the MS5 layer, in sheets of cells rather than cobblestones, whereas the control cells formed normal cobblestones that grew underneath the stromal layer (Figure 4A). To define the nature of these cells, we used flow cytometry to define their lineage-specific cell surface marker profile. The L3MBTL1-KD showed strikingly higher GlyA expression compared with control cells, suggesting that these cells are erythroid progenitors (Figure 4B). Furthermore, when the week 5 culture of the LTC-IC assay cells was plated in methylcellulose, we observed a greater number of BFU-E among the KD cells than the control cells (Figure 4D). Nonetheless, KD of *L3MBTL1* did decrease stem cell frequency in both limiting dilution and bulk CAFC assays (Figure 4C).

These findings suggest that L3MBTL1 knockdown may not only promote the premature differentiation of erythroid committed cells but may also recruit more progenitor cells to differentiate toward the erythroid lineage. Indeed, when we sorted the L3MBTL1-KD cells into the CMP (CD34⁺CD38⁺IL3R α ⁺CD45R α ⁻Lin⁻), MEP (CD34⁺CD38⁺IL3R α ⁻CD45R α ⁻Lin⁻), and GMP (CD34⁺CD38⁺IL3R α ⁺CD45R α ⁺Lin⁻) progenitor cell subsets, we found a modest increase of the MEP and GMP populations, at the expense of the CMP cells (supplemental Figure 5). This implies that loss of L3MBTL1 in progenitor cells can also drive them to differentiate. To further address this issue, we evaluated the ability of L3MBTL1-KD HSPCs to maintain CD34 expression over time. Whereas CD34 expression was initially higher in the KD cells, by day 11 we found no difference in CD34 expression

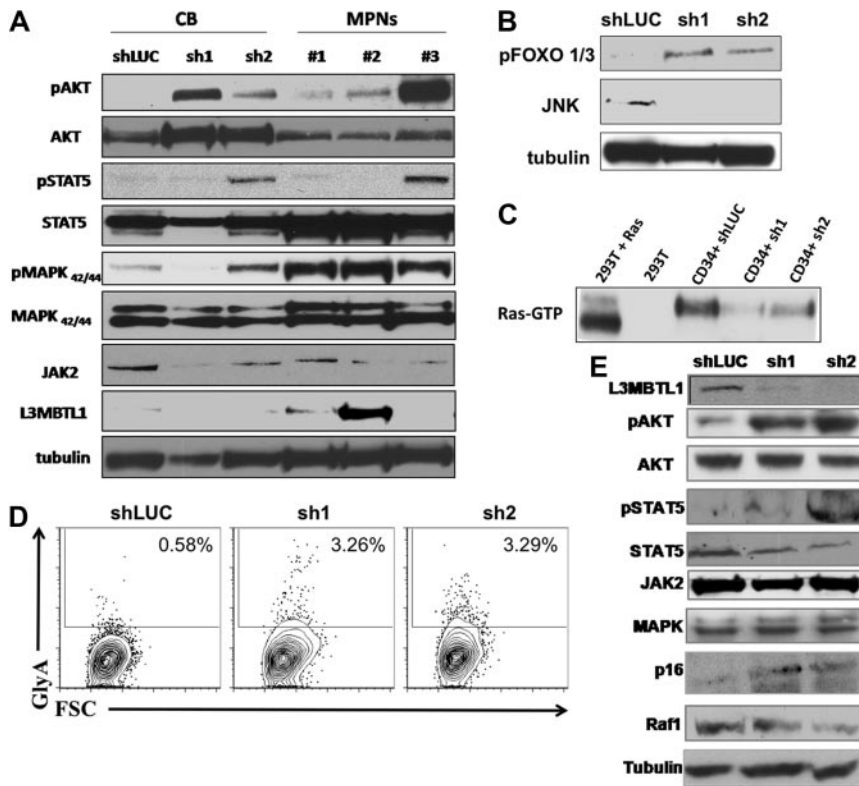


Figure 6. Primary hematopoietic cells lacking L3MBTL1 show Epo-independent phosphorylation of STAT5, AKT, and MAP kinase. (A) Primary GFP⁺ CD34⁺ cells were harvested after one week in erythroid culture and lysed, according to standard protocols. Cultured CD34⁺ cells from MPN patients bearing the *JAK2V617F* mutation were harvested after 1 week of culture in Epo. Phosphorylation of STAT5, AKT, and MAPK was assessed by Western blot. The protein levels of JAK2, STAT5, AKT, MAPK, and L3MBTL1 were also assessed. (B) Primary GFP⁺ CD34⁺ cells were harvested after one week in erythroid culture and FOXO phosphorylation, and JNK expression levels were assessed by Western blot assay. Tubulin serves as a loading control for panels A, B, and E. (C) A total of 2×10^7 GFP⁺ CD34⁺ cells, plated in erythroid culture conditions, were tested for Ras activation, by detection of GTP-bound Ras. Cells were lysed and incubated with (GST)-Raf-RBD fusion protein coupled to glutathione agarose beads. GTP-bound Ras was detected by Western blotting using an isoform-specific antibody. (D) Expression of the erythroid markers CD71 and GlyA was evaluated on L3MBTL1-KD CB cells cultured without Epo, in SCF, FLT-3, IL-6, and TPO. (E) After 1 week in culture without Epo, the GFP⁺ CD34⁺ cells were lysed, and phosphorylation of STAT5 and AKT was assessed by Western blot analysis. The protein levels of JAK2, STAT5, AKT, MAPK, Raf-1, p16, and L3MBTL1 were also assessed.

between the KD and the control cells (Figure 5A). Given these findings, we evaluated whether the commitment toward the erythroid lineage that follows L3MBTL1 down-modulation impairs the proliferative potential of HSPCs. Cell counts at each time point (days 7, 9, and 11) revealed slower growth of KD-HSPCs compared with control cells in liquid cultures with SCF, IL-3, TPO, and FLT-3 (Figure 5B), or Epo, G-CSF, and TPO (data not shown). We also evaluated the clonogenic ability of sorted CD34⁺ L3MBTL1-KD HSPCs in CFU assays and found decreased progenitor frequency compared with controls; all types of colonies were less frequent (Figure 5C).

As the cell's proliferative potential appears to be slightly decreased after L3MBTL1-KD, we tested the sensitivity of HSPCs to transforming growth factor- β (TGF- β). We treated CD34⁺ cells with 200pM TGF- β , which induces the expression of p57²⁰; we observed a greater induction of p57 mRNA in L3MBTL1-KD cells at 2 hours compared with control cells (Figure 5D); no change in p57 expression was observed in the KD cells in the absence of TGF- β .

L3MBTL1-KD alters the Epo-dependent and Epo-independent phosphorylation of STAT5, AKT, and MAP kinase

To investigate the effect of L3MBTL1-KD on intracellular signaling pathways, we prepared lysates from CD34⁺ L3MBTL1-KD cells cultured in Epo for 1 week and performed Western blot analyses. We found increased signaling downstream of the Epo receptor, with consistently greater phosphorylation of AKT, FOXO 1/3, and MAPK and variably increased phosphorylation of JAK2 and STAT5, compared with controls (Figure 6A-B). RAS-GTP and Raf-1 protein levels were decreased in the L3MBTL1-KD cells, consistent with the enhanced erythroid maturation (Figure 6C,E). Overall, this pattern of activation mirrors the activation of signaling pathways seen in similarly cultured CD34⁺ HSPCs isolated from JAK2V617F⁺ MPN patients (Figure 6A).

To determine whether knockdown of L3MBTL1 can contribute to the Epo-independent erythroid cell growth found in MPN patients, we placed sorted CD34⁺ L3MBTL1-KD cells in Epo-free culture media supplemented with SCF, IL-6, FLT-3, and TPO for 1 week and found a small GlyA-positive (ie, erythroid progenitor) cell population in the L3MBTL1-KD cells (Figure 6D). Despite the absence of Epo, phosphorylation of STAT5 and AKT was clearly seen (Figure 6E). Moreover, L3MBTL1-KD cells also displayed increased p16^{INK4a} expression (Figure 6E), a protein associated with the induction of erythropoiesis in primary PV samples.^{21,22}

To assess whether decreased *L3MBTL1* expression could be implicated in the pathogenesis of non-20q- MPNs, we evaluated the expression of *L3MBTL1* in granulocytes obtained from 75 MPN patients, 28 patients with PV, and 47 patients with ET (who did not show loss of 20q) and compared it with the level of expression in granulocytes obtained from 10 normal donors using Affymetrix HGU133a.2 arrays. We observed a more than or equal to 20% decrease in the expression of *L3MBTL1* in 43% of the PV samples (12 of 28) and 62% of the essential thrombocythemia samples (29 of 47) compared with the normal controls ($P < .001$ and $P < .001$, respectively; data not shown). This suggests that down-regulation of L3MBTL1 may also play a role in non-20q- myeloproliferative neoplasms.

L3MBTL1 restricts erythroid differentiation

To address the function of L3MBTL1 in 20q- disorders and to explore the mechanism by which L3MBTL1 affects erythroid differentiation, we overexpressed the full-length L3MBTL1-HA c-DNA in 3 human 20q- hematopoietic cell lines (ie, HEL, CMK, and U937 cells) and in K562 cells. We sorted the GFP⁺ cells and evaluated GlyA expression by FACS analysis: L3MBTL1-HA expressing cells showed decreased expression of glycoprotein A

Figure 7. L3MBTL1 restricts erythroid differentiation.

(A) GlyA expression was assessed by FACS in the L3MBTL1-HA expressing CMK, U937, HEL, and K562 cells compared with the MIGR1 (empty vector) transduced cells. (B) p16 protein expression levels were determined by Western blot analysis in L3MBTL1-HA HEL cells versus the MIGR1 (empty vector) control HEL cells. JNK and L3MBTL1 levels are also shown. Tubulin served as the loading control. (C) GlyA expression in L3MBTL1-HA expressing CD34⁺ cells after 3 days of culture with SCF 100 ng/mL and Epo 6 IU/mL, compared with the MIGR1 (empty vector) transduced cells. (D) L3MBTL1 mRNA expression levels in retrovirally infected CD34⁺ cells, quantified by quantitative PCR (n = 3).

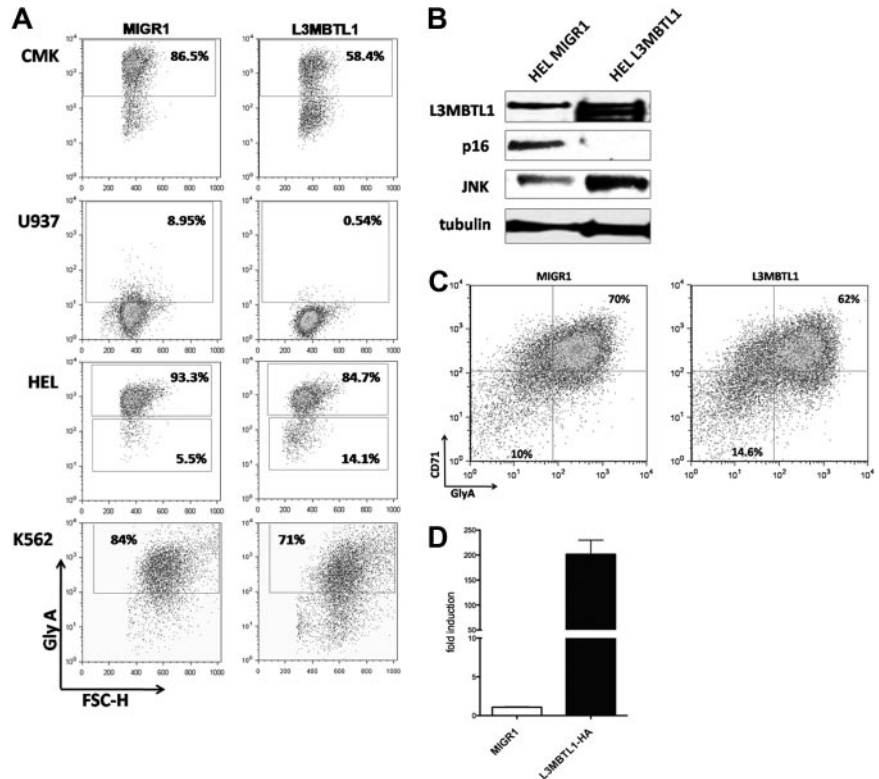


(Figure 7A), suggesting that L3MBTL1 restricts erythroid differentiation. The decreased GlyA expression was seen in CMK (58% vs 86%) and U937 cells (0.5% vs 9%), as well as in HEL (85% vs 93%) and K562 cells (71% vs 84%).

We also overexpressed L3MBTL1 in primary human CD34⁺ cells, obtaining an almost 200-fold increase in L3MBTL1 expression, as documented by quantitative RT-PCR (Figure 7D). We placed the sorted GFP⁺ CD34⁺ cells in Epo-induced liquid culture and consistently found a decreased percentage of CD71⁺/GlyA⁺ cells (62% vs 70%) after 3 days of culture (Figure 7C). The milder decrease in GlyA expression seen in primary human CD34⁺ cells, compared with the 20q⁻ cells, may reflect the normal genetic background of the transduced cells and their intrinsic growth rates. Overexpression of L3MBTL1 in HEL cells did decrease the expression of p16^{INK4} (Figure 7B), further suggesting that L3MBTL1 may affect erythropoiesis by regulating (ie, repressing) p16 expression. Further studies are needed to address this issue.

Discussion

Haploinsufficiency of the polycomb group (PcG) gene *L3MBTL1* has been identified in patients with 20q⁻-associated myeloid malignancies,^{11,12} but whether this has functional relevance for these disorders has not been previously determined. We have demonstrated that L3MBTL1 loss induces the erythroid differentiation of human HSPCs and therefore could contribute to the most common 20q⁻-associated hematologic disorder, PV. Further, L3MBTL1-KD CD34⁺ cells show an enhanced response to Epo, resulting in the more rapid development of immunophenotypically and morphologically mature erythroblasts with increased hemoglobin content, compared with control cells. We have demonstrated the increased sensitivity of L3MBTL1 knockdown hematopoietic stem/progenitor cells to Epo at different concentrations of Epo and

at very early time points. The erythroid commitment that follows L3MBTL1-KD occurs early, based on the erythroid progenitor cell expansion seen in the LTC-IC assay. However, the observed changes in the frequency of the different human progenitor cell subsets (decreased CMP and increased GMP and MEP cells) may indicate a second effect, in the committed progenitor cell population.

L3MBTL1 is classified as a polycomb group protein, and recent evidence suggests that PcG proteins regulate stem cell pluripotency by maintaining the repression of lineage-specifying genes that trigger the differentiation process.^{23,24} *L3MBTL1* is down-regulated on Epo- or hemin-induced erythroid differentiation. *L3MBTL1* is also down-regulated, or at least is less abundant in MEP cells compared with more immature stem cells or progenitor cell populations (such as CMP), which suggests that erythroid differentiation may require “silencing” of L3MBTL1 function. As a compactor of euchromatin, *L3MBTL1* could serve as an epigenetic brake on erythroid commitment. Gene expression profiling of cells treated with Epo supports this hypothesis, as *L3MBTL1* is one of the genes most strongly down-regulated on Epo exposure.²⁵ Pr-Set7, an H4K20-specific methyltransferase that physically associates with L3MBTL1 and is responsible for the H4K20 methyl mark that serves as a docking site for L3MBTL1 binding, is also down-regulated in hemin-treated K562 cells,^{9,26} which suggests that, by binding chromatin and maintaining repression of its target genes, L3MBTL1 impairs erythroid differentiation.

Recently, the ability of reactive oxygen species to trigger the precocious differentiation of *Drosophila* stem cells into all 3 mature blood cell types has been linked to down-regulation of PcG expression.²⁷ This down-regulation is associated with JNK activation, and it triggers differentiation toward lamellocyte but not plasmacyte or crystal cell differentiation, somewhat similar to the effects of L3MBTL1 KD on erythroid, but not myeloid or megakaryocytic, lineages. Reactive oxygen species triggers FOXO activation²⁷; similarly, we found increased phosphorylation/

activation of the STAT5, AKT/FOXO, and MAPK pathways in *L3MBTL1-KD* HSPCs, even in the absence of Epo. Such Epo-independent signaling is a hallmark of the MPNs, especially PV. PcG members specifically repress the JAK-STAT pathway in the *Drosophila* eye imaginal disc,²⁸ and our data suggest that *L3MBTL1* acts in a fashion similar to regulate erythroid differentiation.

We also found increased expression of p16^{INK4a} in *L3MBTL1-KD* cells. Increased expression of p16^{INK4A} is also found in erythroid colony-forming cells isolated from patients with PV.²¹ p16 has been linked to erythroid differentiation and apoptosis in erythroleukemia cells²² and may play a role in mediating the effects of *L3MBTL1* in erythropoiesis because we also observed down-regulation of p16 after *L3MBTL1* overexpression. Like p16 up-regulation, down-regulation of FoxOs by *L3MBTL1-KD* could also contribute to the decreased CAFC frequency seen after *L3MBTL1-KD*.²⁹ Although we previously reported that *L3MBTL1-KD* can increase c-myc levels in some cell types, and cyclin E or cyclin A levels in others,^{10,30} we did not observe such increases in the human CD34⁺ cells at the time points assayed (data not shown). Such increases are seen in terminally differentiated cells (such as 293T cells) and may be needed for cells to manifest a strong proliferative response to *L3MBTL1-KD*.

In future studies, we wish to determine whether *L3MBTL1* loss can cooperate with the constitutively activated mutant JAK2 kinases found in patients with MPNs. There appears to be a relationship between del20q and the occurrence of the JAK2 V617F mutation. In one study of 29 patients with 20q deletion, 28 were found to be JAK2 V617F⁺.³¹ In another study of MPN patient samples, the JAK2V617F/JAK2 burden was 2% to 25% of the clonal cells, even though all of the clonal cells had del20q.³² Whereas these studies suggest that the 20q deletion may represent one of several pre-JAK2 events (others being mutations in TET2, ASXL1, c-CBL, or currently unknown proteins),^{33,34} Schaub et al have reported that del20q may occur after the acquisition of *JAK2V617F* in some clones.³⁵ It is possible that, during the genesis of the MPNs, the acquisition of additional genetic mutations (ie, *JAK2V617F*) allows *L3MBTL1*-deficient cells to override the antiproliferative mechanisms elicited by p16 or MAPK activation.

L3MBTL1 plays a key role in hematopoiesis by regulating the erythroid differentiation of HSPCs. Given that *L3MBTL1* is located within the common deleted region on 20q seen in patients with PV, our data suggest that loss of *L3MBTL1* is important in the pathogenesis of such disorders.

Acknowledgments

We thank Christopher Park for the analysis of human progenitor cells, Benjamin Ebert for providing MPN patient samples, and Emanuela Romano and James Young for providing important reagents.

This work was supported by Associazione Cristina Bassi contro le leucemie acute dell'adulto and American Italian Cancer Foundation postdoctoral fellowships to F.P.; and NCI R01 grant 102202 to S.D.N.

We dedicate this paper to the late Bruno Rotoli, whose devotion to his patients, his mentees, and his profession will always be remembered, and to the late Piernicola Bocconi, whose prior investigations of *L3MBTL1* made this study possible.

Authorship

Contribution: F.P. conducted experiments, analyzed the data, and wrote the paper; N.G. designed shRNAs, performed experiments, and analyzed the data; R.H.-A. designed shRNAs and performed the Ras pull-down experiments; O.A.-W. and R.L.L. analyzed the MPN patient database and helped with the progenitor cell analysis; T.A. helped perform the long-term colony assays; F.V. and S.M. helped with cell cultures and plasmids; L.W., F.L., and X.Z. provided technical expertise; and S.D.N. supervised the experimental design and helped write and edit the paper.

Conflict-of-interest disclosure: The authors declare no competing financial interests.

Correspondence: Stephen D. Nimer, Memorial Sloan-Kettering Cancer Center, 1275 York Ave, New York, NY 10065; e-mail: s-nimer@mskcc.org.

References

- Dewald GW, Schad CR, Lilla VC, Jalal SM. Frequency and photographs of HGM11 chromosome anomalies in bone marrow samples from 3,996 patients with malignant hematologic neoplasms. *Cancer Genet Cytogenet*. 1993;68(1):60-69.
- Bench AJ, Nacheva EP, Hood TL, et al. Chromosome 20 deletions in myeloid malignancies: reduction of the common deleted region, generation of a PAC/BAC contig and identification of candidate genes. UK Cancer Cytogenetics Group (UKCCG). *Oncogene*. 2000;19(34):3902-3913.
- Fenaux P, Morel P, Lai JL. Cytogenetics of myelodysplastic syndromes. *Semin Hematol*. 1996;33(2):127-138.
- Heim S, Mitelman F. Cytogenetic analysis in the diagnosis of acute leukemia. *Cancer*. 1992;70(6 suppl):1701-1709.
- Wismar J, Loffler T, Habtemichael N, et al. The *Drosophila melanogaster* tumor suppressor gene lethal(3)malignant brain tumor encodes a proline-rich protein with a novel zinc finger. *Mech Dev*. 1995;53(1):141-154.
- Gateff E, Loffler T, Wismar J. A temperature-sensitive brain tumor suppressor mutation of *Drosophila melanogaster*: developmental studies and molecular localization of the gene. *Mech Dev*. 1993;41(1):15-31.
- Bocconi P, MacGrogan D, Scandura JM, Nimer SD. The human L(3)MBT polycomb group protein is a transcriptional repressor and interacts physically and functionally with TEL (ETV6). *J Biol Chem*. 2003;278(17):15412-15420.
- Wang WK, Tereshko V, Bocconi P, MacGrogan D, Nimer SD, Patel DJ. Malignant brain tumor repeats: a three-leaved propeller architecture with ligand/peptide binding pockets. *Structure*. 2003;11(7):775-789.
- Kalakonda N, Fischle W, Bocconi P, et al. Histone H4 lysine 20 monomethylation promotes transcriptional repression by *L3MBTL1*. *Oncogene*. 2008;27(31):4293-4304.
- Trojer P, Li G, Sims RJ 3rd, et al. *L3MBTL1*, a histone-methylation-dependent chromatin lock. *Cell*. 2007;129(5):915-928.
- MacGrogan D, Kalakonda N, Alvarez S, et al. Structural integrity and expression of the *L3MBTL1* gene in normal and malignant hematopoietic cells. *Genes Chromosomes Cancer*. 2004;41(3):203-213.
- Bench AJ, Li J, Huntly BJ, et al. Characterization of the imprinted polycomb gene *L3MBTL1*, a candidate 20q tumour suppressor gene, in patients with myeloid malignancies. *Br J Haematol*. 2004;127(5):509-518.
- Moffat J, Grueneberg DA, Yang X, et al. A lentiviral RNAi library for human and mouse genes applied to an arrayed viral high-content screen. *Cell*. 2006;124(6):1283-1298.
- Ivanova N, Dobrin R, Lu R, et al. Dissecting self-renewal in stem cells with RNA interference. *Nature*. 2006;442(7102):533-538.
- Elbashir SM, Lendeckel W, Tuschl T. RNA interference is mediated by 21- and 22-nucleotide RNAs. *Genes Dev*. 2001;15(2):188-200.
- Park CY, Majeti R, Weissman IL. In vivo evaluation of human hematopoiesis through xenotransplantation of purified hematopoietic stem cells from umbilical cord blood. *Nat Protoc*. 2008;3(12):1932-1940.
- Dean A, Erard F, Schneider AP, Schechter AN. Induction of hemoglobin accumulation in human K562 cells by hemin is reversible. *Science*. 1981;212(4493):459-461.
- Fawcett D, Jensch RP. *Hemopoiesis*. New York, NY: Chapman and Hall; 1997.
- Kim A, Dean A. Developmental stage differences in chromatin subdomains of the beta-globin locus. *Proc Natl Acad Sci U S A*. 2004;101(18):7028-7033.
- Scandura JM, Bocconi P, Massague J, Nimer SD.

- Transforming growth factor beta-induced cell cycle arrest of human hematopoietic cells requires p57KIP2 up-regulation. *Proc Natl Acad Sci U S A*. 2004;101(42):15231-15236.
21. Dai C, Krantz SB. Increased expression of the INK4a/ARF locus in polycythemia vera. *Blood*. 2001;97(11):3424-3432.
 22. Minami R, Muta K, Umemura T, et al. p16(INK4a) induces differentiation and apoptosis in erythroid lineage cells. *Exp Hematol*. 2003;31(5):355-362.
 23. Boyer LA, Plath K, Zeitlinger J, et al. Polycomb complexes repress developmental regulators in murine embryonic stem cells. *Nature*. 2006;441(7091):349-353.
 24. Lee TI, Jenner RG, Boyer LA, et al. Control of developmental regulators by Polycomb in human embryonic stem cells. *Cell*. 2006;125(2):301-313.
 25. Bodo E, Kromminga A, Funk W, et al. Human hair follicles are an extrarenal source and a nonhematopoietic target of erythropoietin. *FASEB J*. 2007;21(12):3346-3354.
 26. Sims JK, Rice JC. PR-Set7 establishes a repressive trans-tail histone code that regulates differentiation. *Mol Cell Biol*. 2008;28(14):4459-4468.
 27. Owusu-Ansah E, Banerjee U. Reactive oxygen species prime *Drosophila* hematopoietic progenitors for differentiation. *Nature*. 2009;461(7263):537-541.
 28. Classen AK, Bunker BD, Harvey KF, Vaccari T, Bilder D. A tumor suppressor activity of *Drosophila* Polycomb genes mediated by JAK-STAT signaling. *Nat Genet*. 2009;41(10):1150-1155.
 29. Tothova Z, Kollipara R, Huntly BJ, et al. FoxOs are critical mediators of hematopoietic stem cell resistance to physiologic oxidative stress. *Cell*. 2007;128(2):325-339.
 30. Trojer P, Reinberg D. Beyond histone methylation: lysine binding: how malignant brain tumor (MBT) protein L3MBTL1 impacts chromatin structure. *Cell Cycle*. 2008;7(5):578-585.
 31. Campbell PJ, Baxter EJ, Beer PA, et al. Mutation of JAK2 in the myeloproliferative disorders: timing, clonality studies, cytogenetic associations, and role in leukemic transformation. *Blood*. 2006;108(10):3548-3555.
 32. Kralovics R, Teo SS, Li S, et al. Acquisition of the V617F mutation of JAK2 is a late genetic event in a subset of patients with myeloproliferative disorders. *Blood*. 2006;108(4):1377-1380.
 33. Delhommeau F, Dupont S, Della Valle V, et al. Mutation in TET2 in myeloid cancers. *N Engl J Med*. 2009;360(22):2289-2301.
 34. Sanada M, Suzuki T, Shih LY, et al. Gain-of-function of mutated C-CBL tumour suppressor in myeloid neoplasms. *Nature*. 2009;460(7257):904-908.
 35. Schaub FX, Jager R, Looser R, et al. Clonal analysis of deletions on chromosome 20q and JAK2-V617F in MPD suggests that del20q acts independently and is not one of the predisposing mutations for JAK2-V617F. *Blood*. 2009;113(9):2022-2027.

ETV6-ABL1-positive “chronic myeloid leukemia”: clinical and molecular response to tyrosine kinase inhibition

While great progress has been achieved in the clinical management and molecular understanding of Ph⁺ chronic myeloid leukemia (CML), little is known about the optimal approach to monitor and treat patients with ETV6-ABL1⁺ myeloproliferative neoplasms. Nine BCR-ABL1-negative CML patients with a variant *ABL1* gene (9q34) rearrangement, involving fusion to ETV6 aka TEL (12p13) have been reported thus far.¹⁻⁹ The ETV6-ABL1 fusion gene has also been identified in 3 patients with chronic myeloproliferative neoplasms other than “chronic myeloid leukemia” (cMPN) as well as 7 patients with BCR-ABL1 negative acute lymphoblastic leukemia and 4 patients with acute myeloid leukemia.^{10,11} Of the 9 cases of ETV6-ABL1⁺ chronic myeloid leukemia, only 2 were treated with a TKI in chronic phase^{4,5} and only one of these reached a complete remission with a modest follow up of seven months (no molecular monitoring was performed).⁴ Among the other published ETV6-ABL1⁺ reports, one patient was treated with a second generation TKI for a relapsed cMPN.¹² We provide the first molecular documentation of sustained remission of ETV6-ABL1⁺ chronic phase “chronic myeloid leukemia” (CML requires a BCR-ABL1 fusion according to the most recent 2008 WHO classification) to TKI. Molecular monitoring for the ETV6-ABL1 transcript is important given the fact that conventional karyotyping frequently fails to detect a cryptic translocation, i.e. the t(9;12). We provide evidence that treatment of ETV6-ABL1⁺ “chronic myeloid leukemia” with imatinib results in downregulation of C-MYC, BCL-XL, ID1 and NUP98, mediators of BCR-ABL1 transforming activity. Moreover, we found no associated mutations in *UTX*, *ASXL1*, *EZH2*, *TET2* and *IDH1/2* suggesting that ETV6-ABL1⁺ “chronic myeloid leukemia” may be as tyrosine kinase focused as BCR-ABL1 driven disease.

The patient is a 36-year male who was found to have splenomegaly and a total white blood cell (WBC) count

of $55 \times 10^9/L$ (57% neutrophils, 6% lymphocytes, 1% monocytes, 3% eosinophils, 2% basophils, 7% metamyelocytes, 24% myelocytes). Lactate dehydrogenase was elevated at 653 IU/L. Bone marrow biopsy revealed myeloid hyperplasia suggestive of a myeloproliferative disorder. qRT-PCR for BCR-ABL1 translocation was negative. No BCR-ABL1 fusion signal was observed in interphase FISH analysis using BCR (22q11.2) and ASS-ABL1 (9q34) probes. Instead, 80% of interphase nuclei showed a variant signal pattern consisting of two signals for BCR and three signals for ASS-ABL1 consistent with rearrangement of ABL1 at 9q34 but not BCR at 22q11. Cytogenetic G-banding analysis and FISH showed t(9;12)(q34;p13) in an otherwise normal karyotype (Figure 1A and B). RT-PCR detected the ETV6-ABL1 translocation and the patient was diagnosed with ETV6-ABL1⁺ CML-like disorder. Given the persistence of night sweats and fevers, and the persistent disease despite hydroxyurea at 1,000mg daily (WBC decreased to 7×10^9 cells/L after one month of hydroxyurea) imatinib mesylate, 400mg daily, was initiated. The patient tolerated imatinib and achieved a complete hematological remission after three months of treatment (WBC 5.6×10^9 cells/L). FISH testing after three months of imatinib revealed no evidence of rearrangement at the BCR or ETV6 loci (Figure 1B).

To follow the patient’s response to therapy more sensitively, qRT-PCR was performed using primers for ETV6 and ABL1 (*Online Supplementary Appendix*). Quantification of the ETV6-ABL1 transcript level in peripheral blood cells one month prior to initiation of imatinib revealed $2,160 \times 10^3$ ETV6-ABL1 copies/ μ g RNA. After one month of treatment, ETV6-ABL1 transcript level dropped to 495×10^3 copies/ μ g RNA. The ETV6-ABL1 transcript became undetectable by seven months of treatment, indicating a complete and rapid molecular response. The patient’s molecular response closely mirrored normalization of the WBC count (Figure 2A). We also evaluated the expression of BCR-ABL1 target genes *C-MYC*, *BCL-XL*, *ID1* and *NUP98*, pre- and post-imatinib treatment (Figure 2B). The expression of these genes closely mirrored ETV6-ABL1 expression: imatinib downregulated their expression. The patient has continued to

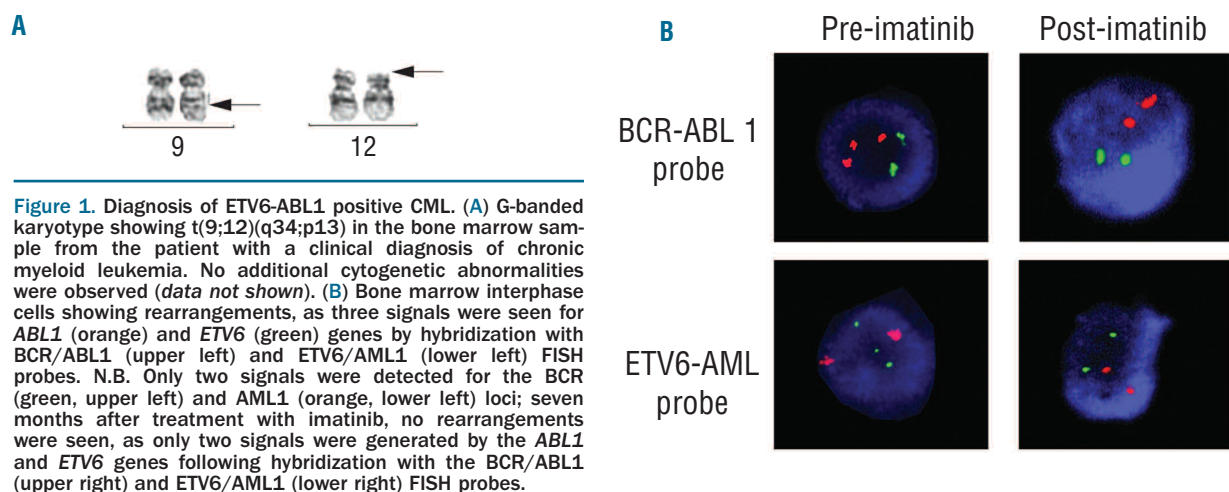


Figure 1. Diagnosis of ETV6-ABL1 positive CML. (A) G-banded karyotype showing t(9;12)(q34;p13) in the bone marrow sample from the patient with a clinical diagnosis of chronic myeloid leukemia. No additional cytogenetic abnormalities were observed (*data not shown*). (B) Bone marrow interphase cells showing rearrangements, as three signals were seen for ABL1 (orange) and ETV6 (green) genes by hybridization with BCR/ABL1 (upper left) and ETV6/AML1 (lower left) FISH probes. N.B. Only two signals were detected for the BCR (green, upper left) and AML1 (orange, lower left) loci; seven months after treatment with imatinib, no rearrangements were seen, as only two signals were generated by the ABL1 and ETV6 genes following hybridization with the BCR/ABL1 (upper right) and ETV6/AML1 (lower right) FISH probes.

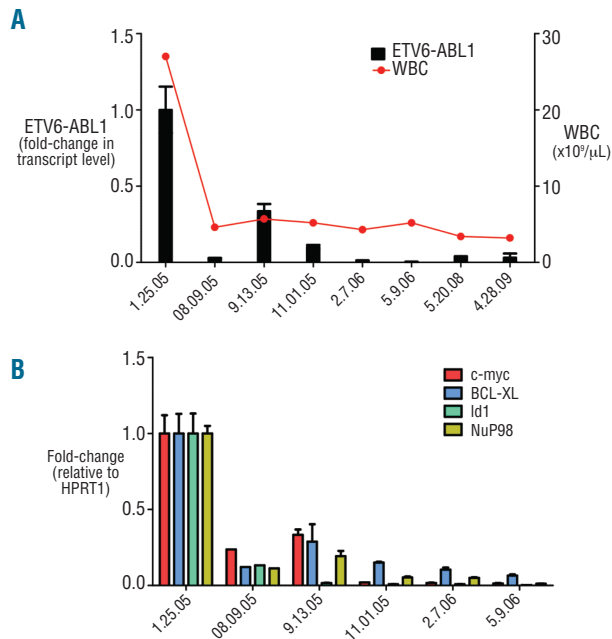


Figure 2. Response to Imatinib in an ETV6-ABL1 positive chronic myeloid leukemia. (A) White blood cell count and peripheral blood qRT-PCR analysis of ETV6-ABL1 transcript levels pre-imatinib and throughout imatinib treatment. (B) Concomitant with decreases in ETV6-ABL1 transcript levels, decreases in C-MYC, ID1, BCL-XL, and NUP-98 transcripts were also seen. The patient remains in hematological remission with no identifiable ETV6-ABL1 transcripts in the peripheral blood after approximately five years of imatinib.

do well on imatinib 400mg/day with no evidence of ETV6-ABL1 transcript by qRT-PCR for the past five years.

Somatic mutations in *UTX*, *ASXL1*, and *TET2* have been reported in chronic myeloid leukemia and mutations in *EZH2* and *IDH1/2* in myeloid malignancies other than CML. We found no somatic alterations in these genes in the DNA extracted from whole blood prior to imatinib treatment, nor when the patient was in a molecular remission.

Our studies indicate that ETV6-ABL1⁺ “chronic myeloid leukemia” can be sensitive to imatinib and there is significant overlap of molecular targets of ETV6-ABL1 with those of BCR-ABL1, suggesting that the ETV6-ABL1 fusion protein may trigger similar oncogenic cascades as BCR-ABL1. Finally, we were able to exclude mutations in any of the recently identified “myeloid” genes including *UTX*, *ASXL1*, *EZH2*, *TET2* and *IDH1/2* suggesting that the pathogenesis of ETV6-ABL1⁺ “chronic myeloid leukemia” may be as tyrosine kinase focused as BCR-ABL1 driven disease.

Fabiana Perna,¹ Omar Abdel-Wahab,² Ross L. Levine,² Suresh C. Jhanwar,³ Kazunori Imada,⁴ and Stephen D. Nimer¹

¹Molecular Pharmacology and Chemistry Program, Sloan Kettering Institute, New York, USA; ²Human Oncology and Pathogenesis Program, Memorial Sloan Kettering Cancer Center, New York, USA; ³Dept. of Pathology, Memorial Sloan Kettering Cancer Center, New York, USA; and ⁴Dept. of Hematology/Oncology, Kyoto University Hospital, Kyoto, Japan.

Acknowledgments: the authors thank Masakatsu Hishizawa and

Takashi Uchiyama from the Department of Hematology/Oncology, Kyoto University Hospital, Japan for following the patient in Japan, Tony DeBlasio for collecting and storing the samples, and Emily Dolezal for generating the database that facilitated our analysis.

Correspondence: Stephen D. Nimer, MD, Memorial Sloan Kettering Cancer Center, 1275 York Avenue, New York, NY 10065, USA. Phone: international +1.646.8883040.

Fax: international +1.646.4220246. E-mail: s-nimer@mskcc.org

Key words: myeloproliferative, neoplasm, imatinib, molecular response.

Citation: Perna F, Abdel-Wahab O, Levine RL, Jhanwar SC, Imada K, and Nimer SD. ETV6-ABL1-positive “chronic myeloid leukemia”: clinical and molecular response to tyrosine kinase inhibition with imatinib. *Haematologica* 2011; 96(02):342-343. doi:10.3324/haematol.2010.036673

References

- Andreasson P, Johansson B, Carlsson M, Jarlsfelt I, Fioretos T, Mitelman F, et al. BCR/ABL-negative chronic myeloid leukemia with ETV6/ABL fusion. *Genes Chromosomes Cancer*. 1997;20(3):299-304.
- Barbouti A, Ahlgren T, Johansson B, Hoglund M, Lassen C, Turesson I, et al. Clinical and genetic studies of ETV6/ABL1-positive chronic myeloid leukaemia in blast crisis treated with imatinib mesylate. *Br J Haematol*. 2003;122(1):85-93.
- Brunel V, Lafage-Pochitaloff M, Alcalay M, Pelicci PG, Birg F. Variant and masked translocations in acute promyelocytic leukemia. *Leuk Lymphoma*. 1996;22(3-4):221-8.
- Kawamata N, Dashti A, Lu D, Miller B, Koeffler HP, Schreck R, et al. Chronic phase of ETV6-ABL1 positive CML responds to imatinib. *Genes Chromosomes Cancer*. 2008;47(10):919-21.
- Kelly JC, Shahbazi N, Scheerle J, Jahn J, Suchen S, Christacos NC, et al. Insertion (12;9)(p13;q34q34): a cryptic rearrangement involving ABL1/ETV6 fusion in a patient with Philadelphia-negative chronic myeloid leukemia. *Cancer Genet Cytogenet*. 2009;192(1):36-9.
- Keung YK, Beaty M, Steward W, Jackle B, Pettnati M. Chronic myelocytic leukemia with eosinophilia, t(9;12)(q34;p13), and ETV6-ABL gene rearrangement: case report and review of the literature. *Cancer Genet Cytogenet*. 2002;138(2):139-42.
- Lin H, Guo JQ, Andreeff M, Arlinghaus RB. Detection of dual TEL-ABL transcripts and a Tel-Abl protein containing phosphotyrosine in a chronic myeloid leukemia patient. *Leukemia*. 2002;16(2):294-7.
- Tirado CA, Sebastian S, Moore JO, Gong JZ, Goodman BK. Molecular and cytogenetic characterization of a novel rearrangement involving chromosomes 9, 12, and 17 resulting in ETV6 (TEL) and ABL fusion. *Cancer Genet Cytogenet*. 2005;157(1):74-7.
- Van Limbergen H, Beverloo HB, van Drunen E, Janssens A, Hahlen K, Poppe B, et al. Molecular cytogenetic and clinical findings in ETV6/ABL1-positive leukemia. *Genes Chromosomes Cancer*. 2001;30(3):274-82.
- Janssen JW, Ridge SA, Papadopoulos P, Cotter F, Ludwig WD, Fonatsch C, et al. The fusion of TEL and ABL in human acute lymphoblastic leukaemia is a rare event. *Br J Haematol*. 1995;90(1):222-4.
- Zuna J, Zaliava M, Muzikova K, Meyer C, Lizcova L, Zemanova Z et al. Acute leukemias with ETV6/ABL1 (TEL/ABL) fusion: poor prognosis and prenatal origin. *Genes Chromosomes Cancer*. 2010; 49(10):873-84.
- Nand R, Bryke C, Kroft SH, Divgi A, Bredeson C, Atallah E. Myeloproliferative disorder with eosinophilia and ETV6-ABL gene rearrangement: efficacy of second-generation tyrosine kinase inhibitors. *Leuk Res*. 2009;33(8):1144-6.

Cytogenetically complex SEC31A-ALK fusions are recurrent in ALK-positive large B-cell lymphomas

Fusion tyrosine kinases involving anaplastic lymphoma kinase (ALK) are central to the pathogenesis of numerous malignancies, in which they represent impor-

L3MBTL1 polycomb protein, a candidate tumor suppressor in del(20q12) myeloid disorders, is essential for genome stability

Nadia Gurvich^a, Fabiana Perna^a, Andrea Farina^b, Francesca Voza^a, Silvia Menendez^a, Jerard Hurwitz^b, and Stephen D. Nimer^{a,1}

^aMolecular Pharmacology and Chemistry Program and ^bMolecular Biology Program, Sloan-Kettering Institute, Memorial Sloan-Kettering Cancer Center, New York, NY 10065

Contributed by Jerard Hurwitz, November 17, 2010 (sent for review August 2, 2010)

The *l3mbtl1* gene is located on the long arm of chromosome 20 (q12), within a region commonly deleted in several myeloid malignancies. L3MBTL1 is a human homolog of the *Drosophila* polycomb L(3)MBT tumor suppressor protein and thus a candidate tumor suppressor in del(20q12) myeloid disorders. We used the loss-of-function approach to explore the possible tumor suppressive mechanism of L3MBTL1 and found that depletion of L3MBTL1 from human cells causes replicative stress, DNA breaks, activation of the DNA damage response, and genomic instability. L3MBTL1 interacts with Cdc45, MCM2-7 and PCNA, components of the DNA replication machinery, and is required for normal replication fork progression, suggesting that L3MBTL1 causes DNA damage, at least in part, by perturbing DNA replication. An activated DNA damage response and genomic instability are common features in tumorigenesis and a consequence of overexpression of many oncogenes. We propose that the loss of L3MBTL1 contributes to the development of 20q⁻ hematopoietic malignancies by inducing replicative stress, DNA damage, and genomic instability.

H4K20me1/2 binding protein | chromatin reader

The *l3mbtl1* gene is located on the long arm of chromosome 20q, within a region on 20q12 commonly deleted in several myeloid malignancies, including myeloproliferative neoplasms, myelodysplastic syndromes, and acute myeloid leukemia (1). It has been proposed that the 20q12 locus contains one or more tumor suppressors, which when lost contribute to the development of these disorders. L3MBTL1 is a human homolog of the *Drosophila* polycomb group (PcG) protein L(3)MBT. Homozygous mutations of the *Drosophila l3mbt* gene cause malignant transformation of the adult optic neuroblasts and ganglion mother cells in the larval brain (2). Somatic, focal deletions of other human L3MBTL family members, the *l3mbtl2* and *l3mbtl3* genes, have recently been found in human medulloblastoma (3). These findings suggest that L3MBTL1 is a candidate tumor suppressor gene in myeloid malignancies associated with 20q12 deletions.

The L3MBTL1 protein contains three MBT repeats, which assume a three-bladed propeller-like architecture, as well as a Zn finger and an SPM dimerization domain (4, 5). We previously demonstrated that L3MBTL1 functions as an HDAC-independent transcriptional repressor (6) that binds preferentially to mono- and dimethylated lysines of histones via the second of its three MBT repeats (7, 8). The three MBT domains of L3MBTL1 are sufficient to compact nucleosomal arrays. This compaction requires that the nucleosome contain a mono- or dimethylated lysine 26 on histone H1b or lysine 20 on histone H4 (H4K20) (7). L3MBTL1 binds to chromatin most prominently during the S phase of the cell cycle, concomitant with the appearance of the monomethylated H4K20 (H4K20me1) mark (8), suggesting that the biological function of L3MBTL1 may be related to DNA replication.

The accurate duplication of DNA during replication is essential for maintaining genomic stability, as uncorrected errors made during this process can lead to DNA breaks, which gen-

erate mutations and/or chromosomal translocations that can promote tumorigenesis (9). DNA breaks resulting from replicative stress trigger an ATM/ATR-dependent DNA damage response (DDR), which prevents the proliferation of cells with damaged DNA by inducing either cell cycle arrest or apoptosis. An activated DDR is present in precancerous lesions from tissues of different origins, and many overexpressed oncogenes cause replicative stress and activation of the DDR. When coupled with mutations in checkpoint and/or DNA repair genes, these abnormalities can lead to cancer (10–12).

In this study we examined the function of L3MBTL1 in mammalian cells and found that L3MBTL1 interacts with several components of the DNA replication machinery. Depletion of L3MBTL1 in cells was sufficient to trigger the DDR and promote genomic instability. Thus, L3MBTL1 is essential for maintaining DNA replication, providing a mechanism for its role as a putative tumor suppressor protein.

Results

Depletion of L3MBTL1 Inhibits Cell Proliferation and Causes G2/M Arrest.

To assess the role of L3MBTL1 in cell cycle regulation, we depleted L3MBTL1 mRNA and protein in U2OS cells using lentiviral vectors that expressed several shRNAs directed against its ORF. Down-regulation of L3MBTL1 mRNA and protein was achieved efficiently with three different shRNAs ($\geq 90\%$ knock-down; Fig. 1 *A* and *B*). The depleted cells were monitored for S phase entry by using BrdU incorporation, and we detected a marked decrease of S phase cells and the accumulation of cells in the G2/M phase (Fig. 1*C* and Fig. *S1A*). This effect was also observed in MRC5 normal diploid fibroblasts, Cal51, T98G, and K562 cells following L3MBTL1 knockdown (Fig. *S1 B–D*), demonstrating that it is not cell-type specific; it occurred in non-cancerous cells as well as hematopoietic K562 cells. These findings indicate that these cell cycle effects are relevant to the myeloid compartment.

Depletion of L3MBTL1 Generates DNA Breaks.

Cell cycle alterations triggered by L3MBTL1 depletion suggest that cells may be experiencing replicative stress, leading to DNA damage. To verify this hypothesis, we examined two DNA damage markers, the production of the phosphorylated histone H2A.x (γ H2A.x), which localizes to sites of double-stranded DNA breaks (DSBs) (13), and the distribution of 53BP1, which is recruited to DNA within minutes following DNA damage by binding to H4K20me2 and possibly other modified histones (14). We observed an increase in both γ H2A.x and 53BP1 foci following L3MBTL1 de-

Author contributions: N.G. designed research; N.G., F.P., A.F., F.V., and S.M. performed research; N.G. analyzed data; and N.G., J.H., and S.D.N. wrote the paper.

The authors declare no conflict of interest.

¹To whom correspondence should be addressed. E-mail: nimers@mskcc.org.

This article contains supporting information online at www.pnas.org/lookup/suppl/doi:10.1073/pnas.1017092108/-DCSupplemental.

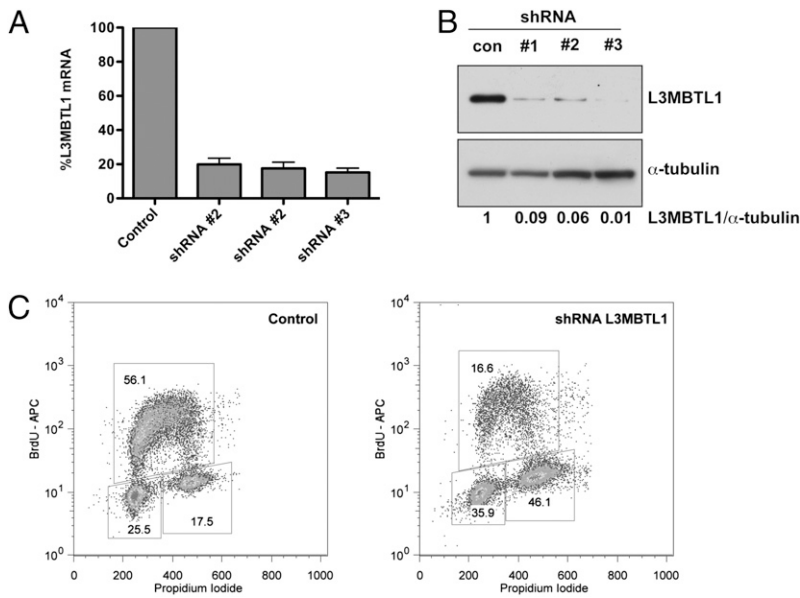


Fig. 1. L3MBTL1 depletion inhibits cell proliferation and causes G2/M arrest. U2OS cells were infected with control shRNA or one of several different lentiviral shRNAs targeting L3MBTL1. Levels of L3MBTL1 mRNA (A) and protein (B) were measured by quantitative RT-PCR and immunoblotting 48 h after infection. L3MBTL1 mRNA levels detected were adjusted for loading discrepancies using Hprt mRNA as the loading standard, and the levels of mRNA detected were plotted as a percent of the L3MBTL1 observed in U2OS cells infected with control shRNA. To quantitate depletion of L3MBTL1, the relative protein levels of L3MBTL1 were adjusted using the α -tubulin loading control and quantified relative to the protein level present in the control sample (set as 1). (C) U2OS cells were infected with control shRNA or with L3MBTL1 shRNA #3. After 48 h, cells were incubated with BrdU, stained with BrdU-APC antibody and propidium iodide (PI), and analyzed by flow cytometry. The distribution of BrdU (y axis) and PI (x axis) is plotted.

pletion with all three shRNAs in U2OS (Fig. 2A and B) and in MRC5 fibroblasts (Fig. S24).

We also measured the formation of DNA strand breaks in L3MBTL1-depleted cells using the comet assay, which visualizes damaged DNA on a single-cell level (15). Comet tails were detected in depleted U2OS cells (Fig. 2C and Fig. S2B), MRC5 and Cal51 cells (Fig. 2D), indicating DNA strand breakage. We treated MRC5 fibroblasts with varying doses of gamma irradiation to establish a range of tail moments (Fig. 2D) and determined that depletion of L3MBTL1 caused extensive DNA damage, similar to that induced by 5 Gy of irradiation.

Loss of L3MBTL1 Activates the DDR and Affects H4K20 Methylation Status. DNA damage triggers a checkpoint response that prevents

cells from progressing into mitosis. To explore this pathway, we first examined the phosphorylation of the ATM kinase, one hallmark of the DDR pathway (16), and detected increased phospho-ATM foci that overlapped with 53BP1 foci in L3MBTL1-depleted cells (Fig. 3A). We also examined whether the downstream components of the ATR/ATM-triggered DDR pathway were activated following L3MBTL1 depletion using immunoblotting to monitor changes in phosphorylation of the key components of this system, including Chk1 and Chk2. As shown in Fig. 3B, increased levels of phospho-Ser317-Chk1, phospho-Ser345-Chk1, and phospho-Thr68-Chk2 were detected in cells at 24, 48, and 72 h postinfection, similar to that observed in cells irradiated with 10 Gy.

Depletion of L3MBTL1 altered the activities as well as the levels of a number of proteins associated with checkpoint regu-

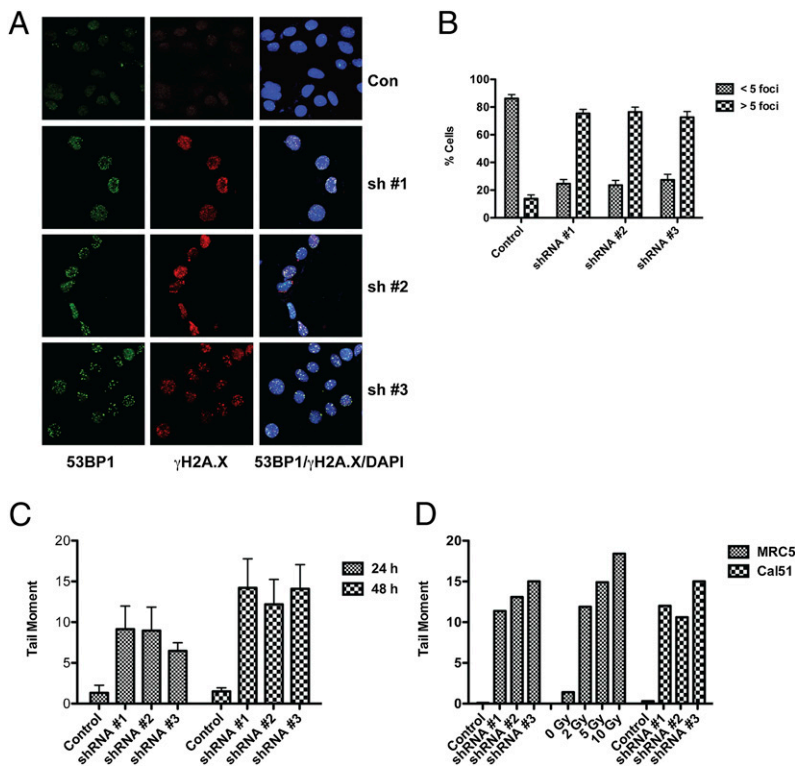


Fig. 2. Depletion of L3MBTL1 generates DNA breaks. (A) U2OS cells infected with one of several shRNAs against L3MBTL1 or with control shRNA were stained with antibodies against 53BP1 and γ H2A.x. (B) DNA damage foci were quantitated in control and L3MBTL1 knockdown cells based on whether they contained more or less than five foci per cell. (C) The tail moment was calculated and plotted from three independent comet assays of U2OS cells treated with control shRNA or L3MBTL1 shRNA U2OS cells at 24 and 48 h after infection. (D) Calculated tail moments from comet assays of control and L3MBTL1-depleted MRC5 and Cal51 cells 48 h after infection are plotted. The tail moment was calculated from comet assays of control MRC5 cells vs. cells irradiated with the indicated dose of gamma irradiation and the data plotted.

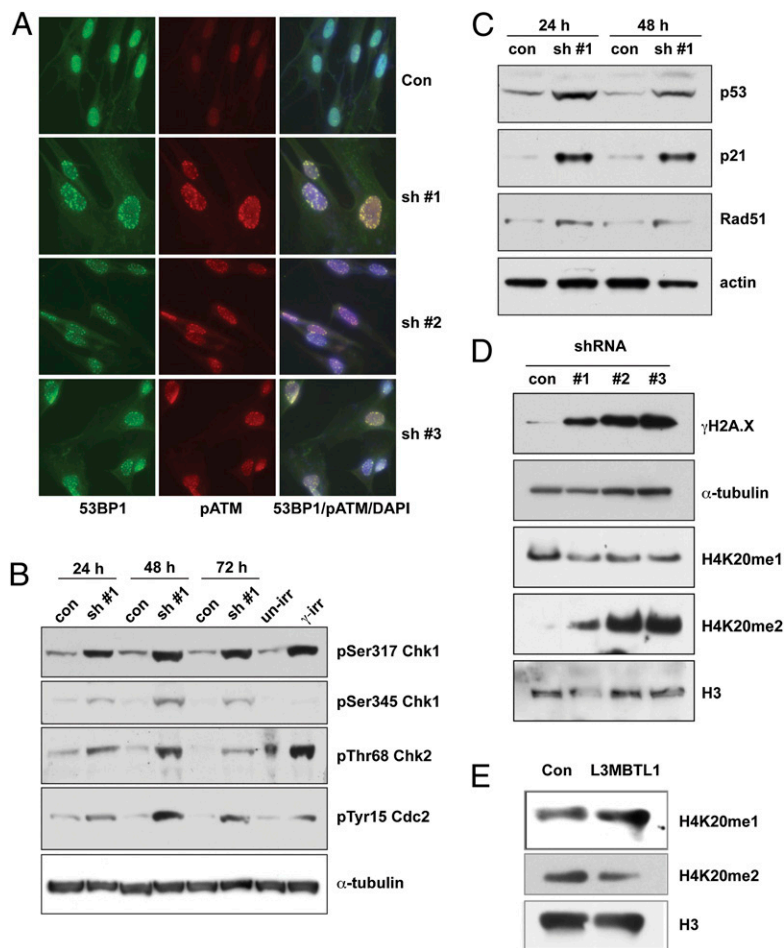


Fig. 3. Depletion of L3MBTL1 activates the DDR. (A) Control and L3MBTL1-depleted U2OS cells were stained with antibodies against 53BP1 and phospho-ATM (pATM) 48 h post-infection. (B) U2OS cells infected with control or L3MBTL1 shRNAs were harvested 24, 48, and 72 h postinfection and immunoblotted with the indicated antibodies to detect activation of the DDR. Unirradiated cells (unirr) and cells harvested 1 h following 10 Gy of gamma irradiation (γ -irr) were used as negative and positive controls for activated DDR proteins. (C) Lysates from control and L3MBTL1-depleted U2OS cells were isolated 24 and 48 h postinfection, and the levels of Rad51, p53, p21, and actin determined by immunoblotting with the indicated antibodies. (D) Lysates from U2OS cells infected with three different shRNAs against L3MBTL1 were harvested at 48 h and immunoblotted with antibodies directed against γ H2A.x, H4K20me1, H4K20me2, histone H3, and tubulin. (E) Histones were extracted from U937 cells that overexpress L3MBTL1 or that contain empty vector control and immunoblotted for H4K20me1, H4K20me2, and histone H3 (loading control).

lation and the DDR pathway (Fig. 3B–D). These include: (i) the formation of phospho-Tyr15-Cdc2, a modification that inhibits Cdc2 kinase activity, which is required for cell cycle progression into mitosis (17) (Fig. 3B and Fig. S3A); (ii) the up-regulation of p21 and p53, downstream effectors of the DDR pathway, as well as Rad51, which plays a key role in double-strand break repair by homologous recombination (Fig. 3C and Fig. S3B), and (iii) an increase in the level of γ H2A.x (Fig. 3D and Fig. S3C), in keeping with the data shown in Fig. 2. We also observed an increase in the amount of H4K20me2 (40- to 90-fold), which plays important roles in DNA replication and DNA damage recognition (18), but detected little effect on the levels of H4K20me1. Conversely, overexpression of L3MBTL1 in U937 cells that have monoallelic loss of the commonly deleted region of 20q had the opposite effect, namely, a decrease in H4K20me2 and an increase in H4K20me1 (Fig. 3E). Collectively, these data show that the DDR pathway is strongly activated following depletion of L3MBTL1 and suggest that changes in the level of H4K20 dimethylation could contribute to these effects.

We, and others, have found L3MBTL1 complexed with Rb/E2F proteins repressed the activation of some E2F target genes, including c-myc and Cyclin E1, two established oncogenes (7, 8, 19, 20). We tested whether these genes were up-regulated in L3MBTL1 knockdown cells, but noted no changes in their levels at 48 h following lentiviral infection with shRNAs against L3MBTL1 (Fig. S3D). Thus, induction of the DDR following L3MBTL1 depletion cannot be explained by the enhanced expression of c-myc or Cyclin E1.

L3MBTL1 Depletion Slows the DNA Replication Forks Movement. The presence of DNA damage and activation of the DDR suggest that

depletion of L3MBTL1 may trigger defects in DNA replication. We examined DNA replication fork progression by DNA fiber analyses. For this purpose, control and L3MBTL1-depleted cells were sequentially pulsed for 1 h each with IdU and CldU, lysed, and DNA fibers spread on slides. The fibers were labeled with antibodies to IdU and CldU and fluorescence-labeled secondary antibodies. Fibers containing green IdU fluorescent label flanked on each side with the red CldU fluorescent label represent DNA molecules formed by bidirectional movement of replication forks. Fig. 4A shows DNA fibers isolated from control and L3MBTL1-depleted MRC5 fibroblasts. The length of the green IdU-labeled fibers, indicating DNA replicated from origins, was shorter in depleted cells than in fibers isolated from control cells. Furthermore, the total length of red CldU- and green IdU-labeled fibers was shorter in L3MBTL1-depleted cells than in control cells, indicating slower replication fork movement. The average length of DNA fibers from L3MBTL1-depleted cells and control cells was 16.8 μ m and 31.7 μ m, respectively (Fig. 4B); 78% of the DNA fibers from L3MBTL1-depleted cells were <20 μ m, whereas 33% of fibers from control cells were this length (Fig. 4C). Similar data were obtained using U2OS cells, indicating that this effect is not cell-type specific (Fig. 4D and E). The average rate of fork progression in L3MBTL1-depleted cells was \sim 40% slower than in control cells, indicating that L3MBTL1 is required for the normal progression of DNA replication forks.

L3MBTL1 Interacts with Components of DNA Replication Machinery. Because L3MBTL1 appears to play a role in replication fork progression, we tested whether it interacted with components of the DNA replication machinery. We overexpressed HA-tagged L3MBTL1 in 293T cells, and examined its interaction with mem-

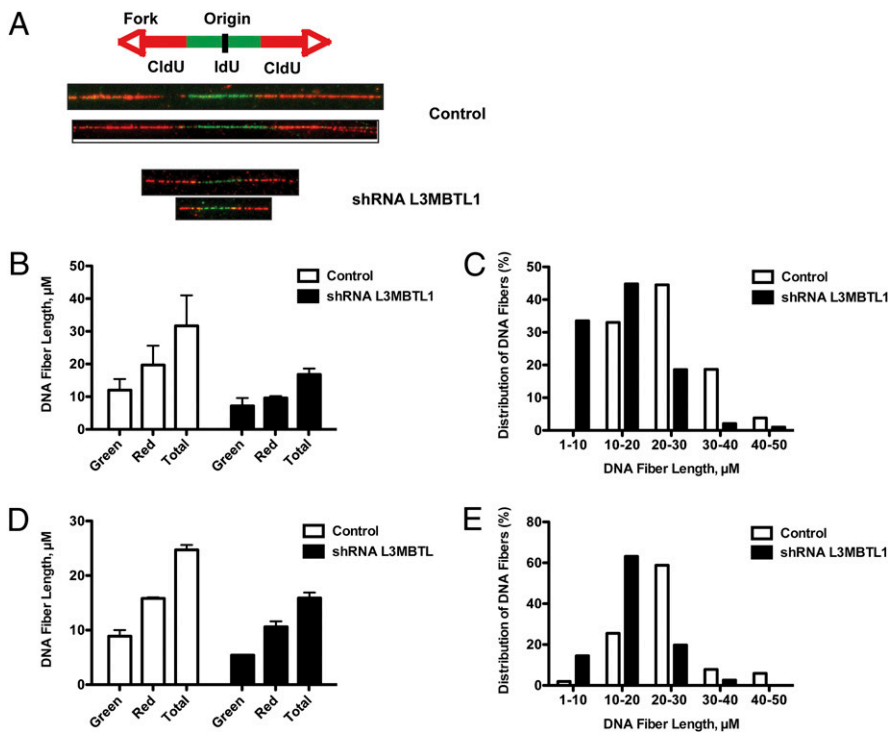


Fig. 4. Depletion of L3MBTL1 alters the progression of DNA replication forks. MRC5 and U2OS cells infected with control or L3MBTL1 shRNA were incubated for 1 h with IdU followed by 1 h incubation with CldU and then subjected to analysis of replication fork movement. (A) Individual replication units were visualized by immunofluorescence for incorporated halogenated nucleotides in isolated DNA fibers, as described in *Materials and Methods*. Images of fibers from MRC5 cells infected with control or L3MBTL1 shRNAs are shown. (B) The mean DNA fiber length from MRC5 cells infected with control or L3MBTL1 shRNA was calculated by measuring at least 100 fibers in each experiment, and the results plotted. (C) The data for one representative experiment with MRC5 cells are plotted as percentage of DNA fibers with each specified length. (D) Mean DNA fiber length for U2OS cells infected with control or L3MBTL1 shRNA was calculated by measuring at least 100 fibers in each experiment and plotted. (E) The data derived from an experiment using U2OS cells are plotted as percentage of replication forks with the specified DNA fiber length indicated.

bers of the MCM2-7 complex, a critical component of the putative replicative helicase. As shown in Fig. 5A, HA-tagged L3MBTL1 interacted with the MCM2-7 complex, and L3MBTL1 was immunoprecipitated by antibodies against MCM2 and MCM5 (Fig. 5B). Cdc45 and the GINS complex form a replicative helicase complex with MCM2-7 (CMG complex) (21) that travels with the replication fork (22). These findings prompted us to examine whether L3MBTL1 interacted with these components as well as other replication proteins. As shown in Fig. 5A, the interaction of L3MBTL1 with Cdc45 was detected, whereas an interaction with Sld5 (a subunit of the GINS complex) was not observed. Interactions with PCNA, the DNA sliding clamp required for processivity of the replicative DNA polymerases, were also noted, whereas interaction with Fen-1, an enzyme involved in DNA repair and lagging strand processing, was not observed (Fig. 5A). We also examined whether the levels of replication proteins were affected by depletion of L3MBTL1 in U2OS cells. As shown in Fig. S4, we did not find significant changes. Thus, L3MBTL1 interacts with a number of proteins that play roles in different stages of DNA replication, consistent with the notion that it affects replication. The mechanisms contributing to these effects remain to be investigated.

Discussion

In this study we demonstrate that depletion of L3MBTL1 induces DNA damage and slows cell cycle progression by arresting cells in the G2/M phase. L3MBTL1 interacts with components of the DNA replication machinery (MCM2-7 proteins, Cdc45, and PCNA) and is required for the normal movement of DNA replication forks. These findings suggest that L3MBTL1 influences multiple aspects of DNA replication and repair.

The methylation status of H4K20 is important in DNA replication and DDR pathways (18). SUV4-20 methyltransferase catalyzes the di- and trimethylation of H4K20, and Suv4-20 knockout mice, which can only form the H4K20me1 derivative, are more sensitive to DNA damage than wild-type mice (23). Loss of Pr-Set7, a histone methyltransferase that monomethylates lysine 20 on histone H4, induces DNA damage in human, mouse, and *Drosophila* cells. Pr-Set7 has also been implicated in DNA replication (24–29). We previously established that L3MBTL1 binds to mono-

and dimethylated H4K20, and interacts directly with PR-Set7. The binding of L3MBTL1 to chromatin occurs during S phase, coincidental with the appearance of H4K20me1, suggesting that it binds to the mark to exert its effects (8). Depletion of L3MBTL1 resulted in a marked increase in H4K20me2 levels (Fig. 3D), possibly by allowing dimethylation of H4K20 by Suv4-20 histone methyltransferase. The biological effects observed following depletion of L3MBTL1 closely parallel those resulting from the loss of Pr-Set7, suggesting that the ability of L3MBTL1 to recognize and bind to the H4K20me1 mark produced by Pr-Set7 plays an important role in maintaining genomic stability.

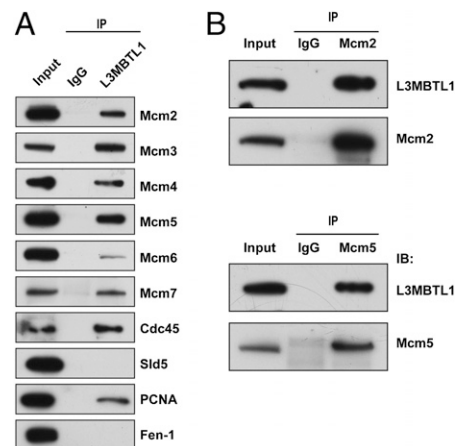


Fig. 5. L3MBTL1 interacts with components of the DNA replication machinery. (A) HA-L3MBTL1 was overexpressed in 293T cells, and cell lysates were immunoprecipitated and immunoblotted with the HA or rabbit IgG antibodies. (B) Flag-L3MBTL1 was overexpressed in 293T cells, and cell lysates were immunoprecipitated with antibodies against Mcm2, Mcm5, or rabbit IgG. Following SDS/PAGE separation, gels were immunoblotted with Flag antibody to detect L3MBTL1. The immunoprecipitation of Mcm2 and Mcm5 proteins was verified by immunoblotting with the corresponding antibodies, using rabbit IgG as a control.

At present, it is unclear how L3MBTL1 contributes to genomic stability and influences fork progression. Its role in fork progression may relate to its function in maintaining genomic stability, as L3MBTL1 depletion triggers the DDR, which leads to checkpoint activation and a halt in replication. Recently, Qin et al. (30) found that loss of L3MBTL1 in mice does not alter H4K20 methylation or result in tumor formation. Differences between the Qin et al. study (30) and ours may reflect the effects caused by the acute loss of L3MBTL1 vs. its chronic absence in the knockout mice, where functional compensation by another L3MBTL1 family member could occur. Furthermore, H4K20 methylation levels may be controlled differently in ES cells than in the normal, human diploid fibroblasts that we have studied. As oncogenesis is a multistep process, it seems highly likely that additional molecular events are needed to induce tumorigenesis.

Interactions between L3MBTL1 and Cdc45 and MCM2-7 suggest that L3MBTL1 may have a more direct role in DNA replication; however, further studies will be required to define the functional significance of these interactions and to determine whether the position of L3MBTL1 is within or external to nucleosomes, because nucleosome deposition occurs behind the fork on newly synthesized DNA. L3MBTL1 may also prevent the conversion of the H4K20me1 mark to H4K20me2 by Suv4-20, as we detected an increase in H4K20me2 in cells depleted of L3MBTL1. Though L3MBTL1 is degraded during mitosis (8), depletion of L3MBTL1 before the G2/M transition leads to the generation of the H4K20me2, which recruits 53BP1, thereby promoting the DDR and hindering normal replication. Normally, Suv4-20 acts during the M and G1 phases to convert H4K20me1 to H4K20me2 (31). This methylation step may occur primarily in the absence of chromatin-bound L3MBTL1. Consistent with this notion, we found that L3MBTL1 depletion slowed replication fork progression and increased the formation of 53BP1 foci. Whether removal of L3MBTL1 from the H4K20me1 mark is required for the DDR, by triggering the H4K20me2 generation and subsequent binding of 53BP1, will require further investigation.

DNA damage and genomic instability promote oncogenesis (32), and tumor samples isolated from patients at diagnosis often show constitutive activation of DNA damage signaling (10, 11). This DDR activation is most prominent in early, preinvasive stages of a diverse group of cancers. Overexpression of activated oncogenes, such as c-myc, H-Ras, Cdc25A, cyclin E1, and E2F1, in multiple cell types leads to a strong DDR activation (10, 33–35) and recapitulates the findings seen in precancerous lesions. This phenomenon is also relevant to hematopoietic malignancies, as both the PML-RAR α and AML1-ETO leukemia-associated fusion proteins trigger the DDR in normal hematopoietic cells (36). Mechanistic studies implicate oncogene-induced DNA replication stress, including replication fork collapse and formation of double-stranded breaks, as the stimulus that evokes the DDR response (12), and in the case of c-myc, the induction of DNA damage was shown to result from its direct involvement in DNA replication (37). Although this response acts as a barrier against oncogene-induced transformation, acquired mutations in DNA-damage checkpoint proteins, such as p53 or ATM, could permit cells with damaged DNA to slip through the checkpoints and progress to a full-blown cancer (38).

We have shown that the depletion of L3MBTL1, a candidate tumor suppressor gene, leads to the activation of the DDR. Failure to correct DNA damage caused by the loss of L3MBTL1 could lead to genomic instability and the development of a myeloid malignancy. Indeed, we detected an increased number of specific breaks, gaps, and exchanges in metaphase chromosome spreads of L3MBTL1 knockdown cells (Fig. S5). Drosophila L3MBTL1 was found to be part of the Myb/E2F2/RBF complex, which has roles in both transcription and replication (18, 39), and human L3MBTL1 is also found in similar complexes (7). Moreover, Lin-61, the *Caenorhabditis elegans* homolog of L3MBTL1, has been implicated in maintaining genomic integrity (40, 41). These observations suggest that the role of L3MBTL1 in DNA replication and genome stability may be evolutionary conserved,

implying that the loss of L3MBTL1 contributes to the development of 20q12 hematopoietic malignancies by causing DNA damage and genomic instability.

Materials and Methods

Lentiviral and Retroviral Transduction. Lentiviral shRNA constructs were purchased from the TRC shRNA library at Thermo Scientific Open Biosystems and modified by subcloning the GFP gene instead of the puromycin gene into the pLKO.1 vector as a marker of viral integration. shRNA sequences against L3MBTL1 were gcctgcactttgatgggtatt (shRNA 1), gctggagctatgctatgatt (shRNA 2), and gcagtcactcacaacaagaat (shRNA 3). shRNA with scrambled sequences in the same vector was used as a negative control. To produce lentiviruses, 293T cells were transfected with the shRNA constructs and helper plasmids (the envelope construct pMD2G and the packaging construct psPAX2) using the calcium phosphate method. To produce the retroviruses for the overexpression assays, Phoenix-A cells were transfected with either HA-tagged L3MBTL1 or empty MIGR1 vector construct. Lentiviruses or retroviruses were harvested by collecting and filtering supernatants 48 and 72 h after transfection, and concentrated by centrifugation at 4 °C for 2 h at 25,000 rpm in a Beckman L7-55 Ultracentrifuge. Target cells were infected with concentrated virus in the presence of 8 μ g/mL polybrene by centrifugation at 450 \times g for 45 min.

Cell Cycle Analysis by Flow Cytometry. Cells were collected by trypsinization and fixed in 70% ethanol. They were washed with PBS, stained with 50 μ g/mL propidium iodide and 0.5 μ g/mL RNase A (both from Sigma-Aldrich), and analyzed by flow cytometry. For BrdU/propidium iodide staining, cells were incubated with 1 mM BrdU for 1 h and then stained with BrdU-APC antibody and propidium iodide, according to the instructions in the BrdU Flow Kit (BD Biosciences). Minimally, 10⁵ cells were analyzed on the BD FACSCalibur flow cytometer, and the data were collected using BD Cell Quest Pro software and analyzed using FlowJo software (Tree Star).

Immunoblotting and Coimmunoprecipitations. U2OS cells were lysed in lysis buffer [20 mM Tris-HCl (pH 8), 0.5% Nonidet P40, 0.5% Tween 20, 1 mM EDTA, 1 mM DTT, 150 mM NaCl, 1 mM PMSF and protease inhibitor mixture (Calbiochem)], and then briefly sonicated and centrifuged. The protein concentration was measured using the Bradford assay (Bio-Rad), and equal amounts of protein were loaded on NuPage gels (Invitrogen). Protein transfer was conducted onto Immobilon-P PVDF membrane (Millipore), and the membranes immunoblotted with antibodies to the following proteins: phospho-Ser-317 Chk1, phospho-Ser354 Chk1, phospho-Thr68 Chk2, phospho-Tyr15 Cdc2, p53 (all from Cell Signaling), actin, Rad51, p21, geminin (all from Santa Cruz), α -tubulin (Sigma Aldrich), γ H2A.x (Biolegend), H4K20me1, H4K20me3, H3 (all from Millipore). The anti-L3MBTL1 antibody was described previously (6). For coimmunoprecipitations, whole-cell extracts were prepared from 293T cells overexpressing HA-tagged L3MBTL1 using the same lysis buffer as above. The lysates for coimmunoprecipitations were treated with 1,000 units/mL of benzonase (Sigma Aldrich) overnight at 4 °C to degrade DNA and RNA. They were also treated with 50 μ g/mL ethidium bromide to disrupt DNA-protein complexes and exclude DNA-mediated protein-protein interactions (42). The lysates were incubated overnight at 4 °C with HA-agarose beads (Roche) or normal rat IgG serum (Santa Cruz) followed by protein A agarose beads (Roche). The coimmunoprecipitates were washed four times with lysis buffer containing 250 mM NaCl before immunoblotting for the following proteins: MCM2-7 (all from Bethyl Laboratories), PCNA (Millipore), Cdc45, Fen-1, Sld5 (all from Santa Cruz). For reciprocal coimmunoprecipitation, Flag-tagged L3MBTL1 was overexpressed in 293T cells, and lysates treated as above were immunoprecipitated with antibodies against Mcm2, Mcm5, or rabbit IgG, followed by adsorption to protein A agarose beads.

Quantitative RT-PCR. U2OS cells were harvested and RNA prepared by RNeasy Plus Mini Kit (Qiagen); cDNA was synthesized using SuperScript III RT-PCR kit (Invitrogen). Quantitative PCR was conducted on an ABI7500 Real-Time PCR system using SYBR Green PCR mix (both from Applied Biosystems) and primers corresponding to the genes of interest. Primer sequences are available upon request.

Comet Assay. DNA breaks were measured using the Comet Assay Reagent Kit (Trevigen) with minor modifications. Briefly, cells embedded in low-melting point agarose on a slide were lysed, treated with alkali, and electrophoresed in 1 \times TBE buffer for 40 min at 1 V/cm, stained with propidium iodide, and imaged under the fluorescent microscope. To evaluate the extent of DNA damage present in each sample, the average tail moment (a product of

percent DNA in tail and tail length) of 100 cells was calculated using Cometscore software (Tritek).

Immunocytochemistry. Cells were plated on coverslips, then fixed in methanol, permeabilized with 0.25% Triton-X/PBS, blocked in 2% FBS/PBS, and incubated with primary antibody for 1 h, followed by secondary antibody conjugated with a fluorescent probe for 30 min, both at room temperature. Cells were stained with DAPI, mounted onto coverslips in mounting medium (Vector Labs), and imaged on Leica Upright confocal microscope or Carl Zeiss fluorescent microscope using appropriate filters. The primary antibodies used were directed against γ H2A.x (Millipore), 53BP1 (Novus Biologicals), and phospho-Ser1981 ATM (Cell Signaling), and secondary antibodies used were anti-rabbit Alexa488 and anti-mouse Alexa568 (both from Invitrogen). Quantitation of the DNA damage foci was determined by scoring foci of at least 100 cells per treatment used.

DNA Fiber Analyses. Control and L3MBTL1 knockdown U2OS and MRC5 cells were sequentially labeled with 50- μ M IdU and 250- μ M CldU for 1 h each. DNA fiber spreads were prepared as described previously with some modifications (43). Briefly, three aliquots of cells were resuspended in PBS at 1×10^6 cells/mL, spotted onto a microscope slide, and lysed with 15 μ L of spreading buffer [0.5% SDS in 200 mM Tris-HCl (pH 7.4), 50 mM EDTA]. After 6 min, slides were tilted 15° to allow lysates to slowly move down the slide, and the resulting DNA spreads were air-dried, fixed in 3:1 methanol/acetic acid, and stored at 4 °C overnight.

- Dewald GW, Schad CR, Lilla VC, Jalal SM (1993) Frequency and photographs of HGM11 chromosome anomalies in bone marrow samples from 3,996 patients with malignant hematologic neoplasms. *Cancer Genet Cytogenet* 68:60–69.
- Gateff E, Löffler T, Wismar J (1993) A temperature-sensitive brain tumor suppressor mutation of *Drosophila melanogaster*: Developmental studies and molecular localization of the gene. *Mech Dev* 41:15–31.
- Northcott PA, et al. (2009) Multiple recurrent genetic events converge on control of histone lysine methylation in medulloblastoma. *Nat Genet* 41:465–472.
- Wang WK, et al. (2003) Malignant brain tumor repeats: A three-leaved propeller architecture with ligand/peptide binding pockets. *Structure* 11:775–789.
- Min J, et al. (2007) L3MBTL1 recognition of mono- and dimethylated histones. *Nat Struct Mol Biol* 14:1229–1230.
- Bocconi P, MacGrogan D, Scandura JM, Nimer SD (2003) The human L(3)MBT polycomb group protein is a transcriptional repressor and interacts physically and functionally with TEL (ETV6). *J Biol Chem* 278:15412–15420.
- Trojer P, et al. (2007) L3MBTL1, a histone-methylation-dependent chromatin lock. *Cell* 129:915–928.
- Kalakonda N, et al. (2008) Histone H4 lysine 20 monomethylation promotes transcriptional repression by L3MBTL1. *Oncogene* 27:4293–4304.
- Paulsen RD, Cimprich KA (2007) The ATR pathway: Fine-tuning the fork. *DNA Repair (Amst)* 6:953–966.
- Bartkova J, et al. (2005) DNA damage response as a candidate anti-cancer barrier in early human tumorigenesis. *Nature* 434:864–870.
- Gorgoulis VG, et al. (2005) Activation of the DNA damage checkpoint and genomic instability in human precancerous lesions. *Nature* 434:907–913.
- Halazonetis TD, Gorgoulis VG, Bartek J (2008) An oncogene-induced DNA damage model for cancer development. *Science* 319:1352–1355.
- Foster ER, Downs JA (2005) Histone H2A phosphorylation in DNA double-strand break repair. *FEBS J* 272:3231–3240.
- Schultz LB, Chehab NH, Malikzay A, Halazonetis TD (2000) p53 binding protein 1 (53BP1) is an early participant in the cellular response to DNA double-strand breaks. *J Cell Biol* 151:1381–1390.
- Liao W, McNutt MA, Zhu WG (2009) The comet assay: A sensitive method for detecting DNA damage in individual cells. *Methods* 48:46–53.
- Shih Y (2003) ATM and related protein kinases: Safeguarding genome integrity. *Nat Rev Cancer* 3:155–168.
- Norbury C, Blow J, Nurse P (1991) Regulatory phosphorylation of the p34cdc2 protein kinase in vertebrates. *EMBO J* 10:3321–3329.
- Yang H, Mizzen CA (2009) The multiple facets of histone H4-lysine 20 methylation. *Biochem Cell Biol* 87:151–161.
- Lewis PW, et al. (2004) Identification of a *Drosophila* Myb-E2F2/RBF transcriptional repressor complex. *Genes Dev* 18:2929–2940.
- Lu J, Ruhf ML, Perrimon N, Leder P (2007) A genome-wide RNA interference screen identifies putative chromatin regulators essential for E2F repression. *Proc Natl Acad Sci USA* 104:9381–9386.
- Moyer SE, Lewis PW, Botchan MR (2006) Isolation of the Cdc45/Mcm2-7/GINS (CMG) complex, a candidate for the eukaryotic DNA replication fork helicase. *Proc Natl Acad Sci USA* 103:10236–10241.
- Gambus A, et al. (2006) GINS maintains association of Cdc45 with MCM in replisome progression complexes at eukaryotic DNA replication forks. *Nat Cell Biol* 8:358–366.
- Schotta G, et al. (2008) A chromatin-wide transition to H4K20 monomethylation impairs genome integrity and programmed DNA rearrangements in the mouse. *Genes Dev* 22:2048–2061.
- Jörgensen S, et al. (2007) The histone methyltransferase SET8 is required for S-phase progression. *J Cell Biol* 179:1337–1345.
- Tardat M, Murr R, Herceg Z, Sardet C, Julien E (2007) PR-Set7-dependent lysine methylation ensures genome replication and stability through S phase. *J Cell Biol* 179:1413–1426.
- Sakaguchi A, Steward R (2007) Aberrant monomethylation of histone H4 lysine 20 activates the DNA damage checkpoint in *Drosophila melanogaster*. *J Cell Biol* 176:155–162.
- Oda H, et al. (2009) Monomethylation of histone H4-lysine 20 is involved in chromosome structure and stability and is essential for mouse development. *Mol Cell Biol* 29:2278–2295.
- Huen MS, Sy SM, van Deursen JM, Chen J (2008) Direct interaction between SET8 and proliferating cell nuclear antigen couples H4-K20 methylation with DNA replication. *J Biol Chem* 283:11073–11077.
- Houston SI, et al. (2008) Catalytic function of the PR-Set7 histone H4 lysine 20 monomethyltransferase is essential for mitotic entry and genomic stability. *J Biol Chem* 283:19478–19488.
- Qin J, et al. (2010) Chromatin protein L3MBTL1 is dispensable for development and tumor suppression in mice. *J Biol Chem* 285:27767–27775.
- Pesavento JJ, Yang H, Kelleher NL, Mizzen CA (2008) Certain and progressive methylation of histone H4 at lysine 20 during the cell cycle. *Mol Cell Biol* 28:468–486.
- Luo J, Solimini NL, Elledge SJ (2009) Principles of cancer therapy: Oncogene and non-oncogene addiction. *Cell* 136:823–837.
- Denko NC, Giaccia AJ, Stringer JR, Stambrook PJ (1994) The human Ha-ras oncogene induces genomic instability in murine fibroblasts within one cell cycle. *Proc Natl Acad Sci USA* 91:5124–5128.
- Bartkova J, et al. (2006) Oncogene-induced senescence is part of the tumorigenesis barrier imposed by DNA damage checkpoints. *Nature* 444:633–637.
- Di Micco R, et al. (2006) Oncogene-induced senescence is a DNA damage response triggered by DNA hyper-replication. *Nature* 444:638–642.
- Viale A, et al. (2009) Cell-cycle restriction limits DNA damage and maintains self-renewal of leukaemia stem cells. *Nature* 457:51–56.
- Dominguez-Sola D, et al. (2007) Non-transcriptional control of DNA replication by c-Myc. *Nature* 448:445–451.
- Bartek J, Bartkova J, Lukas J (2007) DNA damage signalling guards against activated oncogenes and tumour progression. *Oncogene* 26:7773–7779.
- Beall EL, et al. (2002) Role for a *Drosophila* Myb-containing protein complex in site-specific DNA replication. *Nature* 420:833–837.
- Pothof J, et al. (2003) Identification of genes that protect the *C. elegans* genome against mutations by genome-wide RNAi. *Genes Dev* 17:443–448.
- Harrison MM, Lu X, Horvitz HR (2007) LIN-61, one of two *Caenorhabditis elegans* malignant-brain-tumor-repeat-containing proteins, acts with the DRM and NuRD-like protein complexes in vulval development but not in certain other biological processes. *Genetics* 176:255–271.
- Méndez J, Stillman B (2000) Chromatin association of human origin recognition complex, cdc6, and minichromosome maintenance proteins during the cell cycle: Assembly of prereplication complexes in late mitosis. *Mol Cell Biol* 20:8602–8612.
- Jackson DA, Pombo A (1998) Replicon clusters are stable units of chromosome structure: Evidence that nuclear organization contributes to the efficient activation and propagation of S phase in human cells. *J Cell Biol* 140:1285–1295.

L3MBTL1 Deficiency Directs the Differentiation of Human Embryonic Stem Cells Toward Trophectoderm

Ruben Hoya-Arias,¹ Mark Tomishima,² Fabiana Perna,¹ Francesca Voza,¹ and Stephen D. Nimer¹

Human embryonic stem cells (hESCs) can be used to study the early events in human development and, hopefully, to understand how to differentiate human pluripotent cells for clinical use. To define how L3MBTL1, a chromatin-associated polycomb group protein with transcriptional repressive activities, regulates early events in embryonic cell differentiation, we created hESC lines that constitutively express shRNAs directed against L3MBTL1. The L3MBTL1 knockdown (KD) hESCs maintained normal morphology, proliferation, cell cycle kinetics, cell surface markers, and karyotype after 40 passages. However, under conditions that promote spontaneous differentiation, the L3MBTL1 KD cells differentiated into a relatively homogeneous population of large, flat trophoblast-like cells, unlike the multilineage differentiation seen with the control cells. The differentiated L3MBTL1 KD cells expressed numerous trophoblast markers and secreted placental hormones. Although the L3MBTL1 KD cells could be induced to differentiate into various embryonic lineages, they adopted an exclusive trophoblast fate during spontaneous differentiation. Our data demonstrate that depletion of L3MBTL1 does not affect hESC self-renewal, rather it enhances differentiation toward extra-embryonic trophoblast tissues.

Introduction

HUMAN EMBRYONIC STEM CELLS (hESCs) are derived from the inner cell mass of early preimplantation blastocysts; they self-renew and are pluripotent. They can be maintained in an undifferentiated state, but can also be induced to differentiate into cell types characteristic of all 3 germ layers and of extra-embryonic tissues, offering the potential to model aspects of mammalian development and disease. Indeed, progress made over the past decade has determined that directing hESCs toward specific cell fates requires similar kinetics and signaling pathways as those required during development [1].

The trophoblast is an essential extra-embryonic tissue that arises from pluripotent trophoctoderm (TE) during mammalian development. Interplay between transcriptional, epigenetic, and physiological factors governs TE cell fate. Several transcription factors including Cdx2, Tead4, Eomes, Gata3, Elf5, Ets2, and Tcfap2c are involved in TE lineage specification and its further expansion [2–8]. Differential epigenetic modifications including DNA methylation [9] and the distribution of histone modifications and their modifying enzymatic complexes [10–13] contribute to lineage identity in the early embryo by regulating the appropriate gene expression profiles. Because in vitro cell fate decisions are similar to those made during development in vivo, hESCs

can be exploited to reveal critical aspects of human development.

The *Drosophila* lethal 3 malignant brain tumor protein, D-l(3)mbt, functions as a tumor suppressor in the larval brain [14]. The gene encoding its human homolog, L3MBTL1, is located on chromosome 20q12, within a region commonly deleted in myeloid malignancies [15], suggesting that it may also function as a tumor suppressor in mammals. L3MBTL1 functions as a transcriptional repressor [16] and chromatin compactor [17]; in vitro biochemical studies have shown that the L3MBTL1 MBT domains can compact nucleosomal arrays dependent on the mono- or dimethylation of histone H4K20 and H1bK26 [17,18]. We have recently demonstrated that L3MBTL1 depletion enhances the differentiation of hematopoietic stem cells toward the erythroid lineage [19], and its depletion from differentiated, malignant cell lines causes replicative stress, DNA breaks, activation of the DNA damage response, and genomic instability [20].

We hypothesized that as a chromatin-associated protein with repressor properties, changes in the level of L3MBTL1 activity could alter the chromatin structure and influence the ability of hESCs to either self-renew or commit to differentiation. To test this hypothesis, we generated and characterized 2 independent and stable clones of L3MBTL1-depleted hESCs, using a lentiviral vector system to express short hairpin RNAs (shRNAs) directed against L3MBTL1 mRNA.

¹Molecular Pharmacology and Chemistry Program and ²SKI Stem Cell Research Facility, Sloan-Kettering Institute, Memorial Sloan-Kettering Cancer Center, New York, New York.

Although the self-renewal properties of L3MBTL1 knock-down (KD) hESCs were retained, we observed striking morphological changes when L3MBTL1 KD hESCs spontaneously differentiated and established that they spontaneously differentiate into trophoblast-like cells. L3MBTL1 appears to be an important regulator of early cell fate decisions during mammalian development.

Materials and Methods

shRNA design and cloning

The design and cloning of shRNAs into the H1P-Hygro/EGFP lentiviral plasmid was done essentially as previously described [21]. RNA sequences were selected using the Dharmacon SMARTselection design software. Forward and reverse oligonucleotides were resuspended at a concentration of 5 μ M, heated to 95°C for 5 min, and allowed to cool to RT overnight. After annealing, the duplexes were cloned into *SmaI/XbaI* sites of an H1P shRNA cassette. The sequences targeted by the shRNAs are as follows: L3MBTL1 shRNA1: 5'-GTAGTGAGTTGTAGATAAAA-3'; L3MBTL1 shRNA2: 5'-GTGGAATCATTGACAGAAA-3'; luciferase control shRNA: 5'-CCCGGAAAGACGATGACGG-3'.

Cell culture and differentiation protocols

hESC line H9 (WA-09) cells were cultured on a feeder layer of mouse embryonic fibroblast (MEFs), purchased from GlobalStem, and plated on gelatin-coated tissue culture plates. ES cells were maintained in an undifferentiated state in human ES (HES) media (DMEM:F12; Invitrogen) supplemented with 20% knockdown serum replacement (Invitrogen), 1% nonessential amino acids (Invitrogen), 0.1 mmol/L 2-mercaptoethanol (Invitrogen), 1 mmol/L L-glutamine (Invitrogen), and 6 ng/mL FGF2 (R&D Systems). Cells were passaged using Dispase (neural protease; Worthington Bioscience).

Spontaneous differentiation was induced by plating control and L3MBTL1KD cells in feeder-free conditions on Matrigel (BD Bioscience)-coated dishes in HES medium without FGF2 for 2 weeks; cells were fed daily. The day on which the cells were seeded was defined as day 1.

Embryoid bodies (EBs) were generated by culturing control and L3MBTL1 KD cells in low-cell-binding dishes for 14 days with the same medium used in spontaneous differentiation. EBs were collected by gravity and fed every other day.

The directed differentiation to trophoblast was achieved by culturing the cells on Matrigel-coated dishes in HES medium in the presence of exogenous BMP4 (100 ng/mL), as previously described [22]. Differentiation toward neuroectoderm was performed using a published protocol [23]. Briefly, control and L3MBTL1 KD cells were cocultured on MS-5 stroma cells and fed with KSR medium supplemented with SB431542 (10 μ M/mL) and dorsomorphin (600 nM/mL) during the first 7 days; then cells were fed only with KSR medium until day 14.

Production of stable L3MBTL1-deficient embryonic stem cell lines

The H1P-HygroEGFP plasmid expressing shRNA against L3MBTL1 was cotransfected with plasmids pMD2.G and

psPAX2 into 293T cells to make lentiviral particles. Virus-containing media was collected, filtered, and concentrated by ultracentrifugation. Viral titers were measured by serial dilution on 293T cells followed by flow cytometry analysis after 48 h. For transduction, lentiviral vectors were added to H9 cells maintained without feeders on Matrigel-coated plates. To select clones, colonies were treated with Accutase (Innovative CT/ISC Bioexpress) for 30 min at 37°C, leaving a single-cell suspension. The Accutase was neutralized with 3 volumes of HES medium and the cells were resuspended by pipetting before being filtered using a 70- μ m nylon filter (Falcon, BD Bioscience). The cells were centrifuged and washed 2 \times with HES media and then 2 \times in ice-cold PBS with 1% BSA. The pelleted cells were resuspended in 100 μ L ice-cold PBS with 1% BSA supplemented with 10 μ M Y27632 (ROCK inhibitor purchased from Calbiochem). GFP-positive cells were sorted using a BD FACSAria cell sorter (BD Bioscience) and resuspended in HES media with 10 μ M Y27632 and penicillin/streptomycin 1,000 U/mL and replated on MEF feeders. Y27632 and penicillin/streptomycin were maintained in the medium until the first colonies appeared. Several clones for each shRNA construct were selected and quantitative polymerase chain reaction (qPCR) analysis was performed to ascertain viral copy number and the efficiency of L3MBTL1 knockdown.

Reverse transcriptase and real time polymerase chain reaction

Total RNA was isolated from undifferentiated and differentiated hESCs growing as monolayers using the RNeasy[®] Plus Kit (Qiagen). cDNA was synthesized from 1 μ g total RNA using Moloney murine leukemia virus RT (Promega) in 1 \times transcription buffer containing 0.5 μ mol/L oligo dT (Promega) and 400 μ mol/L deoxyribonucleotides (dNTPs). Reverse transcriptase (RT) qPCR was performed with the ABI 7500 real-time PCR system with SYBR green (ABI) and 200 nM of forward and reverse primers. A standard curve was generated for each primer pair, and genes of interest were assigned a relative expression value interpolated from the standard curve using the threshold cycle (Ct). Gene expression was normalized against the level of GAPDH expression. All reactions were done in duplicate, and at least 4 technical and 2 biological replicates were performed. PCR primer sequences are shown in Table 1 and Supplementary Table S1.

Immunofluorescence

Cultured cells were washed twice with PBS before being fixed in 4% paraformaldehyde at room temperature. Cells were washed 3 times with PBS before permeabilization with wash buffer (0.3% Triton X-100 and 1.0% bovine serum albumin in PBS) for at least 5 min. The primary antibody (diluted in wash buffer) was added to the cells for 2 h at room temperature, and then the cells were washed 3 times in wash buffer before the addition of the secondary antibody (diluted in wash buffer) for 1 h at room temperature. The cells were washed 3 times with PBS and stored at 4°C. The primary antibodies OCT-3/4 (4 μ g/mL; sc-5279), HAND1 (0.4 μ g/mL; Ab11846), and L3MBTL1 (1:50 dilution) previously described [16] were detected using the appropriate secondary

TABLE 1. LIST OF OLIGONUCLEOTIDES USED IN REVERSE TRANSCRIPTASE qPCR

Gene	Forward	Reverse
L3MBTL1	AGAGGAAGCGCAGGGAATA	CACGACCAGCATTCTTCTT
OCT4	CCTCCAGCAGATGCAAGAA	ATTGGAAGGTTCCAGTCG
NANOG	CCTCCAGCAGATGCAAGAA	ATTGGAAGGTTCCAGTCG
CDX2	GTCTTTTTTCTCTCCCTTCCC	CAACAACACAAACTCCCC
SOX2	ACCAGCGCATGGACAGTTA	ATGTAGGTCTGCGAGCTG GT
AFP	CTTCCAAACAAAGGCAGCA	ATGTACATGGGCCACATCC
SOX1	ATGCACCGCTACGACATGG	CTCATGTAGCCCTGCGAGTTG
ACTC1	CCCTGGAGAAGAGCTATGAAC	GGAAGGTAGATGGAGAGAGAA G
CGB	GTGGAGAAGGAGGGCTGC	GGCGGCAGAGTGCACATT
HAND1	TGCCTGAGAAAAGAGAACCAG	ATGGCAGGATGAACAAACAC
KRT 7	TGAATGATGAGATCAACTTCTCAG	GCAGTCCCAGATCTCCGACA
KRT 8	GATCGCCACCTACAGGAAGCT	ACTCATGTTCTGCATCCCAGACT
GCM1	GAGCCTGGAGACCGAGAAC	TGCGAAGATCTGAGCCC
PAX6	CGGAGTGAATCAGCTCGGTG	CCGCTTATACTGGGCTATTTTGC
GAPDH	GGTCGGAGTCAACGGATT	CCCCACTTGATTTTGGAG

l3mbtl1, l(3)mbt-like 1 (*Drosophila*); OCT4, POU class 5 homeobox 1; NANOG, nanog homeobox; CDX2, caudal type homeobox 2; SOX2, SRY (sex-determining region Y)-box 2; AFP, alpha-fetoprotein; SOX1, SRY (sex-determining region Y)-box 1; ACTC1actin, alpha, cardiac muscle 1; GCB, chorionic gonadotropin, beta polypeptide; HAND1, heart and neural crest derivatives expressed 1; KRT7/8, keratin 7/8; GCM1, glial cells missing homolog 1; PAX6, paired box 6; GAPDH, glyceraldehyde-3-phosphate dehydrogenase.

antibodies conjugated with Alexa Fluor 546 (Molecular Probes). Negative controls consisted of no primary antibody, no secondary antibody, or the appropriate IgG isotype control as indicated. DAPI counterstaining was performed on fixed cells to visualize all cellular nuclei.

Western blot analysis

Total cellular protein extracts were prepared using RIPA buffer (SIGMA R0278) supplemented with Halt Protease Inhibitor Cocktail (Thermo Scientific 78430) according to the manufacturer's instructions. Nuclear and cytoplasmic extracts were prepared using the PIERCE kit (78833) for subcellular fractionation; 40 µg of protein extracts were electrophoresed on a 4–12% denaturing gel and electroblotted onto a nitrocellulose membrane. The membrane was incubated with different antibodies at 4°C overnight and then incubated with the indicated secondary antibodies at room temperature for 1 h. The Pierce Enhanced Chemiluminescence kit was used to detect antibody reactivity, according to the manufacturer's instructions.

Cell cycle/DNA and flow cytometry analysis

To analyze DNA content, control and L3MBTL1 KD ES cells were cultured on Matrigel-coated tissue culture-treated dishes, harvested by trypsinization, washed with PBS, and fixed in 70% EtOH at 4°C. The cells were washed with PBS, resuspended in propidium iodide solution (5 µg/mL) containing 10 mg/mL RNase, mixed, and incubated 45 min at 37°C. Flow cytometric data were acquired on a BD FACSCalibur (BD Biosciences) using CellQuest Pro version 6.0. Propidium iodide was excited by the 488 nm laser and fluorescence emission was measured in fluorescence parameter 3 (FL3) with the standard 670LP filter. Doublets were excluded by gating out high FL3-W (width) cells. Single cells were analyzed for percentages of G1/G0, S, and G2/M in MultiCycle AV (Innovative Cell Technologies).

Detection of trophoblast marker HLA-G in L3MBTL1 KD spontaneously differentiated cells was performed by immunostaining with an APC-labeled anti-human HLA-G (eBioscience 17-9957 clone 87G) using 0.125 µg/sample; 7-AAD (5 µg/mL) staining served to exclude dead cells from subsequent analysis. For each sample, 5×10^4 cells were analyzed on a FACS Calibur flow cytometer (BD Biosciences) using CELLQuest (BD Biosciences); data analysis was performed using the FlowJo software (Tree Stars, Inc.).

Immunoassays

Media were collected from growing cells and stored at –20°C until assay. Chorionic gonadotropin (CG-β) and progesterone levels were measured using ELISA kits, as indicated by the manufacturer (Calbiotech).

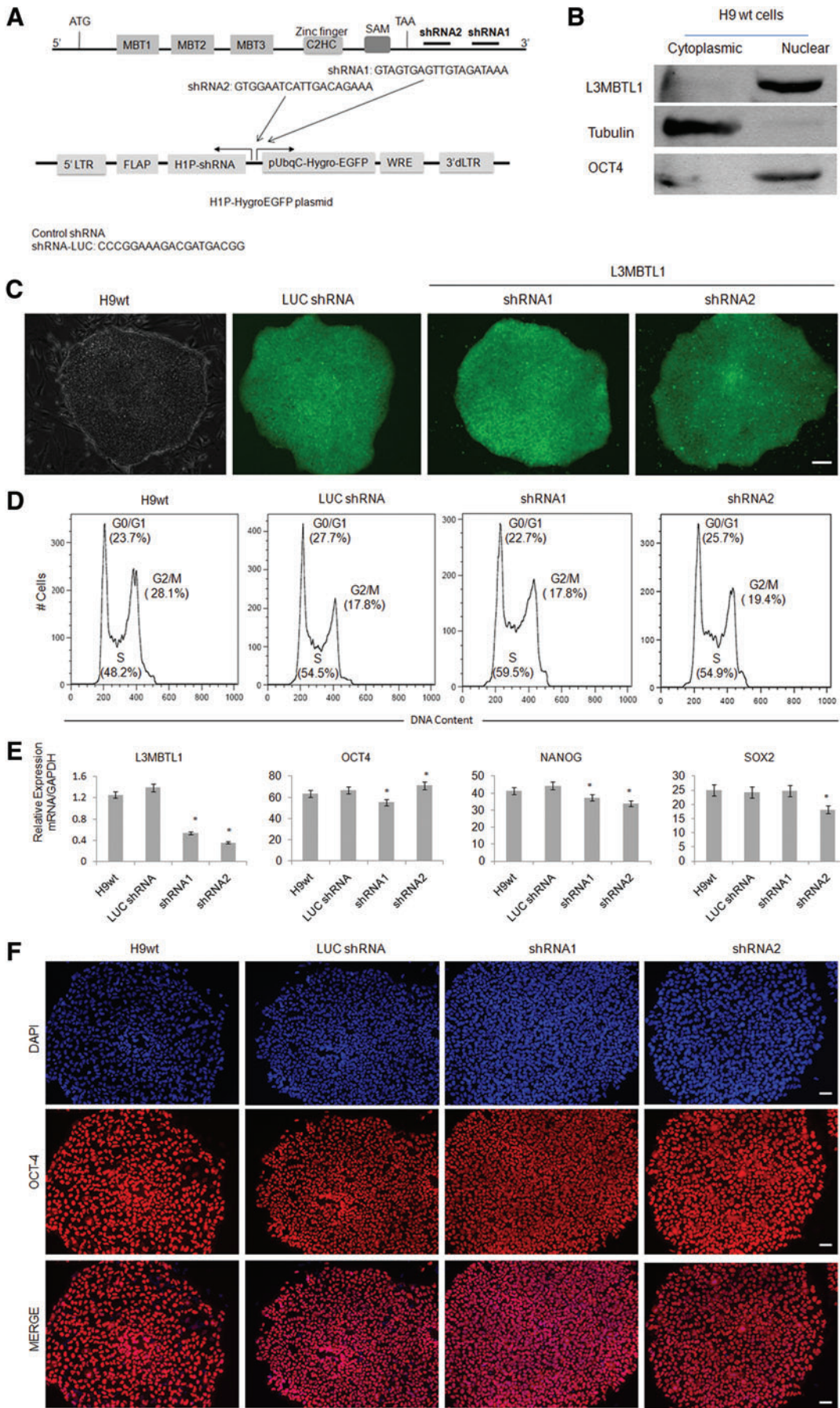
Statistical analysis

Data were analyzed using PRISM Version 5.04 (GraphPad Software, Inc.). Sample comparison was performed using 1-way analysis of variance (ANOVA) followed by a post-hoc Tukey test or 2-way ANOVA followed by a post-hoc Bonferroni test, with the level of significance set at $P < 0.05$.

Results

L3MBTL1 knockdown does not affect embryonic stem cell renewal

We initially screened 10 different shRNAs that target L3MBTL1 using K562 cells (data not shown) and used the 4 most efficient shRNAs to transduce H9 hESCs. Ultimately, 2 shRNAs were used (shRNA1 and shRNA2) (Fig. 1A) that most consistently knocked down L3MBTL1 in H9 cells compared with the H9 cells expressing a nontargeting, luciferase-specific hairpin (LUC shRNA) and the parental H9 cell line. Overall, 11 L3MBTL1 KD ES cell clones were generated. Western blot (Fig. 1B) and immunofluorescence analysis (Supplementary Fig. S1; Supplementary Data are



available online at www.liebertonline.com/scd) confirm the nuclear localization of L3MBTL1 in ES cells. The L3MBTL1 KD hESCs showed normal colony morphology (Fig. 1C), normal cell cycle kinetics (Fig. 1D), an unchanged pattern of cell surface markers, and a normal karyotype in prolonged culture (data not shown) when cultured under normal hESC growth conditions. We obtained an ~70% reduction in L3MBTL1 mRNA levels (using either shRNA1 or shRNA2) and observed a small decrease in the levels of the pluripotency-promoting OCT-4, NANOG, and SOX2 transcription factor mRNAs (Fig. 1E). Immunofluorescence analysis confirmed the normal expression and localization of OCT-4 protein in all cell lines (Fig. 1F). Thus, L3MBTL1 depletion does not detectably affect the undifferentiated state of hESCs.

L3MBTL1 knockdown impairs embryonic cell production during spontaneous differentiation

To determine whether loss of L3MBTL1 affects differentiation, we withdrew FGF2 from HES media and grew the hESCs under either adherent or nonadherent conditions, inducing their spontaneous differentiation. hESCs were maintained for 2 weeks under adherent culture conditions as colonies, using Matrigel-coated dishes. Depletion of L3MBTL1 had clear morphological consequences, as all 11 clones derived from the shRNA1- or shRNA2-expressing hESCs generated differentiated colonies composed of large, flat mononucleated cells by days 7–14. In contrast, the control luciferase knockdown H9 cells and the parental line H9 generated mixed colonies composed of many different cell morphologies (Fig. 2A and data not shown). We also observed morphological consequences in the EBs generated from L3MBTL1 KD cells under nonadherent conditions; in contrast to the control cells, the L3MBTL1 KD cells failed to give rise to typical EB structures containing differentiated cell types. Starting at day 5 of differentiation, the L3MBTL1 KD EBs underwent significant cell death that continued until day 14, indicating defects in differentiation, whereas control cells developed into characteristic EB structures (Fig. 2B). Flow cytometric analysis for Annexin V binding and 7-AAD permeability confirmed an increased cell death in the L3MBTL1 KD cells compared with the control cells at day 7 of differentiation (Fig. 2C).

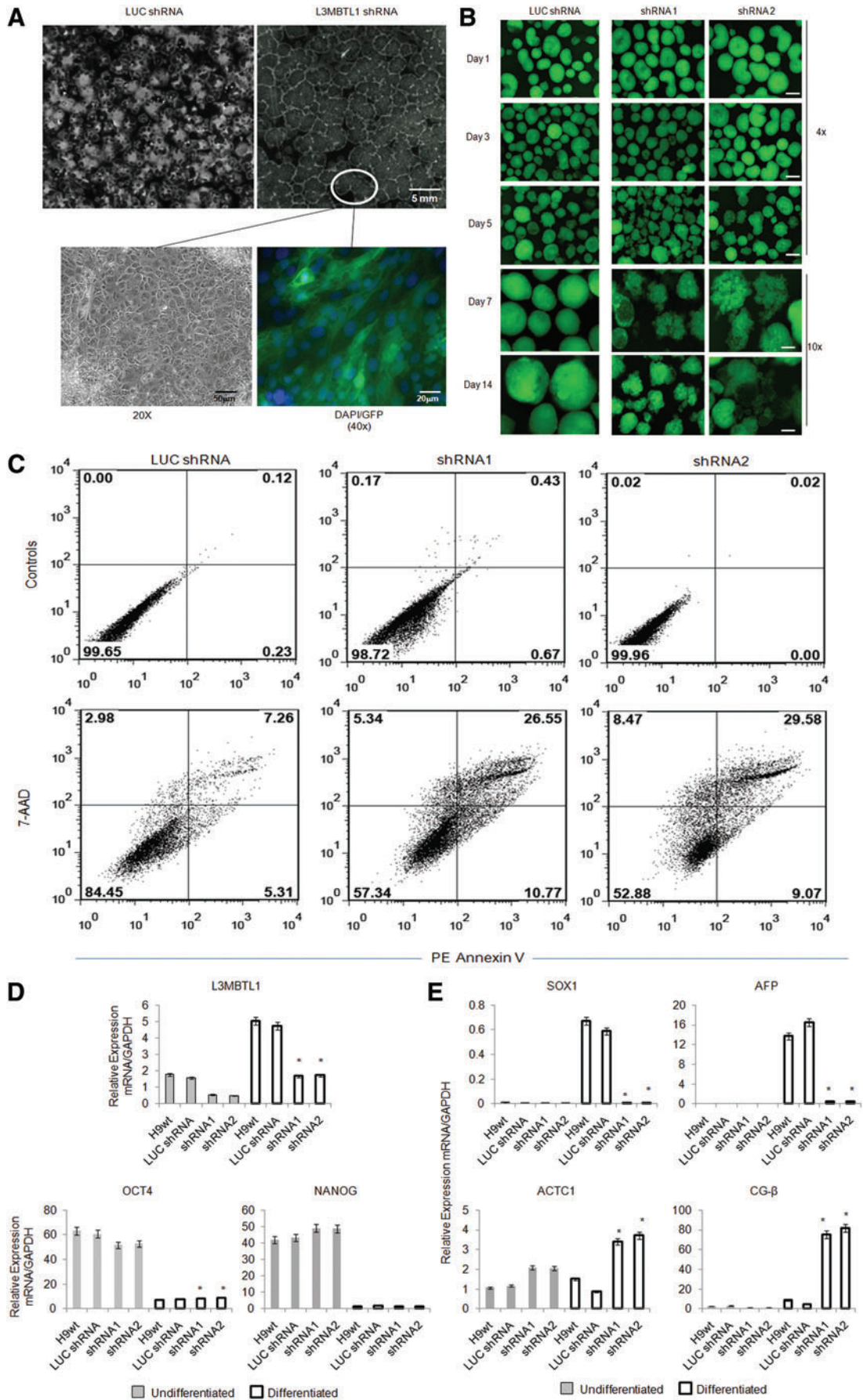
To characterize the differentiation state of the L3MBTL1 KD cells in monolayer cultures, we performed reverse transcriptase qPCR analysis to quantify the expression of a variety of pluripotent and lineage-specific markers. Differentiated control and L3MBTL1 KD cells were evalu-

ated and significant differences were seen. As expected, the pluripotency markers OCT-4 and NANOG were reduced in both the L3MBTL1 KD and the control KD cells compared with the undifferentiated cells (Fig. 2D). Of note, L3MBTL1 levels were upregulated at least 3-fold in the differentiated controls compared with the undifferentiated controls, suggesting a potential role for L3MBTL1 in the earliest stages of differentiation. However, the shRNA constructs continued to suppress L3MBTL1 mRNA levels despite the increased expression that have occurred during normal differentiation (Fig. 2D). Quantification of lineage marker expression shows downregulation of the SOX1 (ectoderm) and AFP (endoderm) markers in the L3MBTL1 KD cells, compared with their increased levels in the differentiated controls. Interestingly, we observed a substantial upregulation in the expression of ACTC1 (mesoderm) and the trophoblast marker chorionic gonadotropin (CG- β) in the L3MBTL1 KD in contrast to the differentiated control cells (Fig. 2E). We also performed reverse transcriptase qPCR analysis to assess the expression of additional lineage markers including NEUROD1, SOX2, MAP2 (ectoderm); HNFA4, FOXA2, PECAM1 (endoderm); and MIXL1, RUNX1, and RUNX2 (mesoderm). These studies confirmed that ectoderm, endoderm, and mesoderm derivatives are severely reduced, and of the mesodermal markers, only RUNX1 was upregulated in the L3MBTL1 KD cells (3-fold) compared with the differentiated control cells (Supplementary Fig. S2). Consistent with this finding, RUNX1 has been reported to be an L3MBTL1 target gene in K562 cells [24]. These results show that L3MBTL1 KD cells have a bias to differentiate into trophoblast following FGF2 withdrawal, whereas ectoderm and endoderm differentiation appears to be blocked.

L3MBTL1 knockdown promotes differentiation of hESCs toward trophoblast

The flat cell morphology (Fig. 2A) and the greater than 18-fold upregulation of CG- β in the differentiated L3MBTL1 KD cells (Fig. 2E) led us to examine the expression of other trophoblast markers, including CDX2 [25–27], HAND1 [28–31], KRT7, KRT8, and GCM1 [22,27,31–34]. CDX2 mRNA upregulation parallels the appearance of morphological changes in spontaneously differentiated L3MBTL1 KD cells by days 6–7, reaching a peak on day 9; in contrast, HAND1, KRT7, KRT8, and GCM1 mRNAs peak at day 14. The expression pattern of these markers further indicates that L3MBTL1 KD cells primarily differentiate into trophoblast cells (Fig. 3A, B). We have confirmed that HAND1 protein is

FIG. 1. Characterization of undifferentiated control and L3MBTL1 knockdown (KD) human embryonic stem cells. (A) Schematic representation of L3MBTL1 gene showing the location for the short hairpin (shRNA) sequences cloned into the H1P-HygroEGFP lentiviral plasmid. (B) Western blot of cytoplasmic and nuclear fractions from H9 parental cells shows nuclear location of L3MBTL1. Oct4 (nuclear) and tubulin (cytoplasmic) were used as controls. (C) Microscopic images showing the undifferentiated stage for the wt parental, LUC shRNA, L3MBTL1-shRNA1, and shRNA2 H9 cells based on their expression of GFP. Whole colonies were imaged on an Olympus epifluorescence system under a 10 \times objective. Scale bar represents 100 μ m. (D) Cell cycle analysis of undifferentiated control and L3MBTL1KD ES cells. Relative DNA content, assessed by PI staining, shows the proportion of cells in the G1, G2, and S phases. A representative example of 3 independent experiments is shown. (E) Reverse transcriptase qPCR analysis comparing the level of L3MBTL1, OCT-4, NANOG, and SOX2 mRNA expression in control and L3MBTL1-depleted cells. Statistical analysis was performed by 1-way ANOVA and Tukey posttest ($*P < 0.05$). Error bars represent the standard deviation ($n = 3$). (F) Fluorescent microscopy images of OCT-4 with a DAPI DNA counterstain using the Olympus epifluorescence system under a 20 \times objective. Scale bar represents 50 μ m. Color images available online at www.liebertonline.com/scd



expressed in differentiated L3MBTL1 KD cells by immunofluorescence (Fig. 3C) and that more than 80% of the cells analyzed at day 14 of differentiation have trophoctoderm phenotype, as indicated by the expression of HLA-G (Fig. 3D).

To further examine the differentiation of L3MBTL1 KD cells into trophoblasts, we directed control cells toward trophoblasts using BMP4 [22]. We compared the gene expression pattern of the BMP4-treated control (LUC shRNA) cells with the spontaneously differentiated L3MBTL1 KD cells and found similar but higher trophoblast marker expression (CG- β and HAND1) in the BMP4-treated control cells (Fig. 4A). Of note, L3MBTL1 expression decreased at least 4-fold in the control cells treated with BMP4 compared with untreated LUC shRNA control, which is also consistent with the notion that downregulation of L3MBTL1 allows trophoblast formation to proceed in hESCs (Figs. 2D and 4A). To further investigate the role of BMP signaling, we measured the level of phosphorylated SMAD proteins (SMAD 1/5/8) during the spontaneous differentiation of the LUC shRNA and L3MBTL1 KD cells. We found an increased level of phospho-SMAD 1/5/8 in differentiated L3MBTL1 KD cells compared with the control cells (Fig. 4B). We also measured the secretion of the placental hormones CG- β and progesterone into the medium from spontaneously differentiated L3MBTL1 KD cells and also the untreated and BMP4-treated controls. L3MBTL1 KD and BMP4-treated control cells show a continuous increase in the concentration of both hormones, with the hormone secretion by the knockdown cells being nearly as high as from the BMP4-treated control (Fig. 4C). These results show that L3MBTL1 KD cells differentiate into functional trophoblast cells, which indicates the role of L3MBTL1 in regulating the spontaneous differentiation of embryonic derivatives.

Directed differentiation is not impaired in L3MBTL1 KD cells

L3MBTL1 KD cells did not express ectoderm markers under conditions that allow spontaneous differentiation (Fig. 2D). However, to determine whether directed differentiation was affected in L3MBTL1 KD cells, we induced neural differentiation by coculturing them on MS-5 stromal cells for 2 weeks according to an established protocol [23]. We observed neuronal rosette formation on day 8 with all clones (Fig. 4D, upper panel), demonstrating that L3MBTL1 KD cells can differentiate into neuroectoderm if provided with a suffi-

ciently strong signal. Further, reverse transcriptase qPCR analysis found a similar level of induction of the neuroectodermal markers SOX1 and PAX6 in the knockdown versus the control cell lines (Fig. 4D, lower panel). We also directed the differentiation of L3MBTL1 KD hESC toward hematoendothelial cells (CD31⁺CD34⁺) using a previously reported protocol [35] and found that the KD cells responded to these differentiation signals as well, albeit less efficiently than to the controls (data not shown). These results indicate that L3MBTL1 KD does not impair hESC differentiation toward embryonic neuroectoderm or hematoendothelial cells when potent differentiation-promoting signals are provided.

Discussion

Undifferentiated ES cells generally contain more permissive chromatin with higher levels of activating marks (lysine acetylation) and lower levels of repressive marks (H3 lysine K9 and K27 methylation), whereas differentiated ES cells generally display silenced chromatin structure [36]. One of the great challenges in human stem cell biology is to understand the mechanisms that selectively silence certain gene-rich regions of the genome, to allow the production of the full range of cell types found in the adult. Compacted chromatin is generally found during differentiation, but very little is known about the individual proteins that differentially silence genes and affect the outcome of differentiation.

In this study, we found that knocking down the epigenetic “reader” L3MBTL1 strongly influences the differentiation potential of hESCs toward trophoctoderm under conditions wherein spontaneous differentiation occurs, without affecting hESC self-renewal in the undifferentiated state. L3MBTL1 KD hESCs can be cultured continuously with no noticeable changes in their behavior, morphology, or cell cycle status and only minor changes in the RNA levels of the pluripotency markers OCT-4, NANOG, or SOX2 (Fig. 1C–E), which suggests that L3MBTL1 does not play a critical role in maintaining the undifferentiated status or self-renewal potential of hESCs.

Nonetheless, L3MBTL1 KD clearly impaired the developmental potential of hESCs in spontaneous differentiation assays. Withdrawal of FGF2 triggered profound changes in the differentiated L3MBTL1 KD cells under adherent conditions with loss of ectoderm, endoderm, and mesoderm marker expression; this implies that L3MBTL1 KD cells have limited pluripotency. The differentiated L3MBTL1 KD cells

FIG. 2. Morphological changes of spontaneously differentiated control and L3MBTL1 KD cells. **(A)** Photographs showing the morphological contrast between LUC shRNA and L3MBTL1 KD cells (*left and right upper row*, respectively); images were acquired using the Gel Doc System Quantity One software (BioRad). Lower row shows a magnified view of the differentiated L3MBTL1 KD cells (*white circle*); black lines show a phase-contrast image (*left*) and a DAPI/GFP fluorescence image (*right*). **(B)** L3MBTL1 KD cells fail to develop proper embryoid bodies. Fluorescent microscopic images showing EB derivation based on GFP expression for the LUC shRNA, shRNA1, and shRNA2 cell lines. Scale bars: 0.2 mm (4 \times); 100 μ m (10 \times). Representative images of 3 independent experiments are shown. **(C)** Flow cytometry assay shows increasing cell death for the differentiated L3MBTL1 KD EB cells. Top plots show unstained control and L3MBTL1 KD EB cells and bottom plots show PE-Annexin V versus 7-AAD permeability profiles in the same cells. Apoptotic cells on the plots are Annexin V positive and PI negative (*lower right quadrant*), whereas necrotic cells are Annexin V positive and PI positive (*upper right quadrant*). **(D)** Expression of L3MBTL1, OCT-4, and NANOG in undifferentiated and differentiated state measured as relative level of mRNA/GAPDH. **(E)** mRNA expression levels of lineage cell markers SOX1 (ectoderm), AFP (endoderm), ACTC1 (mesoderm), and CG- β (trophoblast) in undifferentiated and differentiated states measured as relative level of mRNA/GAPDH. Statistical analysis was performed by 1-way ANOVA and Tukey posttest ($*P < 0.05$). Error bars represent the standard deviation ($n = 3$). Color images available online at www.liebertonline.com/scd

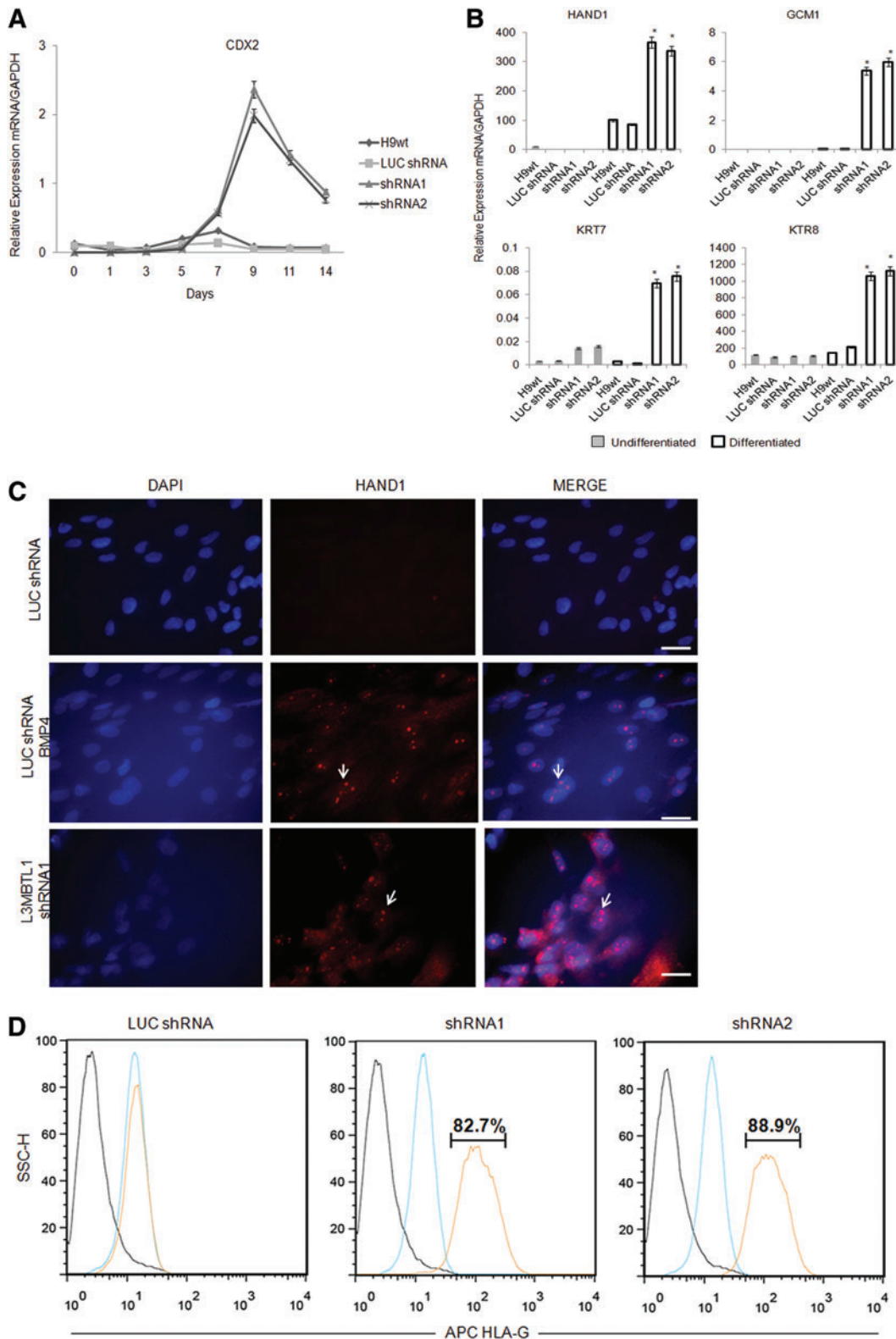


FIG. 3. Reverse transcriptase qPCR analysis for lineage cell markers. **(A)** Relative levels of mRNA expression of trophoblast marker CDX2. Error bars represent the standard deviation ($n=3$). **(B)** Trophoblast cell markers HAND1, GCM1, KRT7, and KRT8 in undifferentiated and differentiated states measured as relative level of mRNA/GAPDH. Statistical analysis was performed by 1-way ANOVA and Tukey posttest ($*P<0.05$). Error bars represent the standard deviation ($n=3$). **(C)** Immunofluorescent detection of HAND1. *White arrows* indicate the nuclear location of HAND1 protein. Microscopy performed with Olympus epifluorescence system under a $40\times$ objective. Scale bar represents $50\ \mu\text{m}$. Representative images of 3 independent experiments are shown. **(D)** FACS analysis shows the percentage of spontaneously differentiated control and L3MBTL1 shRNA1 and shRNA2 cells expressing the trophodermal (TE) marker HLA-G (red). Isotype control antibody staining is shown (black). Undifferentiated LUC shRNA and L3MBTL1 KD cells were used as negative controls for HLA-G staining (blue). Color images available online at www.liebertonline.com/scd

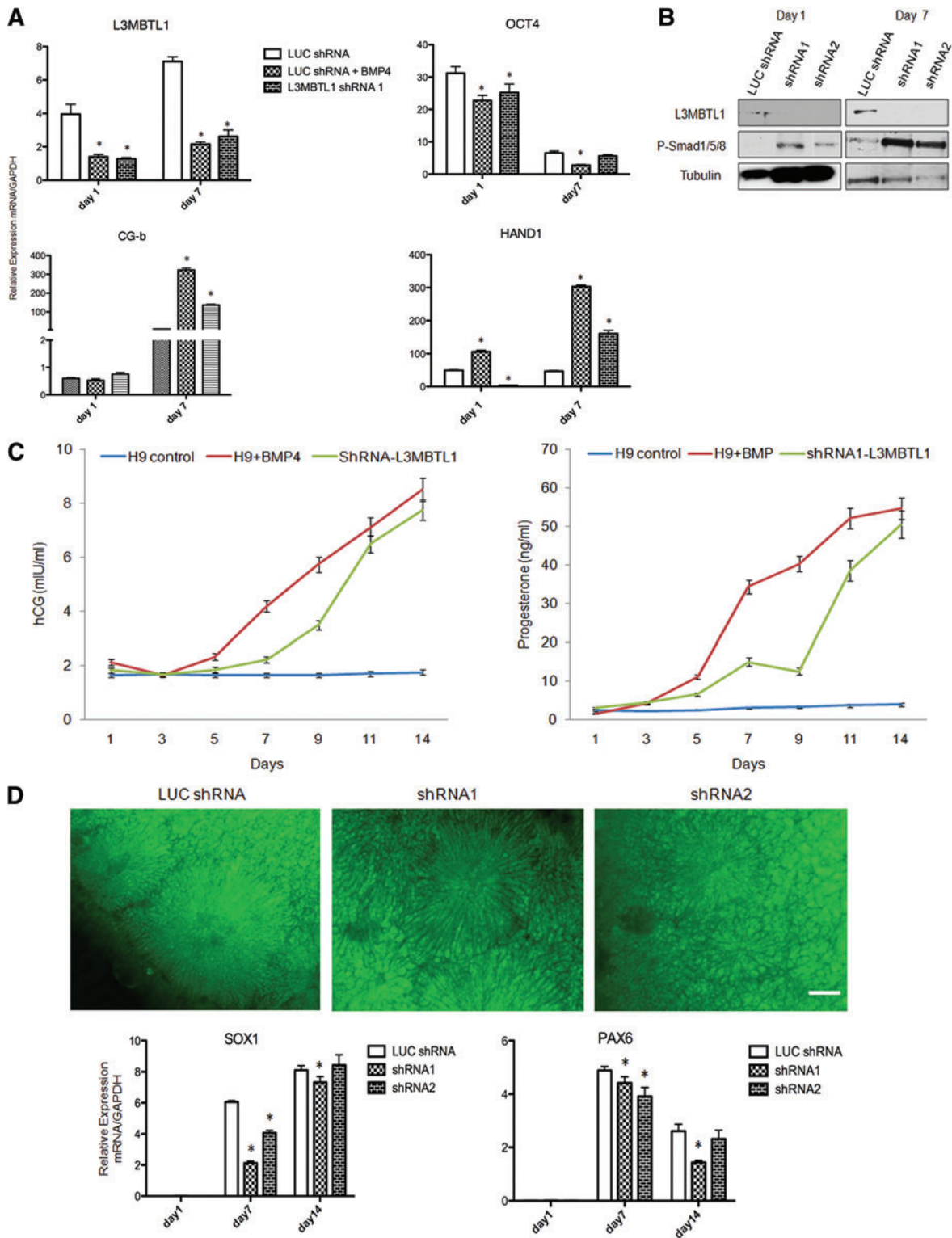


FIG. 4. L3MBTL1 knockdown mimics trophoblast differentiation induced by BMP4. Luciferase control with or without BMP4 and L3MBTL1 KD cells were cultured for 7 days. **(A)** Reverse transcriptase qPCR analysis for L3MBTL1, OCT-4, CG- β , and HAND1 mRNA expression. Statistical analysis was by 2-way ANOVA and Bonferroni posttest ($*P < 0.05$). Error bars represent the standard deviation ($n = 3$). **(B)** Phosphorylation of SMADS1/5/8 was examined by Western blot analysis in the homogenates of undifferentiated (day 1) and spontaneously differentiated (day 7) control LUC shRNA and L3MBTL1-KD cells. **(C)** Immunoassay for placental hormones CG- β and progesterone. Error bars represent the standard deviation ($n = 3$). **(D)** L3MBTL1 KD cells differentiate under defined conditions. Fluorescence images of typical neuronal rosette structures at day 9 of directed neuroectoderm differentiation for control LUC shRNA and L3MBTL1 KD cell lines (upper panel) are shown. Scale bar represents 50 μ m. Representative images of 3 independent experiments are shown. Reverse transcriptase qPCR analysis results for neuroectoderm markers SOX-1 and PAX6 mRNA expression (bottom panel) are also shown. Statistical analysis was performed by 2-way ANOVA and Bonferroni posttest ($*P < 0.05$). Error bars represent the standard deviation ($n = 3$). Color images available online at www.liebertonline.com/scd

do express trophoblast markers (Figs. 2E and 3B, D), and in fact, the increased expression of CDX2 is consistent with the L3MBTL1 KD cells being restricted to a trophoblast fate (Fig. 3A) [37]. Cdx2 acts early in the lineage hierarchy and its overexpression triggers embryonic stem cells to differentiate into trophoblast stem cells [26,27]. Overall, these changes could explain the failure of these cells to form typical EB structures in nonadherent assays. It is also possible that genomic instability during EB development could explain the increased cell death seen in L3MBTL1 KD cells (Fig. 2B, C), as we recently reported [20]. In contrast, the differentiated control cells maintained expression of embryonic lineage markers, and consistent with their upregulation of L3MBTL1, the expression of trophoblast markers was absent.

The production of extra-embryonic trophoblast cells from the L3MBTL1 KD cells resembles the effect of BMP4 on hESCs [22]. BMP4 directs hESCs toward trophoblast with increased SMAD 1/5/8 phosphorylation, CG- β secretion, and HAND1 expression, which occurs concomitantly with a marked decrease in L3MBTL1 expression (Fig. 4A, B). Both the BMP4-stimulated hESCs and the L3MBTL1 KD cells secrete placental hormones, demonstrating that knockdown of L3MBTL1 drives hESCs to become trophoblast-like cells (Fig. 4C). The lack of other embryonic cell types derived from L3MBTL1KD cells is not absolute, as L3MBTL1 KD cells can still form neural tissue and hematoendothelial cells in response to strong inductive signals. This suggests that L3MBTL1 may promote the retention of pluripotency of hESCs, at least in part by blocking trophoblast differentiation.

Thus, L3MBTL1 may play a role in the earliest cell fate decisions involved in human development, most likely by repressing genes involved in trophoblast differentiation. Such a phenotype was recently described for Mbd3, a component of the Mi-2/NURD repressor complex [38]. L3MBTL1 may promote chromatin compaction via its recognition of mono- and dimethylated states of H4K20 by L3MBTL1 [17,18] or by recruiting additional chromatin remodelers to block the trophoblast differentiation of hESCs. In *Drosophila*, dl(3)MBT has been shown to bind histone H4 K20 monomethyl in close association with the dRPD3 histone deacetylase, resulting in deacetylation of histone H4 K5/K12 [39]. However, we found that L3MBTL1 can repress gene expression in an HDAC-independent fashion [16]. L3MBTL1 could be a central component of a repressive complex that loses its function after L3MBTL1 KD. It is likely that multiple chromatin regulators control the differentiation process. For instance, the histone methyltransferase SETDB1 was recently shown to repress trophoblast differentiation of mouse ESCs via H3K9 methylation [40]. The degree of histone H4K20 methylation is dynamically regulated during hESC differentiation. Mass spectrometry (MS) studies have revealed that a large percentage of histone H4 is dimethylated in undifferentiated hESCs (~65%) with some unmethylated (~20%) and some monomethylated (~10%) or trimethylated (~5%) residues. Following TPA treatment, unmethylated lysines are largely converted to dimethyllysines, and electron transfer dissociation-MS experiments have identified histone H4 K20 as the target of both methylation events [41]. Mice deficient for Suv4-20 h1/2, a H4K20 methyltransferase, display loss of di- and trimethyl H4K20 with consequent embryonic lethality [42]. ESCs have a poised epigenetic state that maintains chromatin in a structure ready for quick cell fate decisions

[10]. The inner cell mass and trophoblast possess different gene expression profiles. Consequently, their epigenetic profiles should also differ. We have not seen noticeable differences in the level of HP1 γ , which binds L3MBTL1, or in H3K9 trimethylation, a heterochromatin mark recognized by HP1 γ , between the spontaneously differentiated trophoblast cells and the induced neuroectoderm cells (Supplementary Fig. S3A). Nonetheless, epigenetic disturbance during the early events of differentiation may be a consequence of knocking down L3MBTL1, explaining the lineage selectivity of hESCs toward the trophoblast fate.

In summary, L3MBTL1 KD hESCs proliferate normally in the undifferentiated state, but are impaired in their ability to spontaneously differentiate toward embryonic tissues, and preferentially differentiate into trophoblast tissue (Supplementary Fig. S3B). Further studies are required to establish the molecular basis of the lineage selectivity that occurs after L3MBTL1 knockdown.

Summary

To define how L3MBTL1, a chromatin-associated polycomb group protein with transcriptional repressive activities, regulates early events in embryonic cell differentiation, we created hESC lines that constitutively express shRNAs directed against L3MBTL1. Although the L3MBTL1 KD cells could be induced to differentiate into embryonic neuroectoderm, they adopted an exclusive trophoblast fate during spontaneous differentiation. The data suggest that L3MBTL1 depletion does not affect hESC self-renewal but impacts pluripotency; depletion of L3MBTL1 directs hESC differentiation toward extra-embryonic tissues, rather than embryo-derived tissues.

Acknowledgments

This work was supported by grants from The Starr Foundation and NIH (R01 grant CA102202 to S.D.N.) and by Lymphoma Research Foundation.

Author Disclosure Statement

The authors declare that no conflicts of interest exist.

References

1. Keller G. (2005). Embryonic stem cell differentiation: emergence of a new era in biology and medicine. *Genes Dev* 19:1129–1155.
2. Auman HJ, T Nottoli, O Lakiza, Q Winger, S Donaldson and T Williams. (2002). Transcription factor AP-2gamma is essential in the extra-embryonic lineages for early post-implantation development. *Development* 129:2733–2747.
3. Donnison M, A Beaton, HW Davey, R Broadhurst, P L'Huillier and PL Pfeffer. (2005). Loss of the extraembryonic ectoderm in Elf5 mutants leads to defects in embryonic patterning. *Development* 132:2299–2308.
4. Ralston A, BJ Cox, N Nishioka, H Sasaki, E Chea, P Rugg-Gunn, G Guo, P Robson, JS Draper and J Rossant. Gata3 regulates trophoblast development downstream of Tead4 and in parallel to Cdx2. *Development* 137:395–403.
5. Russ AP, S Wattler, WH Colledge, SA Aparicio, MB Carlton, JJ Pearce, SC Barton, MA Surani, K Ryan, MC Nehls, V Wilson and MJ Evans. (2000). Eomesodermin is required for

- mouse trophoblast development and mesoderm formation. *Nature* 404:95–99.
6. Strumpf D, CA Mao, Y Yamanaka, A Ralston, K Chawengsaksophak, F Beck and J Rossant. (2005). *Cdx2* is required for correct cell fate specification and differentiation of trophoctoderm in the mouse blastocyst. *Development* 132:2093–2102.
 7. Yagi R, MJ Kohn, I Karavanova, KJ Kaneko, D Vullhorst, ML DePamphilis and A Buonanno. (2007). Transcription factor TEAD4 specifies the trophoctoderm lineage at the beginning of mammalian development. *Development* 134:3827–3836.
 8. Yamamoto H, ML Flannery, S Kupriyanov, J Pearce, SR McKercher, GW Henkel, RA Maki, Z Werb and RG Oshima. (1998). Defective trophoblast function in mice with a targeted mutation of *Ets2*. *Genes Dev* 12:1315–1326.
 9. Christophersen NS and K Helin. Epigenetic control of embryonic stem cell fate. *J Exp Med* 207:2287–2295.
 10. Bernstein BE, TS Mikkelsen, X Xie, M Kamal, DJ Huebert, J Cuff, B Fry, A Meissner, M Wernig, K Plath, R Jaenisch, A Wagschal, R Feil, SL Schreiber and ES Lander. (2006). A bivalent chromatin structure marks key developmental genes in embryonic stem cells. *Cell* 125:315–326.
 11. Peters AH, D O'Carroll, H Scherthan, K Mechtler, S Sauer, C Schofer, K Weipoltshammer, M Pagani, M Lachner, A Kohlmaier, S Opravil, M Doyle, M Sibilia and T Jenuwein. (2001). Loss of the *Suv39h* histone methyltransferases impairs mammalian heterochromatin and genome stability. *Cell* 107:323–337.
 12. Pasini D, AP Bracken, MR Jensen, E Lazzarini Denchi and K Helin. (2004). *Suz12* is essential for mouse development and for *EZH2* histone methyltransferase activity. *EMBO J* 23:4061–4071.
 13. Torres-Padilla ME, DE Parfitt, T Kouzarides and M Zernicka-Goetz. (2007). Histone arginine methylation regulates pluripotency in the early mouse embryo. *Nature* 445:214–218.
 14. Wismar J, T Loffler, N Habtemichael, O Vef, M Geissen, R Zirwes, W Altmeyer, H Sass and E Gateff. (1995). The *Drosophila melanogaster* tumor suppressor gene *lethal(3)-malignant brain tumor* encodes a proline-rich protein with a novel zinc finger. *Mech Dev* 53:141–154.
 15. Nimer SD. (2008). Myelodysplastic syndromes. *Blood* 111:4841–4851.
 16. Bocconi P, D MacGrogan, JM Scandura and SD Nimer. (2003). The human *L(3)MBT* polycomb group protein is a transcriptional repressor and interacts physically and functionally with *TEL* (*ETV6*). *J Biol Chem* 278:15412–15420.
 17. Trojer P, G Li, RJ Sims 3rd, A Vaquero, N Kalakonda, P Bocconi, D Lee, H Erdjument-Bromage, P Tempst, SD Nimer, YH Wang and D Reinberg. (2007). *L3MBTL1*, a histone-methylation-dependent chromatin lock. *Cell* 129:915–928.
 18. Kalakonda N, W Fischle, P Bocconi, N Gurvich, R Hoya-Arias, X Zhao, Y Miyata, D Macgrogan, J Zhang, JK Sims, JC Rice and SD Nimer. (2008). Histone H4 lysine 20 monomethylation promotes transcriptional repression by *L3MBTL1*. *Oncogene* 27:4293–4304.
 19. Perna F, N Gurvich, R Hoya-Arias, O Abdel-Wahab, RL Levine, T Asai, F Voza, S Menendez, L Wang, F Liu, X Zhao and SD Nimer. Depletion of *L3MBTL1* promotes the erythroid differentiation of human hematopoietic progenitor cells: possible role in 20q- polycythemia vera. *Blood* 116:2812–2821.
 20. Gurvich N, F Perna, A Farina, F Voza, S Menendez, J Hurwitz and SD Nimer. *L3MBTL1* polycomb protein, a candidate tumor suppressor in *del(20q12)* myeloid disorders, is essential for genome stability. *Proc Natl Acad Sci USA* 107:22552–22557.
 21. Ivanova N, R Dobrin, R Lu, I Kotenko, J Levorse, C DeCoste, X Schafer, Y Lun and IR Lemischka. (2006). Dissecting self-renewal in stem cells with RNA interference. *Nature* 442:533–538.
 22. Xu RH, X Chen, DS Li, R Li, GC Addicks, C Glennon, TP Zwaka and JA Thomson. (2002). *BMP4* initiates human embryonic stem cell differentiation to trophoblast. *Nat Biotechnol* 20:1261–1264.
 23. Lee H, GA Shamy, Y Elkabetz, CM Schofield, NL Harrision, G Panagiotakos, ND Socci, V Tabar and L Studer. (2007). Directed differentiation and transplantation of human embryonic stem cell-derived motoneurons. *Stem Cells* 25:1931–1939.
 24. Sims JK and JC Rice. (2008). *PR-Set7* establishes a repressive trans-tail histone code that regulates differentiation. *Mol Cell Biol* 28:4459–4468.
 25. Beck F, T Erler, A Russell and R James. (1995). Expression of *Cdx-2* in the mouse embryo and placenta: possible role in patterning of the extra-embryonic membranes. *Dev Dyn* 204:219–227.
 26. Tolkunova E, F Cavaleri, S Eckardt, R Reinbold, LK Christenson, HR Scholer and A Tomilin. (2006). The caudal-related protein *cdx2* promotes trophoblast differentiation of mouse embryonic stem cells. *Stem Cells* 24:139–144.
 27. Niwa H, Y Toyooka, D Shimosato, D Strumpf, K Takahashi, R Yagi and J Rossant. (2005). Interaction between *Oct3/4* and *Cdx2* determines trophoctoderm differentiation. *Cell* 123:917–929.
 28. Riley P, L Anson-Cartwright and JC Cross. (1998). The *Hand1* bHLH transcription factor is essential for placentation and cardiac morphogenesis. *Nat Genet* 18:271–275.
 29. Hemberger M, M Hughes and JC Cross. (2004). Trophoblast stem cells differentiate *in vitro* into invasive trophoblast giant cells. *Dev Biol* 271:362–371.
 30. Martindill DM, CA Risebro, N Smart, M Franco-Viseras Mdel, CO Rosario, CJ Swallow, JW Dennis and PR Riley. (2007). Nucleolar release of *Hand1* acts as a molecular switch to determine cell fate. *Nat Cell Biol* 9:1131–1141.
 31. Scott IC, L Anson-Cartwright, P Riley, D Reda and JC Cross. (2000). The *HAND1* basic helix-loop-helix transcription factor regulates trophoblast differentiation via multiple mechanisms. *Mol Cell Biol* 20:530–541.
 32. Jaquemar D, S Kupriyanov, M Wankell, J Avis, K Benirschke, H Baribault and RG Oshima. (2003). Keratin 8 protection of placental barrier function. *J Cell Biol* 161:749–756.
 33. Simmons DG and JC Cross. (2005). Determinants of trophoblast lineage and cell subtype specification in the mouse placenta. *Dev Biol* 284:12–24.
 34. Mi S, X Lee, X Li, GM Veldman, H Finnerty, L Racie, E LaVallie, XY Tang, P Edouard, S Howes, JC Keith, Jr. and JM McCoy. (2000). Syncytin is a captive retroviral envelope protein involved in human placental morphogenesis. *Nature* 403:785–789.
 35. Vodyanik MA and II Slukvin. (2007). Hematoendothelial differentiation of human embryonic stem cells. *Curr Protoc Cell Biol Chapter 23:Unit 23.6*.
 36. Meshorer E and T Misteli. (2006). Chromatin in pluripotent embryonic stem cells and differentiation. *Nat Rev Mol Cell Biol* 7:540–546.

37. Jedrusik A, DE Parfitt, G Guo, M Skamagki, JB Grabarek, MH Johnson, P Robson and M Zernicka-Goetz. (2008). Role of Cdx2 and cell polarity in cell allocation and specification of trophectoderm and inner cell mass in the mouse embryo. *Genes Dev* 22:2692–2706.
38. Zhu D, J Fang, Y Li and J Zhang. (2009). Mbd3, a component of NuRD/Mi-2 complex, helps maintain pluripotency of mouse embryonic stem cells by repressing trophectoderm differentiation. *PLoS One* 4:e7684.
39. Scharf AN, K Meier, V Seitz, E Kremmer, A Brehm and A Imhof. (2009). Monomethylation of lysine 20 on histone H4 facilitates chromatin maturation. *Mol Cell Biol* 29:57–67.
40. Lohmann F, J Loureiro, H Su, Q Fang, H Lei, T Lewis, Y Yang, M Labow, E Li, T Chen and S Kadam. (2009). KMT1E mediated H3K9 methylation is required for the maintenance of embryonic stem cells by repressing trophectoderm differentiation. *Stem Cells* 28:201–212.
41. Phanstiel D, J Brumbaugh, WT Berggren, K Conard, X Feng, ME Levenstein, GC McAlister, JA Thomson and JJ Coon. (2008). Mass spectrometry identifies and quantifies 74 unique histone H4 isoforms in differentiating human embryonic stem cells. *Proc Natl Acad Sci USA* 105:4093–4098.
42. Schotta G, R Sengupta, S Kubicek, S Malin, M Kauer, E Callen, A Celeste, M Pagani, S Opravil, IA De La Rosa-Velazquez, A Espejo, MT Bedford, A Nussenzweig, M Buslinger and T Jenuwein. (2008). A chromatin-wide transition to H4K20 monomethylation impairs genome integrity and programmed DNA rearrangements in the mouse. *Genes Dev* 22:2048–2061.

Address correspondence to:

Dr. Stephen D. Nimer

Molecular Pharmacology and Chemistry Program

Sloan-Kettering Institute

Memorial Sloan-Kettering Cancer Center

1275 York Avenue, Box 575

New York, NY 10065

E-mail: nimers@mskcc.org

Received for publication September 29, 2010

Accepted after revision February 22, 2011

Prepublished on Liebert Instant Online February 22, 2011

Posterior reversible encephalopathy syndrome (PRES) during induction chemotherapy for acute myeloblastic leukemia (AML)

Giorgia Battipaglia · Simona Avilia · Emanuela Morelli · Ferdinando Caranci · Fabiana Perna · Andrea Camera

Received: 20 October 2011 / Accepted: 28 December 2011 / Published online: 13 January 2012
© Springer-Verlag 2012

Dear Editor,

Posterior reversible encephalopathy syndrome (PRES) is a neurological condition characterized by headache, visual disturbances, seizures, and altered mental status, associated with computed tomography (CT) and magnetic resonance (MR) findings of symmetrical edema mainly in the posterior cerebral areas [1]. Controversy exists on the pathogenesis of PRES, considered to be probably caused by either vasogenic edema due to a loss of the autoregulatory mechanisms of cerebral flow [2, 3] associated with acute blood pressure (BP) increase or by direct endothelial damage.

We report two adult patients with acute myeloblastic leukemia (AML) who developed PRES during induction chemotherapy. The first case was a 22-year-old woman diagnosed with AML associated to multilineage dysplasia. Chemotherapy consisted of daunorubicin, etoposide, and standard dose (100 mg/m²) cytarabine by continuous infusion (c.i.) for 10 days. While the patient was still aplastic, she developed posterior headache, emesis, generalized seizures, and hypertension (BP, 170/100 mmHg). Brain CT showed bilateral hypodense areas due to edema in the temporo-occipito-parietal white matter; MR allowed to define more clearly the extensive and nearly symmetrical hyperintense areas on long TE sequences in cortical and subcortical regions of the temporo-occipito-parietal lobes

of both hemispheres (Fig. 1a). Treatment consisted of diuretics, glycerol, and phenobarbital, and her condition improved in a few days. After 2 weeks, MR showed an improvement of the edema (Fig. 1b). Complete remission was documented on day +50. After the consolidation treatment, the patient relapsed in 4 months, before any attempt to perform autologous stem cell transplant could be made, and died of disease progression.

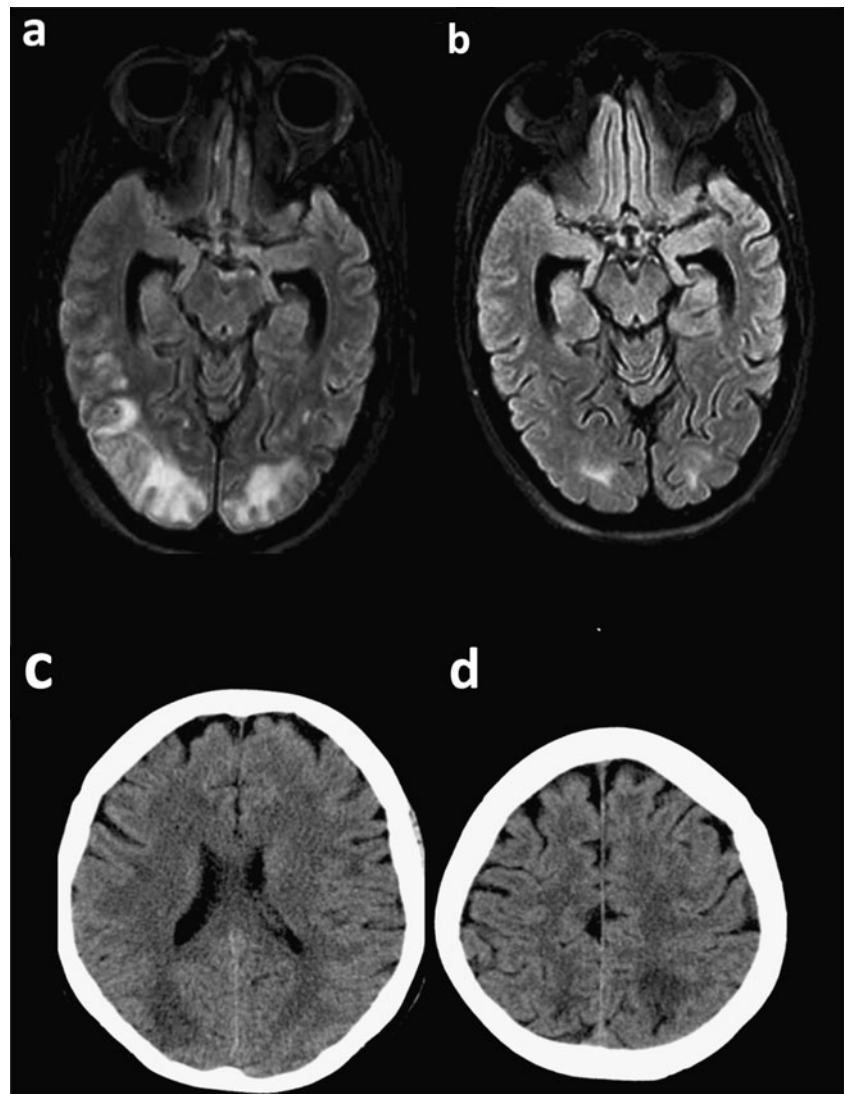
The second patient was a 57-year-old woman suffering from idiopathic hypertension and diagnosed with AML secondary to a 2-year history of myelodysplasia. Cytogenetics showed a complex karyotype. She started chemotherapy with daunorubicin, etoposide, and standard dose cytarabine by c.i. for 7 days. On day +3, blood pressure rapidly increased probably due to fluid overload. On day +8, while in cytopenia, the patient developed septic shock from *E. coli* complicated by SIRS with multiple organ failure, followed shortly after by the onset of neurological symptoms (i.e., confusion, visual disturbances with right hemianopsia, aphasia, left hemiparesis). Brain CT showed cortico-subcortical mildly hypodense areas in both parieto-occipital lobes, predominantly in the right hemisphere, described as an ischemic process (Fig. 1c and d). Despite supportive therapy including diuretics and mannitol, the neurological and clinical conditions rapidly worsened precluding the possibility to perform an MR examination; the patient died within 3 days.

Even if hypertensive encephalopathy, eclampsia, immunosuppressive treatments, and renal failure are the most commonly reported causes of PRES, this syndrome has also been described during cytotoxic treatment for hematological malignancies in the pediatric setting [4–7]. In adults, PRES has been reported in patients with NHL after CHOP or different regimens and, in one patient, with multiple myeloma [8, 9]. This is the first report of PRES in adults with AML,

G. Battipaglia · S. Avilia · E. Morelli · F. Perna · A. Camera (✉)
Department of Biochemistry and Medical Biotechnology,
Federico II University,
via Pansini 5,
80131, Naples, Italy
e-mail: ancamera@unina.it

F. Caranci
Diagnostic Imaging and Radiotherapy, Federico II University,
Naples, Italy

Fig. 1 **a** Case 1: Brain MR imaging (FLAIR sequence), showing hyperintense lesions in the subcortical white matter of the temporo-occipital regions with some cortical involvement consistent with vasogenic edema. **b** Case 1: Follow-up MR image (FLAIR sequence) obtained 2 weeks later, showing almost complete resolution of the lesions. **c, d** Case 2: Non-enhanced CT. Mildly hypodense areas involving both cortical and subcortical matter in the right occipito-parietal region associated to subcortical matter involvement in the left parietal region, with some sulcal effacement



where cytotoxic chemotherapy, BP lability, and sepsis play a key role in the pathogenesis of this neurological syndrome which should be promptly recognized and treated to avoid irreversible damage.

References

- Hinchey J, Chaves C, Appignani B et al (1996) A reversible posterior leukoencephalopathy syndrome. *N Engl J Med* 334:494–500
- Striano P, Striano S, Tortora F et al (2005) Clinical spectrum and critical care management of posterior reversible encephalopathy syndrome (PRES). *Med Sci Monit* 11:549–553
- Javed MA, Sial MSH, Lingawi S et al (2005) Etiology of posterior reversible encephalopathy syndrome (PRES). *Pak J Med Sci* 21:149–154
- Greaves P, Oakervee H, Kon SSC, Jones R, Farah N (2006) Posterior reversible encephalopathy syndrome following anti-lymphocyte globulin treatment for severe aplastic anaemia. *Br J Hematol* 134:251
- Cooney MJ, Bradley WG, Symko SC, Patel ST, Groncy PK (2000) Hypertensive encephalopathy: complication in children treated for myeloproliferative disorders-report of three cases. *Radiology* 214:711–716
- Lucchini G, Grioni D, Colombini A et al (2008) Encephalopathy syndrome in children with hemato-oncological disorders is not always posterior and reversible. *Pediatr Blood Cancer* 51(5):629–633
- Won SC, Kwon SY, Han JW, Choi SY, Lyu CJ (2009) Posterior reversible encephalopathy syndrome in childhood with hematologic/oncologic diseases. *J Pediatr Hematol Oncol* 31(7):505–508
- Edwards MJ, Walker R, Vinnicombe S, Barlow C, MacCallum P, Foran JM (2001) Reversible posterior leukoencephalopathy syndrome following CHOP chemotherapy for diffuse large B-cell lymphoma. *Ann Oncol* 12:1327–1329
- Tam CS, Galanos J, Seymour JF, Pitman AG, Stark RJ, Prince HM (2004) Reversible posterior leukoencephalopathy syndrome complicating cytotoxic chemotherapy for hematologic malignancies. *Am J Hematol* 77:72–76

Aplastic anemia: immunosuppressive therapy in 2010

Antonio M. Risitano, Fabiana Perna

Department of Biochemistry and Medical Biotechnologies, Federico II University of Naples, Naples, Italy

Abstract

Acquired aplastic anemia (AA) is the typical bone marrow failure syndrome characterized by an empty bone marrow; an immune-mediated pathophysiology has been demonstrated by experimental works as well as by clinical observations. Immunosuppressive therapy (IST) is a key treatment strategy for aplastic anemia; since 20 years the standard IST for AA patients has been anti-thymocyte globuline (ATG) plus cyclosporine A (CyA), which results in response rates ranging between 50% and 70%, and even higher overall survival. However, primary and secondary failures after IST remain frequent, and to date all attempts aiming to overcome this problem have been unfruitful. Here we review the state of the art of IST for AA in 2010, focusing on possible strategies to improve current treatments. We also discuss very recent data which question the equality of different ATG preparations, leading to a possible reconsideration of the current standards of care for AA patients.

Introduction

Aplastic anemia (AA) is the most typical example of bone marrow failure, characterized by an empty or fatty bone marrow leading to the subsequent pancytopenia.¹ Recently it has been reported that in some adults AA may be due to inherited abnormalities.² However, idiopathic AA is usually considered an immune-mediated disease.³ According to the most accepted view, self-reactive T cells cause a damage of the hematopoietic stem cells (and possibly of committed progenitors) through a cell-cell interaction (via Fas/Fas-L, granzyme, perforine)⁴ and the production of inhibitory cytokines such as IFN- γ , TNF- α and TGF- β .⁵⁻⁷ The role of T cells was confirmed by the identification, *in vivo*, of oligoclonal T cells,⁸⁻¹⁰ and by the demonstration of their pathogenic role either *in vitro* or *in vivo*.^{10,11} All these findings make the immune system the therapeutic target in AA patients; immunosuppressive (IS) regimens have been largely developed in the past

years, exploiting agents that affect distinct steps of the immune response.

Immunosuppression for aplastic anemia

The standard immunosuppression: anti-thymocyte globuline plus cyclosporine A

Initial observations showed that some AA patients failing donor engraftment following allogeneic stem cell transplantation rescued autologous hematopoiesis¹² and that in other patients treatment with anti-lymphocyte globuline (ALG) resulted beneficial.^{13,14} In fact, the efficacy of immunosuppressive treatment (IST) by ALG was confirmed in a prospective, placebo-controlled, randomized trial, in 1983.¹⁵ In order to improve the response rate and reduce the risk of subsequent relapse, several immunosuppressive agents have been associated to anti-thymocyte globuline (ATG) or ALG (such as corticosteroids,¹⁶ androgens)^{17,18} but cyclosporine A (CyA) only resulted in an increased response rate,¹⁹ with an improved long-term failure-free survival.²⁰ Since the early '90s, ATG + CyA was considered the standard IST for AA patients, with an expected 50-60% probability of response and 60% overall survival at one year.²¹⁻²³

The most recent studies have shown improved overall survival (above 80% at 1 year), regardless of the initial response to IST;²⁴⁻²⁶ likely due to a better supportive care and salvage treatment (mainly SCT). However, treatment-failure remains a major problem after first-line IST. In fact, about one third of AA patients do not respond to their initial IST; in addition, within responders patients, half of them require long-term IS maintenance treatment by CyA to sustain the response. In fact, recent studies showed that CyA-dependency ranges between 25 and 50% of patients and the patients who require long-term CyA treatment present the higher risk to relapse (about 30-50% of responders).²²⁻²⁴ Furthermore, the development of clinical paroxysmal nocturnal hemoglobinuria is seen in about 10% of AA patients after IST;²⁷ clonal evolution to myelodysplastic syndromes (MDS) or acute leukemias (AML) accounts for about 10-15% of treatment-failures,^{24,28} and solid tumors account for an additional 10%.²⁹ Thus, a substantial fraction of AA patients cannot be considered cured by IST, and understanding the underlying causes is necessary to develop salvage strategies.³⁰ While secondary failures suggest a flare-up of the underlying immune process, the causes accounting for primary failures (which occur in one third of patients) may include: i) non-immune pathophysiology (e.g., due to misdiagnosis of hypoplastic MDS, or to inherited forms associated to mutation in telomerase complex genes);³¹ ii) an insufficient delivered IS (in fact, some refractory patients may respond to further IST);³²⁻³⁴

Correspondence: Antonio M. Risitano, Department of Biochemistry and Medical Biotechnologies, Federico II University of Naples, Via Pansini 5, 80131 Naples, Italy.
Tel: +39 081 7462037 - Fax: +39 081 7462165.
E-mail: amrisita@unina.it

Key words: aplastic anemia, immunosuppressive therapy.

Received for publication: 4 May 2011.

Accepted for publication: 4 June 2011.

This work is licensed under a Creative Commons Attribution NonCommercial 3.0 License (CC BY-NC 3.0).

©Copyright A.M. Risitano and F. Perna, 2011
Licensee PAGEPress, Italy
Pediatric Reports 2011; 3(s2):e7
doi:10.4081/pr.2011.s2.e7

iii) a third explanation is the exhaustion of the hematopoietic stem cells, which would hamper any hematological recovery regardless the control of the pathogenic immune-attack. This latter hypothesis seems supported by the recent data showing that baseline telomere length is the most powerful predictor of long-term survival in AA patients receiving IST.³⁵ In fact, shorter telomeres were associated with increased relapse rate and clonal evolution (including monosomy 7), suggesting that they are a reliable marker for functional hematopoietic stem cell damage (possibly linked to the replicative stress of residual cells). If confirmed, these data will provide an informative tool to identify AA patients who may benefit from an early transplant strategy rather than IST.

Improving standard ATG-based immunosuppression: additional or alternative IS agents

To improve the results obtained with the standard ATG + CyA, several investigators tried to deliver an intensified IS by adding a third IS agent, possibly with a distinct (hopefully synergistic) mechanism of action. However, this strategy did not result in a substantial benefit. The purine synthesis inhibitor mycophenolate mofetil (MMF) was tested in a prospective study conducted at NIH, but did not result in either increased response (62% at 6 months) or decreased relapse (37%, despite maintenance therapy with MMF) in comparison to historical data.³⁶ The mammalian target of rapamycin (mTOR) inhibitor rapamycin/sirolimus (RAPA)³⁷ was also tested in a randomized trial conducted at NIH; the addition of RAPA to the standard ATG + CyA resulted in a response rate of 51%, which was comparable to that of the control arm (ATG + CyA, 62%), with similar relapse and survival rates.³⁸

Some investigators developed different strategies of IST, with the aim of retaining (or possibly increasing) a marked IS activity, ideally with a better toxicity profile. They used lymphocyte depleting agents other than ATG, such as cyclophosphamide (CTX) or alemtuzumab. High-dose CTX (50 mg/kg intravenously on 4 consecutive days) was mainly tested at the Johns Hopkins University; the initial results were excellent, with a response rate of about 70% (even if the time-to-response appeared delayed in comparison to that expected with ATG).³⁹ This single-center experience continues to show interesting results, with the most recent follow up reporting 44 naïve AA patients showing response rate, overall survival and event free survival of 88%, 71% (the majority complete) and 58%, respectively.⁴⁰ However, most investigators do not consider CTX as a feasible treatment option for AA patients, based on the results of the randomized study versus ATG + CyA conducted at NIH. This study was early stopped due to increased fatal infectious complications in the experimental arm (CTX + CyA), related to the prolonged neutropenia resulting from CTX myelotoxicity;⁴¹ in addition, the latest follow up did not confirm Johns Hopkins' data suggesting that CTX may reduce the risk of MDS/AML development.⁴²

Another candidate agent for inducing lymphocyte depletion in AA patients is the anti-CD52 monoclonal antibody alemtuzumab, which specifically kills CD52-bearing cells via both antibody-dependent cellular cytotoxicity and complement-mediated lysis. We have recently reported, in collaboration with the EBMT Working Party for Severe Aplastic Anemia (WPSAA), that an alemtuzumab-based IS regimen (also including low-dose CyA) was feasible, safe and effective for the treatment of AA patients.⁴³ Alemtuzumab was given subcutaneously with negligible injection-related side effects, and the low rate of infectious complications ruled out most safety concerns; preliminary efficacy data suggested response rates not below standard IS regimen (58%), with easy re-treatment in case of relapse. These data confirms observations from smaller series.^{44,45} However, recent data from NIH seem only partially confirm these positive results;⁴⁶ in fact, alemtuzumab resulted in a 56% response rate in relapsed AA (n=23) and 36% in refractory AA (n=25). However, quite surprisingly, as front line treatment alemtuzumab resulted in a response rate as low as 19% (on 16 patients only); it has to be remarked that in the NIH experience alemtuzumab was used as single agent, without CyA.

Other IS agents may be also hypothesized for the treatment of AA; in the past years, the anti-CD25 monoclonal antibody daclizumab was used for moderate forms of AA, with a response rate of about 40%.^{47,48} Given the proven

role of cytokines in suppressing the hematopoiesis in AA,⁷ some cytokine inhibitors have been hypothesized for the treatment of AA, especially the already available TNF- α inhibitors etanercept (a TNF-receptor/Ig fusion protein),⁴⁹ infliximab (a chimeric anti-TNF- α mAb) and adalimumab (a fully humanized anti-TNF- α mAb). One could also hypothesize that in the future additional IS agents will be investigated in AA, such as alefacept,⁵⁰ efalizumab,⁵¹ anti-IFN agents⁵² or even immunomodulation by mesenchymal stem cells.⁵³

Current immunosuppression: the matter of different ATG preparations

ATG is a heterologous anti-serum obtained by injecting human lymphocytes in animals; various ATG preparations exist, which differ in stimulating antigens (peripheral lymphocytes, thymocytes or even T cell lines), and/or in the host animal (either horse or rabbit). Thus, even if comprehensive descriptions of the composition of each anti-serum are limited, they are obviously different;⁵⁴⁻⁵⁶ in addition, at least in the past, inter-lot variation due to manufacturing processes cannot be excluded.⁵⁷ The majority of available data coming from large randomized clinical trials refer to polyclonal ATGs obtained from horse (h), which have to be considered the gold standard for AA treatment. Of note, US and Japanese investigators utilized hATG (ATGAM®, Upjohn; 40 mg/kg/day for 4 days),^{24,25} which is different from the hATG preparation used in Europe (Lymphoglobuline®, Genzyme; 15 mg/kg/day for 5 days).^{20,26} Even if a formal head-to-head comparison has been never conducted, both h-ATG preparations resulted in response rates ranging between 50% and 70%;^{20,24-26} thus, they are considered equivalent as standard IST for AA. However, since 2008 Lymphoglobuline is no longer available in Europe, and physicians were forced to utilize other ATG preparations. Alternative polyclonal ATGs may be obtained from rabbits (r); two rATGs are currently available (Thymoglobuline®, Genzyme; ATG-Fresenius®) but to date the clinical results with these agents are less robust for the lack of large randomized trials. Thymoglobuline has been utilized in AA patients, and both retrospective data and prospective series have demonstrated a substantial efficacy. In most cases, rATG was used as second-line IST (after initial hATG) to prevent side effects due to possible sensitization to horse proteins, resulting in response rates up to 68% (in relapsed patients).^{33,34} As a front-line therapy, the experience with Thymoglobuline is quite limited; the only prospective trial is currently ongoing at NIH, where investigators are comparing head-to-head h-ATG (ATGAM) and r-ATG (Thymoglobuline), both arms with CyA, as first line treatment for AA patients (NCT00260689). The

recruitment is now closed (60 patients per arm), and preliminary data were just presented at the 2010 ASH meeting;⁵⁸ very surprisingly, r-ATG was markedly inferior to h-ATG in terms of response rate (33% vs 62% and 35% vs 68% at 3 and 6 months, respectively). Of note, lymphocyte depletion after r-ATG was markedly longer-lasting in comparison to h-ATG, raising the question that lymphocyte depletion may be not sufficient to achieve hematological remission in AA patients. Based on this data, one could hypothesize that additional immune or non-immune mechanisms may be involved in the pathophysiology of AA, and that h-ATG may target them more efficiently than r-ATG. For instance, regardless the antibodies resulting in T cell depletion, h-ATG might contain antibodies targeting immune cytokines involved in the inhibition or in the damage of hematopoietic stem cells. The NIH data were in agreement with a retrospective study from Brazil,⁵⁹ which showed a 34.5% response rate with Thymoglobuline in comparison to the 59.5% achieved with Lymphoglobuline (patients were 42 and 29, respectively). However, other retrospective experiences are in contrast with the results of this randomized study: investigators at the Cleveland Clinic treated 22 naïve AA patient with Thymoglobuline, showing a response rate of 50% and 54% at 6 and 12 months, respectively; these results were comparable to the historical control of 67 AA patients who have received initial treatment with ATGAM (59% response rate at 6 and 12 months).⁶⁰ A similar retrospective study was conducted by the Spanish group,⁶¹ which showed that 75 AA patients receiving front-line treatment with Thymoglobuline (2.5 mg/kg for 5 days) had a response rate of 45%, which was comparable to the 49% of the 35 patients who have received Lymphoglobuline. Additional studies are currently ongoing to investigate the efficacy of Thymoglobuline: the EBMT is retrieving its retrospective registry to assess the actual response rate. In addition, the EBMT is running a pilot study (NCT00471848) to investigate whether 2.5 mg/kg/day of Thymoglobuline (for 5 days) may be equivalent to the most utilized dose (3.75 mg/kg/day). Indeed, based on these data, at the moment h-ATG + CyA seems the safest treatment for AA patients; Thymoglobuline, which have in any case a substantial efficacy, should be recommended only if h-ATGs are not available, or within prospective trials. Finally, ATG-Fresenius should not be used as IST for AA patients, given that its use is limited to anecdotic and disappointing experiences.⁶²

Conclusions

To date, ATG + CyA remains the standard IST for AA patients. All the attempts to improve

the results obtained with this regimen have been unfruitful. Unexpectedly, recent observations have confounded rather than clarified our knowledge of IST in AA; in fact, the dogma that different ATG preparations may be equally effective has been unexpectedly debunked. The fact that hematological response does not correlate with lymphocyte depletion also suggest that h-ATG may work through unknown mechanisms of actions, even other than immune, leading to a possible dispute of AA pathophysiology itself. Even if these data have to be confirmed, at the moment h-ATG seems the best standard of care for AA patients; this represents a urgent challenge for those Countries (i.e., Europe) where h-ATG is no longer available. At the moment, it is not clear whether novel IS agents or strategies may be useful to improve the results of current IST; the design of large, co-operative prospective studies seems the only way to unravel the open issues in IS for the treatment of AA.

References

- Young NS. Acquired aplastic anemia. In: Young NS, ed. Bone marrow failure syndromes. Philadelphia: WB Saunders. 2000;1-46.
- Young NS, Calado RT, Scheinberg P. Current concepts in the pathophysiology and treatment of aplastic anemia. *Blood* 2006;108:2509-19.
- Young NS, Maciejewski J. The pathophysiology of acquired aplastic anemia. *N Engl J Med* 1997;336:1365-72.
- Maciejewski JP, Selleri C, Sato T, et al. Increased expression of Fas antigen on bone marrow CD34+ cells of patients with aplastic anaemia. *Br J Haematol* 1995; 91:245-52.
- Zombos NC, Gascon P, Djeu JY, Young NS. Interferon is a mediator of hematopoietic suppression in aplastic anemia in vitro and possibly in vivo. *Proc Natl Acad Sci U S A* 1985;82:188-92.
- Sloand E, Kim S, Maciejewski JP, Tisdale J, et al. Intracellular interferon-gamma in circulating and marrow T cells detected by flow cytometry and the response to immunosuppressive therapy in patients with aplastic anemia. *Blood* 2002;100:1185-91.
- Dufour C, Ferretti E, Bagnasco F, et al. Marrow Failure Study Group of the AIEOP. Changes in cytokine profile pre- and post-immunosuppression in acquired aplastic anemia. *Haematologica* 2009;94:1743-7.
- Zeng W, Nakao S, Takamatsu H, et al. Characterization of T-cell repertoire of the bone marrow in immune-mediated aplastic anemia: evidence for the involvement of antigen-driven T-cell response in cyclosporine-dependent aplastic anemia. *Blood* 1999;93:3008-16.
- Risitano AM, Kook H, Zeng W, et al. Oligoclonal and polyclonal CD4 and CD8 lymphocytes in aplastic anemia and paroxysmal nocturnal hemoglobinuria measured by V beta CDR3 spectratyping and flow cytometry. *Blood* 2002;100:178-83.
- Risitano AM, Maciejewski JP, Green S, et al. In-vivo dominant immune responses in aplastic anaemia: molecular tracking of putatively pathogenetic T-cell clones by TCR beta-CDR3 sequencing. *Lancet* 2004;364:355-64.
- Nakao S, Takami A, Takamatsu H, et al. Isolation of a T-cell clone showing HLA-DRB1*0405-restricted cytotoxicity for hematopoietic cells in a patient with aplastic anemia. *Blood* 1997;89:3691-9.
- Mathé G, Schwarzenberg L. Treatment of bone marrow aplasia by mismatched bone marrow transplantation after conditioning with antilymphocyte globulin—long-term results. *Transplant Proc* 1976;8:595-602.
- Speck B, Gluckman E, Haak HL, van Rood JJ. Treatment of aplastic anaemia by antilymphocyte globulin with and without allogeneic bone-marrow infusions. *Lancet* 1977;2:1145-8.
- Speck B, Gratwohl A, Nissen C, et al. Treatment of severe aplastic anaemia with antilymphocyte globulin or bone-marrow transplantation. *Br Med J (Clin Res Ed)* 1981;282:860-3.
- Champlin R, Ho W, Gale RP. Antithymocyte globulin treatment in patients with aplastic anemia: a prospective randomized trial. *N Engl J Med* 1983;308:113-8.
- Doney K, Pepe M, Storb R, et al. Immunosuppressive therapy of aplastic anemia: results of a prospective, randomized trial of antithymocyte globulin (ATG), methylprednisolone, and oxymetholone to ATG, very high-dose methylprednisolone, and oxymetholone. *Blood* 1992;79:2566-71.
- Champlin RE, Ho WG, Feig SA, et al. Do androgens enhance the response to antithymocyte globulin in patients with aplastic anemia? A prospective randomized trial. *Blood* 1985;66:184-8.
- Bacigalupo A, Chaple M, Hows J, et al. Treatment of aplastic anaemia (AA) with antilymphocyte globulin (ATG) and methylprednisolone (MPred) with or without androgens: a randomized trial from the EBMT SAA working party. *Br J Haematol* 1993;83:145-51.
- Frickhofen N, Kaltwasser JP, Schrezenmeier H, et al. Treatment of aplastic anemia with antilymphocyte globulin and methylprednisolone with or without cyclosporine. The German Aplastic Anemia Study Group. *N Engl J Med* 1991;324:1297-304.
- Frickhofen N, Heimpel H, Kaltwasser JP, Schrezenmeier H; German Aplastic Anemia Study Group. O Antithymocyte globulin with or without cyclosporin A: 11-year follow-up of a randomized trial comparing treatments of aplastic anemia. *Blood* 2003;101:1236-1242.
- Rosenfeld SJ, Kimball J, Vining D, Young NS. Intensive immunosuppression with antithymocyte globulin and cyclosporine as treatment for severe acquired aplastic anemia. *Blood* 1995;85:3058-65.
- Marsh J. Making therapeutic decisions in adults with aplastic anemia. *Hematology Am Soc Hematol Educ Program* 2006:78-85.
- Bacigalupo A. Aplastic anemia: pathogenesis and treatment. *Hematology Am Soc Hematol Educ Program* 2007;23-28.
- Rosenfeld S, Follmann D, Nunez O, Young NS. Antithymocyte globulin and cyclosporine for severe aplastic anemia: association between hematologic response and long-term outcome. *JAMA* 2003;289: 1130-5.
- Teramura M, Kimura A, Iwase S, et al. Treatment of severe aplastic anemia with antithymocyte globulin and cyclosporin A with or without G-CSF in adults: a multicenter randomized study in Japan. *Blood* 2007;110:1756-61.
- Locasciulli A, Oneto R, Bacigalupo A, et al. Outcome of patients with acquired aplastic anemia given first line bone marrow transplantation or immunosuppressive treatment in the last decade: a report from the European Group for Blood and Marrow Transplantation (EBMT). *Haematologica* 2007;92:11-8.
- Scheinberg P, Marte M, Nunez O, Young NS. Paroxysmal nocturnal hemoglobinuria clones in severe aplastic anemia patients treated with horse anti-thymocyte globulin plus cyclosporine. *Haematologica* 2010;95: 1075-80.
- Locasciulli A, Arcese W, Locatelli F, et al. Treatment of aplastic anaemia with granulocyte-colony stimulating factor and risk of malignancy. *Lancet* 2001;357:43-4.
- Socié G, Henry-Amar M, Bacigalupo A, et al. Malignant tumors occurring after treatment of aplastic anemia. *European Bone Marrow Transplantation-Severe Aplastic Anaemia Working Party. N Engl J Med* 1993;329:1152-7.
- Maciejewski JP, Risitano AM. Aplastic anemia: management of adult patients. *Hematology Am Soc Hematol Educ Program* 2005;110-7.
- Calado RT. Telomeres and marrow failure. *Hematology Am Soc Hematol Educ Program* 2009;338-43.
- Tichelli A, Passweg J, Nissen C, et al. Repeated treatment with horse antilympho-

- cyte globulin for severe aplastic anaemia. *Br J Haematol* 1998;100:393-400.
33. Di Bona E, Rodeghiero F, Bruno B, et al. Rabbit antithymocyte globulin (r-ATG) plus cyclosporine and granulocyte colony stimulating factor is an effective treatment for aplastic anaemia patients unresponsive to a first course of intensive immunosuppressive therapy. Gruppo Italiano Trapianto di Midollo Osseo (GITMO). *Br J Haematol* 1999;107:330-4.
 34. Scheinberg P, Nunez O, Young NS. Retreatment with rabbit antithymocyte globulin and ciclosporin for patients with relapsed or refractory severe aplastic anaemia. *Br J Haematol* 2006;133:622-7.
 35. Scheinberg P, Cooper JN, Sloand EM, et al. Association of telomere length of peripheral blood leukocytes with hematopoietic relapse, malignant transformation, and survival in severe aplastic anemia. *The Journal of the American Medical Association*, 2010;304:1358-64.
 36. Scheinberg P, Nunez O, Wu C, Young NS. Treatment of severe aplastic anaemia with combined immunosuppression: antithymocyte globulin, ciclosporin and mycophenolate mofetil. *Br J Haematol* 2006;133: 606-11.
 37. Sehgal SN. Rapamune® (RAPA, rapamycin, sirolimus): mechanism of action immunosuppressive effect results from blockade of signal transduction and inhibition of cell cycle progression. *Clin Biochem* 1998;31:335-40.
 38. Scheinberg P, Wu CO, Nunez O, et al. Treatment of severe aplastic anemia with a combination of horse antithymocyte globulin and cyclosporine, with or without sirolimus: a prospective randomized study. *Haematologica* 2009;94:348-54.
 39. Brodsky RA, Sensenbrenner LL, Jones RJ. Complete remission in severe aplastic anemia after high-dose cyclophosphamide without bone marrow transplantation. *Blood* 1996;87: 491-4.
 40. Brodsky RA, Chen AR, Dorr D, et al. High-dose cyclophosphamide for severe aplastic anemia: long-term follow-up. *Blood* 2010; 115:2136-41.
 41. Tisdale JF, Dunn DE, Geller N, et al. High-dose cyclophosphamide in severe aplastic anaemia: a randomised trial. *Lancet* 2000; 356:1554-9.
 42. Tisdale JF, Maciejewski JP, Nunez O, et al. Late complications following treatment for severe aplastic anemia (SAA) with high-dose cyclophosphamide (Cy): follow-up of a randomized trial. *Blood* 2002;100:4668-70.
 43. Risitano AM, Selleri C, Serio B, et al. Alemtuzumab is safe and effective as immunosuppressive treatment for aplastic anaemia and single-lineage marrow failure: a pilot study and a survey from the EBMT WPSAA. *Br J Haematol* 2010;148: 791-6.
 44. Gómez-Almaguer D, Jaime-Pérez JC, Garza-Rodríguez V, et al. Subcutaneous alemtuzumab plus cyclosporine for the treatment of aplastic anemia. *Ann Hematol* 2010;89:299-303.
 45. Kim H, Min YJ, Baek JH, et al. A pilot dose-escalating study of alemtuzumab plus cyclosporine for patients with bone marrow failure syndrome. *Leuk Res* 2009;33:222-31.
 46. Scheinberg P, Wu CO, Scheinberg P, et al. Alemtuzumab (Campath) monotherapy for severe aplastic anemia. *Blood* 2010;116: 1167a.
 47. Maciejewski JP, Sloand EM, Nunez O, et al. Recombinant humanized anti-IL-2 receptor antibody (daclizumab) produces responses in patients with moderate aplastic anemia. *Blood* 2003;102:3584-6.
 48. Sloand EM, Olnes MJ, Weinstein B, et al. Long-term follow-up of patients with moderate aplastic anemia and pure red cell aplasia treated with daclizumab. *Haematologica* 2010;95:382-7.
 49. Dufour C, Giacchino R, Ghezzi P, et al. Etanercept as a salvage treatment for refractory aplastic anemia. *Pediatr Blood Cancer* 2009;52:522-5.
 50. Krueger GG. Selective targeting of T cell subsets: focus on alefacept - a remittive therapy for psoriasis. *Expert Opin Biol Ther* 2002;2:431-41.
 51. Cather JC, Cather JC, Menter A. Modulating T cell responses for the treatment of psoriasis: a focus on efalizumab. *Expert Opin Biol Ther* 2003;3:361-70.
 52. Dumont FJ. Fontolizumab Protein Design Labs. *Curr Opin Investig Drugs* 2005;6: 537-44.
 53. Fouillard L, Bensidhoum M, Bories D, et al. Engraftment of allogeneic mesenchymal stem cells in the bone marrow of a patient with severe idiopathic aplastic anemia improves stroma. *Leukemia* 2003;17:474-6.
 54. Smith AG, O'Reilly RJ, Hansen JA, Martin PJ. Specific antibody-blocking activities in antilymphocyte globulin as correlates of efficacy for the treatment of aplastic anemia. *Blood* 1985;66:721-3.
 55. Kawano Y, Nissen C, Gratwohl A, Speck B. Immunostimulatory effects of different antilymphocyte globulin preparations: a possible clue to their clinical effect. *Br J Haematol* 1988;68:115-9.
 56. Bourdage JS, Hamlin DM. Comparative polyclonal antithymocyte globulin and antilymphocyte/antilymphoblast globulin anti-CD antigen analysis by flow cytometry. *Transplantation* 1995;59:1194-200.
 57. Raefsky EL, Gascon P, Gratwohl A, et al. Biological and immunological characterization of ATG and ALG. *Blood* 1986;68:712-9.
 58. Scheinberg P, Wu CO, Scheinberg P, et al. A randomized trial of horse versus rabbit antithymocyte globulin in severe acquired aplastic anemia. *Blood* 2010;116: LBA-4.
 59. Atta EH, Dias DS, Marra VL, de Azevedo AM. Comparison between horse and rabbit antithymocyte globulin as first-line treatment for patients with severe aplastic anemia: a single-center retrospective study. *Ann Hematol* 2010;89:851-9.
 60. Afable M, Shaik M, Sugimoto Y, et al. Efficacy of rabbit anti-thymocyte globulin (ATG) compared to horse ATG in severe aplastic anemia. *Blood* 2010;116:2236a.
 61. Vallejo C, Montesinos P, Rosell A, et al. Comparison between lymphoglobuline- and thymoglobuline-based immunosuppressive therapy as first-line treatment for patients with aplastic anemia. *Blood* 2009; 114:3194a.
 62. Zheng Y, Liu Y and Chu Y. Immunosuppressive therapy for acquired severe aplastic anemia (SAA): A prospective comparison of four different regimens. *Exp Hematol* 2006;34:826-831.

Hepatitis C Virus Infection in Ocular Adnexal Lymphomas

Diego Strianese, MD, PhD; Fausto Tranfa, MD; Marialuisa Finelli, MD, PhD; Amalia De Renzo, MD; Stefania Staibano, MD; Roberta Schiemer, MD; Domenico Cardone, MD; Roberto Pacelli, MD; Fabiana Perna, MD; Massimo Mascolo, MD; Gaetano De Rosa, MD; Giulio Bonavolontà, MD

Objective: To assess the influence of hepatitis C virus (HCV) infection on disease appearance and outcome of ocular adnexal non-Hodgkin lymphoma (ONHL).

Design: Retrospective comparative study (from January 1, 1992, through December 31, 2006).

Methods: The medical records of 129 patients with ONHL were retrospectively reviewed. All the patients were tested serologically for the presence of HCV infection. Patients were divided into 2 groups according to the presence or absence of HCV infection.

Main Outcome Measures: Prevalence of HCV infection, staging to evaluate the extent of disease at the onset, and clinical outcome data on overall and disease-free survival.

Results: The prevalence of HCV infection among the patients with ONHL was 17.8%. Seropositivity for HCV infection was significantly associated with extraorbital lymphoma at the onset ($P = .006$).

High prevalence of mucosa-associated lymphoid tissue disease (79.8%) was registered. Protocol therapy included radiotherapy and chemotherapy, depending on the stage of the disease. Complete remission was achieved in 99 patients (76.7%). A total of 23.6% of patients with HCV-seronegative status and 21.7% of those with HCV-seropositive status experienced relapse of the lymphomatous disease. No significant differences in the 5-year overall survival and disease-free survival between the 2 groups were observed.

Conclusions: Prevalence of HCV infection in patients with ONHL is a relevant issue, accounting for 17.8% of the examined patients. Infection with HCV may influence the initial appearance of ONHL because it is associated with more widespread disease at the onset. However, the overall and disease-free survival of the infected patients are not statistically different than that of patients who are not infected.

Arch Ophthalmol. 2010;128(10):1295-1299

Author Affiliations:

Department of Ophthalmological Sciences (Drs Strianese, Tranfa, Finelli, Schiemer, Cardone, and Bonavolontà), Pathology Section, Department of Biomorphological and Functional Sciences (Drs Staibano, Mascolo, and De Rosa), and Departments of Diagnostic Imaging and Radiation Oncology (Dr Pacelli) and Haematology (Drs De Renzo and Perna), University of Naples Federico II, Naples, Italy.

HEPATITIS C VIRUS (HCV) represents a viral pandemic and is well known as the causative agent of chronic viral hepatitis, which has been linked to the development of hepatocellular carcinoma.¹ Hepatitis C virus is a hepatotropic virus that can also replicate in lymphoid cells. The virus has been shown to sustain clonal expansion of B lymphocytes in patients with HCV infection.² This observation raised the question of whether HCV is a lymphomagenic virus and has led to evaluation of the potential role of HCV infection within B-cell non-Hodgkin lymphoma, as well as other hematologic malignant neoplasms.³⁻⁶ A pathogenic link between HCV and non-Hodgkin lymphoma (NHL), mostly marginal zone lymphoma of mucosa-associated lymphoid tissue (MALT), has been suggested.³⁻¹⁰ In contrast, other

authors¹¹⁻¹³ have not confirmed such an association.

Ocular adnexal non-Hodgkin lymphoma (ONHL) (eg, conjunctiva, lachrymal gland, and orbital soft tissue) is one of the most common forms of extranodal lymphomas and usually displays limited stages of disease, an indolent clinical course, and a tendency to remain localized for several years.¹⁴ Only 1 study¹⁰ shows a positive association between HCV infection and the development of ONHL. The authors of this previous article state that HCV infection concomitant to ONHL is associated with more disseminated disease at the diagnosis and with poor prognosis. The current study aims to assess whether HCV infection plays a role in determining the clinical features of HCV-seropositive orbital lymphomas, especially regarding the prognosis.

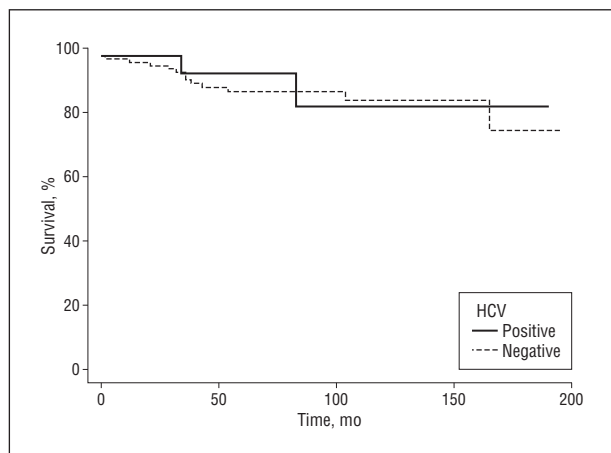


Figure 1. Comparison of the overall survival between the 2 groups of patients (hepatitis C virus [HCV] seropositive and seronegative) assessed by Kaplan-Meier curves ($P=.79$).

Table 1. Clinical Characteristics at Disease Onset

Characteristic	No. (%) of Patients by HCV Status (N=129) ^a		P Value
	Seropositive	Seronegative	
No. of patients	23 (17.8)	106 (82.2)	...
Age, median (range), y	64.34 (43-84)	62.88 (26-93)	...
Sex, M/F	4/19	45/61	...
Orbital lymphoma	10 (43.5)	86 (81.1)	<.001
Conjunctival lymphoma	2 (8.7)	10 (9.4)	>.99
Eyelid lymphoma	1 (4.3)	8 (7.5)	>.99
Lacrimal gland	9 (39.1)	22 (20.8)	.10
Extraocular muscles	1 (4.3)	1 (0.9)	.32
Stage			
1	15 (65.2)	96 (90.6)	.004
2	0	0	...
3	0	0	...
4	8 (34.8)	11 (10.4)	.006
Positive BMB	8 (34.8)	10 (9.4)	.004

Abbreviations: BMB, bone marrow biopsy; ellipses, not applicable; HCV, hepatitis C virus; M, male; F, female.

^aData are number (percentage) of patients unless otherwise indicated.

METHODS

STUDY GROUP

A retrospective study of a series of 129 patients with orbital ONHL, who had been referred from January 1, 1992, through December 31, 2006, to the Orbital Unit of the University of Naples Federico II, was performed. The patients included in this study had the onset symptom of orbital localization of ONHL. Data concerning age, sex, mass localization, and follow-up were available for all the examined patients. All the patients had a diagnosis of orbital lymphoma based on pathologic examination of an incisional biopsy specimen. The patients with ONHL diagnosed according to the previous classification for NHL (Working Formulation classification) were reclassified according to the latest criteria of the World Health Organization classification¹⁵ by pathologic reevaluation with additional immunohistochemical examinations.

The staging workup consisted of physical examination, biochemical blood profile, total-body computed tomography, and

bone marrow biopsy. In patients with conditions diagnosed after 2002, positron emission tomography was also performed.

Each patient underwent tests for antibodies to HCV assayed by a second-generation enzyme-linked immunoassay (HCV RNA qualitative reverse-transcriptase polymerase chain reaction standardized method) and determination of HCV genotype. Furthermore, we analyzed the presence of chronic hepatic disease. The patients who had HCV-seropositive status underwent liver biopsy with the aim of evaluating the hepatic disease associated with the viral infection. The chronic liver disease was classified according to criteria developed by Ishak et al.¹⁶

First-line treatment consisted of radiotherapy, in proportions of 1.8 or 2.0 Gy, 5 times per week, with total doses ranging from 34.2 to 50.0 Gy, when the disease was localized at the only orbit. When the lymphomatous disease appeared to be disseminated, according to the staging, a conventional protocol therapy based on cyclophosphamide, doxorubicin hydrochloride, vincristine sulfate, and prednisone (CHOP) chemotherapy or a CHOP-like scheme was administered. In selected patients whose conditions were diagnosed after 2002, rituximab was added.

After antineoplastic treatment, 6 patients with HCV-seropositive status who had ONHL were treated with interferon alfa (3 000 000 units 3 times a week for 12 months) subcutaneously. They were also given ribavirin, 1000 mg/d, orally.

All patients were followed up every 3 months with clinical evaluation and laboratory tests. They were also followed up every 6 months with ultrasonography and computed tomography (with positron emission tomography and computed tomography after 2002).

STATISTICAL ANALYSIS

Clinical characteristics and disease extent at onset of the HCV-seropositive and HCV-seronegative groups were verified with the χ^2 test and t test for nominal and continuous clinical variables, respectively. Cumulative risk for relapse of ONHL (ie, disease-free survival) or death (ie, overall survival) during the follow-up was assessed by Kaplan-Meier curves, and a comparison between HCV-seropositive and HCV-seronegative patients with NHL was performed with the log-rank test.

Overall survival was calculated starting from the date of pathologic diagnosis to death or to the latest date of follow-up visit, whereas time to progression and disease-free survival were calculated from first day of treatment to relapse, time to progression and time of death, or the latest date of follow-up visit.

RESULTS

The follow-up varied from a minimum of 12 months to a maximum of 185 months, with an average of 75 months. The frequency of the different histologic types of ONHL is shown in **Figure 1**. The clinical characteristics of the 129 patients included in this study are summarized in **Table 1**. The median age of the patients was 62.88 years (range, 26-93 years), and the male to female ratio was 0.61.

Twenty-three patients (17.8%) were infected with HCV. In all patients, the diagnosis of HCV infection preceded the diagnosis of lymphoma. All patients had HCV RNA detectable by polymerase chain reaction.

Mucosa-associated lymphoid tissue is the most frequent type of lymphoma, resulting in 79.8% of cases. A similar percentage was found among patients with HCV-seropositive status. No significant differences were found between the 2 groups in terms of distribution of the dif-

ferent histopathologic subtypes (**Table 2**). The histologic analysis of the hepatic tissue in the HCV-seropositive patients showed chronic active hepatitis in 6 patients (26.1%) and no signs of liver disease in the remaining 17 patients (73.9%). The apparent disease duration was calculated as the time passed by the first known risk of infection (eg, major or minor surgery, transfusion, tattooing, or intravenous drug abuse) to the time of the diagnosis of the orbital lymphoma. The average time was 22.6 years (SD, 13.9 years).

As reported in Table 1, the extent of the disease was significantly different between the 2 groups: 8 (34.8%) patients with HCV-seropositive status had stage IV disease at the diagnosis vs 11 (10.4%) patients with HCV-seronegative status. Infection with HCV was significantly associated with extraorbital disease at the onset ($P = .006$).

Radiotherapy treatment was administered in 108 patients (83.7%) as single-line therapy, whereas 21 patients (16.3%) were treated with a combination of radiotherapy and chemotherapy. The therapeutic outcome is summarized in **Table 3**. Ninety-nine patients (76.7%) achieved complete remission of the NHL. Thirty patients experienced relapse of the disease with extranodal localization: 25 (23.6%) of these patients had HCV-seronegative status and 5 patients (21.7%) had HCV-seropositive status ($P = .99$). The median time to disease progression was 57.6 and 55.0 months for the HCV-seronegative and HCV-seropositive groups, respectively. The 5-year overall survival and disease-free survival were not significantly different in the 2 groups ($P = NS$) (Figure 1 and **Figure 2**).

COMMENT

The association between HCV infection and NHL has been postulated in several studies.¹⁻¹⁰ This correlation has been mostly observed in countries such as Italy, the United States, and Japan.^{6,8-10} However, this issue remains controversial based on additional studies.^{12,17} In Italy a prevalence of HCV infection in NHL ranging from 15% to 30% has been reported.^{4,6}

In the literature there are few studies^{10,12,13,18} that explore the association of HCV infection and ocular adnexal lymphomas (eg, conjunctiva, lachrymal gland, and orbital soft tissue), even though the ocular region is one of the most common sites of extranodal lymphomas. Ferreri and coworkers¹⁰ have shown clinical implications of HCV infection in MALT-type lymphoma of the ocular adnexa. Of 55 patients, 13% tested seropositive for HCV. The concomitant HCV infection was associated with more disseminated disease and aggressive behavior in ocular adnexal lymphoma. By contrast, in an Austrian study,¹² only 2 of 45 patients (4%) had a concomitant HCV infection, and neither influence of HCV on clinical course nor risk of relapse was found. In a short report,¹³ performed in France, of 40 analyzed patients with ONHL, only 1 patient had HCV-seropositive status.

In the present study, the prevalence of HCV infection in the examined population with ONHL was 17.8%, similar to what has been reported in other Italian studies on patients from other districts with NHL localized in differ-

Table 2. Distribution of Different Disease Subtypes Between the 2 Groups of Patients

Subtype	HCV Seropositive, No.	HCV Seronegative, No.	P Value
MALT	18	85	.78
Diffuse	2	9	>.99
Follicular	0	9	.36
Mantle	3	3	.69

Abbreviations: HCV, hepatitis C virus; MALT, mucosa-associated lymphoid tissue.

Table 3. Study Outcome Data

Outcome	No. (% of Patients by HCV Status (N=129) ^a		P Value
	Seropositive (n=23)	Seronegative (n=106)	
Relapse rate	5 (21.7)	25 (23.6)	>.99
Local relapse	0	12 (11.3)	.12
Systemic relapse	4 (17.4)	12 (11.3)	.48
Systemic and local relapse	1 (4.3)	1 (0.9)	.32
Follow-up, median, mo	71.7	77.4	...
TTP, median, mo	55.0	57.6	...

Abbreviations: ellipses, not applicable; HCV, hepatitis C virus; TTP, time to progression.

^aData are number (percentage) of patients unless otherwise indicated.

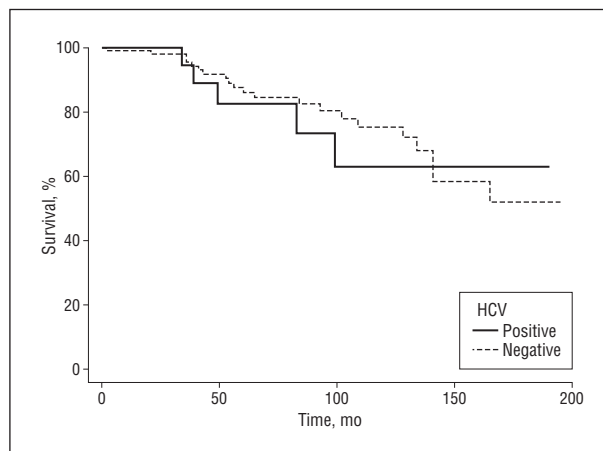


Figure 2. Comparison of the progression-free survival between the 2 groups of patients (hepatitis C virus [HCV] seropositive and seronegative) assessed by Kaplan-Meier curves ($P = .53$).

ent sites.^{3,12} The variable worldwide prevalence of HCV together with different environmental and genetic factors could explain these contrasting results. In fact, the prevalence of HCV infection in Italy is high (3%-5%).⁵ For comparison, the role of *Chlamydia psittaci* in ocular adnexal lymphoma appears to be especially pronounced in Italy,¹⁹ whereas widely varying rates of infection could be found in different geographic regions.²⁰

Recently, an increasing amount of biologic data have been found that support the role of HCV in lymphomagenesis.²¹⁻²³ It seems that the long-term antigenic stimulation provided by these agents may elicit host immune

responses able to promote and sustain clonal B-cell expansion.³ A significant increase of NHL in patients with more than 15 years of HCV infection has been reported.⁶ In our study the median duration of HCV infection was 22 years, with 34.8% of patients with HCV-seropositive status having disseminated disease at onset and only 9.4% of patients with seronegative status having widespread disease at onset ($P=.004$) (Table 1). This finding supports the hypothesis that HCV infection allows spreading of the lymphoma, sustaining its clonal expansion. Although the HCV genome and its replicative intermediates have been detected in peripheral blood mononuclear cells and in lymphoid tissues of chronically infected patients,²¹ its role as a trigger agent of a frank B-cell neoplastic disorder is not clear yet.²¹⁻²³ In fact, because the virus lacks reverse transcriptase, it is unable to integrate into the host genome and to encode for any known oncogenesis. Considering this possible pathogenic mechanism, the need for analysis of the biopsied tissue for the presence of HCV is uneventful, as advocated by some authors.¹⁸

A history of liver disease may be considered a possible pathogenic factor on the progression of lymphoma staging in patients with HCV-seropositive status.⁴ However, only 6 of 23 patients in our cohort had an active viral liver disease. Considering these data, we were not able to state that liver disease gravity may have conditioned lymphoma staging in our group of patients.

Patients included in this study received radiotherapy alone or with adjuvant chemotherapy, depending on the stage of the disease. As we previously reported in primary NHL with different site distribution, the use of an appropriate therapeutic option also resulted in a favorable outcome for this subset of patients with extranodal lymphomas.⁵ The overall outcome resulted in a complete remission of NHL in 99 patients (76.7%). A total of 25 (23.6%) of the patients with HCV-seronegative status and 5 (21.7%) of those with HCV-seropositive status experienced relapse of the disease; however, we did not observe a statistically significant difference in the 5-year overall survival and disease free survival between the 2 groups (Tables 1 and 3 and Figures 1 and 2). It can be argued that the appropriate use of the protocol therapy based on a careful evaluation of the stage or extent of the disease can minimize the negative effect of HCV infection.

The results of this study were compared with those of the only previously published large Italian study¹⁰ in the PubMed database, to our knowledge, which concerned the positive link between HCV infection and ocular adnexal lymphoma. The authors of the other study similarly found that HCV infection is associated with a more aggressive clinical stage at the onset, but they conversely reported that patients with HCV-seropositive status had a poor prognosis over time compared with those with HCV-seronegative status. Possible explanations of the difference regarding the outcome between these reported data and our own data may be ascribed to differences in the first-line therapy choices.

In a study²⁴ performed with a French population that demonstrated the link between HCV infection and the diffuse large cell lymphoma, the authors suggested that specific protocols, including antiviral therapy, should be designed for patients affected by lymphoma. Recent re-

ports, attesting to the efficacy of antiviral treatment on the course of HCV-related B-cell NHL, strengthen the hypothesis of a link between HCV infection and B-cell lymphoma.^{25,26} The value of the antiviral therapy was ruled out by the statistical analysis of this study because of the paucity of patients with HCV-seropositive status treated. Nevertheless, the use of antiviral therapy may improve the outcome of patients infected with NHL, as we reported in a previous study.²⁵

To summarize, HCV infection has a potential negative effect on patients infected with ocular lymphoma because it is associated with a more diffuse dissemination at the onset. Discrepancy with previous studies in terms of the incidence of HCV-seropositive cases among patients infected with ONHL may be explained by the geographic variations of this infection. Therefore, although an influence of HCV infection on lymphoma exists, the different prevalence can modify its role as a prognostic factor. Outcome seems to be slightly modified by the presence of this infection, probably because the effectiveness of the recent first-line treatment could minimize the influence of this risk factor. However, future studies will be necessary to better assess the influence of infectious agents and malignant neoplasms and the possible role of antiviral therapy. It must be considered that the data reported herein were collected in a single referral center.

Submitted for Publication: April 25, 2009; final revision received November 20, 2009; accepted November 28, 2009.

Correspondence: Diego Strianese, MD, PhD, Department of Ophthalmological Sciences, University of Naples Federico II, Via Pansini 5, Naples 80131, Italy (strianese@unina.it).

Financial Disclosure: None reported.

REFERENCES

1. Saito I, Miyamura T, Ohbayashi A, et al. Hepatitis C virus infection is associated with the development of hepatocellular carcinoma. *Proc Natl Acad Sci U S A*. 1990;87(17):6547-6549.
2. King PD, Wilkes JD, Diaz-Arias AA. Hepatitis C virus infection in non-Hodgkin's lymphoma. *Clin Lab Haematol*. 1998;20(2):107-110.
3. Luppi M, Grazia Ferrari M, Bonaccorsi G, et al. Hepatitis C virus infection in subsets of neoplastic lymphoproliferations not associated with cryoglobulinemia. *Leukemia*. 1996;10(2):351-355.
4. Gisbert JP, Garcia-Buey L, Pajares JM, Moreno-Otero R. Prevalence of hepatitis C virus infection in B-cell non-Hodgkin's lymphoma: systematic review and meta-analysis. *Gastroenterology*. 2003;125(6):1723-1732.
5. De Renzo A, Perna F, Persico M, et al. Excellent prognosis and prevalence of HCV infection of primary hepatic and splenic non-Hodgkin's lymphoma. *Eur J Haematol*. 2008;81(1):51-57.
6. Mele A, Pulsoni A, Bianco E, et al. Hepatitis C virus and B-cell non-Hodgkin lymphomas: an Italian multicenter case-control study. *Blood*. 2003;102(3):996-999.
7. Duberg A-S, Nordström M, Törner A, et al. Non-Hodgkin's lymphoma and other nonhepatic malignancies in Swedish patients with hepatitis C virus infection. *Hepatology*. 2005;41(3):652-659.
8. Takeshita M, Sakai H, Okamura S, et al. Prevalence of hepatitis C virus infection in cases of B-cell lymphoma in Japan. *Histopathology*. 2006;48(2):189-198.
9. Morgensztern D, Rosado M, Silva O, et al. Prevalence of hepatitis C infection in patients with non-Hodgkin's lymphoma in South Florida and review of the literature. *Leuk Lymphoma*. 2004;45(12):2459-2464.
10. Ferreri AJM, Viale E, Guidoboni M, et al. Clinical implications of hepatitis C virus infection in MALT-type lymphoma of the ocular adnexa. *Ann Oncol*. 2006;17(5):769-772.
11. Grünberger B, Wöhrer S, Streubel B, et al. Antibiotic treatment is not effective in patients infected with *Helicobacter pylori* suffering from extragastric MALT lymphoma. *J Clin Oncol*. 2006;24(9):1370-1375.

12. Gruenberger B, Woehrer S, Troch M, et al. Assessment of the role of hepatitis C, *Helicobacter pylori* and autoimmunity in MALT lymphoma of the ocular adnexa in 45 Austrian patients. *Acta Oncol.* 2008;47(3):355-359.
13. Arnaud P, Escande M-C, Lecuit M, et al. Hepatitis C virus infection and MALT-type ocular adnexal lymphoma. *Ann Oncol.* 2007;18(2):400-403.
14. Svoboda J, Andreadis C, Downs LH, Miller WT Jr, Tsai DE, Schuster SJ. Regression of advanced non-splenic marginal zone lymphoma after treatment of hepatitis C virus infection. *Leuk Lymphoma.* 2005;46(9):1365-1368.
15. Harris NL, Jaffe ES, Diebold J, et al. World Health Organization classification of neoplastic diseases of the hematopoietic and lymphoid tissues: report of the Clinical Advisory Committee meeting-Airlie House, Virginia, November 1997. *J Clin Oncol.* 1999;17(12):3835-3849.
16. Ishak K, Baptista A, Bianchi L, et al. Histological grading and staging of chronic hepatitis. *J Hepatol.* 1995;22(6):696-699.
17. Besson C, Canioni D, Lepage E, et al; Groupe d'Etude des Lymphomes de l'Adulte Programs. Characteristics and outcome of diffuse large B-cell lymphoma in hepatitis C virus-positive patients in LNH 93 and LNH 98 Groupe d'Etude des Lymphomes de l'Adulte programs. *J Clin Oncol.* 2006;24(6):953-960.
18. Verma V, Shen D, Sieving PC, Chan CC. The role of infectious agents in the etiology of ocular adnexal neoplasia. *Surv Ophthalmol.* 2008;53(4):312-331.
19. Ferreri AJM, Guidoboni M, Ponzoni M, et al. Evidence for an association between *Chlamydia psittaci* and ocular adnexal lymphomas. *J Natl Cancer Inst.* 2004;96(8):586-594.
20. Chanudet E, Zhou Y, Bacon CM, et al. *Chlamydia psittaci* is variably associated with ocular adnexal MALT lymphoma in different geographical regions. *J Pathol.* 2006;209(3):344-351.
21. Machida K, Cheng KT-N, Sung VM-H, et al. Hepatitis C virus induces a mutator phenotype: enhanced mutations of immunoglobulin and protooncogenes. *Proc Natl Acad Sci U S A.* 2004;101(12):4262-4267.
22. Chan CH, Hadlock KG, Fong SKH, Levy S. *V_H1-69* gene is preferentially used by hepatitis C virus-associated B cell lymphomas and by normal B cells responding to the E2 viral antigen. *Blood.* 2001;97(4):1023-1026.
23. Marasca R, Vaccari P, Luppi M, et al. Immunoglobulin gene mutations and frequent use of *VH1-69* and *VH4-34* segments in hepatitis C virus-positive and hepatitis C virus-negative nodal marginal zone B-cell lymphoma. *Am J Pathol.* 2001;159(1):253-261.
24. Hermine O, Lefrère F, Bronowicki JP, et al. Regression of splenic lymphoma with villous lymphocytes after treatment of hepatitis C virus infection. *N Engl J Med.* 2002;347(2):89-94.
25. La Mura V, De Renzo A, Perna F, et al. Antiviral therapy after complete response to chemotherapy could be efficacious in HCV-positive non-Hodgkin's lymphoma. *J Hepatol.* 2008;49(4):557-563.
26. Vallisa D, Bernuzzi P, Arcaini L, et al. Role of anti-hepatitis C virus (HCV) treatment in HCV-related, low-grade, B-cell, non-Hodgkin's lymphoma: a multi-center Italian experience. *J Clin Oncol.* 2005;23(3):468-473.

This Month in Archives of Ophthalmology Online @ www.archophthalmol.com

FREE This Month's Free Article

Canadian Glaucoma Study 3: Impact of Risk Factors and Intraocular Pressure Reduction on the Rates of Visual Field Change

View Last Month's

- Most Viewed Articles
- Most Sent Articles
- Most Viewed Collections



Sign Up for Free

- Table of Contents E-mail Alerts
- Topic Collection E-mail Alerts
- RSS Feeds

See Also

- Calendar of Events
- Physician Jobs
- Backfiles of Articles Back to 1929

Supplementary Online-Only Content

- Risks of Mortality, Myocardial Infarction, Bleeding, and Stroke Associated With Therapies for Age-Related Macular Degeneration
- Blue Sclera With and Without Corneal Fragility (Brittle Cornea Syndrome) in a Consanguineous Family Harboring *ZNF469* Mutation (p.E1392X)

Early-Release Article

Canadian Glaucoma Study 3: Impact of Risk Factors and Intraocular Pressure Reduction on the Rates of Visual Field Change



Clinical Challenge: You Make the Diagnosis

Skin and Corneal Ulceration in a 73-Year-Old Woman



CME Course

Canadian Glaucoma Study 3: Impact of Risk Factors and Intraocular Pressure Reduction on the Rates of Visual Field Change

Assessment of Metabolic Response to Radioimmunotherapy with ^{90}Y -Ibritumomab Tiuxetan in Patients with Relapsed or Refractory B-Cell Non-Hodgkin Lymphoma¹

Giovanni Storto, MD, FEBNM
Amalia De Renzo, MD
Teresa Pellegrino, MD
Fabiana Perna, MD
Teresa De Falco, MD
Paola Erra, MD
Anna Nardelli, PhD
Antonio Speranza, PhD
Michele Klain, MD
Bruno Rotoli, MD
Leonardo Pace, MD

Purpose:

To prospectively compare the assessment of metabolic response to yttrium 90 (^{90}Y)-ibritumomab tiuxetan radioimmunotherapy (RIT) by using fluorine 18 (^{18}F) fluorodeoxyglucose (FDG) combined positron emission tomographic-computed tomographic (PET/CT) imaging at 2 and 6 months to determine the most appropriate time to detect therapeutic response in refractory non-Hodgkin lymphoma (NHL) patients treated with RIT.

Materials and Methods:

The ethical committee of the university approved the protocol and all patients signed informed consent. Twenty-three consecutive patients (10 women, 13 men; mean age, 51.8 years \pm 7.3 [standard deviation]) treated by using RIT for relapsed or refractory follicular NHL were enrolled. For all patients, ^{18}F FDG PET/CT scanning was performed at baseline and at 2 and 6 months after RIT. Response was assessed by using the International Workshop Criteria (IWC) and revised criteria (IWC + PET) as well as the criteria of the European Organization for Research and Treatment of Cancer. One-way analysis of variance for repeated measures, receiver operator curve analysis, and Kaplan-Meier curves were used for statistical analysis.

Results:

PET/CT performed at 2 months revealed complete ($n = 12$) or partial ($n = 4$) metabolic response in 16 of 23 patients with complete or partial clinical response. These findings were all confirmed at 6-month scanning. PET/CT indicated refractory or persistent disease at 2 and 6 months in the remaining seven patients. Better overall survival was observed for patients with a reduction in the maximum standard uptake value of 49% or higher (both at 2 and 6 months after RIT) when compared with those with a decrease of less than 49% ($P < .05$).

Conclusion:

Early assessment of response to RIT by using PET/CT might be useful in the identification of patients needing additional therapeutic strategies.

© RSNA, 2010

Supplemental material: <http://radiology.rsna.org/lookup/suppl/doi:10.1148/radiol.09090603/-/DC1>

¹ From the Istituto di Ricerca e Cura a Carattere Scientifico (IRCCS), Centro di Riferimento Oncologico di Basilicata, Rionero in Vulture, Italy (G.S.); Dipartimento di Biochimica e Biotecnologie Mediche (A.D.R., F.P., B.R.), Istituto di Biostrutture e Bioimmagini, Consiglio Nazionale delle Ricerche (T.P., A.S.), and Dipartimento di Scienze Biomorfologiche e Funzionali (P.E., A.N., M.K., L.P.), Università "Federico II," Via Pansini 5, 80131 Naples, Italy; and IRCCS, Fondazione Istituto di Diagnostica Nucleare, Naples, Italy (T.D.F., L.P.). Received April 6, 2009; revision requested May 27; revision received July 9; accepted August 4; final version accepted August 10. Address correspondence to G.S. (e-mail: gio24@hotmail.com).

© RSNA, 2010

Follicular lymphoma is one of the most frequently occurring types of non-Hodgkin lymphoma (NHL), accounting for 70% of all indolent cases. The overall prevalence of NHL in the European Union is approximately 230 000, with an annual incidence of about 70 000. Approximately 18 500 new cases of follicular lymphoma are diagnosed annually in the United States (1,2). Although the therapeutic options for patients with NHL have improved over the past 20 years, most patients with low-grade lymphoma ultimately die of their disease, regardless of the treatment used (3).

Targeted radioimmunotherapy (RIT) is attractive as an approach toward treatment because follicular lymphoma cells are intrinsically extremely sensitive to radiation. Yttrium 90 (^{90}Y)-ibritumomab tiuxetan (Zevalin; Schering AG, Berlin, Germany) for RIT is currently approved for adult patients with relapsed or refractory CD20+ follicular B-cell NHL in Europe and the United States (4-6). It combines the tumor-targeting ability of an anti-CD20 monoclonal antibody and the tumor-destroying power of ^{90}Y radiation confined to a small area. This treatment ensures a high bioavailability at tumor sites and prevents the radioactivity from being distributed through the body by circulating lym-

phocytes by coating them beforehand with rituximab.

Recently, fluorine 18 (^{18}F) fluorodeoxyglucose (FDG) combined positron emission tomographic-computed tomographic (PET/CT) imaging has been recognized as a suitable tool for staging, follow-up, and tumor response assessment of NHL patients (7-9). It offers the advantage of functional tissue characterization by measuring glucose uptake, which is independent of morphologic or size criteria. However, no consensus has been reached regarding the optimal timing for performing ^{18}F FDG PET/CT after RIT in lymphoma patients. Therefore, the aim of our study was to prospectively compare the assessment of metabolic response to RIT by performing ^{18}F FDG PET/CT at 2 and 6 months after treatment to determine the most appropriate time to detect therapeutic response in refractory NHL patients treated with ^{90}Y -ibritumomab tiuxetan RIT.

Materials and Methods

Patients

The ethical committee of our university approved the study protocol. All patients undergoing RIT and imaging studies signed informed consent in accordance with the Declaration of Helsinki.

Twenty-three consecutive patients (mean age, 51.8 years \pm 7.3 [standard deviation]; range, 43-76 years) consisting of 10 women (mean age, 53.5 years \pm 8; range, 43-65 years) and 13 men (mean age, 54.4 years \pm 9; range, 49-76 years) were referred for ^{90}Y -ibritumomab tiuxetan treatment of low-grade follicular NHL that was relapsed after or refractory to chemotherapy and immunotherapy (Table E1 [online])

Implication for Patient Care

- Early assessment of response to RIT by using PET/CT might be useful in the identification of patients needing additional therapeutic strategies or to avoid ineffective therapies and diagnostic procedures.

between November 2005 and April 2008. Refractory/relapsed disease was confirmed in all patients before RIT by using clinical, laboratory, and/or imaging or histologic findings obtained from biopsy results. Before RIT, 17 patients received combined cyclophosphamide-doxorubicin-vincristine-prednisone and six received a fludarabine-mitoxantrone (Fludara, Schering, Berlin, Germany; Onkotrone, Baxter, Rome, Italy) regimen. One patient had undergone bone marrow autologous transplantation and two had undergone local external-beam radiation therapy. Nine had multiple remissions and subsequent relapses. All patients received at least one course of rituximab therapy. All patients strictly fulfilled recommended inclusion criteria, which were as follows: relapsed or refractory low-grade or follicular B-cell NHL, having less than 25% lymphoma marrow involvement and/or impaired bone marrow reserve, and absence of severe thrombocytopenia (ie, a platelet count of $>100\,000$ per mm^3).

All patients underwent comprehensive evaluation, including clinical and hematologic data, as well as neck ultrasonography and chest, abdominal, and

Advances in Knowledge

- Fluorine 18 (^{18}F) fluorodeoxyglucose (FDG) PET/CT assessment of metabolic response to radioimmunotherapy (RIT) in non-Hodgkin lymphoma (NHL) patients performs equally well at both 2 and 6 months, with an accuracy of 91% in predicting clinical outcome at 12-month follow-up.
- ^{18}F FDG metabolic data after RIT showed significant difference in maximum standard uptake value (SUV_{max}) between responders and nonresponders with a better overall survival in NHL patients with a 49% or higher reduction in SUV_{max} .

Published online

10.1148/radiol.09090603

Radiology 2010; 254:245-252

Abbreviations:

EORTC = European Organization for Research and Treatment of Cancer

FDG = fluorodeoxyglucose

IWC = International Workshop Criteria

NHL = non-Hodgkin lymphoma

RIT = radioimmunotherapy

SPD = sum of the product of the diameters

SUV = standard uptake value

SUV_{max} = maximum SUV

Author contributions:

Guarantors of integrity of entire study, G.S., A.D.R., T.P., A.N., A.S.; study concepts/study design or data acquisition or data analysis/interpretation, all authors; manuscript drafting or manuscript revision for important intellectual content, all authors; approval of final version of submitted manuscript, all authors; literature research, G.S., A.D.R., T.P., F.P., A.N., A.S., B.R.; clinical studies, G.S., A.D.R., T.P., F.P., T.D.F., P.E., A.N., A.S., M.K., B.R.; statistical analysis, G.S., A.D.R., T.P., F.P., A.N., A.S., L.P.; and manuscript editing, G.S., A.D.R., T.P., A.N., A.S., B.R.

Authors stated no financial relationship to disclose.

pelvic CT at baseline, at 6 months after RIT, as well as mid-term follow-up (mean, 12.8 months \pm 5.9; range, 7–20 months). In particular, clinical findings, including signs and symptoms such as painless swelling in the lymph nodes of the neck, axilla, or groin, unexplained fevers, drenching night sweats, fatigue, unexplained weight loss, itching, reddened patches on the skin, nausea, vomiting, or abdominal pain, correlated with the results of complete blood counts, serum electrolytes, liver and kidney function tests, and serum lactate dehydrogenase levels. No patients showed bone marrow involvement before RIT. A majority of relapses or evidence of refractory disease was seen following physical examination during scheduled or unscheduled visits.

A baseline ^{18}F FDG PET/CT scan at restaging was performed 10–14 days (mean, 12 days \pm 1) before RIT. ^{18}F FDG PET/CT examinations to help evaluate responses were performed 2 (mean, 2.1 months \pm 0.3; range, 1.7–2.4 months) and 6 (mean, 5.6 months \pm 0.2; range, 5.4–6.3 months) months after RIT and their results were compared with those of the baseline imaging examination, as well as with the clinical and hematologic data.

Treatment Procedures

Patients underwent ^{90}Y -ibritumomab tiuxetan treatment according to a standardized regimen: an initial dose of rituximab (250 mg per square meter of body surface area) was administered intravenously on day 1; on day 8, a second identical dose of intravenous rituximab was followed by a single intravenous injection of ^{90}Y -ibritumomab tiuxetan (14.8 MBq/kg), for a maximum of 1169 MBq. No treatment other than RIT was administered between the baseline and follow-up ^{18}F FDG PET/CT examinations; moreover, no changes in therapy resulted from the early (2-month) patient evaluation.

Imaging Technique

^{18}F FDG PET/CT was performed with a commercial PET/CT scanner (Discovery LS; GE Healthcare, Milwaukee, Wis) that combines a PET scanner (Ad-

vance NXi; GE Healthcare) and a four detector-row CT system (LightSpeed Plus; GE Healthcare). In all studies, PET/CT imaging was performed 75–90 minutes after intravenous administration of 12–15 mCi (444–555 MBq) of ^{18}F FDG. Multidetector CT (pitch, 1.5; tube charge, 120 mAs; and tube voltage, 120 kVp) was performed without intravenous and/or oral contrast medium as part of the PET/CT examination. PET scanning was subsequently performed with 4 minutes per bed position and six to eight bed positions per patient, depending on patient height. Raw CT data were reconstructed in transverse images with a 4.25-mm section thickness. Sagittal and coronal CT images were generated by means of reconstruction of the transverse data. Raw PET data were reconstructed both with and without attenuation correction in transverse, sagittal, and coronal images. Attenuation correction was performed on the basis of the attenuation coefficients, which were determined by using iterative reconstruction. Patients fasted for 4–6 hours prior to imaging and blood glucose level was determined in all patients before ^{18}F FDG administration. A cutoff value of less than 160 mg/dL (8.8816 mmol/L) was considered appropriate to perform the examination.

At the mid-term evaluation, unenhanced CT scans of the neck, chest, abdomen, and pelvis were performed with a multidetector scanner (Toshiba Aquilion; Toshiba Medical Systems, Otawara, Tochigi, Japan) by using the following parameters: pitch, 1.0; tube charge, 240 mAs; and tube voltage, 120 kVp.

Imaging Evaluation

All images were reviewed at a workstation by using PET/CT fusion software (Volumetrix for PET-CT; GE Healthcare, Waukesha, Wis). Each set of baseline and follow-up PET/CT studies, as well as the final CT scans, were interpreted by two experienced nuclear physicians (G.S. and L.P., each with 15 years experience) in consensus, one of whom (L.P.) is a radiologist. Images were interpreted promptly after acquisition. At that moment, readers were aware only of the timing of follow-up. The examin-

ers first evaluated the CT images alone. Mass sizes were visually estimated and those considered as potentially clinically important were measured by using electronic calipers for at least two maximum diameters. A lesion in the baseline study was defined as an identifiable mass or lymph node larger than 1 cm in minimum diameter with soft-tissue mediastinal window settings. Then, maximum standardized uptake values (SUV_{max}) were determined and corrected for body weight.

Response Assessment

Response assessment was performed for PET/CT scans by using three methods: International Workshop Response Criteria (IWC) (10); revised IWC + PET criteria (11,12), and PET response criteria of the European Organization for Research and Treatment of Cancer (EORTC) (13) (Table E2). The IWC evaluation performed at mid-term follow-up was considered as a reference standard together with clinical and hematologic evaluation. The accuracy of each method in predicting the results of the comprehensive assessment (ie, clinical and hematologic and imaging), carried out at mid-term follow-up, was tested.

At baseline PET/CT scanning, all lymph nodes and extranodal masses were systematically evaluated according to topographic criteria and up to eight of the hottest (those with the highest levels of uptake) representative lesions (>1 cm in size) per patient were identified as target lesions. SUV_{max} and bidimensional tumor size measurements were obtained for each target lesion and in the location of the treated lesion (background) when tumor uptake was no longer visually detectable. The presence and metabolic activity of new lesions were also recorded. The percentage change in SUV_{max} and in tumor size (sum of the product of the diameters [SPD]) between baseline and both 2 and 6 months post-RIT scans were calculated for each target lesion.

Response to RIT was classified according to IWC criteria (10) and further categorized according to revised IWC + PET criteria (11,12) and EORTC PET response criteria (13) at both 2

and 6 months after RIT. In particular, metabolic tumor response was assessed visually (IWC + PET) and semiquantitatively (EORTC). Briefly, EORTC criteria for PET responses define progressive metabolic disease as an increase in ^{18}F FDG tumor SUV_{max} of greater than 25% in a target lesion defined on a baseline scan, a visible increase in the extent of ^{18}F FDG tumor uptake (>20% in the longest dimension), or the appearance of new tracer uptake; stable metabolic disease as an increase in SUV_{max} of less than 25% or a decrease of less than 15%; and a partial response as a reduction in SUV_{max} of 25% or more. Complete metabolic response would be a complete resolution of ^{18}F FDG uptake in the tumor mass so that it was indistinguishable from surrounding normal tissues.

Clinical Follow-up

Performance status and status of disease (assessed by means of clinical parameters and on the basis of imaging results) were monitored during follow-up. The final assessment at mid-term follow-up was performed according to clinical and dimensional criteria obtained at the last CT examination (IWC) (9–11). In particular, this system defines categories of complete response, partial response, stable disease, and progressive disease. For the statistical evaluation, responder patients were defined as those with complete or partial response. Nonresponder patients were those with no response or progressive disease. RIT side effects were also recorded, if any, by using laboratory data and medical records.

Blood glucose level was stable in each patient ($91 \text{ mg/dL} \pm 28$ vs $93 \text{ mg/dL} \pm 21$ vs $89 \text{ mg/dL} \pm 23$; $P = .82$ over time) and none of the patients experienced significant weight loss during the study ($67 \text{ kg} \pm 6$ vs $66 \text{ kg} \pm 6$ vs $67 \text{ kg} \pm 6$; $P = .95$ over time).

Statistical Analysis

Differences between mean values were assessed by using the Student *t* test (two-tailed probability) for paired data. The McNemar test was used to compare proportions. The one-way analysis of variance for repeated measures was also used. The post hoc analysis was performed with a Bonferroni correction. Receiver operator curve analysis was performed to estimate the optimal cutoff of percentage of SUV_{max} decline for differentiating metabolic responders from nonresponders. Both 2- and 6-month responses to RIT were correlated with overall survival, which was defined as time from RIT until death from any cause or time of last censor. Overall survival was computed by using Kaplan-Meier curves. A *P* value of less than .05 was considered to indicate a significant difference.

Results

Seven patients were classified as Ann Arbor stage 2B, one as stage 2BE (ie, involvement of two lymph node groups on the same side of the diaphragm and of a single extranodal site next to the nodal groups with presence of lymphoma-related symptoms), 12 as stage 4B, two as stage 4BE (ie, extensive disease

in one site with involvement of a single extranodal site and lymphoma-related symptoms), and one as stage 4BX (ie, extensive disease in one site with bulky disease and lymphoma-related symptoms) at reevaluation before RIT.

FDG PET/CT Response Assessment after RIT

The 2-month CT scan (IWC) resulted in six complete response, 10 partial response and seven nonresponse outcomes, while the 6-month scan showed 10 complete response, six partial response and seven nonresponse (Table 1) outcomes. Assessment of response by using IWC + PET and ^{18}F FDG PET/CT scanning (EORTC) at both 2 and 6 months helped identify 12 complete response, four partial response and seven nonresponse outcomes.

Two patients showing complete response at 12-month follow-up were classified as metabolic partial response by using IWC + PET criteria (Fig 1). Both showed at least a 50% decrease in SPD of their ^{18}F FDG PET/CT results at 2 (–51% and –52%, respectively; $P < .05$) and 6 (–51% and –55%, respectively; $P < .05$) months, and continued to show FDG uptake in the previously involved sites.

The overall accuracy at the 2-month assessment was 65% (15 of 23) for IWC and 91% (21 of 23) for both IWC + PET and EORTC ($P < .05$ vs IWC), while at the 6-month evaluation, accuracy was 83% (19 of 23) and 91% (21 of 23), respectively ($P = .39$).

Of the 14 patients with persistent complete response at mid-term follow-up,

Table 1

Overall Response Assessed at Mid-term Follow-up

Response	2-month Follow-up			6-month Follow-up			Mid-term Follow-up
	IWC	IWC + PET	EORTC	IWC	IWC + PET	EORTC	Comprehensive Assessment
Complete	6/23 (26)	12/23 (53)*	12/23 (53)*	10/23 (44)	12/23 (53)	12/23 (53)	14/23 (61)
Partial	10/23 (44)	4/23 (17)†	4/23 (17)†	6/23 (26)	4/23 (17)	4/23 (17)	2/23 (9)
Nonresponders (progressive + stable disease)	7/23 (30)	7/23 (30)	7/23 (30)	7/23 (30)	7/23 (30)	7/23 (30)	7/23 (30)

Note.—Numbers are raw data; percentages are in parentheses.

* $P < .05$ vs IWC.

† $P < .01$ vs IWC.

Figure 1

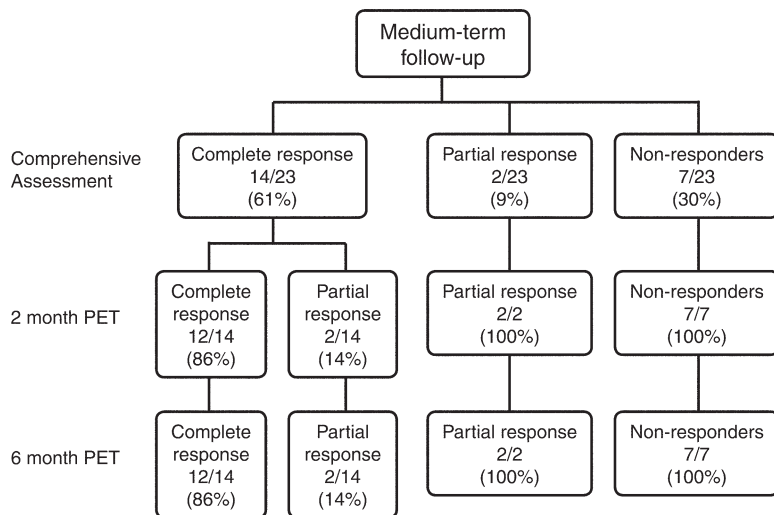


Figure 1: Overall responses assessed by using PET (IWC + PET) related to comprehensive assessment at mid-term follow-up.

12 were correctly identified by using 2- and 6-month IWC + PET, while IWC detected only six of them at 2 months and 10 at 6 months (Table 2).

Of seven patients who progressed at 2- and 6-month ¹⁸F FDG PET/CT, one had both a new lesion and showed changes in target lesions, while the others presented changes in target lesions only.

There was no difference in the number of locations at baseline between responders and nonresponders (3.9 ± 2.0 vs 4.3 ± 1.8; *P* = .69). At 2-month ¹⁸F FDG PET/CT, the mean change in the SPD of the target lesions was 83% ± 163 in nonresponders and -71% ± 23 in responders (*P* < .001); at the 6-month scan, the mean change in SPD was 146% ± 207 in nonresponders and -83% ± 22 in responders (*P* < .0001).

At both 2- and 6-month ¹⁸F FDG PET/CT, the SUV_{max} of target lesions was significantly lower in responder patients as compared with nonresponders (*P* < .05) (Table 3). At 2-month ¹⁸F FDG PET/CT, the mean change in SUV_{max} of the target lesions was 22% ± 67 in nonresponders and -78% ± 17 in responders (*P* < .001); at the 6-month scan, the mean change in SUV_{max} was 28% ± 73 in nonresponders and -79% ± 15 in responders (*P* < .001). In particular, no significant differences were found in SUV_{max} changes after RIT between patients with complete response and those with partial response at both 2- (-76% ± 16 vs -75% ± 16; *P* = .68) and 6- (-77% ± 15 vs -82% ± 8; *P* = .18) month scans. In patients with stable disease, SUV_{max} remained unchanged over time, whereas it increased in those with disease progression.

Clinical Follow-up and Survival

The median follow-up period was 12 months (range, 7–19 months). At the 6-month clinical evaluation, 10 (43%) of 23 patients had continued complaint of disease-related symptoms (no further therapies were implemented at that time), whereas the remaining patients experienced a substantial relief of symptoms, as well as recovery of hematologic parameters. In the latter group, clinical responses remained substantially unmodified thereafter. At mid-term follow-up, 14 (61%) of 23 patients had persistent complete response, two (9%) patients had partial response, three (13%) were considered stable and four (17%) showed progressive disease. None of the responders died or relapsed; in particular, those who achieved partial response showed clinical and hematologic improvement during the study.

In the nonresponders group, two (28%) of seven patients died because of late hematologic complications (severe neutropenia with lethal sepsis), three required red blood cell transfusion, and four patients underwent rescue chemotherapy with the combined regimen of rituximab and cyclophosphamide-doxorubicin-vincristine-prednisone at 12-month follow-up. One patient had evidence of a new location (soft tissue), two presented with a paravertebral relapse and histotype shift to large-cell NHL at biopsy; these findings were evident by 13-months (range, 10–17 months) of follow-up.

Receiver operator curve analysis showed that a reduction in SUV_{max} of 49% at both 2 and 6 months after RIT was optimal for differentiating metabolic responders from nonresponders. Better overall survival (Fig 2) was observed in patients with a reduction in SUV_{max} of 49% or higher (at both 2 and 6 months after RIT) as compared with those with a decrease of less than 49% (median survival, 15 vs 10 months; *P* < .05).

Discussion

Although results of several studies (14–16) have suggested the advantages of

Table 2
Accuracy of Predicting Results of Comprehensive Assessment at Mid-term Follow-up

Follow-up	Complete Response (14/23)		P Value
	Accuracy of IWC + PET (%)	Accuracy of IWC (%)	
2 months	86 (12/14)	43 (6/14)	<.01
6 months	86 (12/14)	71 (10/14)	.40
Agreement for 2 versus 6 months	100	59	

Note.—Numbers in parentheses are raw data used to calculate percentages.

Table 3

Assessment of Metabolic Tumor Response in Target Lesions

Comprehensive Assessment at Mid-term Follow-up	SUV _{max}			P Value
	Baseline	Two Months after RIT	Six Months after RIT	
Responders	5.7 ± 5.1*	1.3 ± 2.2*	1.2 ± 2.3*	<.0001
Complete response	5.7 ± 5.3 [†]	1.3 ± 2.2 [‡]	1.3 ± 2.4 [‡]	<.0001
Partial response	5.1 ± 2.6 [†]	1.2 ± 1.8 [‡]	0.9 ± 1.0 [‡]	<.01
Nonresponders	8.0 ± 4.9	9.9 ± 7.3	10.5 ± 7.7	<.05
Stable disease	5.6 ± 2.4	5.4 ± 3.5	5.9 ± 1.7	.95
Progressive disease	9.6 ± 5.5	12.9 ± 7.7	13.5 ± 7.9	<.05

Note.—Data are the mean ± standard deviation.

* $P < .05$ vs nonresponders.

[†] $P < .05$ vs progressive disease.

[‡] $P < .01$ vs nonresponders.

¹⁸F FDG PET for early chemotherapy result assessment, few trials have supported the benefits of such methods in the early assessment of RIT (17,18). Our study results suggest that metabolic findings obtained by using ¹⁸F FDG PET/CT at 2 months are not different from those at 6 months after RIT, and that both are predictive of clinical response assessment at 12-month follow-up. At present, standard guidelines recommend reassessing patient status after the completion of treatment every 3 months for 2 years, every 6 months for 3 years, and then annually (19).

Our findings further support the fact that ¹⁸F FDG PET/CT performed 8 weeks after RIT may provide useful information to correctly stratify treatment response in these patients (17,18,20). At this point, therapy-induced inflammation, which had been previously thought to affect imaging findings (21–24), does not appear to be a problem. Furthermore, Bodet-Milin et al (18) have recently reported that ¹⁸F FDG-PET imaging performed six weeks after fractionated RIT with humanized anti-CD22 ⁹⁰Y-epiratuzumab is reliable for early disease assessment.

They concluded that the best metabolic response could be determined as early as six weeks after RIT in more than 90% of cases and that the effect of radiation-induced inflammation at ¹⁸F FDG PET/CT is probably not an important consideration after the low-dose irradiation caused by RIT.

Nevertheless, there is a limited amount of data available concerning the optimal time to perform PET/CT studies after RIT (18,20). This is crucial, as early assessment of lesion metabolic response in NHL may be useful in suggesting the need for alternate therapeutic strategies earlier. In our study, results from ¹⁸F FDG PET/CT performed 2 months after RIT were equivalent to those from scans performed at 6 months (91% accuracy; 21 of 23) in evaluating outcome at mid-term follow-up, thus leading to a possible early change in patient management. Our results are consistent with those reported by other authors (25–28) on the response rate to RIT and with previous data on the important value of ¹⁸F FDG PET/CT in the assessment of metabolic response in these patients (11–14,20,29–31).

Morphologic data derived from CT (IWC) by using an independent assessment of images in responding patients showed lower complete response and higher partial response rates when compared with PET/CT results (EORTC or IWC + PET) at both 2 and 6 months. Although morphologic assessment has been considered the standard for helping detect therapy response, the limitations of conventional CT-based disease evaluation for NHL are well-known. The use of anatomic size criteria for lymph nodes is unreliable, since subcentimeter lymph nodes may be malignant and large nodes may be nonmalignant. Moreover, size reduction generally occurs slowly and over time, and posttreatment fibrosis is often difficult to differentiate from residual disease (18,20).

The accuracy of ¹⁸F FDG PET/CT in helping detect complete response in our study was higher than that of CT data alone. The findings of our study confirm those of earlier studies (17,18) that an early (at 2 months) metabolic assessment after RIT by using ¹⁸F FDG

Figure 2

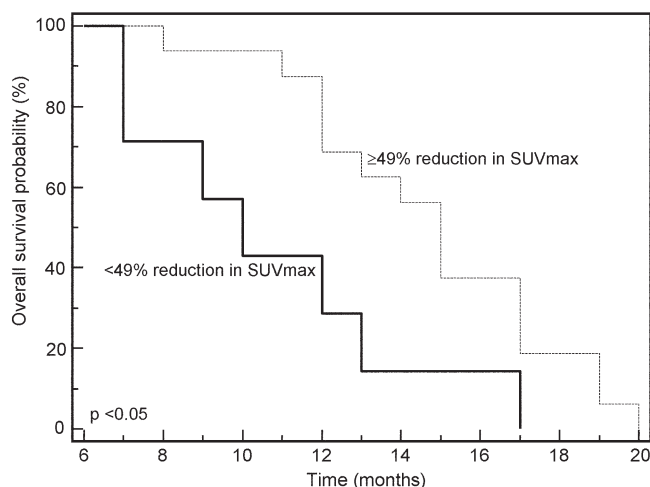


Figure 2: Overall survival versus percentage variations in SUV_{max}. Overall survival is longer for patients with decline in SUV_{max} of 49% or higher than in those with decline in SUV_{max} of less than 49%.

PET/CT provides the same information obtained later on (at 6 months) and correlates well with the clinical outcome resulting from the clinical follow-up, at least for the medium term (12 months). Moreover, our preliminary results demonstrate, as have others (20), that patients who were classified as responders by using 2-month ^{18}F FDG PET/CT data (and 6-month data, as well) had better overall survival as compared with nonresponders. Because even a partial response may suggest the need to alter therapeutic strategies, the advantage of PET/CT over CT alone in correctly helping identify complete responders at 2 months may be clinically relevant.

Quantitative analysis by using SUV with PET/CT examinations is not presently recognized as necessary to determine therapeutic response (11). We explored the utility of stratifying patient response early and predicting outcome after RIT according to the EORTC PET study group recommendations (13). As a result, in both responder and non-responder patients, the SUV variations detected at the quantitative assessment after RIT substantiated the findings obtained by using visual analysis (IWC + PET), further supporting the use of PET/CT for early stratification of patients undergoing RIT. These findings, as well as the data reported by others (16,20), suggest the need for prospectively validated quantitative criteria that can be used to determine response to RIT rather than relying on visual analysis alone. For instance, in our study, the incidental evidence of an increasing SUV in two nonresponders who were classified as stable disease by using IWC + PET criteria suggests the need for this type of study in the future. In addition, the analysis of variations in percentage for SUV_{max} observed after RIT was found to correctly stratify the patients according to overall survival and the ultimate outcome.

Our study had limitations. The first was the small sample size. The small number of patients enrolled derived from our strict entry criteria regarding indications for RIT while allowing the recruitment of a homogeneous group of patients. A second potential limitation

is our use of noncontrast CT. However, this is in keeping with published criteria for CT evaluation of treatment response, which are developed on the basis of mass size modifications and do not consider mass enhancement.

In summary, ^{18}F FDG metabolic data obtained 2 months after RIT correlate well with those obtained 6 months after RIT and with a mid-term clinical evaluation of response to RIT, showing a significant difference in SUV_{max} between responders and nonresponders with a better overall survival in patients with a large reduction in SUV_{max} as compared with those showing less of a decrease. Thus, early assessment of response to RIT by using ^{18}F FDG PET/CT might be useful in implementing further strategies or avoiding undue therapies and diagnostic procedures.

References

1. Kassam S, Montoto S. Oncologic, endocrine & metabolic emerging drugs in B-cell non-Hodgkin's lymphoma. *Expert Opin Emerg Drugs* 2008;13:323-343.
2. Cheson BD, Gregory SA, Marcus R. Emerging treatments for indolent lymphoma. *Clin Adv Hematol Oncol* 2007;5(suppl 8):1-9.
3. Horning SJ. Treatment approaches to the low-grade lymphomas. *Blood* 1994;83:881-884.
4. Lemieux B, Coiffier B. Radio-immunotherapy in low-grade non-Hodgkin's lymphoma. *Best Pract Res Clin Haematol* 2005;18:81-95.
5. Alcindor T, Witzig TE. Radioimmunotherapy with yttrium-90 ibritumomab tiuxetan for patients with relapsed CD20+ B-cell non-Hodgkin's lymphoma. *Curr Treat Options Oncol* 2002;3:275-282.
6. Marcus R. Use of 90Y-ibritumomab tiuxetan in non-Hodgkin's lymphoma. *Semin Oncol* 2005;32(1 suppl 1):S36-S43.
7. Jerusalem G, Beguin Y, Fassotte MF, et al. Whole-body positron emission tomography using ^{18}F -fluorodeoxyglucose compared to standard procedures for staging patients with Hodgkin's disease. *Haematologica* 2001;86:266-273.
8. Castellucci P, Nanni C, Farsad M, et al. Potential pitfalls of ^{18}F FDG PET in a large series of patients treated for malignant lymphoma: prevalence and scan interpretation. *Nucl Med Commun* 2005;26:689-694.
9. Jerusalem G, Beguin Y, Fassotte MF, et al. Whole-body positron emission tomography using ^{18}F -fluorodeoxyglucose for post-treatment evaluation in Hodgkin's disease and non-Hodgkin's lymphoma has higher diagnostic and prognostic value than classical computed tomography scan imaging. *Blood* 1999;94:429-433.
10. Cheson BD, Horning SJ, Coiffier B, et al. Report of an international workshop to standardize response criteria for non-Hodgkin's lymphomas: NCI Sponsored International Working Group. *J Clin Oncol* 1999;17:1244-1253.
11. Juweid ME, Stroobants S, Hoekstra OS, et al. Use of positron emission tomography for response assessment of lymphoma: consensus of the Imaging Subcommittee of International Harmonization Project in Lymphoma. *J Clin Oncol* 2007;25:571-578.
12. Cheson BD, Pfistner B, Juweid ME, et al. The International Harmonization Project on Lymphoma Revised response criteria for malignant lymphoma. *J Clin Oncol* 2007;25:579-586.
13. Young H, Baum R, Cremerius U, et al. Measurement of clinical and subclinical tumour response using [^{18}F]-fluorodeoxyglucose and positron emission tomography: review and 1999 EORTC recommendations—European Organization for Research and Treatment of Cancer (EORTC) PET Study Group. *Eur J Cancer* 1999;35:1773-1782.
14. Spaepen K, Stroobants S, Dupont P, et al. Prognostic value of positron emission tomography (PET) with fluorine-18 fluorodeoxyglucose ([^{18}F] FDG) after first-line chemotherapy in non-Hodgkin's lymphoma: is [^{18}F]FDGPET a valid alternative to conventional diagnosis methods? *J Clin Oncol* 2001;19:414-419.
15. Kostakoglu L, Coleman M, Leonard JP, et al. PET predicts prognosis after 1 cycle of chemotherapy in aggressive lymphoma and Hodgkin's disease. *J Nucl Med* 2002;43:1018-1027.
16. Haioun C, Itti E, Rahmouni A, et al. [^{18}F] fluoro-2-deoxy-D-glucose positron emission tomography (FDG-PET) in aggressive lymphoma: an early prognostic tool for predicting patient outcome. *Blood* 2005;106:1376-1381.
17. Torizuka T, Zasadny K, Kison P, Rommelfanger SG, Kaminski MS, Wahl RL. Metabolic response of non-Hodgkin's lymphoma to ^{131}I anti-B1 radioimmunotherapy: evaluation with FDG-PET. *J Nucl Med* 2000;41:999-1005.
18. Bodet-Milin C, Kraeber-Bodéré F, Dupas B, et al. Evaluation of response to fractionated

- radioimmunotherapy with 90Y-epratuzumab in non-Hodgkin's lymphoma by 18F-fluorodeoxyglucose positron emission tomography. *Haematologica* 2008;93:390-397.
19. Elis A, Blickstein D, Klein O, Eliav-Ronen R, Manor Y, Lishner M. Detection of relapse in non-Hodgkin's lymphoma: role of routine follow-up studies. *Am J Hematol* 2002; 69:41-44.
 20. Jacene HA, Filice R, Kasecamp W, Wahl RL. 18F FDG PET/CT for monitoring the response of lymphoma to radioimmunotherapy. *J Nucl Med* 2009;50:8-17.
 21. Spaepen K, Stroobants S, Dupont P, et al. [18F]FDG PET monitoring of tumour response to chemotherapy: does [18F]FDG uptake correlate with the viable tumour cell fraction? *Eur J Nucl Med Mol Imaging* 2003;30:682-688.
 22. Naumann R, Vaic A, Beuthien-Baumann B, et al. Prognostic value of positron emission tomography in the evaluation of post-treatment residual mass in patients with Hodgkin's disease and non-Hodgkin's lymphoma. *Br J Haematol* 2001;115:793-800.
 23. Wehrauch MR, Re D, Scheidhauer K, et al. Thoracic positron emission tomography using 18F-fluorodeoxyglucose for the evaluation of residual mediastinal Hodgkin disease. *Blood* 2001;98:2930-2934.
 24. MacManus MP, Seymour JF, Hicks RJ. Overview of early response assessment in lymphoma with FDG-PET. *Cancer Imaging* 2007;7:10-18.
 25. Witzig TE, Gordon LI, Cabanillas F, et al. Randomized controlled trial of yttrium-90-labeled ibritumomab tiuxetan radioimmunotherapy versus rituximab immunotherapy for patients with relapsed or refractory lowgrade, follicular, or transformed B-cell non-Hodgkin's lymphoma. *J Clin Oncol* 2002;20:2453-2463.
 26. Morschhauser F, Illidge T, Huglo D, et al. Efficacy and safety of yttrium-90 ibritumomab tiuxetan in patients with relapsed or refractory diffuse large B-cell lymphoma not appropriate for autologous stem-cell transplantation. *Blood* 2007;110:54-58.
 27. Gopal AK, Rajendran JG, Petersdorf SH, et al. High-dose chemo-radioimmunotherapy with autologous stem cell support for relapsed mantle cell lymphoma. *Blood* 2002;99:3158-3162.
 28. Zinzani PL, d'Amore F, Bombardieri E, et al. Consensus conference: implementing treatment recommendations on yttrium-90 immunotherapy in clinical practice—report of a European workshop. *Eur J Cancer* 2008;44:366-373.
 29. Juweid ME. Utility of positron emission tomography (PET) scanning in managing patients with Hodgkin lymphoma. *Hematology Am Soc Hematol Educ Program* 2006;259-265, 510-511.
 30. Juweid ME, Wiseman GA, Vose JM, et al. Response assessment of aggressive non-Hodgkin's lymphoma by integrated International Workshop Criteria and fluorine-18-fluorodeoxyglucose positron emission tomography. *J Clin Oncol* 2005;23:4652-4661.
 31. Ulaner GA, Colletti PM, Conti PS. B-cell non-Hodgkin lymphoma: PET/CT evaluation after 90Y-ibritumomab tiuxetan radioimmunotherapy—initial experience. *Radiology* 2008;246:895-902.